Interpretation of shallow buried maritime archaeological sites, using non-invasive methods, for in situ management and archaeological research purposes

By

Trevor Winton

Thesis
Submitted to Flinders University
for the degree of

Doctor of Philosophy

College of Humanities, Arts, and Social Sciences
11th May 2020

CONTENTS

LIST OF FIGURES

LIST OF TABLES

ABSTRACT

The potential application, and value, of using acoustic methods to map and monitor sub-seabed material found on maritime archaeological sites have been previously identified. Despite their apparent significant advantages, practitioners have not widely adopted in situ management approaches, and the concurrent use of sub-bottom profilers (SBPs). This work extends the application potential of parametric acoustics to in situ management at sites that are potentially 'at risk' from degradational loss of shallow-buried material, and provides a basis for greater practitioner uptake. In addition, for archaeological research planning purposes, preliminary non-invasive SBP data improves the efficacy of subsequent site investigations. The performance of a parametric SBP was assessed in situ on two control sites and on the historic *James Matthews* (1841) shipwreck site, against process driven data requirements from in situ preservation and research frameworks. At these control sites, multiple timber and ferrous 'sleepers' were purpose-buried in different configurations at a range of depths in different sediment environments. Performance attributes associated with the accuracy and reliability of locating buried timber, metal, slate and ballast stones, estimating their depth of burial (DoB) and identifying the lateral extent of a complex shipwreck site were quantified. Measurements of DoB for the keel, ribs and planking timber on the *James Matthews* shipwreck site identified a high risk of ongoing materials degradation, confirmed by previous independent testing. Reflection coefficient analyses based on in situ measurements differentiated the density, and hence degradation state, between the fully saturated and degraded oak timbers found on *James Matthews* and the adjacent partially saturated oak used in the buried sleepers. These analyses also demonstrated that the orientation of the wood buried in the sediment had minimal influence on DoB estimates, and confirmed earlier laboratory-based conclusions that wood orientation may not influence the magnitude of reflection coefficients calculated from in situ acoustic measurements. These are key outcomes since, a priori, the likely grain orientation of buried shipwreck timbers is unknown when gathering initial site data. Acoustically derived reflection coefficients, plotted against the known relationships between DoB, sediment dissolved oxygen profiles and degradation potential for a site, provide a tentative model with which to interpret in situ conditions. These validated outcomes reveal that the performance characteristics of the parametric SBP, utilised in archaeological applications, provide data which supports the theoretical frameworks for the protection of UCH derived from the 1992 European Valetta Convention and the UNESCO 2001 *Convention on the Protection of the Underwater Cultural Heritage*.

DECLARATION

I certify that this thesis does not incorporate without acknowledgment any material previously submitted for a degree or diploma in any university; and that to the best of my knowledge and belief it does not contain any material previously published or written by another person except where due reference is made in the text.

Signed 

Date 20/01/2020

ACKNOWLEDGEMENTS

To Marianna, Mack, Vicki, Wendy and David: Marianna, you helped me dream and lovingly supported my aspirations; Mack you showed me the way to achieve them and Vicki and Wendy, with many others providing assistance along the way, you helped me get there; and David, you observed my journey and aided me in the workshop, and in the field. I want to acknowledge the support and help I received from you and from so many other colleagues and friends—to all of you I owe a great deal of gratitude.

Mack (Michael McCarthy), you have been a long-time mentor, supporter and friend, and showed an enthusiastic volunteer that success in today's maritime archaeology world comes not from individual brilliance, but from harnessing a broad, disparate and changing range of skill sets. As an outsider, you brought me into your team and treated me as an equal. Over many discussions around your desk you graciously guided me along a pathway, over many years, to reach this point in time. Without hesitation, you provided me boating and diving support, both in the field and behind the scenes, and also showed me where to get the best fish burger in town on the way out to the dive site! I truly thank you for this, and hope that I can emulate your wisdom, and your leadership skills, as I further pursue my maritime archaeological interests.

I also am indebted to the support and the long-term friendship given to me by Vicki Richards. Vicky, your advice and shared enthusiasm around in situ management, and your generosity of time and laboratory support during the many hours of sediment and timber analyses, is acknowledged and deeply thanked. Likewise, my thanks and appreciation to others from the Western Australian Museum (WAM). Jeremy Green, you gave me complete and wholehearted approval and backing for the field activities and staff support which I truly appreciated, as well as providing GIS advice. Ross Anderson, Deb Shefi, Nicolas Bigourdan, Jon Carpenter, Rebecca Ryan, Kalle Kasi, Iva Cirkovick, Maddy Fowler and Tash Trenear—I thank you all for your field support, both on the water and on the seabed. I hope that the many slices of Marianna's boiled fruit cake on the boat after diving showed, in part, our gratitude. Thanks too Pat Baker, you directed me to the original archived underwater survey sheets and photography of the *James Matthews* following the 1975/76 excavation, which were key to the SBP verification success.

Despite the generosity of staff time from WAM, the field work could not have been completed without the volunteer assistance from members of the Maritime Archaeological Association of Western Australia (MAAWA). Patrick Morrison, Ian McCann, Kevin Edwards, Steve Wells and Mitch Cadden— thanks for assisting with the offshore field and diving roles, at least now you can all say you know how to dive in near-zero visibility conditions! Thanks too to David Jackson for your help with relocating the historic position of the *K8* submarine for a trial survey, and to Alan Stephens, Ian Warne, Ian McCann, Col Cochran, together with Helen and Sandy McCall, for your valued assistance

with the field work at the Swan River site. This work included the arduous task of standing knee-deep in shallow water shovelling muddy sands in collapsing holes to bury sleepers—truly committed supporters!

And to my supervisors Wendy Van Duivenvoorde, Jonathan Benjamin and Paul Baggaley, and friends at Flinders University. My deepest gratitude Wendy for supporting my ideas and research objectives from the beginning, for the freedom and encouragement to execute my research plan, and for the many chats over coffee and lunch where you provided guidance and advice when needed. You taught me that there are different styles of writing for different occasions, and helped me to improve my own with shorter sentences and better use of the active tense! To Paul and Jonathan, thanks for steering me to the parametric SBP and helping to set my technical direction. Thanks for the friendship, shared beers, encouragement and generous hospitality extended to me by my fellow PhD Candidates during my many visits to campus, especially to you Celeste Jordan, John McCarthy, Enrique Aragon, Katarina Jerbic and Mimi Eldeeb—I wish you all success, and trust that our futures will remain entwined.

Technical support, in conjunction with specialist software, field and laboratory equipment, came from a few key individuals and companies. Special thanks go to you, Doug Bergerson. Your tireless responses to my numerous technical questions regarding software setup and interpretation of SBP field data, especially in the early stages was much appreciated—I think that I would still be bogged down if you hadn't provided that early advice! But especially I want to thank you for providing your time and the Innomar parametric SBP, together with the satellite positioning equipment, for the two field measurement trips. I also want to acknowledge and thank Sabine Mueller, Jens Wunderlich and Jens Lowag from Innomar Technologie GmbH for your wise advice, access to your proprietary software, and for the opportunity to publicly present my initial and final key results for critical technical feedback. Likewise, thanks to QPS for provision of your proprietary Fledermaus software, C.R. Kennedy and Company Pty Ltd for use of your RTK DGPS positioning equipment, and to Fugro Satellite Positioning Pty. Ltd. for access to your Marinestar positioning solutions. At UWA Centre for Offshore Foundation Systems, I would like to thank Conleth O'Loughlin and Ryan Beemer, and the staff from the National Geotechnical Centrifuge Facility Preparation Laboratory and the Soils Laboratory. Access to your advice and facilities enabled me to undertake ex situ sediment density and grain size analyses, respectively.

I acknowledge the financial support provided to me from the award of an Australian Government Research Training Program Scholarship. I also acknowledge and thank Flinders University and the Australasian Institute for Maritime Archaeology (AIMA) for the 2017 Research Higher Degree Project Funding Award, the Research Student Conference Travel Grant, and the 2018 AIMA Scholarship Award, which greatly assisted with field and travel expenses. Also thanks to Alastair Paterson for your support for the costs to undertake the sediment grain size analyses at UWA.

To David, my son: in part I did this work for you. You have grown up alongside most of the people mentioned here, and are part of this story. You have become a great young man, and your future awaits. By undertaking this thesis, I wanted you to understand that with a plan, enthusiasm, commitment, perseverance and support, you too can achieve your dreams, however challenging and ambitious they may be, or how far and wide they may take you.

And once more to Marianna, my wonderful wife, whose love and support has made me a far better person and helped me get to this position. You sacrificed your favourite room in the house so that I could have an office. You put up with me being 'absent' during times of my single focus to complete different components, and carried an additional burden along my PhD journey. You undertook the initial manuscript reviews, complimented me on the bits that were written well, and pointed out where parts didn't make sense—you often said that 'if I couldn't understand what you had written, then others would not either'—so you would get me to tell you what I meant, and when my explanation was clear to you, I then rewrote the words into their current form. Thank you my darling for all of your care, love, patience and encouragement over these past years. I would not have been able to accomplish my dream without you.

1. INTRODUCTION

Framing the thesis

There is a growing world-wide appreciation of the importance of protecting maritime archaeological sites against the loss of UCH material subject to ongoing or accelerated degradation. There have been and still are however, impediments in providing such protection. In Australia there are over 8,000 registered shipwrecks representing the full spectrum of materials associated with ship construction, propulsion systems, weaponry and cargos. In addition to shipwrecks, submerged aircraft with modern alloys are also considered and protected as important maritime archaeological sites. Globally, there are estimates of over three million shipwrecks and tens of thousands of submerged settlement sites (Gregory 2012:368; UNESCO 2001).

In situ management of maritime archaeological sites can reduce the detrimental impacts from recognised in situ, or site-formation processes (Gregory 1996; Gregory 2009; Gregory and Matthiesen 2012a). To understand these site-specific processes, and hence effectively manage underwater archaeological sites, non-invasive baseline and periodic monitoring data are required (Gregory 2009; Oxley 2016:215). These data need to provide information on the extent of the site to be managed, the most significant threats to that site, the types of materials present and their state of preservation. The data also needs to inform mitigation, stabilisation and preservation strategies (Gregory 2009:10–12).

Previously, while considering site management decisions involving potential excavation of shipwreck material, Arnott et al. (2002b:699) noted that 'there were no methods currently available that could provide that information without destroying or disturbing the artefacts….however acoustic methods offer possible solutions'. Gregory also noted the follow up work by Arnott, and others, which demonstrated the potential of marine geophysics to rapidly map the spatial distribution of wreck material in situ, and the state of preservation (density) of those materials (Gregory 2009:2,6). Manders et al. (2008:184) and Gregory and Manders (2015:37) advocated that acoustic sub-bottom profiler (SBP) instruments can provide a non-intrusive view of material below the seabed, and so shipwreck and submerged sites could then be interpreted and/or managed with the UCH material remaining undisturbed in their protective burial environments. Gregory and Manders (2015:37) and (Gregory 2015b:369) further noted that the use of SBPs for site mapping and monitoring purposes is 'a cutting edge method' and would make a 'powerful tool… for managing submerged cultural heritage sites'.

During the past two decades the capacity to qualitatively map selected buried timbers, the sedimentary environment, peat structures and ferrous material has grown. Chirp SBP technology has evolved and been primarily and successfully used in research environments to identify, map and determine acoustic properties of buried shipwreck timbers in the United Kingdom (UK), for example Plets et al. (2008); Plets et al. (2005); Plets et al. (2007b); Quinn et al. (1998a); Quinn et al. (2002); Quinn et al. (1997c). This work encompassed sites with European timber species buried in muds and fine grained siliceous (quartzoze) sands. More recently, parametric SBPs have been applied on European shipwreck and submerged sites (Gregory and Manders 2015:35–37; Missiaen 2010a; Missiaen et al. 2012; Missiaen et al. 2017a). Independently, magnetometer surveys have been used to identify large scale structures and the presence and spatial location of ferrous metals both on and under the seabed (Camidge et al. 2010; McCarthy 2019).

Despite these advances, Oxley and Keith (2016:8) commented that while practitioners have acknowledged the importance of site formation theory, and the resulting approaches to in situ management, they 'have not adopted widespread practices to do so'. These authors argue that this lack of action may arise from 'a lack of funding, limited time and lack of access to the necessary specialists'. It may also come from confusion or lack of confidence on how and when to apply in situ preservation methods (including the use of SBPs), their value and effectiveness. This has been revealed by a practitioner attitude survey (Ortmann 2009:79; Ortmann et al. 2010:36–38) and responded to by UNESCO (2013:20) in their *Manual for Activities Directed at Underwater Cultural Heritage*.

Extensive international research efforts have focussed on improved understanding of in situ processes, in situ preservation and in situ management techniques, for example, Gregory (2015b); Manders (2004); Manders (2010b); Nyström Godfrey et al. (2012); (Richards 2012; Richards et al. 2014). Published SBP research that identifies, maps and characterises a broader range of buried shipwreck material in differing sedimentary environments is, however, still lacking. This includes timber species associated with Australian Colonial shipbuilding practices (1850 to 1899) (O'Reilly 2007:1) as well as those used in European ship construction, iron and non-ferrous metals together with their encrusting corrosion biproducts, and ballast stone and other cargo materials. The mapping and quantification of materials buried in medium–coarse carbonate and siliceous sand environments is missing. With the exception of a buried canister trial and the opportunistic post-survey dredging and recovery of cylinders and poles, published reporting of quantitative performance trials is also lacking. This includes the absence of quantified accuracies of depth of burial (depth of sediment cover)

measurements and of confidence estimates for the identification/interpretation of buried reflectors and/or their derived material properties.

This research, as set out below, consequently examines the process-oriented approach to in situ preservation and management, and identifies how and when SBPs can be effectively applied by practitioners. It addresses some of the application gaps in different sedimentary environments and buried material types. For the first time, this research quantitatively investigates, in situ, the reliability and accuracy of parametric SBPs to map sites, measure depths of burial (DoB) and differentiate between different buried timber species, iron and ballast stones, and timber degradation states. This extends the application potential of parametric acoustic SBPs to in situ management sites that are potentially 'at risk' from loss of archaeological material, as envisaged by Arnott et al. (2002b). Hopefully it also provides greater practitioner confidence for their applicability. The research question is then:

How can non-invasive in situ methods be applied to current theoretical frameworks for UCH management and archaeological research pertaining to shallow buried archaeological material?

The question can be deconstructed into three specific sub-questions. Firstly, how can non-intrusive SBP data, together with complimentary geophysical data, be applied to current theoretical frameworks to improve the assessment and management of maritime archaeological sites potentially 'at risk' from further degradation? Secondly, with what level of confidence can parametric SBPs be used to locate, quantify the depth of sediment cover of shallow (from zero to 50 cm) buried material and determine site extent? And thirdly, how can major types of buried material on a site, together with their state of degradation, be identified in situ using non-invasive measurements?

The research objectives which evolve from these questions are:

- review the theoretical frameworks for UCH management, the influence and outcomes of the UNESCO 2001 *Convention on the Protection of the Underwater Cultural Heritage* on these frameworks, and the important relationships between burial depth of UCH material and *in situ* degradation processes to identify the implementation gaps and needs;
- determine the confidence estimates associated with either correctly or incorrectly identifying modern artefact replicates, comprising different timber and ferrous materials, that were purpose-buried between 10 cm and 50 cm in calcareous and siliceous sediments, using a parametric SES-2000 compact SBP;

- determine the accuracy of Depth of Burial (DoB) measurements for these modern artefact replicates buried under controlled conditions in course calcareous and siliceous sediment environments using the parametric SES-2000 compact SBP;
- determine the horizontal accuracy associated with the use of the parametric SES-2000 compact SBP in locating buried modern artefact replicates;
- analyse the relationships between the parametric SES-2000 compact SBP reflection characteristics (magnitude and phase), and the material properties of the modern artefact replicates, to assess the material type; and for timber, its grain orientation and degradation state; and
- verify the parametric SES-2000 compact SBP performance on an actual complex shipwreck site, which has previously been archaeologically surveyed in three dimensions (3D), to independently test the application of the SBP for in situ management and archaeological purposes.

This thesis contributes new knowledge by quantitatively investigating in situ the applicability of parametric SBPs to UCH management and archaeological research, consistent with the principles of UNESCO's 2001 *Convention on the Protection of the Underwater Cultural Heritage*. It validates for the first time the accuracy of the important depth of sediment cover (DoB) measurements which are key to assessing whether or not sites are potentially 'at risk' from loss of buried archaeological material. It demonstrates the interpretation of in situ derived reflection coefficient analyses, which to the present, have primarily been determined from laboratory analyses. The results also address questions regarding the significance of buried timber orientations on SBP measurements—differences in buried timber axial directions appear to have minimum effect on DoB measurements. Also, differences in axial reflection coefficient values, which can be accurately derived and differentiated in laboratory tests appear to be less significant for archaeological site interpretation due to the influence of other site factors, when measured in situ. In addition, this thesis demonstrates that the combination of accurate SBP derived DoB estimates and measured sediment chemistry, particularly sediment dissolved oxygen profiles, can provide the basis for a site-based risk assessment model of loss of timber and iron based archaeological materials.

Theory and methodological approach

This research takes a scientific archaeological approach, applying processual archaeology and middle-range theory. The application of archaeological science has grown rapidly during the past 20 years (Killick 2015:242–243) and a number of authors have written on this theoretical approach to archaeological research (Cunningham 2008; Johnson 2008; Raab and Goodyear 1998; Shott 1998; Stanish 2008). Stanish (2008:1358–1359) reviewed four kinds of

archaeological research ranging from the least to the most scientific based on their respective philosophical foundations and goals. These were: critical theory; hermeneutic or interpretative archaeology; historicist archaeology; and scientific archaeology. He described scientific theory as a branch of behavioural and social science, associated with 'explanation' and 'causality'. Under this theory, no direct link between material culture and behaviour is assumed, as both natural and cultural processes alter the archaeological record in space and time (Stanish 2008:1362). Contemporary scientific archaeology uses a broad range of systems, including technology and ecology, often combining them to provide complex and multivariable explanations. Whereas processual archaeology used to be synonymous with New Archaeology, Stanish (2008:1362) argues that now it is simply another term for scientific archaeology.

The primary goal of processual archaeology is to 'explain the variability in the archaeological record by reference to general cultural processes' by, in part, 'studying the archaeological record in terms of itself' (Johnson 2008:1894). Frustrated by the lack of existing knowledge to achieve this goal, the focus of processual archaeology turned to developing methods for observing and interpreting the archaeological record and identifiable patterns, with which to explain variability. Johnson (2008:1895) states that this approach is commonly referred to as 'middle-range research' or 'middle-range theory'.

Like processual archaeology, the aim of middle-range research is to identify the causal forces that combine to create the material patterns observable in the archaeological record (Cunningham 2008:1620). 'Testability' and verification are key properties, and scientific studies and experiments are important sources, for middle-range theory (Shott 1998:303–305). Research methodologies using middle range theory include technically sophisticated experimental processes to understand patterns in the archaeological record, and these may specifically be applied to the study of site formation processes (Raab and Goodyear 1998:218). The most successful advances have been the highly technical analyses where the research plan has been theoretically based in the hard sciences to identify a limited number of causal forces affecting the archaeological record (Cunningham 2008:1622). This technical experimental practice is well illustrated in Schiffer's model of n-transforms and c-transforms to account for the natural and cultural formation processes affecting the archaeological record (Caporaso 2017:10–14; Schiffer 1972; 1987). In maritime archaeological applications, it was Muckelroy (1977) who was the first to conduct a systematic study of shipwreck site formation processes using middle-range theory (Delgado 1997:387; Gibbs 2006:4). Subsequent environmental and cultural site formation models expanded Muckelroy's initial work, and applications based on middle-range theory included interpretations of the HMS *Pandora*

(1791) and SS *Xantho* (1872) shipwreck sites (Gibbs 2006; Gibbs and Duncan 2016; McCarthy 2000; Stewart 1999; Veth 2006:21–23; Ward et al. 1998; Ward et al. 1999). Anuskiewicz (1998) provided guidance to maritime archaeologists using geophysical data as a tool for middle-range theory building. In his research using a magnetometer on and around St. Catherines Island, Georgia, USA, the magnetometer signatures for specific maritime features, and their verified archaeological correlates, formed the foundation of middle-range theory for his maritime sites. Anuskiewicz (1998:230) demonstrated that the systematic application of scientific methods and remote sensing equipment, founded on middle-range theory, provided the desired outcomes of the study—identifying the location of modern shipwreck sites, both on St. Catherines Island and other similar physiographic sites.

The research methodology adopted in this thesis was consequently based on the middle-range (scientific) archaeology model, using scientific methods and geophysical tools, to investigate shallow-buried archaeological materials. This approach is appropriate given the proposed in situ testing and verification of SBP measurements associated with shallow-buried archaeological material and environmental markers for site formation processes—and the subsequent interpretation of their combined impact on the risk of further material degradation loss. The model provides a framework in which in situ and ex situ experimental analyses, embedded in the geophysical, physical and biological sciences, can be undertaken to address the research objectives and question. The procedure incorporates a scientifically based two-step experimental process (NATA 2018; NSW Department of Primary Industries 2015) around non-invasive measurements of site formation related variables which affect the archaeological record. The first step involved trialling the SBP performance in situ, under tightly controlled burial conditions—the ‘validation’ step. The performance of the SBP under actual complex wreck-site conditions was then quantitatively assessed in the second step—the ‘verification’ step. The validation step ‘confirms whether or not a specific technology meets its performance target under controlled conditions’, and verification involves ‘monitoring under actual conditions in a non-simulated environment’ (NSW Department of Primary Industries 2015 :1-2). This process provides objective evidence that a method is ‘fit-for-purpose’, meaning that ‘the particular requirements for a specific intended use are fulfilled’ (NATA 2018:4).

The validation step was achieved by trialling the parametric SES-2000 *compact* SBP over 26 purpose-buried timber and ferrous sleepers at a coastal site on the northern side of Woodman Point, and over 18 sleepers at a fluvial site at the confluence of the Swan and Canning rivers, both located within the Perth metropolitan area of Western Australia. In this thesis, these sites are referred to the James Matthews sleeper site to avoid confusion with the adjacent *James Matthews* (1841) shipwreck site, and the Swan River sleeper site, respectively. Sediments

were characterised as medium-fine grained calcareous sands at the offshore site, and medium grained siliceous sands, with a higher proportion of coarse sand, at the river site. The sleepers were fabricated from air dried European oak, freshly cut radiata pine and jarrah (an Australian hardwood), and iron. At both sites they were buried as single sleepers in duplicate or triplicate numbers at multiple depths from 10 to 50 cm sediment cover. Two sets of sleepers were stacked vertically, and while nearly all of the sleepers were buried with the timber's long grain horizontal, some were buried with the long grain oriented vertically and some with the top flat surface inclined 22.5 degrees to the horizontal. Environmental conditions were controlled through in situ measurement of water quality parameters and ex situ measurements of sediment properties from 50 cm long sediment cores collected adjacent to the buried sleepers, and at undisturbed reference sites. Timber moisture and density conditions in the sleepers at the times of SBP measurement were controlled by analysing sacrificial timber blocks of each of the timber types which had been buried at the same time and depths as the sleepers. A representative number of blocks were subsequently removed at the time of SBP measurement for ex situ analyses.

Verification was achieved by using the parametric SES-2000 *compact* SBP to survey the buried remains of the *James Matthews* wrecksite located on the northern side of Woodman Point, adjacent to the James Matthews sleeper site. *James Matthews* was a French composite Snow Brig purpose-built in 1835 for the slave trade which had been subsequently captured and sailed to the newly established Swan River colony. During this last voyage it was carrying four passengers and general cargo including roofing slate, iron bars for blacksmithing and farm machinery (Henderson 2009:67–70, 107–231). Shortly after arrival it foundered during a storm after its anchor cable broke. The wrecksite was discovered in 1973 and the Western Australian Museum (WAM) undertook successive excavations and archaeological surveys between 1974 and 1977, and again in 2000 to undertake a conservation survey (see Chapter 3 for a detailed history of *James Matthews*, the discovery and archaeological surveys of the wrecksite). After each survey period the site was backfilled. While some archaeological material was removed from the site during the 1970s for conservation and display purposes, this site, together with its detailed 3D survey of the remaining buried material, provided the ideal situation to test and verify the SBP. Due to seabed erosion on the site from 2000 onwards and the subsequent exposure of previously buried material, WAM has undertaken numerous archaeological, conservation and site formation studies, formulated an in situ management plan, and carried out reburial actions to protect this significant site from further degradation and loss of material.

Thesis structure

The remainder of this thesis is structured in six chapters which are summarised as follows.

Chapter 2 addresses the first research objective derived from the research question. It discusses the literature associated with in situ methods applied to theoretical frameworks for UCH management and archaeological research. Commencing with Muckelroy's leading study of shipwreck site formation processes and Gregory's alternate model, it progresses through the development of international conventions and documents such as the European Valetta Convention, culminating in the adoption of the UNESCO 2001 *Convention on the Protection of the Underwater Cultural Heritage*. The aspirational rules of these conventions gave rise to numerous scientific research programs investigating site formation, depth related degradation processes, and effective reburial of waterlogged UCH material. The knowledge gained from these programs resulted in further refinements to the theoretical frameworks for UCH management and archaeological research pertaining to shallow-buried archaeological material. The chapter concludes with a review of the past and current use of SBPs in maritime archaeological applications, and acoustic properties in timbers and sediments related to SBP interpretation.

Chapter 3 details the methods used to construct and install the purpose-buried sleepers, and associated timber blocks at both sleeper sites. In situ and ex situ measurement and analyses processes for controlling water quality parameters, sediment and timber variables are presented. SBP data collection procedures using vessel mounted and purpose-built seabed sled mounted transducers across the buried sleepers and the remaining material from the *James Matthews* wrecksite are also described, together with methods used to extract and analyse the SBP data.

Chapter 4 presents all data and results from these sites and SBP measurements. From the controlled sites this includes water quality data, sediment dissolved oxygen and redox profiles, sediment grain size, sediment bulk density and sediment in situ density. Data from recovered sacrificial timber blocks included moisture content, bulk and basic density. Data interpreted from the vessel mounted and seabed sled mounted SBP included mean values and statistical variability around depth of burial, sleeper thickness measurements and reflection coefficients. For verification, original hand-drawn WAM underwater survey recording sheets were digitally transformed into a 3D AutoCAD model of the buried remains of *James Matthews.* Forty-seven transverse and longitudinal SBP runs directly over the *James Matthews* wrecksite were gridded (interpolated) into a 3D volume, from which horizontal depth slices were prepared for visual comparison with the 3D AutoCAD model. Qualitative comparisons were made between

three transverse and three longitudinal seismic cross-sections to the known wrecksite features.

Chapter 5 interprets the data and results from the validation and verification steps, both individually and in combination. The ease and speed of operability, and consistency of data interpretation from vessel and underwater sled-mounted SBP in shallow waters from 0.9 m to 2.8 m deep, were demonstrated. High confidence in correctly identifying the presence of buried material at the experimental sleeper sites, and at the *James Matthews* wrecksite, was established together with the mapping of the aerial extent of the buried material at this complex wrecksite. Following correction to default velocity estimates in the water column and in the sediments using in situ data, the SBP results statistically matched the true burial depths within a 95th percentile range of 0.6 to 2.5 cm. On the *James Matthews* wrecksite burial depths in the range 14 cm to 60 cm were verified. Complimentary surveys with magnetometers afforded insights into the depth and distribution of ferrous material across the site. The SBP data could not alone provide definitive descriptions of material types buried on a site. The data was able to discriminate, however, changes in timber density associated with water logging and degradation, and provide interpretation of buried shipwreck remains, sediment layering and other acoustic interfaces buried throughout the *James Matthews* site.

Chapter 6 discusses the theoretical frameworks for UCH management and the need for non-destructive sub-seabed in situ measurements. These data are used in assessing the risk of further material degradation loss, providing key information with which to make sound in situ management plans, and monitoring the success of those plans. The chapter progresses with a description of how the quantified results from SBP performance verification meet those UHC in situ management and research needs. This includes their applicability to determining site extent, the measurement of the key depth of burial parameter, and estimating buried material types and their density. These outcomes are compared to laboratory derived results and provide in situ verification to tentative conclusions based on the laboratory data regarding the acoustic in situ measurement of timber density buried under the seabed. The chapter concludes with a discussion on how SBP data can help interpret the degradation risks, and provide input into research plans for a complex site such as the *James Matthews* wrecksite.

Chapter 7 summarises the conclusions from this study, and identifies recommended opportunities for future advancement of this work.

2. LITERATURE REVIEW

Introduction

This chapter discusses the literature associated with in situ methods applied to theoretical frameworks for UHC management and archaeological research. As outlined in the previous chapter, the assessment of in situ management encompasses the analysis of in situ protection, conservation and processes, the latter otherwise known as site formation processes. International conventions, legislation and evolving best-practice guidelines applicable to in situ management are reviewed. Non-invasive geophysical techniques, including the growing use of SBPs are summarised. The lack of purpose-specific 'fit for purpose' trials to assess their suitability for archaeological in situ management applications, is highlighted.

Pragmatically, the principles of in situ management for submerged archaeological sites were developed around integrated environmental/coastal zone management philosophies, including key components such as: good data as a pre-requisite for good decision making; developing an understanding of the site's environment; defining site formation transforms and processes of change; baseline and ongoing monitoring; responding to change; and promoting non-intrusive access (Oxley 2001). In developing in situ management strategies for Scotland's underwater cultural heritage, built on contemporaneous international shipwreck management studies, Oxley (1998:160) noted that management success is predicated on a comprehensive understanding of the marine environment in and around shipwreck sites. In addition to comprehending the site's physical environment, measurement and monitoring of the 'deterioration of materials and the various chemical and biological parameters' operating at the site is important. This information is needed to understand the formation of the archaeological record at the site and to manage the ongoing preservation of the UCH materials (Gregory 1996). With some notable exceptions however, the long-term success of in situ management associated with these early projects suffered from either a lack of available site data for guidance, or as a result of strategies driven by short-term, contingency goals (Oxley and Keith 2016:7–8). Further research and technology development, galvanised by international legislation, was needed.

The remainder of this chapter is structured to review the literature pertinent to the research question developed in Chapter 1. The review commences with a discussion on site formation processes as the basis for the initial theoretical framework for underwater cultural heritage management. The subsequent evolution of the theoretical frameworks is traced through the world-wide stimulus for in situ management, and the protection of UCH which grew with the

successive advancement and approval of international conventions and aligned national/state legislation. These aspirational and legally binding requirements fostered international research from which practitioner guidelines, best practise techniques and technologies, and new theoretical models for protection of UCH evolved. These programs and outcomes are summarized as they have created the environment from which the research in this thesis has formed. Finally, the development and use of non-invasive geophysical technologies, specifically sub-bottom profilers as a powerful tool for the process-driven in situ preservation and archaeological research approach, is critically reviewed.

Site formation processes as the theoretical framework for UCH management

Factors that create the archaeological record are known as formation processes (Schiffer 1987:7) and these factors can be both cultural and non-cultural (natural). Terrestrial archaeologists realised in the early 1970s that the archaeological record did not directly reflect past societies, and they began to 'systematically investigate the transformational processes responsible for distortions' (Delgado 1997:386). Clarke developed five theories for interpreting archaeological finds: pre-depositional and depositional human influences; retrieval, connecting materials which survive and are recovered; analytical, the analysis of recovered material; and interpretive, the connection between archaeological patterns and past behaviours. On a parallel track, Michael Schiffer, a behavioural archaeologist, refined archaeological inference by reducing, correcting or controlling for distortions (transforms) inherent in the archaeological record. Schiffer (1972) distinguished between transforms in the systemic context (when artefacts are part of a cultural system, c-transforms) and in the archaeological context (when artefacts interact with the natural environment, n-transforms). The application of transformation process analyses to shipwrecks was first suggested by Schiffer and Rathje in 1973, however it was Muckelroy, influenced by Clarke, who conducted the first systematic study of shipwreck site formation processes (Delgado 1997:387).

Muckelroy's seminal research was based on shipwreck sites around the coast of the United Kingdom (UK) (Muckelroy 1977). From his analysis of historical and archaeological data of the *Kennemerland* site in the Shetland Isles, Muckelroy developed a theoretical site model, depicted as a flow diagram (Muckelroy 1976:282). This diagram represented the evolution of a shipwreck from the process of wrecking through to the observed sea-bed distribution of model was later reproduced in his more comprehensive volume (Muckelroy 1978) and this work was considered to be one of the first attempts to 'develop and apply explicit middle-range theory for maritime archaeology' (Gibbs 2006:4). Based on existing information on the

archaeological remains at 20 wrecksites within the UK, Muckelroy (1977; 1978) studied the environments at those sites and developed a wrecksite classification, as listed here:

- Class 1–sites where a coherent ship's structure substantially survived;
- Class 2–slightly less coherent and complete;
- Class 3–no ship's structure but a substantial amount of surviving organic material and ship's artefacts;
- Class 4–no organic material surviving but still a substantial number of ship's artefacts; and
- Class 5–sites where only heavy metal and stones survive.

Muckelroy (1978:165–181) defined two main shipwreck site formation processes, those being 'extracting filters' and 'scrambling devices'. Extracting filters were mechanisms that took material away from the wreck, such as those during the wrecking event, salvaging and disintegration of materials. Scrambling devices resulted in artefacts being moved around the post-depositional site, including seabed movement, wave action, currents and marine animal disturbance.

Following Muckelroy, site formation research focussed on predictive models to explain the presence of artefacts using correlations between the observed distribution of shipwreck sites and their environmental attributes. Gregory (1996:3) reasoned however, that such retrospective interpretation of formation processes doesn't allow for temporal differences and may be misleading. Muckelroy himself noted (1977:55) that there were very low correlations between artefact survival characteristics and storm conditions, tidal currents and water depth at those sites. Gregory (1996:107) further argued that the natural environment should be studied in order to understand and define the processes which currently affect shipwreck sites, rather than predict which natural processes affected a site based on the observed state of its preservation. Such an understanding of the processes governing the present-day site could be used to predict the preservation or degradation of shipwreck sites, and this knowledge used to develop methods to mitigate these effects.

In addition to Gregory's call, there was a growing awareness of the opportunity and value of studying the inter-relationship between site formation processes, materials conservation and site assessment (see for example (MacLeod and Killingley 1982). A number of investigations encapsulating the physical, biological and chemical processes at specific shipwreck sites followed, for instance those described and summarised in Stewart (1999) and Wheeler (2002). Others articulated theoretical models of shipwreck disintegration, building on Muckelroy's

original flow-chart, but incorporating physical, chemical and biological changes that occur variably through time (Ward et al. 1998; Ward et al. 1999).

While the development of process-oriented formation models was advancing, they were primarily based on site environmental processes. Gibbs (2006:4) lamented that 30 years on from Muckelroy's pivotal work in 1976 'research on the cultural processes which contribute to the creation and modification of shipwrecks remained limited'. He proposed a similar process-oriented framework (his disaster response model), which parallels the physical processes, to 'integrate and synthesize the documentary, oral and archaeological evidence of the human response to shipwreck'.

Today there is a large volume of research reported in the literature describing studies investigating cultural and environmentally based site formation processes. Stewart (1999) summarises formation studies conducted up to the end of the twentieth century at shipwreck sites, intentional ship deposition sites, inundation of coastal sites and sites subject to refuge disposal. He also describes and references post-depositional process studies including: cultural formation processes associate with reclamation, construction, fishing, dredging, and disposal of refuse; and environmental formation processes associated with bioturbation, waves, tides and currents, and the effect of gravity. This author (Winton 2015) provided a bibliographic overview of the physical, biological and chemical processes, along with their environmental and anthropogenic influences that can operate on UCH sites. He also demonstrated that many of these site formation processes are interlinked, forming interactive systems, and that these linkages need to be adequately understood in order to effectively manage submerged archaeological sites in situ. Recently Matthew Keith edited a book *Site Formation Processes of Submerged Shipwrecks* (2016) in which leading researchers wrote chapters dedicated to: natural processes (geomorphological changes, sedimentation, scour, corrosion products and degradation of wood); cultural processes (anthropogenic impacts, trawling and cultural processes affecting shipwrecks and ship mishap sites); and site formation and heritage management (English Heritage's approach, management of deep-water WWII shipwrecks in the Gulf of Mexico, and the *U-166* and *Robert E. Lee* Battlefield).

As Gregory (1996:107) anticipated, site formation process studies are now central to in situ management planning for the protection of underwater archaeological sites and conservation of their artefacts. Examples include: *James Matthews* and *Clarence* (1850) in Australia (Godfrey et al. 2005; Heldtberg et al. 2004; Richards 2001; 2011b; Richards et al. 2007; Richards et al. 2012; Richards et al. 2013; 2014; Shefi et al. 2014; Veth et al. 2013); *Stora Sofia* (1645) wrecked on the west coast of Sweden (Bergstrand 2010); shipwrecks in the Baltic Sea (Björdal 2012a); the Duart Point wreck, UK (Gregory 1999); the many thousands of

artefacts at Nydam Mose, Denmark (Gregory and Matthiesen 2012b); and conservation of World War II wrecks in Chuuk Harbour, Federated States of Micronesia (MacLeod and Richards 2011). In situ management guidelines based on the outcomes from these studies, and from international research projects such as the Monitoring, Safeguarding and Visualizing North-European Shipwreck Sites (MoSS), Preserving cultural heritage by preventing bacterial decay of wood in foundation piles and archaeological sites (BACPOLES), Reburial and Analyses of Archaeological Remains (RAAR), Survey, Assess, Stabilise, Monitor And Preserve underwater archaeological sites (SASMAP) and Managing Cultural Heritage Underwater (MACHU) research projects (Gregory 2015b; Manders 2004; Manders 2010b; Nyström Godfrey et al. 2012), are discussed in the following sections. Firstly though, the international conventions and national/state legislation which provided the research impetus, and politically galvanised in situ protection of underwater cultural heritage, are examined.

International conventions and legislation driving research and implementation frameworks for in situ protection of UCH

This section discusses the development of international conventions, guidance rules and legislation which evolved from world-wide concern for the protection of underwater cultural heritage, and the subsequent implementation research and best practice frameworks which were triggered. This discussion is not intended to be a comprehensive historical analysis of the evolution of these conventions and associated outcomes, as others have well documented this situation (Clément 1996; Firth 1999; González et al. 2009; Shefi 2013; UNESCO 2001). Rather, these advances are examined in the context of the requirements placed on today's practitioners and archaeological researchers to develop and apply effective in situ management strategies and the best-practice implementation role for non-invasive sub-bottom profilers.

Underwater cultural heritage (UCH) means 'all traces of human existence having a cultural, historical or archaeological character which has been partially or totally under water, periodically or continuously, for at least 100 years' (UNESCO 2001). This includes sites, structures, buildings, artefacts and human remains, vessels, aircraft, other vehicles and their cargo or contents—together with their archaeological and natural context—and objects of prehistoric character. There had been great concern for decades by archaeologists and heritage managers about the loss of scientific information and cultural material resulting from unprofessional excavation and salvage of commercially valuable property from shipwrecks. During the period from the 1960s to the 1980s there were unsatisfactory and ineffective changes in the *United Nations Law of the Sea Convention* (UNCLOS I, II and III) to protect UCH from salvage (Clément 1996:309–310; Shefi 2013:111–117). As a result, separate

initiatives were developed to provide internationally recognised protection, which ultimately coalesced into the drafting of the UNESCO 2001 *Convention on the Protection of the Underwater Cultural Heritage* (UNESCO 2001).

The *Convention for the Protection of Archaeological Heritage in Europe (revised)* (the Valetta Convention) was adopted in 1992 and replaced and updated the original London Convention (Council-of-Europe 1992). The Valetta Convention reflected the change in threats to the archaeological heritage from the unauthorised excavations in the 1960s to the major construction projects carried out all over Europe from 1980 onwards. It aims to protect European archaeological heritage, both on land and underwater, preferably in situ, and requires provisions to be made where possible for in situ conservation. It was from this treaty, which was progressively backed up by national legislation, that preservation in situ became the preferred option (Gregory and Matthiesen 2012a).

The International Council on Monuments and Sites (ICOMOS) is an established global organisation with professionals working in all disciplines associated with cultural heritage places. ICOMOS is an Advisory Body to the UNESCO World Heritage Committee, but does not derive legislation (ICOMOS 1996). The 1996 ICOMOS *Charter on the Protection and Management of Underwater Cultural Heritage* encourages the protection and management of underwater cultural heritage in inland and inshore waters, in shallow seas and in the deep oceans. It was drafted as a supplement to the ICOMOS *Charter for the Protection and Management of Archaeological Heritage* 1990 which sets out best practices for the protection of for UCH management, including: ethical standards, professional qualifications, preservation of sites in situ, and recommendations that any disturbance survey and excavation should be preceded by non-invasive general surveys, from which a suitable management plan can be developed.

Another global professional body prepared a draft convention on the protection of UCH for UNESCO. The International Law Association (ILA) submitted a draft document at the 1992 ICOMOS Conference. The final text was adopted by ILA two years later and submitted as a draft convention to UNESCO for consideration. The ILA defined UCH as ‘all underwater traces of human existence provided these have been lost or abandoned and have been underwater for at least 100 years’ (O'Keefe 1996) with the same inclusions as defined in the UNESCO 2001 Convention. While the text suggests that all sites greater than 100 years should be protected, it stipulated that not all sites require the same level of in situ management effort. UCH is deemed abandoned if the rightful owner has not made a claim for the lost items and/or shipwreck after 25 years following discovery of new research and recovery technology. If appropriate technology does not exist or is too difficult to obtain, the rightful owner has 50

years to ‘keep the claim afloat’ (O'Keefe 1996:300). The above provisions do not apply to wrecked warships and other sites where Member States have established sovereign immunity over government owned vessels (Staniforth et al. 2009).

Neither the ICOMOS 1996 Charter nor the ILA draft convention have any legally binding stature within member countries. By comparison, the UN and UNESCO are supranational organisations driven by governmental representations by member States (Shefi 2013:109). As such, once conventions proposed by these organisations are signed and then ratified by their member States, they become international law. In 1997 the UNESCO General Conference decided that the protection of the underwater cultural heritage should be regulated by an international convention at the international level. The preliminary text was based on the integration of the ILA draft convention, the 1996 ICOMOS Convention and the European Convention. A number of review meetings were held with experts from State Parties, members from the UN Division for Ocean Affairs and the Law of the Sea (DOALAS) and the International Maritime Organization. In addition, there were observers from non-member States and non-governmental bodies at these meetings. At the Plenary Session of the 31st General Conference of UNESCO on November 2, 2001 the *Convention on the Protection of the Underwater Cultural Heritage* was adopted, ready for ratification by Member States.

The 2001 UNESCO Convention (UNESCO 2001) consists of the main text (Articles) and an Annex which sets out the ‘Rules for activities directed at underwater cultural heritage’. The convention ‘rebuts pillage and the commercial exploitation of heritage for individual profit…. embraces the concept that heritage is a common asset, and encourages responsible public access, knowledge sharing and public enjoyment’. Through the Articles, the four main principles of the convention are designated, which are: the obligation to preserve underwater cultural heritage; in situ preservation as the first option; no commercial exploitation; and training and information sharing. There are 36 rules in the Annex covering: general principles; project design; preliminary work; project objectives; methodology and techniques; funding; project duration-timetable; conservation and site management; and documentation. These rules are clarified and explained in the UNESCO guideline and capacity building publications *Manual for Activities directed at Underwater Cultural Heritage* and *Training Manual on UCH Management in Asia and the Pacific* (UNESCO 2013).

Article 2.5. of the UNESCO convention states that the ‘preservation in situ of underwater cultural heritage shall be considered as the first option before allowing or engaging in any activities directed at this heritage’. Rule 1 elaborates (UNESCO 2001):

> The protection of underwater cultural heritage through in situ preservation shall be considered as the first option. Accordingly, activities directed at underwater cultural heritage shall be authorized in a manner consistent with the protection of that heritage, and subject to that requirement, may be authorized for the purpose of making a significant contribution to protection or knowledge or enhancement of underwater cultural heritage.

This rule was forged in 'recognition of the importance of the interplay between the site, its story and its context' with authenticity and context being important drivers for preserving heritage where it is found (UNESCO 2013:23–24). It has been described as the most debated and least understood rule. In a practitioner attitude survey, there was a dichotomy of views regarding how to apply in situ preservation, its value and its effectiveness (Ortmann 2009:79; Ortmann et al. 2010:36–38). They also reported the interpretation (or justification) from this rule, by some, to equate in situ preservation with a passive 'do nothing' approach (Ortmann 2009:66; Ortmann et al. 2010:34). The UNESCO *Manual for Activities directed at Underwater Cultural Heritage* elaborates further on this rule and states that the 'first option' is not the same as the 'only option' nor the 'preferred option' (UNESCO 2013:25–28). It states that partial or total excavation may be necessary, or appropriate under certain circumstances, such as when external factors like proposed development or site instability due to environmental conditions adversely affect the site. In addition, there are also substantive reasons to partially or fully excavate, if the intention is to make a significant contribution to the protection, knowledge and enhancement of the UCH located at that site. In this case, the planned excavation 'must meet the maximum requirements of state-of-the-art archaeological projects' and be based on a research design with pertinent research questions. This position was described by Manders (2008) and recently emphasised in June 2019 at the UNESCO Brest Conference. The Secretariat of the 2001 UNESCO convention clarified beyond any doubt that 'in situ preservation as a first option is written into the 2001 convention so that objects are not removed without a plan. In situ preservation does not limit archaeological excavation and scientific study' (Benjamin 2019).

Rule 4 of the UNESCO convention states the preference for non-destructive in situ techniques. Specifically:

> Activities directed at underwater cultural heritage must use non-destructive techniques and survey methods in preference to recovery of objects. If excavation or recovery is necessary for the purpose of scientific studies or for the ultimate protection of the underwater cultural heritage, the methods and techniques used must be as non-destructive as possible and contribute to the preservation of the remains.

UNESCO's guideline acknowledges that 'research and management depend on data, and that data gathering by non-destructive techniques is essential'. Further, 'in all activities, non-destructive techniques come first' and are 'preferred to intrusive methods' (UNESCO 2013:41–42). It also acknowledges that intrusive approaches will continue to be important, but the efficacy of those intrusive methods will be significantly improved if informed by preliminary non-destructive techniques. While anticipating the development of further non-destructive techniques, the guidelines identify suitable current hydrographical and geophysical survey methods, including magnetometers, side scan sonars, swath-bathymetry (MBES) and sub-bottom profilers.

In developing a management plan to preserve a site in situ, UNESCO's Rule 16 applies where 'the methodology shall comply with the project objectives, and the techniques employed shall be as non-intrusive as possible.' If a site is unstable and there is the potential for loss of UCH, then under Rule 24 'the conservation programme shall provide for the treatment of the archaeological remains during the activities directed at UCH, during transit and in the long term'. Temporary consolidation of the site may be appropriate, or alternatively, a longer term in situ solution may be preferable through the creation of an underwater archive in which the UCH is protected and available when the archive is reopened. The guidelines provide examples of techniques for site stabilisation and in situ protection (UNESCO 2013:120–124).

In addition to the *Manual for Activities directed at Underwater Cultural Heritage* UNESCO have published a list of 'Best Practices' (UNESCO 2017). The purpose of this initiative is to help foster public and practitioner awareness of excellent project examples of protection of UCH. Best practice projects are judged by the Scientific and Technical Advisory Body based on: a special and outstanding effort to make the project site accessible to the public; promotion of the Convention and the implementation of national juridical frameworks for protection; supporting scientific research in accordance with the Convention; and appropriate conservation of the heritage. Currently there are seven best practice examples published on the UNESCO 2001 convention's web page. The projects provide examples of excavation, on-site protection, monitoring by archaeologists and biologists, site access by amateur divers and knowledge sharing and dialogue through travelling and stationary exhibitions, publication and documentary screenings.

To date, 63 Member States have ratified the convention and have aligned national legislation (UNESCO 2019a; 2019b). Additionally, there are a further six countries who have formally deposited their instruments of acceptance of the convention. Beyond these, other countries have national and/or state legislation which are aligned with the intent of the UNESCO 2001 convention, or otherwise provide protection to UCH. For example, the first state-based

legislation in the world to protect historic shipwrecks from looting and damage was the 1963 Amendment to the *Western Australian Museum Act*, which was then superseded by the Western Australian *Maritime Archaeology Act* of 1973 (Jeremy Green pers. comm. 2019). This act protected shipwrecks lost in state waters prior to 1900, shipwreck survivor camps, relics associated with historic ships, historic maritime infrastructure and whaling stations. These sites can be situated below low water, at intertidal locations, or on land (Government-of-Western-Australia 1973). The contemporaneously enacted national *Historic Shipwrecks Act* 1976 automatically protected all shipwrecks older than 75 years that lie within Australian waters, extending from the low tide mark along open coasts to the edge of the continental shelf. This commonwealth act has now been superseded by one of the world's most recent legislation to protect UCH—the *Commonwealth Underwater Cultural Heritage Act* 2018 (Australian-Government 2018). This new act adopts the same definition for UHC as per the UNESCO 2001 Convention. From 1st of July 2019 this act automatically protects all UCH including historic shipwrecks, sunken aircraft and their associated relicts over 75 years old, as well as artefacts on land directly associated with historic shipwrecks or sunken aircraft. A site containing protected underwater cultural heritage can be declared as a protected zone, and activities undertaken in that protected zone can be regulated or prohibited. It also prohibits the damage, sale, export or import of protected articles.

While the UNESCO and Valetta Conventions provided the galvanizing impetus to protect UCH material in situ, gave rule interpretations through manuals and Best Practice showcase examples, extensive scientific research was needed to effectively implement the rules of the conventions. Some of this research had already commenced by 2001, but a number of other projects commenced shortly there-after. These projects developed practitioner guidelines which are described in the following section, with emphasis on those outcomes related to in situ measurement and monitoring.

Research programmes and best-practice guidelines developed for in situ management of UCH

The Netherlands commenced in situ protection in the 1980s with shipwrecks found on the former Zuiderzee-bed in the Flevopolder, and followed in 1988 with physical and legal protection of the BZN 3 wreck, a ship of the East India Company (Manders 2004:279). Manders noted however, that despite the work undertaken on these projects there was insufficient scientific data to support methods and approaches to effectively respond to the ICOMOS 1996 charter and the UNESCO 2001 Convention. Specifically, data was needed to answer questions relating to the mechanisms and speed of shipwreck deterioration, the time period that shipwrecks can be protected in situ, and the validity of current approaches for long term

management. Consequently, and together with Finland, Germany, Sweden, UK and Denmark, the Netherlands started an EU-project called Monitoring, Safeguarding and Visualising North-European Shipwreck Sites (MoSS). This four-year pilot project commenced in 2001 with the aim to gain insight into shipwreck degradation processes and their consequences. Research was undertaken on the wrecks and surrounding environments of the Burgzand Noord (BZN) 10 (The Netherlands), *Vrouwe Maria* (Finland), Darsser Cogg (Germany) and *Eric Nordevall* (Sweden) shipwrecks (Manders 2004:279–280). The BACPOLES project was commenced very shortly afterwards. This EU-project focussed on bacterial wood degradation on land and underwater. The two underwater sites included the BZN 3 and BZN 15 wrecks found in Dutch waters (Manders 2004:285–287).

Rule 24 of the UNESCO 2001 Convention and associated discussion in the *Manual for Activities directed at Underwater Cultural Heritage* described the need for in situ conservation and the protection of UCH artefacts through reburial in an 'underwater archive'. In order to effectively respond to this approach, the Reburial and Analyses of Archaeological Remains (RAAR) project was initiated. Its purpose was to 'evaluate reburial as a method for long-term storage of waterlogged archaeological remains' and material samples have been buried since 2001, retrieved systematically, analysed and results reported (Bergstrand and Godfrey 2007; Nyström Godfrey et al. 2012). For clarification purposes, the project defined 'reburial in situ' and reburial 'ex situ'. The former definition applies when 'artefacts are recovered, recorded and reburied on the same site from which they originated', the latter when 'artefacts are recovered, recorded and reburied on a specially created site outside the original site—in artificially created reburial depots' (Nyström Godfrey et al. 2012:361). The project reburied material from the ship *Fredericus* which sank in Marstrand harbour, Sweden in 1717, together with modern materials to a depth of approximately 50 cm. An environmental monitoring program was conducted as part of the project from 2003 to 2006. Its purpose was to develop methods to assess and monitor the reburial environment, to measure the ongoing aerobic and anaerobic processes therein, and to estimate the ongoing deterioration of the material placed in the reburial trench. The program included in situ measurements of dissolved oxygen, pH and redox potential in the pore waters of the sediment, and ex situ measurement of the same parameters plus sediment porosity, organic content and sulphide (Gregory et al. 2008b). The reburial sediments were sandy with low porosity and low organic matter. Dissolved oxygen content in the sediment cores taken from the reburial trench were suboxic after the first few centimetres, and below that bordering on anoxic. The predominant biological processes acting in the sediments were sulphate reducing, especially at the depths of material burial, and that there was sulphate available for the deterioration of the organic materials. Further examination

of the sulphate availability at depths of burial greater than 50 cm was recommended (Gregory et al. 2008b:149).

Publication and dissemination of the results of these European and other research programmes, were presented at a series of international conferences. These conferences collectively became known as the PARIS (Preserving Archaeological Remains In Situ) conferences (Gregory and Matthiesen 2012a). They presented the results of almost 20 years of study from the practitioners' and stakeholders' (cultural resource managers) perspectives along four themes: degradation of archaeological material; monitoring and mitigation; protocols, standards and legislation for monitoring and management; and preserving archaeological material in situ (Gregory and Matthiesen 2012a:2). Gregory and Matthiessen, as editors for $PARIS_4$, argued for a process-driven approach to in situ preservation—one that identifies the site threats, uses monitoring to assess and quantify these threats and uses baseline data to identify if the site is safe or requires mitigation measures. Delegates at $PARIS_4$ recommended that national standards for monitoring needed to be implemented and evaluated before making international standards, and that 'guidelines for good practice' be created instead of rigid standards (Gregory and Matthiesen 2012a:5).

The MACHU (Managing Cultural Heritage Underwater) project was another EU funded initiative to develop techniques to manage UHC and provide data and information to scientists, policymakers and the general public. The multi-party project started in September 2006 and ended on 1 September 2009 (Manders 2010b). New techniques, including the use of parametric sub-bottom profilers, were introduced and evaluated for use in assessing and monitoring archaeological sites and their environment, and to predict the severity of threats and establish the urgency of measures to protect UCH at those sites. In the MACHU final report, Missiaen (2010b:67–70) discusses seismic imaging, using a parametric SBP, to map exposed and buried remains of two shipwrecks. She noted that while the bottom of the wreck *'T Vliegent Hart* could not be identified, the surveyed results 'agreed well' with information obtain from earlier excavations. There were, however, no quantitative comparisons to evaluate this subjective statement. Missiaen also commented on the opportunity to obtain additional information using complimentary methods such as coring and other geophysical measurements. In the same volume, Manders (2010a:71) summarised other geophysical research. This involved the combination of chirp sub-bottom profilers with side-scan sonar to detect disturbances in the sedimentation processes and map the thickness of sand layers protecting wrecksites. Manders concluded that more research was needed to assess combined information from multibeam monitoring and sub-bottom profiling, with controlled observations by divers.

Based on Gregory's extensive involvement in many of the above projects, he identified five fundamental steps to ensure that in situ preservation and management is undertaken successfully and in a responsible manner (reflecting the requirements of the European Valetta Treaty and the UNESCO 2001 Convention) (Gregory 2009). These steps determine:

1. the extent of the site to be preserved;
2. the most significant physical, chemical and biological threats to the site;
3. the type of materials located on the site and their state of preservation;
4. strategies to mitigate deterioration and stabilise the site from natural impacts; and
5. subsequent monitoring of a site and implemented mitigation strategies.

The purpose of the SASMAP project was to develop new technologies and best practices in order to address these five steps (Gregory 2015a). This research program commenced in September 2012 and concluded in August 2015. The project prepared two Guideline Manuals, the second of which outlines best practices for locating, surveying, assessing, monitoring and preserving underwater archaeological sites. In this volume, Gregory and Manders (2015) reported on the application of marine magnetometers and sub-bottom profiling using a prototype Innomar parametric SES-2000 quattro transducer array. Magnetometers have been successfully used in isolation for the detection of ferrous objects at known UCH sites and for the detection of large scale buried archaeological sites such as submerged harbours (Camidge et al. 2010). For best practice application, magnetometers should however be accompanied by other non-intrusive geophysical instruments (Gregory and Manders 2015:32). The processed data from the prototype SBP provided 3D images of the sedimentary environment together with the identification and 3D mapping of submerged and buried archaeological remains. In addition to the identification of paleogeographic site formation processes and UCH material, Gregory and Manders (2015:37) noted that the additional use of this SBP for ongoing site monitoring purposes would make it a 'powerful tool… for managing submerged cultural heritage sites'.

Archaeological research, conservation and in situ management studies at the *James Matthews* wrecksite located south of Fremantle in Western Australia, were concurrently and collaboratively undertaken with these European programs. Following the exposure of timbers in 2000, Richards (2001) conducted an extensive conservation pre-disturbance survey on this archaeologically and culturally significant site. The survey involved geological, chemical and biological analysis of the sediment, its pore water and the sediment microbiota through in situ and ex situ analyses, and assessment of the state of degradation of the timbers and iron components (Godfrey et al. 2005). Despite interim protective measures being subsequently

implemented, the site continued to erode. Consistent with the principals of the ICOMOS 1996 and UNESCO 2001 conventions, and with the evolving best-practice implementation knowledge, an in situ management plan for site re-burial was devised and implemented. This scientifically based plan was informed by the results from the pre-disturbance survey, a geomorphological study into the changing in situ physical processes, and the trialling the effectiveness of alternative site protection measures including sediment trapping and cathodic protection. It incorporates a comprehensive long-term conservation monitoring program, the results from which are used to optimise the ongoing effectiveness of the plan (Godfrey et al. 2005; Richards 2011b; Richards et al. 2007; Richards et al. 2012; Richards et al. 2014; Winton and Richards 2005).

A second major Australian interdisciplinary study commenced in 2012 to develop a best-practice strategy for the in situ preservation and rapid reburial of 'at risk' historic shipwrecks. Initially the nineteenth-century schooner *Clarence* (1850), located in Victoria's Port Phillip Bay, was selected as the case study, and a chemical and biological survey of the water column and sediment proceeded. A partial excavation and recording of the vessel's wooden hull structure followed, together with extraction of artefacts for ex situ documentation, including cleaning and X-ray imaging, as required. All artefacts were returned to the site and reburied. Organic materials were reburied in a purposely prepared underwater repository located on the site. Non-organic artefacts were reburied in a trench adjacent to the hull structure. Sacrificial wooden and metal samples were also buried to permit ongoing assessment of material degradation. All reburied materials were covered by overburden, and the site covered by a tarpaulin and sandbags. The project was subsequently extended to include the *James Matthews* site in Western Australia, to allow comparison across reburial techniques. Based on the results of the existing site protection trials, an inert plastic 'road crash barrier' cofferdam was constructed around the *James Matthews* shipwreck. Sacrificial wooden and metal samples were also inserted and the site within the cofferdam filled with sterile sand. Over this a geotextile cloth was placed to reduce wave-induced sand loss from within. At both sites sediment and water chemistry measurements were taken in situ and from cores collected from the reburial and reference sediments to assess the stabilisation of the degraded hull structures and UHC materials (Richards et al. 2013; 2014; Shefi and Veth 2015; Shefi et al. 2014; Veth et al. 2013; Veth et al. 2011).

Following the reburial of *Clarence,* Shefi and Veth (2015) undertook a critical review of the rapid reburial philosophy and proposed criteria to determine if a site is 'at risk'. For the latter, they advocated that 'a range of considerations that should be used to assess the research potential and level of risk of a particular UCH site' and posed multiple questions in areas of:

the site's historic, scientific, aesthetic and social value; whether or not aspects of the site are rare and if the site contains a significant amount of artefacts; and the condition, stability trajectory and the vulnerability of the site to natural or anthropogenic influences (Shefi and Veth 2015:373). The authors inferred that answers to these questions would establish if a site was at risk, however they provided no guidance as how to interpret and answer these questions. The conclusions regarding site risk, based on answers to the questions around the value, condition and vulnerability of a site, may vary significantly with or without knowledge of the presence, lateral extent, material type and depth of burial of UHC material located below the seabed. Interpretation of (only) material known to exist on the site may lead to an appropriate assessment of site risk—however, shallow-buried material otherwise unknown, but located on the site, may subsequently become exposed or further damaged. The value and susceptibility to degradation of this material may change the assessment of site risk. It is also important to understand the full lateral extent of a site. If there is additional UHC material outside the known and managed surficial area, will the management plan mitigate or potentially exacerbate any damage to this material? Likewise, it is crucial to understand the depth of burial of all UHC material, relative to the potential limits of seabed scour and dissolved oxygen penetration. This information provides insight into the potential condition and vulnerability of that material, and hence the critical needs of the in situ management plan.

Depth of Burial – the most influential factor affecting in situ management decisions for shallow-buried materials

Biological and chemical site formation processes for metals and organic materials change with depth of sediment burial. Their associated rates of degradation significantly decrease with burial depth below the seabed surface. Understanding these depth related processes, and the optimal depth of burial below which the degradation of UHC material is minimised, are critical factors influencing in situ management decisions.

Archaeological timber is primarily decomposed by biological processes. The degradation rate varies according to different biological degraders. Their respective dominance is primarily driven by the dissolved oxygen concentration, the presence of iron and manganese ions, and the redox environment within the sediments. These control the utilisation of organic matter through metabolic processes. Organic materials buried in suboxic-anoxic sediments are subject to anaerobic tunnelling and erosion bacteria, avoiding the more aggressive degradation processes by wood borers and white and brown rot fungi on the seabed surface and in aerobic sediments. Soft rot fungi is also known to degrade wood in suboxic water logged conditions (Gregory 2007:4; Gregory et al. 2008a:206). The exacerbating physical processes, such mechanical abrasion, pressure forces and gravitational loads, on exposed and degrading

materials are also avoided when materials are buried. The rate and the complex mechanisms of metal corrosion are controlled by either aerobic or anaerobic chemical processes, the intactness of the resulting corrosion product layers, and the pH and chloride concentrations in the sea and sediment pore waters (MacLeod 2016:92–100). In aerobic waters, dissolved oxygen is the oxidising agent and chloride the most common and effective electrolyte. Corrosion products formed by this reaction interact with and fuel the growth of marine biota encapsulating the metal, separating it from the dissolved oxygen in the surrounding waters. The corrosion mechanism changes within this microenvironment, with anaerobic bacteria stimulating the rate of concretion growth, which further slows the corrosion rate if the protective encrusting layer remains intact. Under anaerobic water and sediment conditions, anaerobic bacteria and their enzymes control the rate of corrosion and corrosion products—these bacteria utilize sulfate ions as a source of energy producing sulphides as a by-product. Micro-organisms concentrate at the aerobic/anaerobic boundary where some bacterial species increase metal corrosion rates due to chemical oxidation, dissimiliatory metal or sulphate reduction (Godfrey et al. 2005:17, 21–24). Consequently, episodic or long-term surface exposure of buried UCH materials due to intermittent periods of scour, or from full or partial excavation, changes the degradation processes and exacerbates the deterioration of those materials. Likewise, for reburial of artefacts, the goal is to ensure that those artefacts are placed at depth in anaerobic conditions to optimise their protection. When assessing a site where UHC material may be buried, information on the presence and lateral extent of buried UCH must be ascertained. The most influential factor affecting the likely state of degradation of those items, and subsequent in situ management decisions, is the depth of burial of the material.

The depth of burial, conducive to material preservation, has been experimentally studied in the numerous reburial and site formation process studies. A depth of 50 cm has generally been adopted, but in most circumstances the researchers have identified that site specific conditions dictate the optimum depth. Following a year-long experimental timber and canvas burial study, Gregory (1998:356) concluded that timber samples buried at 50 cm showed little signs of microbial degradation, in contrast to those placed on the seabed and buried directly underneath. Also, the sediment chemistry and redox conditions at this 50 cm depth were indicative of reducing conditions conducive to preservation. Björdal and Nilsson (2008) recommended a reburial depth of at least 50 cm, based on the results of three years of exposure of birch, oak and pine timber samples situated just above the seabed, and buried 10 cm and 42 cm below the seabed. One of the objectives for the Phase II of the RAAR project was to ascertain whether or not a 50 cm burial depth was sufficient for protection (Nyström Godfrey et al. 2011:12). Physical, nutrient and chemical analyses were undertaken along the

70 cm long sediment cores collected from undisturbed locations, and alongside their burial trenches. All results reflected that the materials previously buried to 50 cm were in conditions conducive to preservation. The authors commented however, that 'the optimal depth of burial… also depends on the type of sediment, its properties and the processes occurring within it.' More specifically, porosity and organic content have an effect on the rates of microbial activity, and the lower they are the better for preservation of archaeological materials (Nyström Godfrey et al. 2011:28). At the *James Matthews* site, sediments were characterised as medium to coarse grained calcareous sands with low levels of organic material. Godfrey et al. (2005:57) identified high concentrations of iron and manganese in the depth range 30–50 cm. They concluded that the redox boundary may lie at this depth and recommended that in order to reduce the rate of degradation of organics and metals, materials should be buried well below these depths. Based on further research at this site and elsewhere, Richards (2011b:34) advocated that the proposed remediation strategy for *James Matthews* required a sediment cover of at least 50 cm over the entire site. This depth of burial was also adopted for the *Clarence* reburial project (Shefi and Veth 2015:376).

Non-invasive geophysical (acoustic) techniques for in situ management applications

Marine seismic reflection techniques have been progressively used since the early 1950s to investigate a range of submerged palaeolandscapes and archaeological sites. These techniques include: Single-Beam and Multi-Beam Echo Sounders (SBES, MBES), Side Scan Sonar (SSS), Synthetic Aperture Sonar (SAS) and Sub-Bottom Profilers (SBP) (Bjørnø 2017c; 2017d; Dix et al. 2008; Missiaen et al. 2017b; Quinn 2012). Single beam acoustic ground discrimination systems (AGDS) are based on SBES and used to classify seabed type and map submerged archaeological materials lying on the seabed (Lawrence and Bates 2001). Electrical resistivity tomography (ERT) has rarely been used for maritime archaeological applications, but has been recently applied to map submerged ancient walls in Greece and a sunken barge in shallow turbid waters in Australia (Simyrdanis et al. 2019; Simyrdanis et al. 2016). Electrical resistivity systems are also used to map sediment geomorphology in marine and freshwater systems (OEMGGlobal). The echo sounders, side scan and synthetic aperture sonars have traditionally been used for mapping the seabed bathymetry and objects on, or above, the seabed. Shallow sub-seabed imaging is carried out with the high-frequency sub-bottom seismic profiling systems. Significant advances in SBP technology, analysis and software imaging processes have occurred in the past two decades (Bull et al. 2005; Gregory and Manders 2015:35–37; Missiaen 2005; Müller et al. 2005; Plets et al. 2009; Wunderlich and Müller 2003b) and new SBP devices developed (Wilken et al. 2019). These

developments, together with the outcomes from test trials in both the MACHU and SASMAP research projects, have progressively attracted interest for UCH in-situ management. Manders et al. (2008:184) and Gregory and Manders (2015:37) have advocated that SBP instruments can provide a non-intrusive view of material below the seabed, and so shipwreck and submerged sites could then be interpreted and/or managed with the UCH material remaining undisturbed in their protective burial environments.

Research projects using Chirp SBPs have dominated the archaeological literature up to 2016. Chirp systems were first developed in 1981, and from 2001 the towed array system was optimized and enhanced for maritime archaeological applications, initially as a two-dimensional (2D) system, and subsequently as three-dimensional (3D), at the University of Southampton. Chirp systems transmit computer generated, linearly swept frequency pulses which are amplitude and phase compensated. The Chirp waveform is weighted in the frequency domain to possess a Gaussian spectrum with its autocorrelated form being the zero-phase Klauder wavelet (Quinn et al. 1998b). The initial 2D Chirp towed transducer system comprised four transducers coupled to a plate and a single-section hydrophone. Pole and hull-mounted Chirp systems are now commercially available (Edgetech) and were previously available through Teledyne Marine. The high-resolution 3D towed system comprises a 2.2 m by 2.5 m rigid frame containing an array of four Chirp transducers in a Maltese Cross configuration, 60 receiver groups, plus GPS positioning and attitude antennas. The principle processing steps of the recorded uncorrelated Chirp data includes bandpass filtering, cross-correlation, geometry processing, binning, normal move-out correction, instantaneous amplitude calculation, stacking, and automatic gain control (Plets et al. 2009).

Descriptions of research and application projects using the Chirp SBP is given by Arnott et al. (2005); Cvikel et al. (2017); Dix et al. (2008); Forrest et al. (2005); Grøn and Boldreel (2013); Grøn and Boldreel (2014); Grøn et al. (2015); Lafferty et al. (2006); Plets et al. (2005); Plets et al. (2008); Plets et al. (2009); Quinn et al. (1997a); Quinn et al. (1997b); Quinn et al. (1998a); Quinn et al. (1998); and Vardy et al. (2008). Initially the SBP instruments were used to survey, and qualitatively improve understanding of site formation processes, on *Invincible* (1758)*, Mary Rose* (1545)*, La Surveillante* (1797) and *Pandora* shipwreck sites (Forrest et al. 2005; Quinn et al. 1998a; Quinn et al. 2002; Quinn et al. 1997a; Quinn et al. 1997c). Subsequently, quantitative analysis of shipwreck sites became possible following improvements in data processing and data interpretation processes. In these situations, reflection coefficients derived from the recorded acoustic data were used to predict the degradation state of the buried ship's timbers (Arnott et al. 2005; Bull et al. 1998; Quinn et al. 1997b) and the 3D shape of the buried ship remains (Plets et al. 2008; Plets et al. 2009). Chirp SBPs have also been

used on submerged harbour sites (Oniz 2018) and on prehistoric sites to map palaeoshorelines, palaeochannel systems, shell midden accumulations and possible tool remnants (Cawthra et al. in press; Grøn and Boldreel 2014; Grøn and Hermand 2015; Grøn et al. 2007; Missiaen et al. 2017b). Recently, Vardy et al. (2017) used Chirp SBP profiles as part of their evaluation of current techniques for geophysical characterization of shallow subsurface sediments.

There were, however, logistical difficulties in using the towed Chirp systems for in-situ management purposes, especially in shallow (<5 m) water depths. These difficulties arose from vessel-induced bubble turbulence, restricted acoustic geometry of the system, wide acoustic beam patterns and inability to discriminate in the top 30 cm. Towed Chirp systems can be pulled by divers to avoid boat noise interference (Plets et al. 2008; Plets et al. 2009; Plets et al. 2007b) and data processing techniques can be used to correct for geometry and optimize the processing of the collected data. The Edgetech development to combine the multi-channel hydrophones and the transducers into pole/hull mounted options overcome these issues, but their field operability is still never-the-less difficult (Bjørnø 2017d). Chirp SBPs use wide acoustic beam patterns (20–30 degrees) which limits horizontal resolution. Vertical resolution in shallow water depths has progressively improved from approximately 2–3 m (Plets et al. 2008), to 0.4–0.7 m resolution (Plets et al. 2009), 'decimeter resolution' (Gutowski et al. 2015) and 6–10 cm (Edgetech). Finer resolution to around 4.5 cm can be achieved, but only in 3D by expert use of post-processing software (Justin Dix 2017 pers. comm. 22 December). Small lateral variations in the very-near surface sediments have a profound effect on Chirp acoustic returns in the top 30 cm of the seabed (Bull et al. 1998). This results in high uncertainty in very shallow sub-bottom measurements, which from an in situ management perspective, is in the seabed penetration range of maximum importance. The array of the new PingPong system (Wilken et al. 2019) is attached via a hinge to the bow of the survey vessel to eliminate vessel noise interference and operates with a horizontal and vertical resolution of 15 cm. Wave motion effects cannot be corrected and consequently this system can only be used in calm water and weather conditions.

SBPs based on nonlinear acoustic phenomena have operational and resolution advantages for in-situ management applications of shallow buried archaeological material, compared with the Chirp SBPs (Bjørnø 2017d:916). Nonlinear (parametric) SBPs utilize inherently different acoustic wave characteristics than linear (Chirp) systems. Parametric SBPs generate two simultaneous high frequency (~ 100 kHz) sound waves at high sound pressure, which are transmitted at slightly different frequencies. Through the interaction of these primary acoustic waves, short low-frequency (4–15 kHz) pulses are generated. These low frequency pulses

have advantageous operational and seabed penetrating qualities including: narrow (+/- 2 degrees) beam width with consequential high horizontal resolution; short pulses combined with narrow beam width which result in high vertical resolution; very low side-lobe levels, which reduce clutter and signal-to-noise ratios and enhance separation of backscattering from seafloor and sub-surface reflectors—this leads to an improved ability to detect very shallow and acoustically weak reflectors; high pulse repetition rates allowing more 'hits' per target and higher boat survey speeds; and a smaller combined transmitter/receiver array—this significantly improves field operability as it can be vertically mounted from a vessel to avoid propeller wash noise interference, or attached to an autonomous underwater vehicle (AUV), rather than towed in an array (Bjørnø 2017a; 2017d; Caiti et al. 1999; Wunderlich et al. 2005a; Wunderlich et al. 2005b). Commercially available parametric SBPs include: Atlas Hydrographic GmbH (Parasound), Germany; Kongsberg Defence Systems (TOPAS PS and Geopulse Pinger systems), Norway; Innomar Technologie GmbH, Germany (SES-2000); Teledyne Marine (Parasound); and Tritech (SeaKing) (Bjørnø 2017a). The TOPAS PS and SES-2000 systems are available in different optimized models which operate in very shallow waters to full ocean depths.

The initial applications of parametric SBPs to maritime archaeology came through the deployment of a prototype SBP on a ROV in deep water off the Israeli coast in 1999 to map two Phoenician ships (Mindell and Bingham 2001), and the trial of the Innomar SES-2000 in the Baltic to identify a narrow 0.2 m diameter wooden post and other embedded wooden archaeological objects (Müller and Wunderlich 2003; Wunderlich et al. 2005a; Wunderlich et al. 2005b). In 2007 Missiaen used a parametric SBP to survey the remains of Roman dykes and human activities, including salt/peat exploitation in prehistoric tidal gullies along the Belgium coast at Ostend, and of an exposed shipwreck on the Buiten Ratel sandbank (Missiaen 2010a). Again in 2010, Missiaen undertook a seismic survey of the scattered remains of the Dutch East Indiaman *'t Vliegent Hart* using a parametric SBP (Missiaen et al. 2012). More recently Innomar Technologie GmbH introduced a multi-transducer sub-bottom profiler to capture very high data density in shallow waters (SES-2000 quattro). The data from this instrument can be subsequently viewed in 3D using gridding and visualisation software. The prototype version was used in the SASMAP research project to map submerged sites in Greece and Denmark (Gregory and Manders 2015:35–37). Missiaen et al. (2017a) conducted 3D seismic surveys using the now commercialised SES-2000 quattro across shallow intertidal areas at the coastal site of Oostende-Raversijde, Belgium. This complemented the previous 2D parametric surveys on this site and provided an image of the complex peat exploitation patterns, the features of which matched with old aerial photographs. The 2D version has been used on other prehistoric sites identifying palaeochannels and shell middens (Astrup et al.

2019) and for the detection of surface and shallow buried steel pipelines, cables, spheres and steel canisters (Kozaczka et al. 2013; Vasudevan et al. 2006; von Deimling et al. 2016). Lately parametric SBPS have also been used in the recording of complex geomorphological structures in a shallow nearshore zones, tidal estuaries and lake sediments (Barklage et al. 2019; Ghinassi et al. 2019; Menard et al. 2019; Missiaen et al. 2008; Novak et al. 2020; Sitkiewicz et al. 2020) and for the study of mounded morphology of benthic assemblages (Alevizos et al. 2018; Chronis et al. 2014).

Wang et al. (2019) attempted to experimentally measure the vertical resolution of a SES 2000 parametric SBP in a large-scale anechoic tank. They compacted a 0.1–1.4 m wedge-shaped clay layer on the bottom of the sloping concrete tank, and compacted a 0.7 m sand layer on top. The tank was then filled with fresh water to a depth of five meters. While the seabed layer and the horizontal sand/clay interface were detected, the researchers were not able to detect the sloping clay/concrete boundary. They hypothesised that the experimental conditions did not allow for natural sedimentary processes to form effective acoustic interfaces. They were consequently not able to quantify the vertical resolution of the SBP by direct measurement. Based on measurements of the SBP's variable frequency and pulsewidth settings, Wang et al. (2019:190–192) used the method of duration of reflection event to estimate vertical resolution. They determined that the SBP's vertical resolution varied with pulsewidth from 36.2 cm (secondary wave frequency 4 kHz–500 μs) to 11.6 cm (secondary wave frequency 15 kHz–67 μs). Wang et al. (2019:193) concluded that actual resolution of the SES 2000 SBP 'related to the environmental conditions and the geological conditions of the seabed'.

Except for the buried canister trial undertaken by (Kozaczka et al. 2013) and the post-measurement dredging and recovery of cylinders and poles (Gutowski et al. 2015; Vardy et al. 2008), there has been no reported purpose-specific in situ verification for either linear or non-linear SBP performance. This lack of performance verification extends to quantitative assessments of the measurement accuracy of depth of sediment cover, confidence estimates associated with the correct identification and interpretation of a buried reflector, and assessment of differentiating reflector material types.

Chapter summary

Pragmatically, the principles of in situ management for submerged archaeological sites were developed around integrated environmental/coastal zone management philosophies, including key components such as: good data as a pre-requisite for good decision making; developing an understanding of the site's environment; defining site formation transforms and processes of change; baseline and ongoing monitoring; responding to change; and promoting

non-intrusive access. These arose as an outcome of progressive scientific in situ management studies, driven by international legislation to protect UCH, in response to concerns regarding loss of material to natural and anthropogenic factors.

Theoretically, the principles of in situ management arose from the challenge to understand the transformational (site formation) processes acting on underwater and submerged archaeological sites in order interpret the archaeological record. Muckelroy conducted the first systematic study of shipwreck site formation processes in the mid-1970s. He developed a theoretical site model representing the evolution of a shipwreck from the process of wrecking, through to the observed sea-bed distribution of artefacts. His seminal work was considered one of the first attempts to develop and apply explicit middle-range theory for maritime archaeology. Following Muckelroy, site formation research focussed on predictive models to explain the presence of artefacts using correlations between the observed distribution of shipwreck sites and their environmental attributes. These theoretical constructs did not allow for temporal affects and failed to identify the processes which affected a site based on the observed state of its preservation—and hence the models may be non-predictive and misleading. Gregory proposed an alternate model where the natural environment is studied to understand and define the processes which currently affect shipwreck sites in order to understand their current state of degradation. Using this knowledge, methods could then be developed to mitigate these effects. With this scientific approach there was a growing awareness of the opportunity and value of studying the inter-relationship between site formation processes, materials conservation and site assessment. Today there is a large volume of research reported in the literature describing studies investigating cultural, physical, chemical and biological site formation processes. These studies, and the knowledge gained therefrom, are now central to in situ management planning for the protection of underwater archaeological sites and conservation of their artefacts.

Concurrently, there was a growing concern by archaeologists and heritage managers regarding the loss of scientific information and underwater cultural heritage material. This demise arose from unprofessional excavation and salvage of commercially valuable property from shipwrecks, and also from the impacts associated with onshore, coastal and deep-water development projects. During the period from the 1960s to the 1980s there were unsatisfactory and ineffective changes in the *United Nations Law of the Sea Convention* (UNCLOS I, II and III) to protect UCH from salvage. As a consequence, separate initiatives were undertaken to provide national and internationally recognised protection. These included: 1) the *Convention for the Protection of Archaeological Heritage in Europe (revised)* (the Valetta Convention), adopted in 1992, as an updated replacement for the original London Convention. This

convention aims to protect European archaeological heritage, both on land and underwater, preferably in situ, and requires provisions to be made where possible for in situ conservation; 2) the preparation of the 1996 ICOMOS *Charter on the Protection and Management of Underwater Cultural Heritage* which encourages the protection and management of underwater cultural heritage in inland and inshore waters, in shallow seas and in the deep oceans. It was drafted as a supplement to the ICOMOS *Charter for the Protection and Management of Archaeological Heritage* 1990 which sets out best practices for the protection of UCH management; 3) a draft convention on the protection of UCH by the International Law Association (ILA); and 4) national and state-based legislation. While neither the ICOMOS 1996 Charter nor the ILA draft convention had any legally binding stature, the UNESCO General Conference decided in 1997 that the protection of the UCH should be regulated by an international convention at the international level. The preliminary text was based on the integration of the ILA draft convention, the 1996 ICOMOS Convention and the European Convention. In 2001 the UNESCO *Convention on the Protection of the Underwater Cultural Heritage* was adopted, ready for ratification by Member States.

The four main principles of the UNESCO 2001 convention are: the obligation to preserve underwater cultural heritage; in situ preservation as the first option; no commercial exploitation; and training and information sharing. Article 2.5 (Rule 1) of the convention states that the 'preservation in situ of underwater cultural heritage shall be considered as the first option before allowing or engaging in any activities directed at this heritage'. This has been described as the most debated and least understood rule of the convention, with a dichotomy of practitioner interpretations of in situ preservation ranging from 'no excavation allowed' to 'do nothing'. UNESCO's *Manual for activities directed at Underwater Cultural Heritage* clarifies that the 'first option' is not the same as the 'only option' nor the 'preferred option', and that partial or total excavation may be necessary, or appropriate under certain conditions. These conditions include when site instability or proposed development threaten the site, or for scientific study. If a site is unstable and there is the potential for loss of UCH, then a conservation programme should be implemented during the activities protecting UCH, in transit and in the long term (Rule 24). Such a program should provide for the treatment of the archaeological remains either in situ, through temporary consolidation or long term in an underwater archive (reburial) in which the UCH is protected and available at a later date, or following recovery. UNESCO's guideline manual acknowledges that research and in situ management are dependent upon data, and that non-destructive techniques come first and are preferred over intrusive methods (Rule 4)—but intrusive methods remain important and their efficacy will be significantly improved if informed by preliminary data gathered using non-invasive techniques.

While the UNESCO and Valetta Conventions provided the galvanizing impetus to protect UCH material in situ, gave rule interpretations through manuals and Best Practice showcase examples, extensive scientific research was needed to effectively implement the rules of the conventions. Specifically, data was needed to answer questions relating to the mechanisms and speed of shipwreck deterioration, the time period that shipwrecks could be protected in situ, and the validity of approaches for long term management. Some of this research had already commenced by 2001, but a number of other European and Australian projects progressively commenced and shared learnings during the following two decades. While not an exhaustive list, the initial projects included: the MoSS project to better understand shipwreck degradation processes and their consequences; a study on bacterial wood degradation on land and underwater (BACPOLES); the RAAR project which evaluated reburial as a method for long-term storage of water logged archaeological remains; and the MACHU project which developed techniques to manage UCH and provide data and information to scientists, policymakers and the general public.

Publication and dissemination of the results from these research programmes were presented at a series of international conferences which collectively became known as the PARIS conferences. On the basis of the new scientific data and the principles of the UNESCO 2001 and Valetta Conventions, Gregory and Matthiessen as editors for the fourth PARIS conference, argued for a process-driven approach to in situ preservation—one that identifies the site threats, uses monitoring to assess and quantify these threats and uses baseline and ongoing data to identify if the site is safe and if mitigation measures or modification to the in situ management plan is required. Gregory identified five fundamental steps to successfully deliver this process driven in situ preservation approach. These steps determine:

- the extent of the site to be preserved;
- the most significant physical, chemical and biological threats to the site;
- the type of materials located on the site and their state of preservation;
- the strategies to mitigate deterioration and stabilise the site from natural impacts; and
- the subsequent monitoring of a site and implemented mitigation strategies.

The SASMAP research project subsequently commenced to develop new technologies and best practices to address these five steps. Gregory and Manders prepared two practitioner Guideline Manuals based on the results from the SASMAP program. In addition to highlighting the performance of a number of new tools, or their combined use with existing technologies, they reported in their guidelines on the use of magnetometers and a prototype parametric SES-2000 quattro SBP transducer array. Specifically, they noted, the use of this SBP for

ongoing site monitoring purposes would make it ‘a powerful tool... for managing submerged cultural heritage sites’.

Process-driven archaeological research, conservation, in situ management and reburial studies at the *James Matthews* wrecksite, located south of Fremantle in Western Australia, were concurrently and collaboratively undertaken with these European programs. A second major Australian interdisciplinary study commenced in 2012 at the site of the nineteenth-century schooner *Clarence* (1850), located in Victoria’s Port Phillip Bay, to develop a best-practice strategy for the in situ preservation and rapid reburial of ‘at risk’ historic shipwrecks. This project was extended to include the *James Matthews* site in order to contrast different reburial techniques. The reburial goal of both projects was to achieve a depth of sediment burial of at least 50 cm. This value was based on the in situ results from the numerous reburial and site formation process studies, including those at the *James Matthews* site, representing the depth where the chemical and microbiological conditions were conducive to the preservation of archaeological materials.

As noted above, the use of SBPs for monitoring purposes would be a powerful tool for in situ management of UCH sites. They could, however, provide a greater value in providing preliminary data to inform the process-driven approach to in situ preservation and/or archaeological research. Consistent with the principles and rules of the UNESCO and Valetta conventions, SBPs have the potential to provide non-invasive data: identifying archaeological material buried below the seabed; defining the lateral extent of that buried material; defining the depth of burial of that material and geomorphological structures, from which an understanding of the current influence of physical, biological and chemical site formation processes could be deduced; interpreting the degradation state of buried materials; and informing subsequent invasive sampling and excavation activities, if required, as part of the archaeological research and in situ management planning for the site.

Marine seismic reflection techniques, which include SBP instruments, have been progressively used since the early 1950s to investigate a range of submerged palaeolandscapes and archaeological sites. Significant advances in SBP technology, analysis and software imaging processes have occurred in the past two decades. This has resulted in their use to survey shipwreck and submerged cultural heritage sites. These surveys were initially conducted in 2D, and then on shipwreck sites interpreted in quasi-3D, to qualitatively assess site formation processes and to provide quantitative data to interpret structure and degradation states of buried materials. Research projects using Chirp SBPs dominated the archaeological literature up to the mid-2010s. More recently the advantageous performance characteristics of parametric SBPs (higher horizontal and vertical resolution, improved ability

to detect very shallow and acoustically weak reflectors, improved field operational capabilities) have been reported in practitioner guidelines derived from the SASMAP and the earlier MACHU research programs, and from single demonstration/application projects. With the exception of a buried canister trial, and the opportunistic post-measurement dredging and recovery of cylinders and poles, there has, however, been no reported purpose-specific in situ verification—in terms of measurement accuracy, confidence estimates from the identification/interpretation of buried reflectors or derived material properties—for either Chirp or parametric SBP performance.

3. METHODS

Site-formation processes, as a middle-range processual (scientific) theory, provides the basis for the overall methodological framework for this research. Chapter 2 reviewed and assessed the available literature pertaining to relevant theoretical frameworks, site-formation processes, and the application of non-invasive methods to archaeological research and in situ management of maritime archaeological sites. The review of non-invasive methods focussed specifically on the sub-bottom profiler (SBP). This chapter describes the approach and specific methods used to undertake in situ experimental and comparative field studies to quantitatively assess whether or not SBPs are capable, and fit-for-purpose, for this application.

Chapter 2 identified a number of factors affecting the performance of SBPs and their ability to detect and accurately quantify shallow-buried maritime archaeological artefacts. There are a number of application examples using SBP technology on maritime archaeological sites. With only a few exceptions, however, quantitative performance trials have not been undertaken, or the results there-from published. These exceptions include a buried canister trial by Kozaczka et al. (2013), and the post-measurement dredging and recovery of measured cylinders and poles by Gutowski et al. (2015) and Vardy et al. (2008). Zisi (2016), Arnott et al. (2002a) and Arnott et al. (2005) conducted laboratory based research to examine specific variables that affect SBP measurements. This research has yet to be fully verified on complex wrecksite environments. When assessing the potential site management and archaeological application of SBPs, the major gap in the literature relates to performance documentation. This is particularly important for in situ site assessment, where performance and purpose-specific limitations need to be understood within the context of key site variables.

The methodological approach described in the following section provides a scientifically-based framework for in situ SBP performance assessment, under controlled site-related variables, to generate sufficient evidence and reasoned discussions to answer the research question. How this evidence is collected in the field, through laboratory tests and 3D computer modelling, and then subsequently analysed, is described in the latter part of this chapter under the various ‘methods’ headings.

Methodological framework

A two-step scientifically-based approach was adopted in this research. The first step involved trialing SBP performance in situ, under tightly controlled burial condition parameters (e.g. precisely known depth of burial, buried material type/characteristics, sediment characteristics). This step is known as the ‘*validation’* step. In the second step the performance of the SBP

under actual complex wrecksite conditions was quantitatively assessed—the '*verification*' step. Put simply, the validation step confirms that a specific technology meets its performance target under controlled conditions, and verification involves monitoring under actual conditions in a non-simulated environment (NSW Department of Primary Industries 2015 :1-2). This methodological approach was selected since 'method validation and verification provide objective evidence that a method is fit for purpose, meaning that the particular requirements for a specific intended use are fulfilled' (NATA 2018:4). While the NATA 2018 guidelines specifically pertain to the requirements for laboratory method accreditation, the principles never-the-less are 'applicable to most activity types of testing' (NATA 2018:4). Consequently, by identification of key variables and performance testing under controlled conditions, the approach quantifies the ability of the SBP to meet performance requirements dictated by the research question.

SBPs can successfully identify buried objects and their depth under the seabed (or the interface depth between different sediment layers) depending on: the strength of the reflection coefficient associated with that object or interface; the size of the object; and the ability for the SBP to discriminate acoustic signals reflecting from those buried objects against background 'noise' and from those signals reflecting off the seabed. From acoustic theory, a reflection coefficient (K_R) is the numerical expression for the strength of the reflection of the acoustic wave from a boundary (seabed surface, the interface between two sedimentary layers or a buried object). Simply, they represent the ratio of the energy reflected to the amount of energy transmitted across the boundary (Telford et al. 1990). A portion of the energy of acoustic sound waves reflect from a boundary if a contrast exists between the elastic properties (acoustic impedances) of the two media that form the boundary. The remaining portion is transmitted across the boundary. The acoustic impedance of each media is simply the product of its density, ρ, and its compressional P-wave velocity, V_p. In terms of the material properties of each media, the reflection coefficient K_R derives from:

$$K_R = (\rho_2 V_{p2} - \rho_1 V_{p1}) / (\rho_2 V_{p2} + \rho_1 V_{p1}) \quad (1)$$

The depth of burial of an object below the seabed is determined from the difference in the recorded two-way travel time (TWT) of generated acoustic waves reflecting off a buried object, and off the seabed surface, and returning to the acoustic receiver. This requires the acoustic waves to travel through both the water column and the seabed for the buried object, and travel only through the water column for the seabed surface. The depth to the seabed, d_b and depth to the buried object, d_o are calculated by multiplying 0.5 x TWT by the speed of sound in water and in the sediment, respectively. Depth of Burial (DoB) then simply becomes:

$$DoB = d_o - d_b \quad (2)$$

where

$d_b = 0.5 \times TWT_w \times V_w$ (3)

and

$d_o = 0.5 \times (TWT_w \times V_w + TWT_s \times V_s)$ (4)

$TWT_{w,\,s}$ is two-way travel time of the acoustic wave in water, sediment

$V_{w,\,s}$ is speed of the acoustic wave in water, sediment

From the above equations, three sets of parameters become critical in situ related experimental variables. These include: the speed of the acoustic (sound) wave in the water column; the density and speed of sound in the upper (sediment) layer; and the density and speed of sound in the lower (object) layer. The performance capabilities of the SBP, in terms of the instrument's sampling rate, horizontal and vertical resolution, signal-to-noise ratio and other acoustic wave properties, dictate the influence of other site variables such as object size and thickness, sediment microlayers/fluctuations, seabed cover and vessel speed.

The acoustic wave speed in the water column is dependent upon the water salinity, temperature and pressure (Lovett 1978:1713). Sediment density is a function of the sediment facies, grain size, porosity, environmental sedimentation conditions and hydraulic saturation (Richardson and Jackson 2017: 500). The speed of sound in sediment is a function of these same variables (Bjørnø 2017b:327; Richardson and Jackson 2017:506–512; Robb et al. 2005). For buried timber objects, their density varies according to timber type, the degree of seasoning/water saturation and their state of degradation (Arnott et al. 2005; Bucur and Chivers 1991; Schniewind 1989). Likewise, the speed of sound in timber is a function of these same parameters, as well as the orientation of the timber grain to the incoming acoustic wave path (Arnott et al. 2005; Quinn et al. 1997b; Zisi 2016). For other objects of interest, the speed of sound travelling through these materials is a function of their density and elastic qualities (Bjørnø 2017b:304).

Academic researchers and maritime archaeologists have used Chirp SBPs since the late 1990s, for example from Quinn et al. (1997b) to Cvikel et al. (2017), to map and characterise buried maritime archaeological artefacts (Bjørnø 2017d:913–916). Despite these successful applications, however, there are difficulties in the use of (linear) Chirp SBP systems for in situ management purposes, especially in shallow (less than five metre) water depths. These operational difficulties are associated with vessel-induced bubble turbulence, restricted acoustic geometry of the system, wide acoustic beam patterns and inability to discriminate in the top 30 cm of the sediment column. While divers can pull Chirp systems through the water to avoid boat noise interference (Plets et al. 2008; 2009; 2007a), and operators can use data

processing techniques to correct for geometry and optimize the processing of the collected data, their field operability is still difficult (Bjørnø 2017d:916). Chirp SBPs use wide acoustic beam patterns (20–30 degrees) which limits horizontal resolution. Instrument technical improvements have progressively improved resolution in shallow water depths from approximately 2–3 m (Plets et al. 2008) to 0.4–0.7 m resolution (Plets et al. 2009) and 'decimeter resolution' (Gutowski et al. 2015). Finer resolution to 0.25 cm (horizontal) and around 4.5 cm (vertical) can be achieved in 3D, but requires expert use of post-processing software (Justin Dix pers. comm. 2017). Bull et al. (1998) also report that small lateral variations in the very-near surface sediments have a profound effect on Chirp acoustic returns in the top 30 cm of the seabed. This results in high uncertainty in very shallow sub-bottom measurement. Unfortunately, this uncertainty occurs in the depth range of maximum importance for in situ management application.

An Innomar non-linear (parametric) SES-2000 compact SBP was selected for this research to take advantage of numerous field deployment advantages. Results from this research will also test Wunderlich's (2005b:123) assertion that 'nonlinear acoustics (parametric SBP systems) offer many advantages compared to linear sound generation (Chirp SBPs) ….that can be exploited for the detection of small (buried) objects especially in shallow water areas'. Non-linear SBPs simultaneously generate two high sound pressure, higher-frequency sound waves transmitted at slightly different frequencies. These primary waves interact to produce low-frequency seabed penetrating pulses (secondary frequencies). This secondary sound beam is narrow (+/- 2 degrees) and results in high horizontal resolution with no significant side lobes. The resulting benefits are twofold: reduced reverberation, ambiguous reflections and clutter; and improved signal-to-noise ratios and separation of backscattering from seafloor and sub-surface reflectors. In addition, the produced wave pulses have no ringing effect and can be as short as one sine wave cycle. These features lead to improved vertical resolution and ability to detect very shallow and acoustically weak reflectors (Bjørnø 2017a:873–875; 2017d:916; Caiti et al. 1999:1105; Wunderlich et al. 2005a:1). Beneficial field operational characteristics include the compact size of the SES-2000 SBP, and of particular importance the combined transducer/receiver unit. The latter permits hull or pole mounting options for vessels (forward of the motors) or integration into an autonomous underwater vehicle (AUV). These facilitate improved positional accuracy, avoid vessel induced bubble noise and significantly simplify data processing. High pulse repetition rates, independent of water depth, permit higher detection capabilities through more 'hits' per target and higher vessel survey speeds. Accurate seabed profiles and near surface features are also simultaneously recorded from the return of the high frequency sound waves (Wunderlich and Müller 2003a:7).

In situ experimental surveys—validation step

The validation step was undertaken in two stages following the identification of the key validation variables and field challenges to undertake replicated performance tests under controlled conditions. The first stage, undertaken in 2017, trialed and tested SBP deployment and measurement along a number of purpose-buried, replicated buried modern timber artefacts (known as 'sleepers') at one site. Analysis techniques for quantitative assessment of DoB and material type were established, and 'proof of concept' results from this stage published for peer review (Winton 2019). Based on the experience gained and learnings achieved, the second stage, executed in 2018, involved the additional burial of modern timber and ferrous (steel) artefacts at the original sleeper site. Furthermore, a second site with different sediment characteristics was added. In situ sampling, coupled with laboratory analyses, was included to characterize timber properties of the buried sleepers and key sediment properties from both sites. The development and use of a purpose-specific underwater SBP sled in the second stage facilitated multiple measurement runs across all buried modern artefacts. This provided a high degree of positional control with centimetric accurate recording.

Multiple oak, pine and jarrah timber and high-tensile steel sleepers were buried at shallow depths (10, 20, 30 and 50 cm) in different sediment types at two locations—the James Matthews site and the Swan River site (Figure 3.1). The former is located adjacent to the *James Matthews* wrecksite on the northern side of Woodman Point, approximately seven km south of Fremantle, Western Australia (Figure 3.2). This site is known as the 'James Matthews sleeper site', to differentiate it from subsequent measurements undertaken directly on the *James Matthews* wrecksite. Here, water depths range from 1.5 to 2.8 m. The Swan River site is located in very shallow waters (0.1 to 1.0 m) at Coffee Point, within the lease area boundaries of the South of Perth Yacht club, approximately five km south of Perth's central business district (CBD).

The key parameters for the in situ experimental survey are listed in Table 3.1 and were chosen to be representative of equipment measurement capabilities and in situ conditions that may be encountered on a range of wrecksites. European oak and pine represent timbers commonly used in European shipbuilding (Zisi 2016), whereas Australian hardwood was mainly used in Australian colonial-period construction (O'Reilly 2007; Pemberton 1979; Staniforth and Shefi 2014). Iron was incorporated in the construction of composite-built ships—from iron deck knees and diagonal iron strapping to fully iron framed ships—since the early 1800s (Sexton 1991). The cross-sectional dimensions of the timber samples were based

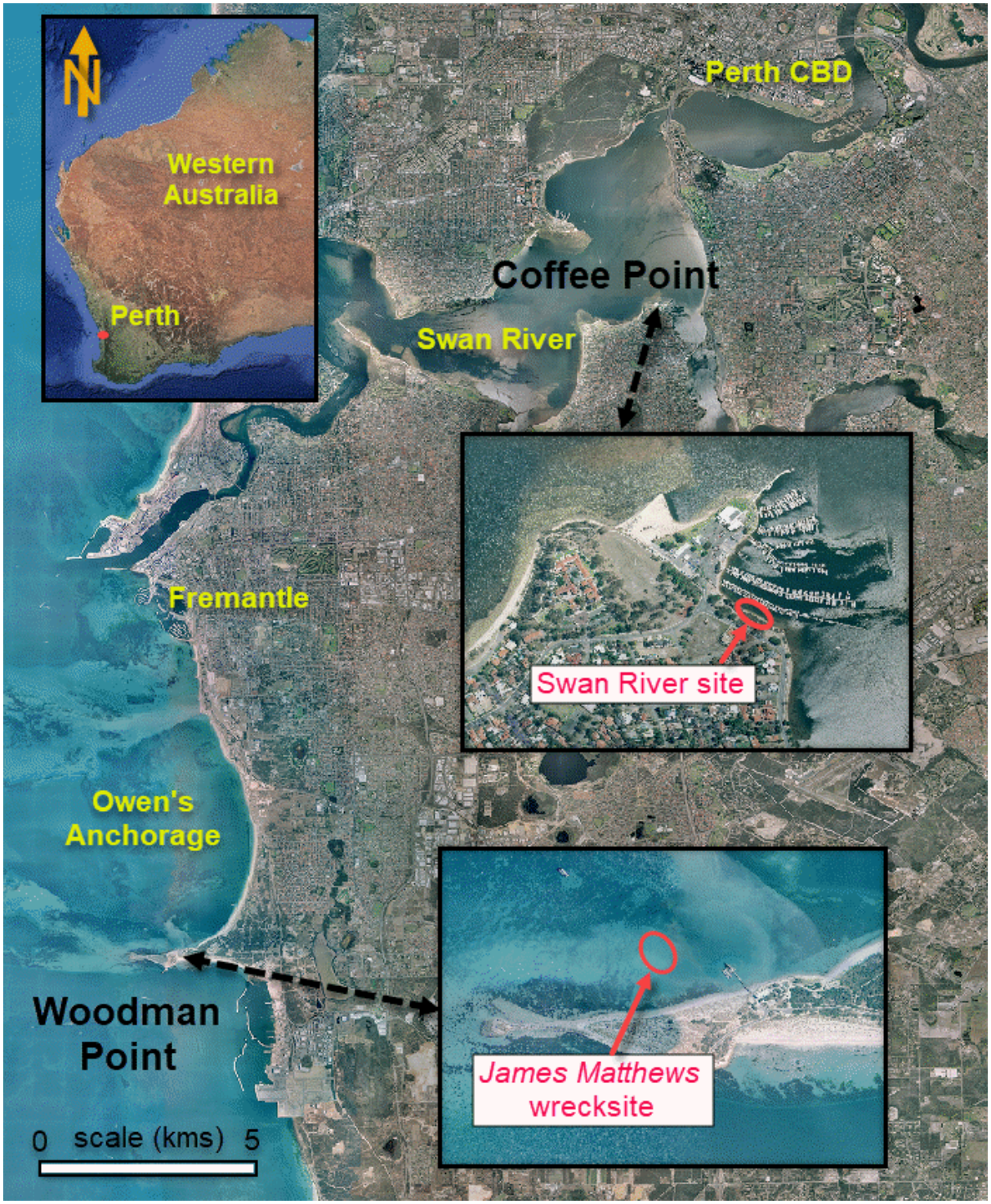

Figure 3.1 Location map of *James Matthews* and Swan River sites.

on the theoretical measurement resolution of the SBP (<5 cm vertical and 5–10 cm horizontal, respectively, in water depths 1.5–2.8 m with burial depths 0.1–0.5 m (Doug Bergersen pers. comm. 2016)). Timber grain orientation results in different acoustic properties for timber (Arnott et al. 2005) and the horizontal/vertical orientations and surface inclinations tested are indicative of those likely to be found on complex shipwreck sites (Zisi 2016). Stacking of the

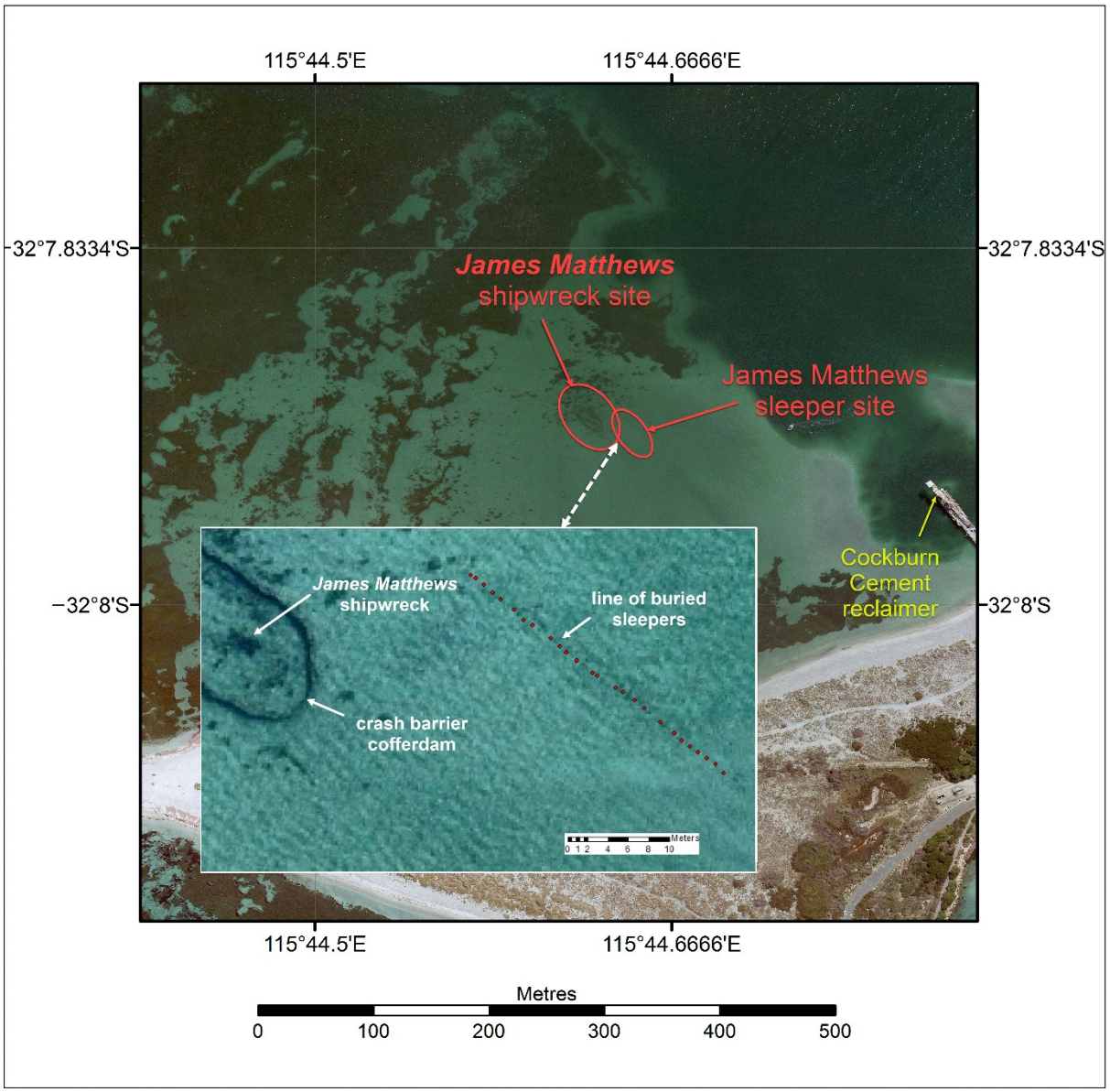

Figure 3.2 Site map of *James Matthews* shipwreck site and James Matthews sleeper site.

timbers mimics the multiple layers of timbers found on some wrecksites. It also allows for the testing of the ability and acoustic strength of the SBP system to measure multiple layers of timbers. Oak, pine and jarrah timber samples were analysed prior to sleeper burial to determine pre-submerged density for later comparison. Multiple pine, oak and jarrah sacrificial blocks were also buried at both sites, at the same depths and the same times as the sleepers. Concurrent with SBP measurements a selection of these blocks were recovered in order to measure the in situ density of the corresponding insonified timber sleepers. Sediment characteristics at each site were determined to quantify sediment in situ density and estimate sediment acoustic velocities from literature sources. Sediment DO and Eh profiles were used to interpret the degradation potential in the sediments for the buried timbers. The acoustic

wave speed in the overlying water column was estimated based on water temperature and salinity measurements. The final replicated numbers and corresponding depths of burial of sleepers and blocks at each site are listed in Table 3.2.

Table 3.1 In situ experimental parameters

parameter	included within in situ experimental burial survey
Sediment environment	Mid-coarse grained calcareous sands Coarse grained silicious sands
Sleeper material types	Timber: European Oak (*Quercus* robur) Pine (*Pinus* radiata) Jarrah (*Eucalyptus* marginate) Ferrous metal (steel)
Timber sample size (nominal)	50 cm x 12.5 cm x 12.5 cm (sleepers) 12.5 cm x 12.5 cm x 12.5 cm (blocks)[a]
Burial Depths / depths of sediment cover	10 cm, 20 cm, 30 cm and 50 cm
Replication	Mostly triplicates, duplicates when restricted
Grain/sleeper orientation	Longitudinal grain placed horizontally and vertically
Upper surface inclination	Zero (parallel to seabed surface) 22.5 degree sideways inclination
Sleeper stacking	Single beam multiple 10 cm + 30 cm beams, multiple 10cm + 30 cm + 50 cm beams
SBP survey time after timber burial	1.5 months, 4 months and 15 months
Timber density	Measured prior to burial Measured at time of SBP survey
Sediment characteristics	Sediment type Particle size distribution In situ density and porosity DO and Eh profiles
Seawater characterisitcs	Water temperature Salinity

[a] for ease of removal, blocks with depths of burial of 20 cm, 30 cm and 50 cm were cut with a 45^0 taper on top. Blocks with 10 cm depth of burial remained with flat top, otherwise taper would protrude above seabed surface.

Table 3.2 In situ experimental design

sleeper type/DoB	James Matthews sleeper site				Swan River sleeper site[S2]			
	10 cm	20 cm	30 cm	50 cm	10 cm	20 cm	30 cm	50 cm
pine	3 x horiz'l 1 x 10/30[a] 1 x 10/30/50[b]	3[S2] (2 x 22.5 deg. 1 x horiz'l)	3 x horiz'l 3 x vert'l	3 x horiz'l	2 x horiz'l	2 x horiz'l	2 x horiz'l	1 x horiz'l
oak		1[S2] x horiz'l	3 x horiz'l				2 x horiz'l	
jarrah		1[S2] x horiz'l	1[S2] x horiz'l			2 x horiz'l	2 x horiz'l	2 x horiz'l
ferrous		1[S2] x horiz'l	1[S2] x horiz'l	1[S2] x horiz'l		1 x horiz'l	1 x horiz'l	1 x horiz'l
block type								
pine	6 x		6 x	6 x		2 x	1 x	1 x
oak			6 x				1 x	
jarrah						2 x	1 x	

[S2] Buried in stage 2; [a] two sleepers horizontally stacked with 10 cm and 30 cm DoB; [b] three sleepers horizontally stacked with 10 cm, 30 cm and 50 cm DoB; horiz'l /vert'l: horizontal/vertical long grain orientation

In situ comparative wrecksite surveys—verification step

The second methodological step, verification, directly compares the results from SBP measurements with actual shallow-buried artefacts from a complex wrecksite environment. For this purpose, the wreck of *James Matthews* was selected for in situ comparison. This site was excavated during the 1975–1976 field season by archaeologists from the Western Australian Museum (WAM) Department of Maritime Archaeology, under the leadership of Graeme Henderson. Once excavated, the exposed shipwreck remains were archaeologically surveyed in 3D (Baker and Henderson 1979). While some artefacts were removed, the archaeologists reburied the bulk in the shallow-water site located on the northern side of Woodman Point, WA (Figure 3.2). Original survey sheets are stored in the WAM Department of Maritime Archaeology's archives. Records of the survey are contained in the excavation Day Book (Henderson 1977a) and survey methods and list of recovered artefacts have been described in published accounts by Baker and Henderson (1979) and Henderson (1975; 1976; 1977b). Conservators from the WAM Department of Conservation excavated a series of test trenches on the *James Matthews* site in 2000 to measure the nature and degradation state of the hull remains. This conservation pre-disturbance survey is described by Richards (2001).

The ship, identified as *James Matthews*, had a 'chequered history' as described by Henderson (2009:67–70, 107–231). It operated under three different names, initially as a slaver, then as a cargo vessel, and finally as an emigrant ship. The vessel was built in Bordeaux, France as

a slaver by Gabriel Giraud and launched as *Voltigeur* on 1st of January 1835. Following several voyages to Brazil, the brig was sold in 1836 to Don Francisco Felix de Souza, the notorious slave dealer of Whydah, Africa, and entered the Atlantic slave trade under the Portuguese flag as D*on Francisco.* By 1837 the ship was in poor condition and with 433 slaves onboard was run-down and captured by HMB *Griffon* near the Caribbean island of Dominica. The vessel was sold, repaired and renamed as *James Matthews*. It entered general cargo duties, and was further resold in London, UK when Henry de Burgh took a mortgage over the vessel in March 1841 with the purpose of sailing it to the newly established Swan River Colony. On this journey it carried general cargo, farm implements, 7,000 slate tiles, iron for blacksmithing, 15 crew and four passengers. *James Matthews* arrived safely in Fremantle on or around 21st of July 1841 and moored in Owen's Anchorage. The following night during a gale, the anchor cable broke, the vessel drifted towards Woodman Point and having struck the bottom, sank broadside in heavy seas (Henderson 2009:255–259). Varying aspects of this history and the wrecking event are also described in other accounts (Henderson 1975:40; 1976:245–246; 1977b:79; 2008:40–46; Henderson and Stanbury 1983:16).

Following the discovery of the *James Matthews* wrecksite in July 1973, WAM undertook multiple archaeological surveys and excavations of varying extent on this site between 1974 and 1977. Following each excavation season, the site was back-filled with stockpiled sand to provide protection to the otherwise exposed shipwreck remains. The aim of the 12-week 1975–1976 excavation was to record the entire ship's structure and cargo, and complete the raising of small artefacts for protection, conservation and display (Baker and Henderson 1979; Henderson 1975; 1976; 1977a; 1977b). Exposure of the full extent of the *James Matthews'* starboard hull, from stern to bow and from keel to deck level, required an airlift excavation of 30 x 6 x 0.5–1.5 m of sand. Once the timbers were cleared, archaeologists assembled a 3D recording grid frame and commenced recording (see Figure 3.3). The frame consisted of steel square hollow piping: four legs were initially hammered into the seabed at the stern end; 6 m long sides and 1 m long ends were connected to the legs using purpose fabricated 'sleeves'; all sides and end frames were levelled to form an elevated horizontal plane; all key features along the edges and within the 6 x 1 m section of the hull were recorded in their horizontal (A, B) and vertical (C) positions relative to the top corner of the frame and the distance below the elevated horizontal plane; once all recording was completed within that section, new legs were driven into the seabed a further 1 m towards the bow with their sleeves set to maintain the same horizontal plane (and vertical height control); and the sides and end frames reconnected.

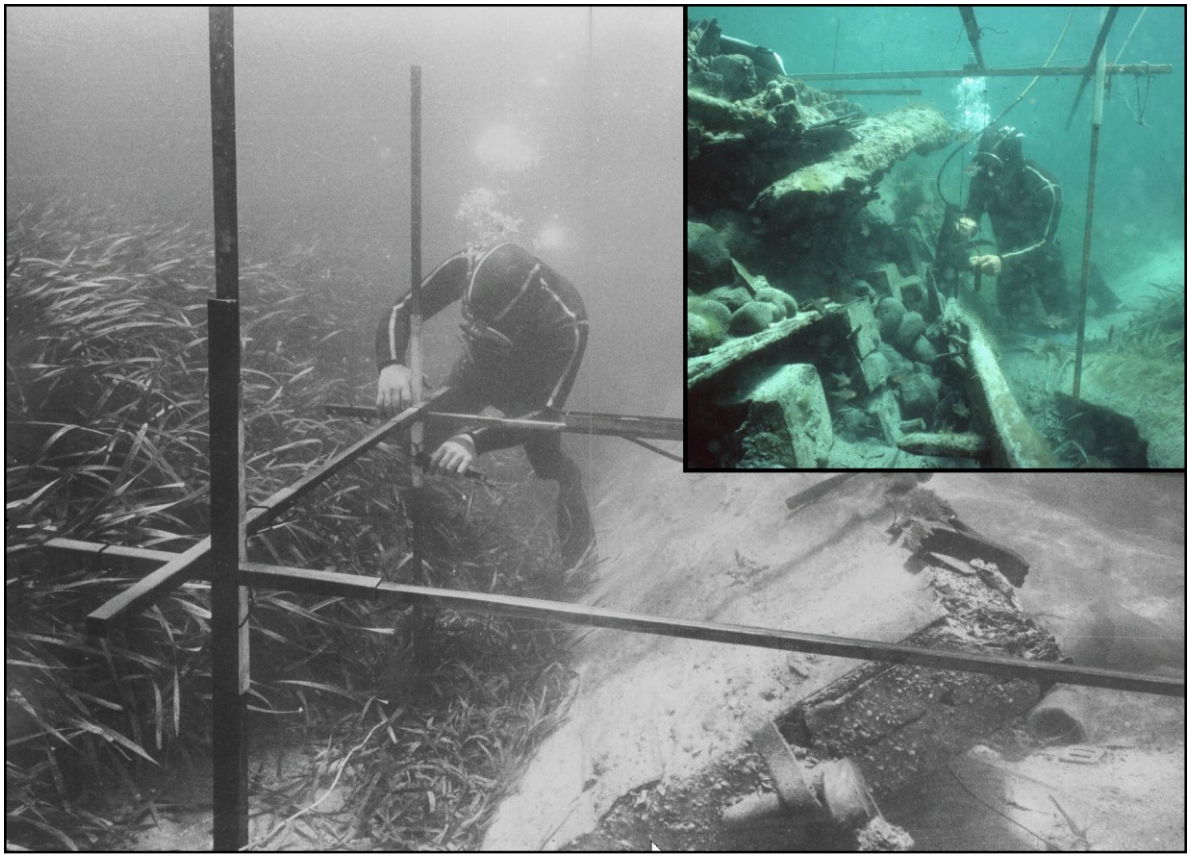

Figure 3.3 Recording grid frame set up on seabed over excavated hull remains, (insert) diver recording in 3D (photographs by Patrick Baker).

The archaeologists recorded all key features of the entire length of the hull in 3D by continuously 'leapfrogging' the frame every 1 m (Baker and Henderson 1979: 231–234; Henderson 1977b:75–78). All A, B, C measurements and associated location sketches were recorded by hand on underwater plastic film (Figure 3.4). In addition, underwater photography was extensively used to document the excavation. This included overlapping vertical stereoscopic coverage along 27 survey sections, each 6 x 1 m, to aid interpretation of the recorded survey data (Henderson 1977b:237–243).

Henderson drew a two-dimensional (2D) site plan based on interpolations between all recorded A and B co-ordinates, supplemented by the plan sketches and stereoscopic photomosaics. Preliminary lines plans were also drawn based on selected A, B and C co-ordinates (Baker and Henderson 1979:235–237; Henderson 2009:289). It is important to note that the archived survey sheets, plans and photographic records represent what was found on the *James Matthews* site immediately following excavation, and not necessarily what currently remains on site after reburial at the end of the excavation. The bulk of items removed

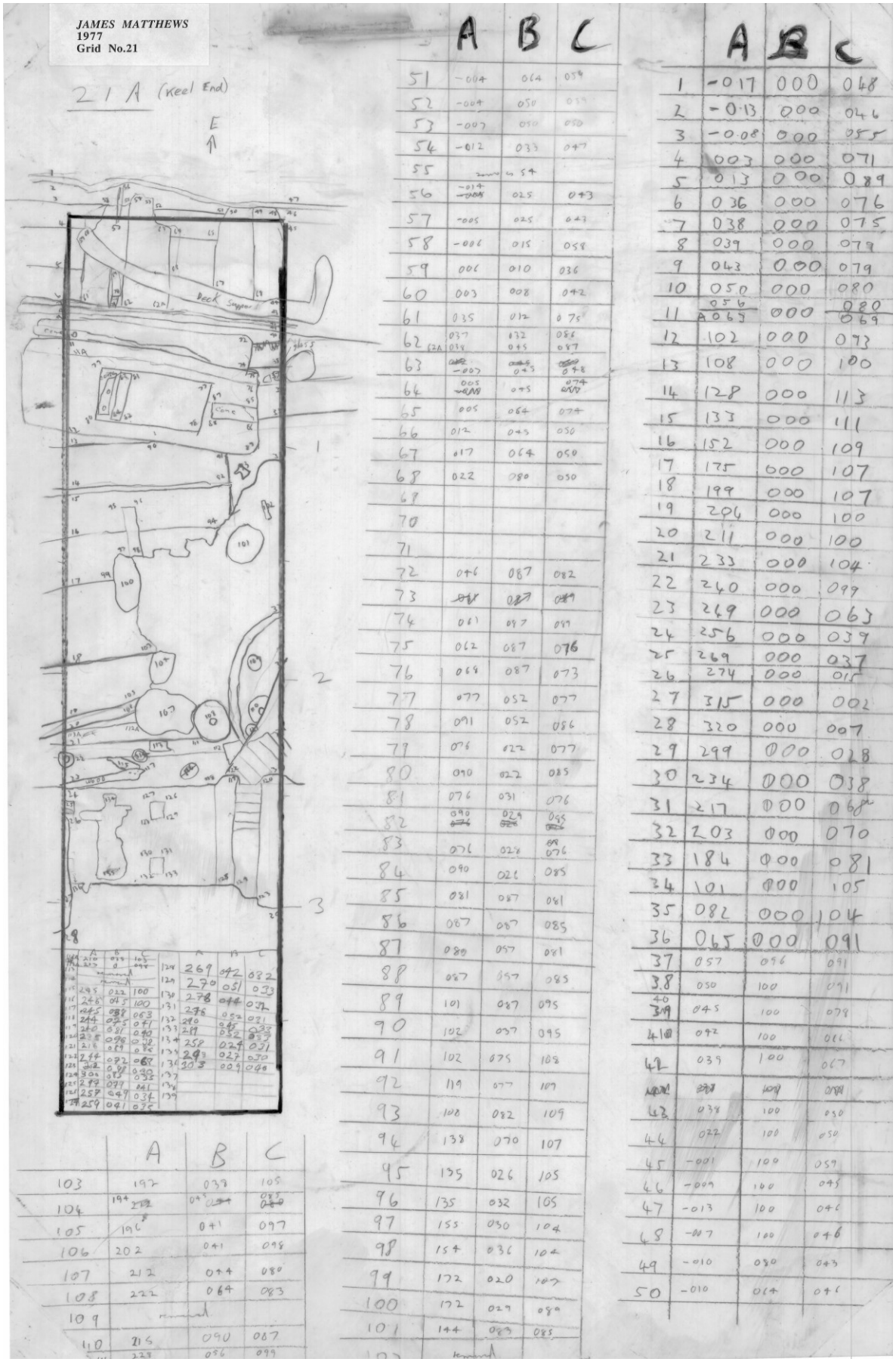

Figure 3.4 Scanned copy of typical underwater survey recording sheet.

consisted of granite ballast stones which were moved to one side of the site, and around 7,000 pieces of intact and broken slate which were raised (Henderson 1977b:77,79). Other small artefacts raised included construction items (window panes, door hinges and bundles of iron rods presumably intended for blacksmithing), carpenters' tools, domestic items and ship's equipment including rigging, skylights, rope, nails, bolts and loose wooden structures.

In response to an observed increase in timber exposure on the seabed and significant loss of sand coverage over the site, WAM undertook a conservation pre-disturbance survey in 2000. The purpose of this survey was to determine the condition of the hull remains and their suitability for potential recovery, conservation and exhibition (Richards 2001). Conservators dredged six test trenches (each approximately 2 m x 2 m x 2 m) at various locations to measure the extent of degradation of exposed and buried timbers and the corrosion potential of iron structural components. Sediment cores were also collected for chemical, geological and bacterial analyses. Like previous excavations, the test trenches were backfilled to rebury the hull timbers. Sediment erosion continued to occur on the site, and consequently WAM strategically placed sandbags on the site as a short-term measure. They subsequently developed an in situ management plan based around the conservation surveys, burial trials and monitoring programs. In 2013 WAM commenced a large-scale reburial of the site by installing a cofferdam, consisting of interlocking medium density polyethylene road 'crash barriers', on the seabed around the known dimensions of the buried and partially exposed shipwreck area (Figure 3.5). This cofferdam was then partially back-filled with clean sand and covered with a geotextile cloth (Richards et al. 2014).

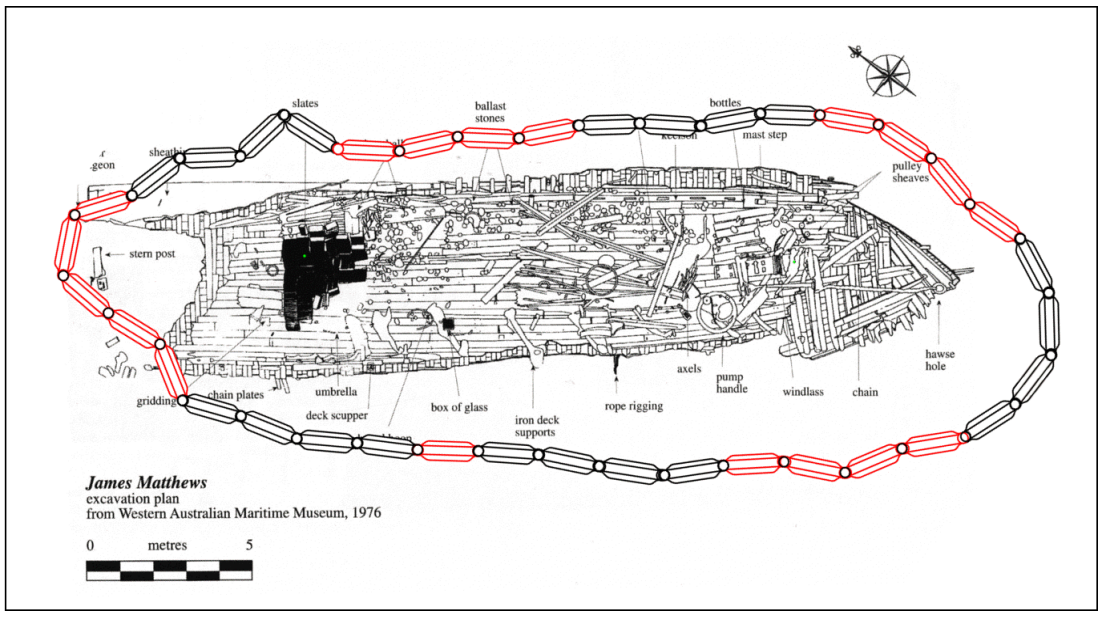

Figure 3.5 Henderson's annotated 2D plan of the *James Matthews* shipwreck site and surrounding 'crash-barrier' cofferdam.

In situ experimental methods

Buried timber sleepers and blocks

Fabrication of sleepers and blocks

Untreated pine and European oak timbers with the minimum required dimensions for the experimental burial were not available in Australia through the normal retail outlets. In early 2017, WAM's Fremantle workshop generously supplied European oak (*Quercus* robur) which was originally sourced from Poland for the construction of the 1999 replica Dutch jacht *Duyfken*. Freshly sawn green pine (Pinus radiata) was sourced from a local sawmill. Extra lengths of green pine and lengths of jarrah (Eucalyptus marginate) were sourced in December 2017. All timbers were used for the fabrication of timber sleepers and blocks. The oak was cut from a large left-over irregular-shaped piece into sections approximately 50 cm long and 12.5 cm by 9–12.5 cm square for the sleepers, the final dimensions being dependent on the quality and variable size of the remaining pieces. Likewise, smaller sections of the oak were cut into blocks measuring 12.5 cm in length, 12.5 cm in width and 6–12.5 cm in thickness. The freshly milled green timbers were delivered in 3.6 m or 4.2 m lengths, each 12.5 cm x 12.5 cm square. These were subsequently cut into 50 cm lengths (for sleepers), 25 cm lengths and 12.5 cm lengths (for flat topped blocks). The 25 cm lengths were cut diagonally at 45 degrees to create the tapered top blocks (Figure 3.6).

All timber sleepers were fabricated as a single beam, with longitudinal grain horizontal, except where two and three beams were respectively vertically stacked with 7.5 cm gaps between the inner faces (Figure 3.7a). Three pine sleepers were each cut into 16.5 cm lengths, each section then rotated through 90 degrees such that the end grain was vertical. These rotated sections were horizontally drilled and pinned, using pine dowels and PVA timber glue, to form three 38 cm long vertical grained sleepers. In late 2017 two pine sleepers were prepared by rotating each along the horizontal axis by 22.5 degrees. Once drilled, pinned and buried, the top face of these sleepers lies at an angle of 22.5 degrees to the seabed surface.

Three ferrous sleepers were fabricated for burial at each of the James Matthews and Swan River sleeper sites. Innomar technical specialists advised that a minimum beam thickness of 5 cm was required to ensure SBP delineation of the upper beam surface from the overlying sediment (Jens Lowag pers. comm. 2017). This beam thickness however would not necessarily allow for the SBP identification of the lower beam surface and underlying sediment interface. Scrap metal yards were unsuccessfully searched to find suitable sized

Figure 3.6 Timber sleepers and blocks: (a) lengths of freshly milled jarrah and pine; (b) cutting timbers to length; (c) oak sleepers and blocks; (d) pine sleepers and blocks (photographs by Trevor Winton).

Figure 3.7 Assembled sleepers and blocks: (a) multiple stacked timber sleepers;(b) ferrous sleeper and endplate connector; (c) single pine sleepers for 20 cm and 50 cm DoB measured from top face of timber surface to underside of plank inserted in slot; and (d) pine, jarrah and oak blocks (photographs by Trevor Winton).

single ferrous beams. Instead, scrapped truck leaf suspension systems were purchased and dissembled. These leaf springs measure 9 cm in width by 1.84 cm in thickness. They were made from hardened high-tensile steel and were cut into 50 cm lengths at an engineering shop. Three springs stacked tightly on top of each other weighed 18 kgs and provided the required minimum beam thickness for SBP discrimination. Due to safety concerns about lifting and manipulating beams heavier than this on the surface as well as underwater, the ferrous sleepers were limited to three stacked steel leaf springs. Attempts to drill and bolt these together failed due their hardness, so they were held in place using mild-steel clamps with attachment brackets for the endplates (Figure 3.7b).

Endplates cut from inert 12 mm PVC sheeting were attached to both ends of the timber and ferrous sleepers, and on one side of each block (Figure 3.8). These endplates facilitated identification, multiple stacking of sleepers, accurate burial, precise measurement of actual sediment cover over each sleeper at times of SBP measurement, and ultimate retreival of the sleepers and blocks. These endplates were securely attached to each timber sleeper/block by driving two 25 mm diameter PVC dowels through holes drilled in the endplates into slightly undersized holes in the ends of each timber sleeper/block. The varying length of each PVC endplate, from the upper surface of the sleeper to the underside of a pre-cut slot, enabled accurate placement below the seabed and subsequent measurement of actual depth of sediment cover. The depth of burial was determined by subtracting the distance measured from the seabed surface to the underside of the slot from the endplate distance between the underside of the slot and the upper face of the sleeper (see Figure 3.7c). For retrieval of blocks, and ultimately the sleepers, an air lift bag or rope can be tied to the slot(s) and the entire sleeper/block lifted out from under the seabed.

Identifying labels for each sleeper/block were engraved and blackened into the PVC endplates using a soldering iron and engraved color-coded PVC cattle tags were also attached via nylon cable ties. For the shallowest buried sleepers and blocks (DoB = 10 cm) additional weights were added (gravel in 12 cm diameter PVC tubing at each end) to compensate for the timbers' unsaturated buoyancy and the relatively smaller weight of sediment cover. For these sleepers and blocks, any loss of sediment cover may result in the sleeper or block floating away.

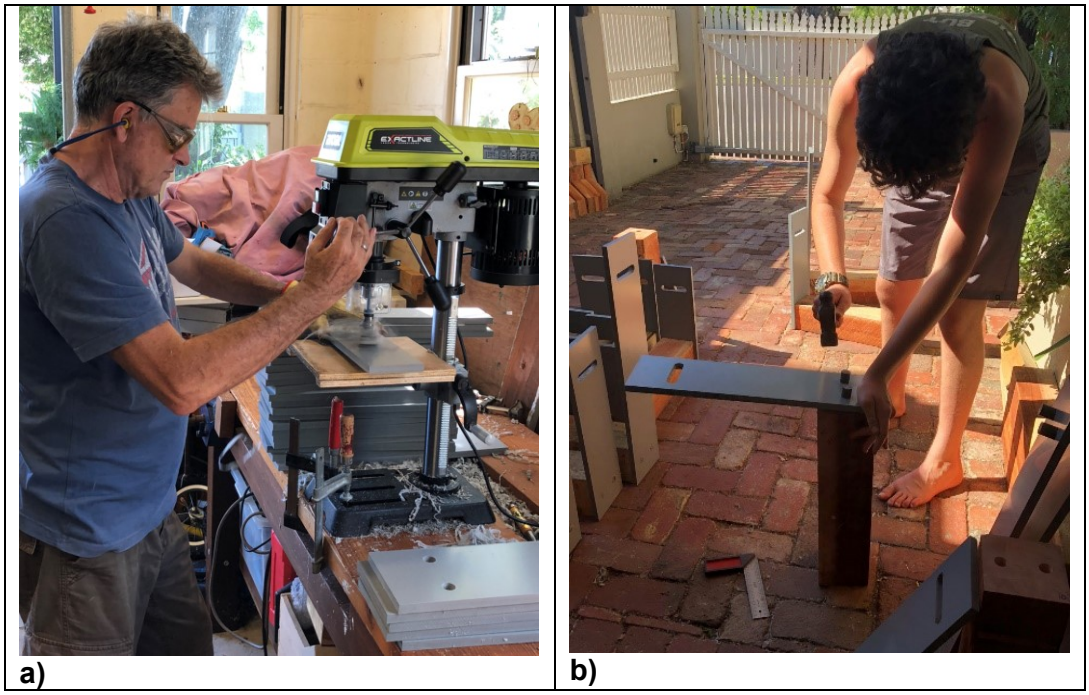

Figure 3.8 Sleeper endplates: (a) fabricating; and (b) assembling (photograph (a) by David Winton, photograph (b) by Trevor Winton).

Installation of sleepers and blocks—James Matthews sleeper site

A total of 26 sleepers and 24 blocks were buried at the James Matthews sleeper site during two field seasons using diver-operated water-dredging techniques. The author, as field director and lead diver, was generously supported by staff from the WAM Departments of Maritime Archaeology and Conservation, and volunteers from the Maritime Archaeological Association of Western Australia (MAAWA). The team conducted 19 field trips from February 2017 to May 2019 and undertook 76 individual dives with excess of 4,500 minutes of dive time (Appendix A, Table A.1) to accomplish the site preparation, burial, backfilling/leveling, sleeper location and ultimately block recovery tasks. WAM also provided their new dive and research vessel *Dirk Hartog* as surface support (including surface supplied air, SCUBA, water dredge and dive platform) and supervised all diving under their *Health, Safety and Environment Plan for Fieldwork and Dive Planning, Metropolitan Wreck Inspection and Survey Program.* Mack McCarthy provided his smaller vessel *Seaspray* on some field trips for additional logistical support. The WAM Department of Archaeology is responsible for managing historic shipwreck sites within State waters of Western Australia and all work was undertaken within the designated protected area of the *James Matthews* shipwreck site. As all field work was undertaken under the auspices of WAM, no separate approval was required for the in situ burial and measurement activities at this site.

The diving team buried the timber sleepers side-by-side in a single row more than 20 m away from the bow of the *James Mathews* shipwreck site. This separation was required to avoid any possible degradation or physical impact on the protected shipwreck remains. Site establishment commenced with divers driving two 'star' pickets into the seabed 50 cm apart and 21 m northeast from the bow of *James Matthews*. A measuring tape was then swum 30 m in a southeasterly direction (at right angles to the line of these top star pickets) where two further star pickets were driven 50 cm apart into the seabed. Divers then installed permanent ropes from the crash barrier located adjacent to *James Matthews'* bow to the top pickets (21 m), and from the bottom pickets back to the bow crash barrier (40 m). The purpose of these guide ropes was to facilitate navigation around the site during periods of intermittent low visibility which result from the nearby dumping/reclaiming of dredged shell and release of backwash water from Cockburn Cement Pty Ltd operations. Two semi-permanent 30 m measuring tapes were tautly tied off between the top and bottom pickets forming two parallel lines 50 cm apart. Using the water pump located on the *Dirk Hartog*, the dive team progressively buried the sleepers at right angles and between these two parallel tapes. The separation distance between adjacent sleepers was approximately one metre, but this was varied slightly for deeper sleepers to avoid impacting on those previously buried. Each sleeper hole was dredged by one diver operating the suction head until the required burial depth (10 cm, 20 cm, 30 cm or 50 cm) was achieved, with sand stockpiled on the side (Figure 3.9a). Each sleeper was randomly selected from the vessel, additional temporary weights placed on the timber to overcome its natural buoyancy, and then swum to the seabed. The support diver inserted a long flat plank through the endplate slots and placed the sleeper into the dredged hole, stabilized by concrete 'besser blocks'. If the horizontal plank rested on the natural seabed surface at both ends of the excavated hole, then the correct burial depth had been achieved (Figure 3.9b). Dredging continued until this occurred, at which point the dredge head was reversed and the stockpiled sand was dredged back into the hole, burying the sleeper (Figure 3.9c). During backfilling the support diver progressively removed the besser blocks and temporary weights. Following completion of the burial of all sleepers, the distances from the top pickets to the center-line of each sleeper was recorded. Besser blocks were also placed at the top end and mid-way along the line of buried sleepers to create an acoustic seabed marker of these positions. The location of each sleeper, relative to the top star pickets, was measured using the measuring tapes and these locations are recorded in Appendix A Table A.3 and summarized in Table 3.3. The measuring tapes were then removed and an over-weighted diver, using a weighted horticultural rake, smoothed seabed irregularities around each sleeper position to restore the original seabed profile.

a)

b)

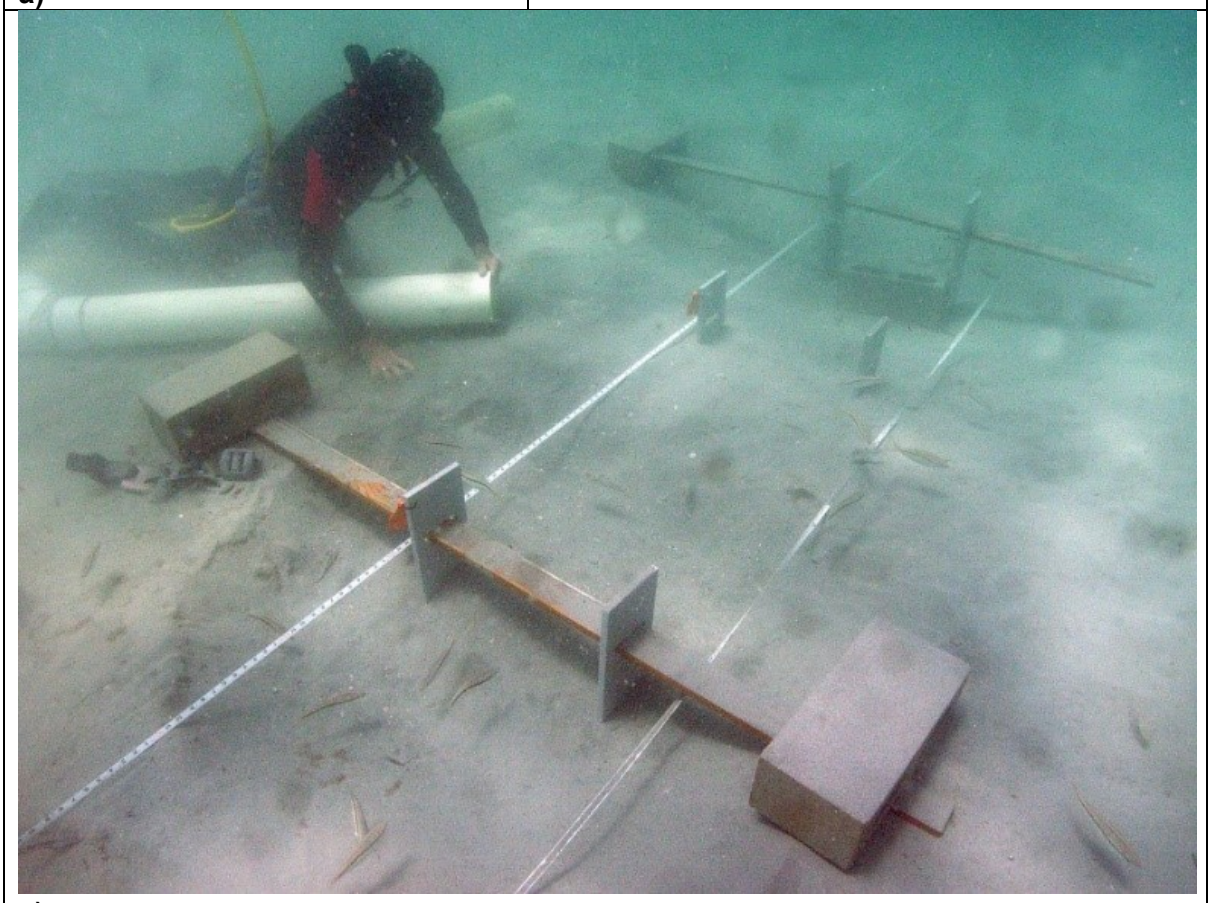

c)

Figure 3.9 Burial of sleepers by author at James Matthews sleeper site: (a) excavation to deepen hole; (b) correct burial depth achieved; and (c) backfilling (photographs by Jon Carpenter).

Table 3.3 James Matthews sleeper burial details.

date of burial	sleeper ID	distance from NE (top) star pickets (m)
April 2018	Besser block	0.6
	$P20_{(22.5)}$	1.0
	P20	1.9
	$P20_{(22.5)}$	2.8
February 2017	$P_{up}30$	3.7
	P30	4.7
	P30	6.1
	P10	7.3
	P50	8.4
	P30	9.2
	P10	10.3
	O30	11.2
	$P_{up}30$	12.3
	Besser block	13.0
	O30	13.9
	$P_{up}30$	15.6
	P50	16.4
	P50	17.3
	O30	18.6
	P10/30	19.7
	P10/30/50	21.6
	P10	23.2
April 2018	O20	24.2
	J20	25.0
	J30	25.7
	S20	26.5
	S30	27.3
	S50	28.2

Legend: P-pine; O-oak; J-jarrah; S-steel; P_{up}-pine with vertical grain; 10/20/30/50-nominal burial depth (cm), $P_{22.5}$ pine inclined at 22.5 degrees to horizontal.

During the first field season in February 2017, the dive team buried 15 single beam pine and oak sleepers with 10 cm, 30 cm and 50 cm DoB, together with two multiple stacked pine sleepers. Divers also buried six rows of three pine blocks (10 cm, 30 cm and 50 cm DoB) and one oak block (30 cm DoB) between the NE pickets and the bow of *James Matthews*. In April 2018 during the second field season, divers buried additional sleepers. These comprised two

jarrah (20 cm and 30 cm DoB), one oak (20 cm DoB), three pine (20 cm DoB, two of which had their top surfaces inclined 22.5 degrees to the horizontal) and three ferrous (20 cm, 30 cm and 50 cm DoB) sleepers. Distance measurements of all buried sleepers measured by tape are listed in Table 3.3, and a site schematic with sleepers and blocks is shown in Figure 3.10. In June 2019, the author recorded the GPS coordinates of all sleeper endplates and besser blocks using a sled mounted Leica GS16 High Precision GNSS RTK Rover in combination with Leica Captivate V3.20 software and CS20 logger. Divers manually located the underwater sled such that a plumb-bob hanging directly under the rover position was centrally located above each sleeper or besser block at the time of each positional recording. All results are presented in Appendix A, Table A.5.

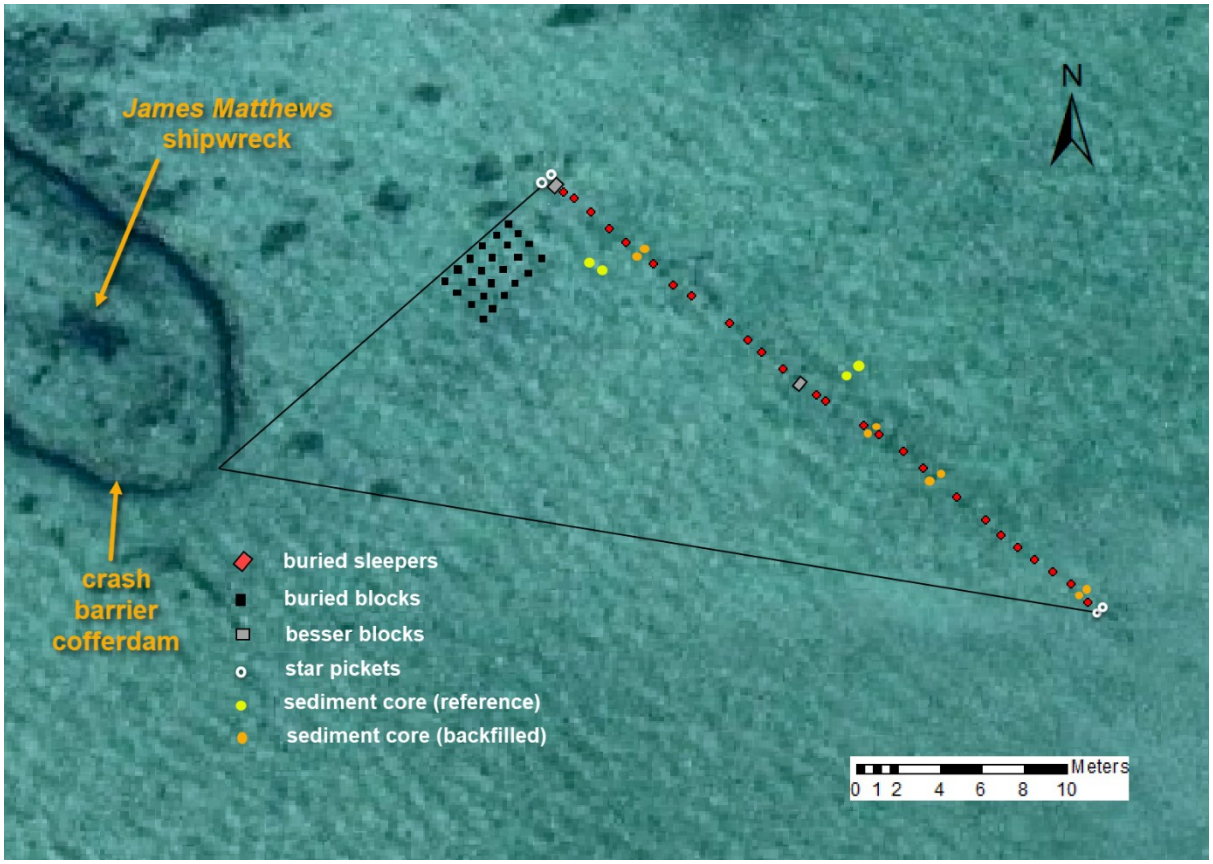

Figure 3.10 *James Matthews* site schematic.

Installation of sleepers and blocks—Swan River sleeper site

The Swan River site was selected to provide a different sediment burial environment and to avoid diver-based dredging and backfilling in black, zero visibility 'fine' sediments. A key site requirement was its tidal range such that the sleepers and blocks could be buried by shovel at spring low tides, yet there would be sufficient water depths at spring high tides to enable successful operation of the SBP. The site at Coffee Point, near the entrance and within the

lease area of the South of Perth Yacht Club (Figure 3.1 andFigure 3.11), was selected and a permit *P12097—Temporary Installation of Timber Sleepers for Scientific Study—Swan River, South of Perth Yacht Club, Applecross* was obtained from WA Department of Biodiversity, Conservation and Attractions, Rivers and Estuaries Division. The permit application described the burial, SBP measurement and removal of multiple timber and steel sleepers and timber blocks, and the permit was granted for two and a half years expiring on the 1st of June 2020.

Supported by volunteers, the field team used shovels to bury eight timber blocks and 18 pine, oak, jarrah and steel sleepers between the 2nd and 4th of January 2018. The author initially set up the site by driving two stakes into the riverbed 30 m apart, parallel to and approximately five meters from the shore, and by tautly tying a single 30 m measuring tape in between. Water depths at the site along the tape varied between 0 cm to approximately 25 cm during periods of spring low tide. The volunteer team, standing in ankle to shin deep water buried the sleepers approximately one metre apart, with the same general approach as used on the James Matthews sleeper site. Holes were dug by shovel between the tapes and when sufficiently deep, a temporarily weighted sleeper was placed in the hole. If the plank fitted through the endplate slots rested on the riverbed, then the sleeper was backfilled by shoveling the spoiled sediment back into the hole. This was relatively easy to achieve for the two shallow burial depths (20 cm and 30 cm DoB), but the deepest holes (62.5 cm deep to give the 50 cm DoB over the 12.5 cm thick sleeper beam) provided significant challenges for this approach. Lateral sediment slumping meant that the size of the hole for each deep sleeper measured at least 1.5 m in width by 1.8 m in length. This required the 'shoveler' to stand waist deep within or on the sides of the hole, resulting in more sediment being unintentionally pushed by foot into the hole than could often be shoveled out. To overcome this limitation, team members hammered temporary side sheeting along one edge of the hole, and sediment was then dug forming a trench away from the sheet wall. The three 50 cm DoB sleepers were progressively placed in this trench and backfilled as the trench was extended. Upon completion the timber sheet was removed. Once all sleepers were installed, the team similarly buried timber blocks in pairs between the tapes at the eastern end of the site.

Following this, the team recorded the position of all sleepers and timber blocks, placed besser blocks as acoustic surface markers at each end of the line of sleepers (Table 3.4 and Figure 3.11) and removed the tape. Team members repeatedly raked the riverbed around the buried sleepers to make smooth, and consolidated (densified) the sand on top of the buried sleepers by foot. The field record for work for preparatory, burial and measurement activities this site, and the measured locations of all installed sleepers and blocks, are summarized in Appendix A, Tables A.2 and A.4. Figure 3.12 shows the pre- and post-burial outcomes at the Swan River

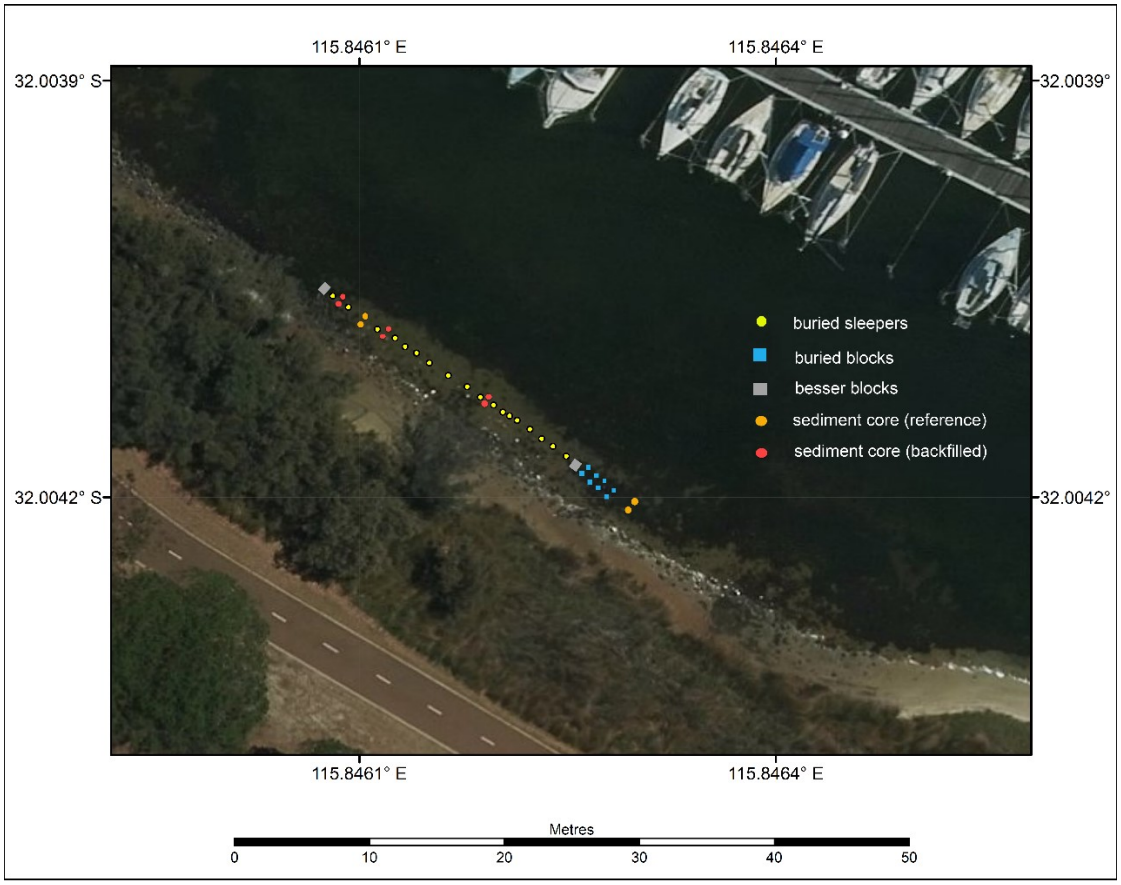

Figure 3.11 Swan River site details.

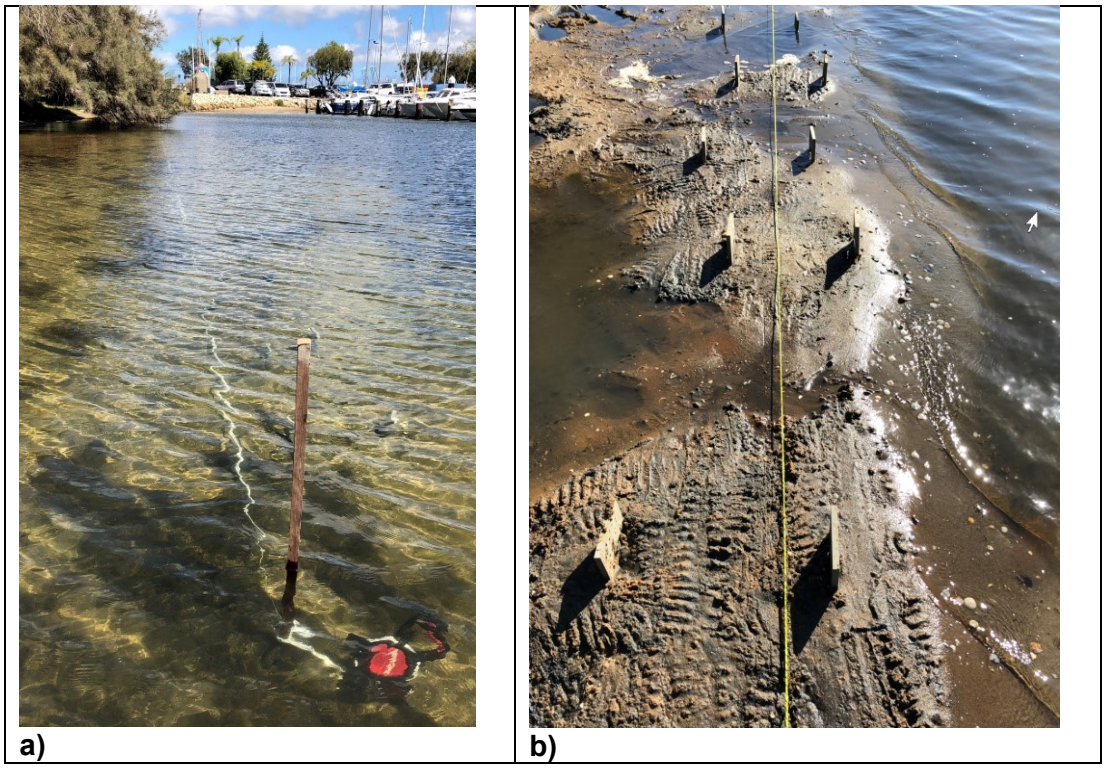

Figure 3.12 Burial of sleepers at the Swan River site: (a) commencement; and (b) completion (photographs by Trevor Winton).

Table 3.4 Swan River sleeper and block burial details.

location	sleeper/block ID	distance from NW stake (m)
	Besser Block	0.5
1	S20	1.02
2	J30	2.26
3	P30	4.72
4	S50	6.00
5	P10	6.82
6	O30	7.80
7	P20	8.81
8	O30	10.28
9	J30	11.77
10	P10	12.90
11	S30	13.94
12	J50	14.73
13	P50	15.27
14	J50	15.83
15	P30	16.87
16	J20	17.80
17	P20	18.76
18	J20	19.87
	Besser Block	20.37
19	$J20_B$ / $J30_B$	20.54
20	$P20_B$ / $P30_B$	21.07
21	$O30_B$ / $P50_B$	21.82
22	$P20_B$ / $J20_B$	22.66

P-pine; O-oak; J-jarrah; S-steel; 10/20/30/50 – nominal burial depth (cm), $_B$ block

sleeper site, and Figure 3.13 shows sleeper burial activities. In May 2018, the author recorded the GPS coordinates of all sleeper endplates at low tide using a pole mounted Leica GS16 High Precision GNSS RTK Rover in combination with Leica Captivate V3.20 software and CS20 logger. All positions are presented in Appendix A, Table A.6.

Figure 3.13 Burying of sleepers at the Swan River site: (a) MAAWA and family volunteers in shallow water; (b) burying 50 cm DoB sleepers; and (c) sheet wall to prevent sediment slumping in deep holes (photographs by Marianna Winton).

Timber characteristics

Pre-burial

Conventional density, also known as basic density or dry bulk density, and wet bulk density were determined following the methods by Jensen and Gregory (2006) from pre-burial samples of freshly sawn radiata pine and jarrah timbers, and from the air-dried European oak. The author cut duplicate 2 cm x 2 cm x 2 cm cubes from three different sections within the three types of timber (Figure 3.14). Each cube was placed on a pre-weighed glass petri dish and their weight measured to four decimal places in a Mettler Toledo AB204-S Analytical Balance. Three sets of dimensional measurements were taken for the width, depth and height, respectively, using a 0.1 mm accurate Toledo calliper (Figure 3.15). The samples were then placed for a minimum 24 hours in a Contherm oven set to 105^0C and following removal, their dry weight measured on the analytical balance. Basic and (non-saturated) bulk density values for each cube were derived by dividing their dry and wet weight, respectively, by their wet volume.

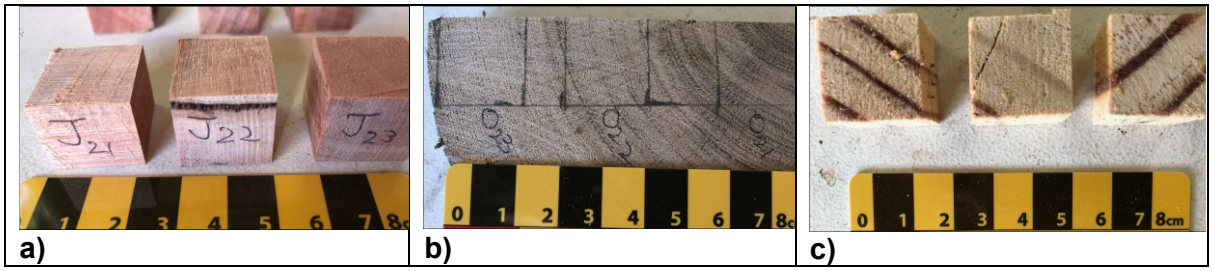

Figure 3.14 Timber cubes cut for density measurements: (a) jarrah; (b) oak; and (c) pine (photographs by Trevor Winton).

Figure 3.15 Volume measurement of timber cubes using toledo calliper (photograph by Trevor Winton).

Maximum water content was determined from pre-burial green Radiata pine, dried European oak and green Jarrah timbers using the methods of (Schniewind 1989:89) and (Jensen and Gregory 2006). Three labelled duplicate 2 x 2 x 2 cm cubes cut from each type of timber were individually placed with water proof labels into separate string bags. The author placed these samples into a large glass vacuum desiccator jar partially filled with freshly collected seawater and slid the lubricated glass lid onto the jar to achieve an airtight tight seal (Figure 3.16a). Rubber hoses connected via a venturi to a water tap created the internal vacuum. All samples initially floated on the seawater. Following weeks of alternating the vacuum on and off, water replaced the air within the cellular structure of the samples, and once fully saturated, the samples sank (Figure 3.16b). Once saturated, each cube was removed, patted dry with a

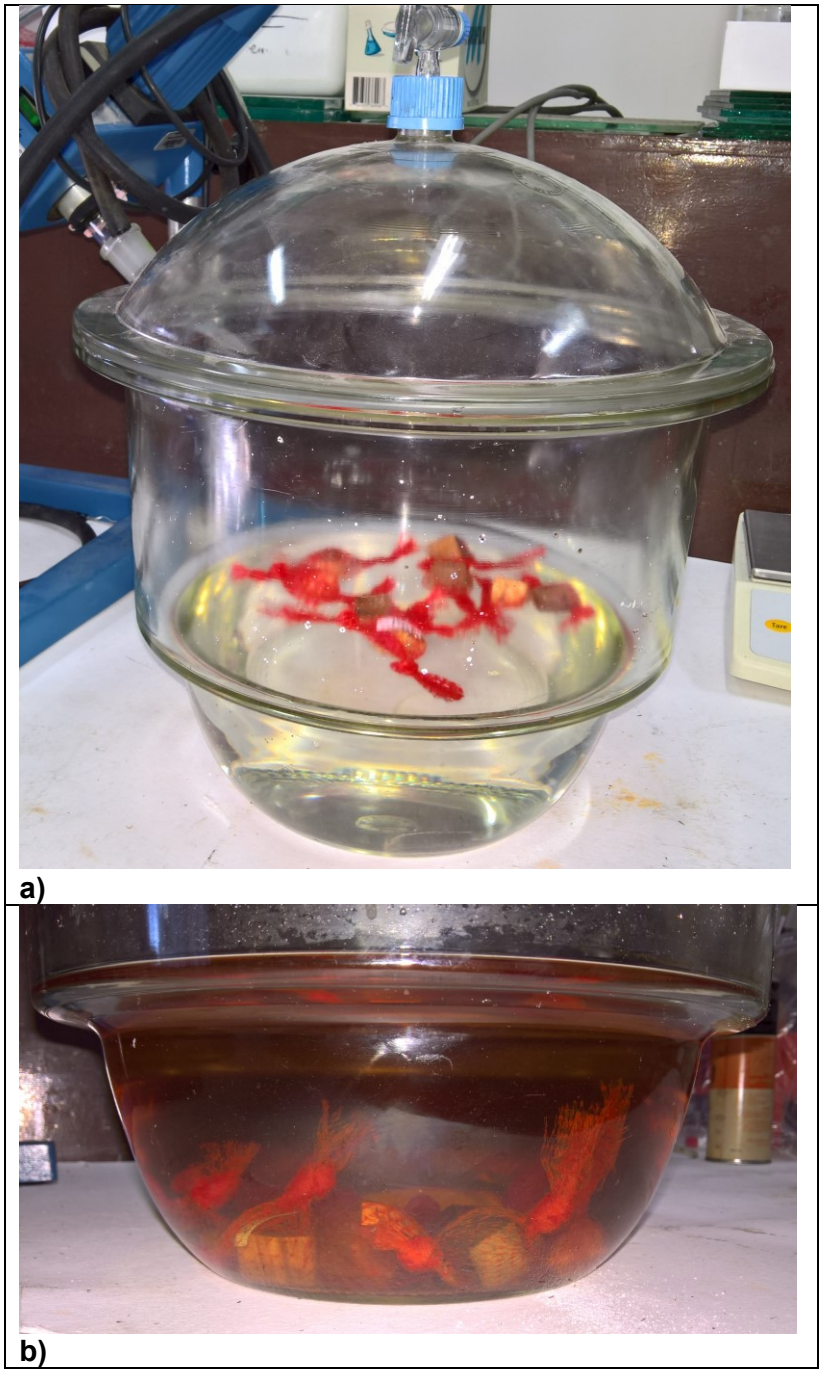

Figure 3.16 Vacuum desiccator jar with timber cubes: (a) floating; and (b) saturated (photographs by Trevor Winton).

paper towel, placed on a pre-weighed glass petri dish and its weight measured to four decimal places in a Mettler Toledo AB204-S Analytical Balance. All samples were then placed for a minimum 24 hours in a Contherm oven set to 105^0C and following removal, their dry weight measured on the analytical balance. Maximum moisture content (%) for each sample was calculated by dividing the difference between the wet mass and dry mass, by its dry mass.

Post-burial

Selected timber blocks buried at the James Matthews sleeper site in March 2017 were recovered by the field team in October 2018. They tied a rope to the endplate slot of each block, passed the rope over the davit of the *Dirk Hartog* and while holding taught, allowed the rocking motion of the boat to break the sediment suction force (Figure 3.17). Selected blocks buried at the Swan River site in January 2018 were also recovered at low tide by shovel. The purpose of the block recovery was to measure any intervening wet and dry bulk density changes, as well as moisture content (MC). Table 3.5 lists the recovered blocks and their respective timber type and burial depths from both sites. Three are shown in Figure 3.18. From each block (the deeper ones with a 45-degree taper at the top) a 2 cm wide vertical slice was first cut in the middle of the front face, followed by a horizontal 2 cm wide slice. From each of these slices 2 cm x 2 cm x 2 cm cubes were cut as shown in Figure 3.19 and Figure 3.20. Changes in colouration and/or appearance of the timbers around the edges was noted to record any effects of water penetration or timber degradation. The wet and dry bulk density of each cube was measured using the same methods as described above for the pre-burial timber cubes. Moisture content, expressed as a percentage, was determined by dividing the difference between wet and dry weights by the dry weight.

Figure 3.17 Author with recovered block Pine 10 cm DoB, James Matthews sleeper site—note attached PVC weight-tube filled with gravel (photograph by Mack McCarthy).

Table 3.5 Timber blocks removed for moisture content and density analyses.

sleeper site	burial depth/timber type			
	10 cm	20 cm	30 cm	50 cm
James Matthews	2 x pine		2 x pine 2 x oak	2 x pine
Swan River		1 x pine 1 x jarrah	1 x pine 1 x oak 1 x jarrah	1 x pine

a) b) c)

Figure 3.18 Recovered blocks: (a) pine 10 cm DoB, James Matthews site; (b) oak 30 cm DoB, Swan River site; (c) pine 20 cm DoB, Swan River site (photographs by Trevor Winton).

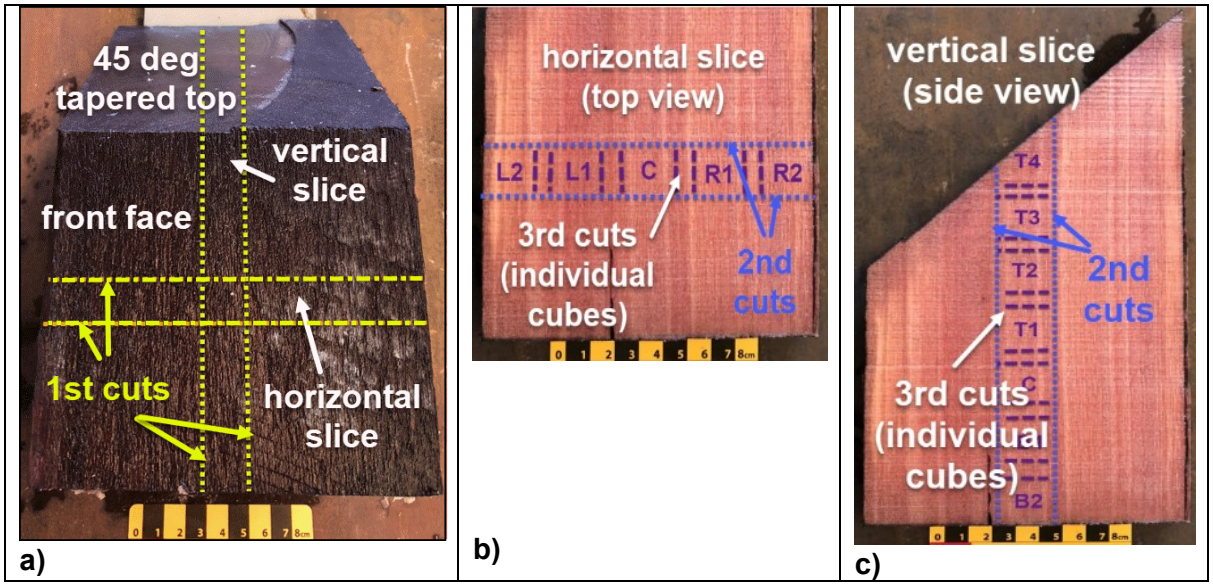

Figure 3.19 Cubes T4 to B2 and L2 to R2 cut from blocks with top 45 degree taper: (a) first vertical and horizontal cuts (yellow) to produce vertical and horizontal slices; second cuts (blue) in (b) horizontal slice and (c) vertical slice; third set of cuts (purple) to form (b) individual cubes L2 to R2 from horizontal slice and (c) cubes T4 to B2 from vertical slice (photographs by Trevor Winton).

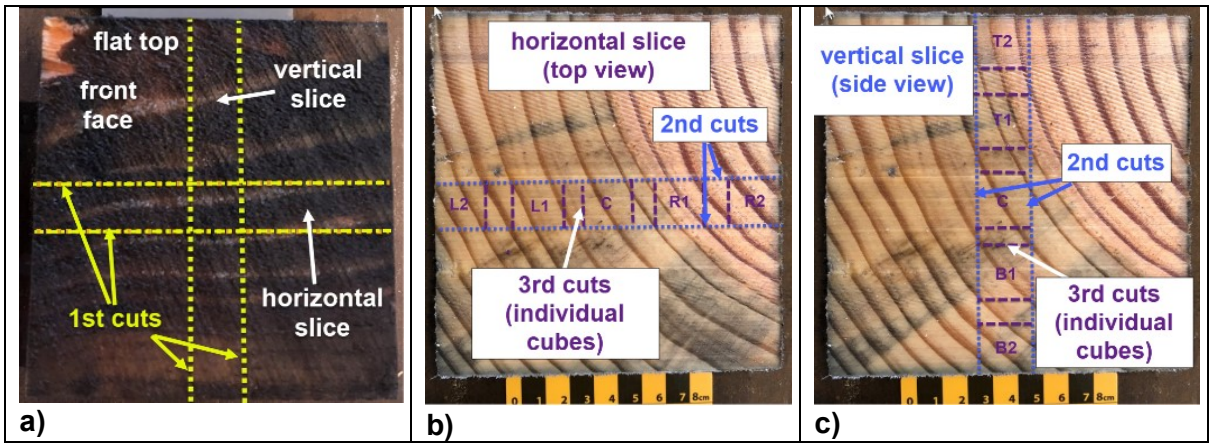

Figure 3.20 Cubes T2 to B2 and L2 to R2 cut from blocks without top 45 degree taper: (a) first vertical and horizontal cuts (yellow) to produce vertical and horizontal slice; second cuts (blue) in (b) horizontal slice (b) and (c) vertical slice; third set of cuts (purple) to form (b) individual cubes L2 to R2 from horizontal slice and (c) cubes T2 to B2 from vertical slice (photographs by Trevor Winton).

Sediment characteristics

Laboratory analyses of sediment cores established key sediment characteristics for undisturbed (reference) and disturbed (backfilled) locations at the James Matthews and Swan River sleeper sites. These characteristics included sediment type, particle size, pore water chemistry, bulk density and porosity, and in situ density. The methods for each of these

parameters are detailed in the following sections. Tables 3.6 and 3.7 show the replicated sediment sampling and analysis plan for both sleeper sites.

Sediment coring

The field teams extracted the sediment cores from reference locations and from immediately adjacent to buried sleepers at both sites (Figure 3.10 and 3.11) following the methods of Gregory (2007) and Richards et al. (2007). A modified diver-operated Shinano compressed air hammer (Figure 3.21a) vertically drove pre-labelled polycarbonate tubes into the seabed until only the last 5–10 cm of the tube protruded. These cores tubes were 60 cm long, with an external diameter of 5.04 cm and internal diameter of either 4.30 or 4.75 cm, and were driven to depth in only five to eight seconds. The diver then inserted a rubber bung in the top of the tube, and the tube and sediment core carefully lifted, trying not to break the 'vacuum seal' created by the top bung. As soon as the bottom of the tube emerged at the seabed surface, the support diver readied a second bung and simultaneously inserted it into the bottom of the tube when the vacuum seal was released by quickly removing and replacing the top bung. The core tube was carefully handled to ensure that the tube remained vertical at all times and that the rubber bungs weren't dislodged. At the James Matthews sleeper site, these cores were temporarily stored underwater in a purpose-built crate while all other cores were

a) b)

Figure 3.21 Sediment core collection at the Swan River site: (a) diver operated compressed air hammer with retrieved sediment core 216; and (b) all cores in crate (photographs by Trevor Winton).

Table 3.6 Sediment sampling and analysis plan—James Matthews sleeper site.

Type	Location	Core ID	Date collected	Time since backfilling	Chemistry (DO, Eh, pH)	Acid test/ microscope inspection	PSD	in situ density	Bulk density and porosity
Reference	Eastern side, midway sleepers	194	15/03/2018	n.a.	yes				
		195			yes				
Reference	Western side, northern end sleepers, near blocks	122	15/03/2018	n.a.	yes		yes x 5		
		20			yes		yes x 5		
		217	09/05/2018				yes x 1	yes	yes
		218					yes x 1	yes^{R}	yes
Backfilled	between P30 & P30	112	15/03/2018	13 months	yes				
		170			yes				
Backfilled	17.3 m between P50 & P50	192	15/03/2018	13 months	yes		yes x 5		
		193			yes		yes x 5		
		215	09/05/2018	15 months				yes	yes
		216						yes	yes
Backfilled	between P10/30 & P10/30/50	100	15/03/2018	13 months	yes				
		155			yes				
Backfilled	between S30 & S50	214	09/05/2018	1 month		yes	yes x 1	yes^{R}	yes
		300					yes x 1	yes	
	totals	*16*			*10*	*1*	*24*	*6*	*6*

yes^{R}	repacked tight and loose
yes x 5	GSD for 5 x 10 cm sections
yes x 1	GSD for 1 x 50 cm core

Table 3.7 Sediment sampling and analysis plan—Swan River sleeper site.

type	location	core ID	date collected	time since backfilling	chemistry (DO, Eh, pH)	acid test/ microscope inspection	PSD	in situ density	bulk density and porosity
Reference	western end, in gap b/w J30 & P30	12	10/04/2018	n.a.	yes		yes x 5		
		17			yes		yes x 5		
		301	28/05/2018				yes x 1	yes	yes
		302				yes	yes x 1	yes^{R}	yes
Reference	Eastern end sleepers	163	10/04/2018	n.a.	yes				
		183			yes				
Backfilled	between S20 & J30	10	10/04/2018	3.25 months	yes				
		162			yes				
Backfilled	between J50 & P50	176	10/04/2018	3.25 months	yes		yes x 5		
		169			yes		yes x 5		
		303	28/05/2018	4.75 months			yes x 1	yes	yes
		304					yes x 1	yes^{R}	yes
Backfilled	between S50 & P10	177	10/04/2018	3.25 months	yes				
		156			yes				
	totals	*14*			*10*	*1*	*24*	*4*	*4*

yes^{R}	repacked tight and loose
yes x 5	GSD for 5 x 10 cm sections
yes x 1	GSD for 1 x 50 cm core

collected. Once this was complete, the crate holding all cores was lifted from the seabed onto the boat and electrical tape wrapped around the bungs at both ends of all cores to minimise any possible water loss from the tubes. At the Swan River site, the cores were walked to shore and immediately taped and placed vertically in the crate (Figure 3.21b). Upon return to the WAM Conservation laboratory, all cores collected for pore water chemistry analyses were immediately placed vertically in a deep freeze and stored at -23.7^{0}C until removed for analysis. Other cores were stored vertically, but not frozen.

DO, Eh, and Ph profiles

Specialist micro-electrodes were used to measure dissolved oxygen (DO), redox potential (Eh) and pH at a minimum 1 cm interval along the length of 20 sediment cores (Tables 3.6 and 3.7) following the method by Gregory (2007). The author pre-drilled the polycarbonate tubes for these cores using a 1/8'' bit (sized to suit diameter of the micro-electrodes) at 1 cm intervals in a line along the length of the tube. These holes were then double sealed with 'gaffer' tape to ensure that when used in the field neither sand nor pore water would escape through these holes (Figure 3.22).

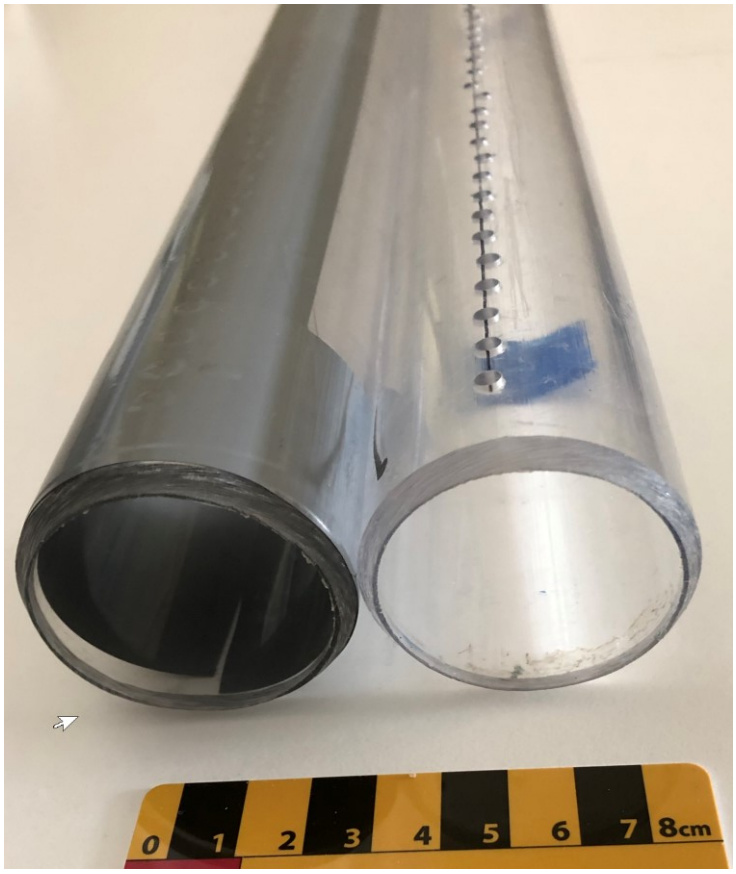

Figure 3.22 Polycarbonate tubes showing pre-drilled holes (uncovered and sealed) (photograph by Trevor Winton)..

In preparation for the measurements, the author removed three cores at a time from freezer storage. The top bung was removed from each, and with light taps from a hammer, the frozen seawater cap sitting above the top of the sediment was fractured and removed, and a solid tube seal inserted. These prepared but still frozen cores were then placed horizontally inside an Argon filled storage bag (Figure 3.23) with the taped tube holes facing downwards. These were left overnight to thaw, and as the sediment core defrosted, the pore water drained towards the holes. During placement and removal of the cores from within the sealed bag, a high flow of Argon was maintained to ensure minimal oxygen presence around the cores. Once removed from the sealed bag, the author placed each core on the laboratory bench, holes upwards, and taped in place to prevent any roll or movement. Prior to insertion of micro-electrodes, the 'gaffer' tape was progressively cut and peeled back exposing only one hole at a time. Following removal of electrodes, the tape was re-sealed over each hole.

Figure 3.23 The author with sediment cores inside argon filled sealed bag and DO, Eh and pH profiling setup (photograph by Jon Carpenter).

A DS-(2) Unisense needle-type oxygen microsensor (OX-N) was inserted into the sediment at each hole, commencing at the top of each core, to measure the dissolved oxygen concentration. This sensor was coupled to a Unisense Picoammeter PA2000 display software set on the 2000 pA (pico-Amp) range scale. The electrode responded linearly in the range 0% to 100% oxygen saturation and was calibrated using a two-point calibration method according to the manufacturer's specifications. The needle sensor was placed for several minutes in an

aerated beaker (air bubbling through) and the pico-amp signal recorded as the 100% DO value. The needle was then removed, wiped with a 'KIMWIPE', and placed into a pre-prepared oxygen scavenger vial. This vial was pre-prepared by the author dissolving 0.4 gm $Na_2S_2O_3$ into 20 mg of water at 30 $^0/_{00}$ salinity, and letting stand for 10 minutes to allow for full scavenging of the oxygen molecules. After two to three minutes in the scavenging vial, the micro-amp signal was recorded as the 0% DO value, and the needle removed, rinsed with deionised water and placed back into the oxygenated beaker. The needle was then removed, wiped and carefully inserted approximately 1 cm into the sediment exposed through the freshly opened tube hole. The micro-amp reading was noted, the needle removed, rinsed with de-ionized water and replaced into the oxygenated beaker. The calibration procedure was undertaken prior to the first sediment DO reading, mid-way through the DO measurements, and at the completion of DO measurements for each core.

Hand-held EUTECH Instruments Cyberscan pH 110 and Cyberscan pH100 electrodes were used to measure the Eh and pH profiles, respectively. These electrodes were calibrated according to the manufacturer's specifications. The calibration of the Eh and pH electrodes are dependent on the solution temperature. The temperature of water, left over the weekend in a beaker adjacent to the buffer solutions, was measured using a mercury thermometer (21.4 ^{0}C). This temperature was used to manually adjust the temperature compensation on both Cyberscan units. The author then placed 20 ml of pH 4 buffer into one small plastic vial and 20 ml of pH 7 buffer into a second vial. Each of these vials was saturated with quinhydrone and vigorously stirred. The temperature of each vial was recorded using the Cyberscan pH 110 electrode, which was then manually changed to measure millivolts (mV). The electrode was then inserted into the pH 4 vial and the Eh millivolt reading recorded. Following removal, the electrode was rinsed with deionized water, then placed in the pH 7 vial to record its Eh millivolt reading. In accordance with the instrument's Operating Instructions the measured potentials should be within 10 millivolts of the tabulated theoretical values. This was achieved most times, however an increasing deviation occurred as the sensors became poisoned with use. This process was repeated using the Cyberscan pH 100 electrode. In this case however, the electrode was placed back and forth four times between the pH 4 and pH 7 solutions without rinsing prior to recording the final pH millivolt reading. These calibrations were undertaken prior to commencement of Eh and pH measurements for each core. Sediment Eh and pH were recorded following the measurement of DO by carefully inserting the respective electrode approximately 1 cm into the exposed sediment through the opened pre-drilled tube hole (Figure 3.24). The author also measured the temperature of the sediment core near the top, around the middle and near the bottom of each core using a EUTECH temperature probe. These sediment core temperatures were used to manually adjust the temperature

compensation on both Cyberscan units. Once the pH electrode and/or the temperature probe was removed, the ‘gaffer’ tape was resealed over the tube hole.

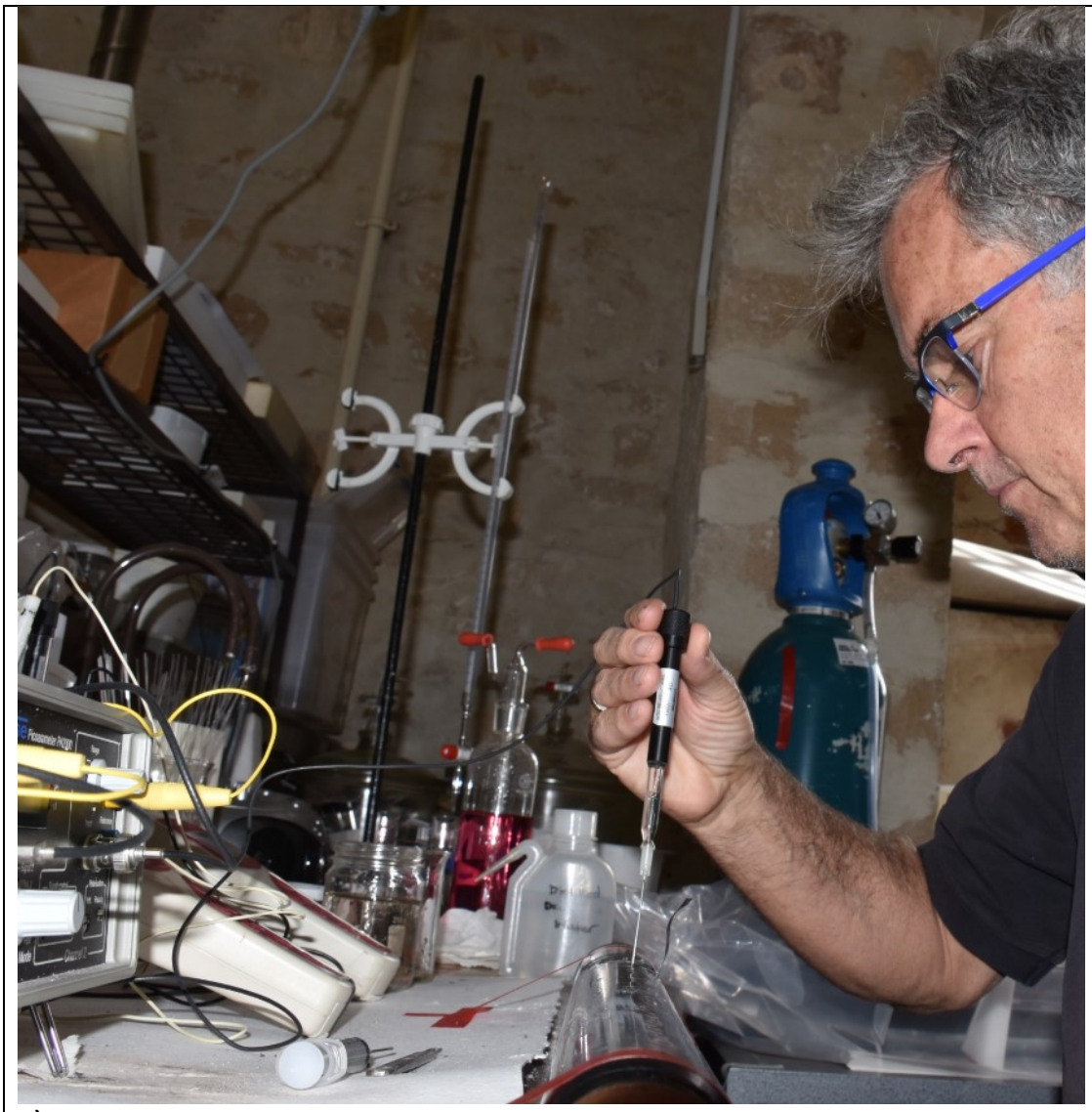

a)

b)

Figure 3.24 DO, Eh, pH and temperature microchemical analyses: (a) author inserting DO probe into sediment core; and (b) sediment core showing progressive uncovering and measurement within tube holes (photographs by Jon Carpenter).

Sediment facies

Chemical and microscopic analyses of sediment sub-samples determined the sediment type at each of the James Matthews and Swan River sleeper sites. In the WAM Conservation laboratory fume hood the author added deionized water and droplets of 37% HCL to a glass beaker containing half a teaspoon of sediment from cores 214 (*James Mathews* site) and 302 (Swan River site). The beaker with the sediment from the offshore *James Matthews* site bubbled and fizzed (see Figure 3.25). This indicated that it was composed mainly of calcareous (carbonate or shell) material. Conversely, only a tiny dot of fizz was seen in the beaker 302. This revealed that the Swan River sediment was composed primarily of siliceous sand with small amounts of shell fragments. Ryan Beemer, Centre for Offshore Foundation Systems, University of Western Australia (UWA), examined samples from the same cores using a desktop microscope. He confirmed that the sediments at the *James Matthews* site consist primarily composed of carbonates with approximately 20% silica and at the Swan River site comprises silica with some shell fragments. He observed that the dark grey colour of the carbonates arose from minerals (FeS_2) incorporated into the pores of the shells during shell formation (Ryan Beemer pers. comm. 2018).

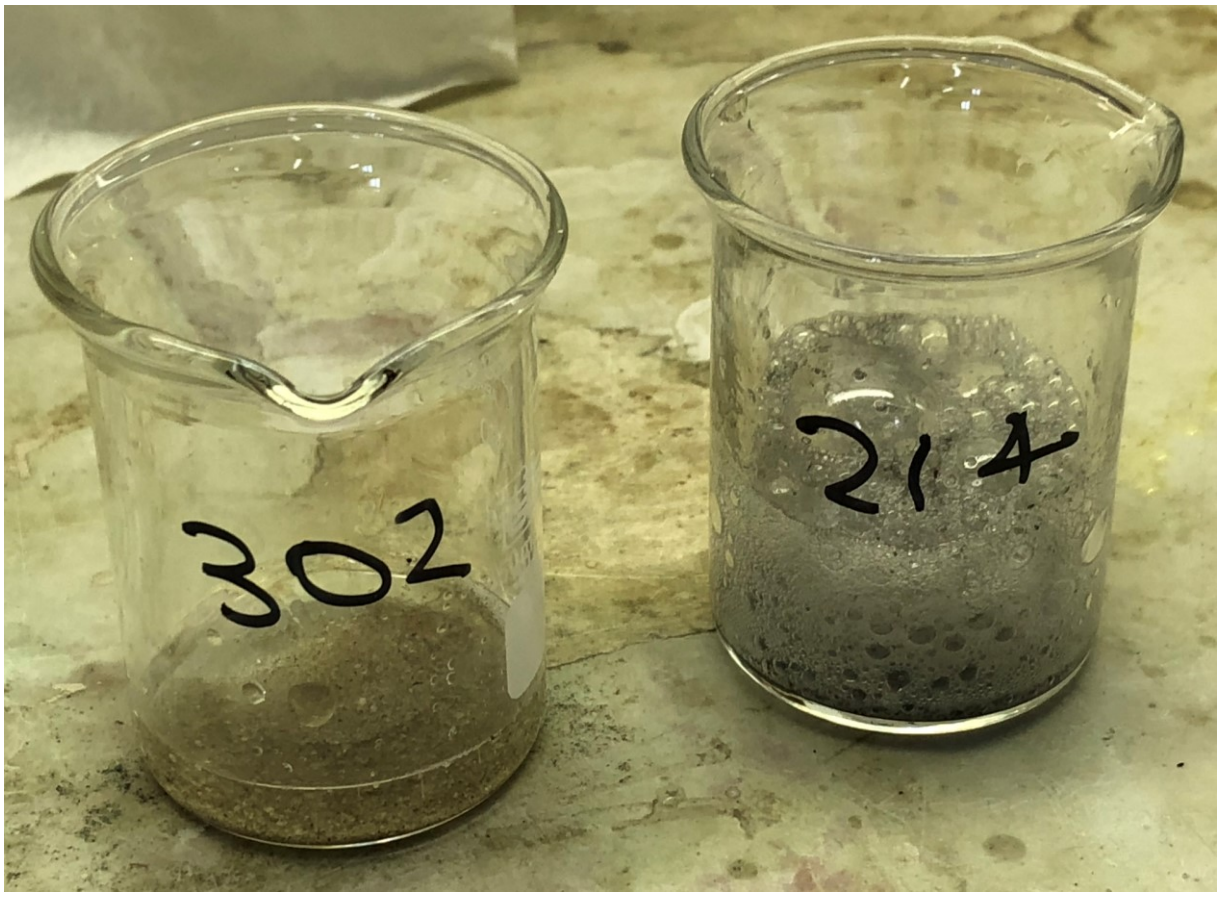

Figure 3.25 *James Matthews* site (214) and Swan River site (302) sediment tests using HCL (photograph by Trevor Winton).

PSD—sieving

Mechanical sieving techniques were used to determine sediment particle size distribution (PSD) on eight replicated cores from each sleeper site. The replicated cores included two sets of duplicates from reference locations and two sets of duplicates from back-filled locations. As shown in **Error! Reference source not found.**, PSD analyses were undertaken on the whole 50 cm+ long cores for one set of duplicated reference cores from each site. In addition, PSD analyses were also undertaken on 5 cm x 10 cm subsamples from the other set of duplicate reference cores. Similarly, PSD analyses were undertaken on duplicate pairs of whole and sub-sampled cores collected at disturbed (backfilled) locations at both the James Matthews and Swan River sleeper sites.

Mechanical sieving of these core samples was undertaken at the UWA Centre for Offshore Foundations Systems' soils laboratory using a complete set of Endecotts Ltd Laboratory Test Sieve ISO 3310-1. The sieving procedure followed Australian Standard AS 1289.3.6.1—2009, Method 3.6.1 *Soil Classification tests—Determination of the particle size distribution of a soil—Standard method of analysis by sieving*. Sediment cores were extruded from the core tubes following completion of the pore water chemistry analyses, or collection from core storage. These extruded samples were either sub-sectioned into 5 cm x 10 cm long samples and each sub-sample individually placed on pre-weighed trays, or the whole extruded sample placed on a pre-weighed tray. These trays were then placed in a laboratory Contherm oven set at 105^0C for a minimum 24 hours. Once dry, the samples were removed from the oven, reweighed and transferred to the UWA soils laboratory. A sub-sample weighing approximately 250 gm was taken from each, accurately weighed using a Mettler Toledo PJ3600 DeltaRange Precision Balance, placed in a pre-weighed tray and soaked with fresh water for 30 minutes. These soaked samples were then washed through a 75-micron sieve until the wash water ran clear. The wash water was collected in a bucket and stored in case it was later needed. The retained sediment was then washed back into its original tray, ensuring that all sediment was recovered, and placed back into a Contherm oven set at 105^0C for a period of at least 24 hours. Once fully dried, samples were again reweighed. Any difference in mass between the pre-washed and post-washed dried samples would represent a loss of fines (<75 micron). If that loss was greater than 10% of the original (pre-wash) mass, then a hydrometer test would need to be undertaken on the wash water stored in the bucket. In all cases, the hydrometer test was not required. The author then obtained a 250 gm sub-sample, representative of each of the dried core samples, and placed it in the top of the nested set of sieves as listed in Table 3.8. Due to the presence of shell material in all samples, the sieves were individually hand shaken, rather than using the mechanical shaker. Following repeated shaking, and once the volume of sediment retained on each sieve did not differ by more than a few percent, the

retained sediment was weighed and recorded against the sieve size. Sediment passing through was placed into the next finer sieve, and the process repeated until the last sieve (<75 micron) was completed.

Table 3.8 AS1289 sieve sizes, nested from coarse to fine.

unit	mm			μm						
AS1289 sieve	4.75	2.36	1.18	600	425	300	212	150	106	75

Sediment bulk density and porosity

Sediment bulk density (sometimes known as sediment wet density) and porosity are measures of the mass and/or volume of sediment particles and pore water fluid in fully saturated sediments (Richardson and Jackson 2017:499). Their methods of determination follow those by Hamilton (1969:25–27). Unfrozen duplicate cores from reference and backfilled locations at both sites were selected for analysis (Tables 3.6 and 3.7) as soon after return from the field as possible. While maintained in the vertical position, the total weight of each core (wet sediment, overlying water cap, polycarbonate tube and rubber end-bungs) was measured using the WAM Conservation Department's 4 kg Mettler Toledo TE 12000 Precision Balance. The column height of the saturated sediment and the height of the seawater cap sitting above the sediment surface were measured using a metre-long steel mm scale. The rubber bungs were then removed, the sediment extruded into a pre-weighed oven tray and placed in a Contherm oven set at 105^0C for a minimum of 24 hours. After allowing the tray and sediment to cool, the tray was re-weighed. Meanwhile, the weight of the individual polycarbonate tube and rubber bungs for each core were measured, and the internal diameter of the tubes recorded using a 0.1 mm accurate Toledo micrometer. The volume of the saturated sediment was calculated using the diameter and column height measurements, and the mass of the seawater cap determined from its volume and assumed density (1.024 kg/m^3 at 23^0C) (Hamilton 1969:18). The mass of saturated sediment was calculated by subtraction of the combined mass of the individual polycarbonate tube, rubber bungs and seawater cap from the total core weight. Sediment bulk density (kg/m^3) for each sample was determined by dividing the mass of saturated sediment by its saturated volume. The difference in mass between the wet sediment and dry sediment equals the mass of seawater evaporated from the saturated sediment while drying. The volume of this evaporated water is this mass divided by its assumed density (1.024 kg/m^3 at 23^0C). Finally, sediment porosity (%) for each sample was calculated using Hamilton's Method A (1969:26) by dividing the volume of evaporated seawater by the volume of the saturated sediment.

In situ density

Ex situ (cone) penetration tests generated density-dependent penetration resistance profiles in sediment cores collected at reference and backfilled locations from both the James Matthews and Swan River sleeper sites. The author conducted these cone penetration tests in the National Geotechnical Centrifuge Facility (NGCF) Preparation Laboratory, UWA. The tests provided a feasible approach to determining relative in situ sediment density following the advice from Mark Randolf, Centre for Offshore Foundation Systems, UWA. Whilst 'the most definitive way is to freeze the saturated sediment in situ, remove the frozen block and slice it into cubes while still frozen, then analyse the mass and volume of the cubes when thawed'—this approach, however, is both 'expensive and logistically difficult' (Mark Randolf pers. comm. 2018). The simpler, but still logistically challenging alternative of using a cone penetrometer in situ was not undertaken either due to the 'highly variable relationship between sediment density and penetrometer resistance'. Randolf advised that 'relative in situ density between reference, backfilled and re-densified sediments could, however, be achieved ex situ with a cone penetrometer'. He also noted that:

> 'in the calcareous and siliceous sands found at the James Matthews and Swan River sleeper sites, a sediment core pushed into the sea/riverbed in under 20 seconds, and subsequently capped on retrieval, should provide a sample suitable for ex situ density analyses. In these situations, the pore water would not have had time to drain away, although there would be some densification adjacent to (within 10 mm of) the inside of the core tube.'

The purpose of a cone penetrometer test (CPT) is to 'determine sub-surface stratigraphy, identify materials present and estimate geotechnical parameters by pushing a cone on the end of a rod into the ground/sediment at a constant speed. Continuous measurements are made of the resistance to penetration of the cone' (Lunne et al. 1997:1–2). At the NGCF laboratory, the smallest diameter cone penetrometer test rod was 10 mm. This rod was dismissed as being relatively too large for the 47 mm diameter sediment core. The surrounding sediment would be constrained as the cone was pushed through, adding unrepresentative additional resistance forces. Consequently, a purpose built small (4 mm) diameter stiff rod, connected to a 1 kilonewton (kN) calibrated load cell with a partially hollowed M10 threaded rod, was fabricated. The rod and load cell were connected to a C72 Standard Actuator and controlled by PACS software to vertically drive the rod into the core at a constant rate. Continuous resistance loads were recorded using DigiDAQ acquisition software. The sediment cores were clamped vertically in place directly below the actuator. Figure 3.26 and 3.27 show this experimental setup.

Figure 3.26 Sediment penetrometer test set up: (a) front view; and (b) side view (photographs by Trevor Winton).

The first trial run revealed that the actuator hit the safety end stop when the rod had only penetrated the sediment core by 30 cm. A 20 cm load cell extender was added, and a 9 cm length cut from the 4mm rod to fit within the physical constraints of the actuator and sediment core lengths. In a second trial, a large 430 N load spike was recorded (the tip of the penetrometer rod was pushing on a large flat shell significantly increasing the resistance area). To protect against equipment damage, the 1 kN load cell was swapped out with a calibrated 10 kN cell. Duplicate unfrozen reference cores from the James Matthews sleeper site were tested, as well as duplicate unfrozen backfilled cores collected one month and 15 months after

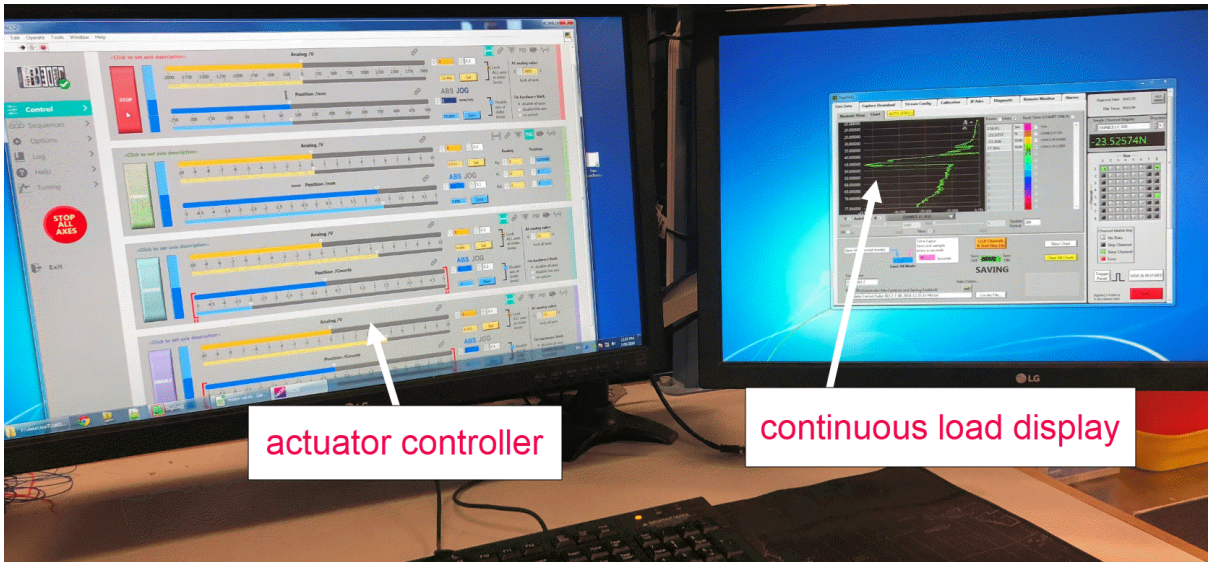

Figure 3.27 Sediment penetrometer PACS and DigiDAQ controls (photograph by Trevor Winton).

backfilling. Likewise, duplicate unfrozen reference cores, and duplicate unfrozen backfilled cores collected 4.75 months after backfilling from the Swan River site, were tested.

To better quantify the relative effect of backfilling and densification on the density-dependent penetration resistance profiles, the probable minimum and maximum penetration resistance profiles were developed. These profiles were generated by testing cores when the sediment was in its loosest and densest state. To achieve this, reference cores 218 and 302 and backfilled cores 214 and 304 (from the James Matthews and Swan River sites, respectively) were physically manipulated. Following their initial non-manipulated penetration test, the sediment from each core was emptied out into a large container, and then repacked back into the core tube. In the first instance this was done by filling the tube with water and slowly pouring the sediment in without any mechanical compaction (the 'light' or loosest compaction test). In the second instance, however, sediment was poured in to create a three cm thick layer within the tube, then vigorously compacted for 30 seconds with a large 10 mm diameter rod. This was repeated until all sediment had been progressively compacted (the 'tight' or densest compaction test). All dimensional and weight data were also recorded in order to calculate the bulk density of the cores in their non-manipulated, lightly compacted and tightly compacted states.

Water quality conditions

The field teams recorded in situ water quality measurements prior to and following SBP profiling measurements. At the Swan River site, a TPS Pty Ltd 90-FLMV water quality logger

was used to measure salinity (%), water temperature (^{0}C), pH and dissolved oxygen (DO, mg/L) at three locations and at three water depths. These locations included in the middle and at each end of the line of sleepers. At each location measurements were recorded near the river bed, mid-depth and near the river surface. At the James Matthews sleeper site, time-averaged water temperature data was recorded using an Oceanic GEO 2 divers' watch, and salinity measured ex-situ in the cap water of sediment core 214 using the TPS water quality logger.

SBP acoustic measurements over buried sleepers

The Innomar SES-2000 *compact* SBP was selected for the sub-bottom measurements. It operates in very shallow coastal waters, from around 50 cm to 400 m water depths, with the transducer pole mounted on a survey or autonomous vessel, forward of propeller wash to avoid problematic acoustic noise (Innomar 2018). The transducer is cable connected to a top-side unit (transceiver) with SESWIN control, data acquisition and real-time data display software. The system has a sampling rate of up to 40 pings/second and data acquisition rate of 70 kHz, allowing for high survey-vessel speeds of 2 m/s. It generates a very narrow transmit beam width (-3dB) of +/- 2^0 which in shallow water depths (<2.8 m) and for shallow (<50 cm) buried timbers, results in an acoustic foot of <10 cm.

Under most marine survey situations, the vessel mounted transducer arrangement provides a more than satisfactory data gathering solution. For the James Matthews sleeper site, however, it was anticipated that it would be difficult to keep the transducer head vertically located over all buried sleepers during a data acquisition run. Operating in even light winds and currents, it is difficult for the WAM survey vessel to maintain a straight-line course of over 30 m with no lateral deviation from the centre-line greater than +/- 20 cm. While more sheltered on the Swan River site, much shallower water depths prohibit the use of the larger survey vessel for SBP measurements. As a consequence, an autonomous floating sled was developed and trialed in February 2017 as a platform to carry the vertically mounted 19 kg SES-2000 *compact* SBP transducer head. A dedicated 20 m cable connected to an adjacent moored vessel (James Matthews site) and the riverbank (Swan River site) provided 240-volt power supply and data connectivity to the transceiver.

This floating sled was constructed of PVC pipes and was laterally constrained along the line of sleepers by taut guidelines. Figure 3.28 shows the concept sketch and prototype sled. The performance of this system was successfully trialed using substitute weights (instead of the transducer). Shortly before mobilizing all equipment to undertake the SBP measurements in June 2017, the field team undertook final sea tests of the sled and support vessels. On this day, a strong easterly breeze pushed the floating sled outside the line of sleepers despite

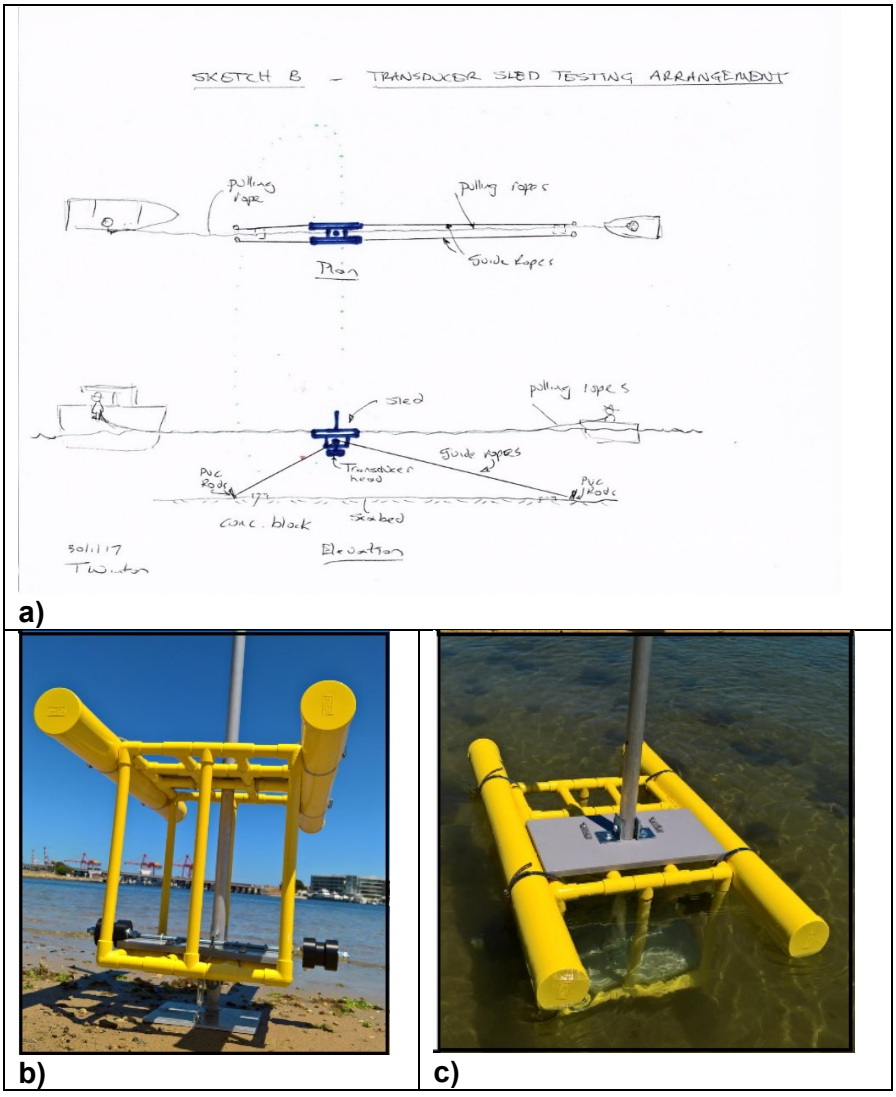

Figure 3.28 Floating sled concept: (a) original sketch; (b) prototype on land (transducer attaches to bottom plate and guide ropes wrap around black rollers); and (c) floating in water (photographs by Trevor Winton).

increasing the tension in the guide ropes. A work-around solution was planned which involved placing lateral restraints mid-way along the line of sleepers. Unfortunately, water visibility was reduced to near zero on the day of survey and a decision was made to cancel diver operations due to safety risks. The survey/dive vessel had already been pre-equipped to survey the buried remains on the *James Matthews* wrecksite using a forward pole-mounted SBP transducer head. As a consequence, the plan to measure the sleepers using the floating sled was abandoned, and reverted to the vessel pole mounted approach.

SBP data collection occurred at the James Matthews sleeper site on the 7th and 8th of June 2017 using the WAM's survey/dive vessel *Dirk Hartog* (Figure 3.29). The transducer was pole mounted amidships with the head positioned 50 cm below sea surface. A Trimble POS MV Surfmaster GNSS G2 real time satellite positioning antenna and heave correction sensor

Figure 3.29 WAM research vessel *Dirk Hartog* showing mounting locations of SES-2000 compact SBP transducer, Trimble GNSS antenna and applanix IMU sensors (photographs by Trevor Winton).

(IMU) (applanix 2019) recorded the position and motion of the transducer head. Offsets from each sensor mounting position relative to the center of the SBP transducer were measured and included into the positioning calculations. Fugro Satellite Positioning Pty. Ltd. supplied Marinestar positioning solution which enabled real time position tracking to approximately 15–20 cm in both the horizontal (x, y) and vertical (z) directions. Following post-processing, two cm accuracy in the horizontal and vertical position was achieved. Surface marker buoys were tethered at each end and midway along the 30 m line of sleepers, and multiple SBP measurement runs were made with the coxswain guided by the surface buoys. The topside transceiver mounted in the cabin provided real time display of the survey results. The on-board data display, confirmed by subsequent data analysis in mid-late 2017, showed that the vessel track veered off from the line directly above the sleepers despite the helmsman's best efforts. SBP data was acquired for only a portion of sleepers, on some runs. An alternate SBP sled was required for subsequent measurements of all sleepers installed at the James Matthews sleeper site, as well as at the depth limited Swan River site.

A new sled was designed to run along the seabed on large, wide pneumatic rubber tyres being pulled from end to end by a single attached rope fed through pulleys centrally located at each end of the line of sleepers. This concept was originally trialled on the Swan River site. This

was to ensure that the sled did not sink into the softer river sediments, and to optimise sled width and wheel diameter to clear all protruding endplates. Despite the weight of the steel rimmed tyres, an additional 40 kgs of ballast was required to keep it on the seabed. The pneumatic tyres were changed to solid rubber, and an aluminium frame constructed to hold the vertically pole mounted SBP transducer. Two removable solid steel bars were added at the base to ensure stability and a bottom skirt added to help the sled deflect off endplates. Figure 3.30 shows images of this new sled following fabrication, entering the water at the Swan River site, and on the seabed at the James Matthews sleeper site. Figure 3.31 shows the sled in operation at the James Matthews sleeper site.

Figure 3.30 Seabed SBP sled: (a) fabricated sled and mast, without transducer and RTK rover; (b) sled entering Swan River site, showing transducer and orange dedicated power/data cable; and (c) sled on seabed at the James Matthews sleeper site (photograph (a) by Trevor Winton, (b) by Col Cochran and (c) by Ian McCann).

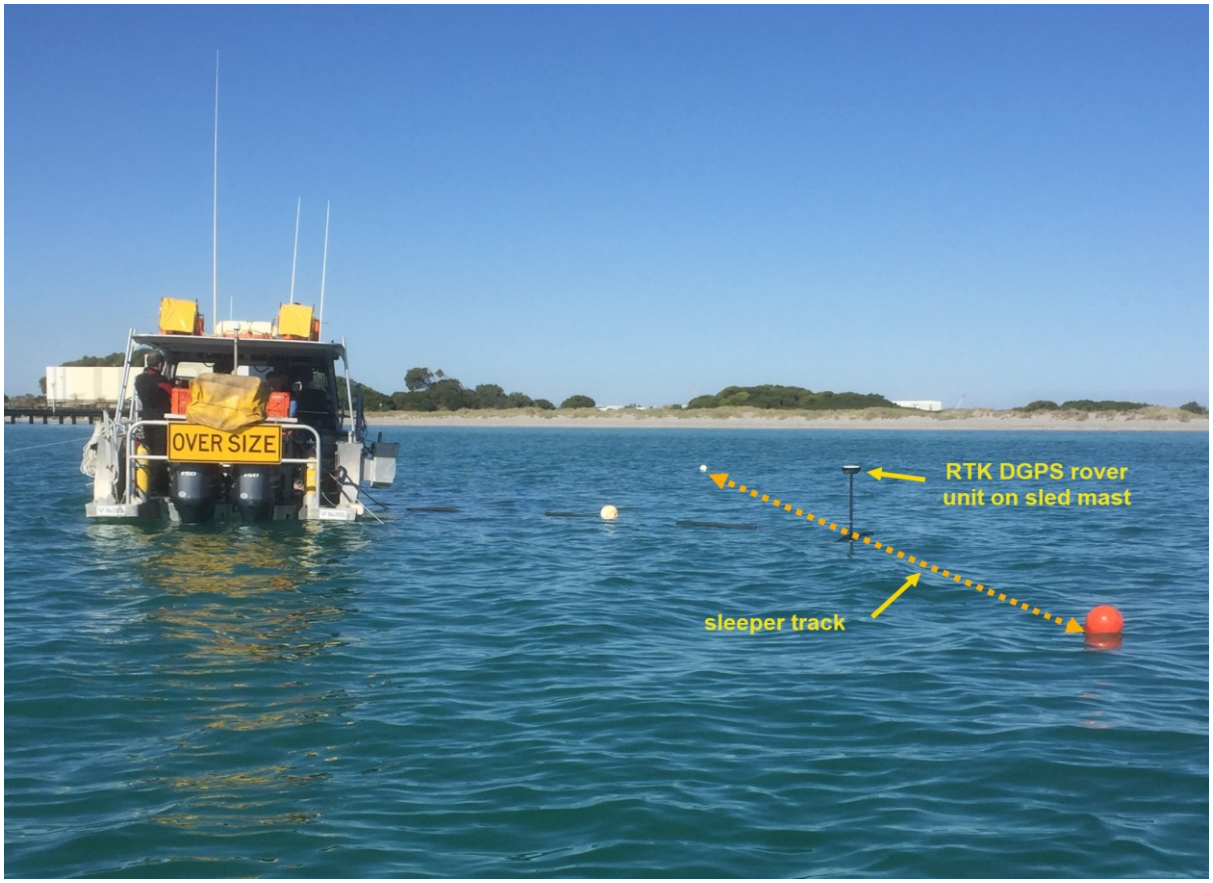

Figure 3.31 Seabed sled operational at the James Matthews sleeper site, running alongside *Dirk Hartog* from red to far white buoy with RTK DGPS rover unit visible on top of sled mast (photograph by Mack McCarthy).

During a spring high tide on 18th of May 2018 water depths peaked at approximately one metre at the Swan River sleeper site. During this period of maximum water depth, MAAWA volunteers pulled the sled mounted Innomar SES-2000 *compact* SBP transducer back and forth along the line of buried sleepers. The vertical position of the transducer head was adjusted so that it was fully submerged with 15 cm of water from the water surface to the underside of the transducer. The resultant distance from the underside of the transducer head to the riverbed was 71.5 cm. The 20 m orange dedicated cable connected the transducer to the transceiver on the river bank and SBP data was viewed in real-time. A portable generator provided 240-volt power to the unit. Positional data of the SBP transducer head was recorded from a Leica GS16 High Precision GNSS RTK Rover mounted directly above the transducer head. This unit operated under the Leica Captivate V3.20 software and was Bluetooth connected with a hand-held CS20 logger to continuously log the co-ordinates.

On the following day the Innomar SES-2000 *compact* SBP was deployed at the James Matthews sleeper site using the seabed sled operated from *Dirk Hartog*. This vessel was positioned midway along, and parallel to the line of sleepers, using both bow and stern

anchors. Divers positioned the sled over the line of sleepers and connected ropes fore and aft to the sled. Each rope was fed through pulleys centrally fastened between the sets of 'star' pickets at the end of the line of sleepers, and the free ends swum back to *Dirk Hartog.* MAAWA volunteers located at the bow and the stern of the vessel then pulled the sled back and forth along the line of sleepers. The vertical position of the transducer head was adjusted to be as high above the seabed as the frame would allow (90.5 cm). This increased the depth of the seabed first multiple reflection, thus minimizing the potential for interference with measurement of the deeper buried sleepers. The horizontal position of the SBP transducer head was continuously logged by the Leica GS16 High Precision GNSS RTK Rover mounted above water on the extended transducer pole. The RTK DGPS data was relayed via Bluetooth back to the CS20 logger held on the deck of *Dirk Hartog*. SBP data was transferred back to the transceiver and real-time display units via the 20 m orange dedicated cable, which was supported in the water by foam tubes. As the sled was rolling across the seabed surface independent of any vessel motion, there was no need to collect simultaneous heave data on the *Dirk Hartog*.

SBP acoustic data analyses

Depth of sediment cover

Following data collection, SBP Echo files (.RAW and .SES) were copied from the field laptop and loaded onto a PC, together with Innomar' s ISE2 software. The internally recorded start and end time of each SBP run was noted. The Leica Point Quality Report was also downloaded and the quality code associated with all RTK DGPS positional data points was assessed. All data points within the SBP run times had the highest quality code indicating that connection to the Smartnet was retained throughout. This ensured that horizontal location accuracies of 6–12 mm were achieved. The SBP files were subsequently processed in ISE2 following the steps described in Table 3.9 to identify and quantify the depths of burial (DoB) and thicknesses of the buried sleepers at both the James Matthews and Swan River sleeper sites. Relevant seismic profiles were exported from ISE2 software using GIF file format for graphical presentation purposes.

Reflection coefficient

The potential relationship between acoustic wave parameters and types and condition of a variety of buried material was evaluated using the original reflection coefficient method by Warner (1990) and reworked in Plets et al. (2008). As introduced in Section 3.1 an acoustic reflection coefficient (K_R) is the numerical expression for the strength of the reflection of the acoustic wave from a boundary (seabed surface, the interface between two sedimentary

Table 3.9 DoB and K_{DR} processing steps.

step	process	comments
1	Load selected low frequency .RAW Echo data file into ISE2. No processing i.e. set: Stacking and Smoothing =1; Prefilter = none; Demodulate = none; Algorithm = AlgoAMP; Palette = 30 Red-White-Black.	No post-processing of .RAW data file. Maintain full .RAW data qualities. AlgoAMP displays the amplitude of the echo envelope.
2	Inspect unprocessed .RAW data file and identify potential buried reflectors, and associated trace numbers, based on the location of inverted red/black hyperbolae (horseshoes)	
3	Select Signal Processing and process .RAW data file. Prefilter = none, Demodulate = Envelope, Algorithm = Algo1P, Palette = 10 Colours	Demodulated .RAW data file. Algo1P displays the gradient of the echo amplitude for better visualisation of amplitude changes.
4	Check buried reflector locations (bright red-yellow blobs) using demodulated .RAW data file, and scan individual trace profiles on LHS of screen.	
5	Block traces from both unprocessed and demodulated .RAW data files associated with each potential reflector (ensuring capture of peak of hyperbolae). Export signal traces and save to (notepad) file. Copy data from each exported trace from value=16 to value=end and paste into Excel sheet.	Minimum number of traces selected for each reflector should be 5-6. Depth increment for each echo trace is [End Range – Start Range]/number of samples ([value=11 – value=10] /value=15). Starting depth is value=10 for *James Matthews* wrecksite and sleeper data.
6	Plot all demodulated .RAW trace data vs. depth for each potential reflector. Identify depth location where the echo envelope is similar/consistent across a minimum of five consecutive traces – mark as a reflector. If echo envelope on one or more demodulated traces is not repeated on adjacent traces, then discard that depth as a non-reflector. Select trace(s) with the minimum reflector depth and maximum acoustic amplitude as the most central above the buried reflector (sleeper). Record the depth of seabed, buried reflector locations and 1st seabed multiple (if profile sufficiently deep). Subtract top reflector and seabed depths to quantify depth (DoB) and multiple reflector depths to quantify thickness of each buried reflector.	Ping rate = 40 pings/sec for SBP data collected with only one LF (15 kHz) channel being recorded. Based on an average vessel speed of 2 m/s this equates to pings (traces) at approximately 5 cm spacings. With a transmit beam width (-3dB) of +/- 2 degrees, this equates to a horizontal resolution of around 7 cm +/- 2.5 cm, depending upon tidal height and sleeper burial depth. For sleepers 12.5 cm wide, this means 2-3 pings centred directly above each sleeper. However, there are additional acoustic recordings for each reflector from non-vertical traces either side of those central 2-3 traces. For these additional non-vertical traces, the acoustic wave path is longer and the depth of the reflector appears slightly greater.

Table 3.9 (cont'd) DoB and K_{DR} processing steps.

step	process	comments
7	Plot depth profiles of unprocessed and demodulated .RAW traces corresponding to those selected in Step 6. For five adjacent and central traces passing through reflectors, record the maximum +ve and -ve adjacent amplitude values at each interface (water:sediment/sediment:reflector/reflector:sediment). Note which is greater of these +ve/-ve maximum amplitudes.	If the greater of these +ve/-ve maximum amplitude pairs is +ve, then there is an increase in acoustic impedance (material density times material compressional wave velocity) across that interface, and vice-versa.
8	Repeat steps 1-7 using high frequency (100 kHz) .RAW Echo file.	Normally low frequency Echo profiles used to map sub-bottom features, however very shallow buried material may be better identified by high frequency data.
9	Calculate magnitude and polarity of Reflection Coefficient (K_{DR}) for each buried reflector interface using corresponding data on depth and amplitude for seabed, reflector and seabed 1st multiple locations.	K_{DR} calculations based on Warner's approach reported in Plets et al. (2008) and v_{DR} as per Dr Jens Wunderlich (*pers. comm.* 2017).
10	Check known lat./long. positions of buried sleepers and compare to the respective traces identified on the unprocessed and demodulated RAW data files. Note any buried sleeper locations not identified in Steps 2-8, and similarly any reflectors identified in Steps 2-8 that do not correspond to known buried sleepers.	Data for confidence analyses.
11	Repeat Steps 5-8 for any sleepers not previously identified.	Identify conditions when sleeper reflectors were not identifiable.

layers or a buried object). This relates to the ratio of the amount of energy reflected to the amount of energy transmitted across the boundary. The material properties (density, ρ and compressional P-wave velocity, V_p) in each of the two adjoining layers are used to derive K_R as per Equation (1). However, the reflection coefficient can also be determined purely on acoustic data collected by SBPs and can used to discriminate buried material types and relative densities.

In Appendix A of Plets et al. (2008) the reflection coefficient for a deeper reflector can be calculated based on acoustic trace properties and known/assumed compressional P-wave velocity values for sediment and the deeper (timber) reflector:

$$K_{DR} = A_{DR} [v_w (TWT_p/2) + v_{DR} (TWT_{DR} – TWT_p)/2] / x \quad (5)$$

where x is a calibration coefficient

$$x = [A_p v_w (TWT_p/2)] / K_p \quad (6)$$

and

$$K_p = [A_m TWT_m] / [A_p TWT_p] \quad (7)$$

K_{DR} – reflection coefficient of deeper reflector

K_p – reflection coefficient of primary (seabed) reflector

v_{DR} – sound velocity in sediment

v_w – sound velocity through water

$A_{DR/p/m}$ – amplitude of deeper reflector/seabed/seabed 1stmultiple

$TWT_{DR/p/m}$ – two-way travel time to deeper reflector/seabed/seabed 1stmultiple

now, knowing that

$TWT_{DR/p/m} = 2d_{DR/p/m}/ v_{DR/p/w}$

d_{DR} – depth from seabed surface to deeper reflector

d_p – depth from water surface to seabed

$v_p = v_w = v_m$

and $TWT_{DR} – TWT_p$ is TWT in seabed = $2d_{DR}/v_{DR}$

then by substituting (7) into (6)

$$x = [A_p^2 \, d_p^2] / [A_m \, d_m] \quad (8)$$

whereby equation (5) simplifies to:

$$K_{DR} = A_{DR} [d_{DR} + d_p] / x \quad (9)$$

and equation (1) becomes

$$K_{DR} = A_{DR} \, A_m \, d_m [d_{DR} + d_P] / (A^2_p \, d^2_p) \quad (10)$$

Amplitudes for the seabed, deeper reflector and seabed 1st multiple, together with their respective depths were tabulated from the Excel plots created for each buried sleeper identified by the steps listed in Table 3.9.

In situ comparative methods

3D digital model reconstruction of the *James Matthews* wrecksite buried materials

The detailed archaeological survey of the excavated *James Matthews'* wrecksite was digitised and a 3D digital model created. The purpose of this model was to verify the accuracy and performance of the non-invasive SBP measurements in quantifying shallow-buried archaeological artefacts at a complex wrecksite environment. A brief description of *James Matthews*, the archaeological surveys conducted by WAM, their methods and artefacts recorded in the 1970s is given in Chapter 3. During the 1975–76 survey, archaeological divers annotated 40 A3 sized recording sheets with location sketches, location ID and horizontal and vertical (A, B and C) measurements across 27 cross-sections, each 6 m x 1 m in dimension. In aggregate, a total of almost 5,000 3D location measurements were recorded underwater. These original recording sheets remain in the WAM Department of Maritime Archaeology archives. The author retrieved and scanned these original sheets at 200 dpi using the Department's HP Designjet T1100 MFP scanner. For safe keeping and future access, these scans were also copied to the Department's computer database as .tif files. Each sheet number, measurement ID and respective A, B and C values were then manually entered into a preformatted Excel spreadsheet. The ability to enlarge the electronic scanned versions of the original sheets by 400+ times became invaluable to help decipher the characteristics of each diver's unique writing style. There were many instances where smudging, feint pencil marking and poor handwriting made it very difficult to read and interpret the numbers on the original sheets. The 2D scale plan drawn by Henderson was also scanned at 200 dpi on the Department's scanner and copied to disc and the Department's computer database as a .tif file.

Quality control checks on the Excel survey data spreadsheet were made to identify and remove any outlier data points generated by errors in digitisation. The spreadsheet was then

imported into Autodesk AutoCAD 2017 (AutoCAD) to create a point cloud of data with which to construct the 3D digital model. The 2D scale plan was also converted into a .dwg file and imported into AutoCAD to be used as a visual background layer, as well as to correctly establish scale. Further quality control checks on the point-cloud data were undertaken to remove any obvious erroneous data. The cross sections of the upper face of ceiling planks were initially drawn at one metre intervals, corresponding to the 6 m x 1 m underwater survey sections, using the QSELECT function in the 3D modelling component of AutoCAD. These cross-sectional locations had the highest density of survey measurements due to the method of survey. Each cross-section was carefully examined against the background plan layer, and the original survey sheets, to identify measurement points associated with the ceiling planks. Any items positioned on top of the ceiling planks were removed and a spline function used to connect the remaining data points to create the initial hull cross-sections. Each cross-section was further examined. Where significant gaps occurred between points along the spine, the cross-sectional shape was improved by interpolating identified nearby ceiling plank survey points into the spline. Once all cross-sections were established, the upper surface of the ceiling planks was created using the AutoCAD LOFT command to smoothly interpolate between all cross-sections. The lower ceiling plank surface was created using the AutoCAD EXTRUDE command based on the average measured thickness of ceiling planks of 6 cm (range 3.5 to 9 cm) from the 2000 Conservation survey. The ceiling planks were then converted into a solid body using the AutoCAD 3D SOLID command. The keel, keelson, the remaining slate mound, pine timber planks, iron ballast and other features located on top of the ceiling planks were subsequently added through similar processes. Each major component type was created on an individual layer within AutoCAD so that they could be viewed in isolation, or by turning on/off various layers, viewed in combination with all other layers.

Clearances, contact and overlap between components on different layers were checked by fully rotating the model in 3D, by turning layers on and off, and by comparing against the background plan and available underwater photographs. Any errors were adjusted to ensure all individual components fitted together without interference. The ship's ribs were drafted in the same manner where they extended beyond the ceiling planking and were exposed and surveyed. The majority of the ribs, however, were only exposed at the deck line and at the keelson with most of their length lying beneath the ceiling planks. In these circumstances, their ends were established from respective survey points and their upper surface shape determined by the shape of the underside of the ceiling planks at that cross-sectional location. These cross-sections were then lofted to the correct width, extruded to the measured thicknesses, and turned into solid 3D shapes. The outer planking was modelled in the same

manner, using survey points on exposed planking where available, then using the underside of the modelled ribs to set their cross-sectional shape. LOFT, EXTRUSION and 3D SOLID commands were used to create a contiguous outer shape to the hull. Figure 3.32 shows the progressive development of the digital model with a plan view, and upper and lower slant views of the stern features.

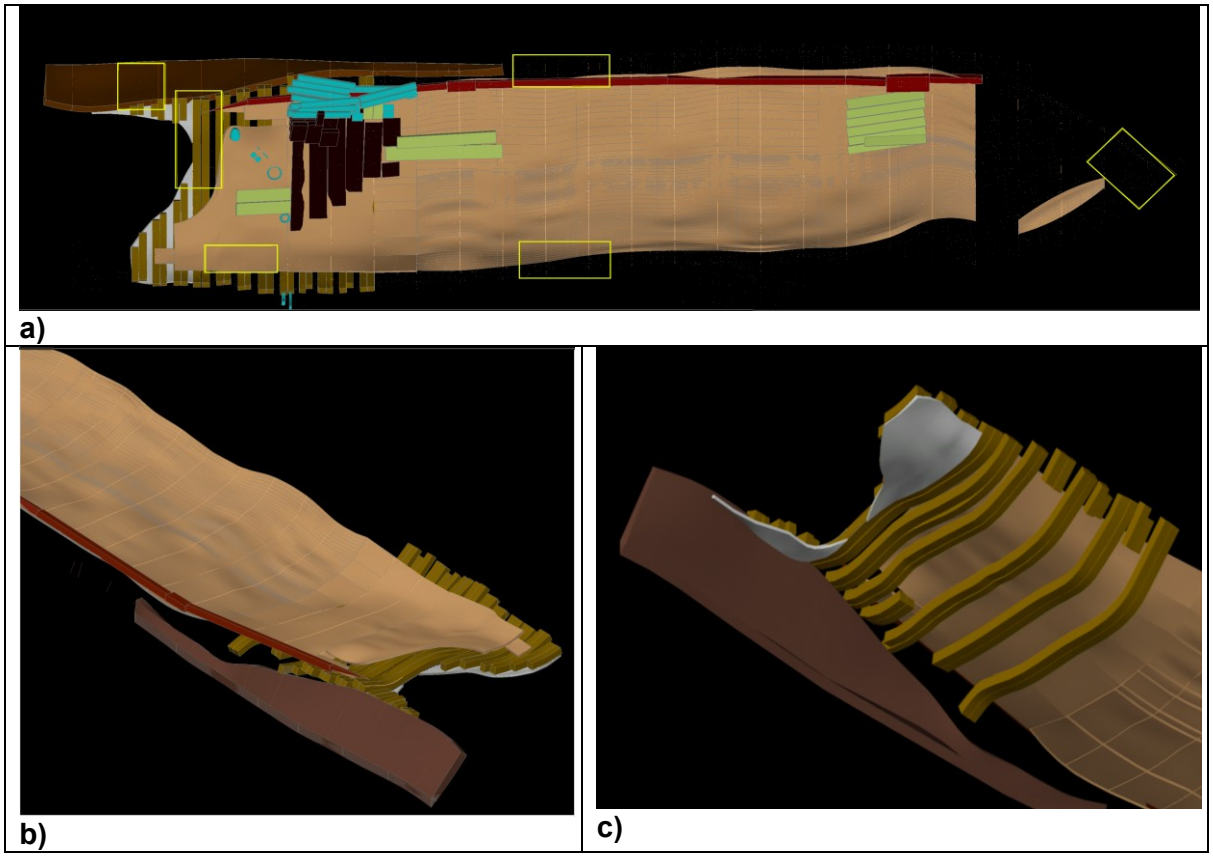

Figure 3.32 Partially complete digital model of the remaining buried features of *James Matthews*: (a) plan view with cargo, total length of buried remains is 26 m and 2000 test trench locations shown as bright yellow boxes; (b, c) expanded upper and lower oblique stern views of vessel structure. Solid and extruded features include keelson and keel (reddish and dark browns), ceiling planks (tan), ribs (mid-brown), outer planking (light grey), iron ballast and curved deck knees (blue), remaining slate mound (black) and pine timber cargo (dull yellow).

SBP wrecksite measurements

SBP measurements over the *James Matthews* wrecksite were recorded on 7th and 8th of June 2017 using the same vessel-mounted instrumentation on *Dirk Hartog* as described in section 3.2.5. A total of 89 long SBP transects (77 east-west and 12 north-south) were run with an average one metre spacing across the site (Figure 3.33). During the runs the coxswain controlled the speed of *Dirk Hartog* to two m/s, and used pre-placed buoys on the bow and stern ends of the wrecksite as visual guides. The transects were extended to a minimum 50

m outside of the crash-barrier cofferdam in order to detect any other potentially buried material isolated from the immediate excavated wrecksite.

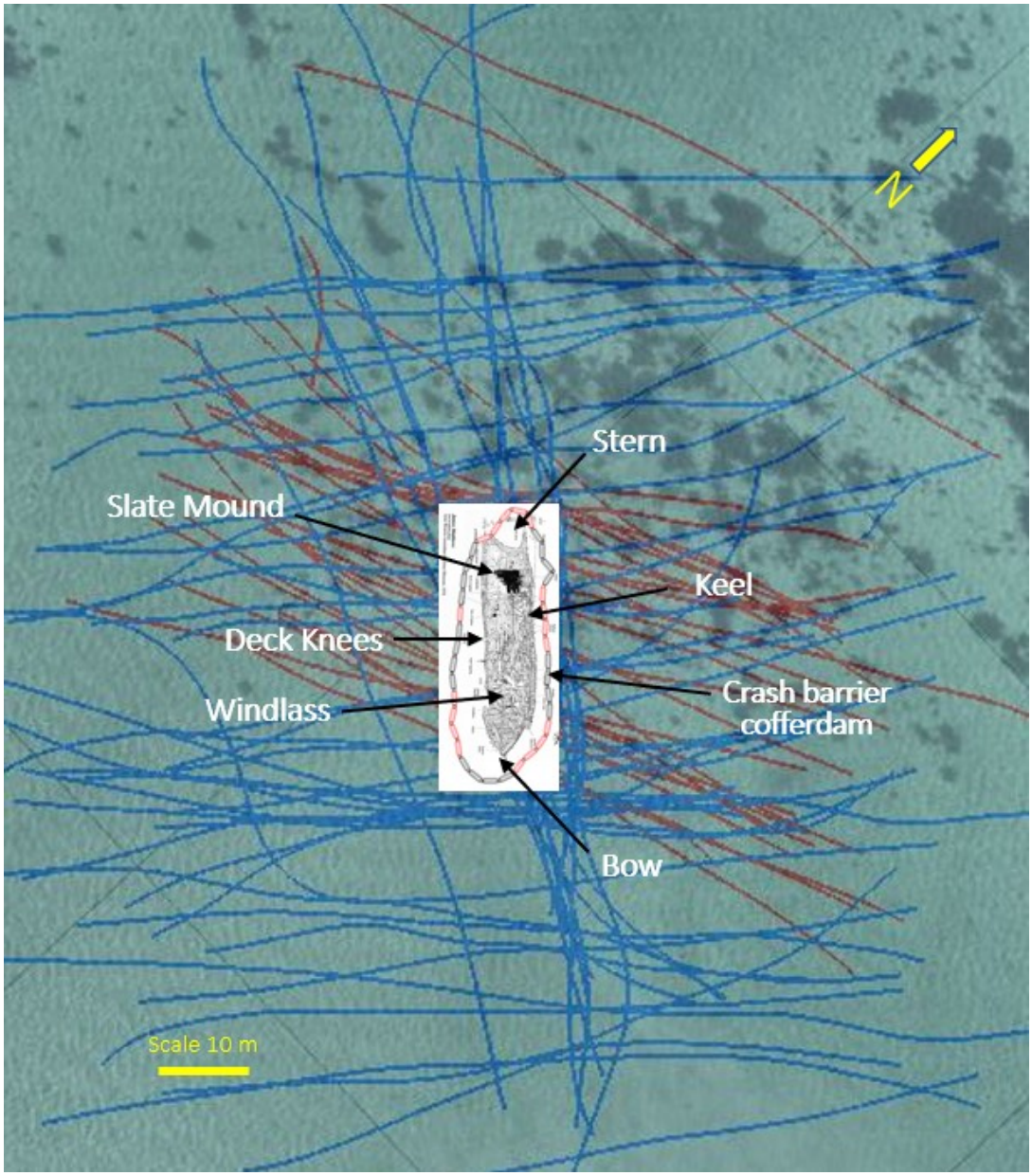

Figure 3.33 Vessel and SBP track lines collected over the *James Matthews* shipwreck site on June 7th (red) and 8th (blue) of June 2017.

Quantitative comparison between actual and mapped remains

The horizontal and vertical co-ordinates for the 1977 *James Matthews* archaeological survey correlate to the survey frame constructed over the site. Converting these local survey grid coordinates to the WGS84 geographic coordinate system would then permit direct comparison with the SBP positional data. At the completion of the 1977 survey the grid frame was totally removed. To rectify all 1977 survey coordinates into the WGS84 coordinate system requires

the accurate measurement of the latitude, longitude and height of a minimum of two (preferably three orthogonal) features on the seabed. These features need to be recognised and accurately located on the original 1977 plan drawing, and be distinguishable on the seabed today. Due to ensuing degradation and recovery of artefacts post-1977 survey, only two such features could be identified. On the 18th of May 2018 the x, y and z position of two survey reference point features (Figure 3.34) were recorded using the Leica GS16 High Precision GNSS RTK Rover mounted on an extended pole. One diver on the seabed held the tip of the pole on each of the two features, and a second diver held the pole vertically in the water column for 30 seconds using a leveling bubble as a guide. The 30 second RTK GPS data burst was relayed via Bluetooth back to the CS20 logger held on the deck of the support vessel *SeaSpray.* The Leica Captivate V3.20 software determined a mean (centroid) seabed position for both features based on all points recorded during the 30 second period (Appendix A, Table A.7).

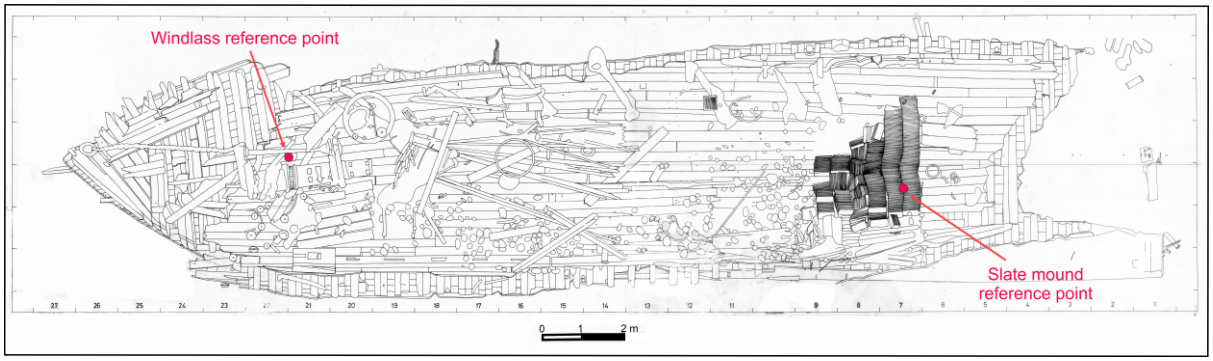

Figure 3.34 *James Matthews* survey reference points.

The AutoCAD model of the buried remains of *James Matthews* was converted to the WGS84 coordinate system using the AutoCAD GEOGRAPHICLOCATION command. The model was geo-referenced by inserting the latitude and longitude co-ordinates when the geographic marker was set to both the windlass and slate mound reference points. Cross-sections of the model, corresponding to the locations of the SBP profiles, were generated using the SECTION command. The upper and lower profile of these cross-sections and features along the cross-sections were directly compared to the respective SBP profiles. All SBP .RAW data files collected over the *James Matthews* wrecksite were also processed and gridded to provide a quasi-3D comparison between the AutoCAD model and the SBP data. For this comparison the .RAW SBP files were interpolated and the lines truncated five metres outside the boundary of the 'crash barrier'. The seabed depth was defined in each file and they were then converted into a binary format (.BIN) using a pre-defined script available in ISE2. The .BIN files were

then imported into Innomar's SESGridder software to create a volumetric cube where acoustic wave trace amplitude values were interpolated across user-specified 3D grid spacings. Extraction of interpolated horizontal slices from the volumetric cube provided a series of progressively deeper plan views of the wrecksite.

Chapter summary

A two-step scientifically-based methodology is described in this chapter. This approach was selected to provide objective evidence supporting the use of non-invasive SBP technology to meet the particular requirements for in situ management and archaeological research purposes. The overarching framework for this research is based on site-formation processes as a middle-range processual (scientific) theory. The first '*validation'* step involves trialing SBP performance in situ, under tightly controlled burial condition parameters (e.g. precisely known depth of burial, buried material type/characteristics, sediment characteristics). With experimental variables either controlled or quantified in situ, the results from this step will confirm whether or not the Innomar SES 2000 parametric SBP technology meets performance targets for in situ management and archaeological research applications. In the second '*verification*' step, the operation of the SBP under actual complex wrecksite conditions is quantitatively assessed and the SBP's capabilities are fit for purpose.

The methods used to undertake the validation and verification steps are extensively detailed in this chapter. These included: the preparation and purpose-burial of modern timber and ferrous artefacts at two sites (adjacent to the *James Matthews* wrecksite and in the Swan River at Coffee Point) under tightly controlled conditions for the validation step; and for verification, 3D computer modeling of archaeologically surveyed, reburied artefacts from the wreck of *James Matthews*. Additionally, the processes for the field collection and subsequent analyses of the primary SBP acoustic data, from those purpose-buried artefacts and from the *James Matthews* shipwreck site, are described. Methods are also outlined on how data is collected and analysed in situ and through laboratory and 3D computer analyses, to quantify site-related experimental variables. The latter encompass: basic and bulk density of timbers pre-burial and post-recovery after submergence; DO, Eh and pH core profiles, PSD, bulk density, porosity and in situ density of sediments; and seawater salinity and temperature.

The individual results from the SBP data analyses and quantification of site-related experimental variables are described, plotted and tabulated in the following chapter. The interpretation of this data is presented in Chapter 5.

4. RESULTS

This chapter presents the results of all field, laboratory and historic data collected and analysed as per the methodologies described in Chapter 3. The results are presented in the following sections for the respective in situ experimental (validation) and in situ comparative (verification) components. The interpretation of these combined data sets, together with information from reviewed literature sources, are presented in the following chapter to address the SBP performance attributes as dictated by the research question.

The in situ experimental component involved the initial burial of timber (European oak, Radiata pine and Jarrah, an Australian hardwood) and ferrous 'sleepers' at varying shallow depths of cover (from 10 cm to 50 cm) at two locations—adjacent to the *James Matthews* shipwreck site, offshore on the northern side of Woodmans Point, and in the Swan River at Coffee Point, WA. In June 2017 a parametric acoustic sub-bottom profiler (the Innomar SES-2000 *compact* SBP) was deployed on multiple runs to measure the position, depth and a number of other acoustic parameters associated with the buried sleepers at the James Matthews sleeper site. The SBP survey was repeated in May 2018 following the burial of additional sleepers at this offshore site, as well as at the newly established Swan River sleeper site. Seawater salinity, timber densities and in situ sediment characteristics are factors which affect both the speed of sound in the water column and in the sediment, and the strength of the acoustic reflection off the buried reflectors. Sediment cores were consequently collected from both sites for subsequent laboratory analyses of their physical and geo-chemical characteristics. Timber samples representative of the buried timber sleepers were also recovered for subsequent measurement of their density. The analyses of these independent variables are required to interpret the accuracy and validity of the acoustic (SBP) results.

A number of closely spaced SBP runs were also made over the *James Matthews* wrecksite where in 1977 the Western Australian Museum excavated, archaeologically surveyed and then backfilled the shipwreck remains. The in situ comparative element of this research involved qualitative interpretation and visualisation of the SBP results in a complex shallow buried shipwreck site, then quantitative comparison against a 3D computer model of the buried remains derived from the 1977 archaeological survey.

In situ experimental (validation) component

The purpose of this section is to present the results of analyses on which the reliability of locating shallow-buried modern archaeological replicas (the sleepers) by parametric SBP surveys can be assessed, as well as the accuracy of the estimates of their depths of sediment

cover. Given the experimental nature of this work, the term depth of burial (DoB) is used to describe the depth of sediment cover over the buried sleepers. In addition, the variability associated with other SBP trace properties (the seabed depth; the depth of the seabed 1st multiple; and the trace amplitudes of the seabed, seabed 1st multiple and buried reflectors) is presented. These parameters, in conjunction with the DoB estimates, are used to calculate the reflection coefficients (RCs) for the sleepers. The derived reflection coefficients are used to identify the relative reflection strengths from each buried reflector, and this reflection strength may differentiate material types buried at the sleeper sites.

The accuracy of the DoB, seabed and depth of the seabed 1st multiple estimates are dependent upon the recorded travel time for acoustic waves to be reflected from those interfaces. This travel time depends on the speed of sound in the water column and in the sediments, which in turn depends on water and sediment properties. Validation of the acoustically derived reflection coefficients is also dependent upon the acoustic impedance (acoustic velocity and density) of the sediment and of the buried sleepers. Accordingly, results are also presented in this section from measurements of: seawater salinity (which affects speed of sound in the water column); sediment characteristics including particle size distribution (PSD) and bulk and in situ density (which affect the acoustic impedance and speed of sound in the sediments); and timber density (which affect the acoustic impedance and speed of sound in the timber sleepers). Changes in submerged buried timber density stem from the waterlogging process and biological degradation, with the latter being dependent on the buried timber's exposure to aerobic or anaerobic conditions. The results of dissolved oxygen (DO) and redox potential (Eh) measurements along the length of the sediment cores will also be presented to identify the degradation environment during burial for each of the sleepers.

As the methodology used in this research requires control (quantification) of the key variables during the SBP performance testing, the results for the water quality, timber and sediment analyses will be presented before the SBP acoustic results.

Water quality data

In June 2017 the average salinity and seawater temperature values measured at the 2 m depth using a TPS Pty Ltd 90-FLMV water quality logger at the James Matthews sleeper site were $35^0/_{00}$ (parts per thousand) and 19^0C, respectively. In 2018 the seabed level salinity was $38.8^0/_{00}$ and the depth averaged seawater temperature, recorded using an Oceanic GEO 2 divers' watch, was 17.6 ^{0}C (Table 4.1).

Table 4.1 Seawater temperature measurement, James Matthews sleeper site, May 2018.

start time	end time	max water depth (m)	average water temperature (^{0}C)
11.00	11.09	2.7	18
12.02	12.59	2.6	17
13.27	13.41	2.8	18

The results of water quality monitoring at the Swan River site using the TPS Pty Ltd 90-FLMV water quality logger is shown in Table 4.2. Water temperature and salinity values averaged over depth and across the site were 19.6°C and 3.93%, or 39.3$^0/_{00}$, respectively. The dissolved oxygen (DO) levels in the water column indicate oxygenated conditions, in line with seasonal surface and bottom level mean values (Department of Water and Environmental Regulation 2018:66). The water depth at the central location along the sleepers immediately following SBP measurements was 0.9 m.

Table 4.2 Water quality measurements at Swan River sleeper site, May 2018.

	time (prior to SBP profiling) 11.51 am					
	central location along sleepers			eastern end of sleepers		
	near bed	mid-depth	near surface	near bed	mid-depth	near surface
salinity (%)	3.90	3.90	3.91	3.94	3.94	3.93
temperature (^{0}C)	19.4	19.4	19.5	19.3	19.3	19.3
DO (mg/L)	NA*	NA	NA	NA	NA	NA

	time (following SBP profiling) 1.10 pm					
	central location along sleepers			eastern end of sleepers		
	near bed	mid-depth	near surface	near bed	mid-depth	near surface
salinity (%)	3.91	3.94	3.94	3.94	3.94	3.94
temperature (^{0}C)	19.8	19.8	20	19.7	19.7	19.9
DO (mg/L)	5.95	5.79	6.06	5.7	5.85	6.01

***** No DO values recorded

In situ sediment analyses

Sediment core samples were collected from reference and back-filled locations at both the James Matthews and Swan River sleeper sites, and brought back to soils and conservation labs to describe their facies, particle size distribution (PSD) and other sediment characteristics. Methods for the collection and analyses of these cores are described in Chapter 3, with the results of those analyses described as follows.

Sediment facies and particle size distribution results

Chemical and microscopic analyses of sediment sub-samples confirmed that the sediments at the James Matthews sleeper site were composed of plate-like, angular but smoothed carbonate grains and coarse particles, with only a few nearshore benthic forams. The smoothed nature of the broken shell material indicated that the sediments have come from, or are still exposed to, a high wave energy climate. By contrast the Swan River sediments are composed of rounded siliceous grains.

PSD analyses were undertaken on two duplicate sets of full 50 cm long reference cores and two sets duplicate sets of full 50 cm long backfilled cores for both sites (see Tables 3.6 and 3.7 for details). Additionally, one of the sets of duplicate reference cores and one of the sets of duplicate backfilled cores from each site were split into 5 x 10 cm sub-cores for individual PSD analyses. Down-core descriptions of all sediment cores are presented in Appendix B, Tables B.1 to B.16, together with particle size distribution plots and photographs of the coarser shell/fragments > 1 mm in size.

The top 50 cm sediments at the James Matthews sleeper site can be characterised as medium-fine grained calcareous sands, with 3–6% coarse to fine gravel sized shell/fragments. This can be seen in the PSD curves for the two sets of duplicate reference cores (cores 20, 122, 217 and 218) in Figure 4.1 which also show negligible variability between duplicates and reference locations. Figure 4.2 reveals the depth related variation in sediment grain size at this offshore site through the plots of PSD for the five sub-core samples of Core 20. This figure shows a finer distribution (fine-medium sands) in the top 20 cm compared with the slightly coarser (medium-fine) in the lower three sub-layers. The down-core descriptions and photographs of the coarser fractions in each sub-core sample for Core 20 are presented in Table 4.3. Following hydraulic dredge excavation and backfilling of the sediments to bury sleepers at the James Matthews sleeper site, the grain size distributions of backfilled sites are slightly coarser than the non-disturbed reference sites (Figure 4.3). The prime change in size fractions comes in the top 20 cm where finer material has been winnowed out during the burial process as shown in Figure 4.4 compared with Figure 4.2.

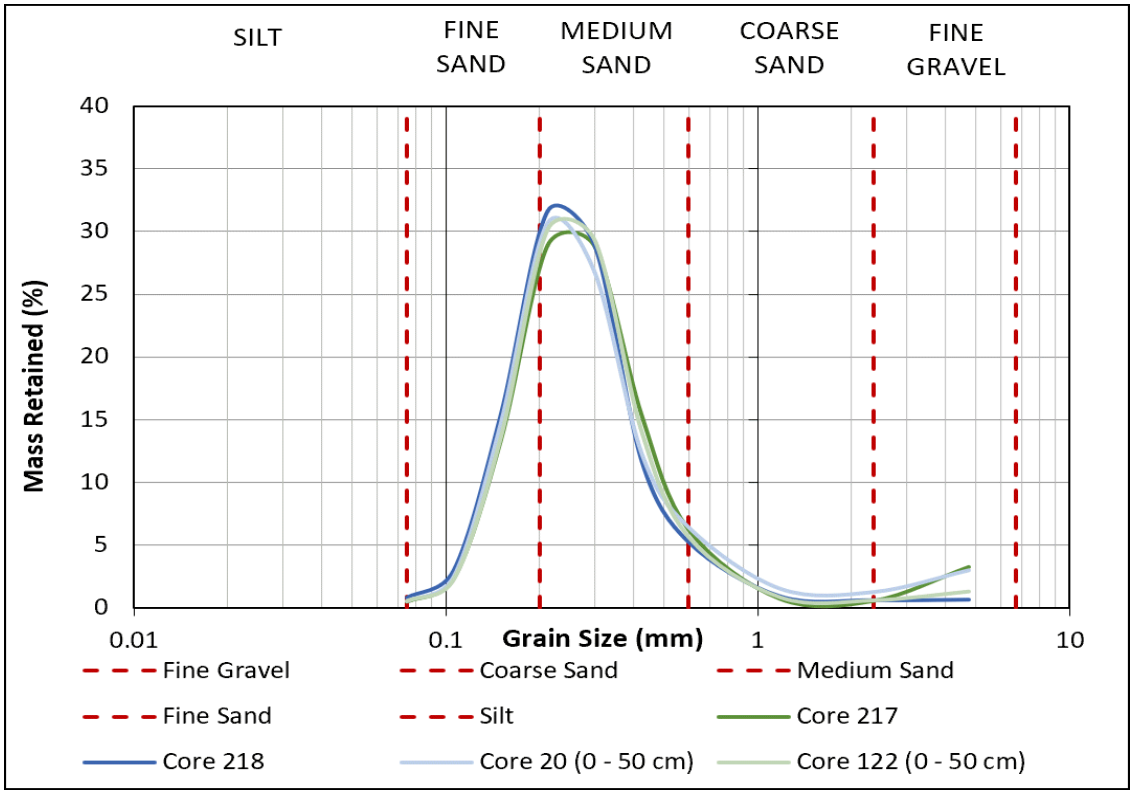

Figure 4.1 Replicate reference cores, James Matthews sleeper site.

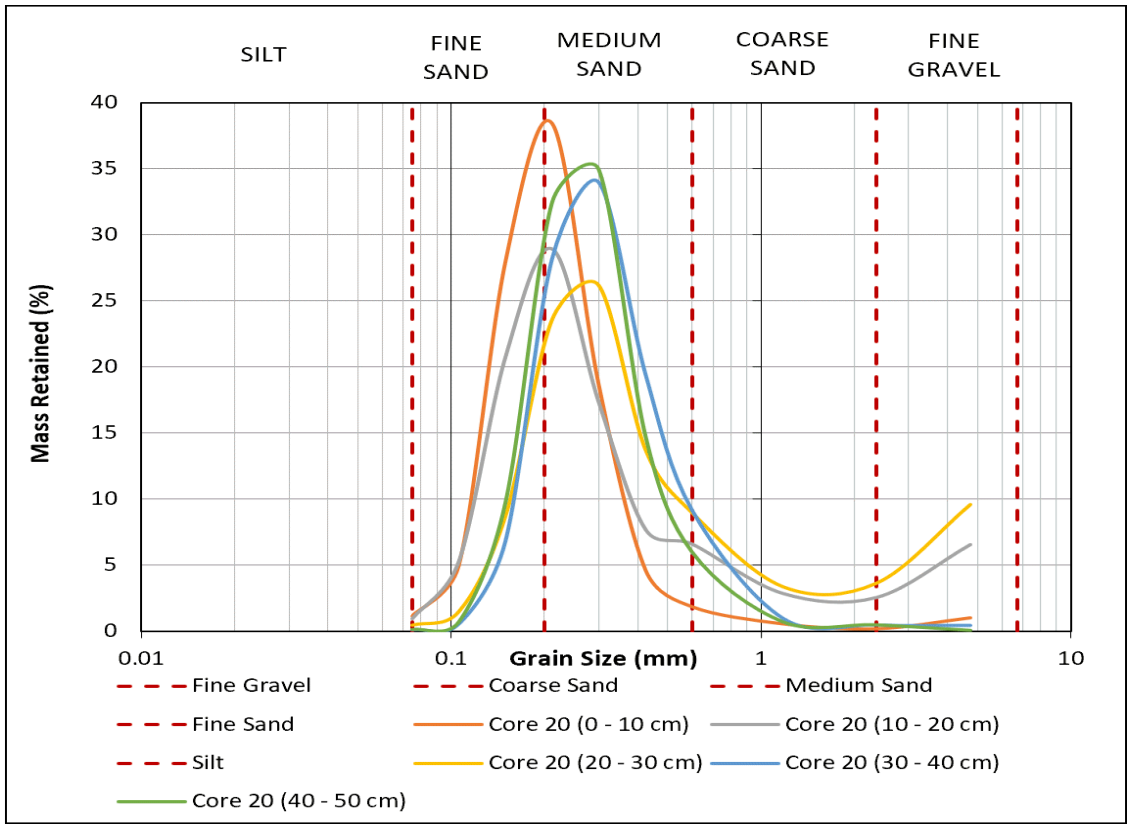

Figure 4.2 Depth related variability, reference core 20, James Matthews sleeper site.

Table 4.3 Down-core sediment description, core 20, James Matthews sleeper site.

depth (cm)	description		shell/frags >1mm at sub-core depth levels
0	yellow	medium-fine grained calcareous sand, 1.7% shell/frags >1 mm	
1			
2	grading grey with depth		
3			
4			
5			
6			
7			
8			
9			
10		medium-fine grained calcareous sand, 11.9% shell/frags > 1mm	
11			
12			
13			
14			
15			
16			
18			
20	lighter yellow grains	medium grained calcareous sand, 16.5% shell/frags >1 mm	
22			
24			
28			
30		medium grained calcareous sand, 1.8% shell/frags >1 mm	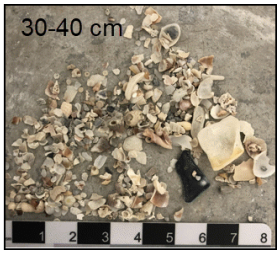
32			
34	yellowish grey		
36			
40			
42		medium grained calcareous sand, 0.7% shell/frags >1 mm	
43			
44			
45			
46			
47			

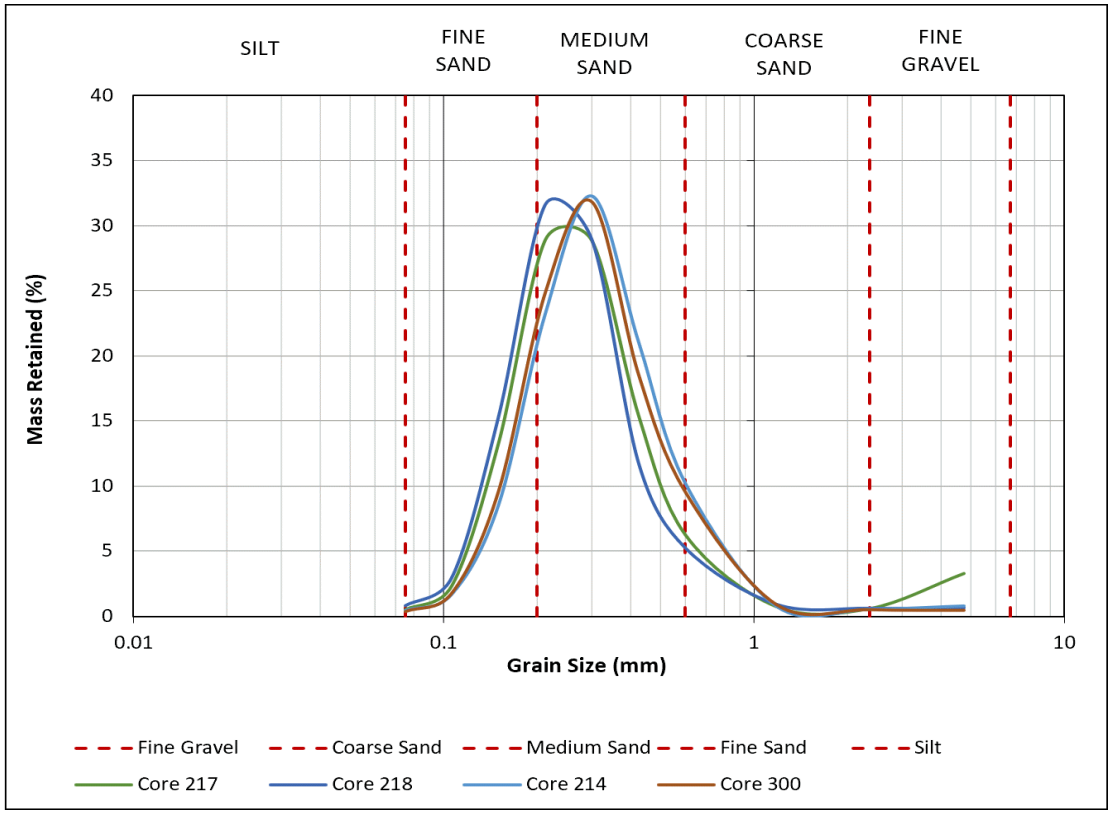

Figure 4.3 Backfilled (214/300) vs reference (217/218) cores, James Matthews sleeper site.

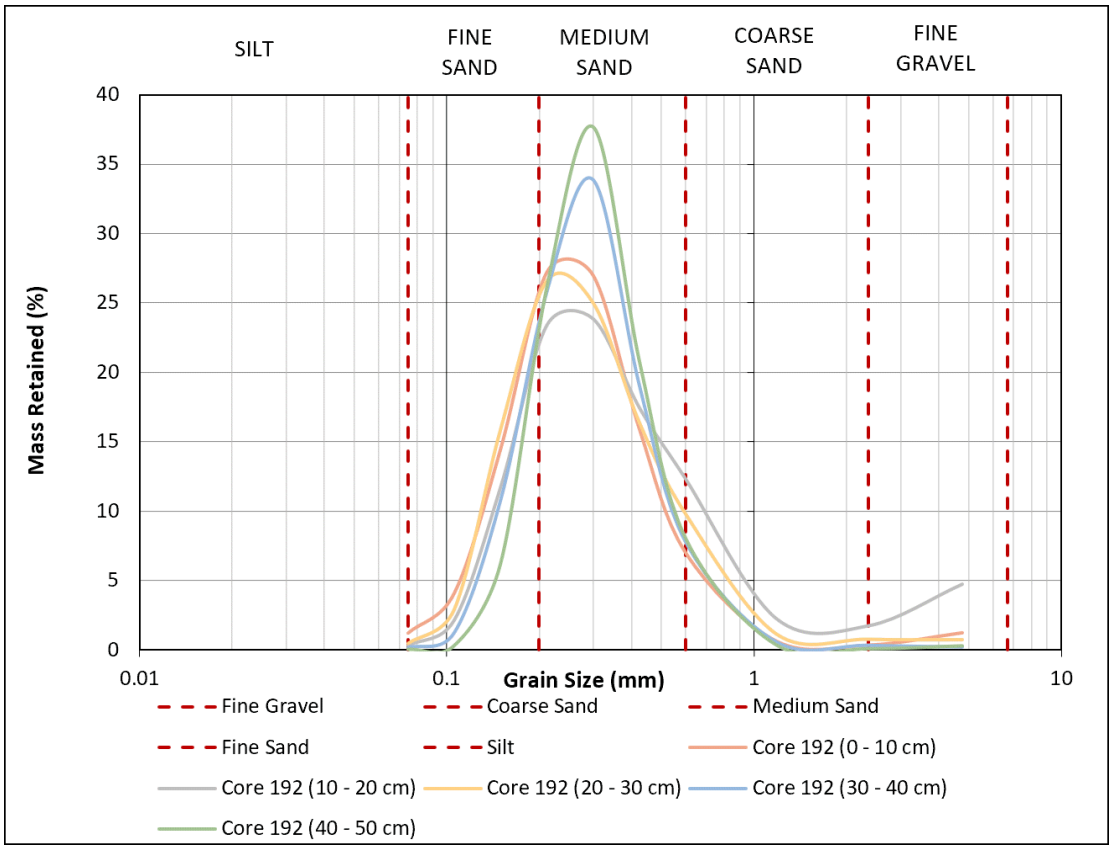

Figure 4.4 Depth variability, backfilled core 192, James Matthews sleeper site.

The same grain size distribution comparisons for the sediments at the Swan River sleeper site are shown in Figures 4.5 to 4.8. The down-core descriptions and photographs of the coarser fractions in each sub-core sample for Core 12 are presented in Table 4.4. The surficial Swan River sediments can be characterised as medium grain sized siliceous sands with 11% fine sands and 1–3% coarse to fine gravel sized shell/fragments. As shown in Figure 4.6, there is minimal depth variability with the exception of a higher proportion of fine gravel sized shell/fragments in the top 20 cm. There is also little variability between reference and backfilled cores (Figure 4.7) and little depth variability at backfilled locations (Figure 4.8). At this site, excavation and backfill of holes to bury the sleepers was undertaken at very shallow water levels using shovels, with little measurable loss of fines.

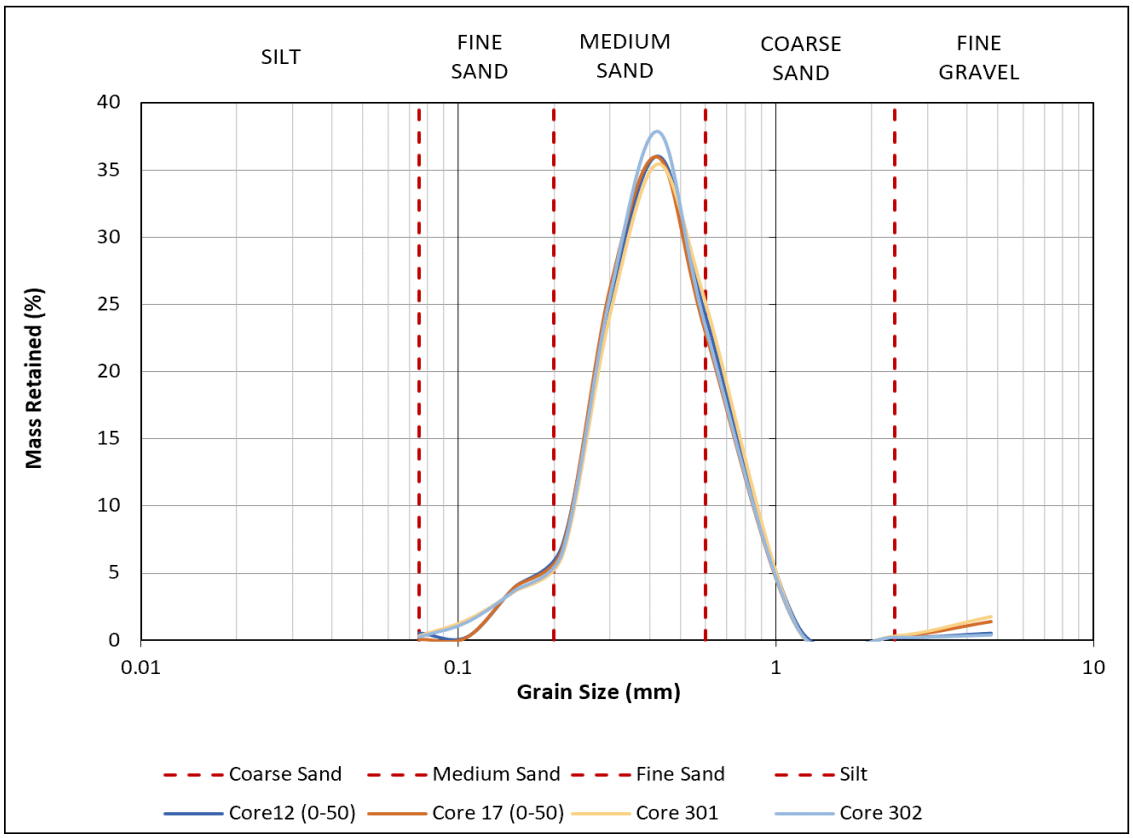

Figure 4.5 Replicate reference cores, Swan River sleeper site.

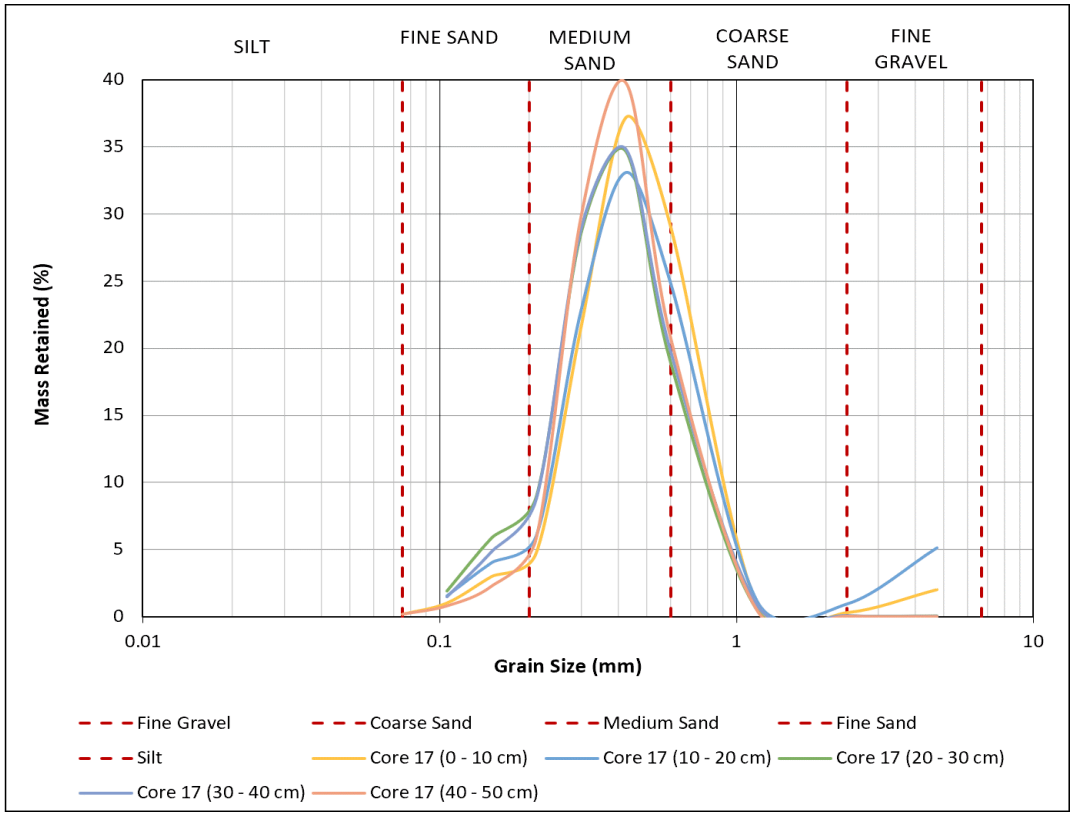

Figure 4.6 Depth related variability, reference core 17, Swan River sleeper site.

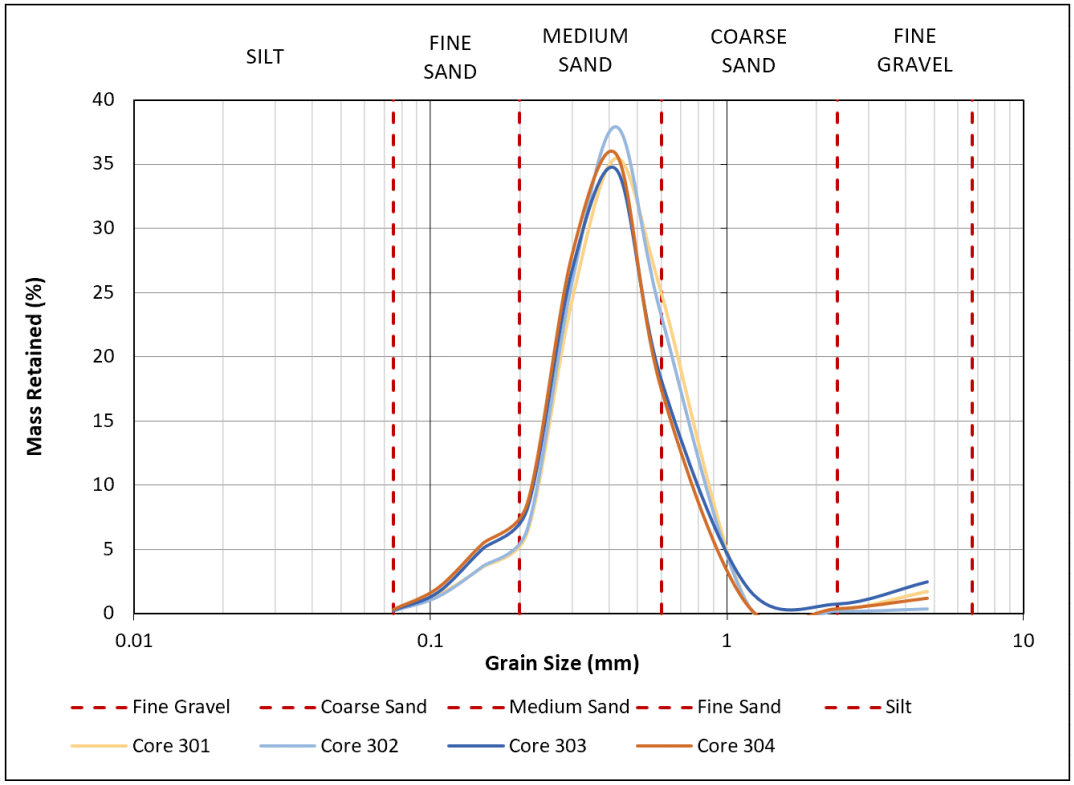

Figure 4.7 Backfilled (303/304) vs reference (301/302) cores, Swan River sleeper site.

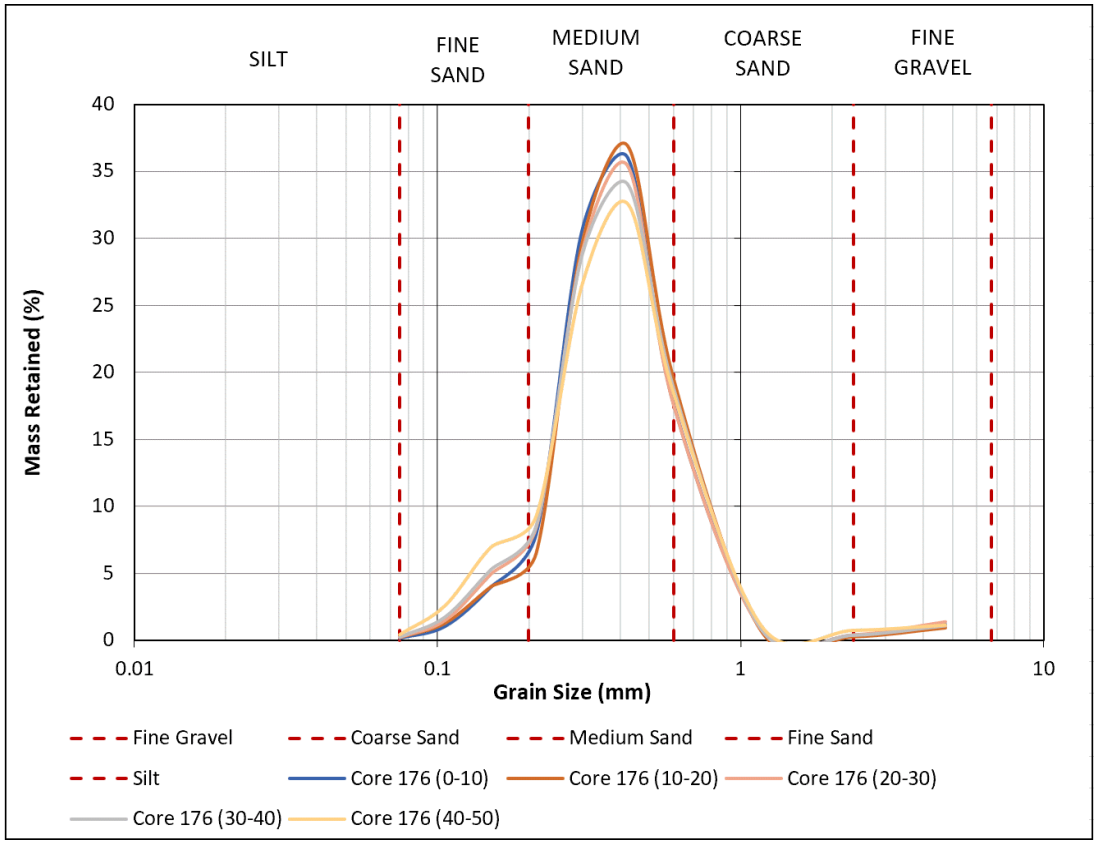

Figure 4.8 Depth variability, backfilled Core 176, Swan River sleeper site.

The relative grain size distribution differences within site, in terms of duplicate reference and backfilled locations, are small when compared to differences across the sites. Figure 4.9 shows duplicate reference cores (217, 218) at the James Matthews sleeper site vs. duplicate reference cores (301, 302) at the Swan River site. Overall, the James Matthews sleeper site sediments are characterised as medium-fine grained calcareous sands. There is, however, a proportionally higher (albeit still a small) percent of fine gravel sized shell/fragments in the offshore sediments, and a much higher fine sand component. The Swan River sleeper site sediments are characterised as medium grained siliceous sands with a higher proportion of coarse sand.

Table 4.4 Down-core sediment description, core 12, Swan River sleeper site.

depth (cm)	description		shell/frags>1 mm at sub-core depth levels
0	yellow, coarser in appearance	Medium to coarse grained siliceous sand, 2.3% shell/frags > 1mm	
1			
2			
3			
4			
5	black, yellow on opposite (lower) side		
6			
7			
8			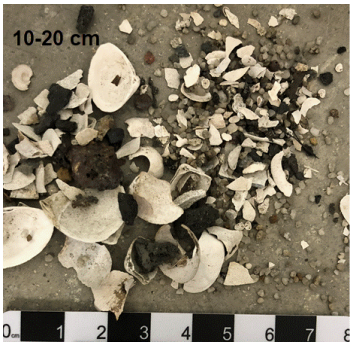
9			
10		Medium to coarse grained siliceous sand, 3.1% shell/frags > 1mm	
11			
12			
13			
14			
15			
16			
17	yellowish grey, coarser in appearance		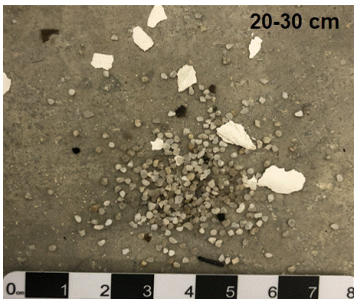
18			
19			
20		Medium grained siliceous sand, 0.6% shell/frags > 1mm	
21			
22			
26	yellow, finer appearance		
32			
34		Medium grained siliceous sand, 1.2% shell/frags > 1mm	
38			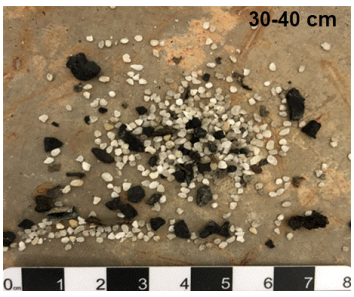
42			
44		Medium grained siliceous sand, 0.7% shell/frags > 1mm	
46			
48			
50			
51			
52			
53			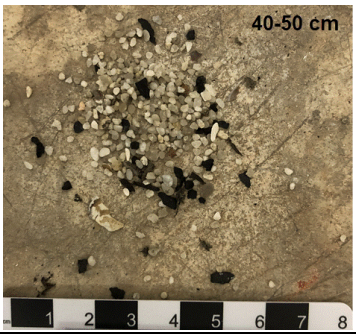

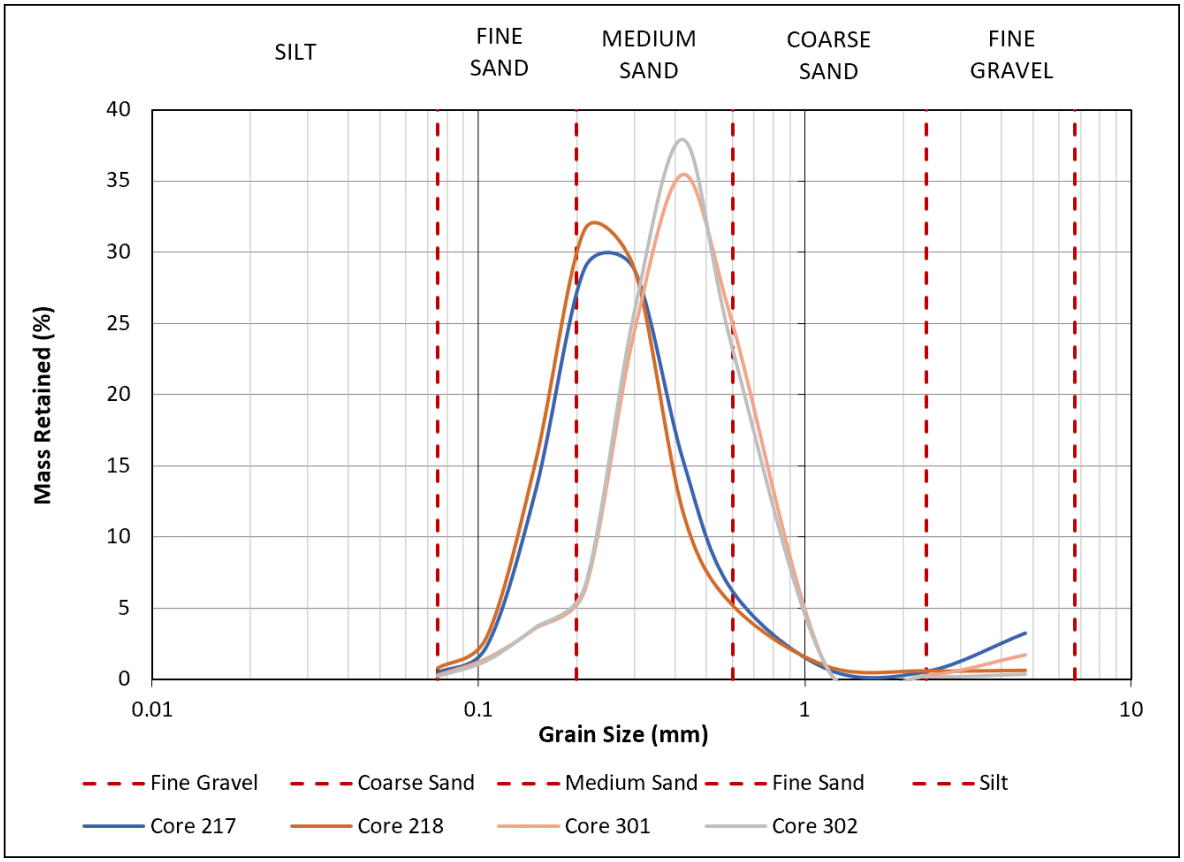

Figure 4.9 Site variability, reference cores (217/218) James Matthews vs reference cores (301/302) Swan River sleeper sites.

Sediment bulk density results

The sediment bulk density and sediment porosity are key parameters used to characterise the mass or volume of sediment particles and their pore-water in fully saturated conditions. Richardson and Jackson (2017:499) describe sediment bulk density as 'the most fundamental sediment property directly affecting acoustic propagation within sediments' and that 'sound speed and bulk density are highly correlated.' To estimate the speed of sound in the sediments during the SBP surveys from literature data, the sediment bulk density of each saturated sediment core was calculated by dividing the mass of the saturated sediment by its volume following the method outlined in Chapter 3. Measurement results for all cores are tabulated in Appendix B Tables B.17 and B.18 and summarised in Table 4.5. The corresponding values for salt corrected porosity, using Hamilton's (1969:28) method A are also included on these tables. The results for manipulated cores 218 and 214 which were repacked in the loosest condition (the 'light' ($_l$) test) and in the densest condition (the 'tight' ($_t$) test) are also shown in these tables.

Table 4.5 Bulk density and porosity of reference and backfilled sediments from the James Matthews and Swan River sleeper sites.

sleeper site	core type	core ID	date core collected for density analyses	sediment bulk density (kg/m^3)	sediment porosity (%)
James Matthews	reference	217	7/11/18	2123.7	46.8
		218	9/05/18	2091.1	50.7
		218_{l1}	9/05/18	1961.7	54.0
		218_{l2}	9/05/18	1958.0	52.5
		218_{t1}	9/05/18	2067.7	44.6
		218_{t2}	9/05/18	2074.3	45.9
	backfilled	214	7/11/18	2100.1	43.7
		215	7/11/18	2084.0	45.6
		216	18/5/18	2084.9	45.1
Swan River	reference	301	11/10/18	2110.7	44.9
		302	11/10/18	2189.3	52.1
	backfilled	303	29/05/18	2066.4	33.8
		304	29/05/18	2031.9	38.7
		304_l	29/05/18	1977.7	41.7
		304_t	29/05/18	2079.3	36.1

Sediment DO and Eh profiles

The results of the DO and Eh profiles measured in sediment cores collected at both the James Matthews and Swan River sleeper sites were used to characterise the environmental conditions within those sediments. These conditions, over time, affect the degradation state and density of shallow buried timber. The profiles will also be used to interpret any measured changes in density in the timber sleepers and blocks buried at these sites (see following section), which in turn may affect the SBP acoustic data. It is not the intent of this research to characterise the nutrients nor microbial levels within the sediments, nor the biogeochemical degradation processes occurring within the timbers. Methods used to produce calibrated DO and Eh sediment profiles are described in Chapter 3. pH profiles were not obtained due to sensor failure.

DO and Eh measurements were made along the length of the 50 cm long duplicate cores collected at duplicate reference and duplicate backfilled locations at each site (refer Tables 3.6 and 3.7 for details). While duplicate cores were collected within a distance of 10–20 cm of each other at each location, there well may be differences in DO and Eh readings between duplicates. These differences can result from very localised (micro-environment) factors

associated with burial of isolated pieces of organic matter (e.g. seagrass blades) and/or burrowing macro-fauna (Vicki Richards pers. comm. 2019). Raw DO values, in picoamps (pA) were calibrated using a two-point calibration method according to the manufacturer's specifications. Zero and 100% saturation values were recorded prior to, mid-way through and post-completion of the profile measurements for each core. These end-point calibration results were linearly applied to the raw measurements—the top third of the raw profile measurements were adjusted by the pre-profile calibration values, the middle third by the mid-way calibration values and the lower third of the raw profile measurements by the post-completion values. Variability of +/- 3 pA in the raw measurements was observed in the 'zero' DO saturation values. Eh raw values were calibrated by adding the calibration voltage, in millivolts (mV) of the redox microelectrode in pH 4 buffer, to the profile measurements. Calibrated DO and Eh profiles for all cores tested are presented in Appendix B, Figures B.17 to B.36.

In the undisturbed sediments at the Swan River site, duplicate cores 12 and 17 show similar DO and Eh profiles (Figure 4.10a, b). DO fluctuates from zero to 70-80% in the upper 17–22 cm of the sediment, below which the values then drop off rapidly to near zero. Eh profiles smoothly vary from around 400–500 mV in the upper 20 cm to around 350–400 mV at 50 cm. In contrast, the DO in cores 163 and 183 (Appendix B, Figures B.32 and B.36) collected at the second reference location were much lower in the upper sediment layer but displayed a slight increase at the bottom of the core. Eh values were more variable and slowly decreased with depth to 300–350 mV. The fluctuating DO profiles in the surficial sediments may be as a result of: near-surface bio-turbation by burrowing macro-fauna; very localised burial of organic matter, which together with the initial aerobic conditions, may have led to aerobic bacterial consumption of the organic matter and ultimate (near) depletion of the DO in the sediments; and the small increase in DO at the base of core 183 may be the un-intended outcome of oxygen diffusion as the core was extruded from the riverbed, prior to insertion of the core end-cap. At backfilled locations (for example cores 10 and 162) at the Swan River site, DO profiles exhibited similar characteristics—variable DO values generally up to 60–70% saturation in the top 5–13 cm, and near zero below that (Figure 4.11a). Visual inspection of the cores indicated excavation/ backfilling effects in the top 32 cm depth for cores 10 and 162. The Eh profiles (Figure 4.11b) reflect this disturbance with a major change in Eh value in core 162 around the 30–35 cm depth. Above this line, Eh values are a little more variable, and slightly, lower than reference site cores. The Eh profiles for alternate backfilled cores 169 and 176 (Appendix B, Figures B.33 and B.34) show considerable variability (visual inspection of these indicated backfilling for full 50 cm depth) but with a general decrease, down-core. This variability may align with the sediment 'clods' shovelled to backfill the hole.

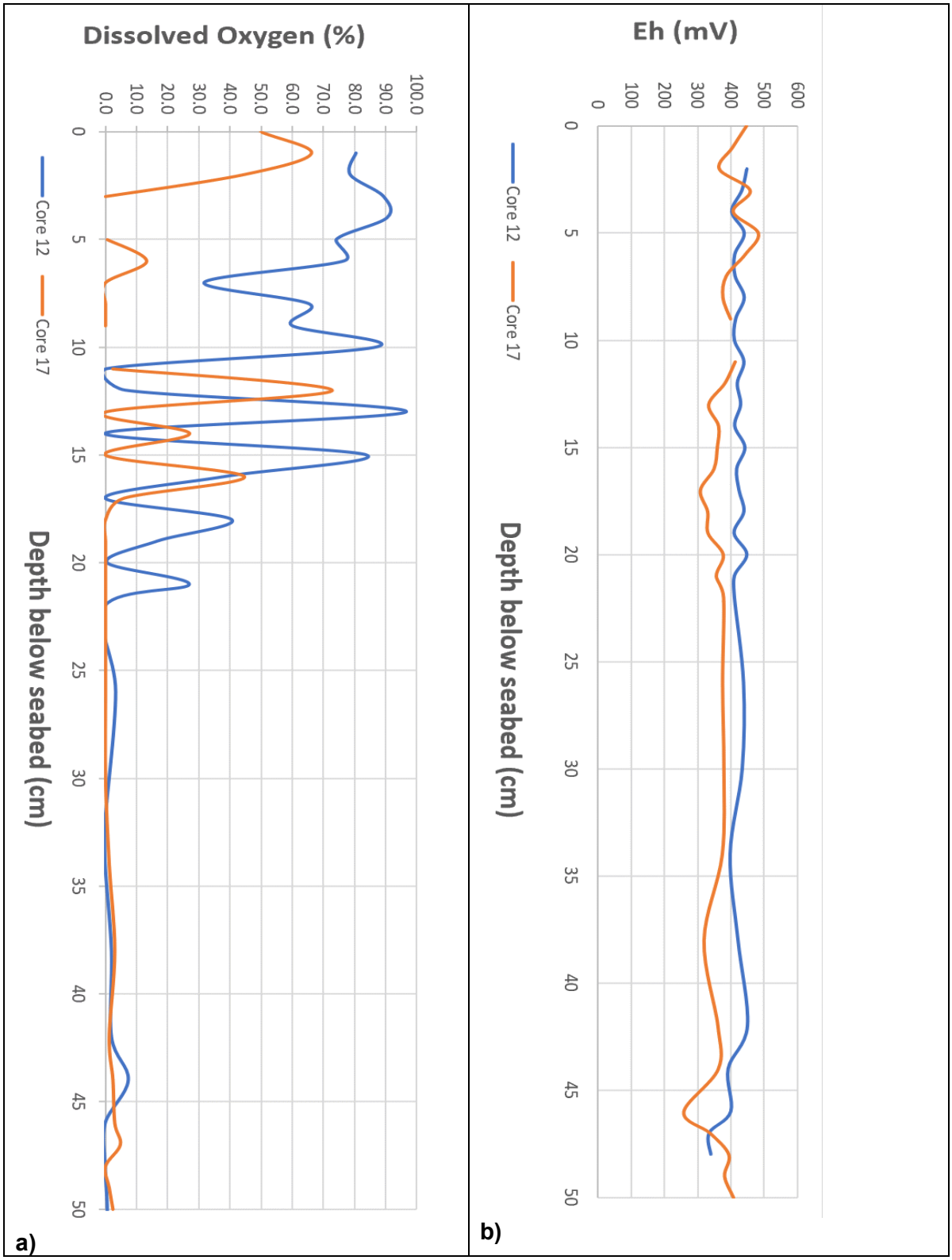

Figure 4.10 Down-core variability in reference cores 12/17, Swan River sleeper site: (a) DO; and (b) Eh.

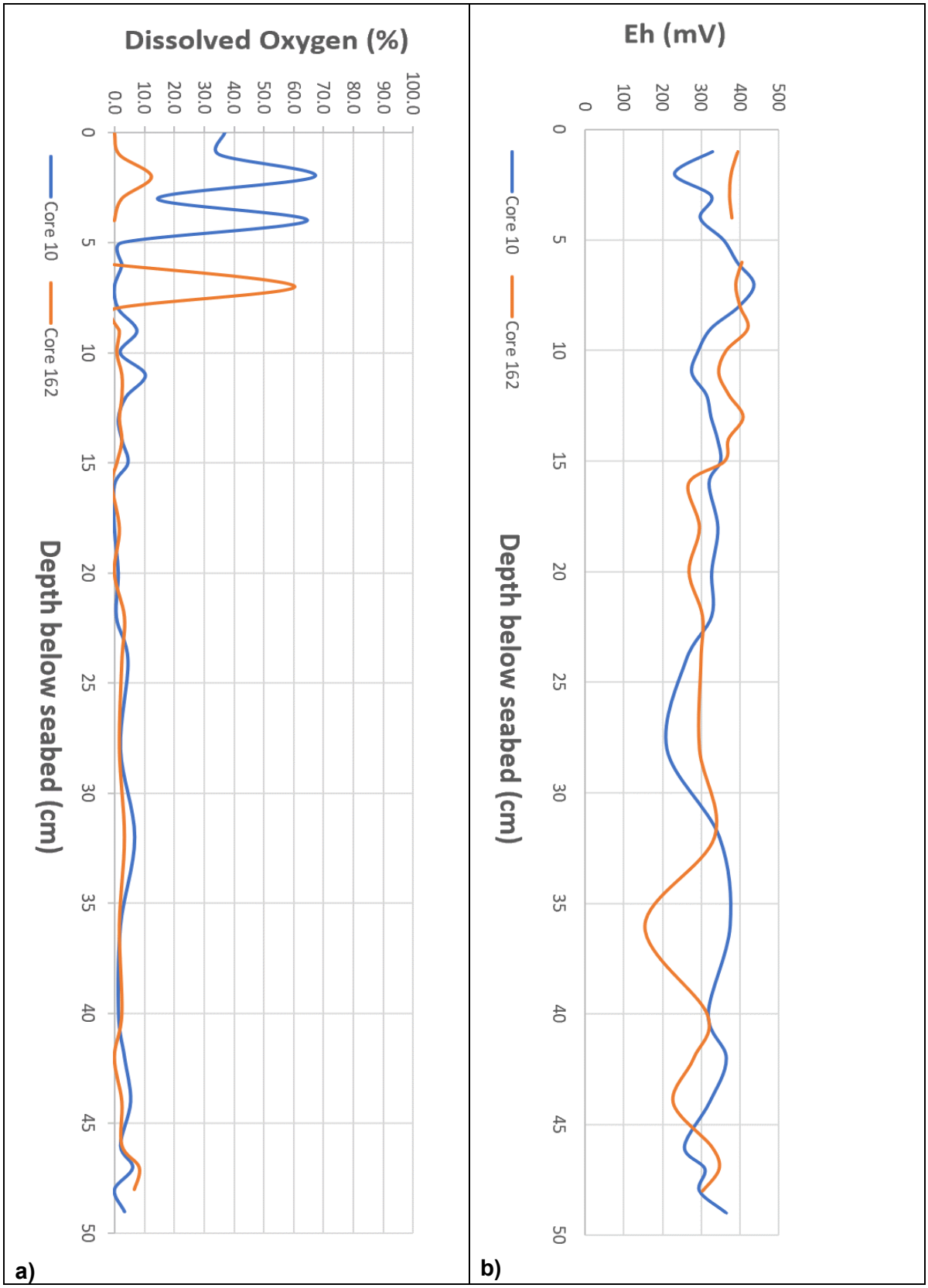

Figure 4.11 Down-core variability in backfilled cores 10/162, Swan River sleeper site: (a) DO; and (b) and Eh.

At the James Matthews sleeper site, reference cores showed greater variability in DO between cores and within each core (Figure 4.12a). The DO profile in core 20 varied between near zero and near saturation in the top 30 cm, then dropped to near zero before rising again at around the 43 cm depth. The upper variability may come from bio-turbation by burrowing macro-fauna in the sediments and localised burial of organic matter. The latter rise may have resulted when the core was extruded from the seabed with aerobic water diffusing into the core prior to the end-cap being inserted. In the adjacent duplicate core 122, DO was near zero percent saturation for the entire core length except for three peaks up to 70% in the top 12 cm, and with a slow rise in DO to around 20% in the lower 10 cm. While on average core 122 had much lower DO values, the variability in the upper and lower core sections may also be due to bio-turbation and end diffusion, respectively. Eh profiles for these two cores (Figure 4.12b) reduced smoothly from around 400–450 mV near the surface to between 350–400 mV at 50 cm depths. At the other reference location, DO in core 194 fluctuated from 0–10% saturation to 80–90% saturation over the full core length (Appendix B, Figures B.25 and B.26). By contrast, DO in the adjacent core 195 decreased from 50% in the upper 6 cm to zero, rose again to 70% between depths 25–30 cm, reduced to sub 10% until 40 cm, then rose again to 60% at the bottom of the core — the latter rise may also be a result of DO diffusion during end-cap placement. Eh profiles for these cores were more variable in the top 15–20 cm compared to the other reference site, and the Eh values in core 195 dropped from 460 to 320 mV in the bottom of the core at the depths where DO rose significantly.

At backfilled locations at the James Matthews sleeper site, very large DO variations were observed between backfilled locations and within cores (Figure 4.13a). This indicates the likely effects of sediment porewater re-oxygenation during excavation/backfilling and the likely, but unintentional, localised burial of organic matter. Core 155 displayed low saturation levels from 1–4 cm, high saturation (80–100%) from 6–20 cm followed by a rapid drop off to less than 10%. This change in DO reflected the observed depth of sediment disturbance from excavation/backfilling. In contrast to its duplicate, core 100 showed very low saturation values for the entire core length, with some fluctuations to 30–40% and a small rise at the base of the core. At the other reference location, core 192 displayed fluctuations along the full core length, but with consistent high saturation values (>90%) between 9 cm and 30 cm (Appendix B, Figures B.23 and B.24). Duplicate core 193 displayed lower values on average with fluctuations up to 40% in the upper 14 cm and a large spike to 85% saturation around 28 cm. Eh profiles for cores 100 and 155 remained reasonably steady with minor fluctuations around 400–450 in the upper 15cm surficial sediments, slowly decreasing with depth to around 350–400 mV to 350 mV (Figure 4.13b). A similar pattern in EH variability was evident for cores 192 and 193, although the magnitude of the surficial fluctuations was slightly greater.

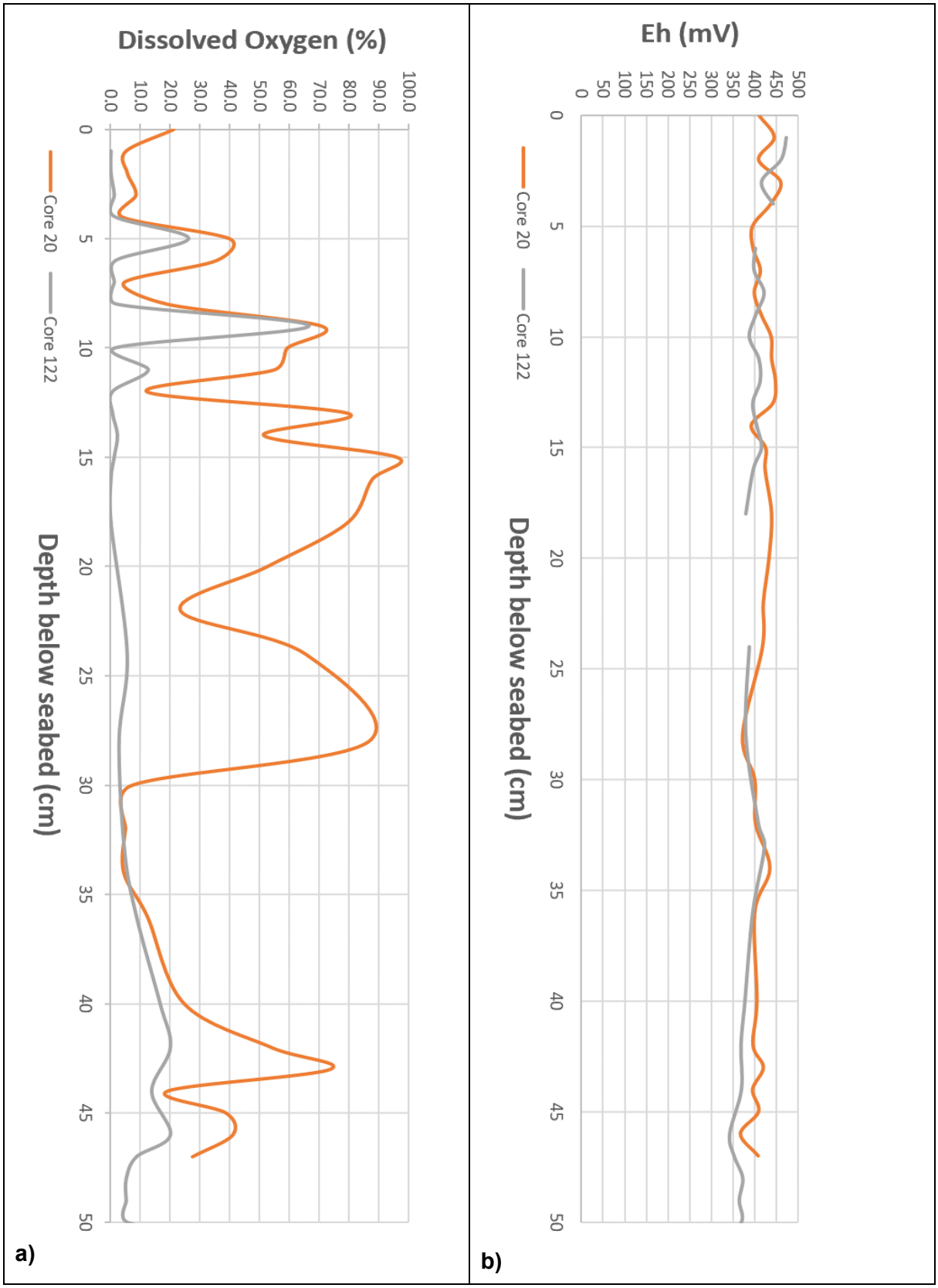

Figure 4.12 Down-core variability in reference cores 20/122, James Matthews sleeper site: (a) DO; and (b) Eh.

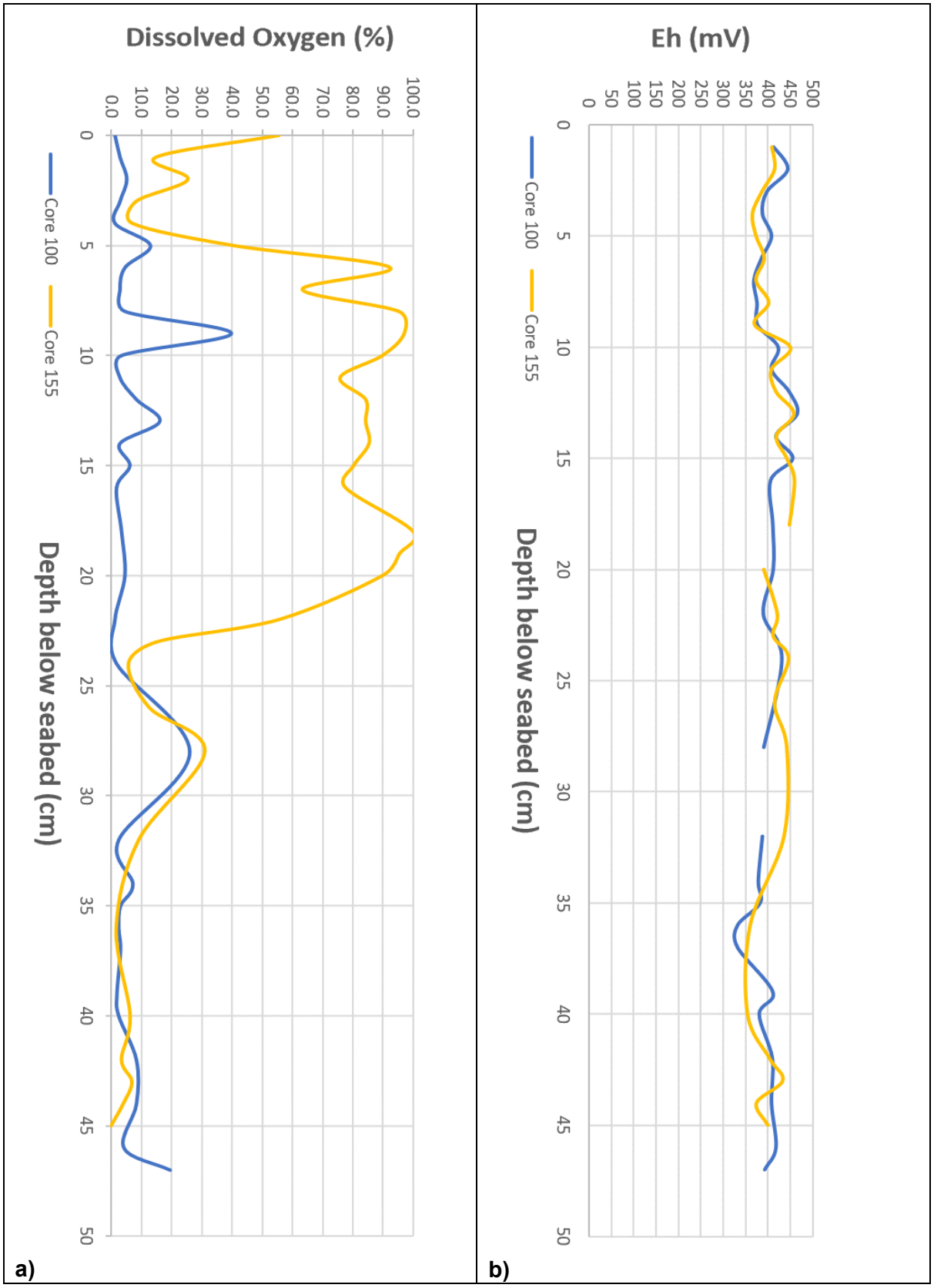

Figure 4.13 Down-core variability in backfilled cores 100/155, James Matthews sleeper site: (a) DO; and (b) Eh.

Sediment in situ density measurement results

For similar types of saturated sediments, in the same sized core tubes and under the same test conditions, penetration resistance profiles reflect in situ sediment density. Penetration resistance is calculated by dividing the measured penetration force by the area of the penetration rod (12.6 mm^2). Penetration force profiles, using the same rod and same penetration speed, and generated following the methods described in Chapter 3, are used for comparative purposes. The methods were applied to cores collected from reference and backfilled locations at both the James Matthews and Swan River sleeper sites. Sediment cores from both sites were also tested following manipulation by repacking the sediment in its loosest condition ('light' compaction) and in its densest condition ('tight' compaction). The relative in situ density for reference, backfilled and manipulated cores within each site were compared, and are described as follows. Due to differing sediment characteristics between the two sites, comparisons between sites were not undertaken.

Penetration force profiles for duplicate cores collected at the James Matthews sleeper site are shown in Figure 4.14. Profiles for duplicate reference cores (Figure 4.14a), for duplicate core collected at locations backfilled 15 months previously (Figure 4.14b) and for duplicate cores collected at locations backfilled one month previously (Figure 4.14c) all show very similar results albeit with slightly different maximum penetration forces. Localised spikes in the profiles indicate that the penetrometer rod pushed against/broke through harder objects like the many small and large shells found at all depths within the cores. Until the rod pushes through or past these shells or hard objects, the shells temporarily increase the effective size of the rod tip, significantly increasing the resistance force. The overall shape of the profile reflects both the sediment density and localised test effects due to the development of internal lateral forces constrained by the core tube. At shallow depths, 'the development of lateral stresses from the penetrating rod are small and influenced by the free surface. At some point (typically 5–10 rod diameters, depending on density and sediment confinement) the behaviour becomes deep and ''steady-state''. With these smaller core diameters however, the steady state depth is difficult to quantify due to the proximity of the rigid tube walls' (Conleth O'Loughlin pers. comm. 2019). For these small core diameter tests, the upper 50–70 mm of the profile indicates very low resistance force under the effect of free state conditions. Following a transition, steady state penetration resistance conditions appear to occur below 230 mm for reference cores and below approximately 200 mm for backfilled cores.

Similar features can be seen in the penetration force profiles for Swan River sediments (Figure 4.15). A shell layer at a depth of around 120–140 mm can be seen by the significant spike in both reference core duplicates. In these cores the steady state penetration resistance

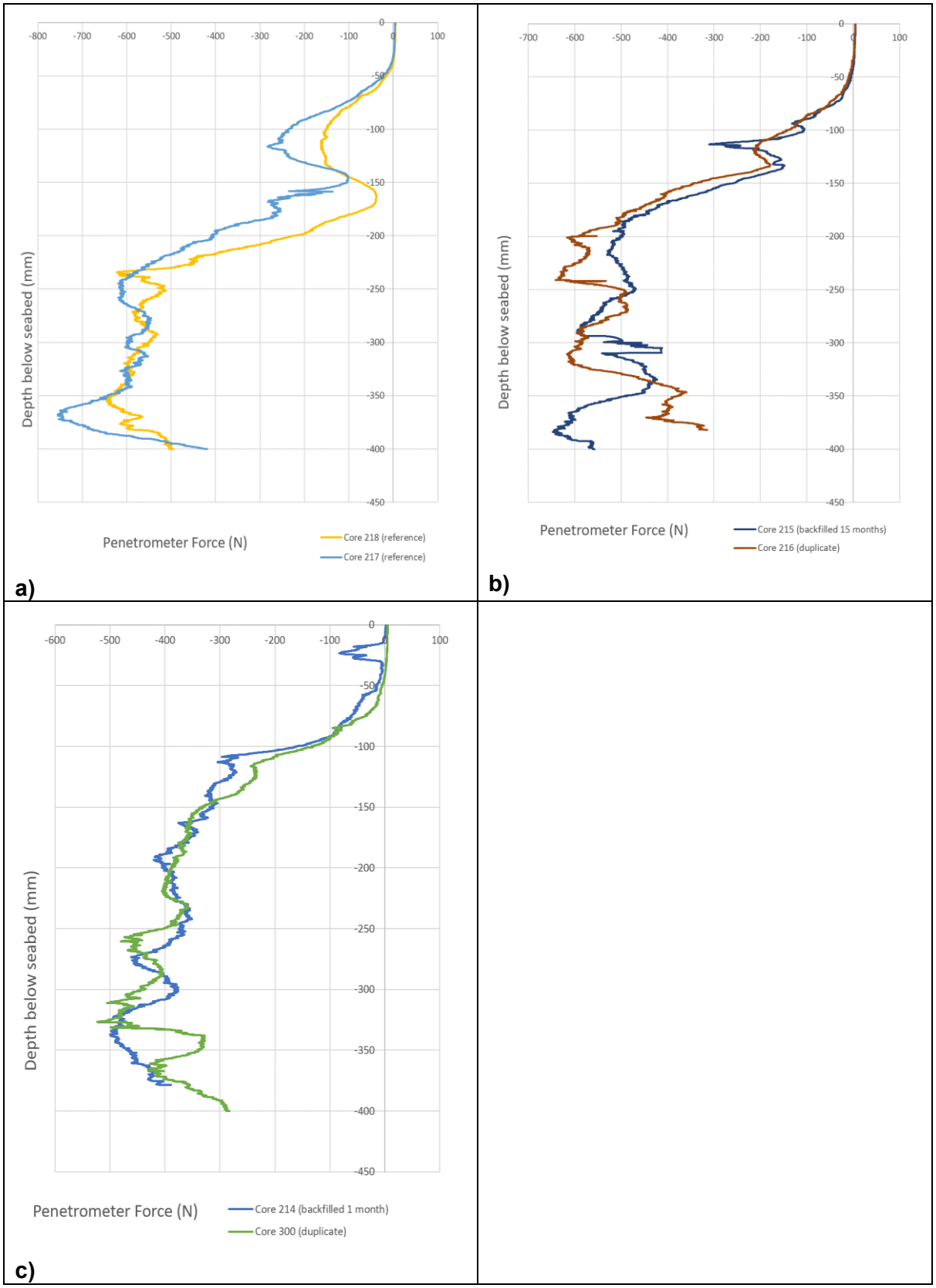

Figure 4.14 Penetration force profiles James Matthews site: (a) duplicate reference cores; (b) backfilled cores (15 months); and (c) backfilled cores (1 month).

conditions appear to occur at a much deeper depth of around 350 to 370 mm (Figure 4.15a), and the steady state resistance force for core 302 is approximately 25% greater than for core 301. While the profile shape is similar for the duplicate cores collected at locations 4.75 months after backfilling, the penetration resistance is much higher for core 303 than for core 304 (Figure 4.15b). Following manual backfilling of the sleepers at this site, the sediment was densified by repeatedly walking over/stamping the loose sediment fill. This process was uncontrolled (i.e. the process of walking/stamping was not evenly applied across buried sleeper locations or around each buried sleeper). Consequently, the differences between the force profiles of backfilled cores 303 and 304 may simply show the real and unintended differences in densification across the Swan River sleeper site.

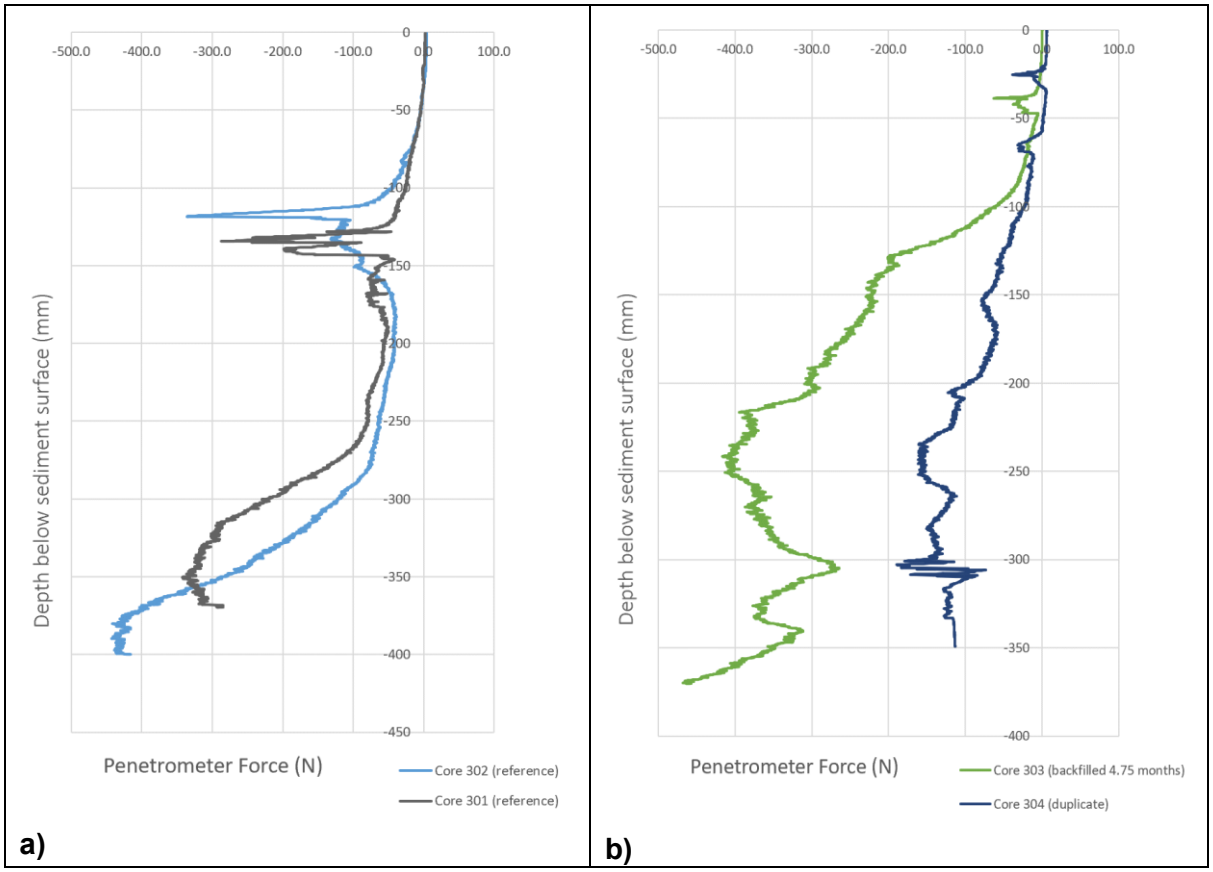

Figure 4.15 Penetration force profiles, Swan River site: (a) duplicate reference cores; and (b) backfilled cores (4.75 months).

In its original backfilled state, the transition to 'steady state' penetration resistance occurs at shallower depths than for the tightly recompacted state. Once achieved however, both have similar steady state resistance forces. These forces are almost an order of magnitude higher than the penetration force profile for the loosest state. It is also possible that steady state conditions may not have been fully achieved in the manipulated cores as the resistance force appears to continue to rise to the 400 mm depth which was the penetration limit of the test.

The same 'order of magnitude' difference in penetration force for the densest state versus the loosest state for Swan River sediments is shown in Figure 4.16b. Two additional features shown in Figure 4.16 are the shallower development of the steady state penetration resistance (from approximately 200 mm) in the tightly compacted case compared to around 370 mm in the lightly compacted case and the smaller-scale periodic variability with depth, also in the tightly compacted cores. The spacing of these fluctuations corresponds to the approximate thickness of each sequential sediment layer after the sediment was poured into the core tube and vigorously compacted with a large diameter rod. By comparison, the smooth profile associated with the light compaction test reflects the continuous addition of sediment with no mechanical compaction of layers.

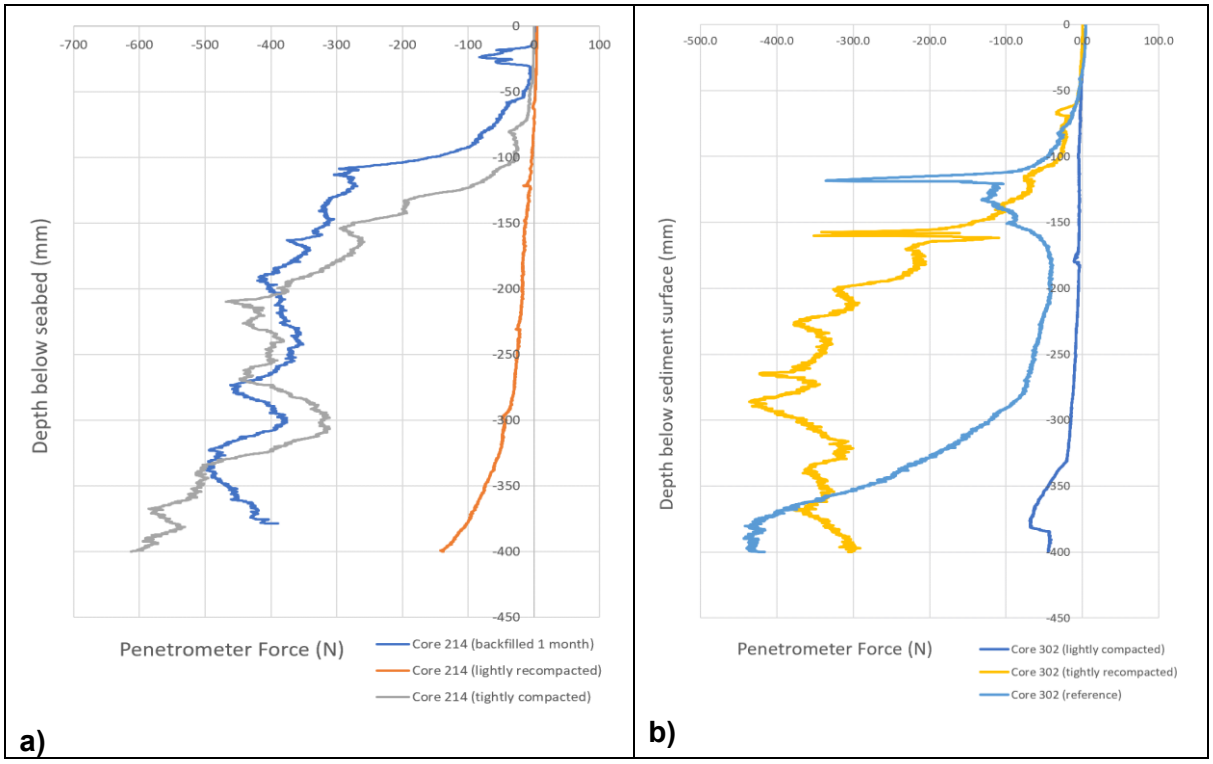

Figure 4.16 Penetration force profiles, light and tight recompaction: (a) James Matthews cores; and (b) Swan River cores.

Buried timber density and moisture content analyses

The purpose for the pre-burial and post-recovery timber analyses of buried blocks is to provide an estimate of the in situ density and moisture content of the timber sleepers at the times of sub-bottom profile surveys. Arnott et al. (2005) and more recently Zisi (2016) undertook laboratory investigations into the relationship between acoustic properties, reflection coefficients and the degradation state of partially-degraded modern pine and European oak

timber samples. They developed mathematical relationships relating velocities in timber and reflection coefficients against timber density, in different sediment types. These authors used conventional or basic density to quantify timber degradation. They used bulk density, however, in the calculation of reflection coefficients as bulk density 'represents the state of the material in its waterlogged condition as encountered by an acoustic signal' (Arnott et al. 2005:138). Jensen and Gregory (2006:551) discussed the merits and practicalities of differing physical parameters to characterize the state of degradation of waterlogged archaeological wood and identified density as a 'benchmark' parameter, even though the maximum water content (U_{max}) is often used (Grattan 1987) to classify types of degraded waterlogged wood. Bulk density is preferred by conservators for fully waterlogged degraded archaeological wood as it 'facilitates the selection of the optimal conservation method' (Gregory et al. 2007:289). These authors noted however, that 'if the timber is not fully waterlogged then the basic density method must be used to assess the level of degradation'. In this study, both basic and bulk densities of the timber samples were determined. This enabled direct comparison with the quantitative experimental relationships developed by Arnott et al. (2005) and Zisi (2016). It also permitted independent calculation of the reflection coefficients at the times of SBP insonification, regardless of whether they were fully waterlogged or not. The maximum moisture content of pre-burial timbers and the moisture content (MC) of post-burial recovered timbers enabled comparison to % saturation levels (U_{max}/MC) associated with reported analyses of maritime archaeological samples. Also, the MC values, relative to their fibre saturation point (FSP), provided insight into the likely effect of MC on the acoustic velocities in timbers. It is not the intent of this research to examine the process of how timbers become saturated and degraded. It is also recognised that the there are many geochemical, environmental and intrinsic timber variables affecting the rate of waterlogging and degradation (Björdal 2012b). Hence these density results, following short-term burial of modern timber, may display much higher levels of variability and may not be representative of fully waterlogged archaeological timbers.

Two duplicate sample cubes each 2 cm x 2 cm x 2 cm were cut from three different locations from each of the freshly cut pine and jarrah timbers, and the air-dried oak timber, prior to their burial. Basic and bulk density and U_{max} characteristics of these pre-burial timbers were measured using the methods described in Chapter 3. All raw data for these 18 sample cubes is tabulated in Appendix C, Table C.1, with results summarised in Table 4.6.

Following 20.5 months of submerged burial, eight duplicate pine and oak blocks from different depths (10 cm, 30 cm, and 50 cm DoB) (Table 4.7) were removed from the James Matthews sleeper site and cut up into 2 cm x 2 cm x 2 cm cubes. As illustrated in Figure 3.15, a 2 cm wide vertical slice (front to back) and a central horizontal slice (side to side), were cut from

Table 4.6 Pre-burial timber densities and maximum moisture content.

	pine		European oak		jarrah	
	mean	**std dev**	**mean**	**std dev**	**mean**	**std dev**
basic density (kg/m^3)	473.7	38.3	580.9	54.1	577.2	25.2
bulk density(kg/m^3)	525.4	56.1	641.7	59.0	877.2	89.1
max moisture content (%)	145.0	10.9	105.2	18.8	91.6	7.2

each recovered block. The individual cubes were cut from these slices to extract samples representing replicated along-grain and cross-grain outer- and inner-sections of each block. Most blocks had 45^0 tapered tops to facilitate easier removal from their buried depths, with the exception of the very shallow buried blocks (DoB =10 cm) which had flat tops. After nine months and one week of submerged burial, six pine, oak and jarrah blocks, from different depths (20 cm, 30 cm and 50 cm DoB) (Table 4.7) were removed from the Swan River site and cut up into cubes in a similar way. After cutting, the sample cubes were stored in zip-locked bags partially filled with seawater. When retrieved for analysis, some of the outer cubes were noted to have sunk, while others still floated, indicating that some of the outer cubes were already waterlogged.

Table 4.7 Blocks recovered for post-burial density and moisture content analyses.

sleeper site	**James Matthews**		**Swan River**		
timber type	**pine**	**oak**	**pine**	**oak**	**jarrah**
Depth of Burial (cm) and numbers recovered	P10 x 2		P20 x 1		J20 x 1
	P30 x 2	O30 x 2	P30 x 1	O30 x 1	J30 x 1
	P50 x 2		P50 x 1		

Basic and bulk density and U_{max} values were determined for all sample cubes cut from the recovered timber blocks using the methods described in Chapter 3. All raw measurement data and density results for each cube sample are tabulated in Appendix C, Table C.2. Bulk and basic density values are summarised in Table 4.8 and 4.9 for blocks recovered from the James Matthews and Swan River sleeper sites, respectively. Associated Box and Whisker charts, developed in XLSTAT and shown in Figure 4.17 and Figure 4.18, display the variability of basic density and bulk density results from pine samples recovered from the James Matthews sleeper site. These charts show the distribution of the results in quartiles, together with median and outlier values—the latter lie beyond the single whisker lines which show the variability outside the upper and lower quartiles. Similar charts are shown in Figure 4.19

Table 4.8 Bulk and basic density values, all blocks recovered 20.5 months post-burial from James Matthews sleeper site.

sample	P10 (D1)		P10 (D2)		P30 (D1)		P30 (D2)	
	bulk density (kg/m3)	basic density (kg/m3)	bulk density (kg/m3)	basic density (kg/m3)	bulk density (kg/m3)	basic density (kg/m3)	bulk density (kg/m3)	basic density (kg/m3)
T4							1022.0	468.5
T3					1002.2#	386.8	872.5	464.2
T2	1102.7	419.3	1006.4	367.2	979.2	388.3	859.5	459.3
T1	1086.9	420.2	958.2	369.8	970.2	401.5	870.3	469.6
C	999.9	386.2	954.4	363.3	942.0	383.2	872.7	475.0
B1	773.0	474.6	995.1	369.3	954.8	373.1	859.6	475.2
B2	822.9	524.4	1033.3	367.6	1025.9#	374.2	1057.7	480.9
L2	1091.5	395.2	656.4	354.4	1002.9#	367.5	747.8	428.7
L1	1022.6	387.5	817.9	396.2	1030.0#	369.4	698.8	481.1
R1	998.3	379.4	1050.2	389.9	713.6	452.1	1077.1	381.7
R2	1080.8	381.5	1129.5	410.1	768.2	416.1	1123.9	451.8
mean	*997.6*	*418.7*	*955.7*	*376.4*	*938.9*	*391.2*	*914.7*	*457.8*
std dev	*120.6*	*49.8*	*140.5*	*18.1*	*108.9*	*26.2*	*137.2*	*29.4*
	long grain top to bottom		long grain top to bottom		long grain top to bottom		long grain top to bottom	

blocks noted to have sunk in seawater

sample	P50 (D1)		P50 (D2)		O30 (D1)		O30 (D2)	
	bulk density (kg/m3)	basic density (kg/m3)	bulk density (kg/m3)	basic density (kg/m3)	bulk density (kg/m3)	basic density (kg/m3)	bulk density (kg/m3)	basic density (kg/m3)
T4								
T3	955.1	443.0	797.0	465.1				
T2	818.1	439.7	719.4	485.1	959.2	452.0	1094.6	647.3
T1	814.5	452.8	703.2	477.8	800.1	422.1	952.0	542.8
C	783.4	454.3	677.6	459.3	781.8	458.0	832.5	484.2
B1	805.2	465.2	718.1	467.9	790.0	449.3	863.8	489.8
B2	1015.3	453.4	1056.4	478.3	913.2	500.8	1037.0	568.1
L2	767.6	505.8	768.6	467.3	670.8	445.4	801.2	445.5
L1	597.1	415.5	710.0	485.5	782.4	458.7	820.0	497.1
R1	1095.4	403.5	1025.9	398.6	719.7	426.9	810.9	480.4
R2	1124.8	456.2	1099.4	416.3	799.7	426.6	850.8	473.5
mean	*877.6*	*448.9*	*827.6*	*460.1*	*801.9*	*448.9*	*895.9*	*514.3*
std dev	*165.3*	*27.7*	*165.1*	*29.4*	*88.0*	*24.0*	*107.0*	*62.0*
	long grain top to bottom		long grain top to bottom		long grain top to bottom		long grain top to bottom	

Table 4.9 Bulk and basic density values, all blocks recovered 9.2 months post-burial from Swan River sleeper site.

sample	J30		O30		P30		P20		P50		J20	
	bulk density (kg/m3	basic density (kg/m3)	bulk density (kg/m3)	basic density (kg/m3)	bulk density (kg/m3)	basic density (kg/m3)	bulk density (kg/m3)	basic density (kg/m3)	bulk density (kg/m3)	basic density (kg/m3)	bulk density (kg/m3)	basic density (kg/m3)
T4	1482.9	698.8			1069.9	489.0			1063.9	432.4	739.7	554.8
T3	1091.8	547.3	1008.9	479.5	738.6	507.6			850.2	439.0	1097.4	556.1
T2	1081.7	546.5	820.4	475.7	693.4	502.8	886.7	449.4	778.3	428.0	1105.0	552.1
T1	992.6	509.8	759.6	492.9	673.0	495.5	1020.7	412.8	790.5	431.9	1119.8	552.8
C	1059.3	557.2	747.7	485.8	656.6	475.4	1093.5	391.9	771.2	432.8	1126.8	558.6
B1	1014.3	554.8	839.1	483.4	690.2	431.0	1144.2	433.5	774.3	438.7	1129.8	551.0
B2	1089.5	562.8	998.7	485.5	1054.7	416.5	1136.4	432.8	1017.7	449.2	1133.2	538.0
L2	985.9	568.0			695.6	446.6	1134.6	436.1	772.5	467.1	1053.7	558.0
L1	1058.2	559.5	734.0	404.4	724.7	534.0	1131.0	428.6	717.9	501.7	1133.2	560.3
R1	1050.6	555.8	800.7	470.0	1136.7	417.9	1138.4	418.6	1131.5	428.2	1129.4	548.6
R2	985.0	551.0			1141.5	467.7	1135.8	419.5	1121.0	440.5	1074.3	556.0
mean	*1081.1*	*564.7*	*838.7*	*472.2*	*843.2*	*471.3*	*1091.3*	*424.8*	*889.9*	*444.5*	*1076.6*	*553.3*
std dev	*139.3*	*47.0*	*108.1*	*28.2*	*206.8*	*39.1*	*86.1*	*16.5*	*159.1*	*22.1*	*114.8*	*6.2*
	long grain top to bottom		long grain top to bottom		long grain top to bottom		long grain left to right		long grain top to bottom		long grain top to bottom	

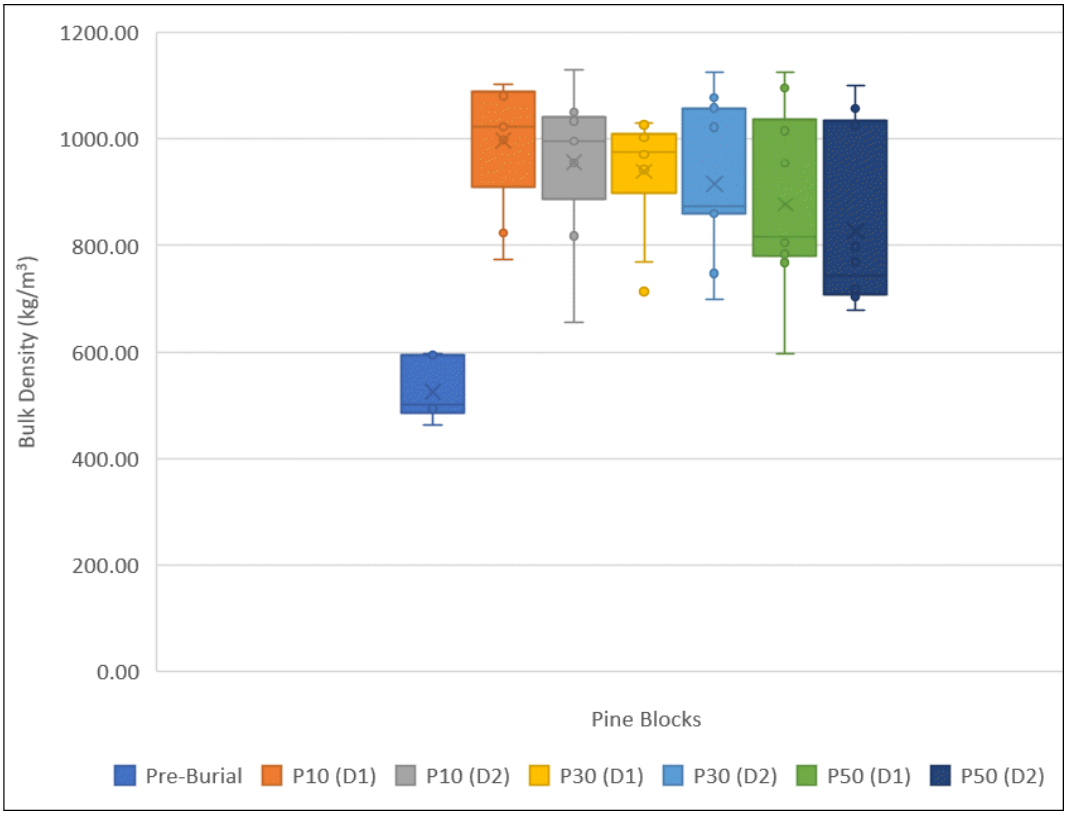

Figure 4.17 Bulk density, pine timber, James Matthews sleeper site.

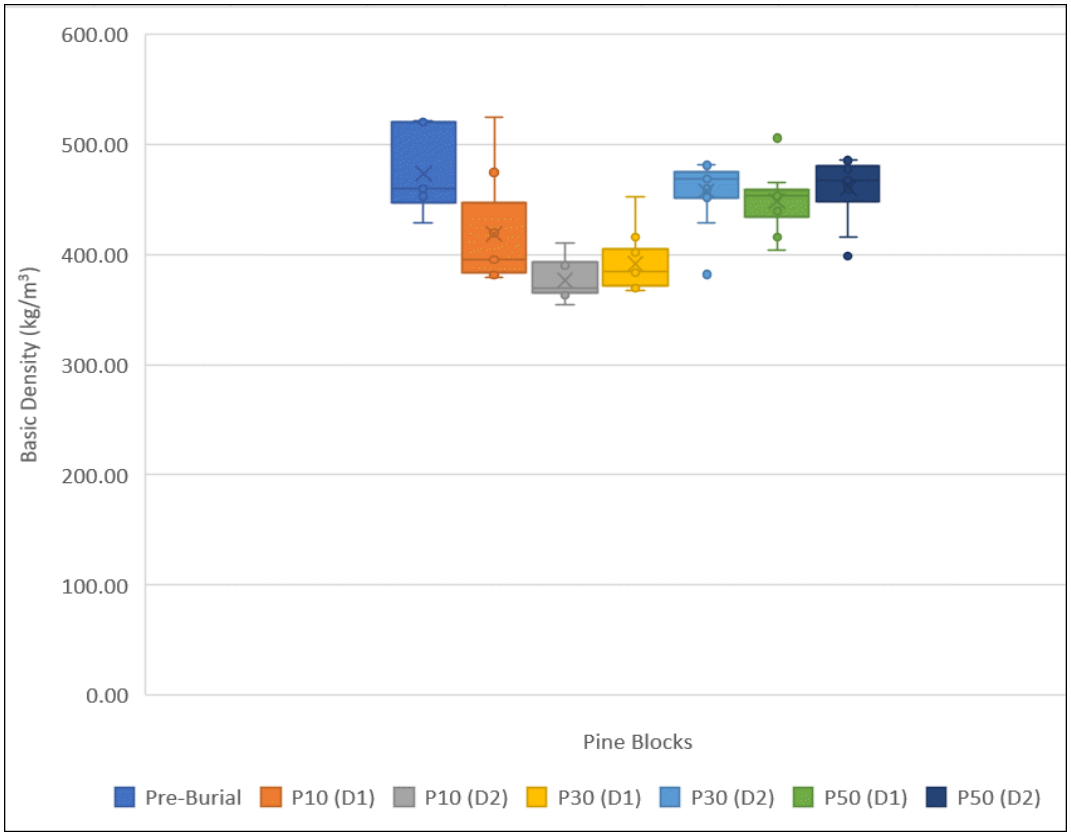

Figure 4.18 Basic density, pine timber, James Matthews sleeper site.

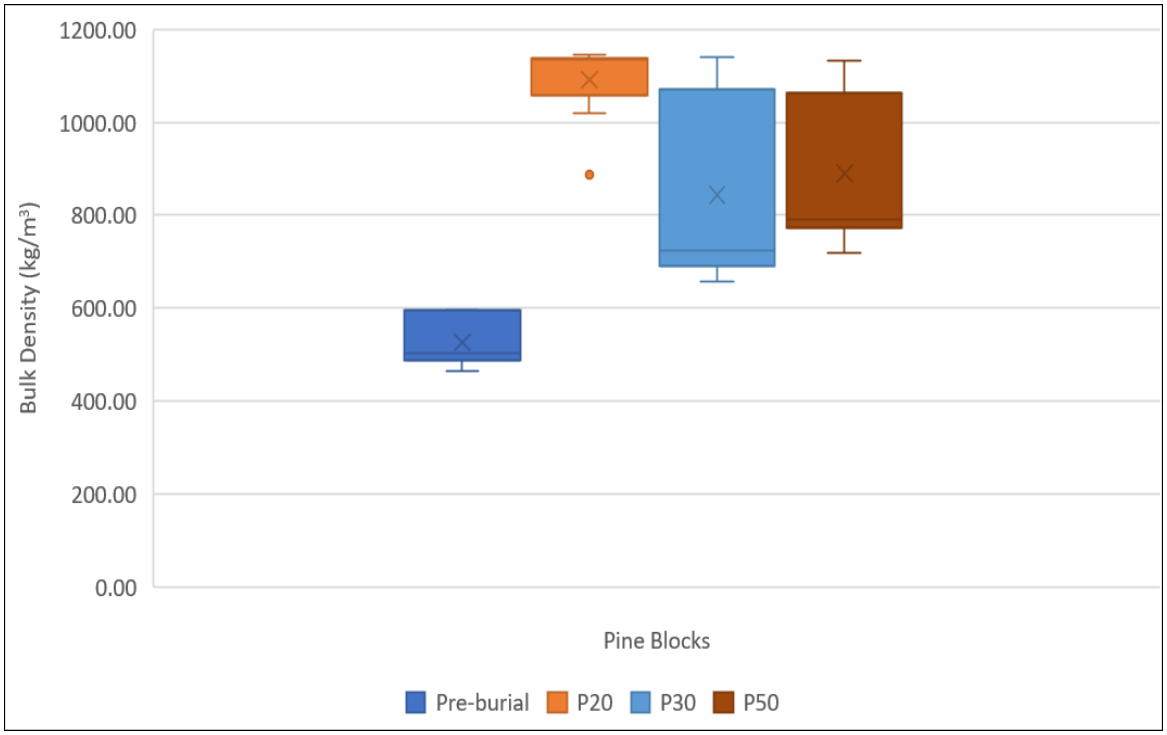

Figure 4.19 Bulk density, pine timber, Swan River sleeper site.

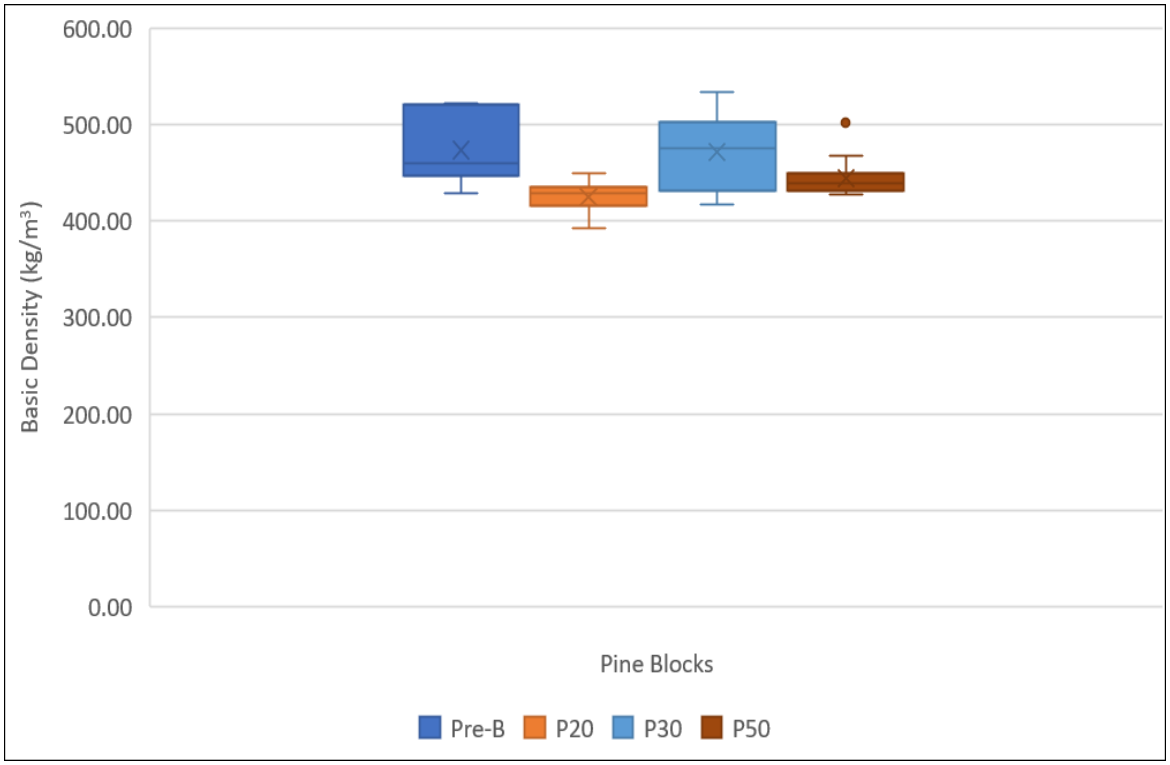

Figure 4.20 Basic density, pine timber, Swan River sleeper site.

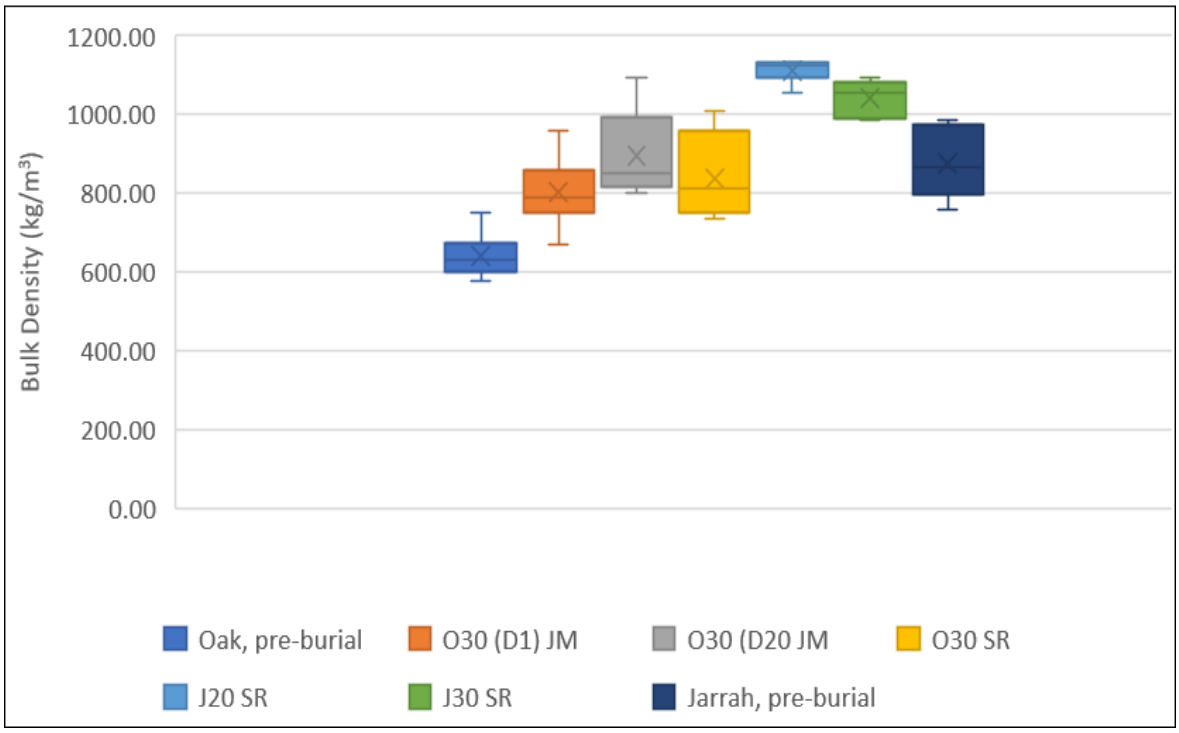

Figure 4.21 Bulk density, oak and jarrah timbers, James Matthews and Swan River sites.

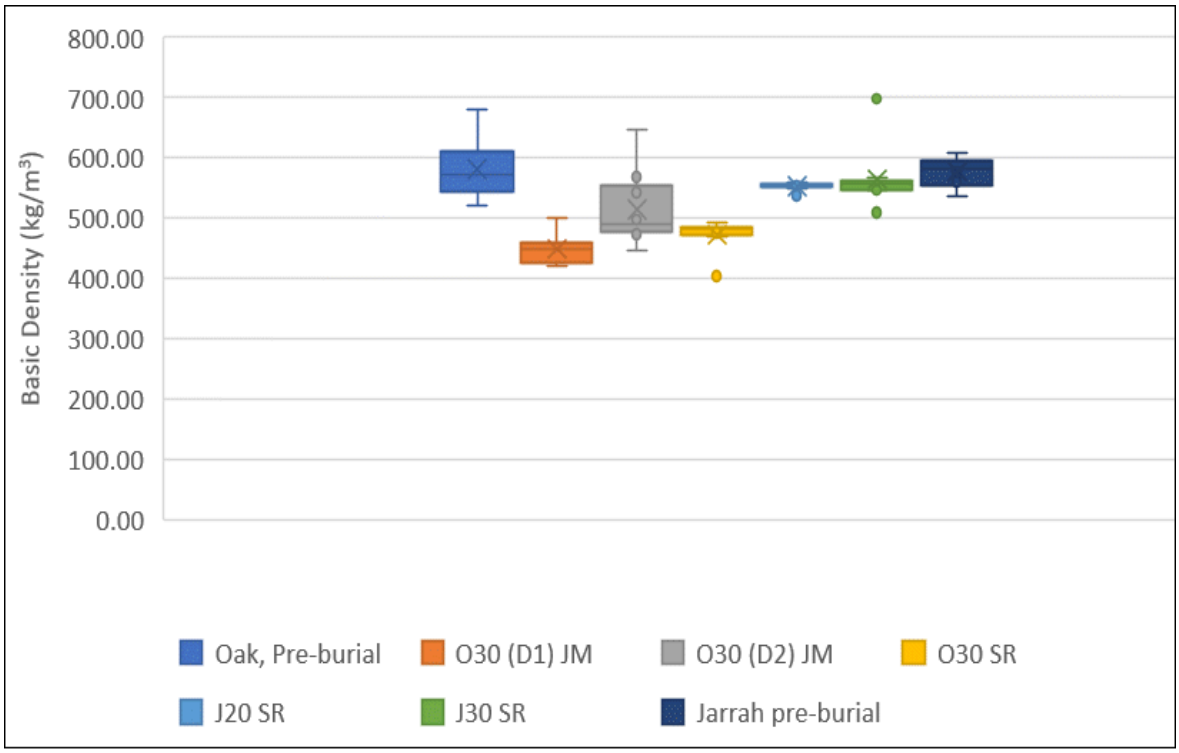

Figure 4.22 Basic density, oak and jarrah timbers, James Matthews and Swan River sites.

through to Figure 4.22 for the pine blocks recovered from the Swan River site and for the oak and jarrah blocks recovered from both sites.

As can be seen from Figure 4.17, there is high variability in the bulk density results for all recovered pine blocks from the James Matthews sleeper site. There is no significant difference in the bulk density values between any of the recovered blocks (duplicates D1, D2 or different burial depths 10, 30, 50 cm), however the average bulk density values of all recovered blocks are significantly greater than their pre-buried value. The basic density values (Figure 4.18) have similar high variability. Only one of the duplicate blocks buried at 10 cm DoB displayed a significant decrease from its pre-burial state and with its mean values also less than the mean values of the other deeper buried blocks. These results are consistent with the processes of waterlogging and degradation of submerged buried timbers as discussed in Chapter 2. During the waterlogging process, timber becomes swollen and seawater fills the internal air-filled pore spaces of the timber, both the capillaries and the microcapillaries (Grattan 1987:55). This leads to an increase in the bulk density of the timber. Biological degradation of waterlogged and buried timber results from attack by ligniferous marine fungi and by marine bacteria. Attack by these micro-organisms results in loss of cellulose, destruction of cell walls and pit membranes, and replacement of cellular material with seawater (Grattan 1987:65; Hoffman and Jones 1989:63). The net effect further increases the bulk density. Following oven drying to constant weight and the consequential removal of the entrained seawater, the loss of cellular material decreases the dry weight of degraded timber and its basic (dry) density.

A similar pattern of high variability, waterlogging and possible degradation is shown for pine timbers recovered 9 months and one week after burial in the Swan River (Figure 4.19 and Figure 4.20). This pattern is also repeated for oak timbers buried at both sites and jarrah timbers buried at the Swan River site (Figure 4.21 and Figure 4.22).

The high within-block density variability is depicted in Figure 4.23 and 4.24 for oak and pine timber blocks recovered 20.5 months after burial at the James Matthews sleeper site. In these figures the bulk densities of the outer cubes (taken from the top and bottom surfaces in the longitudinal grain direction) from duplicate blocks buried at the same depth are individually plotted. Likewise, the bulk densities of the inner cubes from the same blocks are separately plotted. For the oak blocks, the variability within duplicates D1 and D2 buried at 30 cm is explained by the significantly higher bulk density (waterlogging/degradation) in the outer cubes (longitudinal grain direction) vs. the inner cubes (Figure 4.23). This is the same for some, but not all of the pine blocks. The outer cubes in pine blocks D2 at 10 cm DoB, D1 and D2 at 30 cm DoB, and D2 at 50 cm DoB, all had significantly higher bulk densities than their respective inner cubes. The variability of bulk density within the inner cubes for D1 at 30 cm DoB was high, overlapping with the density range in the respective outer cubes. The variability of bulk

density within the inner cubes for D1 at 50 cm DoB was also high which resulted in an overlap of the quartile distribution, but not the mean, with the density of the outer cubes. These outcomes indicate that significant water logging and partial degradation has occurred in the outer 2 cm layer, and primarily in the longitudinal direction, of the blocks buried at the James Matthews sleeper site.

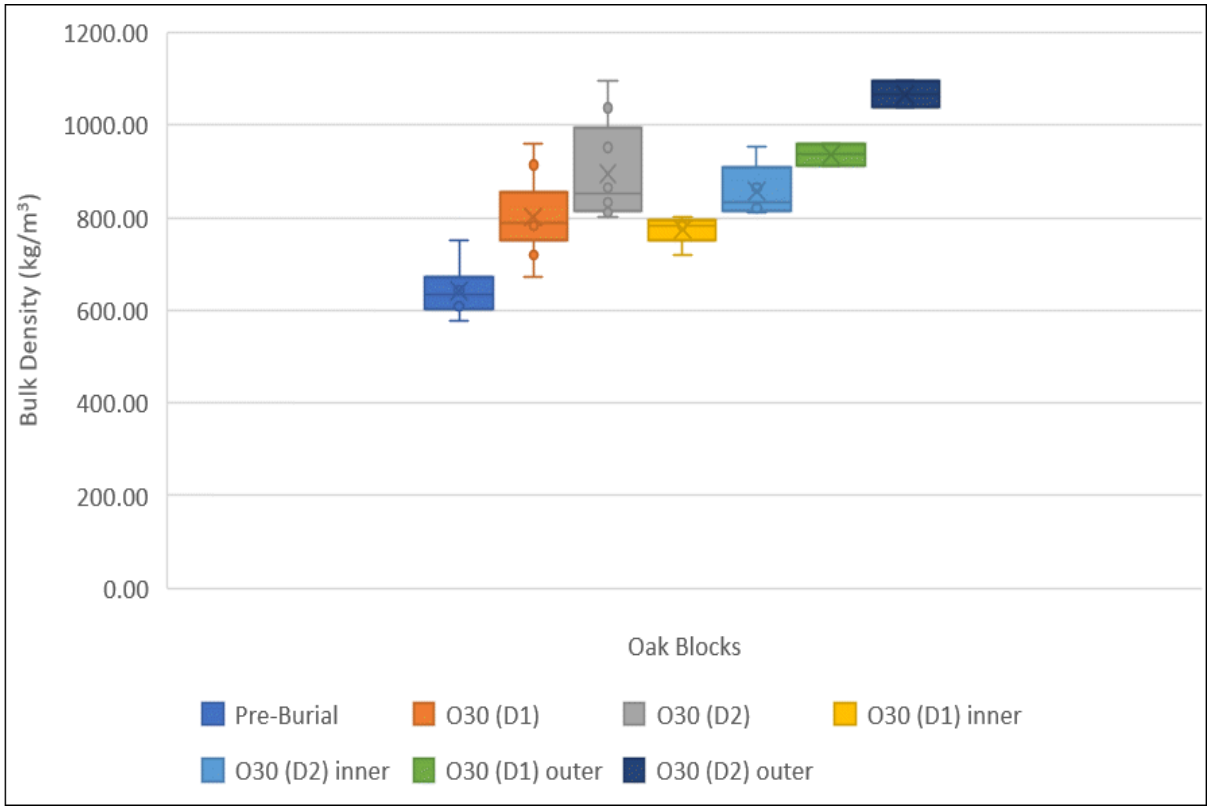

Figure 4.23 Within-block variability, bulk density, oak timber, James Matthews sleeper site.

The moisture content for timber samples collected from the James Matthews and Swan River sleeper sites is presented in Table 4.10 and 4.11, respectively. These tables show that moisture content increases with increasing submerged burial times, with the exception of P50, and with shallower burial depths.

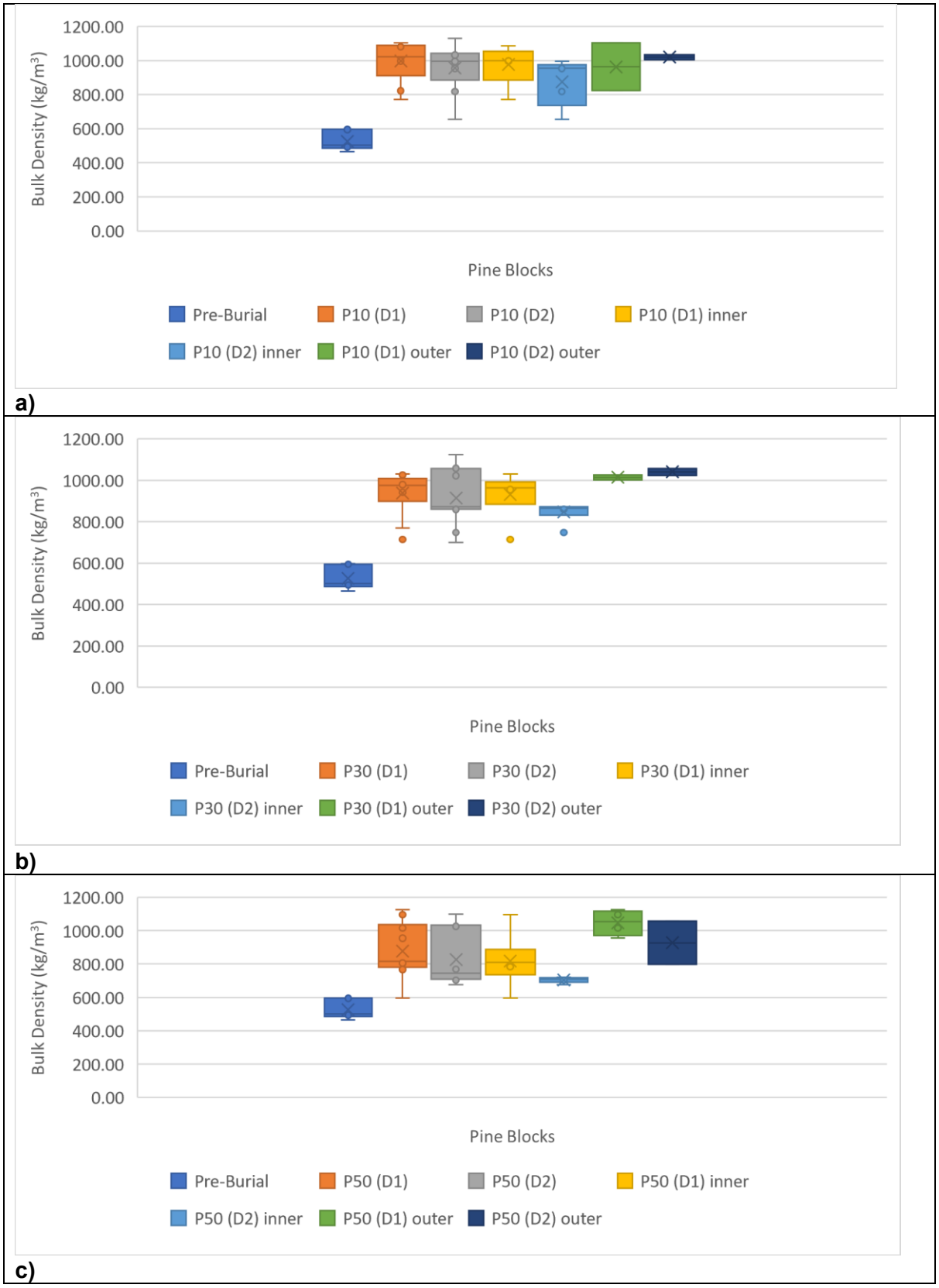

Figure 4.24 Within-block variability, bulk density, pine timber, James Matthews sleeper site: (a) DoB 10 cm; (b) DoB 30 cm; and (c) DoB 50 cm.

Table 4.10 Moisture content in timber samples collected 20.5 months post-burial, James Matthews sleeper site.

sample	P10		P30		P50		O30	
	D1	D2	D1	D2	D1	D2	D1	D2
T4				118.1				
T3			159.1	88.0	115.6	71.4		
T2	162.9	174.1	152.1	87.1	86.1	48.3	112.2	69.1
T1	158.7	159.1	141.6	85.3	79.9	47.2	89.6	75.4
C	158.9	162.7	145.8	83.7	72.4	47.5	70.7	71.9
B1	62.9	169.5	155.9	80.9	73.1	53.5	75.8	76.4
B2	56.9	181.1	174.1	120.0	124.0	120.9	82.3	82.6
L2	176.2	85.2	172.9	74.4	51.8	64.5	97.3	79.8
L1	163.9	106.4	178.9	45.3	43.7	46.3	70.6	64.9
R1	163.1	169.3	57.8	182.2	171.5	157.4	68.6	68.8
R2	183.3	175.4	84.6	148.8	146.6	164.1	87.4	79.7
mean	*143.0*	*153.6*	*142.3*	*101.3*	*96.5*	*82.1*	*83.8*	*74.3*
std dev	*47.8*	*33.8*	*39.9*	*38.3*	*41.6*	*47.1*	*14.5*	*6.0*

Table 4.11 Moisture content in timber samples collected 9.25 months post-burial, Swan River sleeper site.

sample	P20	P30	P50	O30	J20	J30
T4		118.8	146.0		33.3	112.2
T3		45.5	93.7	110.4	97.3	99.5
T2	97.3	37.9	81.8	72.4	100.1	97.9
T1	147.2	35.8	83.0	54.1	102.5	94.7
C	179.0	38.1	78.2	53.9	101.7	90.1
B1	164.0	60.2	76.5	73.6	105.0	82.8
B2	162.6	153.2	126.6	105.7	110.6	93.6
L2	160.2	55.8	65.4		88.8	73.6
L1	163.9	35.7	43.1	81.5	102.3	89.1
R1	171.9	172.0	164.2	70.4	105.9	89.0
R2	170.7	144.1	154.5		93.2	78.8
mean	*157.4*	*81.6*	*101.2*	*77.8*	*94.6*	*91.0*
std dev	*24.2*	*53.9*	*40.0*	*21.0*	*21.2*	*10.6*

Vertical cross-sections of the pine (P50, D2) and oak (O30, D1) timber blocks recovered after 20.5 months of burial at the James Matthews sleeper site are shown in Figure 4.25. Hoffman and Jones (1989:38) note that freshly cut cross-sections of waterlogged wood display zonation, distinguished by differences in colour or hardness. These colour differences are evident in Figure 4.25, with water penetration shown progressing evenly as a darker band approximately 2–3 cm thick in the top and bottom (longitudinal grain direction) of the pine

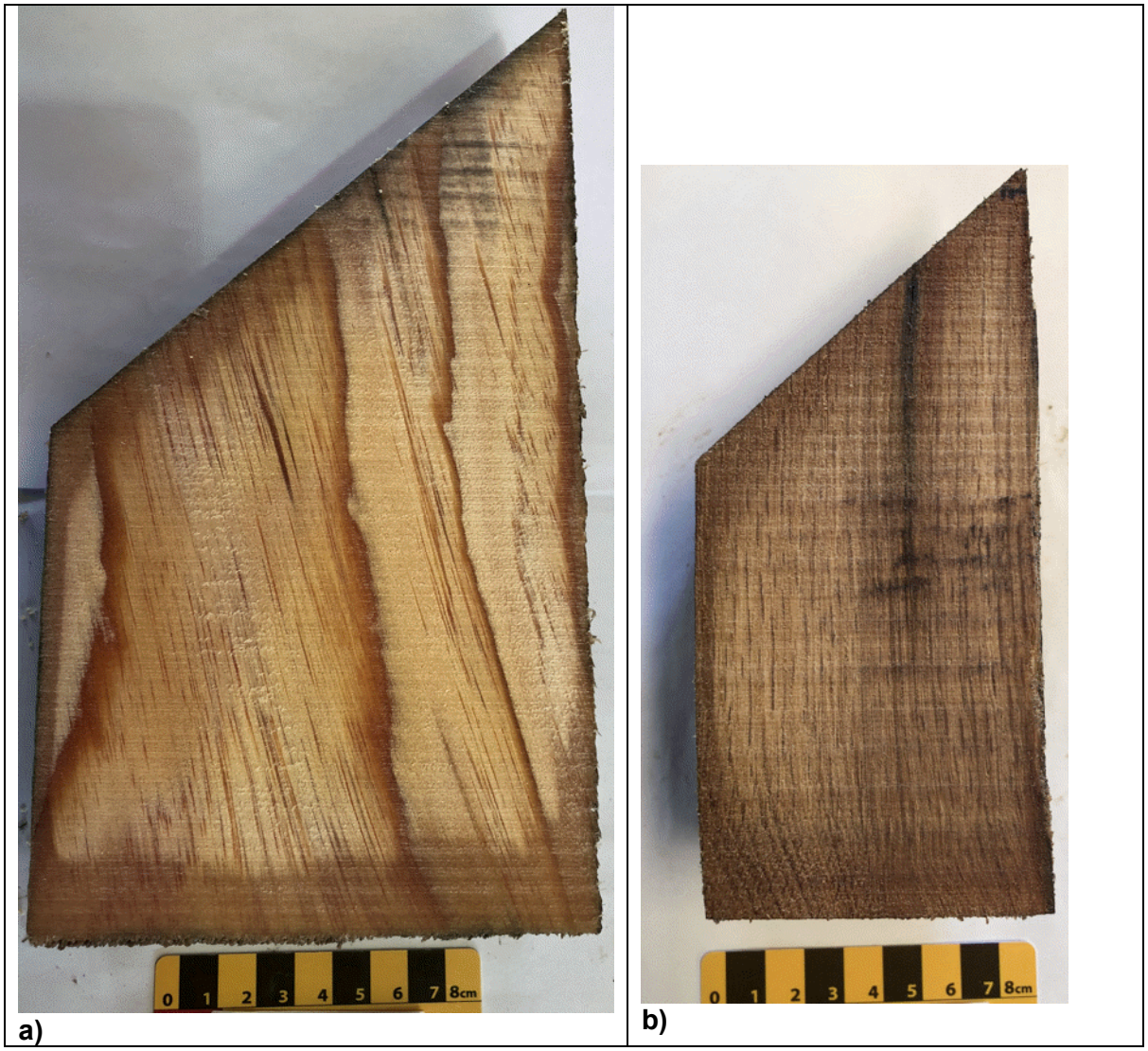

Figure 4.25 Seawater penetration in blocks recovered 20.5 months after burial at James Matthews sleeper site: (a) pine; and (b) oak timbers.

timber block, and 1.5–2 cm thick in the oak timber block. These outer waterlogged bands are narrower (≤0.5 cm) in the cross-grain direction. Waterlogged tracheids, which are long narrow tubular cells running longitudinally in wood, and vessels can also be seen (Grattan 1987:57).

There is less water penetration along the upper tapered edge compared to the flat base. This may have resulted from the diagonal taper cutting through the interconnecting cells (intervascular pits) thus reducing not only the lateral, but also the vertical, passage of seawater. The areas of discolouration match the measured density differences shown in the previous figures between the outer (longitudinal grain direction) and inner cubes of the pine and oak timber blocks. These same features were observed in the vertical cross-sections of pine, oak and jarrah timber blocks recovered after burial in the Swan River (Figure 4.26). The

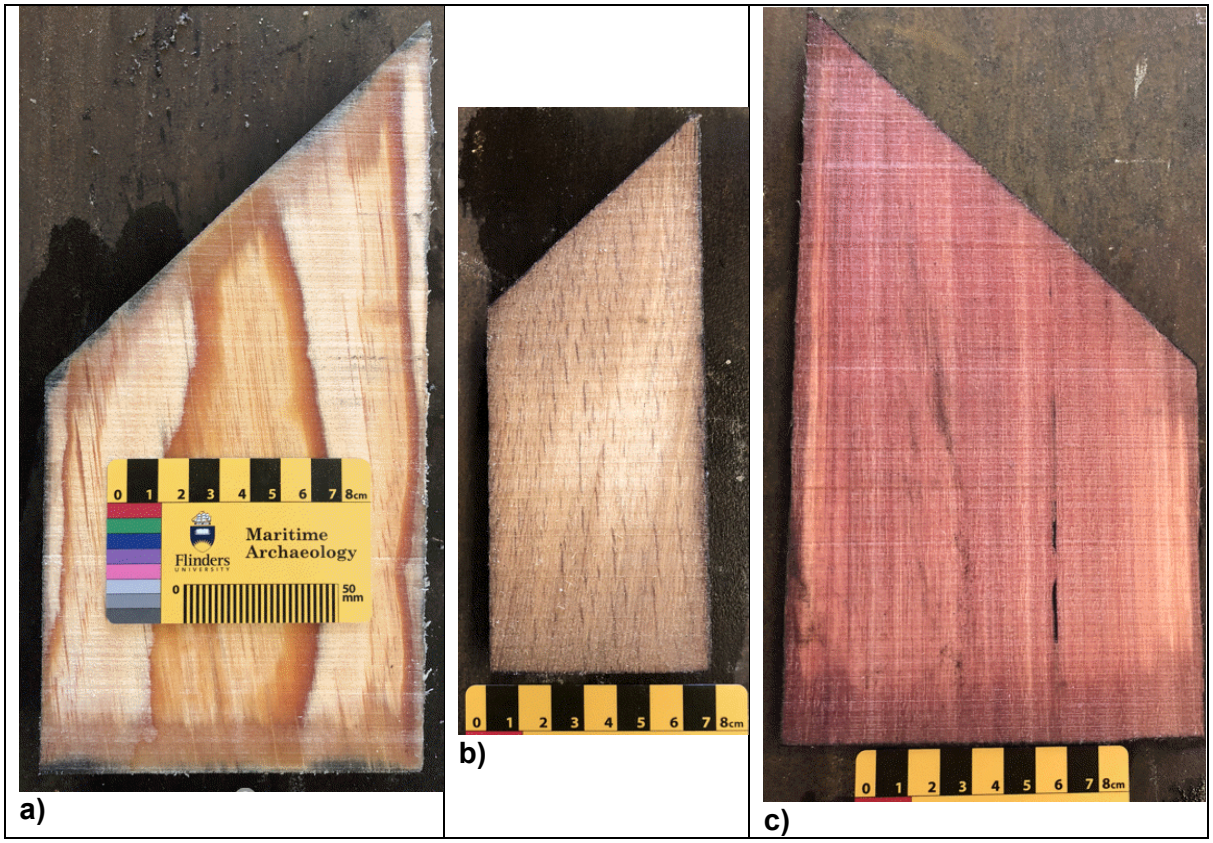

Figure 4.26 Seawater penetration in blocks recovered 9 months 1week after burial at Swan River sleeper site: (a) pine; (b) oak; and (c) and jarrah timbers.

respective difference in the outer and inner cube densities can be seen in the in Table 4.9. Notwithstanding these differences, the current depths of within-block bulk density variability will not be vertically distinguished acoustically for two reasons. Firstly, the timber sleepers are buried with their longitudinal grain in the horizontal direction, with a thinner water penetration layer on the upper face of the sleeper. Secondly, the SBP requires a reflector (a layer of different density or acoustic impedance) of approximately five centimetres thick in order to generate a discernible reflection. As a consequence, the block averaged density values were used to describe the respective timber sleepers at the time when SBP measurements were undertaken.

The timber density duration-variability is depicted in Figures 4.27 to 4.29. These figures respectively show the bulk and basic density time series for pre-burial, 9.2 months post burial and 20.5 months post-burial for oak, pine and jarrah timber blocks. The bulk density of the recovered oak, pine and jarrah timber blocks were all, with one exception, significantly higher than their pre-burial value. However, the variability within the single or duplicate blocks buried for 9.2 and 20.5 months were high, with no significant differences associated with burial times or burial depths. With only several exceptions there were no significant differences between

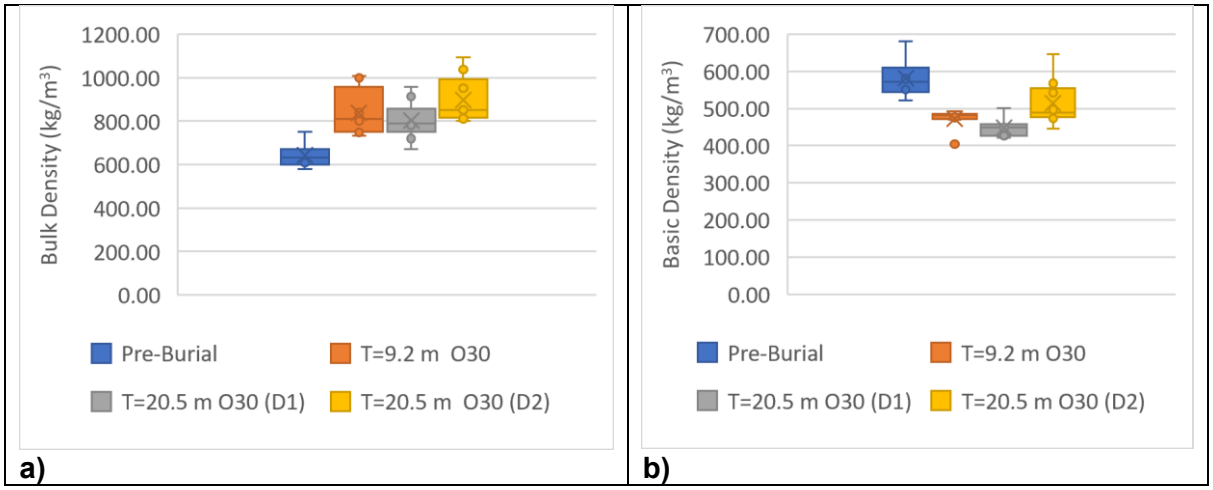

Figure 4.27 Density duration variability, oak timber: (a) bulk density; and (b) basic density.

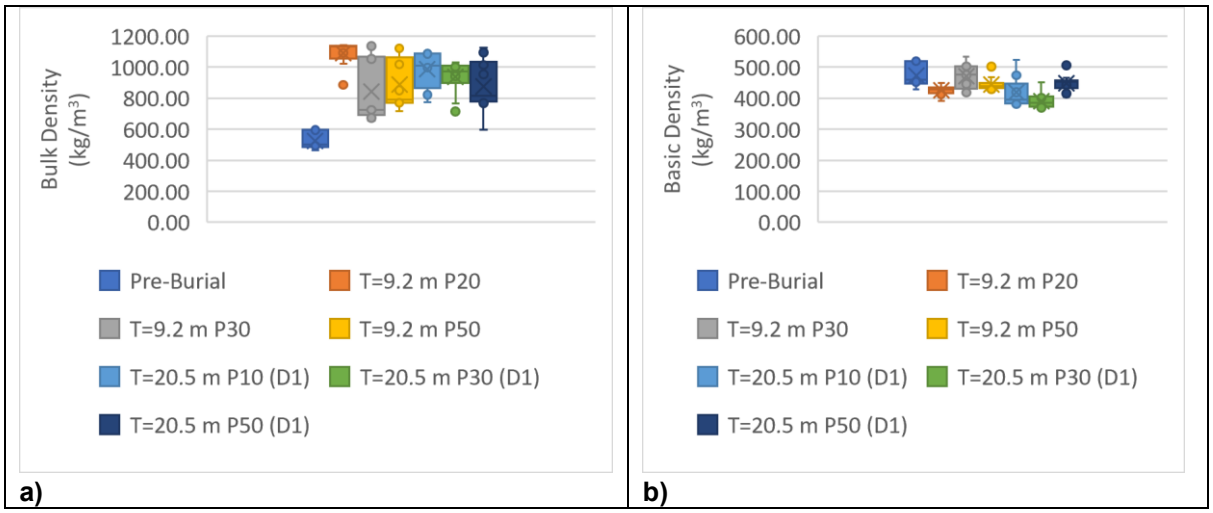

Figure 4.28 Density duration variability, pine timber: (a) bulk density; and (b) basic density.

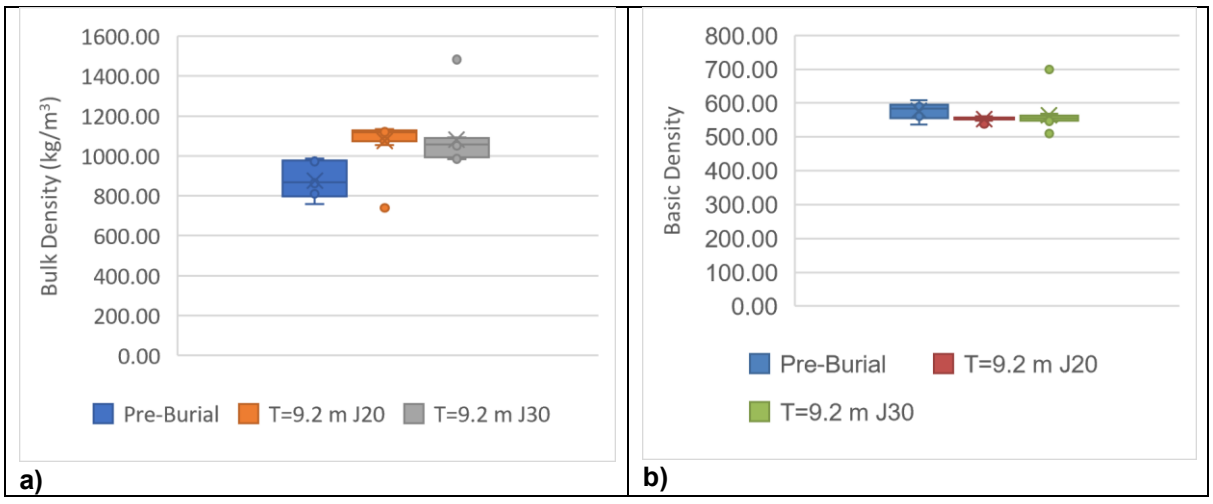

Figure 4.29 Density duration variability, jarrah timber: (a) bulk density; and (b) and basic density.

the post-burial basic density values and their corresponding pre-burial value. The mean values were, however, lower than pre-burial, and like the bulk density values, their variability masked any significant differences associated with burial time and burial depths.

Parametric SBP data

Trace data

The parametric SES-2000 *compact* SBP produces low-frequency (4–15 kHz) seabed penetrating pulses as an outcome of the interaction between two simultaneously generated high sound pressure, high frequency (~100 kHz) sound waves, transmitted at slightly different frequencies. Innomar's data acquisition software (SESWIN) is equipped with online signal processing capabilities. These include real-time screen display of results, incorporation of externally recorded data such as precise x, y and z positional information and heave compensation, as well as digitizing and storing the recorded echo trace data for subsequent data processing (Innomar 2017). During field data collection, the 15 kHz low frequency signal was selected for recording. This followed trials to assess the frequency range (4–15 kHz) which produced the clearest echo trace results. The high frequency signal was also recorded as it produced a better definition of the seabed surface and, under some sedimentary conditions, may also identify reflectors associated with very shallow buried material. Following field activities, all recorded SBP files were exported in RAW format, representing the full wave-form data, into Innomar's proprietary post-processing analysis software (ISE version 2.9.5). Initial visual inspection of all records was undertaken to assess for completeness. This included checking latitude/longitude data for all trace locations, the appearance of reflectors indicating potential buried sleeper locations and/or the appearance of acoustic signatures of sleeper endplates sitting above the seabed.

The ISE software visually presents the acoustic data as echo plots—seismic profiles with a 2D curtain of individual acoustic trace reflection data (vertical) along the length of the SBP run (horizontal)—using a pre-selected acoustic wave speed in both the water column and in the sediment of 1500 m/s. Unprocessed RAW low frequency (LF) (15 kHz) data typically appears as in Figure 4.30. Figure 4.30a displays 525 individual side-by-side vertical traces from trace 600 on the left-hand side to trace 1125 on the right-hand side for run 20170608 025024. These data were collected at the James Matthews sleeper site using the vessel-based transducer mounting. The traces commence at the top of the central screen image at a depth 1 m below the transducer head extending to the bottom of the screen image at a depth of 5 m, and are shown with a four times vertical exaggeration (V.E.). The data is displayed using a greyscale prior to interpretation (Mason 2018). In Figure 4.30b, this same data is interpreted and displayed in the ISE red-white-black colour scale palette to highlight

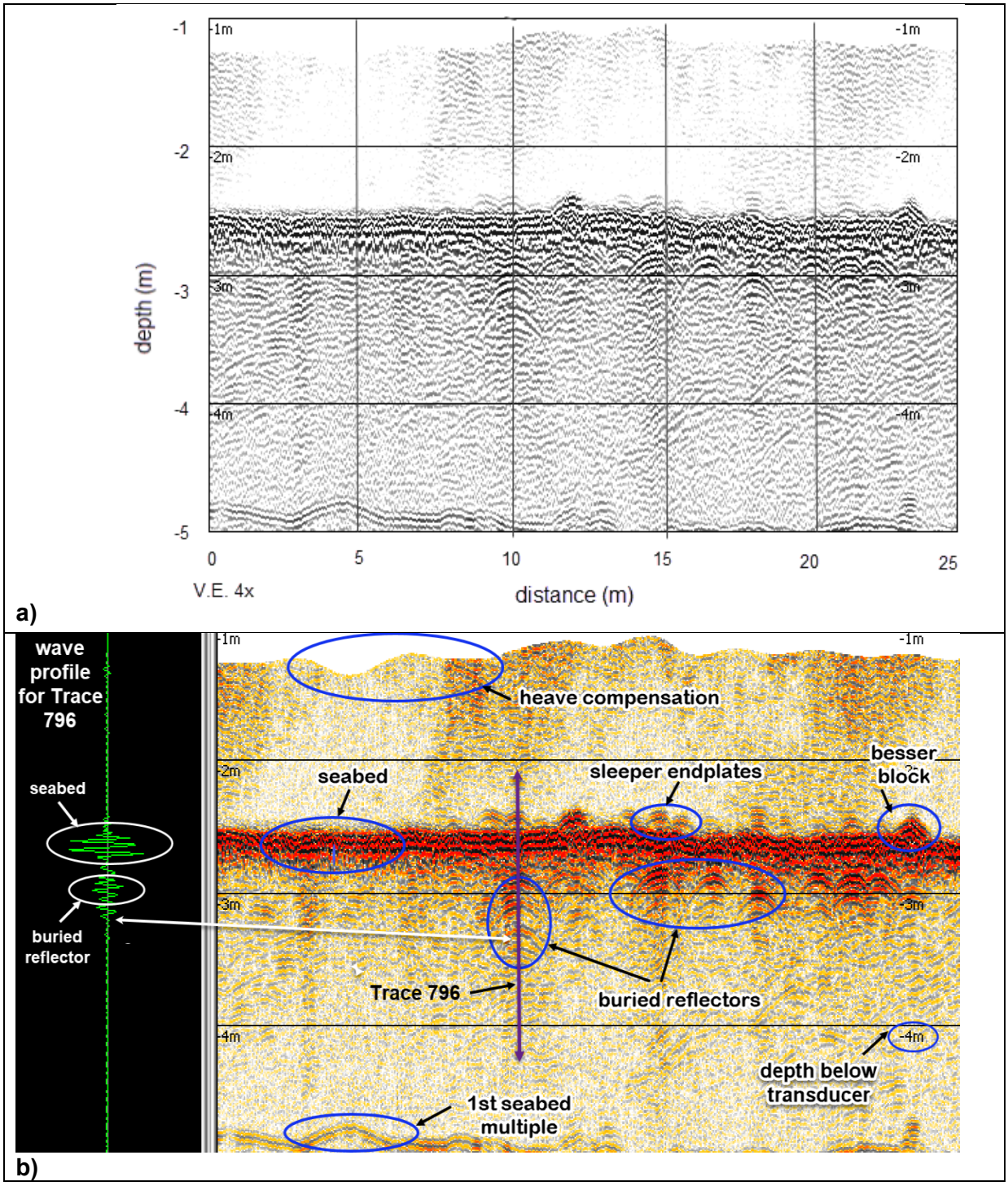

Figure 4.30 LF unprocessed echo plot, from trace 600 to trace 1125, run 20170608 025024; (a) greyscale, uninterpreted; (b) red-white-black colour scale with interpretations.

the location of buried reflectors. Distinguishable features in this echo plot are: the seabed at around 2.5 m below the transducer head; the 1st seabed multiple at approximately twice the seabed depth; the correction for vessel heave at the top of the curtain; reflectors from potential buried sleepers (the 'buried reflectors') shown as inverted hyperbolas below the seabed; and the besser blocks and endplates protruding above the seabed. The colour scale used in this

plot identifies maximum positive amplitudes in black, and maximum negative amplitudes in red, with lesser magnitudes fading in colour from black to grey and from red to a browny-orange, ultimately to white. To the left of the seismic profile is a typical individual echo wave (black background), in this case for trace 796. This wave shows recorded amplitudes of different magnitude as it penetrates through the seabed to a depth of 5 m. On the right-hand side of the (vertical) wave centre-line, the amplitudes are positive, on the left-hand side the amplitudes are negative.

A post-processing option in ISE is to demodulate the RAW full wave-form, the purpose of which can assist in visually identifying buried reflectors. Demodularisation in this case is a process to estimate the envelope of the wave profile using the Hilbert transform (Jens Wunderlich pers. comm. 2019). Figure 4.31 shows the same LF echo plot as in Figure 4.30, but demodulated. The wave profile for trace 796 on the left-hand screen in Figure 4.31b has been converted from full wave form (showing positive and negative amplitudes) to a magnitude only envelope outline. The colour scheme in Figure 4.31b has been changed to the ISE 10-colour scale which reflect the absolute magnitude of the reflected wave traces, with the highest magnitudes shown in red, and with decreasing magnitudes shown in yellow to green to dark and light blue, ultimately to white.

By comparison to Figure 4.30, there is greater visual clarity around buried reflectors which now appear as red ‘blobs’ rather than inverted hyperbolas. Intermittent, low-level reflections appear in the water column which may result from turbidity or suspended sediment particles from the nearby Cockburn Cement reclaimer operations, or in other situations (not in this case due to the forward mounting of the transducer head) from air bubbles caused by propeller cavitation. The colour transition from green to blue approximately 1–1.5 m below the seabed indicates very little acoustic wave energy was reflected beyond this depth. The high frequency (HF) (100kHz) data can also be used to effectively analyse SBP data on sites with shallow-buried reflectors. depicts the same trace range for run 20170608 025024 using demodulated HF data. Here the tops of the endplates which protrude above the seabed are clearly discernable and the seabed interface is sharper with a higher and narrower peak in the individual demodulated wave profile for trace 796. The deeper buried reflectors are, however, no longer distinguishable. Little acoustic wave energy was reflected from depths greater than 0.5 m below the seabed.

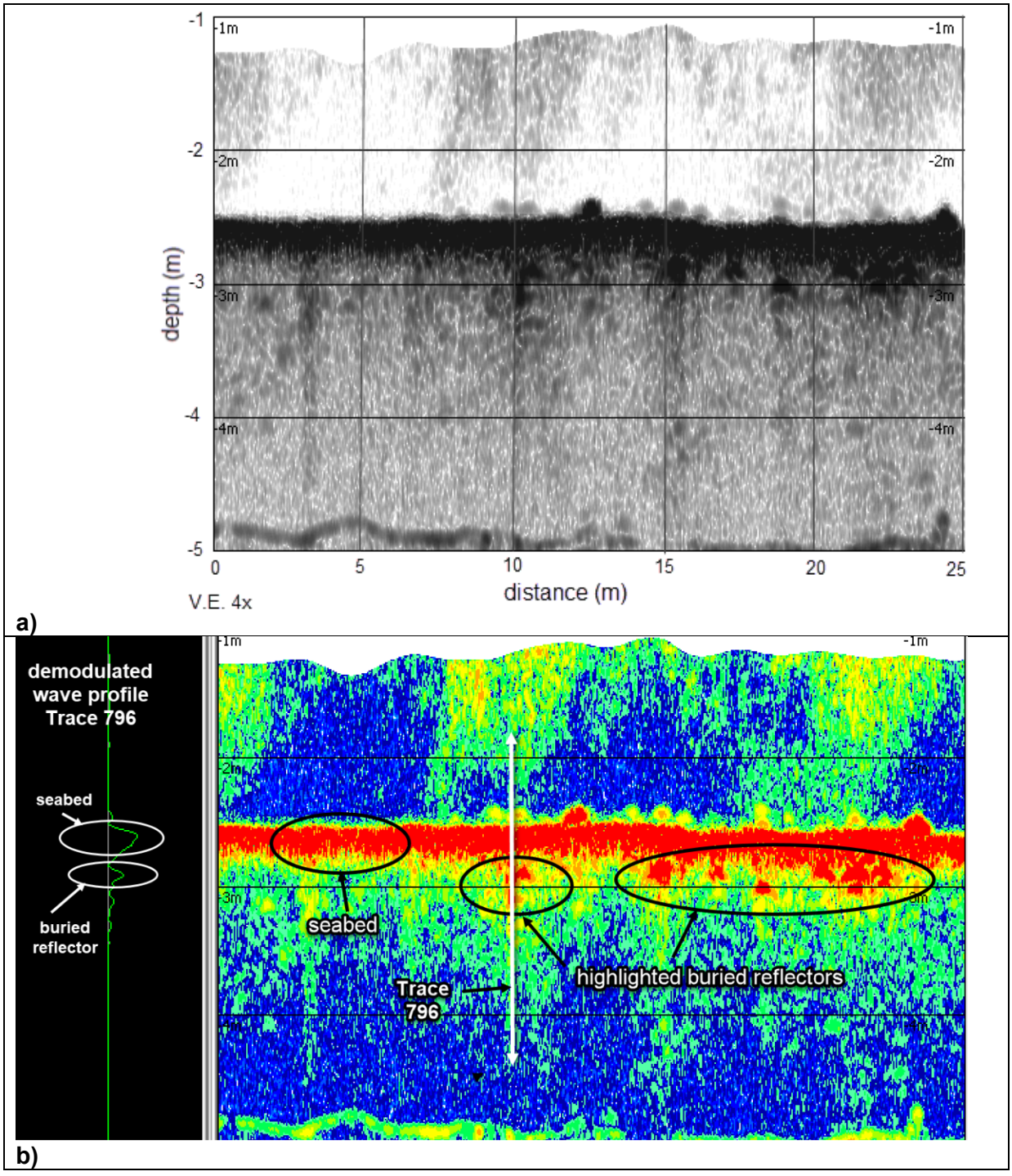

Figure 4.31 LF demodulated echo plot, from trace 600 to trace 1125, run 20170608 025024; (a) greyscale, uninterpreted; (b) 10 colour scale with interpretations.

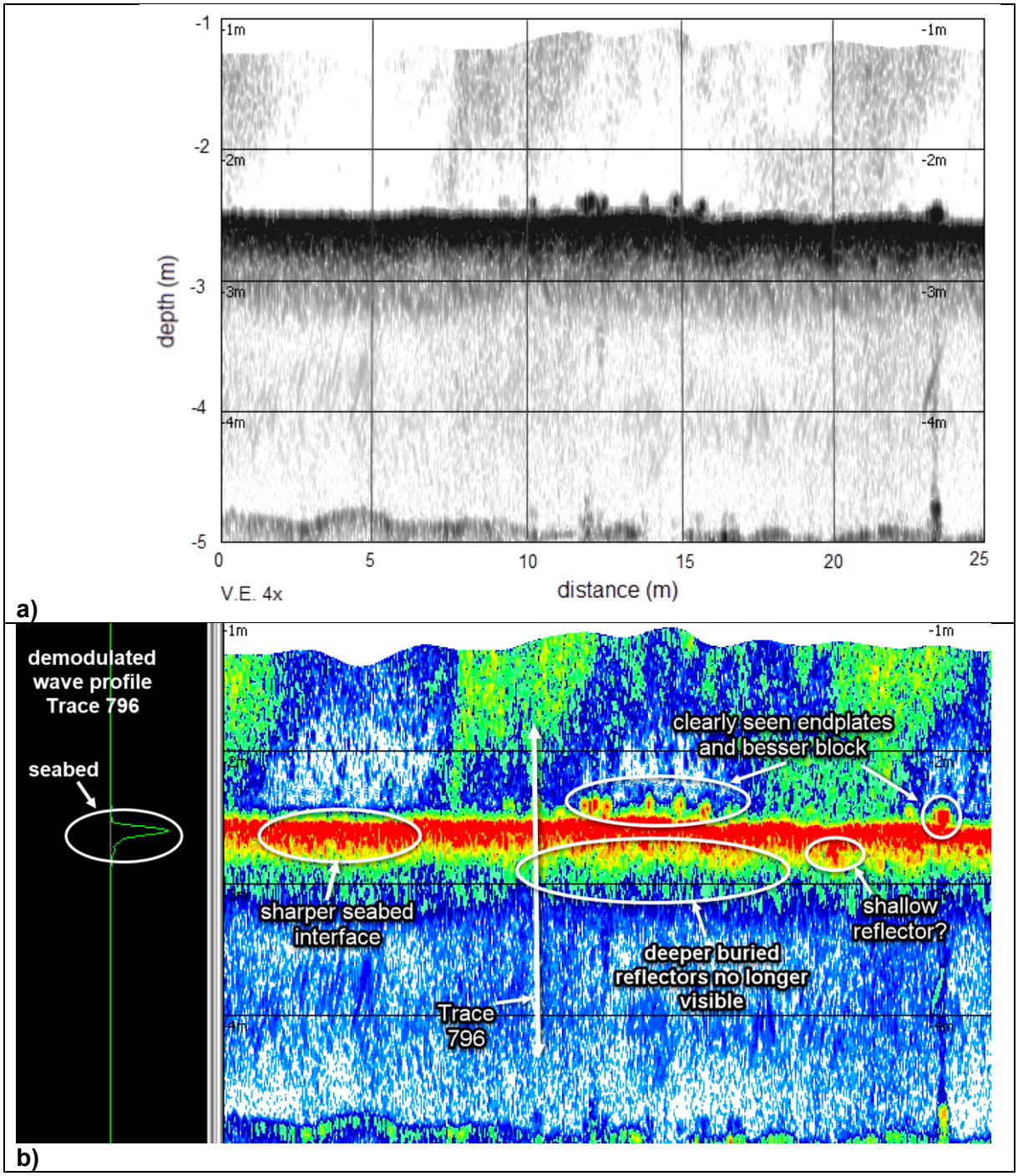

Figure 4.32 HF demodulated echo plot, from trace 600 to trace 1125, run 20170608 025024; (a) greyscale, uninterpreted; (b) 10 colour scale with interpretations.

The survey speed (speed of transducer head traversing the row of buried sleepers) and the height of the transducer head above the seabed change the density of the echo signals and the visual appearance of the echo plots and reflectors. Figure 4.33 LF unprocessed echo plot, from trace 4650 to trace 5500, run 18052018 135105; (a) greyscale, uninterpreted; (b) red-white-black colour scale with interpretations.

to 4.35 respectively depict the LF unprocessed, LF demodulated and HF demodulated echo plots between traces 4650 and 5500 for run 18052018 135105. These data were collected at the same offshore site, but in this case, the transducer head was mounted on the sled rather than from the vessel. Due to the much slower travel speed of the transducer head when mounted on the sled (0.15 m/s compared to 2.0 m/s when vessel mounted) and with the same constant ping rate, a more than a tenfold increase in the number of traces per distance travelled were recorded. Without decimating the data files, the vertical exaggeration has decreased on the figures and the reflectors appear much wider. The 'stacking' function in the ISE2 software can be used to compress the appearance of the data by averaging across a selected number of echo signals, however this function is generally not recommended when assessing fine scale buried objects (Innomar 2017). With the transducer head mounted on the sled 905 mm above the seabed, the nearfield acoustic wave generation zone, located immediate area under the transducer head, is visible in the top 0.5 m in the central screen and in the wave profile screen. This nearfield zone is thinner for the high frequency waves compared to the low frequency waves (Figure 4.35 vs. Figure 4.34).

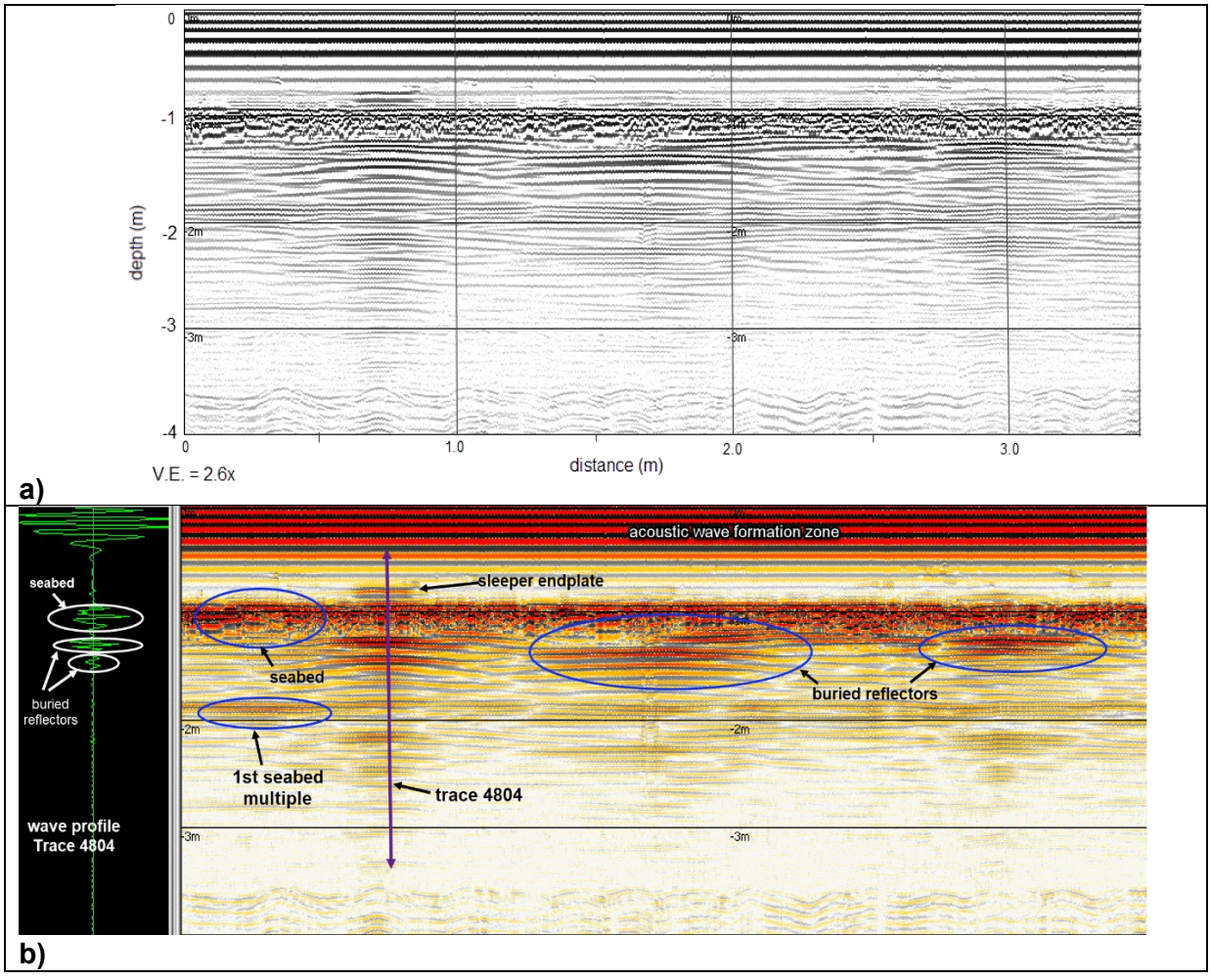

Figure 4.33 LF unprocessed echo plot, from trace 4650 to trace 5500, run 18052018 135105; (a) greyscale, uninterpreted; (b) red-white-black colour scale with interpretations.

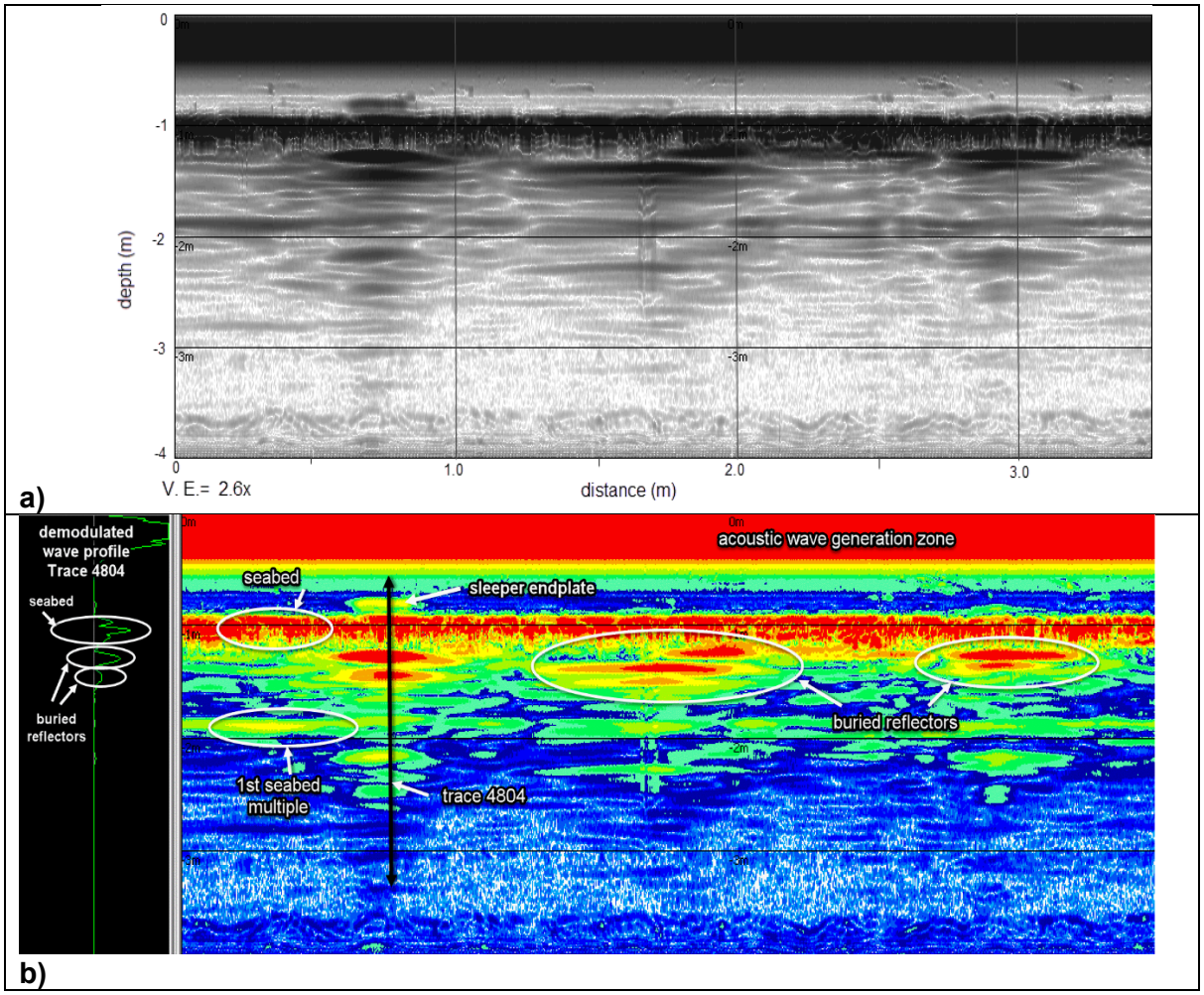

Figure 4.34 LF demodulated echo plot, from trace 4650 to trace 5500, run 18052018 135105; (a) greyscale, uninterpreted; (b) 10 colour scale with interpretations.

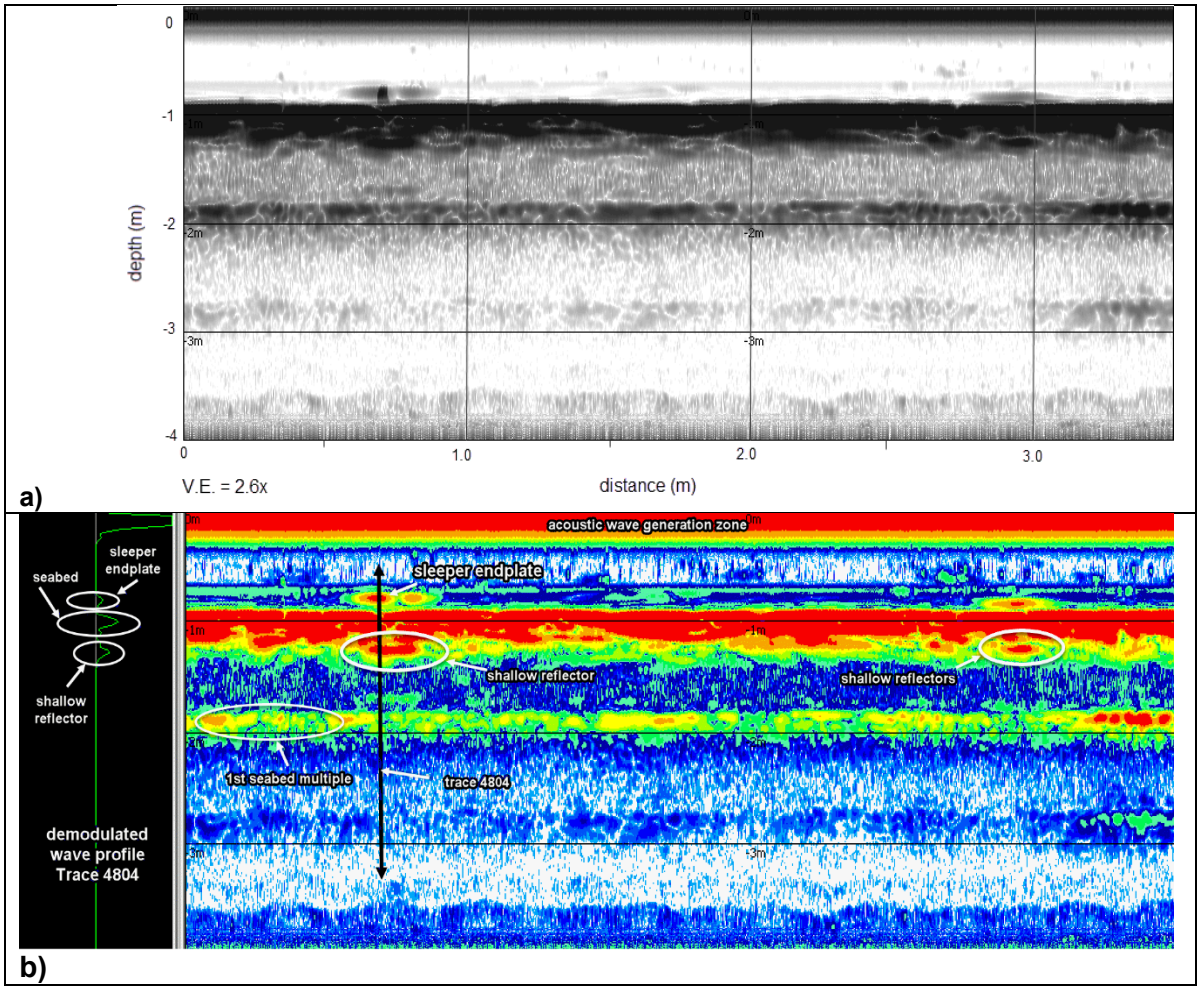

Figure 4.35 HF demodulated echo plot, from trace 4650 to trace 5500, run 18052018 135105; (a) greyscale, uninterpreted; (b) 10 colour scale with interpretations.

A total of eight SBP runs were selected for detailed trace analyses and are listed in Table 4.12. Two of these SBP runs (20170608 -024600, -025024) were undertaken in June 2017 at the James Matthews sleeper site, and as described in Chapter 3, were collected using the vessel mounted SES-2000 *compact* SBP. Whilst a number of other SBP runs were made during this survey, the lack of control over the precise positioning of the vessel along the buried sleeper line due to tide and wind conditions meant that only approximately half of the 17 sleepers buried at the time were identified, most of which were in these selected runs. Four SBP runs were selected from those measured in May 2018 using the sled mounted SBP with the transducer position set to the highest level above seabed. At this time all 26 sleepers were buried at the offshore James Matthews sleeper site. In runs 18052018 -135105 and -135516, the position of each trace was directly recorded and stored in the ISE software with centimetric accuracy. For runs 18052018 -132252 and -135912 Bluetooth© communication issues between the RTK and SES units meant that the precise position of each trace was indirectly

Table 4.12 SBP runs selected for detailed analyses.

								assess variability?			
location	**SBP run**	**date collected**	**vessel or sled mounted transducer**	**height of transducer above seabed (m)**	**lat/long recorded**	**no. of reflectors potentially identified**	**correct / false id of reflectors?**	**reflector locations**	**DoB estimates**	**reflection coefficient estimates**	**comments**
James Matthews sleeper site	024600	June 2017	vessel	2.426	direct	8	yes	yes	yes	yes	with 2018 data allows assessment of changing timber density on RC
	025024			2.593	direct	10	yes	yes	yes	yes	
	135105	May 2018	sled	0.905	direct	26	yes	yes	yes	yes	permits statistical assessment of reflector ID accuracy
	135516				direct	22	yes	yes	yes	yes	
	132252*				time stamp	26	yes	yes	-	-	
	135912*				time stamp	25	yes	yes	-	-	
Swan River sleeper site	125738	May 2018	sled	0.715	direction only	20	no	-	yes	yes	like a site without prior knowledge of actual buried material
	123344					14	no	-	yes	yes	

*analysed only for reflector identification and location accuracy

determined. In this instance both units recorded the same time stamps while the RTK unit additionally recorded the location at each time interval. The identical time stamps recorded in both the SESWIN software and the RTK's CS20 logger were identified, and the trace position in the SESWIN data established from the time-matched RTK records. SBP runs were undertaken at the Swan River sleeper site in May 2018 using the sled with the transducer head set as high as possible off the riverbed, but still ensuring the top of the transducer head was below the water surface. Unfortunately, the same Bluetooth© communication issues occurred, but in this survey (and due to operator error) the RTK unit also failed to record the time stamps and latitude/longitude positions of the moving sled. Two runs (17052018 -125738 and -123344) were selected for detailed analyses, even though there could be no final confirmation that the location of some or all buried sleepers were correctly identified. In the selected runs, either the buried sleeper or endplates were clearly identified, and hence reflector depths and amplitudes could be extracted and analyzed—much like a site where the precise location of buried material is unknown.

Detailed analysis of the selected runs commenced with interpolation of the co-ordinate positions of each trace. The reason for this was that the update rate of the GNSS G2 real time satellite positioning and the RTK DGPS system were slower than the ping rate of the SES-2000 system. For each run, all traces were thoroughly examined on the ISE screen using the LF unprocessed, LF demodulated and HF demodulated echo plots to identify potential reflector locations associated with buried sleepers. Five individual adjacent traces were initially selected for each identified reflector and extracted using the ISE export facility. These traces were centered on the highest point of the hyperbola (LF unprocessed), the mid-point of a red reflector blob (LF demodulated) and/or the central position of the surface protruding end plate (HF demodulated) in the three respective echo plots. The wave profile data from each of these five individual traces, for each potential reflector, and for all runs, were transferred into Excel. Here, larger scale plots of each unprocessed and demodulated LF and HF trace were plotted and examined in detail. One set of typical plots for one reflector are shown in Figure 4.36.

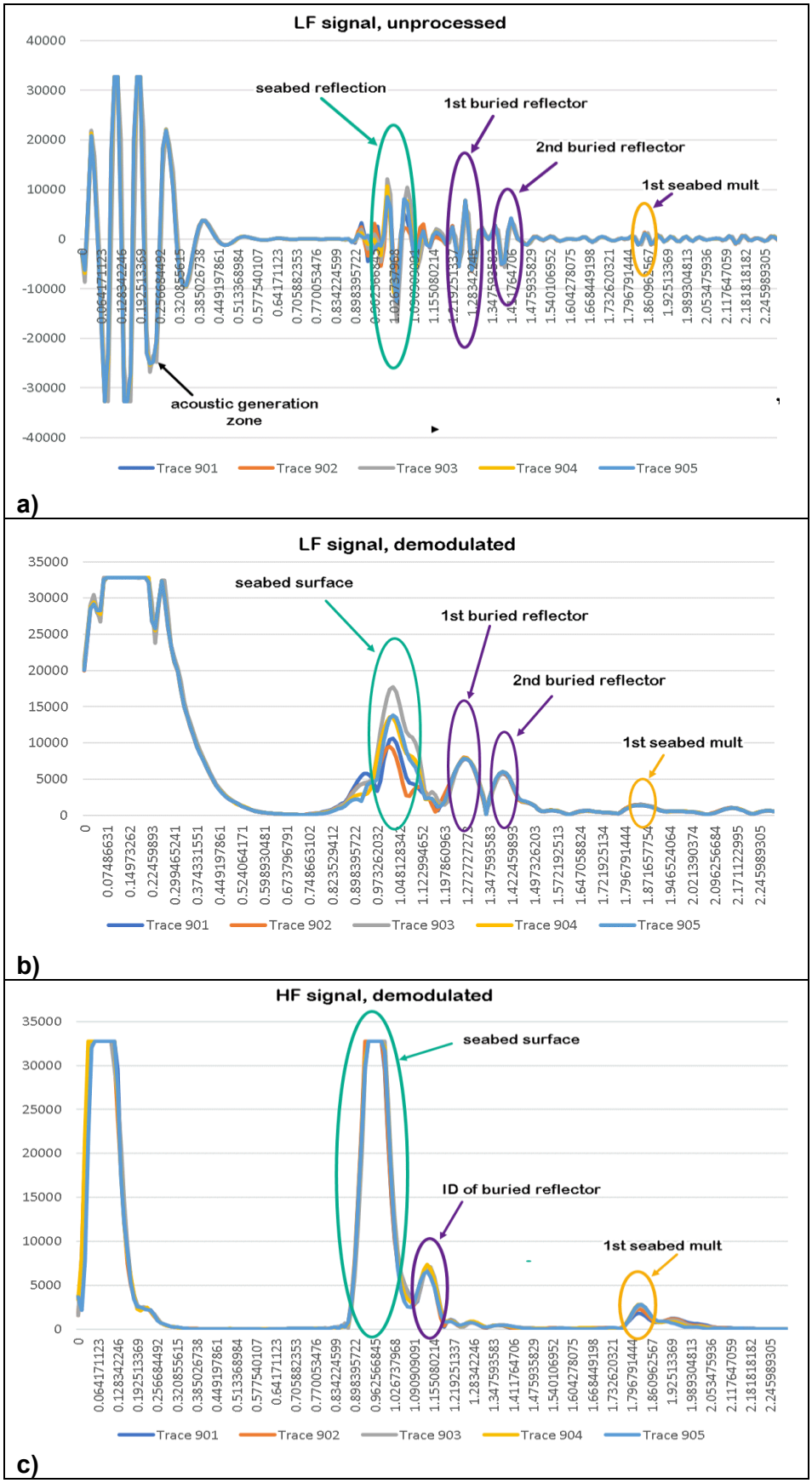

Figure 4.36 Five consecutive wave profile plots for reflector 903, run 18052018 135105; (a) LF unprocessed signal; (b) LF demodulated signal; and (c) HF demodulated signal.

Potential reflector details were tabulated only when: a) there was a consistency across a distinct and separate peak in all five consecutive LF demodulated traces; and b) the magnitude of the unprocessed raw wave-form amplitude increased significantly at the depth corresponding to the LF demodulated peak, as shown in Figure 4.36. If LF demodulated peaks occurred but were composed of fewer than five consecutive traces, or if there were no clear corresponding changes in the unprocessed amplitudes across consecutive traces, then that demodulated peak was not considered to be a reflector associated with one of the buried sleepers. If three or four consecutive traces met the above criteria, but not all five, then additional adjacent traces were extracted and incorporated into the Excel plots. If with the addition of the adjacent traces the consecutive trace criteria was subsequently satisfied, then the central trace of those latter five was noted as the likely reflector location. The HF demodulated plot was used to identify the depth of the seabed surface and the 1st seabed multiple, as well as providing potential identification of shallow reflectors for further assessment using the LF unprocessed and demodulated plots.

Once a potential reflector location was determined, the acoustic properties associated with those five selected wave traces were extracted, tabulated and variances determined. Table 4.13, as an example, depicts the trace data shown in Figure 4.36. Raw amplitude data (both magnitude and sign for the seabed, the first buried reflector, a second buried reflector and the 1st seabed multiple) are shown at the top of the table for five consecutive wave traces centering on trace 903 from run 18052018-135105. The trace phase at each feature is noted as positive or negative depending on the sign of all or the majority of the amplitudes—this phase data will be referred to in the following chapter when interpreting individual traces as they respectively reflect from the top and bottom a buried sleeper. The mean amplitude and standard deviation (SD) values were determined at each feature from the absolute value of the trace amplitudes. The relative, or normalized, standard deviation (RSD) was calculated by dividing the SD value by the mean. The RSD allows comparison of relative variability when mean values are significantly different. For example, in Table 4.13 the mean values for the seabed amplitude, 1st reflector amplitude, 1st seabed multiple amplitude and all associated depths are each one or two orders of magnitude different. It would be otherwise difficult to appreciate the relative variability in each mean or depth value based only on the magnitude of their respective, but varying, standard deviation values. The depth of burial (DoB, in cm) for each identified reflector was determined by subtracting the seabed depth (LF and/or HF value) from the depth of the 1st reflector (LF value). If two buried reflectors are identified, then the second reflector may be the underside of the piece of buried material. In this case the phase of the second reflected amplitude should be the opposite the phase of the first reflected amplitude (+/- or -/+) and the

thickness of the material is obtained by subtracting the depth of the 1st reflector from that of the second.

Table 4.13 Raw data table for reflector 903, run 18052018-135105.

amplitudes	trace 901	trace 902	trace 903	trace 904	trace 905	phase
seabed	-8195	8249	-16731	-11106	-12666	-
1st reflector	7652	7867	6424	7771	7750	+
2nd reflector	-4780	-5166	-5659	-4911	-5059	-
1st seabed multiple	1232	1309	1252	1159	1170	+

						mean	SD	RSD
seabed amp	8195	8249	16731	11106	12666	11390	3546	31%
1st reflector	7652	7867	6424	7771	7750	7492	602	8%
2nd reflector	4780	5166	5659	4911	5059	5115	337	7%
1st seabed multiple	1232	1309	1252	1159	1170	1224	62	5%

depths (LF) (m)	trace 901	trace 902	trace 903	trace 904	trace 905	mean	SD	RSD
seabed	1.027	1.016	1.027	1.016	1.027	1.022	0.006	1%
1st reflector	1.262	1.262	1.273	1.262	1.262	1.264	0.005	0%
DoB	*0.235*	*0.246*	*0.246*	*0.246*	*0.235*	*0.242*	*0.059*	*2%*
2nd reflector	1.390	1.390	1.390	1.390	1.390	1.390	0.000	0%
thickness	*0.128*	*0.128*	*0.118*	*0.128*	*0.128*	*0.126*	*0.005*	*4%*
1st seabed multiple	1.850	1.840	1.850	1.840	1.840	1.844	0.006	*0%*

depths (HF) (m)	trace 901	trace 902	trace 903	trace 904	trace 905	mean	SD	RSD
seabed	0.963	0.963	0.963	0.963	0.963	0.963	0.000	0%
1st reflector	1.134	1.134	1.134	1.134	1.134	1.134	0.000	0%
DoB	*0.171*	*0.171*	*0.171*	*0.171*	*0.171*	*0.171*	*0.000*	*0%*

The graphical and tabulated trace results of all identified reflectors for all SBP runs analysed in full detail are incorporated in voluminous spreadsheets accessible upon request from Flinders University. A summary of amplitude and depth mean, SD and RSD values for each reflector, coded by the central trace number, from each SBP run, are included in Appendix D, Tables D.9 to D.14. In these tables the phase of the amplitudes (+/-) is included.

The seabed level (distance from the underside of the transducer head to the seabed surface) from both the LF demodulated and HF demodulated data was extracted for comparison purposes. For the traces in all five SBP runs, Table D.9 to D.14 show that the HF demodulated seabed levels are lower (typically by 0.027–0.065 m) than those determined from the LF

demodulated data. These HF estimates are closer to the actual depths, 0.905 m at the James Matthews sleeper site and 0.715 m at the Swan River sleeper site, based on the measured distance from the sled mounted transducer head to the seabed surface. This corresponds to Innomar's (2018) recommended use of the HF data to determine seabed levels. For each reflector trace, the RSD values (reflecting the variability between all five traces used to determine the reflector characteristics) ranged from 0% (all values identical) to 3.6%, with mean RSD values across SBP runs ranging from 0.5% to 0.7%. This reveals very low levels of variability, an example of which can be demonstrated with the HF demodulated seabed levels in Table D.9. With a mean of 2.426 m, standard deviation of 0.015 m and RSD of 0.6%, and assuming the trace data seabed levels are normally distributed, then 95% of all derived HF demodulated seabed levels would be expected to lie in the range 2.396–2.456 m.

The variability around the determination of the depths of the 1st buried reflector and the 1st seabed multiple is equally very small as the variability determined for the seabed level. However, the variability was significantly higher for the determination of the DoB for each reflector. For consistency, the depths derived from the LF demodulated traces were used and the DoB determined by subtraction of the seabed depth from the depth of the 1st buried reflector, across all five traces. The mean RSD values across all runs ranged from 4.4–11.9%, with lower mean values in the Swan River, and RSD for individual reflector depths of burial varied from 0% to 30%.

Second (deeper) buried reflectors were identified in over 60% of the cases where the initial reflector was found. The occurrences differed across SBP runs (Table 4.14), were significantly less in the Swan River runs (17052018 -123344, -125738), but were identified across a similar range of burial depths from 13.7 cm to 52.5 cm. Average thicknesses across each run varied from 10.5 to 15.0 cm, with an associated RSD range 0–29.4%. Actual sleeper thickness was 12.5 cm.

The variability in phase associated with amplitude reflections from the seabed and from the 1st buried reflector is shown in Table D.15 in Appendix D. The variability was assessed across the five adjacent traces, for all 49 sleeper reflections identified in SBP runs 135105 and 135516. There was no clear relationship between the trace phases of the seabed and those of the 1st buried reflector. In 80% of the cases, the seabed amplitude phases differed across the five adjacent traces, and correspondingly, 60% of the 1st reflector amplitude phases also differed. The phase was the same (all positive or all negative) across all five traces for 26 (53%) 1st reflector amplitude reflections, however for 19 (39%) of those occurrences, the seabed phase differed.

Table 4.14 Sleeper thickness variability.

SBP Run	number of buried reflectors identified	% of times thickness of buried reflector was determined	range of DoB for buried reflector (cm)	average thickness/std dev (cm)
20170608 024600	10	50	21.0–52.5	14.0/2.5
20170608 025024	11	64	23.9–42.6	15.0/3.4
18052018 135105	25	56	15.2–40.0	12.7/2.3
18052018 135516	23	83*	6.4–45.1	11.7/2.9
17052018 123344	14	12	29.0	10.5/0
17052018 125738	16	38	13.7–36.0	10.9/1.8

*on reflector 3291 the thickness of the upper sleeper wasn't determined, but the gap to the lower (stacked) sleeper was measured.

The variability in estimating wave amplitude reflecting from the seabed surface, the 1st seabed multiple and any buried reflectors is an order of magnitude larger than for estimating their respective depths as presented in Table D.9 to D.14. For each reflector trace, the RSD values associated with seabed amplitudes ranged from 4.7% to 59%, with mean RSD values across SBP runs ranging from 25% to 35%. These much higher levels of variability can be demonstrated with the LF demodulated seabed amplitudes associated with Trace 898 in Table D.9. With a mean value of 23,010 and RSD of 40.1%, and again assuming the trace data seabed amplitudes are normally distributed, then 95% of all derived LF demodulated seabed amplitudes for this reflector would be expected to lie in the range 4,570–41,450 however the upper recording limit is restricted to 32,500. The RSD for the seabed amplitudes averaged across all runs is 29.6%. By comparison the RSD for the 1st seabed multiple averaged across all runs is 19.2%, and similarly, for the 1st buried reflector is 14.6% demonstrating that the greatest variability in acoustic properties is associated with estimating the amplitude of the seabed reflectors.

Location of sleeper reflectors

This section compares the locations of the identified reflectors in each SBP run to the known locations of the buried sleepers. Reliability estimates for these locational data and the accuracy of the DoB values derived from the SBP data are presented in the following chapter.

The latitude and longitude of the location of each buried sleeper is given in Tables A.5 and A.6 in Appendix A for sleepers buried at the James Matthews and Swan River sleeper sites, respectively. While the relative accuracy for each RTK DGPS position record was 6–12 mm, their absolute positional accuracy was an order of magnitude, or more, higher due to the near-zero water visibility conditions restricting the divers positioning the sled and RTK unit precisely

above the centre-line of the buried sleepers. This problem was exacerbated for sleepers 23, 24 and 25 where the accumulation of sand almost fully buried their respective endplates. As a consequence, and under the near-zero water visibility conditions, the sled wasn't located above these sleepers and their locations were not recorded by RTK DGPS. These positions had to be subsequently interpolated from earlier tape measurements between each of these sleepers. The RTK DGPS positions also revealed a tape measurement error between sleepers 8 and 9. The recorded distance using a tape was 0.8 m, however, the locations for sleepers 9–26 were short by one metremetre relative to the RTK DGPS locations. The obvious underwater error of recording 0.8 m instead of 1.8 m occurred due to the decreased water visibility and feint markings on the tape. The position of the two cement 'besser blocks' (BB) placed on the seabed at the NE end and mid-way along the line of buried sleepers were also recorded. The latitude and longitude positions of the best estimate for each sleeper and BBs were plotted using ArcGIS ArcMap 10.6.1 software (Figure 4.37).

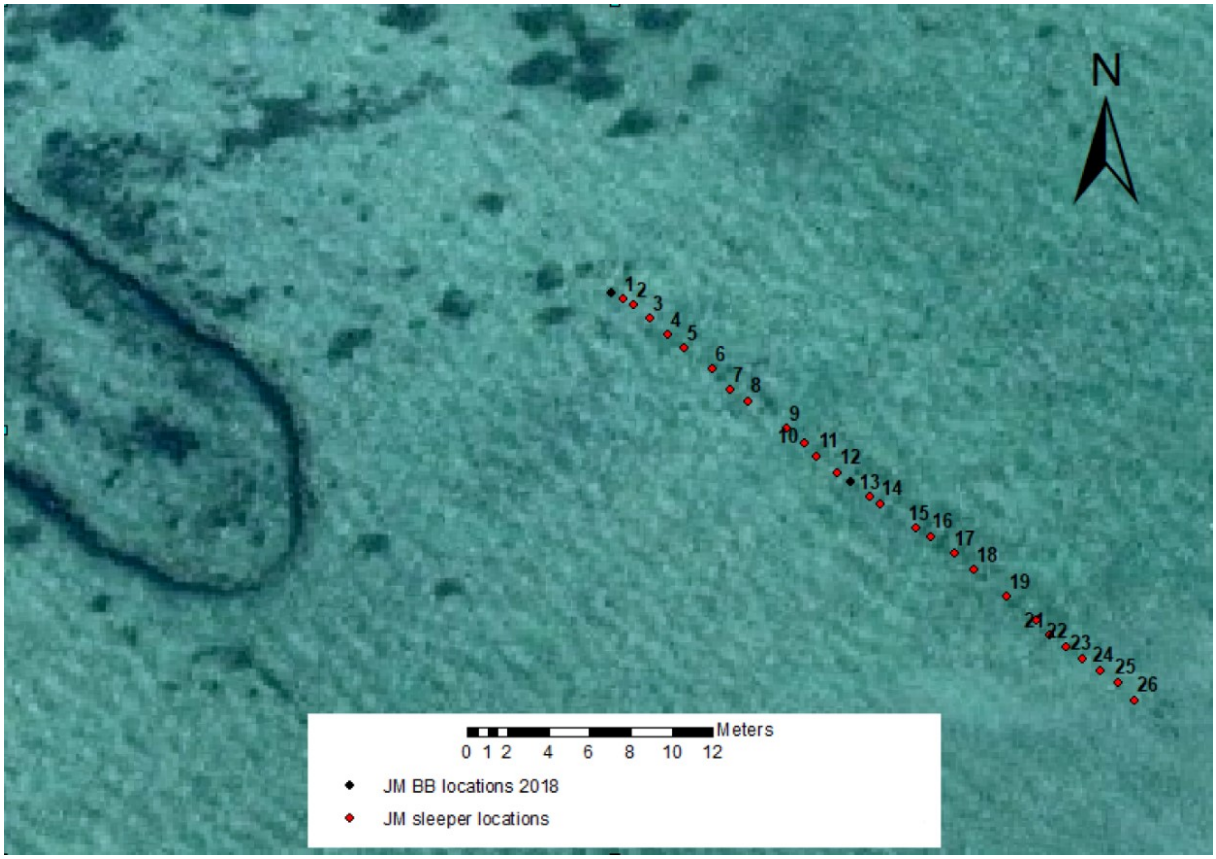

Figure 4.37 Buried sleeper and besser block locations, 2018, James Matthews sleeper site.

As previously discussed and listed in Table 4.12, comparable data for SBP reflectors representing potential sleeper locations are available for six runs at the James Matthews sleeper site. These locations are tabulated in Appendix D, Tables D1 through D6. Due to

Bluetooth© equipment communication failure, acoustic data associated with sleepers at the Swan River sleeper site are only available at relative, not absolute, locations. The latitude and longitude positions of the estimated centre-line locations of each SBP identified reflector, and the besser blocks, for the six runs at the James Matthews sleeper site were plotted against the sleeper locations in ArcMap 10.6.1 (Figure 4.38 toFigure 4.41).

The relative accuracy in determining the centre-line position of each reflector, from each SBP run, was estimated to be 0 cm–21 cm. The variability associated with reading the centre-line position of each reflector in the SBP runs was quantified. Five reflectors (3545–4929) along run 18052018 135516 were examined to determine the range of traces, for each reflector, which could be reasonably interpreted as being ‘over the centre-line’ of the sleeper. The endpoints of these ranges are plotted in Figure 4.42, and the distances between each endpoint

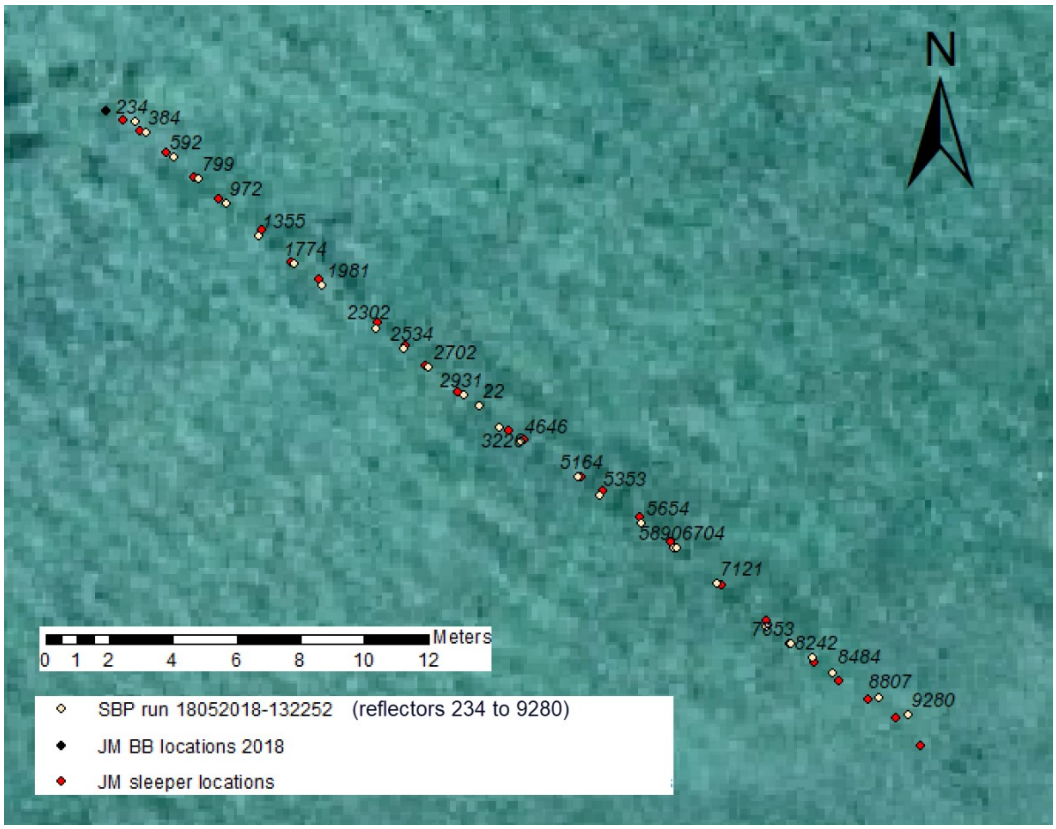

Figure 4.38 Location of sleeper reflectors from SBP run 18052018-132252 vs. sleeper locations.

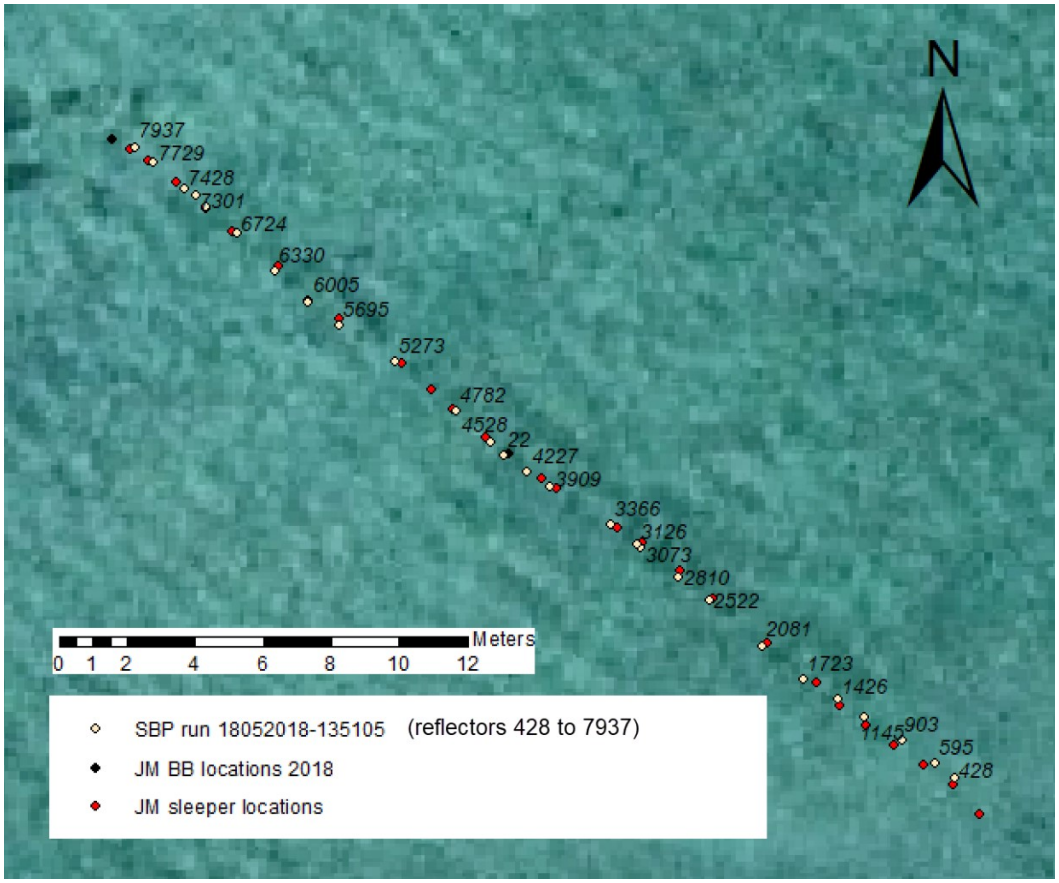

Figure 4.39 Location of sleeper reflectors from SBP run 18052018-135105 vs. sleeper locations.

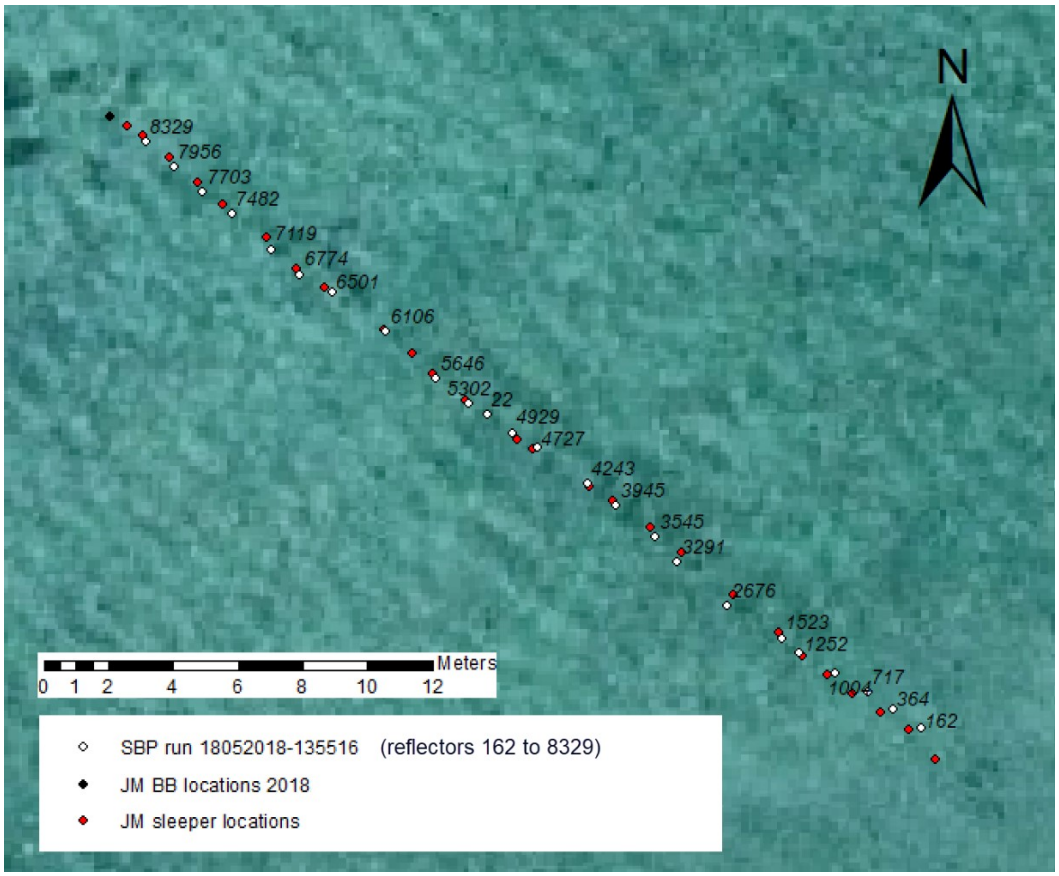

Figure 4.40 Location of sleeper reflectors from SBP run 18052018-135516 vs. sleeper locations.

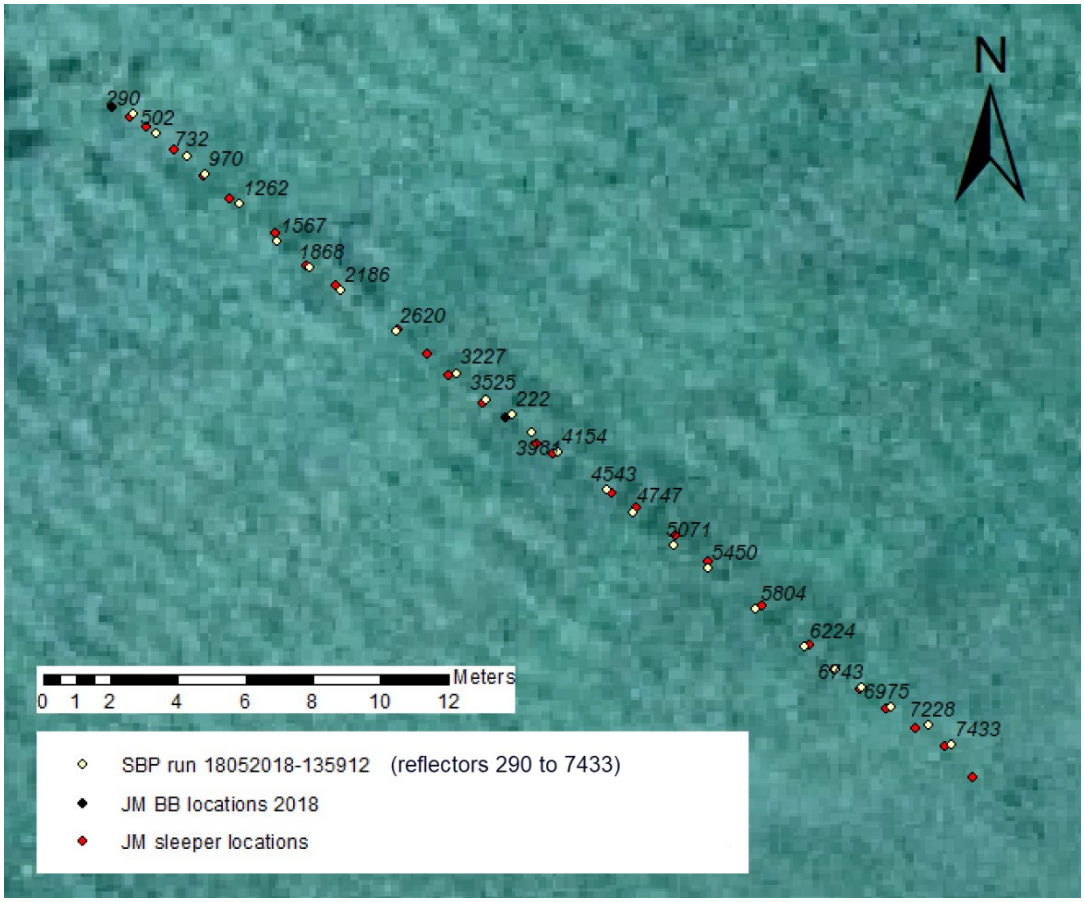

Figure 4.41 Location of sleeper reflectors from SBP run 18052018-135912 vs. sleeper locations.

vary from zero to 15 cm. Separately, the variability in the locations of the central besser block between the RTK DGPS positional survey and their locations from SBP runs 18052018-135105, -133516 and -135912 respectively, ranged from 5 cm to 21 cm. Combining these two sets of location ranges produced the relative accuracy estimate.

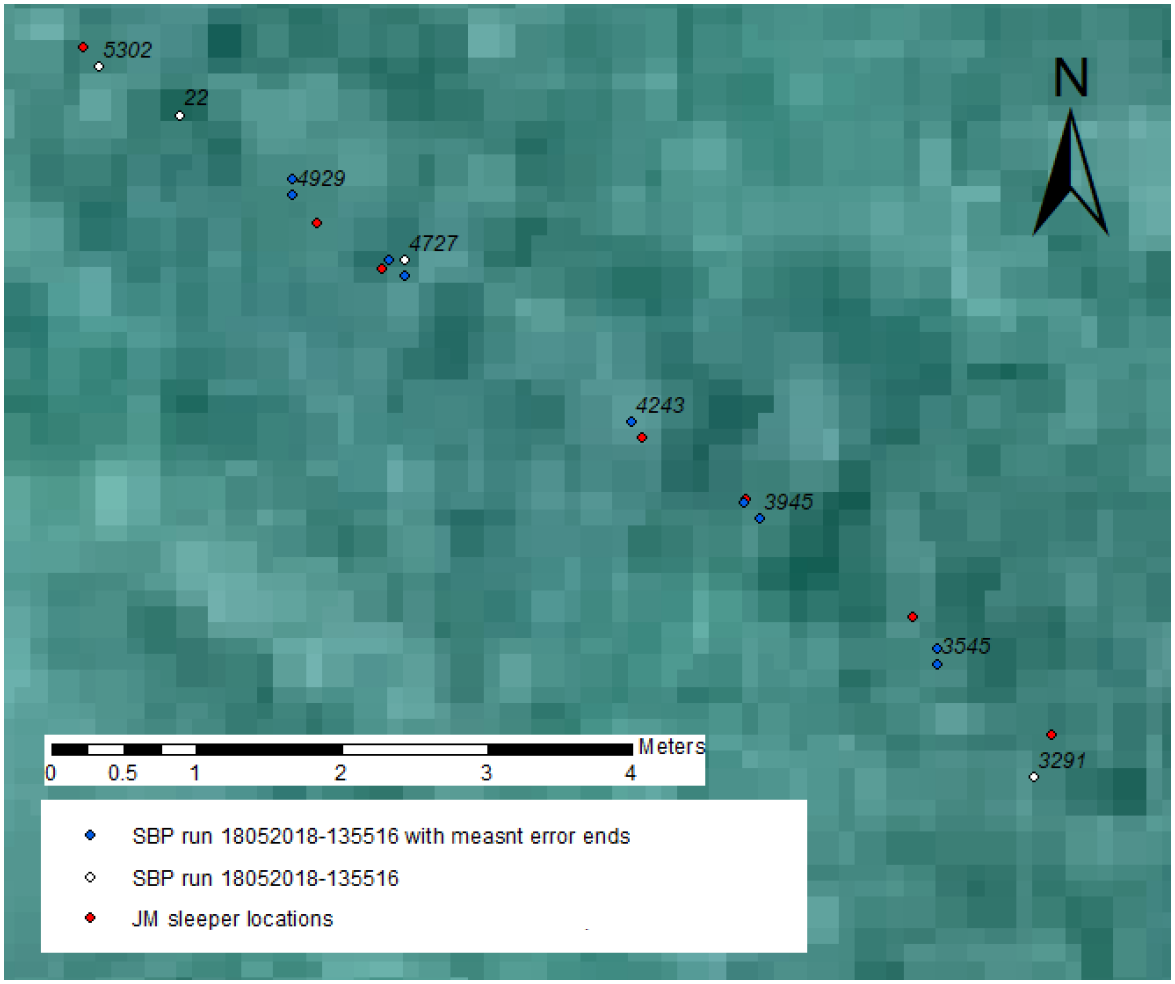

Figure 4.42 Variability of reflector location based on range of reflector interpretation in SBP runs.

The alignment between identified reflectors and sleepers for the four 2018 SBP runs is presented in Table 4.15. Also shown are the distances and directions (for distances greater than 15 cm) separating the SBP reflector location from their respective sleeper location. The match between positions estimated from SBP runs 18052018 -135105 and -135516 lie within the relative accuracy range 0–21 cm for all but a few sleepers along these runs. The exceptions include sleepers 23–25 where there is greater uncertainty on the actual DGPS sleeper location. It appears that the physical dimensions of the sled, relative to the position of the transducer, prevented effective insonification of sleeper 26 on any run. As previously noted, the latitude and longitude data in the SBP record for these runs derived from a direct Bluetooth© link to the RTK DGPS software, with the exception of the very end of run 18052018 135516. This link failed at the time when the sleeper was moving from the position of sleeper 2 toward sleeper 1, and consequentially, no positional record was obtained on this run for the reflector associated with sleeper 1. Likewise, there was no Bluetooth© link for either runs 18052018 32252 and -135912. For these runs the latitude and longitude of each reflector

Table 4.15 Comparison of SBP interpreted reflectors against actual sleeper locations measured in 2018, James Matthews sleeper site.

SBP runs/interpreted buried reflectors								sleeper characteristics (at time of run)		
run 132252		run 135105		run 135516		run 135912				
reflector	distance (cm)	reflector	distance (cm)	reflector	distance (cm)	reflector	distance (cm)	sleeper ID	DoB (cm)	material
234	30 (S)	7937	11	@		290	11 (E)	1	16.8	pine (22^0 rotation)
384	16	7727	17 (S)	8325	17 (S)	502	29 (S)	2	12.5	pine
592	27 (S)	7428	28 (S)	7956	31 (S)	732	33 (S)	3	20	pine (22^0 rotation)
799	15	7301~/7152	midway~/4	7703	33 (S)	970	5	4	30	pine (vert grain)
972	29 (S)	6724	16 (S)	7482	40 (S)	1262	29 (S)	5	26	pine
1355	18	6330	19 (S)	7119	37 (SW)	1567	29 (S)	6	25	pine
1774	11	6002	6	6757	19 (S)	1868	10	7	7	pine
1981	20 (S)	5695	17 (SW)	6501	25 (S)	2186	21 (S)	8	40	pine
2302	20	5273	15 (N)	6106	8	2620	8	9	27	pine
2534Ø	9	*NI*		*NI*		*NI*		10	9.5	pine
2702	10	4782	10	5646	17 (S)	3227	20	11	22.5	oak
2931	23 (S)	4528	16 (S)	5302	16 (S)	3525	11	12	25	pine (vert grain)
3226	24 (N)	4227	39 (N)	4929	25 (N)	3981	33 (N)	13	30	oak
4646	8	3909	16 (N)	4727	15 (W)	4154	14	14	30	pine (vert grain)
5164	7	3366	19 (N)	4243	15 (N)	4543	19	15	47	pine
5353	16	3126	10	3945	12 (S)	4747	15	16	45.5	pine
5654	23 (S)	2810	23 (SW)	3545	37 (S)	5071	32 (SW)	17	30	oak
5890/6704*	19 (S)/25(S)	2522^	12 (W)	3291^	30 (W)	5450	17 (SW)	18	8	pine (mult 10/30)
7121	12	2081 Ø	17 (W)	2676 Ø	34 (W)	5804	18 (W)	19	5.5	pine (mult 10/30/50)
7539^	15	1723	31 (N)	1523	15 (W)	6224^	14	20	11	pine
7853	4	1426	22 (N)	1252	14 (N)	6507	5	21	23.5	oak
8242	15	1145	24 (N)	1004	18 (E)	6743	1	22	23	jarrah
8484	30 (N)	903	23 (E)	717	38 (E)	6975	12	23	35	jarrah
8807	32 (E)	595	32 (E)	364	35 (E)	7228	33 (E)	24	27.5	ferrous
9280	34 (E)	428	20 (E)	162	31 (E)	7433	17 (E)	25	30	ferrous
not insonified								26	46	ferrous
22	0	22	13 (W)	22	5	222	21 (W)	22	surface	Besser Block (midpoint)

^ depth of reflectors identifying lower (not upper) surface of very shallow sleepers; *sled reversal, double measurement; @ lost RTK signal: *NI* no reflector identified; ~ false identification; Ø did not measure the upper stacked sleeper, only the top of the lower sleeper.

position was estimated from the acoustic trace time-record in the SBP data file and the latitude and longitude values associated with that same time in the RTK DGPS record. Using this approach, the distances between the estimated SBP reflector (and besser block) locations and the recorded sleeper (and besser block) locations were consistently higher than the 0–21 cm relative accuracy estimates. One possible cause for this was a non-alignment in the relative timing in the SBP SESWIN and RTK DGPS software. A 3-second difference was identified by comparing the positions of the two besser blocks in each run. The latitude and longitude positions of each of the sleepers in runs 18052018 -132252 and -135912 were then re-estimated using a 3-second delay on the RTK DGPS time record. These new positions resulted in a significant improvement in their relative positional accuracy with nearly all locations within the 0–21 cm accuracy limits. These adjusted results are shown in Table 4.15, Figure 4.38 and in Figure 4.41.

A quantitative assessment of the depth of burial estimates for runs 18052018 -135105 and -135516 is presented in the following chapter. However, a qualitative assessment of the DoB characteristics of each sleeper for all four SBP runs was also undertaken as a final quality check on the alignment of reflectors to sleepers in Table 4.15. Reflector 7301 in run 18052018 135105 had an estimated burial depth of over 36 cm, deeper than the known DoB (20 and 30 cm) of adjacent sleepers. This, together with its plotted location midway between sleepers 3 and 4, suggests an erroneous interpretation from the SBP record. The indicative DoB for reflectors 7539 and 6224, both corresponding to sleeper 20, are in the range 2023 cm and are significantly greater than 11 cm. However, with a sleeper thickness of 12.5 cm, these reflector depths may well represent the second acoustic reflection from the underside, not upper-side, of the sleeper. This will be assessed later using the reflection phase data. Reflectors 5890 and 6704 in run 18052018 -1352252 are both close to the position of sleeper 18 and the estimated depths of burial reasonably match the sleeper's known DoB characteristics. The time record for this run was re-examined and revealed that the sled travelled past the reflector at the time of trace 5890, and then became stationary (presumably jammed against one of the sleeper endplates). The sled operators reversed the direction of sled travel, back close to the position of trace 5890, then traversed forward again around the time of trace 6704. Consequently, the reflector at trace 6704 is a second (independent) measurement of the same reflector associated with sleeper 18. In runs 18052018 -135105, -135516 and -135912 no reflectors were identified from the SBP records for the very shallow-buried sleeper 10. The SBP records were re-examined in this vicinity and confirmed the lack of evidence to identify this very shallow-buried sleeper.

The positions of the reflectors derived from runs 20170608 -024600 and -025024 are shown in Figure 4.43 and the separation distance between the reflectors and sleepers is given in Table 4.21. Both sets of reflector locations consistently sit 1 m–2 m to the north-eastern (starboard) side of the vessel's forward motion, and many appear to be otherwise aligned to sleeper locations. However, the relative locations of the reflectors associated with the besser blocks at the top and mid-way along the runs show a directional change in their relative position, which is also applicable to the sleeper locations. Along the northern portion of run 20170608 025024, a qualitative comparison of the depth of reflectors 900 to 1062 indicated a close match with the DoB of aligned sleepers 11–4, but their north-easterly offset distances varied from 1.0 m to 1.5 m from the sleeper locations. This variability could be indicative of a lower quality GPS solution for all positions, but may well be attributable to the vessel's non-parallel track over the 0.5 m wide sleepers. Of concern, there was no consistency in location nor depth of burial for reflectors 799 to 850 from the southern portion of this run, and little uniformity in location or depth of burial for any of the reflectors from run 20170608 024600. This discrepancy is unlikely to result from measurement set-up or plotting errors as the same coordinate system was used in the sled-mounted RTK DGPS and the vessel-mounted Trimble Surfmaster/Marinestar positioning methods, and both sets of latitude and longitude data were processed to the same decimal units for plotting in ArcGIS. Run 20170608 024600 was undertaken prior to run 20170608 025024, and in the latter run, reflectors 750 to 880 were insonified before reflectors 900 to 1062. While the true reason for the positional discrepancies cannot be fully resolved, it appears that for some reason the DGPS attribute of the Trimble Surfmaster/Marinestar system was lost during run 20170608 024600 and the first half of run 20170608 025024, producing only GPS accuracy in positioning. During the second half of run 20170608 025024, the DGPS capability may have been re-corrected. The north-easterly offset may result from a simple miscalculation of a lever-arm (horizontal distance between Trimble antennae and SBP transducer) in the receiving software. Regardless of the cause, the reflector data from run 20170608 024600 will not be used in further analyses. Data from reflectors 900 to 1062 in run 20170608 025024 will only be used in reflection coefficient analyses, and not in positional accuracy assessment.

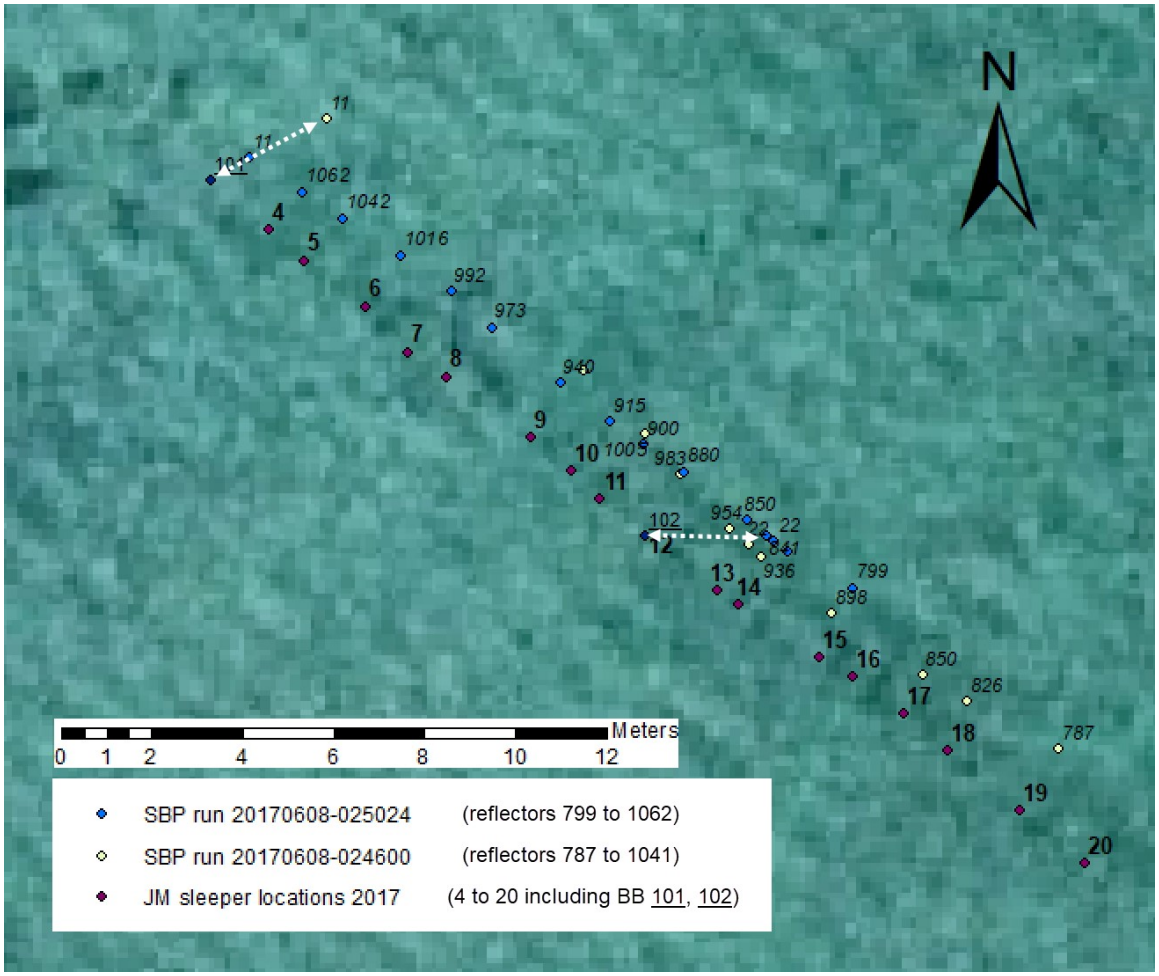

Figure 4.43 Location of sleeper reflectors from SBP runs 20170608-024600 and -025024 vs. sleeper locations.

Table 4.16 Comparison of SBP interpreted reflectors against actual sleeper locations measured in 2017, James Matthews sleeper site.

SBP runs/interpreted buries reflectors				sleeper characteristics (at time of run)		
run 024600		run 025024				
reflector	distance (m)	reflector	distance (m)	sleeper ID	DoB (cm)	material
		1062	1.04	4	28	pine (vert
		1042	1.17	5	29	pine
		1016	1.29	6	27	pine
		992	1.51	7	7	pine
1079	2.00	973	1.39	8	41	pine
1041	1.73	940	1.27	9	29	pine
1020	1.64	917^	1.35	10	10	pine
1005	1.62	900	1.44	11	27	oak

Calculation of reflection coefficients

Reflection coefficients for all identified buried reflectors were calculated using equations (8) and (9) in Chapter 3. Amplitudes for the seabed, buried reflector and seabed 1st multiple, together with their respective depths, are presented in Table D.9 to D.12 for sleepers buried at the James Matthews sleeper site and in Tables D.13 and D 14 for sleepers buried at the Swan River sleeper site. These data are used in the calculations and the reflection coefficient results presented in Table 4.17. Given the variability of the phases associated with the seabed and 1st buried reflectors, and the domination of that variability from the seabed amplitude, reflection coefficients were calculated and subsequently interpreted as their absolute value.

In the following chapter, the reflection coefficients for each reflector and their respective sleeper materials will be compared. The sensitivity of the reflection coefficient value to variations in seabed and burial depths will also be examined. Changes in depth values result from water temperature, water salinity and sediment density effects on the acoustic wave speed in the water column, and in the sediments, respectively. The significant difference between reflection coefficients calculated from SBP data collected in 2017, compared with data collected in 2018 at the James Matthews sleeper site, will also be scrutinised. Table D.9 to D.14 also show that the greatest variability in the reflector characteristics is associated with the estimate of the seabed amplitude, followed by the estimate for the amplitude of the seabed 1st multiple. The impact of this variability on the reflection coefficient values will also be assessed.

In situ comparative (verification) component

This section presents the results from SBP measurements undertaken across the complex shipwreck site of *James Matthews*. While the previous section provided the results of SBP measurements under controlled conditions at the buried sleeper sites, the purpose of the measurements in this section is to assess the performance of the SES-2000 *compact* SBP under actual maritime archaeological conditions in a non-simulated situation. The results initially present a qualitative assessment of six selected SBP runs against the excavated shipwreck survey plan. The interpolated acoustic values from all 51 runs crossing the wrecksite then provide a quasi-3D visual image of the SBP data using a 3D gridding approach. A 3D AutoCAD digital model, generated from the original WAM 1975/76 excavation survey, was finally used to quantitatively assess the accuracy and interpretation of the SBP data across key cross-sections of the buried wreck remains.

The survey team based on the *Dirk Hartog* recorded sub-bottom acoustic data over and surrounding the *James Matthews* wrecksite on 7th and 8th of June 2017 as described in

Table 4.17 Reflection coefficients, James Matthews and Swan River sleeper sites.

James Matthews sleeper site						Swan River sleeper site			
run 20170608-025024		run 18052018-135105		run 18052018-135516		run 17052018-123344		run 17052018-125738	
reflector	K_{DR}	reflector	K_{DR}	reflector	K_{DR}	reflector	K_{DR}	reflector	K_{DR}
900	0.006	428	-0.389	162	-0.107	218	0.41	185	-0.28
917	-0.009	595	-0.034	364	0.124	1138	0.12	559	-0.06
940	-0.006	903	0.176	717	0.527	1967	0.11	1101	0.35
973	-0.005	1145	-0.212	1004	0.052	2276	-0.07	1474	-0.02
992	0.001	1426	-0.268	1252	0.111	2507	0.05	1837	-0.06
1016	-0.009	1723	-0.063	1523	-0.168	2896	-0.21	2068	-0.14
1042	-0.023	2081	0.029	2676	-0.021	3245	0.15	2543	0.06
1062	0.032	2522	0.069	3291	-0.020	3413	0.11	2856	0.05
		2810	-0.245	3545	0.204	3574	-0.04	3238	-0.09
		3126	-0.083	3945	-0.043			3491	-0.03
		3366	-0.240	4243	-0.137			4207	-0.01
		3909	0.028	4727	0.086			4278	-0.02
		4227	0.223	4929	-0.335			4305	-0.14
		4528	0.029	5302	0.021			4583	0.10
		4782	-0.305	5646	0.375			4849	0.23
		5273	0.438	6106	-0.217			5073	0.27
		5695	0.038	6501	0.053			5383	0.77
		6005	-0.004	6757	0.228				
		6330	0.030	7119	0.076				
		6724	0.364	7482	0.350				
		7152	-0.024	7703	-0.330				
		7428	0.045	7956	-0.035				
		7729	-0.069	8325	-0.998				
		7937	-0.081						

Chapter 3. While a total of 89 long SBP transects were measured, only 51 crossed the wrecksite bounded by the 'crash barrier' cofferdam. The remaining transects covered the surrounding areas outside the cofferdam to 50 m in order to detect any other potentially buried material isolated from the immediate excavated wreck-site. For the purposes of qualitative comparison and 3D visualisation with the known and archaeologically surveyed buried material, only those 51 runs which crossed the cofferdam were included in the subsequent analyses. The segments of each of these runs over the wrecksite were extracted and their tracks plotted in Figure 4.44. This figure shows 10 runs tracking 'loosely parallel' and

longitudinally along the shipwreck remains (NW-SE) at an average spacing of 1.4 m. It also shows 37 runs tracking 'loosely parallel' and transversely across the buried structure (SW–NE), at an average 0.8 m spacing. These tracks are listed in Table 4.18. For subsequent analyses, the interpreted seabed profile was manually inserted into the echo plot for each track using a post-processing function within the ISE software package.

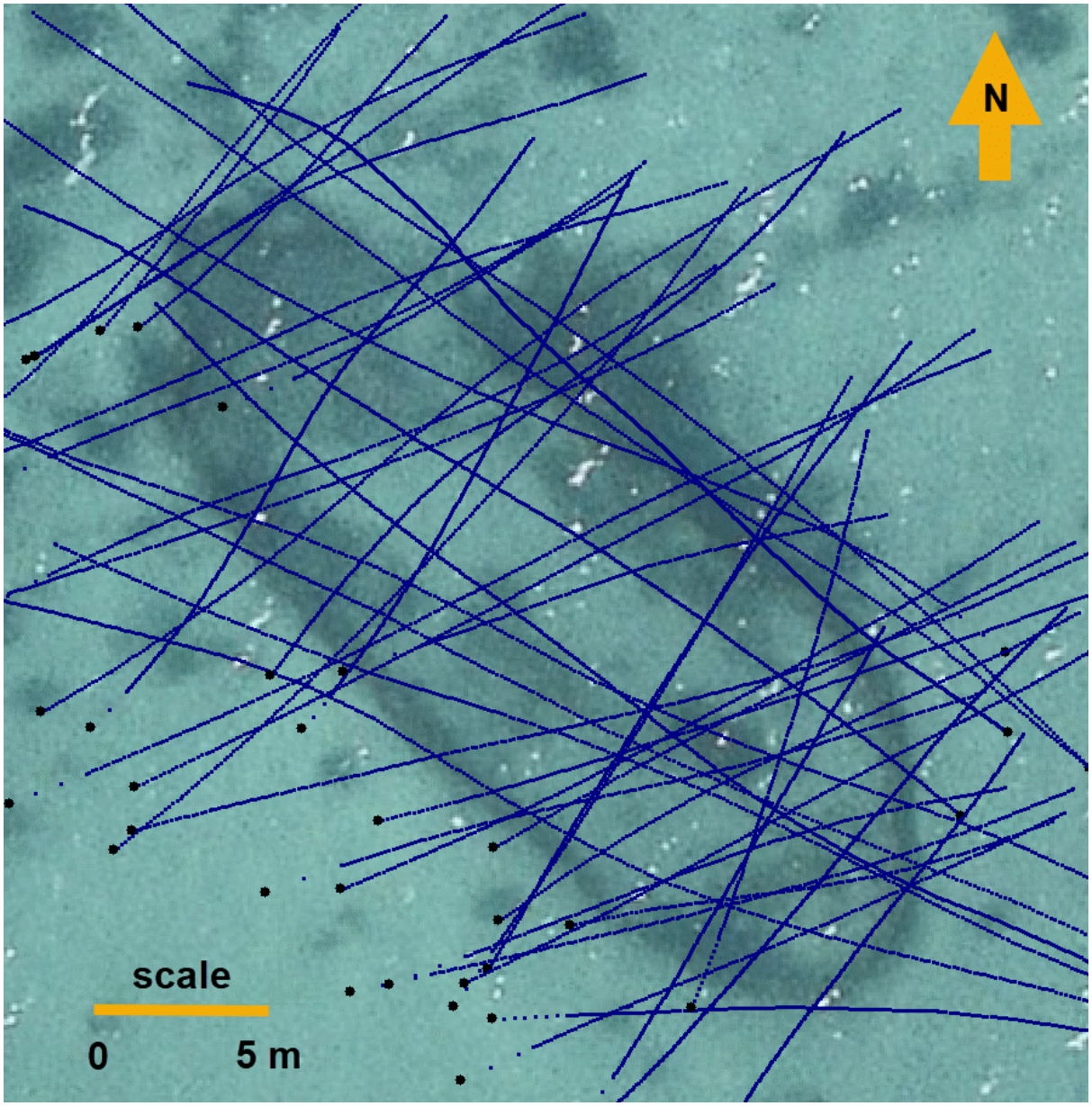

Figure 4.44 SBP tracks crossing *James Matthews* wrecksite cofferdam.

Table 4.18 SBP runs used for qualitative comparison with *James Matthews* buried remains

transverse tracks	transverse tracks
JM_12kHz 20170607 045617	JM_12kHz 20170607 053700
JM_12kHz 20170607 045828	JM_12kHz 20170607 053833
JM_12kHz 20170607 050037	JM_12kHz 20170608 025659
JM_12kHz 20170607 050357	JM_12kHz 20170608 031353
JM_12kHz 20170607 050504	JM_12kHz 20170608 031531
JM_12kHz 20170607 050619	JM_12kHz 20170608 031818
JM_12kHz 20170607 050821	JM_12kHz 20170608 032227
JM_12kHz 20170607 050945	JM_12kHz 20170608 032410
JM_12kHz 20170607 051048	JM_12kHz 20170608 032550
JM_12kHz 20170607 051228	JM_12kHz 20170608 032823
JM_12kHz 20170607 051421	JM_12kHz 20170608 033023
JM_12kHz 20170607 051619	JM_12kHz 20170608 033710
JM_12kHz 20170607 051745	JM_12kHz 20170608 040920
JM_12kHz 20170607 051953	**longitudinal tracks**
JM_12kHz 20170607 052110	JM_12kHz 20170608 041131
JM_12kHz 20170607 052310	JM_12kHz 20170608 041258
JM_12kHz 20170607 052451	JM_12kHz 20170608 041421
JM_12kHz 20170607 052644	JM_12kHz 20170608 041554
JM_12kHz 20170607 052801	JM_12kHz 20170608 041720
JM_12kHz 20170607 052937	JM_12kHz 20170608 041837
JM_12kHz 20170607 053048	JM_12kHz 20170608 042015
JM_12kHz 20170607 053203	JM_12kHz 20170608 042312
JM_12kHz 20170607 053316	JM_12kHz 20170608 042455
JM_12kHz 20170607 053543	JM_12kHz 20170608 042734

Qualitative assessment of the *James Matthews* shipwreck site

Six tracks were selected for individual qualitative assessment with the WAM survey plan drawing (Figure 3.5). These tracks cross key characteristic and identifiable features of the surface visible and buried wreck remains and are shown in Figure 4.45. Images of the key features visible above the seabed surface, including the slate mound, windlass, deck knees and encrusted crash barrier wall, are shown in Figure 4.46. SBP echo plots for each of the six selected runs have been annotated and are shown in Figure 4.47 (transverse runs) and in Figure 4.48 (longitudinal runs). These echo plots display low frequency (12 kHz) data which has been demodulated for easier visual recognition of buried reflectors. A post-processing 'smoothing' function was also applied whereby the value of each trace, at all depths, was

derived by the average of itself plus the values of the trace immediately either side. This results in averaging across a distance of 11.4 cm, but increases the visual recognition of the buried features. Water column noise reduction was also applied based on the defined seabed surface.

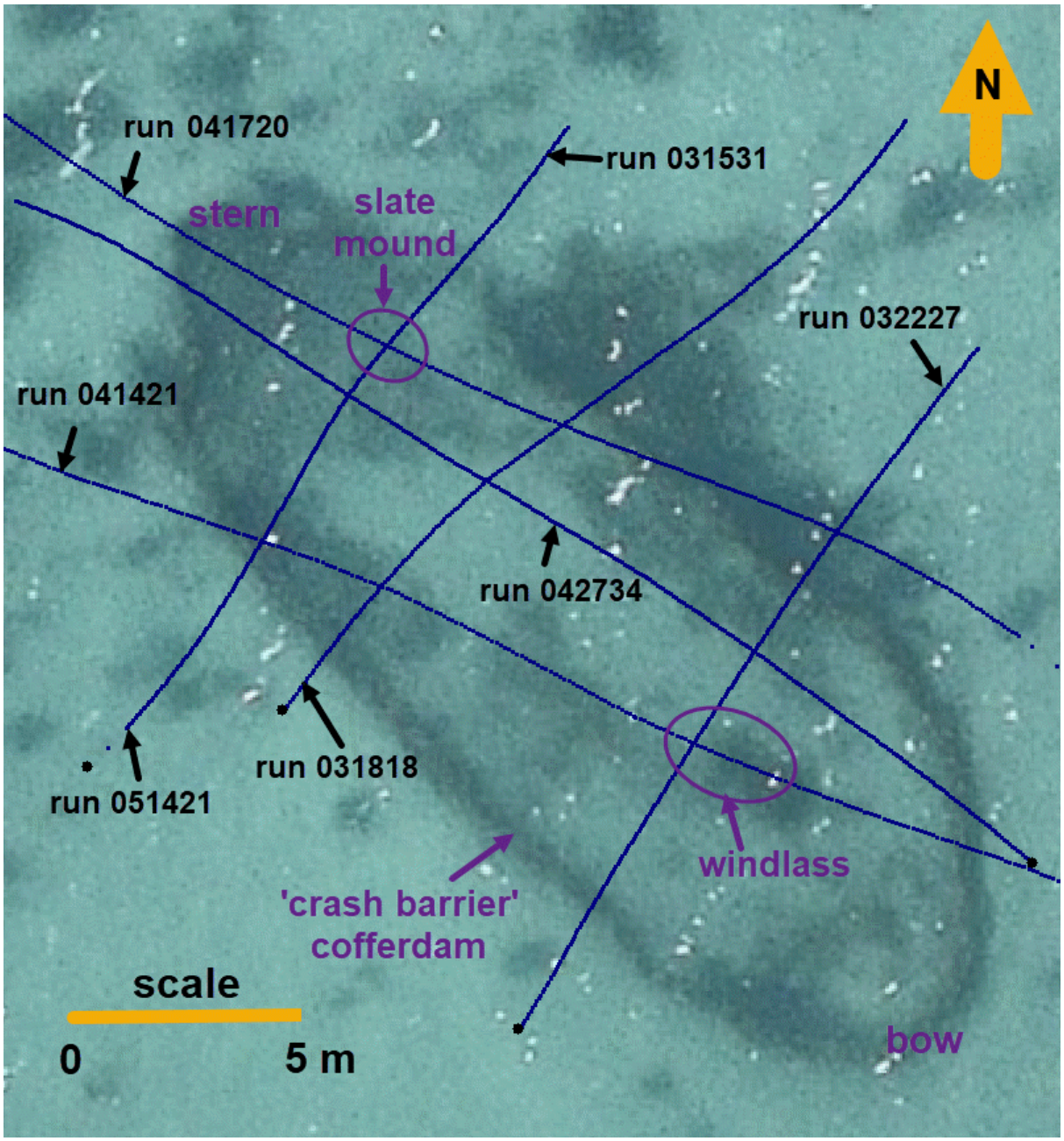

Figure 4.45 SBP tracks selected for individual qualitative comparison with survey plan.

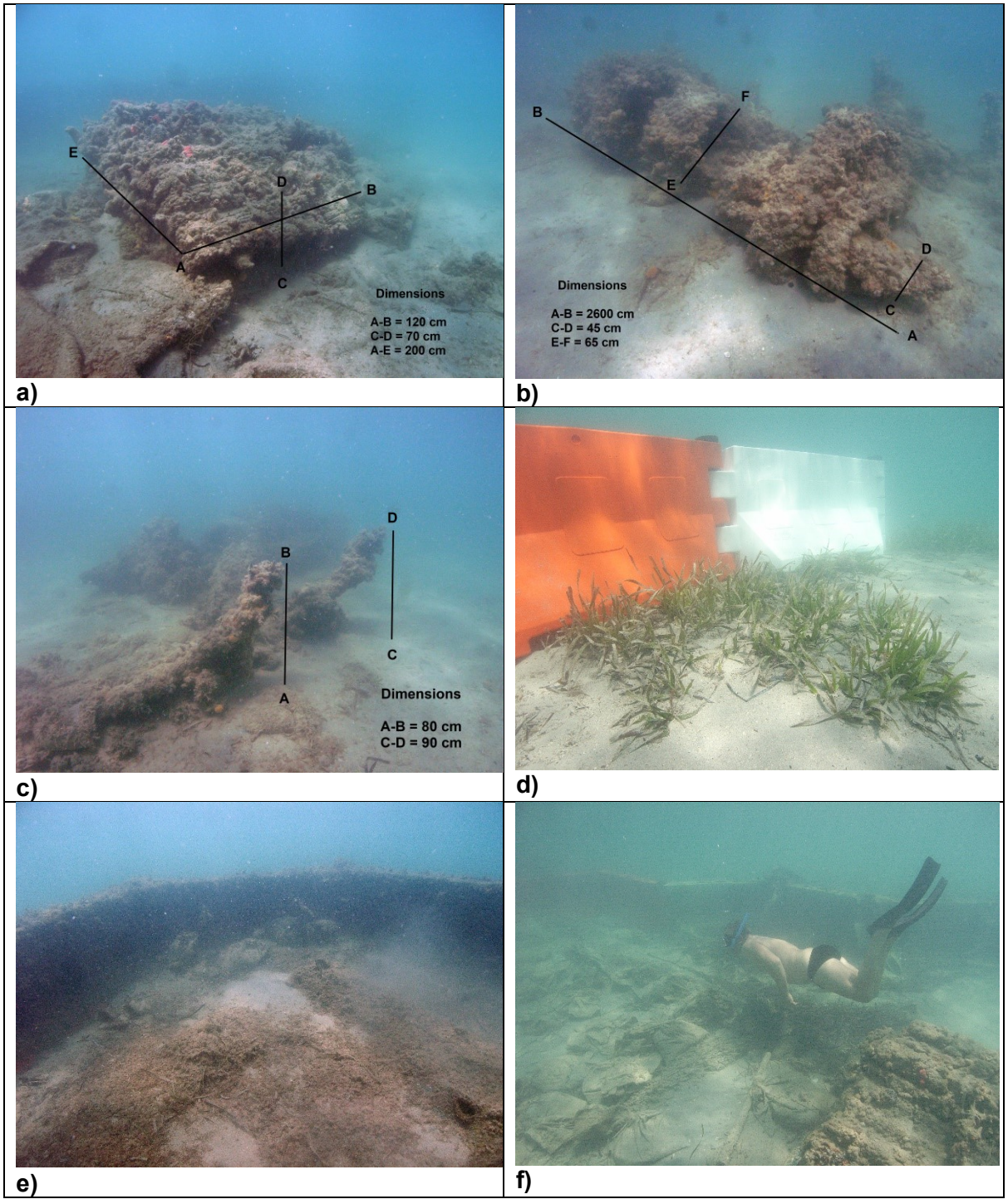

Figure 4.46 Key exposed seabed features on *James Matthews* wrecksite: (a) slate mound from stern end, with sand bags in left foreground; (b) windlass from stern end; (c) deck knees with windlass in background; (d) crash barriers (90 cm high, 200 cm long) shortly after installation; (e) bow end of crash barriers with stockpile sand bags; and (f) crash barrier in background, slate mound in right foreground, sand bags across site (photographs by Jon Carpenter).

Figures 4.47 to Figure 4.49 show three transverse SBP echo plots near the stern, within the stern-end of amidships and near the bow, respectively. The seabed outside the cofferdam varies between 2.3 m–2.6 m below the sea surface, and reflects localised scour or accretion around fixed features. The 0.9 m high plastic road crash barriers, which form the cofferdam surrounding the *James Matthews* wrecksite, can be seen at the ends of each plot. The remains of the slate mound, near the stern, protrudes up to 0.6 m above the seabed (Figure 4.47) and adjacent seabed scour is evident. An iron deck knee (Figure 4.48) can be identified, as well as the windlass near the bow (Figure 4.49), both extending up to 0.3 m above the seabed. The site contains a number of seagrass patches (*Posidonia sinuosa*) which are evident on the seabed as irregular mounds (Figure 4.47). Isolated features which are narrow (typically less than 0.3 m wide) and emerge above the seabed can be identified on all plots both within and outside of the cofferdam. It is thought that the dense foliage of the seasonal brown alga *Sirophysalis trinodis* results in this acoustic feature. This alga was identified from photographs by the Curator of the Western Australian Herbarium, and 'like its closely related genera, it is likely to have a distinct seasonal growth around winter-spring, when the reproductive fronds (as distinct from the vegetative fronds) appear. By end of summer a lot of the growth would have been shed and the plants are often reduced to their inconspicuous basal branches' (John Huisman pers. comm. 2019). The acoustic band associated with the seabed surface is approximately 0.2 m thick, and submerged features can be identified immediately below this layer to a maximum depth of around 1.1 m.

In Figure 4.47, the maximum depth of buried reflectors is 0.8 m on the bulwarks side of the slate mound. From the WAM survey plan this area corresponds to a timber ceiling planking with underlying ribs. Adjacent to this area are the remains of the slate mound, which protrudes above the seabed. Here, the thickness of the surface band is almost 0.4 m (the bottom of which is still above the surrounding seabed level), and below which there is very little signal (see trace 348). This contrasts to the very strong adjacent signal reflections at similar and deeper depths. This indicates that the acoustic energy of the sound wave has been fully reflected from the upper section of the slate mound, forming an acoustic shadow below. The same effect may possibly be seen adjacent to the slate mound on the keel side, an area where metal bars carried as cargo were left in situ. Amidships, in Figure 4.48, the echo plot crosses the timber ceiling planks with minimal cargo left in situ, and it is here that trace 204 shows multiple stacked buried reflectors to a depth of 1.1 m below seabed. At the bulwarks' location along the echo plot, the 0.3 m emerged feature may represent one of the iron deck knees sticking up out of the seabed, with a possible acoustic shadow below the deck concretion. Beyond the plan extent of the shipwreck remains, outside of the bulwarks, a significant reflector is located 0.5 m below the seabed. Similar features are identified in the transverse

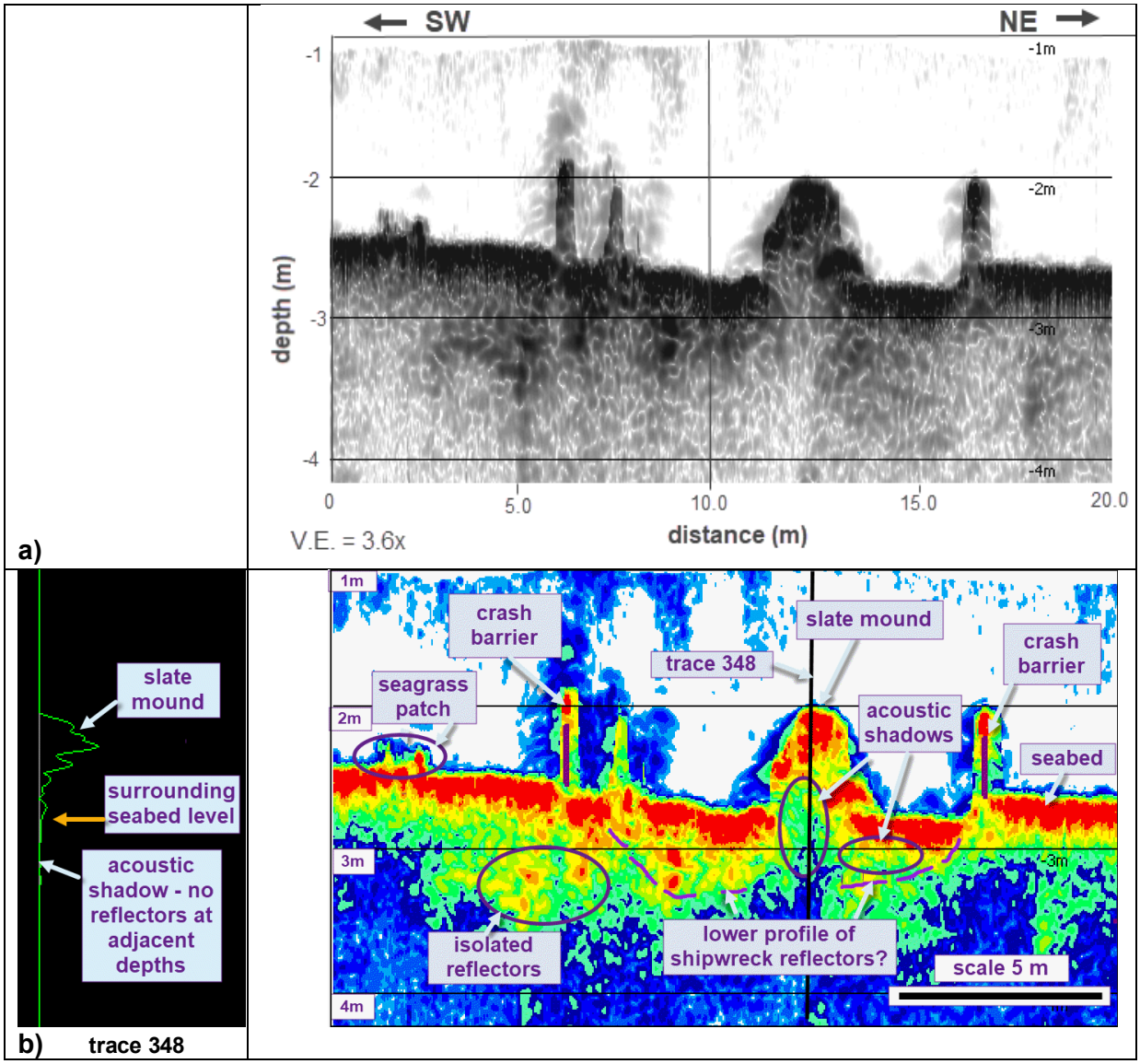

Figure 4.47 Transverse SBP run 20170608 031531 showing qualitative comparison with WAM survey plan of *James Matthews*. The starboard bulwarks are to the left, the keel to the right: (a) greyscale, uninterpreted; (b) 10 colour scale with interpretations.

echo plot near the bow (Figure 4.49). This includes the windlass, which sits above the seabed with its corresponding acoustic shadow below, and an isolated reflector 0.5 m deep below the bulwarks (trace 194).

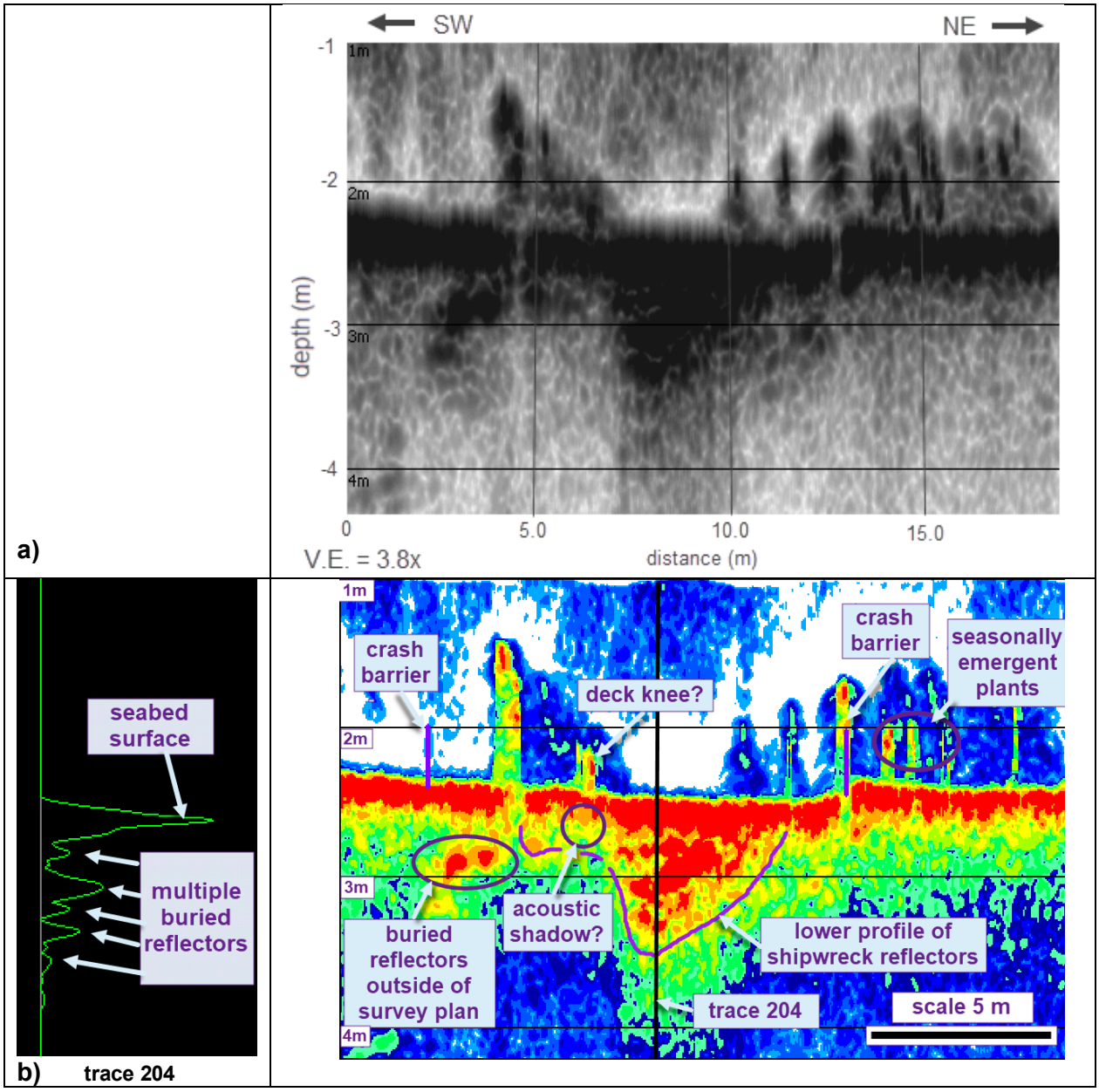

Figure 4.48 Transverse SBP run 20170608 031818 showing qualitative comparison with WAM survey plan of *James Matthews*. The starboard bulwarks are to the left, the keel to the right: (a) greyscale, uninterpreted; (b) 10 colour scale with interpretations.

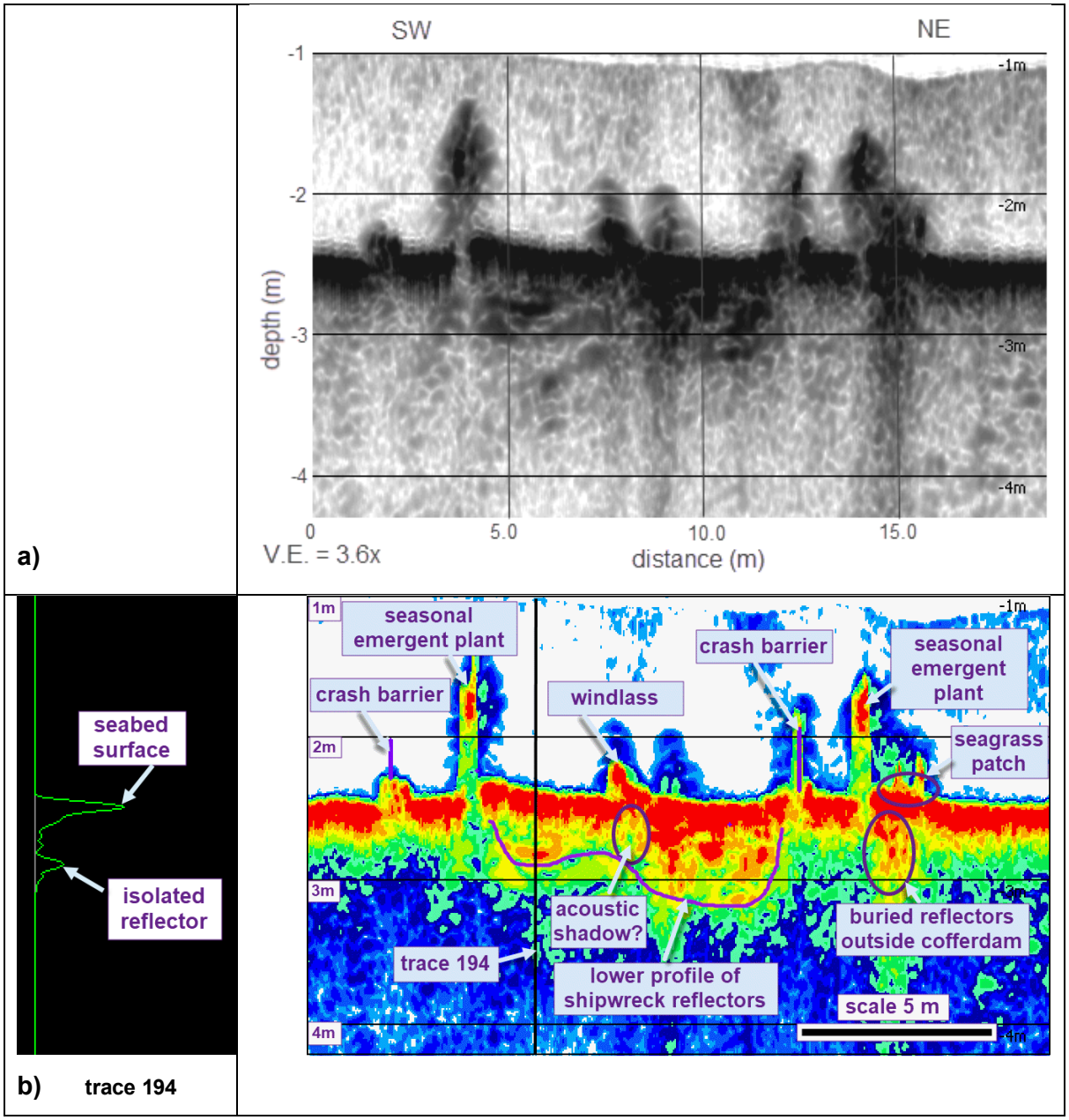

Figure 4.49 Transverse SBP run 20170608 032227 showing qualitative comparison with WAM survey plan of *James Matthews*. The starboard bulwarks are to the left, the keel to the right: (a) greyscale, uninterpreted; (b) 10 colour scale with interpretations.

Figures 4.50 to Figure 4.52 show three parallel longitudinal SBP echo plots partially along the keel (Figure 4.50), between the keel and the starboard bulwarks (Figure 4.51) and from the mid-section of the bow to the bulwarks near the stern (Figure 4.52). The outer two plots (Figures 4.50 and 4.52) show greater seabed irregularity around fixed features and central plot shows a significant dip in the seabed surface 3 m–4 m inside the stern cofferdam wall. The crash barriers forming the cofferdam can be seen on each plot, although it appears wider in Figure 4.50 due the oblique angle of incidence as the echo plot crosses this barrier. Also obvious in these figures are the slate mound in Figure 4.50, the windlass and a deck knee in Figure 4.52 and the seasonally emergent plants in all.

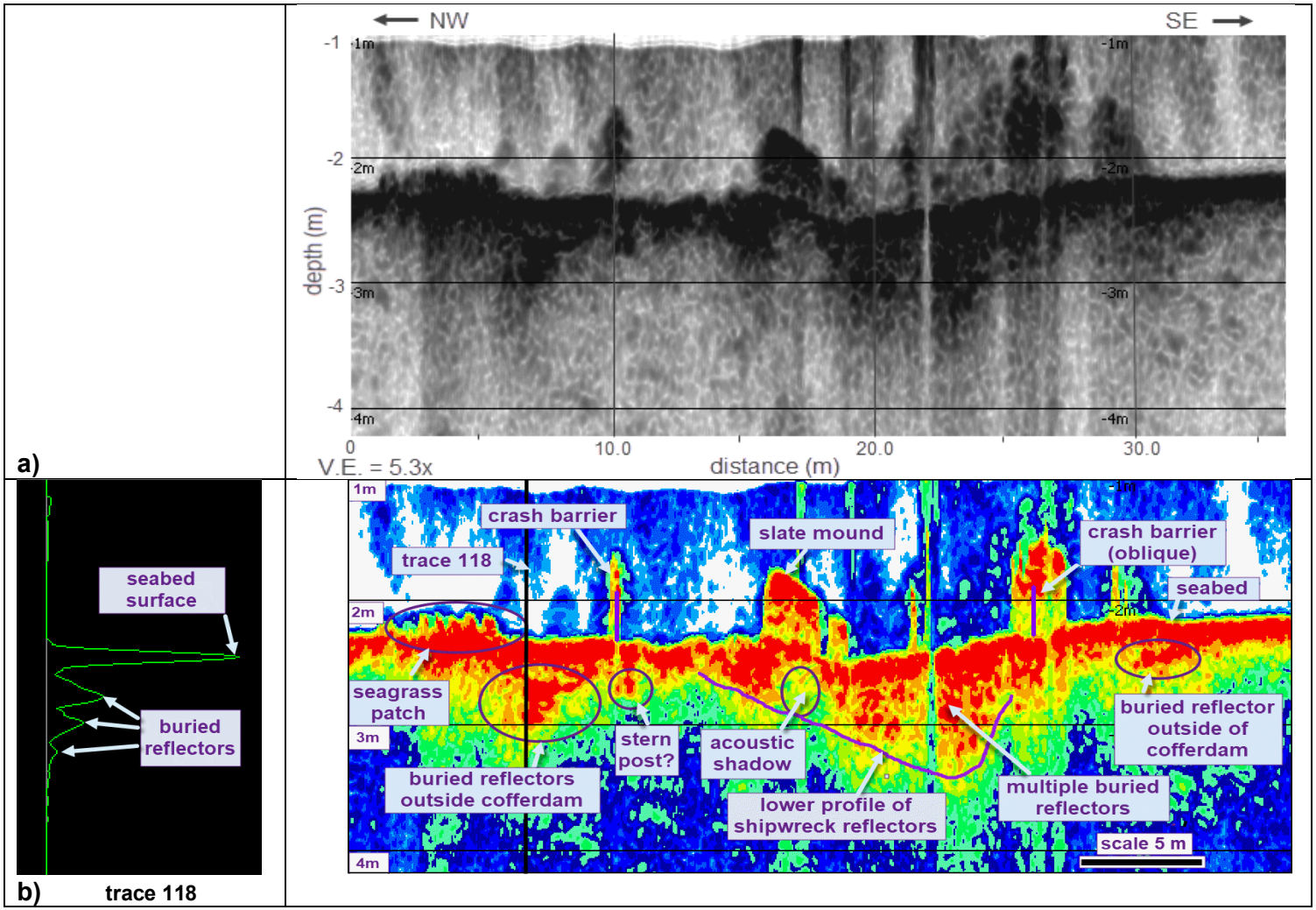

Figure 4.50 Longitudinal SBP run 20170608 041720 showing qualitative comparison with WAM survey plan of *James Matthews*. The stern end of the wrecksite is to the left, the bow to the right: (a) greyscale, uninterpreted; (b) 10 colour scale with interpretations.

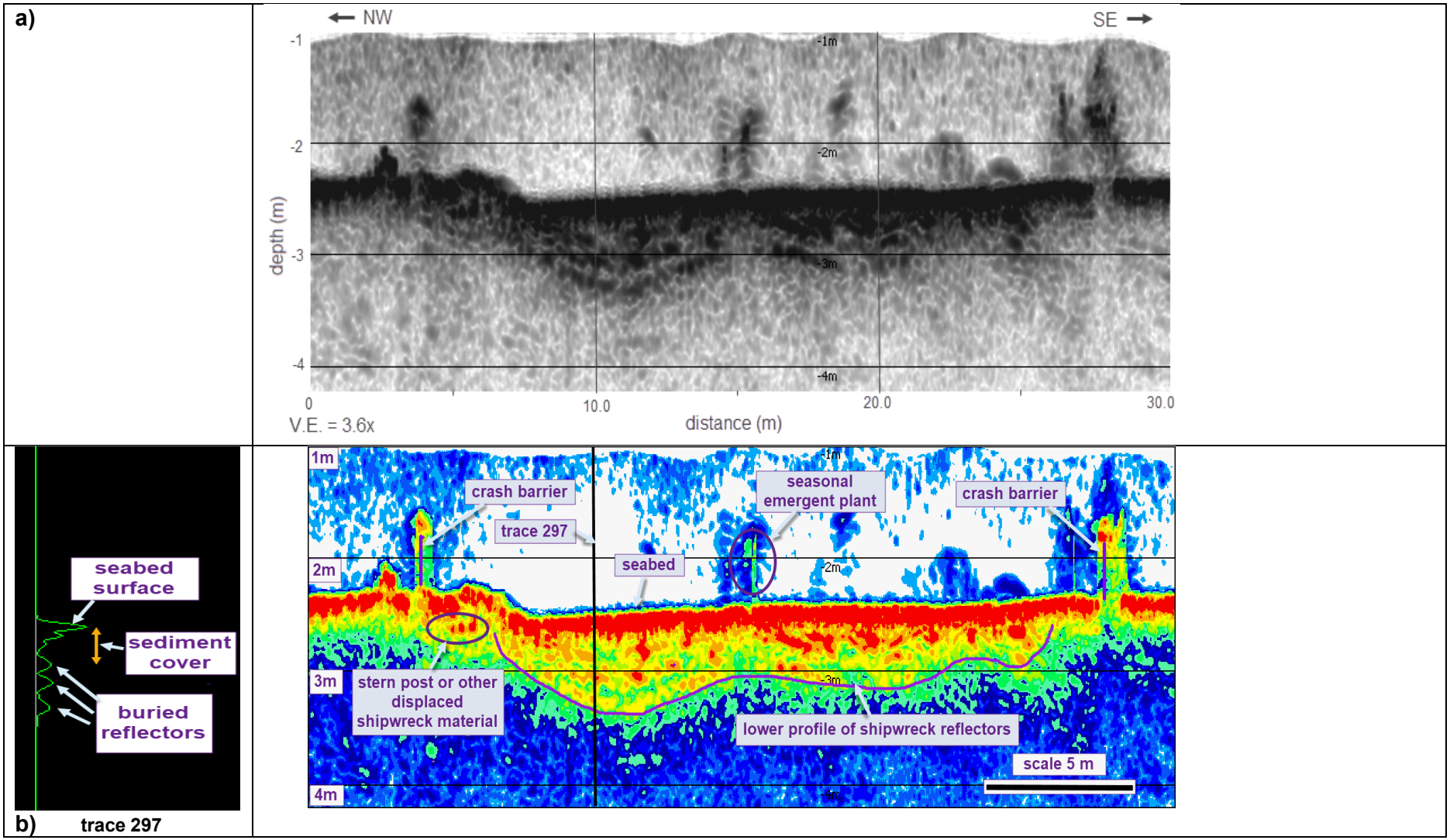

Figure 4.51 Longitudinal SBP run 20170608 042734 showing qualitative comparison with WAM survey plan of *James Matthews*. The stern end of the wrecksite is to the left, the bow to the right: (a) greyscale, uninterpreted; (b) 10 colour scale with interpretations.

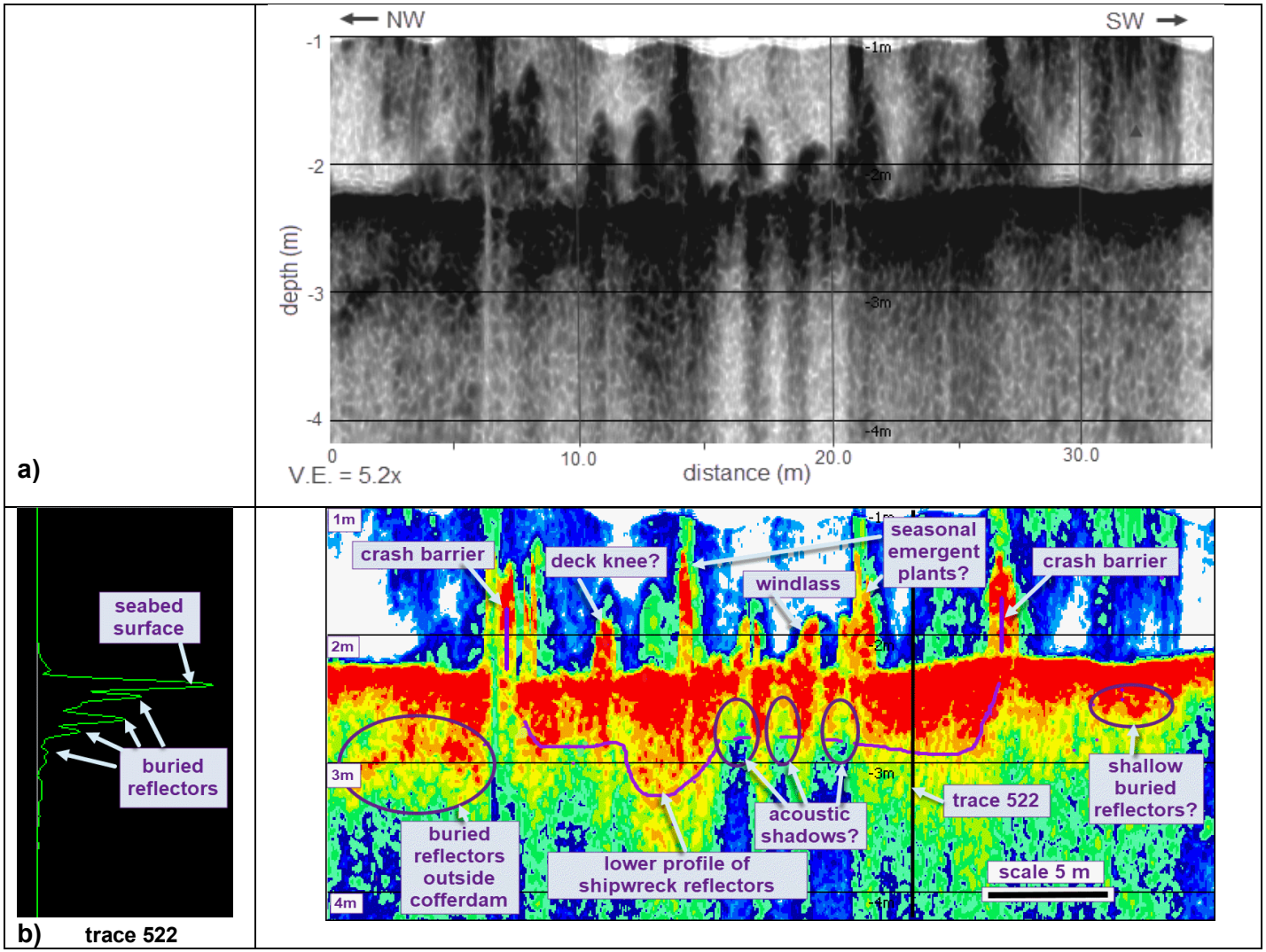

Figure 4.52 Longitudinal SBP run 20170608 041421 showing qualitative comparison with WAM survey plan of *James Matthews*. The stern end of the wrecksite is to the left, the bow to the right: (a) greyscale, uninterpreted; (b) 10 colour scale with interpretations.

In Figure 4.50, the echo plot crosses the keel where there are multiple reflectors at depths to 3.5 m, corresponding to burial depths of 1.0 m. On the stern side of the slate mound, the depths of these reflectors reduce to around 0.5 m, with an acoustic shadow effect evident below the slate mound and iron cargo. An isolated narrow reflector, seen approximately 0.3 m below the seabed level and located 2 m away from the stern, may represent the sternpost of *James Matthews* which was accidently separated from the hull by a dredge. Of equal interest is another significant reflector (trace 118) which is located a further 3 m outside the cofferdam barrier. There is approximately 0.3 m of sediment cover above this multiple reflector, which extends to a depth of 0.9 m below the seabed level. The central longitudinal echo plot (Figure 4.51) displays a lower profile of the shipwreck reflectors, from bow to stern. The maximum depth of these reflectors is approximately 0.9 m below the seabed level (trace 297) located immediately forward of the slate mound. Similar to the profile in Figure 4.50, isolated reflectors can be seen one to two metres from the stern and may also represent (a different portion of) the dislocated stern post. The longitudinal echo plot in Figure 4.52 diagonally crosses the windlass and traverses along the bulwarks amidships. Here the windlass and deck knees are evident, together with acoustic shadows. In between, on uncluttered hull timbers, multiple deep reflectors can be seen to 0.8 m below seabed level forward of the windlass (trace 522), and to 0.9 m amidships. Two areas of multiple isolated buried reflectors are also seen at both ends on the run, outside the line of the cofferdam barriers.

Quasi-3D visualisation of the SBP data

The demodulated amplitudes from the 37 transverse and 10 longitudinal SBP runs were interpolated into a 3D ‘volume’ using Innomar’s SESGridder64 V1020 software. This 3D transformation allows viewing from the front, side and top faces of the ‘volume’, the latter the most enlightening through progressive depth slices from the seabed surface to the base of the acoustic reflectors. Inspection of this series of horizontal slices, each deeper than the previous, enables a quasi-3D interpretation of the shape and depth-related related features across the entire *James Matthews* wrecksite.

The gridding software requires the x and y boundaries of the 3D ‘volume’ to be aligned with lines of latitude and longitude, respectively, and are shown in Figure 4.53. Their minimum and maximum values (in northings and eastings) were selected just outside of the cofferdam to maximise the density and close spacing of runs over the *James Matthews* wrecksite. Maximum and minimum vertical boundaries (z axis) were obtained by trial and error to capture the upper reflectors protruding above the background seabed level, and the deepest reflectors associated with the buried shipwreck material. These boundaries, together with the selected number and dimension of cells (voxels) in each of the three axes, are given in Table 4.19.

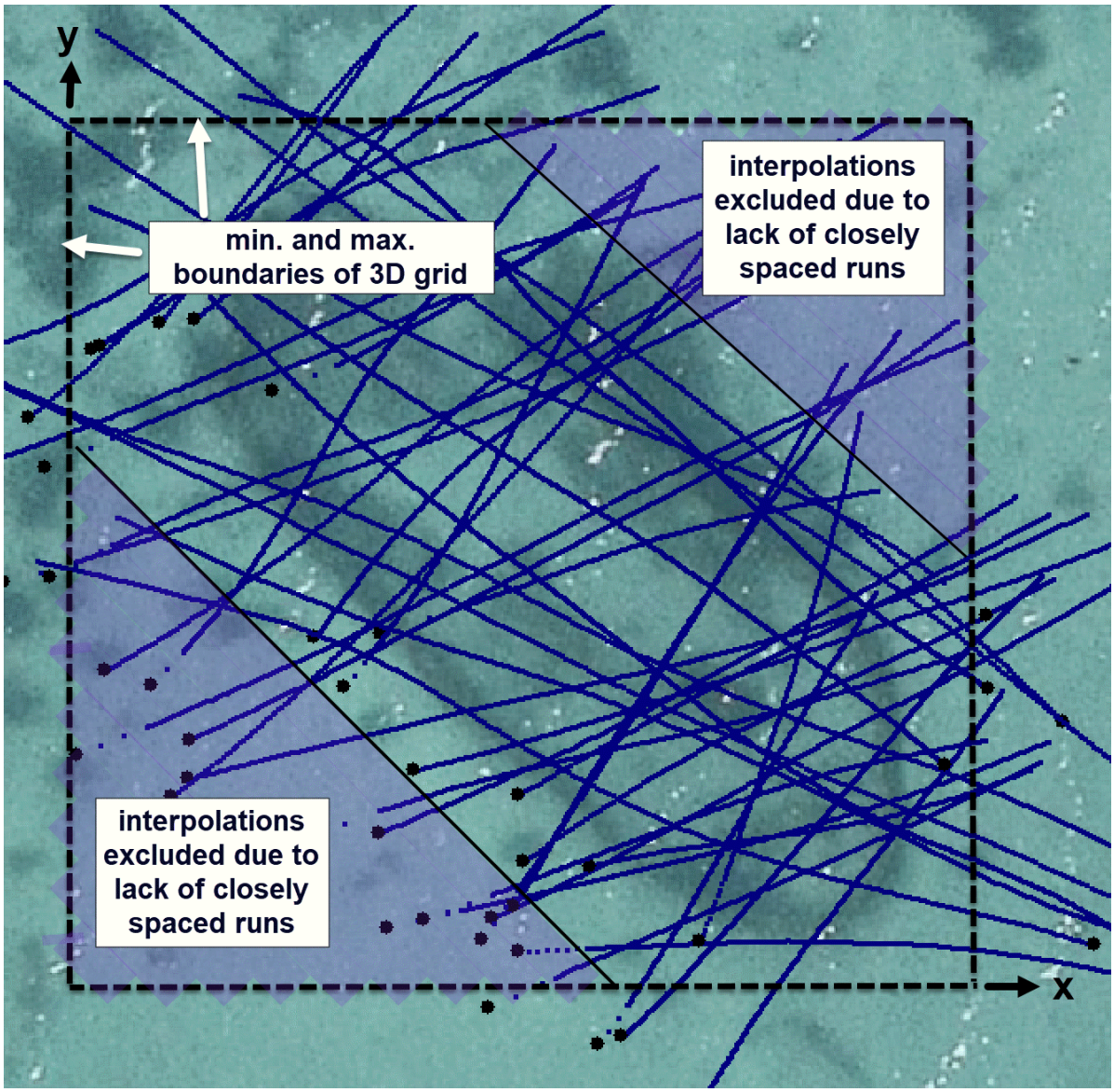

Figure 4.53 3D gridding area and x and y boundaries.

The software calculated a demodulated wave amplitude value at the corners of each voxel based on interpolation of amplitudes from the nearest each echo plot runs. A search radius of four voxels was adopted in this interpolation. The longitudinal axis of the *James Matthews* wrecksite is approximately 45 degrees from the lines of longitude. The density and spacing of runs in the southwest and north-eastern corners of the 'volume' were sparse (Figure 4.53), and in these corners, the interpreted values of the acoustic amplitudes would not be representative. Consequently, the interpolated results in these corners were excluded from interpretation. During field data collection the gain for run 0608 025659 was set at 12 dB (decibel) vs. 6 or 8 dB for the other runs. This resulted in a significant difference in signal

strength and provided very different localised results in the gridded volume compared to other close by or intersecting runs. Consequently, this run was removed from the final grid interpolation lines.

Table 4.19 Grid volume boundaries (in northings and eastings) and cell dimensions

dimension	x	y	z
minimum	381495.0	6444242.0	-33.0
maximum	381524.0	6444270.0	-18.5
no. of voxels	58	56	29
voxel size (m)	0.5	0.5	0.05

The results from the 3D volume interpolation of the SBP runs over the *James Matthews* wrecksite are shown in Figure 4.50. This figure shows the horizontal (x, y) distribution of interpolated demodulated amplitudes in 11 depth layers—the top layer being +0.35 m above the local seabed (layer a), the seabed layer (layer b), and then layers in 0.1 m increments below seabed from -0.1 (layer c) to -0.9 m (layer k). The colour scale, as shown in Figure 4.50l, depicts the interpolated amplitude magnitude from the lowest value (purple) to the maximum value (red).

The top layer (layer a) in Figure 4.54 depicts a plan view at a height of 0.35 m above the localised seabed, and shows a feint outline of the top of the road crash barrier, the slate mound, possible deck knees along the starboard bulwarks, and the isolated occurrences of the brown alga plant. The predominant purple background indicates that there are minimal other reflectors at this level. In the seabed level (layer b), the broad blue areas outside the cofferdam, and centrally within, indicate the seabed surface. Higher intensity amplitudes are seen in patches around the outside of the cofferdam, likely to represent seagrass mounds. These are also seen around the bow end of the site, indicating a small pile of sandbags from earlier site protective works and/or shallower seabed levels relative to the stern. This situation arose following a severe storm which resulted in a failed crash barrier at the stern, with localised currents eroding sand from the stern and depositing it against the bow section of the cofferdam (Vicki Richards pers. comm. 2018). At a depth of -0.1 m (layer c) greater numbers of higher intensity reflectors are seen forward of amidships, around the windlass area, and at several locations alongside the bulwarks. A transverse line of strong reflectors is also seen amidships. The slate mound is more pronounced, surrounded by a deeper seabed. At depths 0.2 m and greater below the localised seabed level, the effect of the continuous seabed band of reflectors is minimised and buried reflectors become identifiable. Between 0.2 and 0.3 m below seabed (layers d and e) the numbers of brighter reflectors reduce around the bow of the shipwreck. This suggests that in these areas there are no immediate reflectors below the

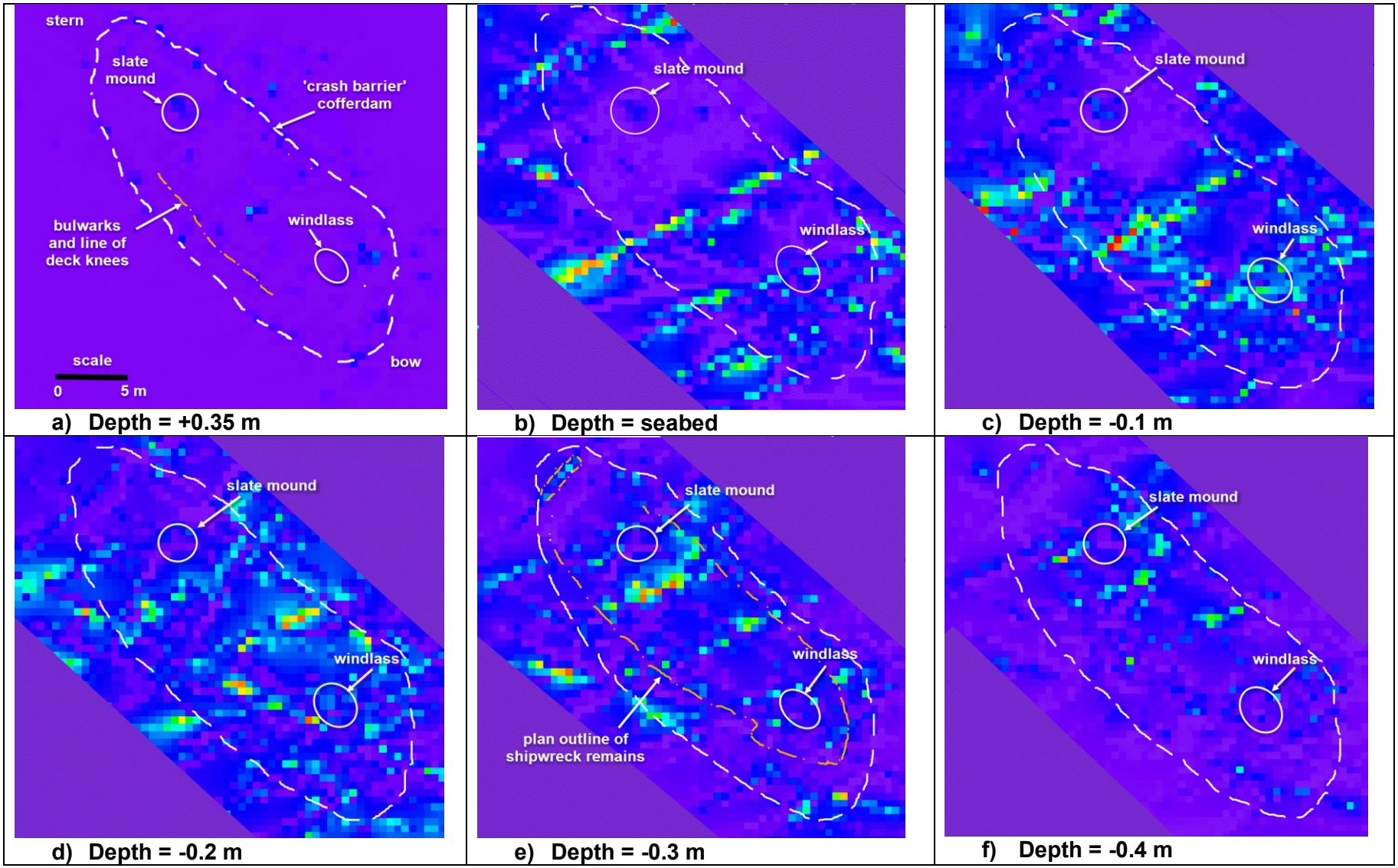

Figure 4.54 Horizontal planes at depths from + 0.35 m to -1.0 m, relative to seabed level, through 3D grid, all at same scale.

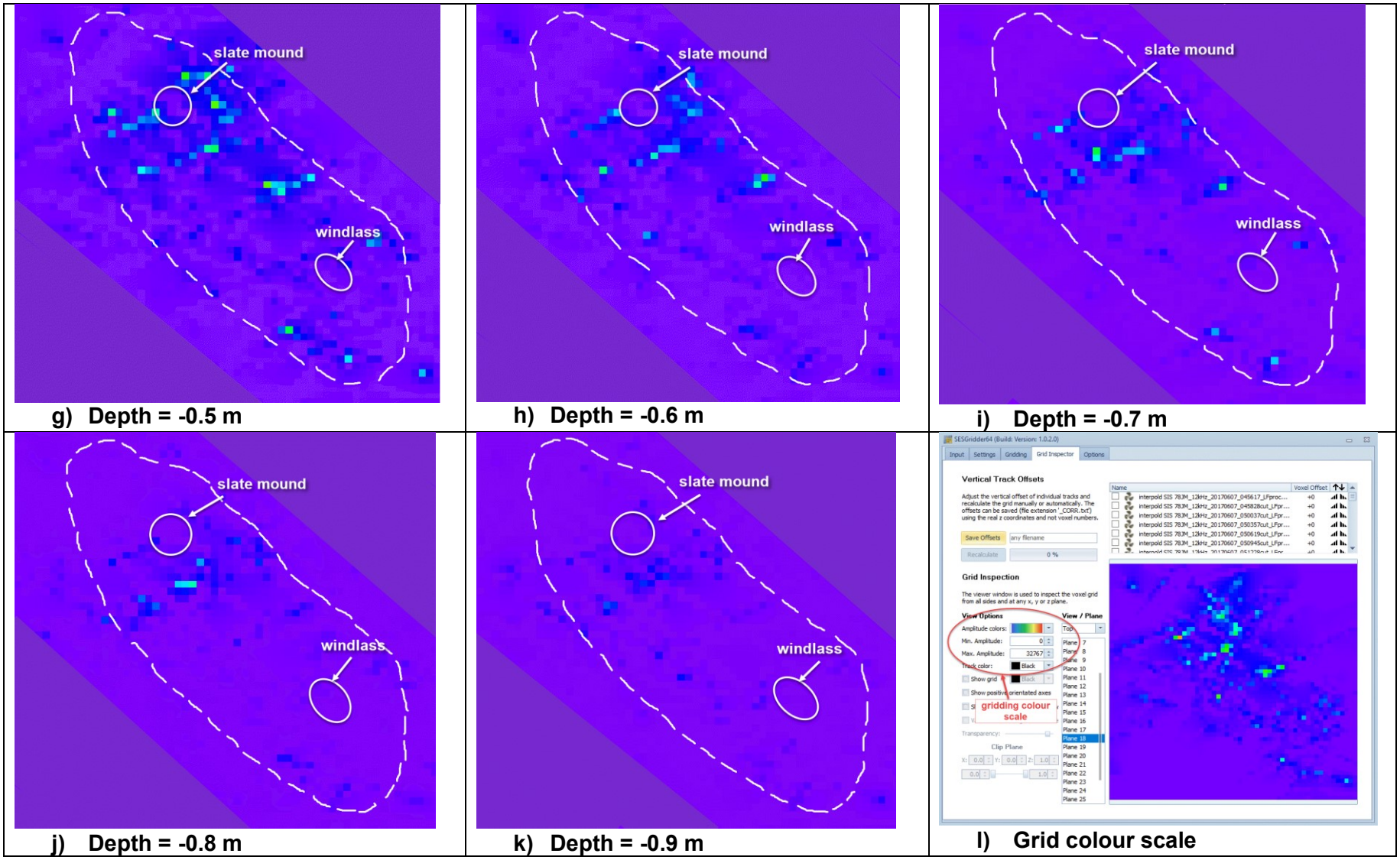

Fig 4.54 (cont'd) Horizontal planes at depths from + 0.35 m to -0.9 m, relative to seabed level, through 3D grid, all at same scale.

seabed. At the same depths bright reflector spots are seen on the immediate inside of the bow crash barrier—these most likely represent sandbags from earlier protective works together with localised sand accumulation. At the slate mound the loss of reflectors indicates the beginning of its underlying acoustic shadow. Surrounding the slate mound however, reflectors appear, signifying deeper seabed levels in this area. Reflectors occur around the base of the windlass, but disappear under it, indicating the top of its acoustic shadow. Bright reflectors appear inside the stern crash barriers at a depth of 0.3 m potentially indicating the stern post which had been separated from the damaged stern remains.

From a depth of -0.4 m (layer f) to -0.9 m (layer k) the shape of the starboard hull and keel can be visualised. Reflectors representing the hull section forward of amidships, with associated ship's fittings and in situ cargo, can still be seen at -0.4 m depth, but gradually disappear by -0.7 m (layer i). In contrast, reflectors from the less cluttered hull section aft of amidships, and especially around the slate mound and keel regions, are relatively much brighter and remain visible at greater depths. At -0.9 m reflectors are still seen just forward of the slate mound, mainly in the central area between the keel and bulwarks. Overall, these gradual changes in reflector locations through depth suggest that that the stern end of *James Matthews* is buried slightly deeper than the bow end, and that the deepest curvature of the starboard hull, forward of the slate mound position, can be identified. In addition, the isolated slate mound with its characteristic acoustic shadow is easily seen, however the windlass is less clearly identifiable against the more cluttered background of cargo and other items laying on the hull timbers. Many isolated bright reflectors are also seen. These may represent iron deck knees, individual items lying on the hull timbers, sandbags from earlier site protection works, effects from surface features including the brown alga, or simply the effects resulting from the 3D interpolation of the irregularly spaced SBP runs.

Quantitative comparison with surveyed remains of *James Matthews* shipwreck

Following the excavation of the *James Matthews* wrecksite in 1976/77, the WAM archaeologists conducted a 3D survey of the exposed remains. Based on those survey records, and following the methodology detailed in Chapter 3, a 3D AutoCAD digital computer model of the stern section of *James Matthews* remains was prepared for direct comparison with SBP data. Oblique cross sections were cut through the AutoCAD model, using the SECTION command, aligning with SBP runs 20170607 051953 and 20170608 031531 (Figure 4.55). These runs were selected as they cross over, or cross forwards of the key identifying feature of the slate mound, as well as the iron bars, the keel, a veneer of slate and multiple layers of hull timbers. The components cut by these two cross sections are

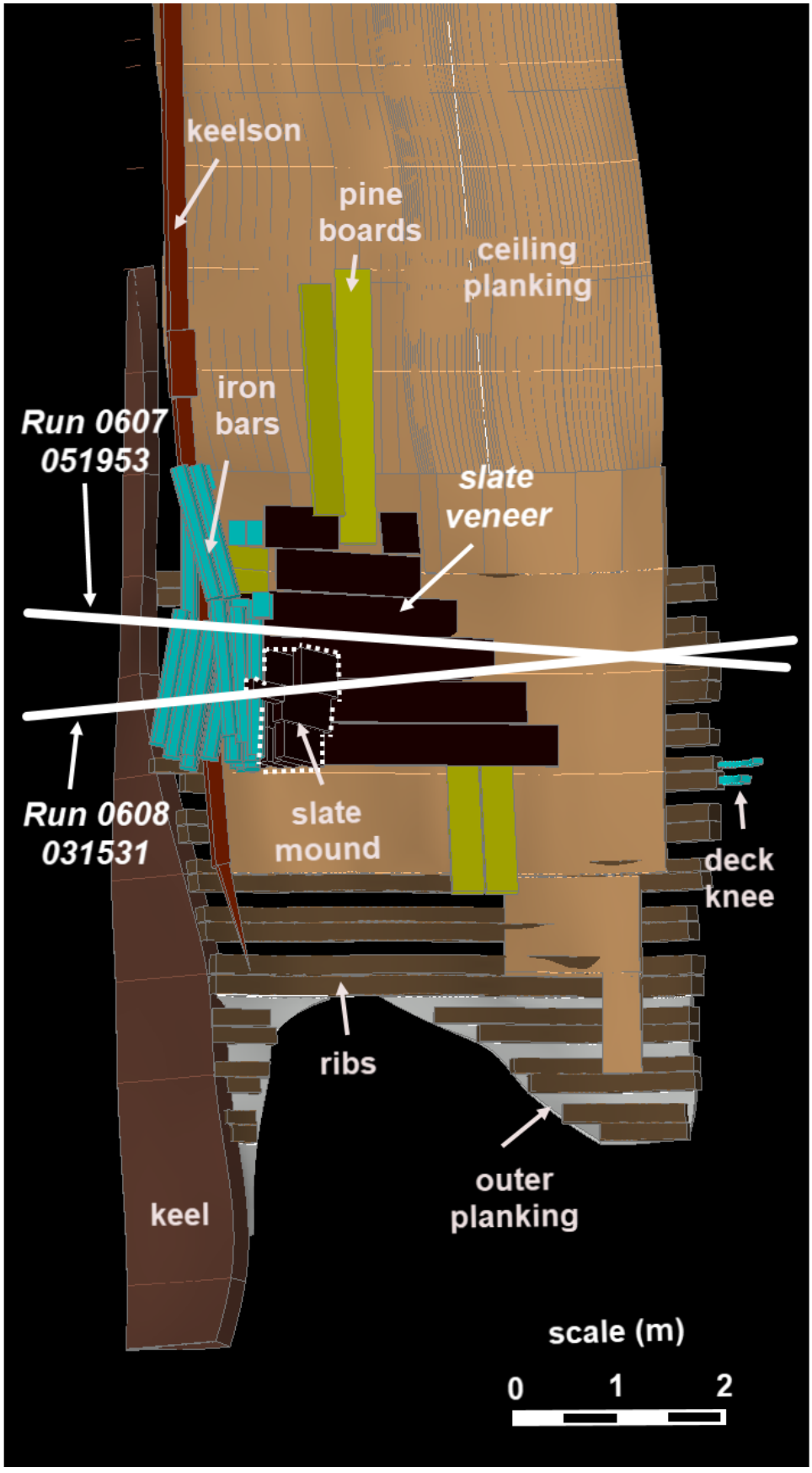

Figure 4.55 Plan view of *James Matthews* AutoCAD model showing the 2017 SBP run locations.

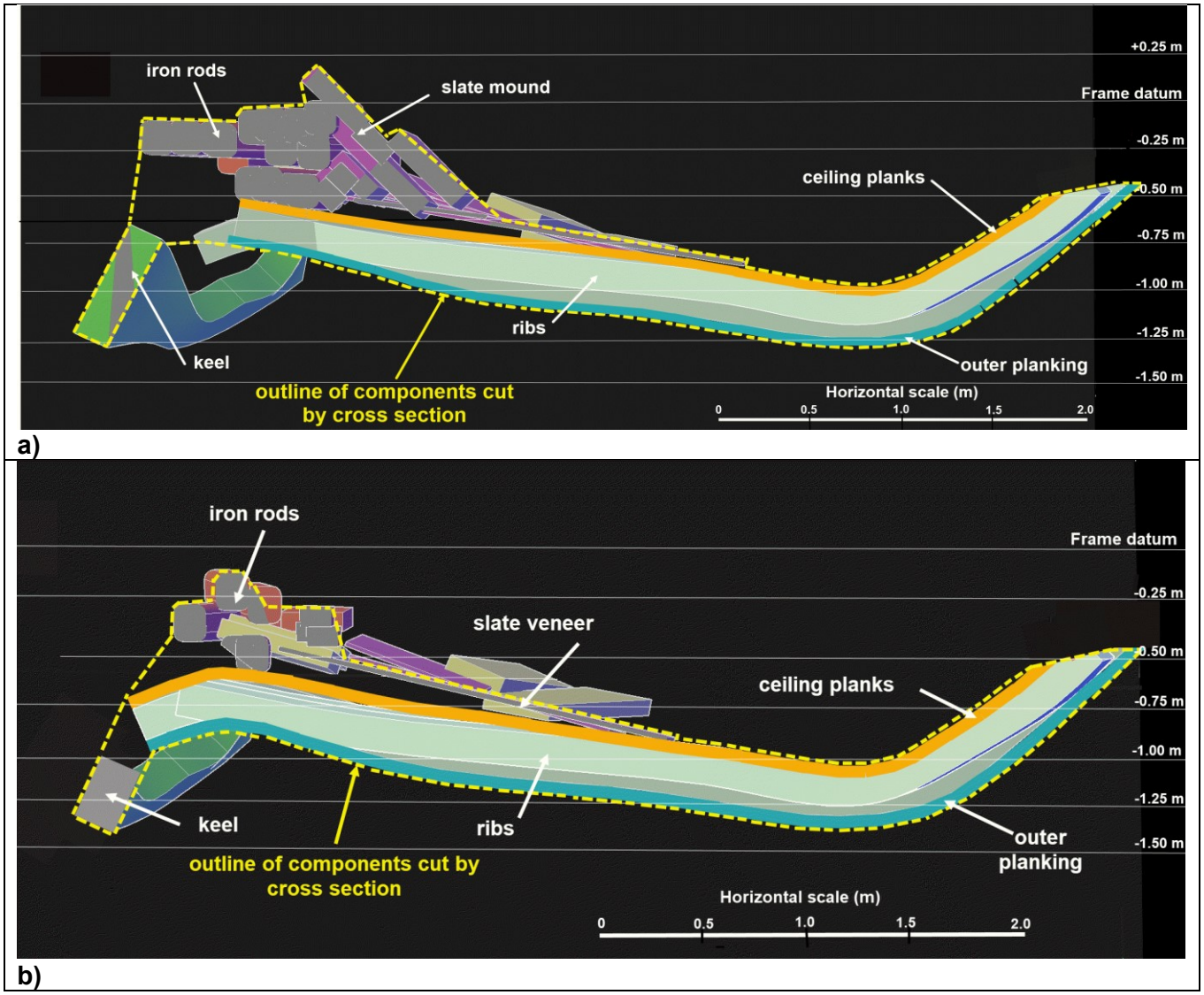

Figure 4.56 Sections through AutoCAD digital model corresponding to SBP locations: a) run 20170608 031531; and b) 20170607 051953.

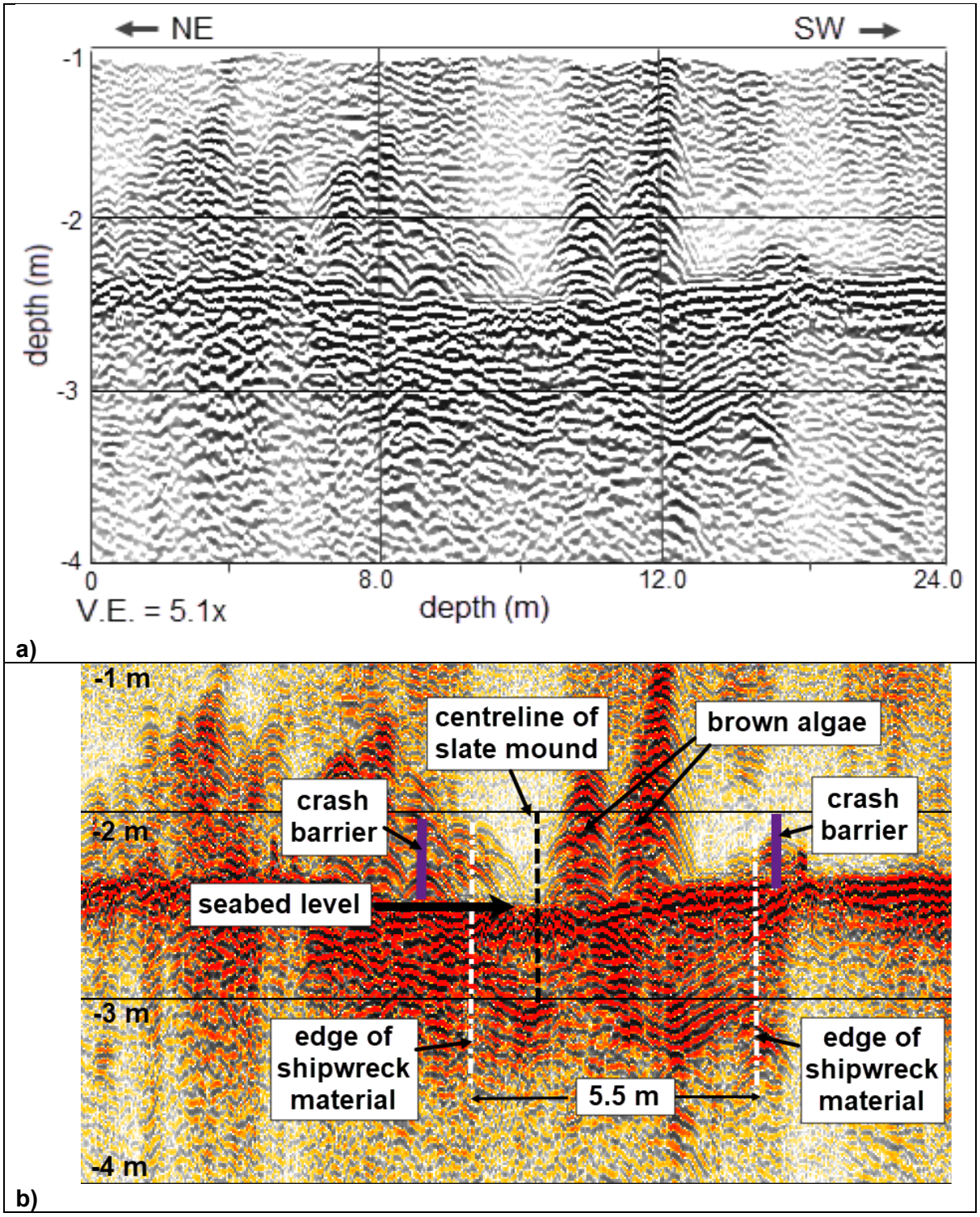

Figure 4.57 SBP section for run 20170607 051953; (a) greyscale, uninterpreted; (b) red-white-black colour scale with interpretations.

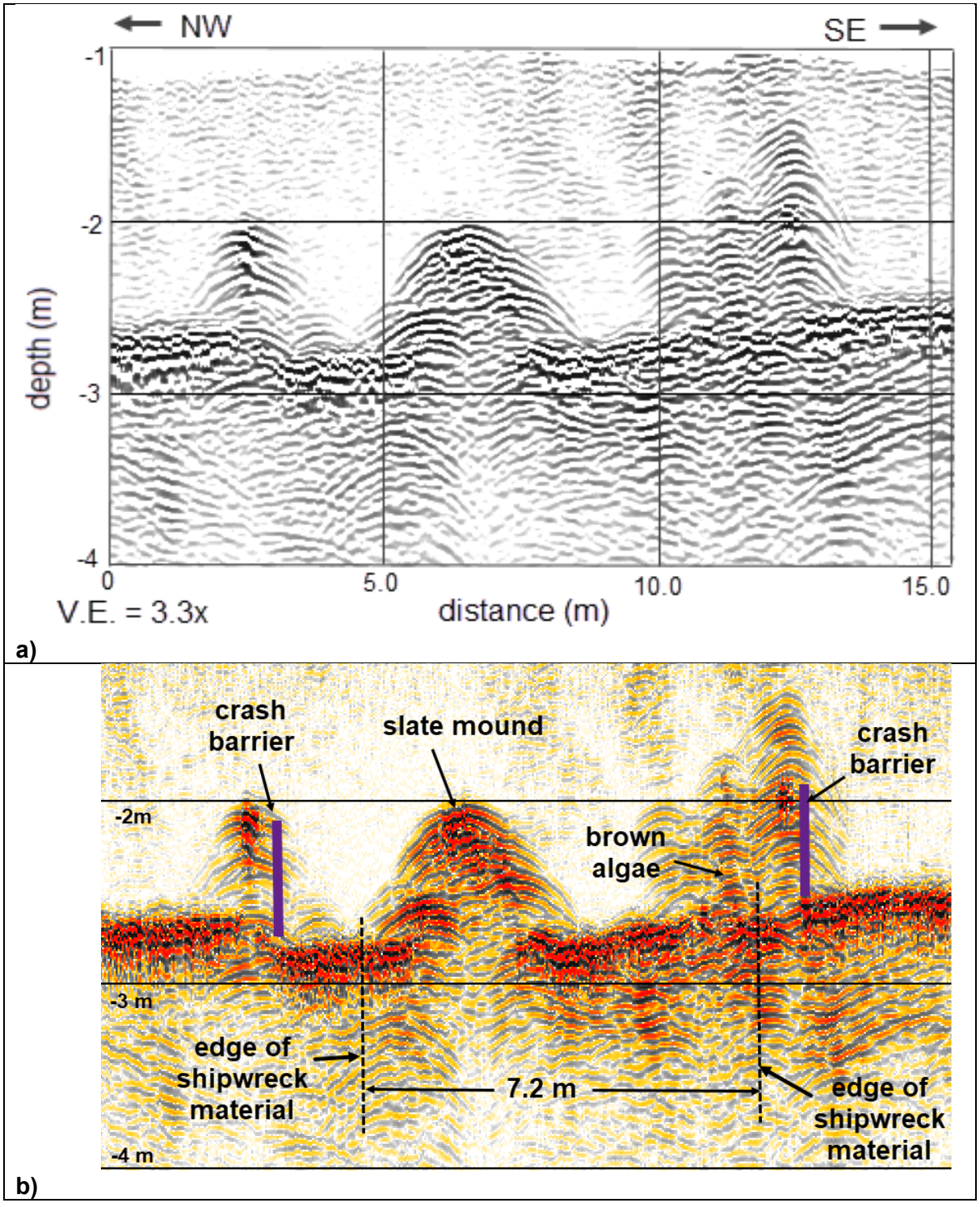

Figure 4.58 SBP sections for run 20170608 031531; (a) greyscale, uninterpreted; (b) red-white-black colour scale with interpretations.

shown in Figure 4.56 and the corresponding SBP cross sections are shown in Figures 4.57 and 4.58. Comparative mapping of burial depths, material thicknesses and comparisons of reflection coefficients to material types, using the SBP and model data, is conducted in the following chapter. Comparative analyses of ship's timbers and cargo forward of amidships was not undertaken. With the exception of the windlass and pine timber boards, the multitude of

shapes of material lying on the ceiling planks, within the curvature of the starboard hull forward of amidships, prevented further development of the AutoCAD model. The complexity of the point cloud of data representing each 3D survey point in this area could not be clearly seen nor individual elements identified.

Chapter summary

Modern timber and ferrous sleepers were buried for SBP verification purposes at different depths from 10 cm to 50 cm, and in different timber grain orientations, at the James Matthews and Swan River experimental sleeper sites. The sediments at the James Matthews sleeper site, located on the north side of Woodman Point, were characterised as medium-fine grained calcareous sands, with a small percent of fine gravel sized shell fragments. At the Swan River sleeper site near the confluence of the Swan and Canning Rivers at Coffee Point, the sediments were characterised as medium grained siliceous sands with a higher proportion of coarse sand.

In shallow water depths, both the salinity and temperature of the water affect the propagation speed of the SBP sound waves. Similarly, sediment bulk density is the most fundamental sediment property directly affecting the speed of sound under the seabed. To correctly validate the performance of the SBP at these sites, the temperature and salinity of the coastal waters at the James Matthews sleeper site were recorded at the times of SBP measurement to be 17.6 ^{O}C –19^{O}C and 35–38.8$^{0}/_{00}$, respectively. Based on volumetric and mass of sediment cores collected at undisturbed (reference) and sleeper (backfilled) locations, the mean sediment bulk density values ranged from 2107–2090 kg/m^3. Likewise at the Swan River sleeper site, the mean temperature and salinity of the aerobic overlying water was 19.6^{O}C and 39.3$^{0}/_{00}$ respectively, and the sediment bulk density ranged 2206–2049 kg/m^3.

The in situ density of the sediments above the buried sleepers was also determined to independently check the SBP based calculation of the reflection coefficient. This coefficient is a measure identifying the strength of the acoustic reflection from the buried sleeper, and is investigated in the following chapter to assess if it can aid interpretation of the buried sleeper material. Cone penetrometer tests were undertaken on reference, backfilled and manipulated (lightly and tightly compacted) cores collected from both experimental sites. For cores collected at the Swan River sleeper site, the cone penetration force profile for the light compaction test resulted in the lowest force profile. The tight compaction test resulted in the highest force profile. The force profile test results for the non-manipulated reference and backfilled cores fell in between these two bounds. Differences in the force profiles for duplicate

backfilled cores, one of which was higher than the reference site cores, demonstrated the unintended effects of post-backfill densification at this site by deliberate (but uncontrolled) walking and stamping on the loose sediment fill. For the James Matthews sleeper site, the light compaction also resulted in the lowest force profile. The force profile associated with the tight compaction test did not result in the highest profile, but was similar to the force profile from the location that was backfilled only one month prior to coring. The force profile was higher for cores that had been backfilled 15 months prior, and the force profile for reference cores at the James Mathews sleeper site was higher again. These results, together with the measured bulk sediment values, will be used in the following chapter to determine the sediment velocity and density (the combination known as the acoustic impedance of the sediment) at the times of SBP measurement (insonification) for each sleeper, buried at different times, at both experimental sites.

Sacrificial timber blocks cut from the same sleeper timbers (European oak (*Quercus* robur), pine (*Pinus* radiata) and jarrah (*Eucalyptus* marginata)) were also buried at the same depths as the timber sleepers at both sleeper sites. A representative proportion of these blocks were then recovered following the SBP surveys for density analyses. From this data the acoustic velocities and acoustic impedance of the timber sleepers, at the time of SBP insonification, were estimated. Pre-burial maximum water content and bulk and basic densities were measured from 2 cm x 2 cm x 2 cm sub-samples cut from of all three timber species. Moisture content, bulk and basic densities were determined from typically 11 similar sized cubes cut sectionally through the blocks post-recovery. These results demonstrated high variability across the cubes, with bulk density values significantly higher in the cubes cut from the outer layer of blocks compared to those cut from the inner sections. These differences were visible in sections cut through the blocks. There were no significant differences in the bulk density values between any of the recovered blocks buried at different depths or for different durations, but their average post-burial values were significantly higher than their pre-burial values. The basic density determined from the recovered blocks showed similar levels of high variability, with a significant decrease compared to pre-burial values in the shallowest buried blocks. The average moisture content in duplicate blocks recovered from the James Matthews sleeper site decreased with depth of burial, and a similar trend of decreasing moisture content with burial depth was also seen at the Swan River sleeper site, despite the shorter (9.25 months as opposed to 20.5 months) burial time at this site compared to the James Matthews sleeper site. These results are consistent with the in situ processes of water logging and timber degradation. Sediment dissolved oxygen and Eh profiles were also measured down the length of reference and backfilled cores collected from both sites. The profiles demonstrated high saturation and high variability in the upper sections of each 50 cm long core, reducing to sub-

oxic and anoxic conditions below, with an oxidising potential at all depths. They reflected variability due to bioturbation, the effects of sediment porewater re-oxygenation during excavation/backfilling and potential localised reburial of organic matter and confirmed the ongoing potential for buried timber degradation as seen in the timber blocks.

Acoustic reflectors potentially associated with buried sleepers were identified from SBP surveys conducted in June 2017 and in May 2018 at the James Matthews sleeper site, and in May 2018 at the Swan River sleeper site. In the June 2017 survey, the SBP transducer was vessel-mounted and two successful runs were achieved, but not all of the sleepers buried at that time were insonified due to wind and tidal drift of the vessel. By May 2018, the SBP transducer was mounted on a remotely controlled purpose-built seabed sled, and the acoustic returns and highly accurate positional data were recorded along all buried sleepers from four opposing runs. At the Swan River site, simultaneous Bluetooth© communication failure between the DGPS instrument and the SBP recording software, and failure of the DGPS internal recording, unfortunately resulted in the recording of acoustic trace data without positional information in two runs. Following a pre-established analysis protocol, the mean values associated with the seabed depth, the depth of reflectors representing buried material interfaces, and the depth of the 1st seabed multiple along all runs from both sites were determined. The variability of these depth estimates was documented using the standard deviation and relative standard deviation for each mean value. Likewise, the amplitude mean values, standard deviations and relative standard deviations for the reflectors associated with the seabed level, buried material interfaces and the 1st seabed multiple were also determined. The largest relative variability was associated with the seabed and buried reflector amplitudes, the least with the seabed and buried reflector depth estimates.

A number of parameters were determined from this SDBP data. The depth of sediment cover over the sleepers, known as the depth of burial (DoB), was calculated by subtracting the depth of the seabed from the depth of the 1st reflector representing buried material. When multiple reflectors were identified below the seabed, the thickness of, or possible gap between the material was calculated by subtracting the depth estimates of the first reflector from the second. Reflection coefficients were calculated based on the mean SBP reflector depth and amplitude data with resulting magnitudes from the 2018 data varying from 0.01 to 0.44. The magnitudes for the reflection coefficient values determined from the 2017 data were an order of magnitude lower. Detailed interpretation of the DoB and material thickness data will be undertaken in the following chapter, once the position of each identified reflector, relative to the known sleeper locations, is confirmed. Likewise, comparative analyses of the reflection

coefficients with their respective sleeper material will be undertaken, as well as an investigation into the significant difference in values from the 2017 to 2018 results.

The positional accuracy of the identified reflectors along the four 2018 SBP runs, relative to the known sleeper locations, was established to be in the range 5 cm–21 cm. Detailed analyses of these results, including the reliability of correctly identifying a buried sleeper, and the likelihood of failing to identify a buried sleeper, is discussed in the following chapter. For the two 2017 vessel based SBP runs at the James Matthews sleeper site, a loss of positional accuracy to around 1+ m, together with an unexplained lateral offset, meant that this 2017 SBP data will only be used for depth and reflection coefficient analyses. Given the uncertainty surrounding the association of reflectors and sleepers buried in the Swan River site, no further analyses beyond the initial calculation of reflection coefficients could be undertaken.

To verify the parametric SBP performance, 89 SBP runs across and surrounding the *James Matthews* wrecksite, located on the northern side of Woodman Point, were undertaken in June 2017. The same vessel-based transducer configuration was used as per the adjacent sleeper site. Of these runs, 37 tracked 'loosely parallel' and transversely across the buried wrecksite material in a SW–NE direction, at an average spacing of 0.8 m. A further 10 runs in a NW-SE direction longitudinally crossed the site at an average spacing of 1.4 m. The echogram plots from three transverse and three longitudinal runs were qualitatively assessed to identify key site features. Current-day exposed material including the protective road crash barrier cofferdam surrounding the wrecksite, the slate mound, windlass and iron deck knees were all recognised. The lateral extent of contiguous reflectors representing the buried shipwreck material across the known site, together with isolated reflectors located outside the cofferdam, were seen. The depth of the buried material, up to a maximum of 1.0 m below seabed level, was also identifiable, as was an area of sand cover up to 0.5 m thick covering portions of the shipwreck material. A quantitative assessment of this interpretation, together with reflection coefficients calculated from known materials and acoustic interfaces, will be undertaken in the following chapter. These will be based on a direct comparison between SBP data from two runs and their corresponding cross-sections from a digital 3D model. This AutoCAD model was constructed using the archived records from the 1976/77 excavation and archaeological survey of the *James Matthews* site conducted by the Western Australian Museum.

The amplitudes from the continuously spaced, vertical traces along all 47 SBP runs across the site, were interpolated into a 29 m x 28 m x 1.45 m 'volume' using gridding software to provide a quasi-3D visualisation of the site. Within this 'volume' amplitudes were calculated at the corners of almost 65,000 elements (voxels), each 0.5 m x 0.5 m x 0.05 m in the horizontal (x and y) and vertical (z) dimensions. The reflector amplitudes within the 'volume' were plotted

in horizontal layers, with each slice from a deeper depth. This revealed the plan shape of the cofferdam, the locations of surficial features, the shallowing slope of the seabed within the cofferdam from stern to bow, the hull buried deeper at the stern than the bow, and the general shape of the starboard hull. In the next chapter the results from independent geophysical surveys will be used to confirm and supplement these observations.

5. INTERPRETATION

Introduction

The results from the sub-bottom profiler (SBP) data collected at the James Matthews and Swan River experimental sleeper sites and the *James Matthews* shipwreck site, together with analyses of site-related controlling variables, were individually presented in Chapter 4. Here, those results are combined and outcomes interpreted to support the response to the research question argued in the final chapter. These conclusions are drawn from the in situ experimental (validation) and comparative (verification) studies.

Validation of the performance of the SBP under controlled burial conditions is the first outcome discussed. Included within this 'fit for purpose' interpretation are the SBP performance characteristics associated with: the ability and reliability to identify shallow-buried modern archaeological replicas (the sleepers); the accuracy and variability associated with measuring their depth of burial (DoB); and the potential to identify their material properties based on measured acoustic parameters. The in situ parameters which control the acoustic properties of the overlying seawater column, the sediments and the timber sleepers are also examined and used to correct SBP interpretations. The operational mode of the SBP and related impacts on the SBP results will be discussed.

The second outcome assessed is the verification performance of the SBP on a real and complex wrecksite. Both qualitative and quantitative comparisons to the known extent of material remaining from the wreck of *James Matthews* will be interpreted. Verification is based on the assessment of accuracy associated with defining the extent of the site plan, site description based on cross-sectional and quasi 3D visualisation comparisons, and quantitative assessment of the DoB and properties of the shallow-buried shipwreck material.

Finally, in this chapter, performance characteristics of the parametric SBP which have been validated and verified, are discussed in the context of their application for the purposes of in situ management and archaeological research.

Validation outcomes

The SBP performance attributes relating to their use in distinguishing purpose-buried sleepers, quantifying the sleepers' DoB, and characterising their material properties are based on interpretation of the results from the experimental sleeper sites. These results, reported in Chapter 4, encompassed the acoustic measurements of precisely buried timber and ferrous sleepers at two sites under different field operational conditions. Single oak, pine, jarrah and

ferrous sleepers, with corresponding sacrificial timber blocks, were purposefully buried adjacent to the *James Matthews* shipwreck site, in nearshore conditions off Woodman Point, WA. Similar sleepers and blocks were also purposefully buried in the Swan River, at the confluence with the Canning River at Coffee Point. The sediment conditions at these two locations are characterised as medium–fine grained calcareous sands, and medium grained siliceous sands, respectively. The sleepers were buried horizontally with depths of sediment cover varying from 10 cm to 50 cm. Additional pine sleepers were buried with the upper face inclined 22.5 degrees to the horizontal, with the longitudinal grain oriented vertically, and with two and three sleepers vertically stacked. Controlling water column parameters were measured in situ and sediment cores collected and sacrificial timber block recovered co-incident with the SBP runs. The water quality and subsequent results from the analyses of the sediment cores and timber blocks were used to calculate actual water and sediment velocities at the time of SBP insonification (measurement). These were used to correct the calculations of the seabed level, the DoB of the sleepers and their reflection coefficients. The results from the sediment and timber analyses were also used to determine their acoustic impedance to validate SBP derived reflection coefficient values.

Identification of sleepers

Detailed examination of the SBP echo plots along multiple runs at the James Matthews sleeper site demonstrated that shallow buried material covered by more than 12 cm of sediment can be identified with high confidence. The likelihood of falsely identifying buried material, or not identifying material when buried deeper than 12 cm, is also very low. This interpretation is based on the analyses of SBP measurements across 17 x 50 cm long sleepers each 12.5 cm wide and 12.5 cm thick, which were buried at the James Matthews sleeper site in February 2017, and a further nine sleepers which were buried in April 2018 (Table 3.3). In June 2017, the sleepers installed at the time were measured using a vessel mounted Innomar SES-2000 *compact* SBP travelling at 2 m/s. In May 2018, all sleepers were measured using the same SBP mounted on a remotely controlled seabed sled travelling at an average speed of 0.15 m/s. The seabed sled was constrained to run along the line of sleepers with the SBP transducer vertically over all sleepers. The vessel-mounted transducer however did not remain directly over the sleepers along the entire 30 m long run of sleepers due to wind and tide conditions. This field operational issue, unrelated to SBP performance, meant that not all sleepers buried at that time were recorded.

The locational accuracy of the SBP identified sleeper reflectors was determined by comparing the relative positions of the SBP reflectors from the 2018 survey with the known sleeper locations. The latitude and longitudinal positions of reflectors identified along four SBP runs,

two in each direction, were compared with the known positions of the buried sleepers (Table 4.20). Using ArcGIS ArcMap 10.6.1 software, the relative accuracy of the centre-line position of each reflector, from each SBP run, was estimated to be 0–21 cm. This accuracy was determined from two components: 1) interpretation of the range of traces in the SBP record, each of which could reasonably be classified as 'over the centre-line of the sleeper'; and 2) from the different plotting position of clearly identifiable besser-brick markers placed on the seabed surface for control purposes. Table 5.1 lists the outcomes from this analysis. Based on the identification of 27 possible sleepers from each of four SBP runs, the SBP reflector interpretation procedure correctly identified sleeper locations 93% of the time. Only one identified reflector did not match a sleeper location. There were two sleeper locations where factors unrelated to SBP performance resulted in a non-identification of those sleepers. Excluding these, three sleeper locations (out of a possible 99) weren't detected. In the two locations with vertically stacked multiple sleepers, rather than a single buried sleeper, the top sleeper was not detected, however the deeper one was. For most sleepers, their position was identified on the SBP record by a reflection from the upper face of the sleeper. The position of four of these sleepers were identified only from the reflection from the lower face (underside) of the sleeper, as the reflection from the very shallow upper face was not discernible. The depth of sediment cover over the upper face of the three sleepers not identified, the four identified only from their lower face, and the two identified by the deeper stacked sleeper, ranged from 5.5–11 cm.

Table 5.1 Identification of sleepers.

run (18052018-)	number of sleepers correctly identified	number of sleepers not identified	number of sleepers falsely identified
132252	26*	1[#]	0
135105	24	3[Ø]	1
135516	23	4 [Ø, ^]	0
135912	24	2	0
totals	97/104 (93%)	5[@] /104 (5%)	1/104 (1%)

* one sleeper measured twice—sled jammed in position, operators reversed sled motion, then reversed forward again, passing same sleeper.
[#] in all runs, the dimensions of the sled and proximity of the end star-pickets prohibited the transducer from positioning over one end sleeper.
[Ø] upper shallowest sleeper not identified, but deeper stacked sleeper was identified.
^ lost RTK positional signal on last sleeper.
[@] excluding those not identified due to mechanical and electronic reasons.

This very shallow depth range (5.5–11 cm) corresponds to the upper portion of a band of high acoustic wave amplitudes associated with the reflection of the acoustic waves at the seawater: seabed interface. Figure 4.30 to Figure 4.34 show that this band extends approximately 20 cm below the seabed surface. With minor exceptions, the higher seabed amplitudes close to the seabed surface mask the amplitudes associated with very shallow buried material. Below this band, strong reflectors from buried material can be identified in the 12–20 cm depth range. At greater depths progressively weaker reflections from multiple interfaces can be seen.

The positional data from the June 2017 SBP runs was not used in this comparative analysis due to unresolved differences in the DGPS positions of the reflectors compared to the sleeper locations (Figure 4.43). Table 4.21 shows similar numerical characteristics, however, to Table 5.1 with eight reflectors aligning with the sequence of sleepers, one of which was identified only through the reflection from the underside of the sleeper. These combined results demonstrated that under controlled conditions, shallow buried sleepers covered by more than 12 cm of sediment can be identified with high confidence. This outcome is applicable whether the transducer is deployed from a survey vessel traveling at 2 m/s, or from a remotely controlled sled traveling at 0.15 m/s over the target area.

DoB and burial characteristics

The burial depths of reflectors based on the pre-set acoustic velocity of 1500 m/s used in the SESWIN data acquisition software strongly correlated to, but underestimated the known DoB of the buried sleepers. This interpretation was based on the comparison of the raw SBP data measured at the James Matthews sleeper site, reported in Table 4.13 through to Table 4.16, with the actual sleeper DoB values at the time of SBP insonification. The reflector DoB corresponding to known sleeper positions are presented in Table 5.2, as well as the measured DoB and material characteristics of each sleeper on the day of the SBP runs. These uncorrected reflector burial depths consistently under-estimated the sleeper DoB, with the exception of those sleepers with a DoB<12 cm. In these very shallow burial cases, the SBP data either over or under estimated the sleeper's DoB, did not identify the sleeper at all, or only identified the underside of the upper sleeper. Each tabulated depth value for each reflector in Table 5.2 is the mean value calculated from five consecutive traces. The associated variability (standard deviation and relative standard deviation) for the depths associated with the seabed level and the seabed 1st multiple, as well as the DoB, is documented in Table 5.3 and 5.4 for SBP runs 18052018-135105 and 18052018-135516, respectively. The standard deviation associated with the DoB estimates for all reflectors averaged across each run (Tables 5.3 and 5.4) are small (1.46 cm to 1.68 cm) and typically

are considerably less than the magnitude of the difference between the SBP predicted and actual sleeper DoB.

Table 5.2 Comparison of mean reflector depths and sleeper DoB measurements.

run 18052018-135105		run 18052018-135516		sleeper characteristics (at time of SBP run)		
reflector	**reflector DoB (cm)**	**reflector**	**reflector DoB (cm)**	**sleeper ID**	**sleeper DoB (cm)**	**material**
7937	15.4	*no positional data*	-	1	16.8	pine (22^0 rotation)
7727	10.1	8325	7.9	2	12.5	pine
7428	15.8	7956	14.3	3	20	pine (22^0 rotation)
7152	22.0	7703	26.3	4	30	pine (vert grain)
6724	21.8	7482	18.0	5	26	pine
6330	18.8	7119	18.4	6	25	pine
6002	12.8	6757	6.4	7	7	pine
5695	32.5	6501	32.3	8	40	pine
5273	20.7	6106	20.5	9	27	pine
not identified				10	9.5	pine
4782	15.4	5646	19.5	11	22.5	oak
4528	24.4	5302	20.3	12	25	pine (vert grain)
4227	25.9	4929	23.3	13	30	oak
3909	22.9	4727	24.8	14	30	pine (vert grain)
3366	31.2	4243	45.1	15	47	pine
3126	35.5	3945	35.5	16	45.5	pine
2810	25.0	3545	23.5	17	30	oak
2522	14.8^/23.3	3291	14.3^/30.8	18	8	pine (mult 10/30)
2081	16.5^/23.5	2676	27.6*	19	5.5	pine (mult 10/30/50)
1691	8.6	1523	14.8	20	11	pine
1426	19.5	1252	18.6	21	23.5	oak
1145	19.5	1004	16.3	22	23	jarrah
903	24.2	717	24.2	23	35	jarrah
595	21.0	364	21.2	24	27.5	ferrous
428	25.5	162	21.0	25	30	ferrous
not insonified				26	46	ferrous

^ underside of top sleeper, * possibly top of 2nd (stacked) sleeper

Table 5.3 Variability associated with reflector depths, SBP run 18052018-135105.

trace	seabed level (m)		DoB (cm)		seabed multiple (m)	
	SD	RSD	SD	RSD	SD	RSD
7937	0.035	3.6%	2.58	15.4%	0.026	1.3%
7727	0.000	0.0%	0.59	5.8%	0.000	0.0%
7428	0.000	0.0%	2.06	13.0%	0.009	0.5%
7152	0.006	0.6%	1.79	8.1%	0.006	0.3%
6724	0.009	0.9%	2.22	10.2%	0.013	0.7%
6330	0.000	0.0%	0.96	5.1%	0.000	0.0%
6002	0.005	0.5%	1.07	8.3%	0.006	0.3%
5695	0.006	0.6%	2.22	6.8%	0.014	0.7%
5273	0.000	0.0%	3.43	16.5%	0.000	0.0%
4782	0.006	0.6%	1.94	12.6%	0.006	0.3%
4528	0.005	0.5%	0.62	2.6%	0.005	0.3%
4227	0.000	0.0%	2.06	7.9%	0.010	0.5%
3909	0.000	0.0%	1.22	5.3%	0.008	0.4%
3366	0.010	1.0%	3.24	10.4%	0.005	0.3%
3126	0.005	0.5%	0.48	1.3%	0.005	0.3%
2810	0.006	0.6%	1.94	7.8%	0.026	1.4%
2522	0.006	0.6%	0.48	3.2%	0.000	0.0%
2081	0.005	0.5%	2.89	17.5%	0.000	0.0%
1723	0.000	0.0%	1.51	17.7%	0.005	0.3%
1426	0.005	0.5%	2.32	11.9%	0.005	0.3%
1145	0.000	0.0%	2.32	11.9%	0.000	0.0%
903	0.000	0.0%	0.59	2.4%	0.006	0.3%
595	0.000	0.0%	0.59	2.8%	0.005	0.3%
428	0.025	2.4%	2.06	8.1%	0.008	0.4%
mean	*0.005*	*0.5%*	*1.68*	*8.6%*	*0.007*	*0.4%*

As previously noted in Chapter 3, water temperature and salinity affect the acoustic velocity in shallow coastal waters. Likewise, sediment facies and their density/porosity affect acoustic velocities in sediments. To evaluate the SBP's true performance relating to DoB estimates, the pre-set acoustic velocity used by the data acquisition software is corrected in the following two sub-sections. These corrections reflect the in situ conditions at the times of the SBP measurement, and detailed correlation analysis using both uncorrected and corrected reflector DoB values follow.

Corrections to seawater velocities

In shallow waters, the acoustic wave speed is dependent upon seawater salinity and temperature Lovett (1978:207). Lovett's equation (3) was used to determine the speed of the SBP acoustic wave in the seawater and in the Swan River at the times of SBP measurements. The raw water quality data is presented in Tables 4.1 and 4.2, and the derived seawater velocities, which are 2.5% to 3% higher than the pre-set value, are shown in Table 5.5.

Table 5.4 Variability associated with reflector depths, SBP run 18052018-135516.

trace	seabed level (m)		DoB (cm)		seabed multiple (m)	
	std dev	RSD	std dev	RSD	std dev	RSD
8325	0.000	0.0%	0.59	7.4%	0.005	0.2%
7956	0.000	0.0%	0.59	4.1%	0.006	0.3%
7703	0.005	0.5%	1.43	5.5%	0.005	0.3%
7482	0.000	0.0%	0.89	5.0%	0.000	0.0%
7119	0.006	0.6%	0.48	2.6%	0.000	0.0%
6757	0.009	0.9%	0	0.0%	0.000	0.0%
6501	0.006	0.6%	1.76	5.4%	0.005	0.3%
6106	0.005	0.5%	2.06	10.0%	0.000	0.0%
5646	0.022	2.1%	2.2	11.3%	0.000	0.0%
5302	0.000	0.0%	2.14	10.5%	0.000	0.0%
4929	0.000	0.0%	2.32	9.9%	0.000	0.0%
4727	0.005	0.5%	3.81	15.4%	0.006	0.3%
4243	0.006	0.6%	0.48	1.7%	0.005	0.3%
3945	0.005	0.5%	2.77	7.8%	0.005	0.3%
3545	0.006	0.6%	2.14	9.1%	0.000	0.0%
3291	0.009	0.9%	1.62	11.3%	0.000	0.0%
2676	0.005	0.5%	1.39	5.1%	0.005	0.3%
1523	0.006	0.6%	2.66	18.0%	0.005	0.3%
1252	0.000	0.0%	0.59	3.1%	0.000	0.0%
1004	0.005	0.5%	0.48	2.9%	0.000	0.0%
717	0.000	0.0%	0.96	4.0%	0.005	0.3%
364	0.006	0.6%	1.17	5.5%	0.000	0.0%
162	0.000	0.0%	0.96	4.6%	0.000	0.0%
mean	*0.005*	*0.5%*	*1.46*	*7.0%*	*0.002*	*0.1%*

Table 5.5 Seawater velocities at times of SBP measurements.

sleeper location/date	seawater temperature (^{0}C)	seawater salinity ($^0/_{00}$)	seawater velocities (m/s)
James Matthews, June 2017	19.0	35.0	1535.8
James Matthews, May 2018	17.6	38.8	1536.1
Swan River, May 2018	19.6	39.3	1542.4

Corrections to sediment velocities

For shallow coastal sub-tidal sediments, regression equations derived by Richardson and Jackson (2017:511) provide the most appropriate relationships to determine sediment velocities. These equations relate the sediment velocity ratios (sediment velocity/water velocity) to measured sediment bulk density values for carbonate sediments (James Matthews sleeper site) and for siliciclastic (silica-based) sediments (Swan River sleeper site).

The sediment bulk density of the surficial sediments covering the sleepers, at the times of SBP measurement, was derived from the combination of the in situ density penetration force profile results (cone penetrometer tests) and sediment bulk density measurements. As discussed in Chapter 4 penetration resistance profiles reflect in situ sediment density for similar saturated sediments under the same test conditions. These profiles were used to understand the relative density differences resulting from the sleeper backfill activities compared with reference (undisturbed) sediments. Together with the results from the manipulated compaction tests, the sediment bulk density values were interpreted for the conditions at the times of SBP insonification.

Figure 5.1a shows the collated results from the cone penetrometer tests undertaken on reference, backfilled and manipulated sediment cores collected in May 2018 at the James Matthews sleeper site. While only one penetration force profile is shown for clarity reasons for the reference and backfilled cores, Figure 4.14 demonstrates the strong similarity between duplicate cores from each of these locations. Given the use of the same 4 mm diameter penetration rod in all tests, the penetrometer force profile, rather than the penetration resistance profile, is shown. The initial expectation was that both the ‘lightly’ recompacted cores and the ‘tightly’ recompacted cores would respectively provide the lower and upper bounds to the penetration force profiles from backfilled and reference cores. This expectation was met with the ‘lightly’ compacted test which had the lowest force profile, indicating the lowest in situ density. This manipulated core reflected the conditions immediately after the sleepers were backfilled by hydraulic dredge at the James Matthews sleeper site. The ‘tightly’ recompacted core however had a similar average steady-state penetration resistance profile to that of the cores which had been backfilled only one month prior to core sampling.

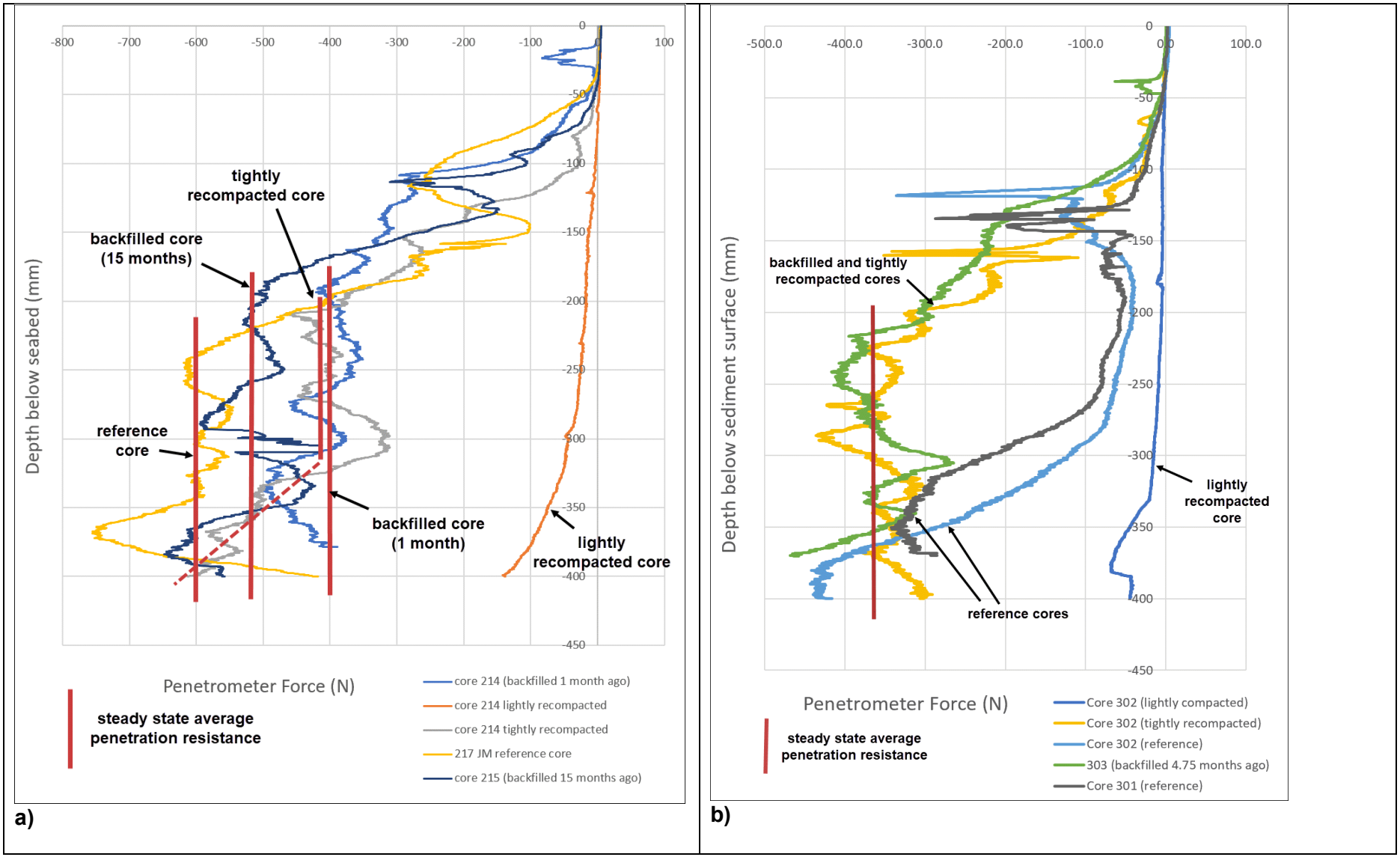

Figure 5.1 Penetration force profiles: (a) James Matthews sleeper site; and (b) Swan River sleeper site.

Furthermore, the average steady-state penetration force was higher for cores which had been backfilled 15 months prior to coring, and the average steady-state penetration force for reference cores was higher again. This suggests that the varying hydrodynamic (pressure) forces associated with the wave and tidal conditions occurring at this site quickly densify the backfilled sediment, from lightly compacted densities (immediate post-backfill) to densities similar to those achieved from mechanical compaction. The sediments gradually further densify to higher levels seen in the undisturbed cores. The penetration force in the 'light' recompaction test was similar to the penetration forces in the top 4–7 cm segment all other cores. In this upper segment the development of lateral test-related stresses was small and had little influence on the force profile. At greater depths, the steady-state penetration force in the 'light' recompaction core rose very slowly and was an order of magnitude lower than the average steady-state penetration forces for all other cores.

Table 5.6 combines these force profile observations with the bulk sediment density measurements undertaken on cores collected from the James Matthews sleeper site (refer Table 4.4). The lowest sediment bulk density value (1960 kg/m^3) was determined from the mean of duplicate 'light' compaction test cores, and this value was applied to the immediate post-backfill conditions. The bulk density of a single core collected seven months after backfilling was 2100.1 kg/m^3. Almost identical bulk density values (2048.0 kg/m^3 and 2084.9 kg/m^3) were determined for cores collected 15 and 21 months after backfilling. For the reference cores, sediment bulk densities were 2091.1 kg/m^3 and 2123.7 kg/m^3, with the latter value derived from a core resampled six months after the first. The duplicate sediment bulk density results for the tightly compacted test were 2067.7 kg/m^3 and 2074.3 kg/m^3. All of these bulk density values were derived as a single average for the entire core. Based on diver observation and the force penetration profiles for all cores, the sediment bulk density from the 'light' compaction test was applied in the upper surficial layer (0–7 cm), with the measured sediment bulk density values for the other cores applied below that, equivalent to the 'steady-state' test depths. There are clear differences in mean sediment bulk density values between the reference cores (2017 kg/m^3), the backfilled cores (2100.1 kg/m^3 to 2084.9 kg/m^3), the 'tightly' compacted cores (2071 kg/m^3) and the lightly compacted cores (1960 kg/m^3). These values are consistent with the relative magnitudes of the force profile results. The differences between the sediment bulk density results from the backfilled locations (7 months against 15–21 months) may indicate the temporal and/or spatial variability associated with this data.

Table 5.6 Sediment bulk densities corresponding to sediment core penetration force profiles, James Matthews and Swan River sleeper sites.

force profile	depth applicability (cm)	bulk density (kg/m^3)	
		James Matthews sleeper site	Swan River sleeper site
'lightly' manipulated	near-surface (0–7 cm)	1960	1978
immediate post-backfill	'steady-state' depths (20–40 cm)	1960	-
'tightly' manipulated		2071	2079
backfilled (1 month)		2071	-
backfilled (7 months)		2100	-
backfilled (4.75 months)		-	2049
backfilled (15–21 months)		2085	-
undisturbed		2107	2150

Figure 5.1b shows the corresponding collated results from the cone penetrometer tests undertaken on reference, backfilled and manipulated sediment cores collected at the Swan River sleeper site. In this case the 'lightly' recompacted core provided lower bound to the penetration force profiles. At the upper bound, the penetration force profile for the 'tightly' recompacted core matched the profile average of the reference cores as well as the backfilled cores. With the exception of a spike due to shell or other hard material buried between 12 cm and 15 cm, the penetrometer force profile for the reference cores slowly rose to around 26 cm below the seabed level. The force then rapidly increased due to lateral stresses at depths greater than 35 cm to an average steady-state value 7–9 times greater than the corresponding force for the 'lightly' recompacted core. In contrast, the penetrometer force profile in the 'tightly' recompacted core and in the backfilled core are similar—they both rose from a low level similar to those in the reference cores at depths of around 10 cm, and reached average steady-state conditions at a shallower depth of 20 cm. The average steady-state penetrometer force was similar in the 'tightly' compacted core, in the backfilled core, and in the reference cores. The backfilling of the sleepers at the Swan River site using shovels, followed by foot compaction, resulted in immediate steady-state resistance conditions occurring at much shallower depths than in non-disturbed reference locations.

The measured sediment bulk density for these Swan River cores are also included in Table 5.6. The 'light' and 'tight' values were 1977 kg/m^3 and 2079 kg/m^3, respectively. Backfilled (4.75 months) values were 2032 kg/m^3 and 2066 kg/m^3, with reference core values 2111 kg/m^3 and 2189 kg/m^3, respectively. The sediment bulk density values for the manipulated and backfilled cores were consistent with the penetration force profile results. The reference core

sediment bulk density values were much higher than that for the 'tightly' compacted core, contrary to the penetration force profile. However, while the cone penetrometer tests were carried out on all cores collected in April 2018, the sediment bulk density measurements for the reference locations were conducted on cores collected 4.5 months later, and the higher sediment bulk density value may reflect temporal and/or spatial variability of the in situ sediment density at this site.

The sediment velocities at the time of SBP measurement were based on the sediment bulk densities at those times. The timeline for the SBP surveys and sleeper burial is shown in Figure 5.2. This timeline is based on the repeated burials (Table 3.3) and SBP surveys at the James Matthews sleeper site, and for the single burial (Table 3.4) and SBP survey at the Swan River sleeper site. This figure shows that SBP surveys were undertaken: 1.5 months after burial of nine sleepers at the James Matthews sleeper site in 2018; four months after burial of the initial 17 sleepers at the James Matthews sleeper site in 2017; four months after burial of all sleepers at the Swan River sleeper site in 2018; and 15 months after burial of the initial 17 sleepers at the James Matthews sleeper site (2017–2018). Based the results shown in Table 5.6, the sediment bulk density values at times of SBP survey are presented in Table 5.7.

Figure 5.2 Timeline for SBP survey and timber burial at the James Matthews and Swan River sleeper sites.

Using Richardson and Jackson's (2017:511) regression equations, the sediment velocity ratio (V_{pR}) was estimated based on the measured sediment bulk density (ρ), (g/cm^3) as follows:

$V_{pR} = 1.878 – 1.2289\rho + 0.4232\rho^2$ (calcareous sediments) (11)

$V_{pR} = 1.585 – 0.8991\rho + 0.3352\rho^2$ (siliciclastic sediments) (12)

$V_{pR} = 1.649 – 0.9807\rho + 0.3595\rho^2$ (siliciclastic+ calcareous sediments) (13)

Table 5.7 Sediment in situ density at times of SBP survey.

sleeper site	sediment depth	time after burial	bulk density (kg/m^3)
James Matthews	near surface (0–7 cm)	–	1960
	20–40 cm	1.5 months	2071
		4 months	2100
		15 months	2085
Swan River	near surface (0–7 cm)	–	1978
	20–40 cm	4 months	2049

Inserting the measured sediment bulk density results from Table 5.7 and the calculated seawater velocities from Table 5.5 into equations (11) and (12), the sediment velocity ratios and sediment velocities for the James Matthews and Swan River sleeper sites are displayed in Table 5.8.

Table 5.8 Sediment velocity ratios and sediment velocities for the James Matthews and Swan River sleeper sites.

sleeper site	sediment depth	time after burial (months)	bulk density (ρ) (g/cm^3)	sediment velocity ratio (V_{pR})	seawater velocity (V_w) (m/s)	sediment velocity (V_s) (m/s)
James Matthews	Near surface (0–7 cm)	–	1.960	1.095	1536.0	1682.1
	20–40 cm	1.5	2.071	1.164		1766.7
		4	2.100	1.164		1787.3
		15	2.085	1.155		1774.8
Swan River	Near surface (0–7 cm)	–	1.978	1.118	1542.4	1724.5
	20–40 cm	4	2.049	1.150		1773.8

Comparison of reflector burial depths with measured sleeper DoB

A strong correlation exists between the SBP reflector burial depths and sleeper DoB. The sediment velocity-corrected mean reflector burial depths are listed in Table 5.9 and are drawn with the measured sleeper D0B as a scatter plot (XLSTAT 2019) in Figure 5.3. The line of best

fit for the uncorrected depths is also drawn in this figure. Corrections to the sediment velocities based on in situ parameters increased the mean reflector burial depths by 2–3 cm in the 5–20 cm depth range, and by up to 5–6 cm in the 30–45 cm depth range. The line of best fit through the mean depth-corrected values in Figure 5.3 shows that the reflector depths matched the measured sleeper depths for the very shallow buried sleepers, but increasingly underestimated the actual sleeper depths for the deeper burials. The variability associated with determining mean burial depths from the SBP data, for each reflector in runs 18052018-135105 and 18052018-135516, is shown in Table 5.3 and 5.4, respectively. From these tables, the average standard deviation across all reflector depths, in each run, was 1.7 cm and 1.5 cm. On the assumption that this variability follows a normal distribution, then the 95% confidence limits for the reflector depths are bounded by the mean value +/- 2 standard deviations. That is, mean depth +/- 3.4 cm for reflectors in run 18052018-135105 and mean depth +/- 3.0 cm for reflectors in run 18052018-1335516. This variability is of similar magnitude to the adjustments added to the mean values for the shallow (5–20 cm) reflectors due to the sediment velocity-corrections. The measurement variability is approximately one half of the magnitude of the depth adjustment to the deeper reflectors due to the sediment velocity-corrections. The average of the confidence limits for the two runs (+/- 3.2 cm) was applied to the line of best fit as depicted in Figure 5.4. Noting the accuracy of the sleeper burial measurements (+/- 1 cm), this figure shows: a) for sleeper DoB values up to 32 cm, the sleeper DoB values lie within the SBP +/- 95% confidence limits; and b) however, across the sleeper D0B range 12–46 cm, the line-of-best-fit (y=0.886x + 1.14) for the velocity-corrected reflector depths under-estimates the measured sleeper depth by 10%.The exceptions to a) tend to be the estimates of reflector depths associated with the deepest buried sleeper, and with the two sets of multiple (vertically) stacked buried sleepers. Here, the reflector depths were estimated based either on the underside of the top sleeper (and not the upper face as per all other sleepers), or the upper face of the lower sleeper (with the seabed amplitude interference masking the top sleeper completely). Confidence in this interpretation was gained from the multiple reflector measurements corresponding to the vertical gap between the stacked sleepers and the upper face of the second stacked sleeper. For the deepest measured sleepers, two estimates were made for the 46 cm buried sleeper on separate runs, yet a large and unexplained variability was recorded.

The 10% under-estimate of the line-of-best-fit in Figure 5.3, based on velocity corrections for calcareous sediments, may possibly result from a consistent underestimate of the sediment velocity. Given the in situ water and sediment characteristics were measured, then a review of the basis for Richardson and Jackson's (2017:509–511) calcareous sediment regression equation is warranted.

Table 5.9 Velocity corrected reflector depth comparisons

run 135105		run 135516		sleeper characteristics (at time of run)			
reflector	**depth of 1st reflector (cm)**	**reflector**	**depth of 1st reflector (cm)**	**sleeper ID**	**time since burial (months)**	**DoB (cm)**	**material**
7937	17.3	*no positional data*	-	1	1.5	16.8	pine (22^0 rotation)
7727	11.3	8325	8.9	2	1.5	12.5	pine
7428	17.7	7956	16.0	3	1.5	20	pine (22^0 rotation)
7152	25.4	7703	30.4	4	15	30	pine (vert grain)
6724	25.2	7482	20.8	5	15	26	pine
6330	21.7	7119	21.3	6	15	25	pine
6002	14.4	6757	7.2	7	15	7	pine
5695	38.5	6501	38.2	8	15	40	pine
5273	23.9	6106	23.6	9	15	27	pine
not identified				10	15	9.5	pine
4782	17.7	5646	22.5	11	15	22.5	oak
4528	28.1	5302	23.4	12	15	25	pine (vert grain)
4227	29.8	4929	26.8	13	15	30	oak
3909	26.4	4727	28.6	14	15	30	pine (vert grain)
3366	36.9	4243	53.4	15	15	47	pine
3126	42.0	3945	42.0	16	15	45.5	pine
2810	28.8	3545	27.1	17	15	30	oak
2522	16.6^/26.8	3291	16.0^/35.5	18	15	8	pine (mult 10/30)
2081	19.1^/27.1	2676	31.8*	19	15	5.5	pine (mult 10/30/50)
1723	8.2	1523	16.6	20	15	11	pine
1426	22.5	1252	21.4	21	15	23.5	oak
1145	22.6	1004	18.9	22	1.5	23	jarrah
903	28.0	717	28.0	23	1.5	35	jarrah
595	24.3	364	24.5	24	1.5	27.5	ferrous
428	29.5	162	24.3	25	1.5	30	ferrous
not insonified				26	1.5	46	ferrous

^underside of top sleeper, * possibly top of 2nd (stacked) sleeper

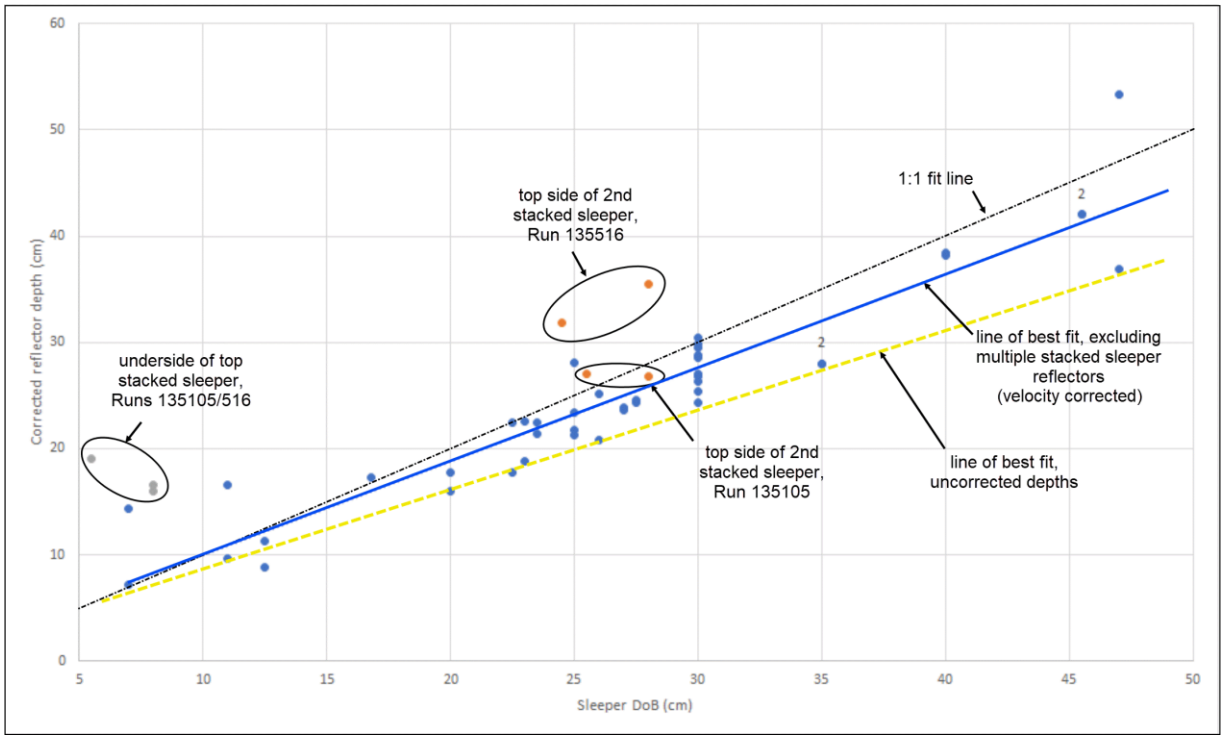

Figure 5.3 Scatter plot showing uncorrected and corrected reflector depth vs. sleeper DoB.

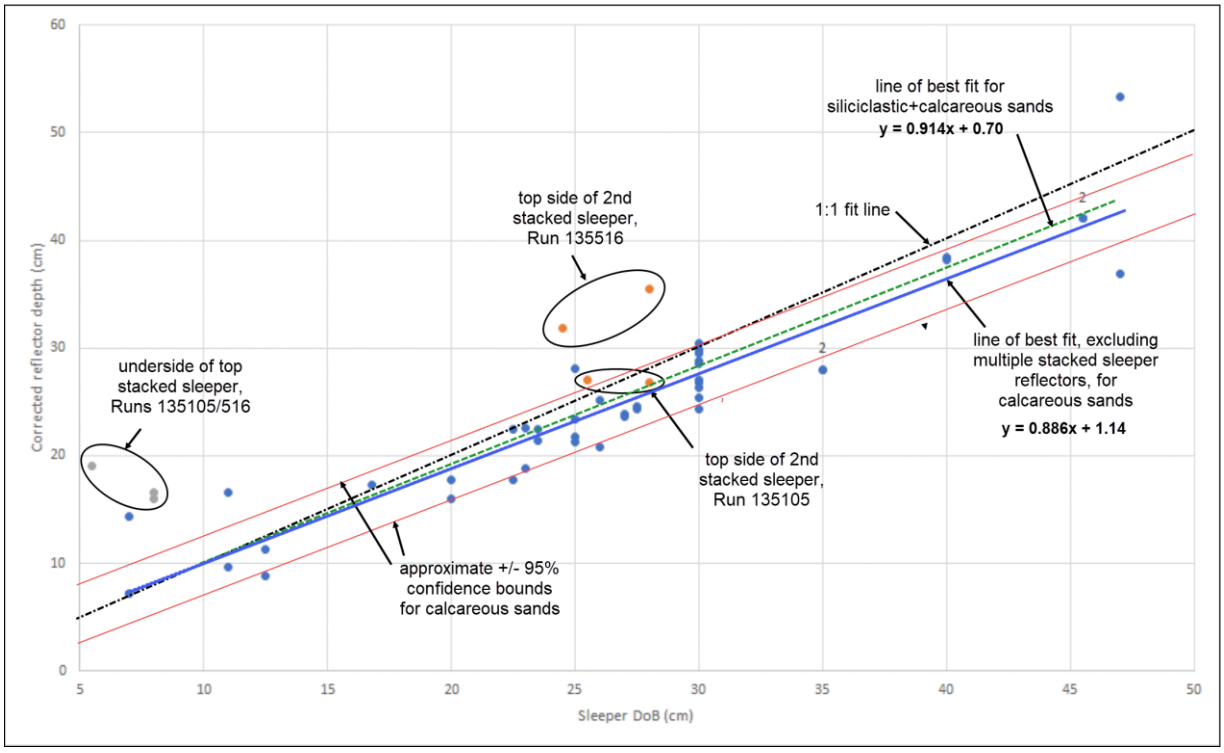

Figure 5.4 Scatter plot showing confidence bounds for line of best fit relationship between corrected reflector depth and sleeper DoB.

Figure 5.5 is a modified copy of their Figure 8.23(c) which shows the regression lines as well as the raw data from which their regression equations were derived. From Table 5.7 the sediment bulk density value for the surficial (0–7 cm) layer at the James Matthews sleeper site was 1.96 g/m^3, and this increased to 2.10 g/m^3 in the depth range 20–40 cm. Both values, especially the value of 2.10 g/m^3, are at the high end of Richardson and Jackson's (2017) data range where small changes in density result in more significant changes in the V_P ratio. Also, the regression curve for calcareous sands falls below the data points at this high end. Consequently, their regression line for siliciclastic + calcareous sands (equation 13), which appears to better fit the data at the high end, was applied to assess any potential significant change to the prediction of sleeper DoB. This change resulted in a marginal revision to the line of best fit (y = 0.914x + 0.70) as shown in Figure 5.4, with the under-estimate of the velocity-corrected reflector depths reducing from 10% to 6%. It thus appears that the divergence of the predicted sleeper depth with increasing DoB is not simply a function of in situ sediment velocity corrections. To achieve a 1:1 fit between the predicted and measured DoB values, a V_p ratio of 1.24 would be required, and this value is well above all of Richardson and Jackson's regression equation lines and would sit outside the range of their raw data.

From an operational perspective, the accuracy of the DoB estimates appear similar regardless of survey speed or transducer mounting. The preceding analyses have been based on two runs from the 2018 SBP survey which have the highest confidence in matching the SBP reflector positions with the measured sleeper locations. These runs were undertaken using the SBP transducer mounted to the remotely mounted seabed sled moving at an average speed of 0.15 m/s. Figure 5.6 compares that data to the results from the 2017 run 20170608-025024 (Table 4.2), albeit with many fewer confirmed sleeper matches. This run was collected using the vessel mounted transducer travelling at 2m/s. Excluding reflector 992 which represented the underside of the sleeper, the comparison between the 2018 and 2017 SBP data shows a similarity in the results from the two modes of field operation. Unfortunately, there are too few data points from the valid 2017 data to quantify the relationship across the full range of sleeper DoB.

These results show that the variability associated with depth of buried reflector measurements using the parametric SBP is very low, regardless of operational deployment. Applying site specific water and sediment velocity corrections to the pre-set 1500m/s velocity value, the DoB for sleepers buried between 12 and 47 cm was under-predicted by 6%.

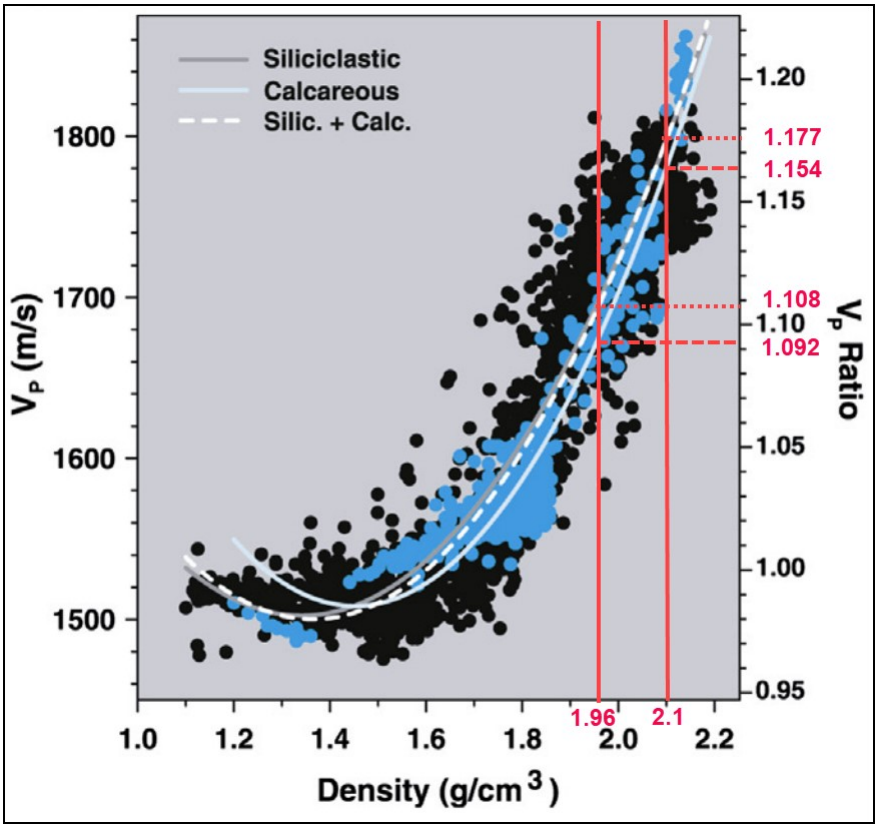

Figure 5.5 V_{pR} vs. sediment density, calcareous and siliciclastic sediments, modified from Richardson and Jackson (2017) Figure 8.23(c) (reproduced with permission from ELSEVIER).

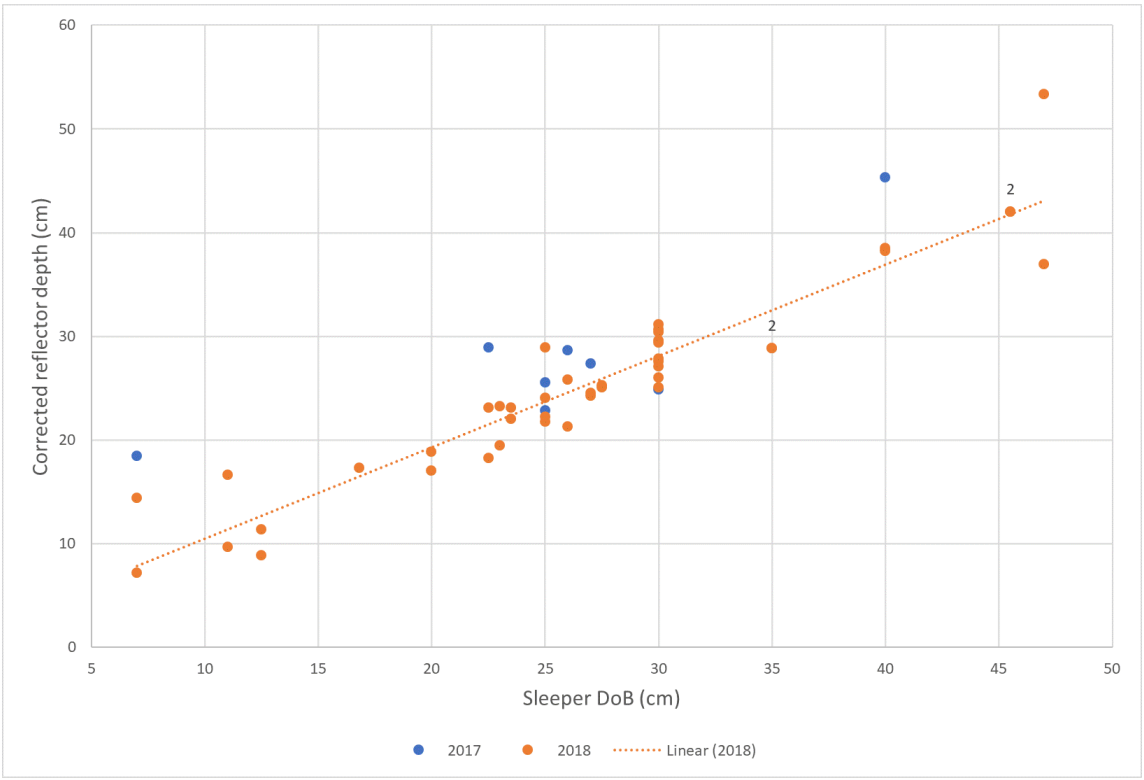

Figure 5.6 Comparison between reflector burial estimates using vessel (2017) and sled (2018) mounted transducer head operations.

Other reflector burial characteristics

The sleeper thickness, and in the case of multiple stacked sleepers the gap between sleepers, were identified in the SBP record. Multiple reflectors below the seabed were identified in 60–78% of the traces corresponding to the sleeper locations at the James Matthews sleeper site. For single sleepers, the first buried reflector typically represented the upper face of the sleeper. Where the phase of the acoustic wave amplitude reversed between reflectors, the second reflector represented the sleeper's lower, underside face. The difference in these depths indicated the sleeper's thickness. Table 5.10 illustrates the percentage of traces with multiple reflectors, velocity-corrected sleeper thickness and variability, and the percentage where amplitude phase changes occurred. The average sleeper thickness determined from the SBP trace data varied from 13.9–17.9 cm, with corresponding standard deviations ranging from 2.7–4.1 cm, across the three SBP runs. These estimates compare to the actual sleeper thickness of 12.5 cm. For multiple stacked sleepers where the first reflector represented the lower, underside face of the top sleeper, then the second reflector represented the upper face of the bottom sleeper—the difference in depth representing the vertical gap between the sleepers. Two sleeper gaps were identified in the SBP trace data, with velocity-corrected thicknesses of 8.7 and 10.3 cm. The stacked sleepers were constructed with a 7.5 cm gap. These results demonstrated that as well as accurately identifying the location and depth of burial of the sleepers, the SBP data also quantified other depth related characteristics for approximately 50% of the sleeper locations.

Table 5.10 Multiple reflector characteristics

SBP run	number of traces with sleeper reflectors	% of multiple reflectors	sleeper thickness (gap) (cm)		% with amplitude phase change
			average	standard deviation	
025024	7	64%	17.9	4.1	71%
135105	13	60%	14.5 (10.3)	2.7	100%
135516	16	78%	13.9 (8.7)	3.5	72%

Reflection coefficients—differentiation of buried material types

Reflection coefficients for boundary interfaces are a function of the acoustic properties of the two media forming those boundaries. In this study, the acoustic properties of the sleepers, buried in two different sediment environments, have been experimentally controlled (different material types, moisture content and degradation state and orientations). The purpose of the following assessment is to examine whether or not the reflection coefficients derived from the SBP data across all sleepers can successfully differentiate the material properties of each

buried sleeper. Reflection coefficients derived from direct in situ measurement of the acoustic properties of the sediments and the sleepers will be used to validate these results.

Reflection coefficients derived from SBP data

The reflection coefficient for a buried reflector (K_{DR}) can be determined from the SBP data using the combination of equations (8) and (9) (from Chapter 3) as follows:

$$x = [A_p^2\ d_p^2] / [A_m\ d_m] \qquad (8)$$

$$K_{DR} = A_{DR}\ [\ d_{DR} + d_p] / x \qquad (9)$$

and following substitution of (8) into (9)

$$K_{DR} = A_{DR}\ A_m\ d_m\ [d_{DR} + d_P] / (A^2_p\ d^2_p) \qquad (10)$$

where x is a calibration coefficient, $A_{DR/p/m}$ are the acoustic wave amplitudes at the buried reflector/seabed/seabed 1st multiple interfaces, respectively, and $d_{DR/p/m}$ are the depths of the buried reflector/seabed/ seabed 1st multiple, also respectively.

Reflection coefficients were initially calculated for known reflectors along SBP runs 18052018-135105, 18052018-135516 and 20170608-025024, using equation (10) and raw SBP amplitude and depth data from Tables 4.14 to 4.16. The results for the 2018 data are shown in Table 5.11 as uncorrected K_{DR} values. All depth values in Tables 4.14 to 4.16 were also corrected, based on in situ sediment velocity estimates using equation (12). These depth-corrected K_{DR} values are also listed in Table 5.11. The sleeper characteristics at the time of SBP measurement are aligned against each identified reflector. Figure 5.7 to 5.10 respectively show the magnitude of the depth-corrected K_{DR} values, plotted against sleeper DoB, for pine, jarrah, oak and ferrous sleepers from each of the two SBP runs. These scatter plots, shown separately for clarity reasons, show considerable scatter due to the high variability of individual values. The uncorrected and depth-corrected K_{DR} values for run 20170608-025024 are depicted in Table 5.12 and reveal results which are an order of magnitude lower than those in Table 5.11. The reasons for that difference are scrutinised later.

Table 5.11 Uncorrected and depth-corrected reflection coefficients, James Matthews sleeper site, 2018 data.

run 135105			run 135516			sleeper characteristics (at time of run)		
reflector	K_{DR}		reflector	K_{DR}				
	uncorrected	corrected		uncorrected	corrected	sleeper ID	DoB (cm)	material
7937	-0.081	-0.083				1	16.8	pine (22^0 rotation)
7729	-0.069	-0.070	8325	-0.998	-1.008	2	12.5	pine
7428	0.045	0.047	7956	-0.035	-0.035	3	20	pine (22^0 rotation)
7152	-0.024	-0.024	7703	-0.330	-0.341	4	30	pine (vert grain)
6724	0.364	0.374	7482	0.350	0.361	5	26	pine
6330	0.03	0.031	7119	0.076	0.077	6	25	pine
6005	-0.004	-0.004	6757	0.228	0.230	7	7	pine
5695	0.038	0.039	6501	0.053	0.055	8	40	pine
5273	0.438	0.452	6106	-0.217	-0.224	9	27	pine
4782	-0.305	-0.313	5646	0.375	0.383	11	22.5	oak
4528	0.029	0.030	5302	0.021	0.022	12	25	pine (vert grain)
4227	0.223	0.230	4929	-0.335	-0.347	13	30	oak
3909	0.028	0.029	4727	0.086	0.088	14	30	pine (vert grain)
3366	-0.24	-0.249	4243	-0.137	-0.144	15	47	pine
3126	-0.083	-0.087	3945	-0.043	-0.045	16	45.5	pine
2810	-0.245	-0.253	3545	0.204	0.210	17	30	oak
2522	0.069	0.070	3291	-0.020	-0.021	18	8	pine (mult 10/30)
2081	0.029	0.030	2676	-0.021	-0.022	19	5.5	pine (mult 10/30/50)
1723	-0.023	-0.023	1523	-0.168	-0.170	20	11	pine
1426	-0.268	-0.275	1252	0.111	0.114	21	23.5	oak
1145	-0.212	-0.218	1004	0.052	0.054	22	23	jarrah
903	0.176	0.182	717	0.527	0.547	23	35	jarrah
595	-0.034	-0.035	364	0.124	0.128	24	27.5	ferrous
428	-0.389	-0.399	162	-0.107	-0.110	25	30	ferrous

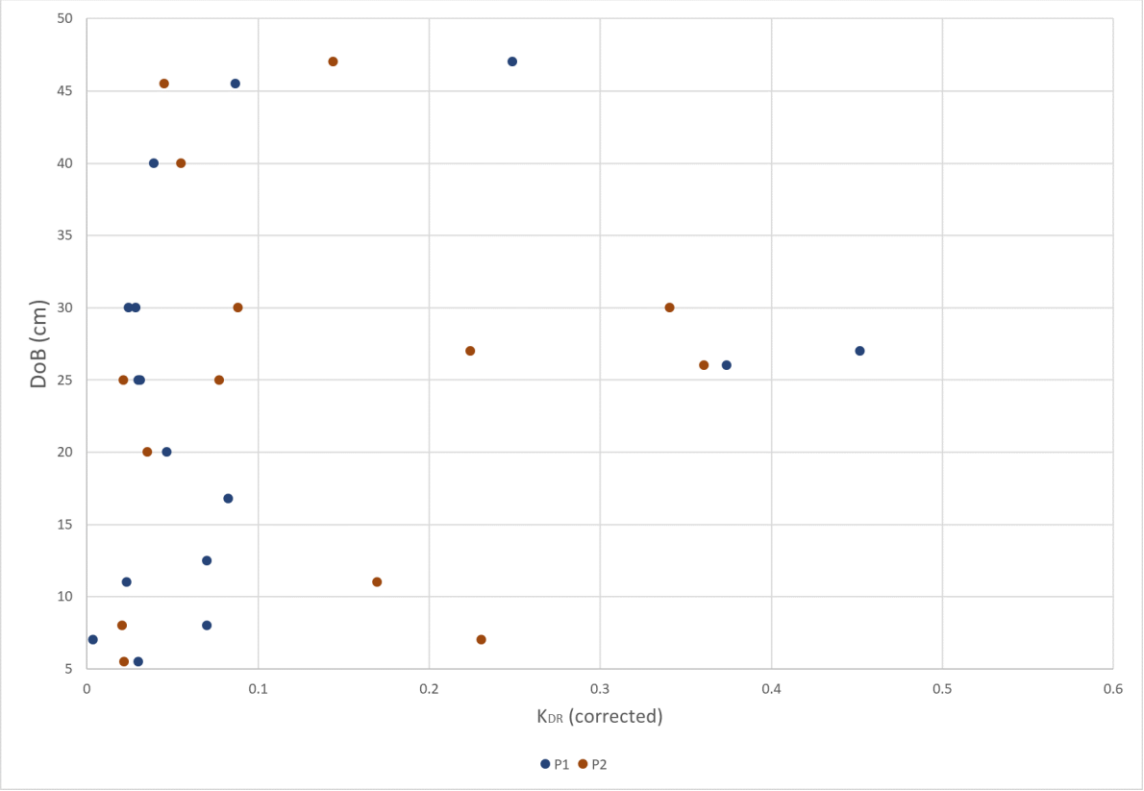

Figure 5.7 Scattering of velocity-corrected K_{DR} values for pine sleepers (P1: run 135105, P2: run 135516).

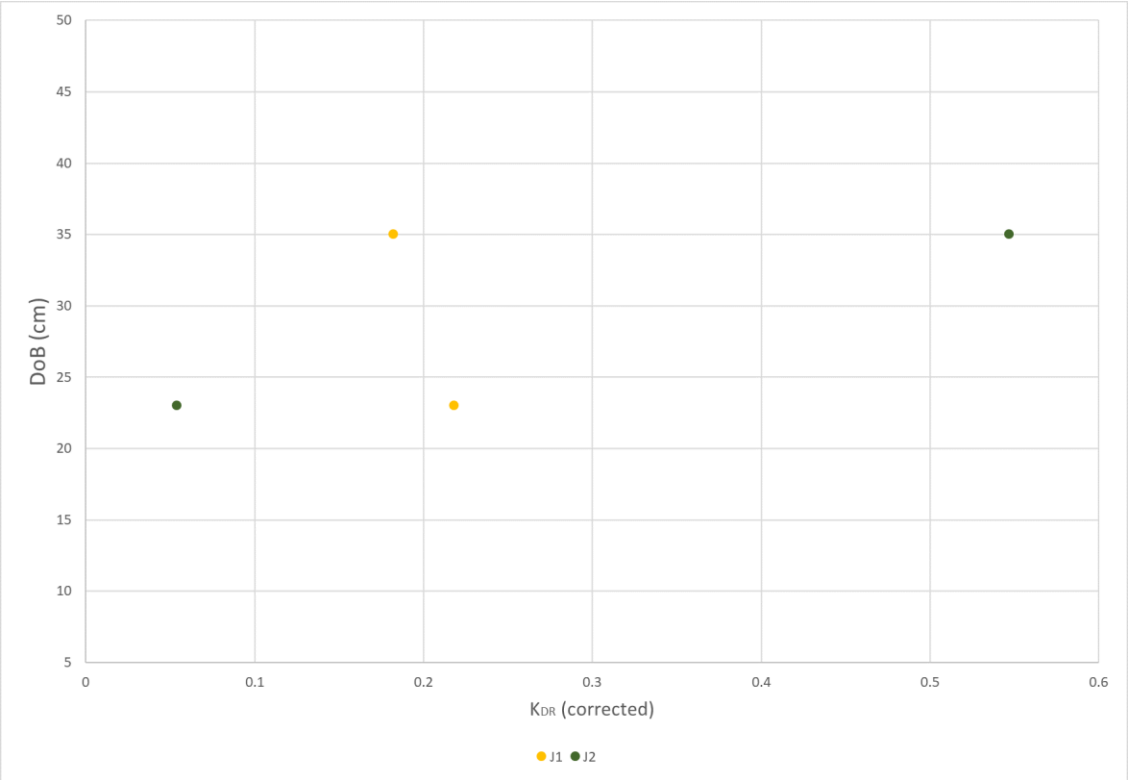

Figure 5.8 Scattering of velocity-corrected K_{DR} values for jarrah sleepers (J1: run 135105, J2: run 135516).

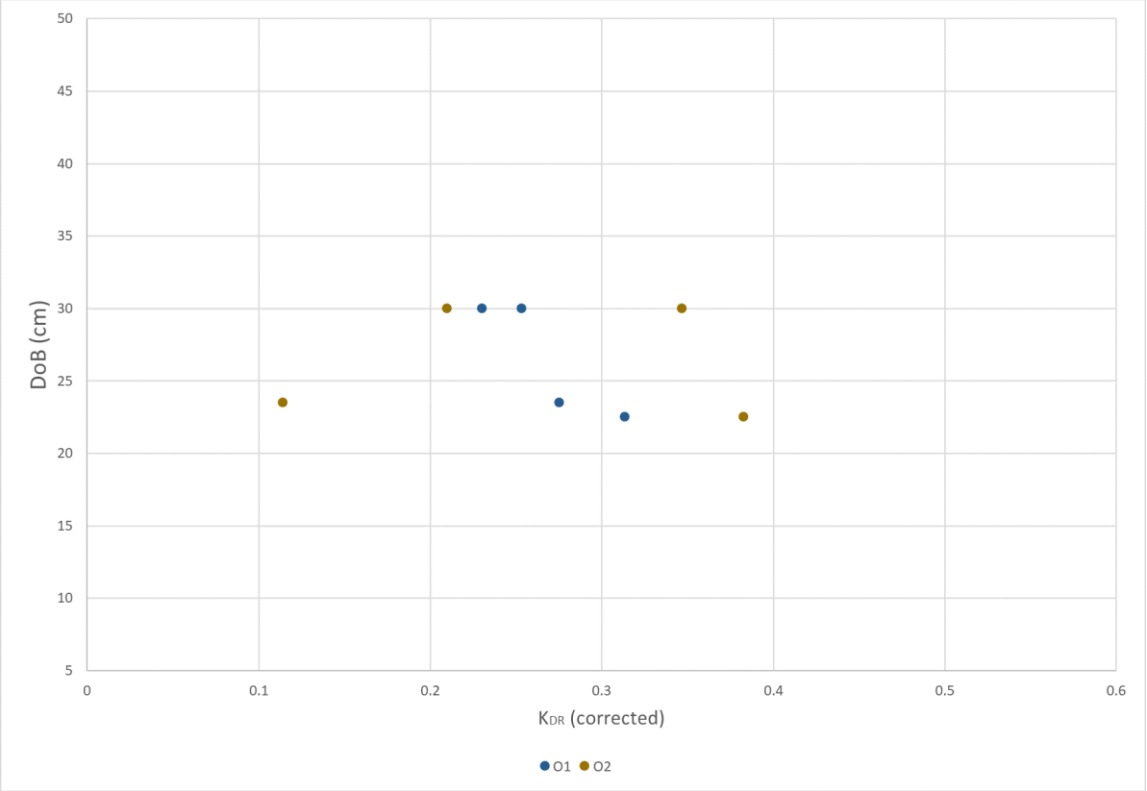

Figure 5.9 Scattering of velocity-corrected K_{DR} values for oak sleepers (O1: run 135105, O2: run 135516).

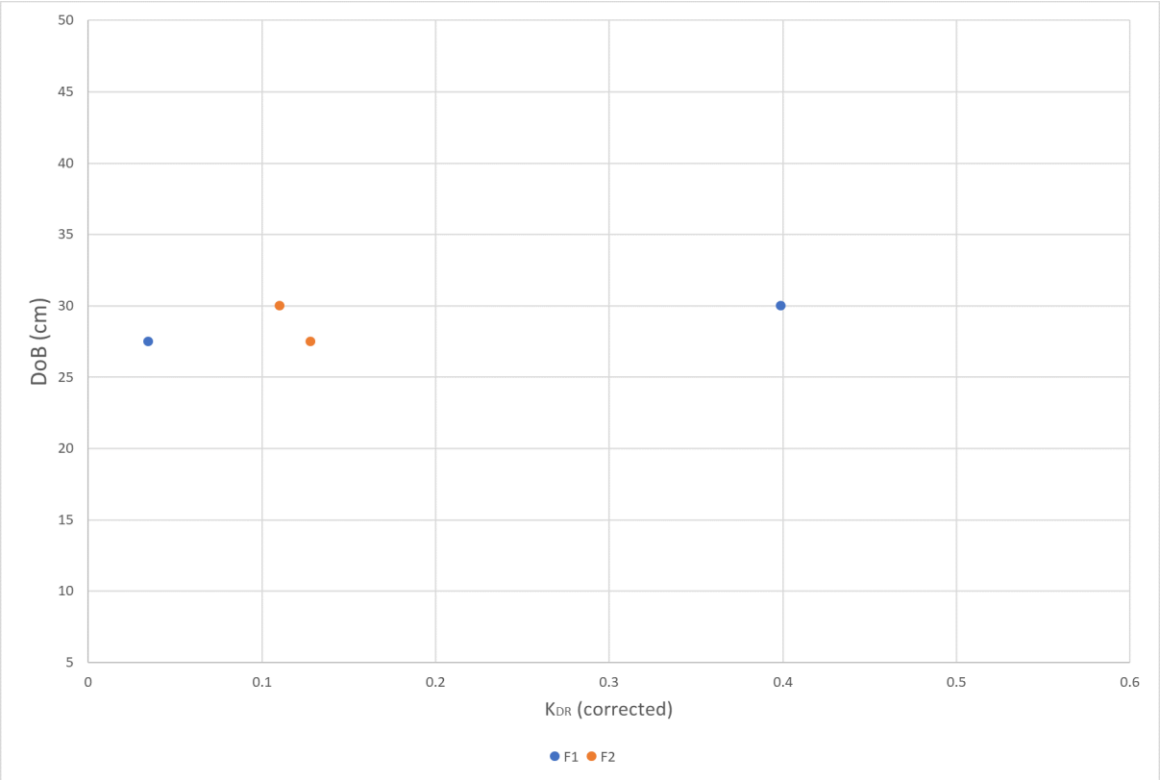

Figure 5.10 Scattering of velocity-corrected K_{DR} values for ferrous sleepers (F1: run 135105, F2: run 135516).

Table 5.12 Uncorrected and depth-corrected reflection coefficients, James Matthews sleeper site, 2017 data.

run 025024			sleeper characteristics (at time of run)		
reflector	K_{DR}				
	uncorrected	corrected	sleeper ID	DoB (cm)	material
1062	0.032	0.032	4	28	pine (vert grain)
1042	-0.023	-0.023	5	29	pine
1016	-0.009	-0.009	6	27	pine
992	0.001	0.001	7	7	pine
973	-0.005	-0.005	8	41	pine
940	-0.006	-0.006	9	29	pine
917	-0.009	-0.009	10	10	pine
900	0.006	0.006	11	27	oak

The high variability in the acoustic reflection amplitudes from the seabed surface between adjacent traces has a strong influence in the variability of the derived reflection coefficient. Examination of the raw SBP data used to calculate the reflection coefficients (Tables 4.15 and 4.16) shows two sets of variability. First, there is a high level of variability between the mean amplitude values across all traces representing different sleeper locations. This amplitude variability, especially the 1st buried reflector, is intrinsically important if the reflection coefficient values can differentiate material type. The second variability is associated with high level of difference between adjacent acoustic waves in the raw trace data. These differences have been extracted into Table 5.13 and 5.14. To identify the reflectors representing a buried sleeper the depths of the buried reflector needed to be consistent across five consecutive traces. Once this condition was met, the amplitudes from each of these five consecutive traces for the buried reflector depth, as well as for the seabed level and 1st seabed multiple, were extracted, averaged to form mean amplitude values, and tabulated under the central trace number. The standard deviation (SD) and relative standard deviation (RSD) values in Table 5.13 and 5.14 show this raw data variability in the five traces surrounding the mean amplitude values for the seabed level, the 1st buried reflector and the 1st seabed multiple used in equation (10). The highest variability is associated with the determination of the seabed level amplitude, which has RSD values averaging 34.9% and 25% for the two runs, compared with RSD values of 9.9/13% and 8.6/11% for the 1st buried reflector and 1st seabed multiple, respectively. This means that the differences in amplitudes between adjacent traces of the seabed reflections have a relatively stronger influence on the derivation of the reflection coefficient than the amplitudes reflecting off the buried sleeper itself. This influence is exacerbated since in the

calculation of the K_{DR} values, the seabed amplitude value found in the denominator of equation (10), is squared, whereas the amplitude values for the buried reflector and seabed multiple are not.

Table 5.13 Variability associated with the calculation of reflector amplitudes, SBP run 18052018-135105.

trace	seabed level		1st reflector		seabed multiple	
	std dev	RSD	std dev	RSD	std dev	RSD
7937	4209	28%	617	9%	101	9%
7727	11582	59%	2036	20%	46	4%
7428	5182	28%	369	5%	78	8%
7152	10452	48%	223	3%	48	9%
6724	411	6%	526	7%	109	12%
6330	6331	50%	829	10%	16	6%
6002	7816	51%	58	7%	94	19%
5695	1930	24%	452	9%	30	17%
5273	1896	32%	529	8%	109	11%
4782	6064	69%	468	5%	129	12%
4528	1999	17%	415	11%	41	9%
4227	2886	41%	943	11%	27	5%
3909	3629	38%	426	14%	14	4%
3366	5088	55%	552	5%	29	4%
3126	3902	39%	262	6%	71	11%
2810	2082	34%	719	8%	33	8%
2522	2462	27%	433	15%	86	10%
2081	8532	40%	1425	16%	36	6%
1723	5508	39%	595	12%	138	12%
1426	4885	40%	1006	8%	58	4%
1145	3122	24%	2452	28%	131	8%
903	3546	31%	602	8%	62	5%
595	4476	29%	388	8%	72	10%
428	1801	35%	297	5%	72	10%
mean	*4416*	*34.9%*	*648*	*9.9%*	*65*	*8.6%*

Plets et al. (2008) used a different approach to computing the calibration coefficient (x) in equation (8). Rather than calculate an individual x value for each reflector, they calculated x values for a large number of locations along the SBP run, selected the 50th percentile value from the distribution of x values, and applied that value as a constant to equation (9). Using

Table 5.14 Variability associated with the calculation of reflector amplitudes, SBP run 18052018-135516.

trace	seabed level		1st reflector		seabed multiple	
	std dev	RSD	std dev	RSD	std dev	RSD
8325	270	6%	2777	16%	57	9%
7956	3316	34%	488	9%	20	7%
7703	958	23%	448	5%	9	3%
7482	899	11%	615	8%	118	10%
7119	2474	26%	494	7%	52	13%
6757	725	9%	3386	32%	53	9%
6501	1467	19%	560	11%	29	12%
6106	837	10%	212	2%	45	7%
5646	2801	43%	368	4%	55	6%
5302	3414	32%	250	11%	71	17%
4929	775	18%	389	6%	22	6%
4727	6133	54%	345	6%	99	12%
4243	2061	2%	1479	8%	52	8%
3945	1854	18%	410	8%	80	25%
3545	1378	26%	285	2%	24	12%
3291	3895	43%	167	6%	48	20%
2676	1497	16%	180	10%	55	14%
1523	2450	35%	977	19%	72	9%
1252	5039	33%	5039	14%	72	5%
1004	3434	12%	1995	16%	181	12%
717	2470	36%	877	11%	119	10%
364	3010	31%	1499	28%	58	6%
162	4110	47%	329	7%	97	13%
mean	*2403*	*25%*	*1025*	*13%*	*65*	*11%*

this approach, the influence of the high intra-variability of the seabed and seabed 1st multiple amplitudes would be reduced. This approach, slightly modified, was applied to the calculation of K_{DR} values. Table 5.15 shows the modified K_{DR} values using Plets et al. approach with x = 69,263 calculated as the 50th percentile value of the distribution of x values. This distribution of 46 individual x values was determined from the velocity-corrected depth and amplitude values in Tables 4.15 4.16.

Table 5.15 Modified calculation of reflection coefficients, based on Plets et al. (2008) calibration factor approach, James Matthews sleeper site.

run 135105			run 135516			run 025024		sleeper characteristics (at time of run)		
reflector	K_{DR}		reflector	K_{DR}		reflector	K_{DR}			
	x = 50th %ile	x = mode		x = 50th %ile	x = mode		x = mode	sleeper ID	DoB (cm)	material
7937	-0.126	-0.197						1	16.8	pine (22^0 rotation)
7729	0.167	0.262	8325	0.288	0.288			2	12.5	pine
7428	0.127	0.199	7956	-0.096	-0.096			3	20	pine (22^0 rotation)
7152	-0.163	-0.255	7703	-0.167	-0.167	1062	0.47	4	30	pine (vert grain)
6724	0.138	0.216	7482	0.137	0.137	1042	-1.23	5	26	pine
6330	-0.147	-0.230	7119	0.138	0.138	1016	-0.59	6	25	pine
6005	0.015	0.023	6757	0.165	0.165	992	-0.31	7	7	pine
5695	0.103	0.161	6501	0.101	0.101	973	-0.42	8	40	pine
5273	0.126	0.197	6106	-0.178	-0.178	940	-0.36	9	27	pine
4782	-0.170	-0.266	5646	0.150	0.150	917	0.19	11	22.5	oak
4528	0.069	0.109	5302	0.043	0.043	900	-1.06	12	25	pine (vert grain)
4227	0.167	0.262	4929	-0.127	-0.127			13	30	oak
3909	0.057	0.089	4727	0.104	0.104			14	30	pine (vert grain)
3366	0.218	0.341	4243	-0.435	-0.435			15	47	pine
3126	0.098	0.154	3945	0.117	0.117			16	45.5	pine
2810	0.175	0.274	3545	0.237	0.237			17	30	oak
2522	-0.053	-0.083	3291	-0.053	-0.053			18	8	pine (mult 10/30)
2081	0.169	0.264	2676	-0.035	-0.035			19	5.5	pine (mult 10/30/50)
1723	-0.036	-0.057	1523	-0.088	-0.088			20	11	pine
1426	-0.231	-0.362	1252	0.150	0.150			21	23.5	oak
1145	-0.159	-0.248	1004	0.225	0.225			22	23	jarrah
903	0.145	0.227	717	0.155	0.155			23	35	jarrah
595	-0.086	-0.135	364	0.099	0.099			24	27.5	ferrous
428	-0.121	-0.190	162	-0.084	-0.084			25	30	ferrous

The histogram showing the distribution of individual x values (Figure 5.11) is highly negatively skewed with a dominant modal value of 44,263. Approximately 46% of all x values are tightly distributed around this value. Consequently, K_{DR} values were also determined using the constant x = 44,263, and are shown in Table 5.15 and in Figure 5.12 to 5.15 for pine, jarrah, oak and ferrous sleepers. These comparisons show that the Plets et al. (2008) methodology significantly reduced the scatter in the K_{DR} values, with the majority of those values for the pine sleepers falling within the range 0.1–0.27. The pine sleepers with their upper face inclined at an angle of 22.5 degrees to the horizontal grouped together, but could not be distinguished from within the broader range of pine sleeper K_{DR} values. Similarly, the change in the insonification orientation, from tangential/radial to longitudinal, could not be distinguished. Likewise, for the jarrah and oak sleepers, a reduction in the scatter resulted in the majority of the modified K_{DR} values falling in the range 0.23–2.5, and 0.2–0.27, respectively. For the ferrous sleepers, the K_{DR} values grouped tightly together in a range 0.13–0.19.

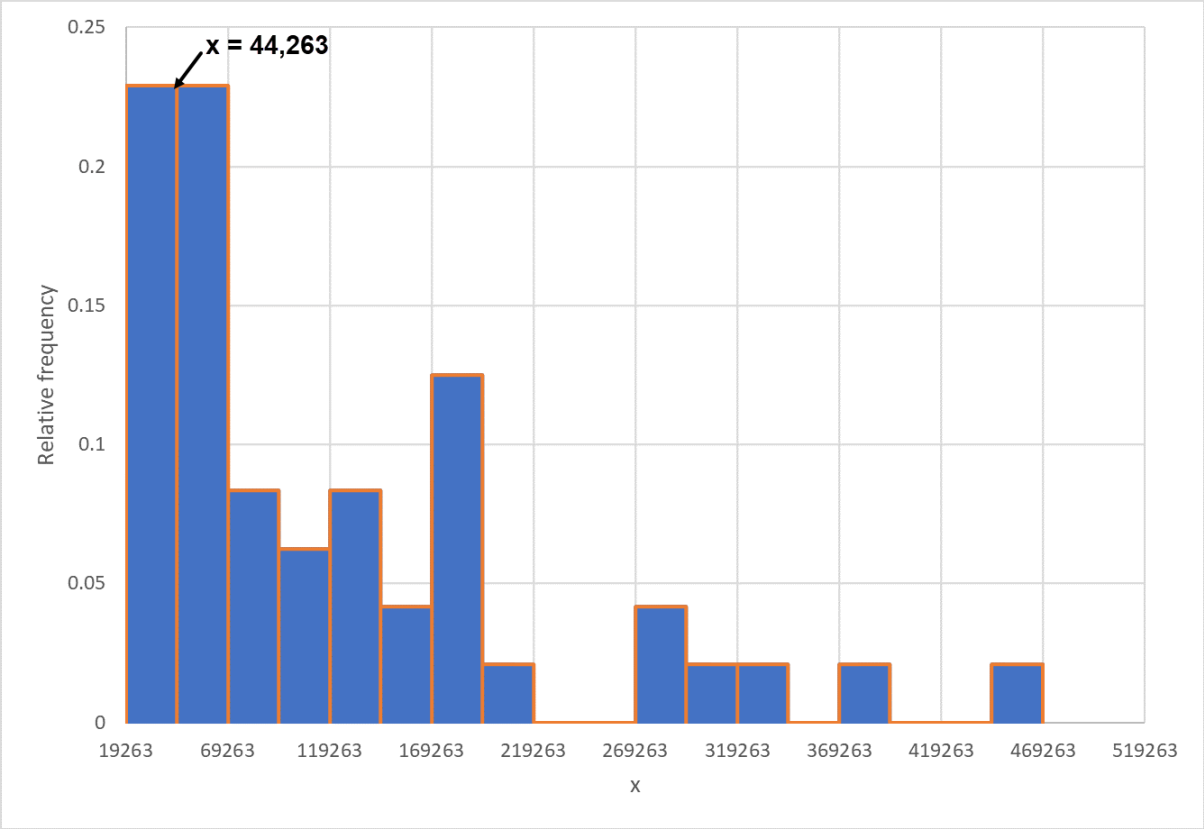

Figure 5.11 Histogram of calibration factor (x) values.

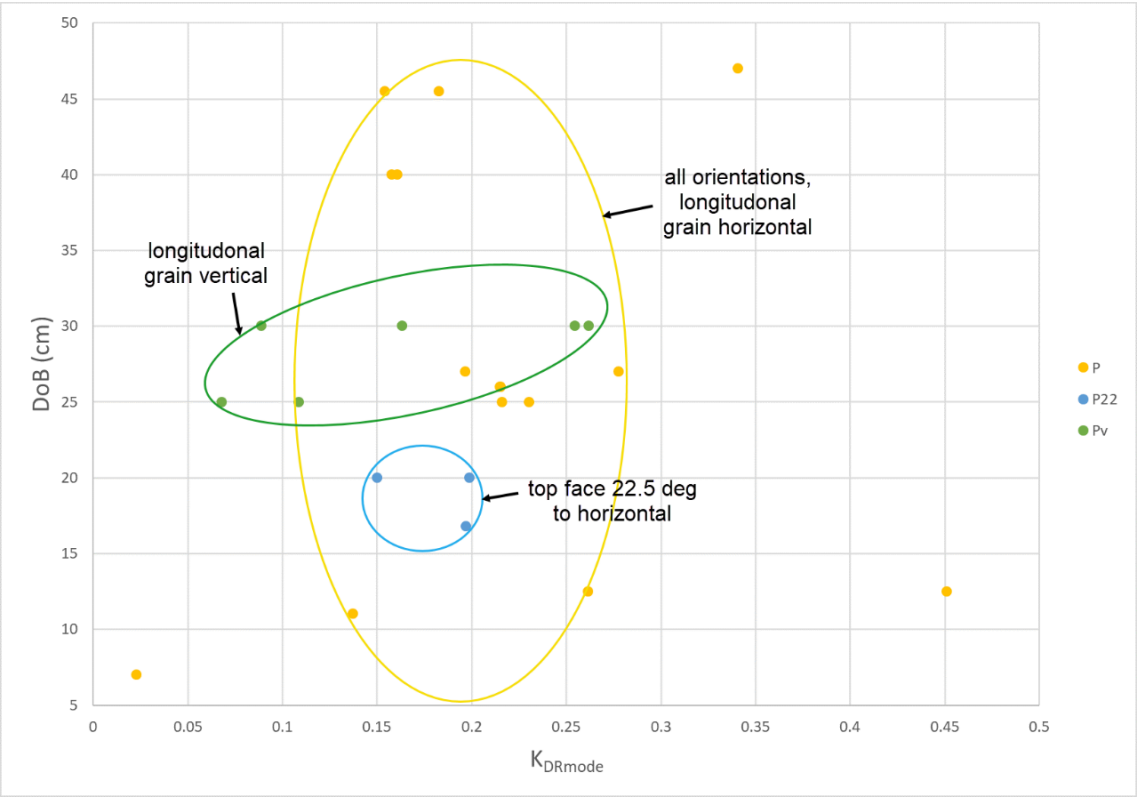

Figure 5.12 Variability of K_{DRmode} values with DoB for pine sleepers.

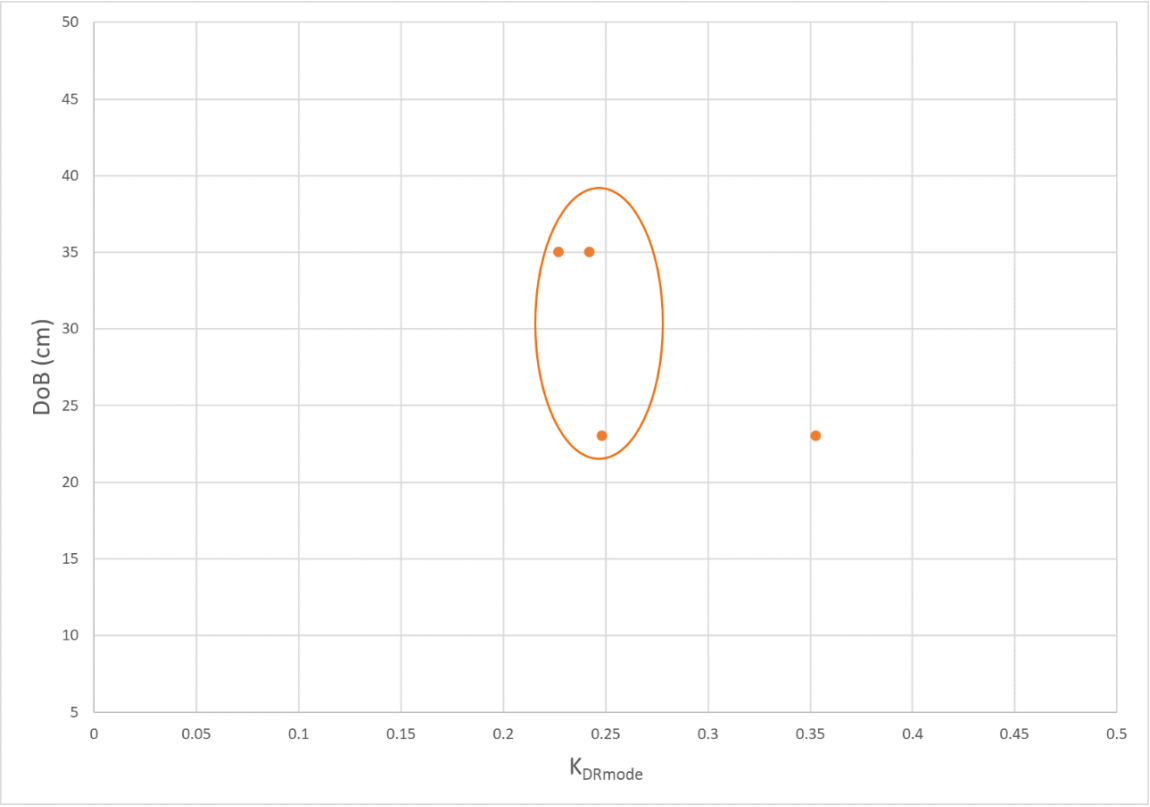

Figure 5.13 Variability of K_{DRmode} values with DoB for jarrah sleepers.

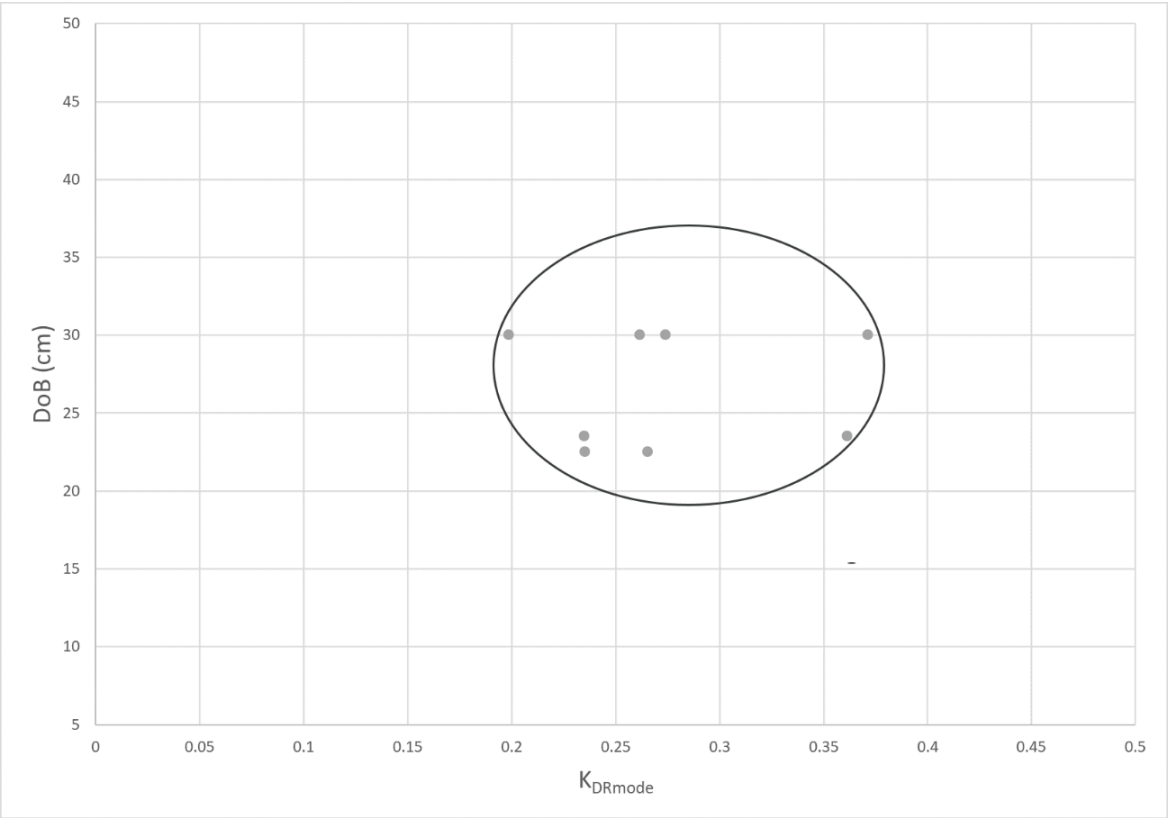

Figure 5.14 Variability of K_{DRmode} values with DoB for oak sleepers.

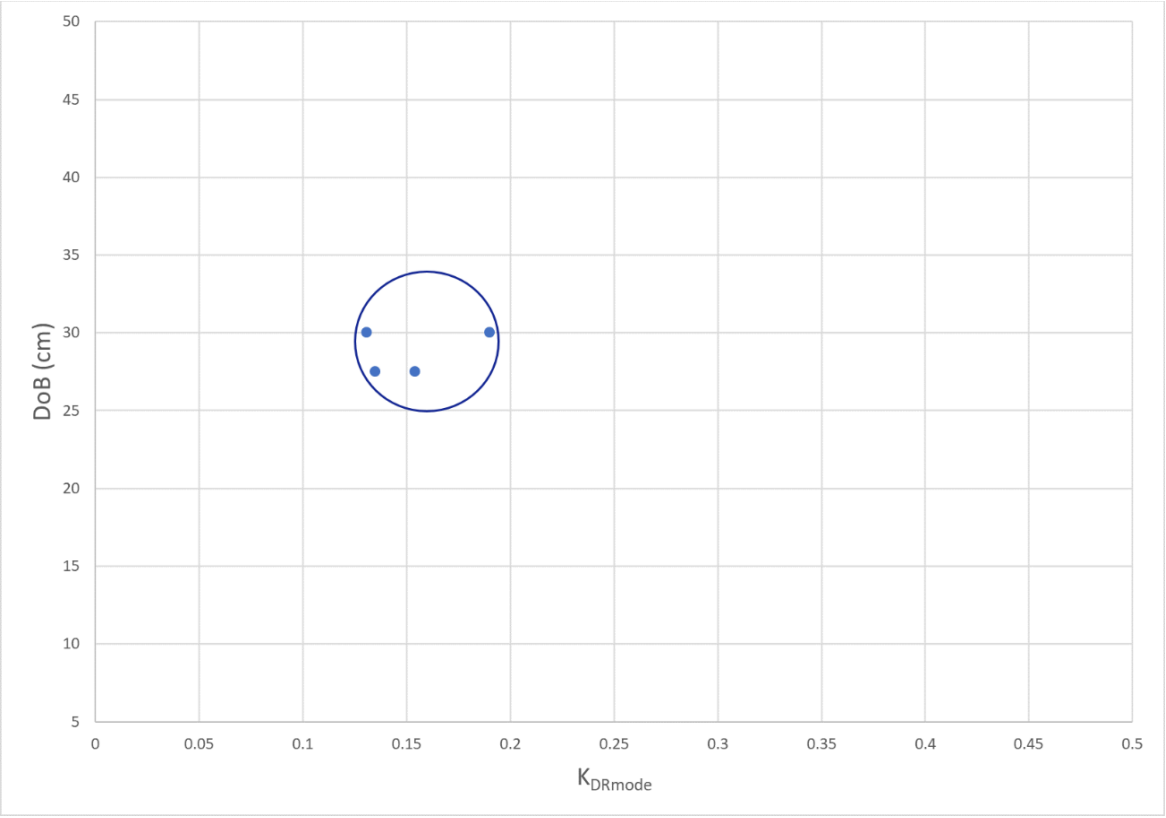

Figure 5.15 Variability of K_{DRmode} values with DoB for ferrous sleepers.

Figure 5.16 displays the groupings of K_{DR} values for all sleeper materials. It shows that while the reflection coefficient values for each material type tend to group together, these groups partially or fully overlap. This means that for the buried sleepers, identification of their respective reflection coefficient from the SBP data cannot be then used to uniquely identify their material composition. However, on a shipwreck site composed of one or two major timber types with ferrous and/or stone (ballast) material, the possibility of identifying several groups from K_{DR} values from non-invasive SBP measurements would provide insight for archaeological interpretation. As a consequence, the above groupings of K_{DR} values identified from SBP data is appraised in the following section against reflection coefficient values determined solely from in situ sediment and sleeper impedance characteristics.

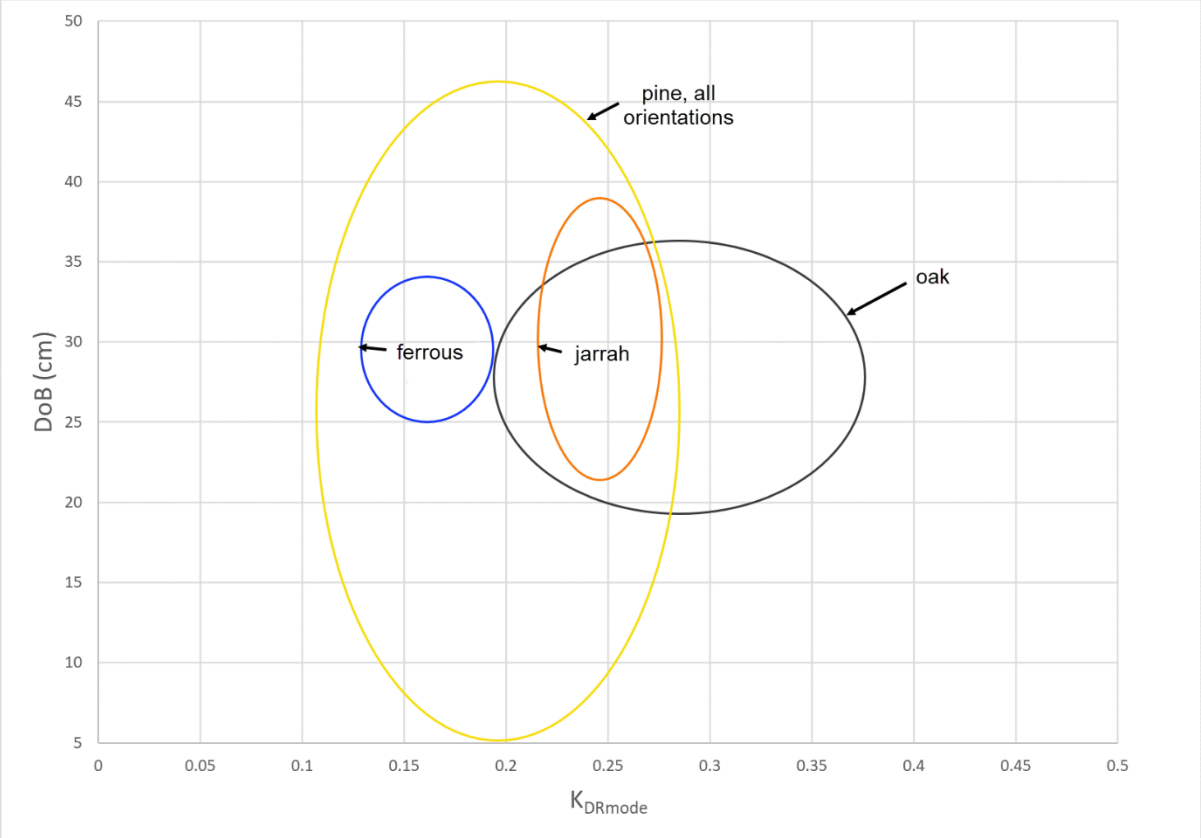

Figure 5.16 Groupings of K_{DRmode} values with DoB for all sleeper materials.

The disparity between the 2017 and 2018 K_{DR} values identified in Table 5.12 derives from the comparatively higher seabed amplitudes, and corresponding lower seabed 1st multiple amplitudes, for the 2017 data. These differences are shown in Table 5.17, which also reveals that the mean amplitudes for the 1st buried reflectors, and their variability described by the respective RSD values, were very similar in 2017 and in 2018. The RSD values were also

similar for seabed level data collected in both years, but significantly higher in 2017 for the 1st seabed multiple.

Table 5.16 Comparison of mean amplitudes and variability from 2017 and 2018 SBP data.

run	seabed level			1st buried reflector			1st seabed multiple		
	amp	std dev	RSD	amp	std dev	RSD	amp	std dev	RSD
18052018-135105	12788	4416	35%	6662	648	10%	826	65	9%
18052018-135516	9560	2403	25%	7801	1025	13%	644	65	11%
20170608-025024	21803	7356	35%	7303	1039	17%	244	86	35%

Examination of the data acquisition software settings for both years revealed a change in the Gain setting from 12-12 dB (decibels) in 2017 to 2-2 dB in 2018. The Decibel Scale is a logarithmic scale whereby every 3dB increase represents a doubling of sound intensity, or acoustic power. In 2017 the higher power settings were used to ensure the desired seabed penetration, whereas in 2018 a lower setting was used, knowing that adequate penetration and buried reflector discrimination had been achieved. This gain amplification explains the reason for the very low K_{DR} values previously published by the author (Winton 2019) as part of the early 'proof of concept' results. The Innomar *compact* SES-2000 is not a calibrated sonar (Doug Bergersen pers. comm. 2019). This means that despite the similarity of the mean amplitudes and associated variability of the 1st buried reflector for both years, the over-amplification of the 2017 seabed amplitude and under-amplification of the corresponding seabed 1st multiple cannot be scaled relative to the 2018 data. The K_{DR} values for run 20170608-025024 were re-estimated using the Plets et al. approach with the calibration coefficient (x_{mode}) derived from the 2018 data. This avoided using the distorted seabed and seabed 1st multiple amplitude values, but retained the buried reflector amplitude and all depth values derived from the 2017 SBP data. These revised K_{DR} values are also shown in Table 5.15, but reveal little similarity to the results from the 2018 data and suggest that SBP data collected with a high gain factor is unsuitable for reflection coefficient analyses.

Reflection coefficients derived from in situ impedance properties

To validate the magnitudes of the reflection coefficients derived solely from the SBP data, reflection coefficients were also independently calculated using the in situ properties of the sediments and sleepers. As introduced in Chapter 3 the reflection coefficient is the numerical

expression for the strength of the reflection of the acoustic wave from a boundary, in this case the seabed and the buried sleepers. From first principles, the in situ impedance properties (density, ρ and compressional P-wave velocity, V_p) in each of the two adjoining layers are used to derive K_R for that interface, as per Equation (1).

$$K_R = (\rho_2 V_{p2} - \rho_1 V_{p1}) / (\rho_2 V_{p2} + \rho_1 V_{p1}) \quad (1)$$

The sediment bulk density and sediment velocities for the James Matthews and the Swan River sleeper sites have been previously derived from in situ measurements and are listed in Table 5.8. The corresponding buried sleeper impedance properties were derived as follows.

The bulk and basic densities of the timber sleepers were both used to derive the acoustic impedance for the timber sleepers. The bulk density was directly used to quantify the timber density in Equation (1) as it 'better represents the water-logged state of the timber as encountered by the acoustic signal' (Arnott et al. 2005:138). In acoustic laboratory studies, basic density has been used to correlate acoustic velocities to corresponding saturated timber degradation states (Zisi 2016:155). The basic density of the timber measured from the recovered blocks was used in this study to derive radial and tangential acoustic velocities for the timber sleepers.

Representative bulk and basic timber densities at the times of SBP survey were estimated from measurements undertaken on the recovered timber blocks. Analyses of sub-samples cut from these recovered blocks identified that the moisture content and densities of the outer sections of the timbers had changed since immersion and burial (see Chapter 4). These changes were associated with the processes of waterlogging and the onset of timber degradation. Measurements of dissolved oxygen and Eh profiles in the top 50 cm sediment layer at the sleeper sites reported in Chapter 4 identified variability, with aerobic conditions in the surficial layers reducing to sub-oxic and anoxic conditions below, and with oxidising potential at all depths. These conditions result in poor timber preservation conditions as per Figure 1 in Gregory et al. (2008a:207). They also confirmed the ongoing potential for buried timber degradation by white and brown rot and soft rot fungi in the surficial sediments at the James Matthews and Swan River sleeper sites.

The timber blocks were recovered from under the seabed after 20.5 months of submergence at the James Matthews sleeper site, and after 9.25 months at the Swan River site. Figure 5.2 shows the timing of the SBP surveys relative to sleeper burial: 1.5 months after burial of pine, oak and jarrah blocks (at the James Matthews sleeper site); four months after burial of pine and oak blocks (at the James Matthews sleeper site); four months after burial of pine, oak and jarrah blocks (at the Swan River site); and 15 months after burial of pine and oak blocks (at

the James Matthews sleeper site). In Chapter 4, Figures 4.27 through 4.29 respectively show the bulk and basic density time series for pre-burial, 9.25 months post-burial and 20.5 months post-burial for oak, pine and jarrah timber blocks. The bulk density of the recovered oak, pine and jarrah timber blocks were all, with one exception, significantly higher than their pre-burial value. However, the within-block variability for the single or duplicate blocks buried for 9.25 and 20.5 months were high, with no significant differences associated with burial times or burial depths. With only several exceptions, there were no significant differences between the post-burial basic density values and their corresponding pre-burial value. However, the mean values were lower than pre-burial, and like the bulk density values, their variability masked any significant differences associated with burial time and burial depths. The variability of these estimates, in terms of their relative standard deviation, is less than 10% for both oak and pine timbers, and less than 2% for jarrah. Consequently, the mean post-burial bulk density from all buried blocks for each timber type were considered to be representative for all SBP survey dates (Table 5.17). Similarly, the mean post-burial basic densities for each buried timber type were also considered to be representative for all SBP survey dates.

Table 5.17 Timber average densities, and their variability, at times of SBP survey.

	pine timber		**oak timber**		**jarrah timber**	
	bulk density (kg/m^3)	**basic density (kg/m^3)**	**bulk density (kg/m^3)**	**basic density (kg/m^3)**	**bulk density (kg/m^3)**	**basic density (kg/m^3)**
mean	928.5	433.9	845.5	478.4	1078.8	559.0
std dev	78.4	28.4	47.4	33.2	3.2	8.0
RSD	8.4%	6.6%	5.6%	6.9%	0.3%	1.4%

The moisture saturation percentage in the recovered timber blocks were in excess of their fibre saturation point (FSP). These values were derived by dividing the timber's moisture content at time of block recovery (Tables 4.9 and 4.10) by the maximum non-degraded (pre-burial) moisture content (Table 4.5) and are presented in Table 5.18. All values exceed their FSP (approximately 30%) and hence their moisture content has minimal influence on the acoustic velocities within the timbers (Zisi 2016:65). Zisi's (2016:155) regression equations (14) and (15) relate radial and tangential velocities to timber density across a range of saturated timber species are therefore appropriate.

$v_R = 1420.3\ d + 1352.5$ (14)

$v_T = 1084.6\ d + 1340.9$ (15)

and where d (g/cm^3) is basic density.

Table 5.18 Moisture saturation values for timbers buried 9.25 and 20.5 months.

Timber type/ burial depth (cm)	Burial duration (months)	
	9.25 (Swan River sleeper site)	**20.5 (James Matthews sleeper site)**
pine (10)		102%
pine (20)	109%	
pine (30)	56%	84%
pine (50)	70%	62%
oak (30)	74%	75%
jarrah (20)	103%	
jarrah (30)	99%	

The resulting timber velocities, derived from substituting the basic density values from Table 5.15 into equations (14) and (15), range from 1811.5 m/s to 2146.4 m/s and are given in Table 5.19. The ferrous sleepers were fabricated from truck leaf springs, which are composed of heat-treated mild steel. The compressional acoustic speed in mild steel is 5920 m/s (Class Instrumentation 2019) and its density is 7870 kg/m3 (AmesWeb 2019).

Table 5.19 Radial and tangential timber velocities, at times of SBP survey.

timber velocities (m/s)	pine timber	oak timber	jarrah timber
radial (v_R)	1968.8	2032.0	2146.4
tangential (v_T)	1811.5	1859.8	1947.2

Reflection coefficients for the varying sleeper material, buried at differing depths in different sediment conditions at both the James Matthews and Swan River sleeper sites, are listed in Table 5.20. These coefficients were calculated using Equation (1) and based on the sediment properties ($\rho_1.V_{p1}$) in Table 5.8, the sleeper properties ($\rho_2.V_{p2}$) in Table 5.17 and 5.19, and the reported mild steel properties.

Table 5.20 Reflection coefficients derived from in situ impedance characteristics for sleepers buried at the James Matthews and Swan River sleeper sites.

			pine		*oak*		*jarrah*		*ferrous*
sleeper location	**sediment depth**	**time after burial (months)**	**K_{Rrad}**	**K_{Rtan}**	**K_{Rrad}**	**K_{Rtan}**	**K_{Rrad}**	**K_{Rtan}**	**K_R**
James Matthews	Near surface	1.5–15	-	-0.324	-	-0.354	-	-0.222	0.868
	20–40 cm	1.5	-	-0.381	-	-0.409	-	-0.282	0.851
		4	-	-0.381	-	-0.409	-	-0.282	0.851
		15	-	-0.375	-	-0.404	-	-0.276	0.853
Swan River	Near surface	1.5–4	-	-0.339	-	-0.369	-	-0.238	0.864
	20–40 cm	4	-	-0.367	-	-0.396	-	-0.267	0.855

The magnitudes of the reflection coefficients derived from in situ impedance characteristics at the James Matthews sleeper site, compared to those derived from SBP data, are shown in Figure 5.17. They are displayed as a range spanning between the radial and tangential values, with the exception for ferrous material (K_{DR} = 0.85–0.87).

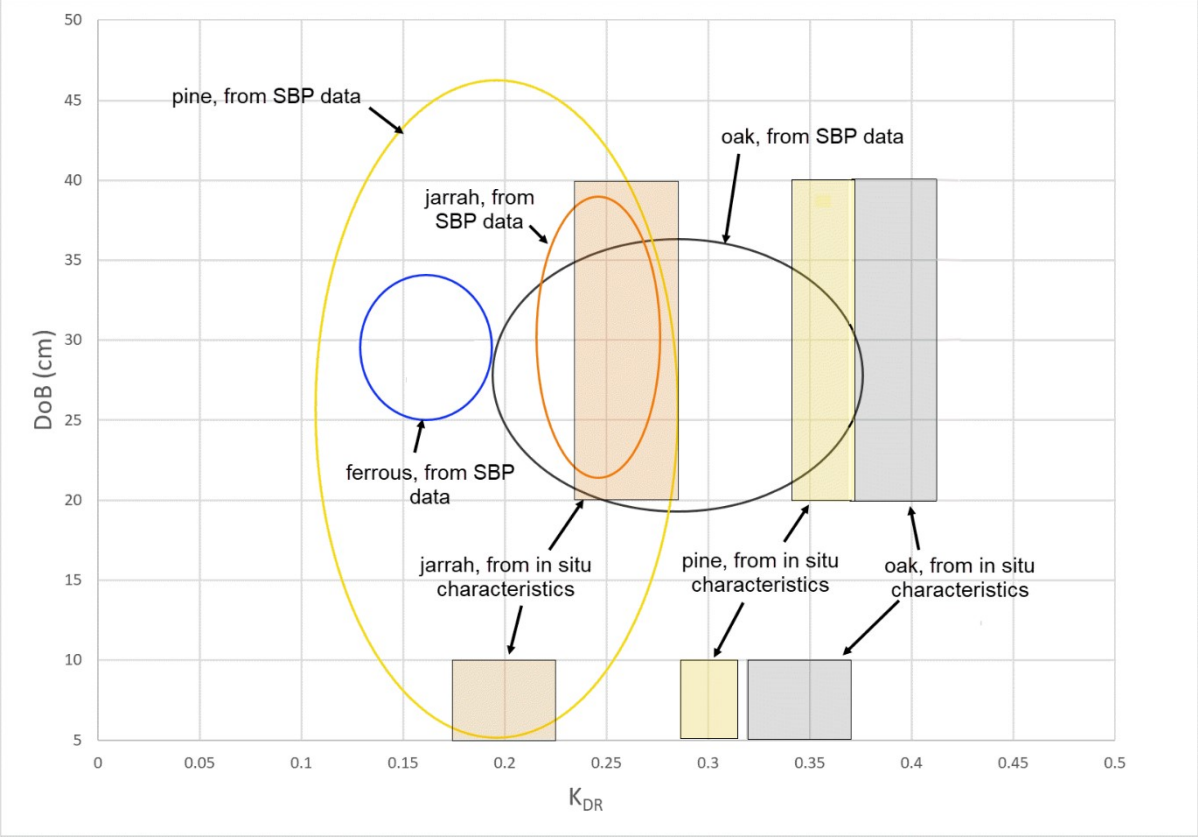

Figure 5.17 Comparison of K_{DR} values derived from SBP data and in situ characteristics.

The reflection coefficient value derived from material impedance characteristics for ferrous sleepers was much larger than the range derived from the SBP data (0.13–0.19). The reason for this large difference is not evident, but may in part be due to: a) the lack of uniformity in the backfilled sediment above one of the ferrous sleepers (trace 248 and 162 in runs 18052018-135105 and 18052018-135516, respectively)—this resulted in the lack of a clear seabed surface interface and inconsistent but significant smaller reflectors within each trace above the top face of the sleeper; b) very high variability between the individual reflection amplitudes from the top face of one sleeper (trace 364 in run 18052018-135516); and c) the ferrous sleepers were not fabricated from one 5.5 cm thick bar, but rather from three individual and slightly curved bars, each 1.84 cm thick, stacked one on top of the other. These bars were selected to allow their curvatures to match together as best as possible, then clamped. There were however some thin air gaps in between each bar, which when buried on site, would have filled with water and possibly a thin veneer of sand. As a composite sleeper, the acoustic reflection may not have been as 'sharp' as with a fully solid sleeper with corresponding changes to the amplitude magnitudes, and by consequence, the reflection coefficient derived from the SBP data.

The reflection coefficient values derived from the radial and tangential insonification of pine timbers were higher than the range calculated from the SBP data. The range of the K_{DR} values derived from the SBP data for pine timber (Figure 5.12) was also the largest for all sleeper material types. This variability may be due to the larger range in values of bulk density in the timbers used to fabricate the pine sleepers as shown in Table 5.17.

There is a closer alignment between K_{DR} values derived from SBP data and in situ characteristics for the jarrah and oak timbers. The envelope grouping the jarrah reflection coefficients derived from the SBP data overlaps the radial–tangential range of the in situ derived values in Figure 5.17. For the oak sleepers, the high end of the envelope matches with the low (radial) end of the in situ derived range. Mathematically, a closer fit for both timbers could be achieved by simply decreasing the value of the calibration coefficient, x, in equation (8). The current value (x = 44,263) was chosen as the modal value in the histogram (Figure 5.11). A slightly lower value of x = 33,000 (still located in the highest frequency range on the histogram) would result in the centroids of the jarrah and oak groups aligning within the in situ radial–tangential range of their respective K_{DR} values. This implies that the absolute magnitude of the K_{DR} values is not critical to potentially identifying that different sleeper material types are present, rather, it is their relative value that is more relevant. If reflection coefficient values were able to be used to predict the actual type of sleeper material at each location, then determining the absolute magnitude of the K_{DR} values would be critical. However as seen in

Figure 5.17, the predictive capability for sleeper material identification is not possible due to the overlap between K_{DR} values.

The ease and consistency of operational deployment and interpretation of the parametric SBP have been validated, giving high confidence in identifying the purpose-buried sleepers. In terms of identifying the varying depths of sediment cover over the sleepers, the results indicate that the SBP is 'fit for purpose'. On a much more complex site, these performance attributes have been assessed and interpreted in the following section. In addition, the potential relationship between buried material properties and acoustically derived reflection coefficients is further examined.

Verification

The verification results presented in Chapter 4 were based on 47 SBP runs directly crossing the *James Matthews* shipwreck site. They were collected in 2017 using the same vessel-mounted transducer set up as was used on the same days for the adjacent sleeper measurements. In this section, these individual results are interpreted with the results from the WAM's 1975/76/77 historic archaeological and 2000 pre-disturbance surveys, and other complimentary geophysical surveys of the wrecksite. The aerial extent of buried reflectors is compared to the known site plan derived from WAM's survey. Qualitative and quantitative comparisons of cross-sections and quasi-3D representations developed from the SBP data are assessed against MBES representation of the seabed surface features, and a 3D digital reconstruction of the buried features developed from the 1975/76 survey. Acoustic characteristics and reflection coefficients derived along specific cross-sections are compared to magnetometer survey data and known material types documented in WAM's 1975/76 and 2000 surveys, to verify site interpretation on the types of buried material.

Plan extent

Reflectors interpreted from the SBP runs across the *James Matthews* wrecksite identify the complexity of the aerial extent of the buried shipwreck remains, as well as isolated buried features. The tracks of the 47 SBP runs crossing the *James Matthews* shipwreck site are shown in Figure 4.44. Of these, 10 align in a NW-SE direction at an average spacing of 1.4 m, and 37 align across the wrecksite in a SW-NE direction at an average spacing of 0.8m. Along each of these runs, the location of reflectors identifying buried material were extracted from the SBP echo plots, and the latitude and longitude of the endpoints of these reflectors recorded. These were mostly contiguous in their extent and are plotted in Figure 5.18. Also

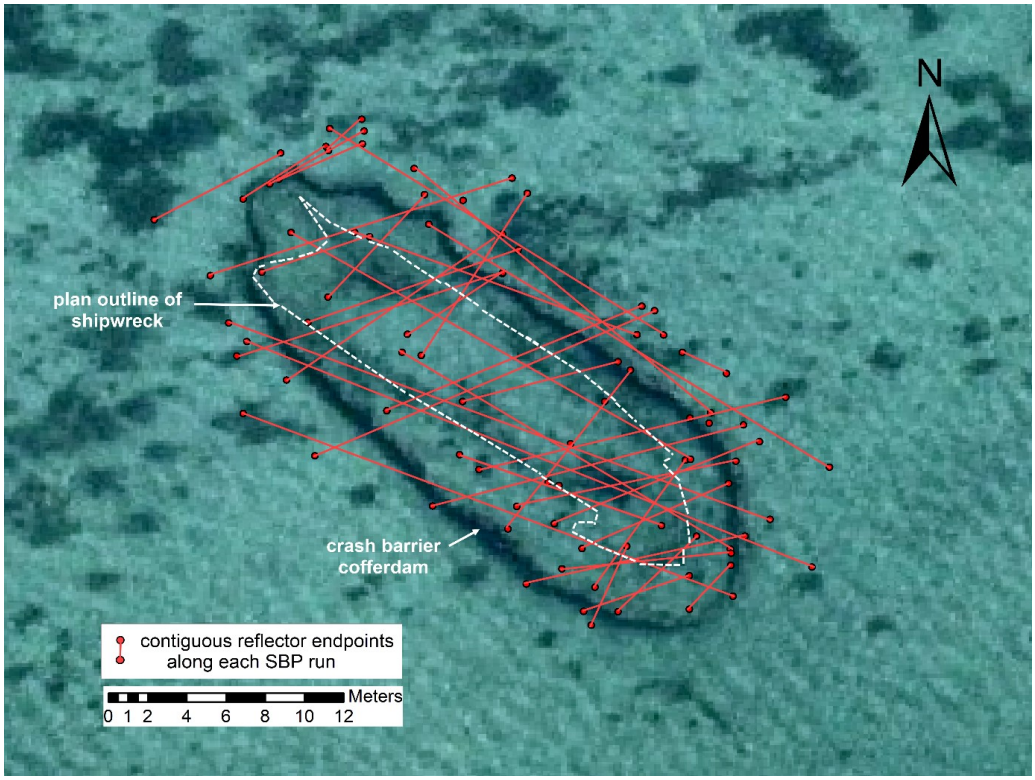

Figure 5.18 *James Matthews* site plan showing extent of contiguous reflectors identified across the wrecksite.

shown on this figure is the surficial crash barrier cofferdam, marking the outer limits of the site protection works, and the plan outline of the intact buried shipwreck material from Figure 3.5.

As can be seen, the lines of contiguous buried reflectors identified from the multiple SBP runs lie mostly within the limits of the cofferdam, with the exception on the north-eastern side where they extend approximately five metres further out. On the south-western side, reflectors extend beyond the plan extent of the shipwreck remains, but generally lie within the line of the crash barrier. On 16 of the SBP runs, groups of additional isolated reflectors were also identified outside the endpoints of the contiguous reflectors, and these are shown on Figure 5.19. Two of these isolated reflectors lie 20–30 m away from the wrecksite to the southwest and east. Of the remainder, half lie up to 5 m outside of the plan outline of the ship wreck material on the southwestern side, co-existent with other contiguous reflectors. The balance are located up to 10 m on the other three sides, mostly outside the area bounded by the contiguous reflectors identified on nearby runs. Without knowledge of the history of this site, interpretation of reflectors from the SBP runs would overestimate the dimensions of the wrecksite by 5–10 m.

Following the extensive 1975/76 excavation, survey and backfill of this site, a fourth and final excavation was undertaken by the archaeologists from WAM from January to March 1977 (Baker and Henderson 1979:228-229; Henderson 1977a:97-113; 1977b:78). The aim of this

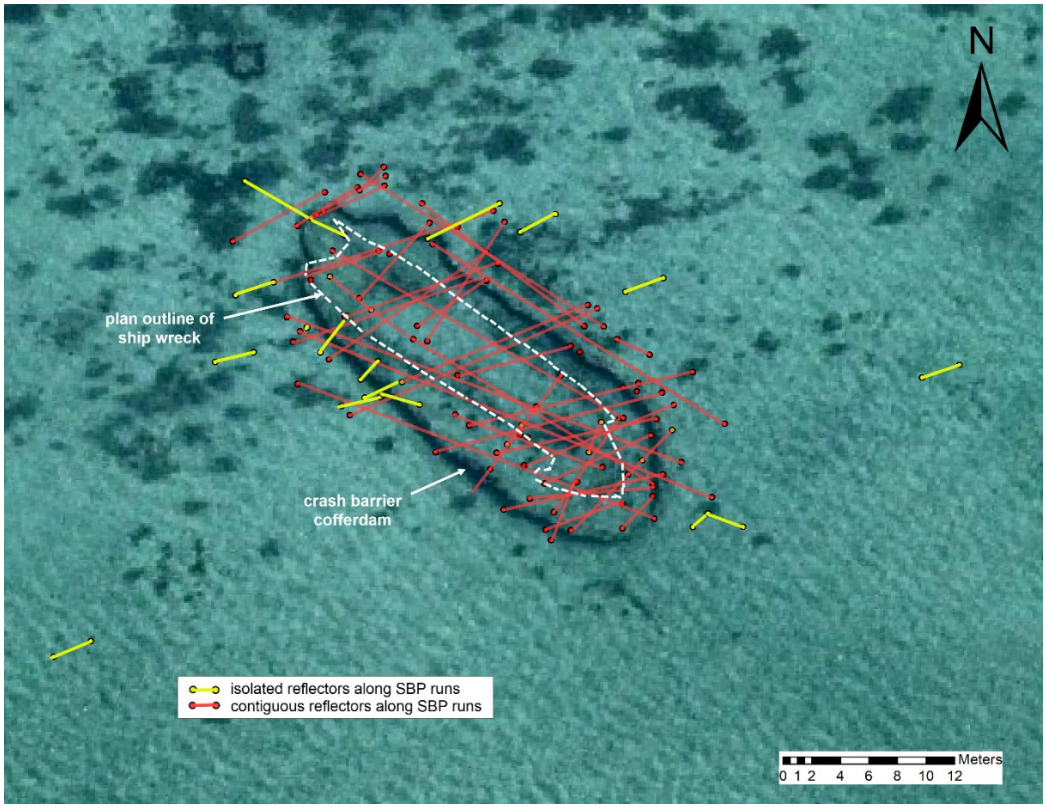

Figure 5.19 *James Matthews* site plan showing extent of contiguous and isolated reflectors across the wrecksite.

last survey was to located and raise any material located outside of the main hull structure previously surveyed. Trenches five metres wide and 1.0–1.5m deep were excavated using an airlift along and under the starboard (south-westerly) side of the wreck, along the bow and along the stern. These are shown in Figure 5.20. Rope from the rigging was found along the starboard side of the wreck, but the bow and stern trenches 'proved to be almost sterile'. During the 1976/77 excavation, broken timbers in quantity were noted to lie along the port side of the vessel. In addition, ballast stones were relocated from the hull to this area. Consequently, a one-metre wide by one-metre deep clearance trench, located five metres out from the keel side of the hull, was excavated in 1976/77 to determine the lateral extent of the broken timbers. All trenches were backfilled with the airlift at the conclusion of the excavation season.

Figure 5.20 shows the context of the locations of the contiguous and isolated reflectors identified from the SBP runs over the site. There are seven isolated reflectors (A–G) that lie outside of the areas excavated in 1975/76 and in 1977. These may or may not be associated with material lost from *James Matthews* during the wrecking event, or subsequently due to wrecksite formation processes. The reflection coefficients for these reflectors were assessed and reported in the following sections, to explore the potential identification of their material

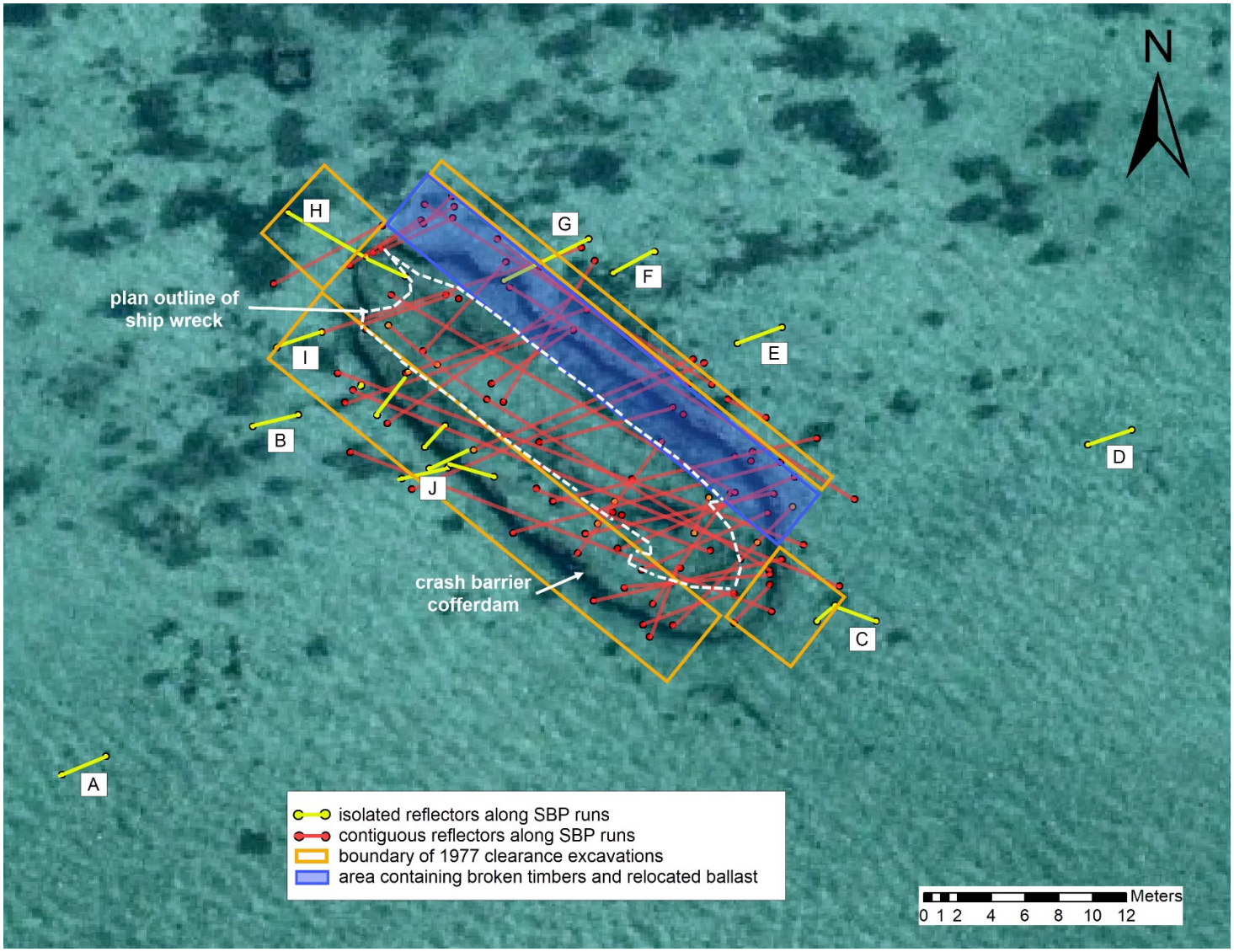

Figure 5.20 *James Matthews* site plan showing extent of contiguous and isolated reflectors and historic excavation limits across the wrecksite.

composition. The remaining isolated reflectors lie within the trench areas excavated and backfilled during the 1976/77 season. The reflection coefficients from reflectors H–J will be examined to see if they reveal characteristics associated with possible sediment layering/interfaces resulting from the hydraulic excavation and backfilling processes, akin to those identified on the *Mary Rose* (1545) site (Quinn 2006; Quinn et al. 1997a; Quinn et al. 1997c). Overall, interpretation of SBP traces collected from 47 runs across *James Matthews* identified the outer dimensions of this complex wrecksite within an accuracy of one metre. The shipwreck remains, including the starboard section of the hull and cargo composed of multiple materials, as well as the effects of multiple seasons of excavation and backfilling over different sections, all added to the complexity of this site.

Depth of burial and cross-sectional features

Qualitative interpretation of SBP echo plots across the buried remains of the *James Matthews* shipwreck in Chapter 4 revealed the lower profile of buried material (hull structure) with multiple layers above, as well as the slate mound and windlass. In addition, isolated reflectors were detected outside the plan area of the shipwreck remains on all sides, consistent with the previous wrecksite plan interpretation. The following detailed verification of SBP profiles documented the slate mound up to 80 cm above the seabed level, and sediment cover from 14 cm to 60 cm deep over the ribs and ceiling planks, with an accuracy of +/- 5–10 cm.

The cross-section verification was undertaken using two transverse SBP runs (0608-013531 and 0607-051953) which cut through, and just forward of the slate mound, respectively (Figure 4.51). The horizontal and depth positions of reflectors representing the seabed surface and buried interfaces along these runs were extracted from every fifth or tenth trace in the SBP LF unprocessed and demodulated echo plots. The complexity of the site, with varied buried materials at different depths, the effects of excavation and backfilling, subsequent erosional protective works placed on the site and seasonal emergent algal growth, resulted in significant variability in the strength and depth of reflectors along both echo plots. Reflectors were interpreted as representing buried interfaces only when their amplitude magnitudes were relatively large, and consistent across a number of adjacent traces. All extracted depths were corrected using the water column and sediment velocities presented in Table 5.8, and the results plotted in Figure 5.21a and Figure 5.22a. The outlines of the corresponding cross sections cut through the 3D digital model of the buried remains of *James Matthews* (Figure 4.52) were co-plotted at the same horizontal and vertical scale with the SBP reflector positions. The vertical datum of the 3D digital model, and hence the model cross sections, was based on the arbitrary height of the underwater survey frame. In Figure 5.21a and Figure 5.22a, the height datum of the model cross sections were adjusted until a match occurred with the upper

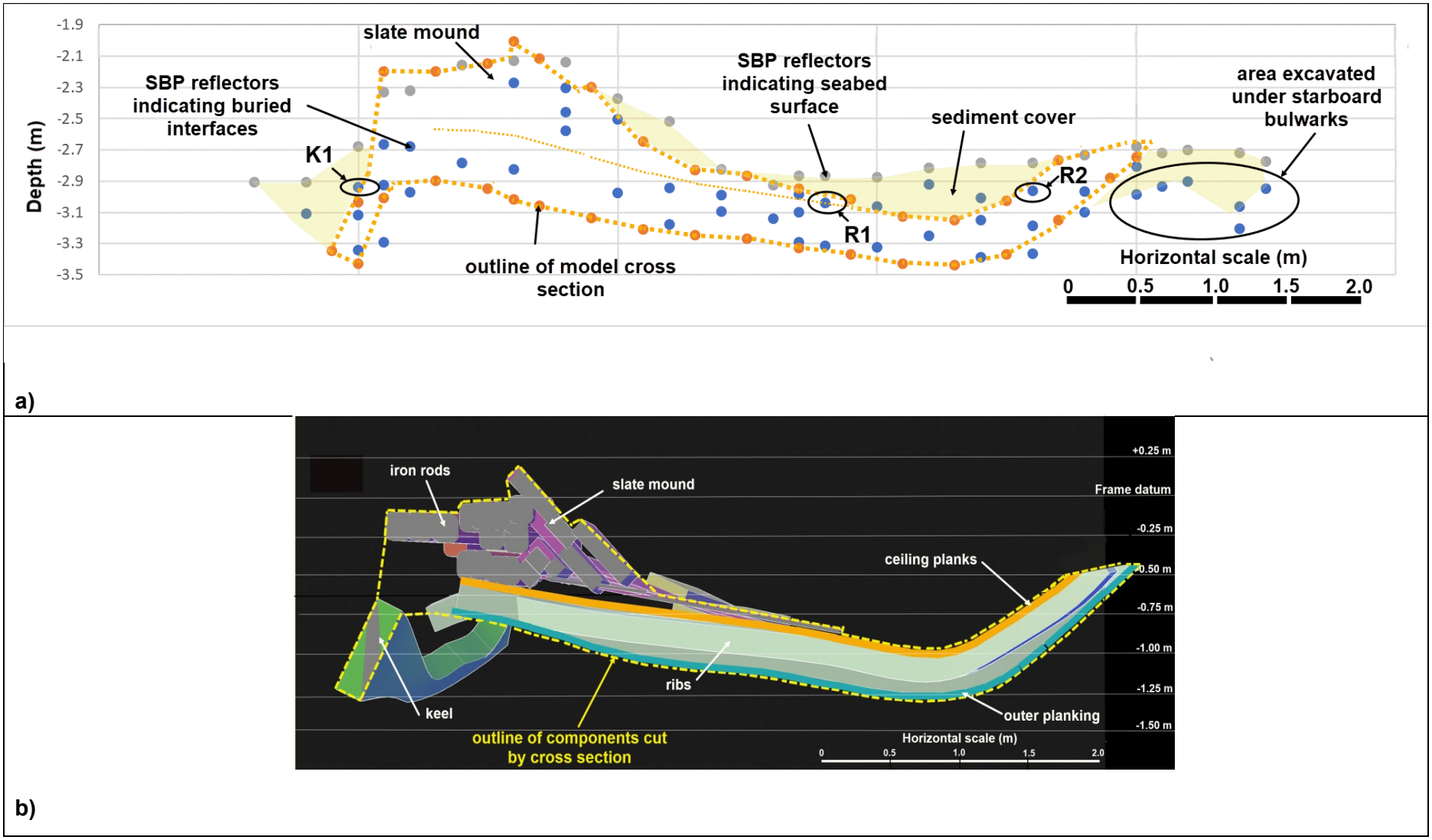

Figure 5.21 Comparison between SBP reflectors identified along run 0608 031531 and outline of corresponding 3D model cross section; and b) details within outline of 3D model cross section

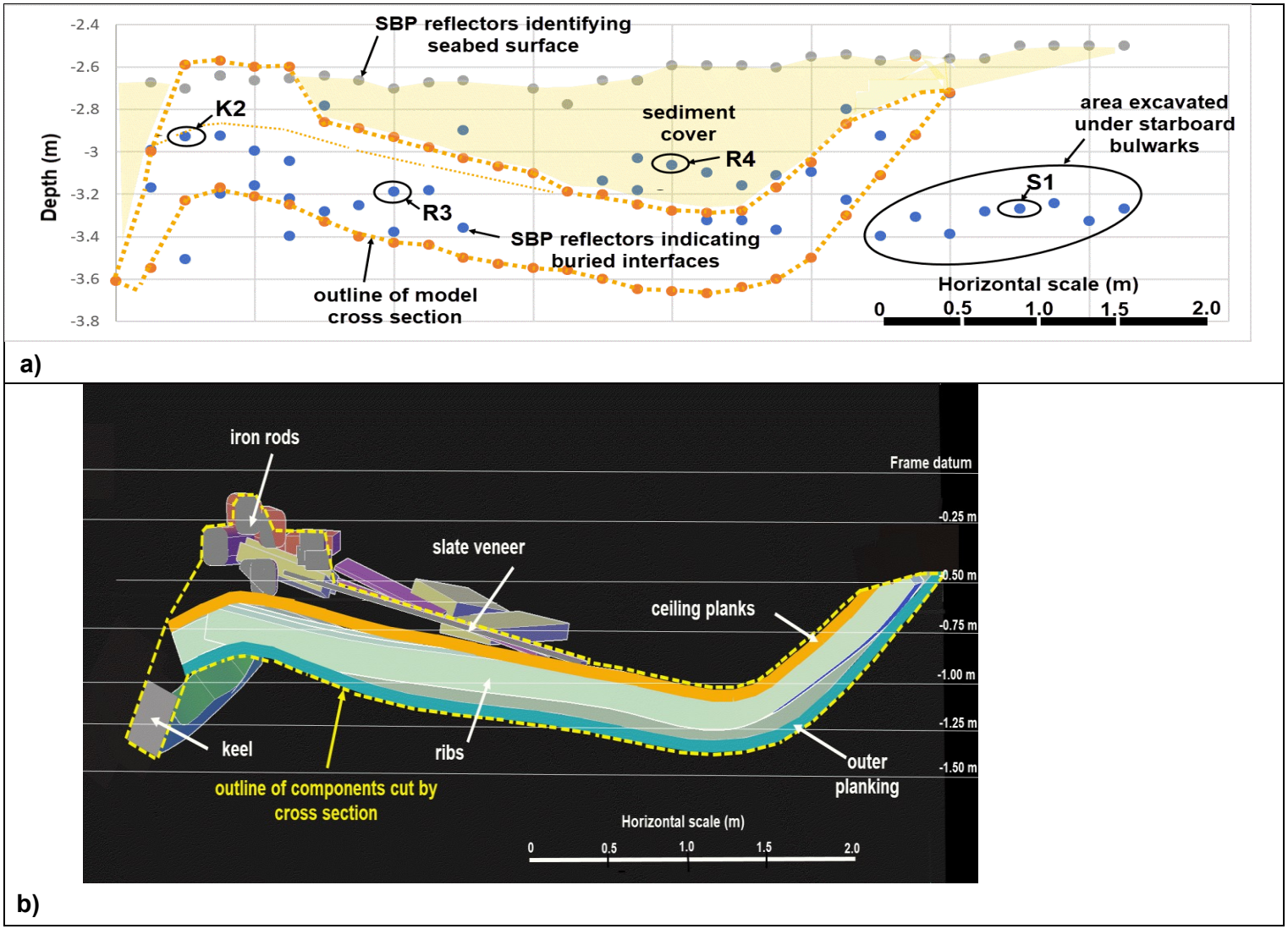

Figure 5.22 Comparison between SBP reflectors identified along run 0607 051953 and outline of corresponding 3D model cross section; and b) details within outline of 3D model cross section.

profile of the slate mound. The relative accuracy of this datum alignment was estimated to be +/- 5–10 cm. For visual interpretation purposes, the cross-sectional detail for both cross sections are also shown in Figure 5.21b and 5.22b, respectively.

The SBP data from run 0608-031531 displayed in Figure 5.21a provided a match to the outline of the buried cross-sectional components extracted from the *James Matthews* digital shipwreck model. SBP reflectors identified the outline of the exposed slate mound and the buried keel and ribs/planking within a horizontal accuracy of 0–15 cm and within the +/- 5–10 cm relative vertical accuracy. Note that the keelson, sitting on top of the keel but under the iron rods, was not depicted in this cross-section. However, SBP reflectors were identified above the keel, and these may well represent the acoustic wave reflecting from the top of the keelson. Importantly the depth of burial, from 14 cm to 30 cm over the ribs/planking, was closely aligned to the upper side of the model cross section. On the starboard side of the exposed slate mound, the SBP data indicated a higher surface level, however this may simply represent a sandbag (see Figure 4.46a) more recently placed as part of the WAM's site protection activities. Beyond the starboard bulwarks, a number of reflectors were identified between 30–55 cm below the seabed level. These may reveal the legacy of the 1977 excavation and backfilling activities along and under the starboard bulwarks.

The comparable results for SBP run 0607-051953 are shown in Figure 5.22. This cross section is located approximately one- metre forward of the slate mound, and was chosen to comparatively assess any interpretation influence from the slate mound. With the exception of the mid-section of the ribs/planking, the SBP reflectors identified the upper and lower sides of the model cross section within the estimated relative vertical accuracy. Extensive algal growth in the water column above the mid-section of this cross section (see Figure 4.53) resulted in numerous high amplitude water column reflections, which quickly decreased below the seabed. This effect may have resulted in the loss of acoustic wave energy at deeper depths, with minimal strength reflections off deeper buried timbers in this section. The depth of burial ranged from 14 cm to 60 cm. A shallower section, 0.75 m long, was indicated on the upper side of the ribs/planking in the same area affected by the red algae. This difference from the surveyed cross section may result from the interference associated with the red algae, or from ballast stones or other items moved and left in situ after the survey was complete. In a similar fashion to the previous cross section, a number of reflectors approximately 80 cm deep were identified outside the starboard bulwarks. These too may reveal the remnant features of the 1977 excavation and backfilling activities.

The results from these quantitative cross-sectional comparisons demonstrate that interpretation of the SBP data depicts the DoB of the *James Matthews* shipwreck remains

within an accuracy of +/- 5–10 cm. A layer of sediment, from 14 cm to 60 cm deep covering the ribs and ceiling planks, was identified by the SBP data. The slate mound, the top of which is located 80 cm above the localised seabed, and iron rods were clearly visible in the SBP record. The cross-sectional outline of these features was equally well represented, within a horizontal accuracy of 0–15 cm. However localised interference on the acoustic records from dense seabed-emergent red algae reduced the interpretation accuracy underneath these emergent plants. The SBP data also revealed buried interfaces which may have resulted from the 1977 excavation and backfilling. For confirmation, the reflection coefficient characteristics of these reflectors (S1) are compared in the following section with those from isolated reflectors H, I and J shown in Figure 5.20. The reflection coefficients associated with keel and rib timbers K1, K2, R1, R2, R3 and R4 marked on Figure 5.21a and 5.22a are also calculated to identify any correlation to material properties.

Material characteristics

Verification of reflection coefficients for known buried materials and for isolated reflectors from the *James Matthews* shipwreck site showed a considerable range of values with no predictive association. These reflection coefficients were derived in the same manner as per the sleeper sites. Mean depth and amplitude characteristics of the reflectors associated with the keel, ribs and excavated sediment locations shown on Figure 5.21a and 5.22b are summarised in Table 5.21. Likewise, properties associated with isolated reflectors A to J shown in Figure 5.20 are also presented in this table. The K_{DR} values were calculated using equation (9) with the calibration coefficient x=44263 based on the 2018 seabed data from the adjacent sleeper site. The absolute value of the derived reflection coefficients for the 2017 *James Matthews* survey may not be accurate using this calibration value due to differences in instrument gain settings between the two SBP data sets. However, any relative difference due to material type shown for *James Matthews* K_{DR} values would still be valid. Reflection coefficient values for *James Matthews* and isolated reflectors are listed in Table 5.21 and plotted against DoB on Figure 5.23.

The most notable feature in Figure 5.23 is the wide spread of reflection coefficient values (0.03–0.5) associated with the isolated reflectors A through J. Within this spread however, reflectors positioned in areas excavated and backfilled during 1976/77 tend to group together with the lowest K_{DR} values (0.03–0.11), with the exception of reflectors G and J. These include reflectors H (stern), C (bow), I (starboard) and S1 (starboard). The K_{DR} value for isolated reflector B also falls within this range, but is located outside of the excavation area. Reflectors G and J are located on the port and starboard edge of the excavated areas, but both have high K_{DR} values of 0.50 and 0.42, respectively. During the 1977 excavations, trenching along

Table 5.21 Reflector properties, model cross sections and isolated reflectors.

			depths				amplitudes			
run	**reflector**	**reflector location/seabed nature**	**seabed level (m)**	**DoB (cm)**	**1st seabed mult. (m)**	**reflection coefficient (magnitude)**	**seabed**	**1st buried reflector**	**1st seabed mult.**	**instrument gain (dB)**
0608 031531	K1	keel/adjacent to ferrous rods	2.78	20.3	2.82	0.14	4685	-8313	-197	6-6
	R1	upper side ribs	2.79	11.8	2.93	0.09	12111	-5215	-426	6-6
	R2	upper side ribs	2.71	16.1	2.88	0.06	10013	-3744	5	6-6
0607 051953	K2	keel/under ferrous rods	2.56	25.7	2.83	0.19	-20302	-11753	-155	8-8
	R3	mid-level ribs	2.57	41.7	3.05	0.18	-17165	10306	-193	8-8
	R4	above (?) ribs	2.53	38.5	2.93	0.26	-32757	15877	-483	8-8
	S1	sand excavation	2.33	62.0	3.09	0.08	-19177	4995	341	8-8
0607 050945	A	clear sand	2.35	43.9	4.58	0.17	-29237	10426	1147	8-8
0607 051048	B	clear sand	2.38	57.8	4.31	0.08	-32741	-4484	-738	8-8
0608 041131	C	clear sand, next to seagrass patch	2.35	32.1	4.59	0.10	27206	5449	200	6-6
0607 053048	D	one isolated spike, not seagrass	2.19	23.5	4.37	0.29	-24242	-21223	2631	8-8
0607 051745	E	clear sand	2.24	17.1	4.79	0.21	-32757	-14988	-1732	8-8
0607 051953	F	(dense) seagrass patch	multiple mixed shallow reflectors							8-8
0608 041720	G	tall red algae	2.47	34.2	4.71	0.50	-32662	-31171	-1694	8-8
0607 050504	H	clear sand, next to seagrass patch	2.39	33.4	4.62	0.03	-5806	-2016	-421	6-6
0607 051745	I	small (red algae?) irregularities	2.51	73.8	4.49	0.11	19242	-6193	728	8-8
0607 050821	J	clear sand	2.33	26.7	4.60	0.42	-27713	-28471	1058	8-8

the sides of the wreck material commenced on January 30th and backfilling concluded on 4th March. During this time, detrital and seagrass material may have accumulated in the trenches as a result of local summer seabreeze conditions and/or the backfilling from adjacent sand piles. Consequently, the variability in acoustic reflections from these trenches may represent a rapid change in sediment density from hydraulically back-filled sands sitting on denser un-disturbed sands, the remnants of vegetative clumps or mats, or both. The isolated reflectors located the furthest from the wrecksite (A, D and E) fall in the mid-range of the scatter plot with K_{DR} values ranging from 0.16–0.29. The reflection coefficients for the timbers identified from the model cross sections further confound any consistent interpretation of Figure 5.23. In SBP run 0607-051953, the sediment reflector S1 is separated from the grouping of K_{DR} values for the timbers in this cross-section, however the S1 value lies in the middle of the K_{DR} range for timbers from run 0608 031531. The K_{DR} values associated with keel and ribs/planking timbers from SBP run 0608 031531 also fall in a similar range to reflectors H, C and I. For these timber reflectors, R1 and R2 have similar K_{DR} values (0.056–0.08) which are lower than the value (0.145) for the keel timber K1. Comparably, K_{DR} values associated with keel and ribs/planking timbers from SBP run 0607-051953 are higher and fall in a similar range to reflectors A, E and D. In this situation, there is no differentiation of the keel timber (K2) from the ribs/planking timbers (R3, R4).

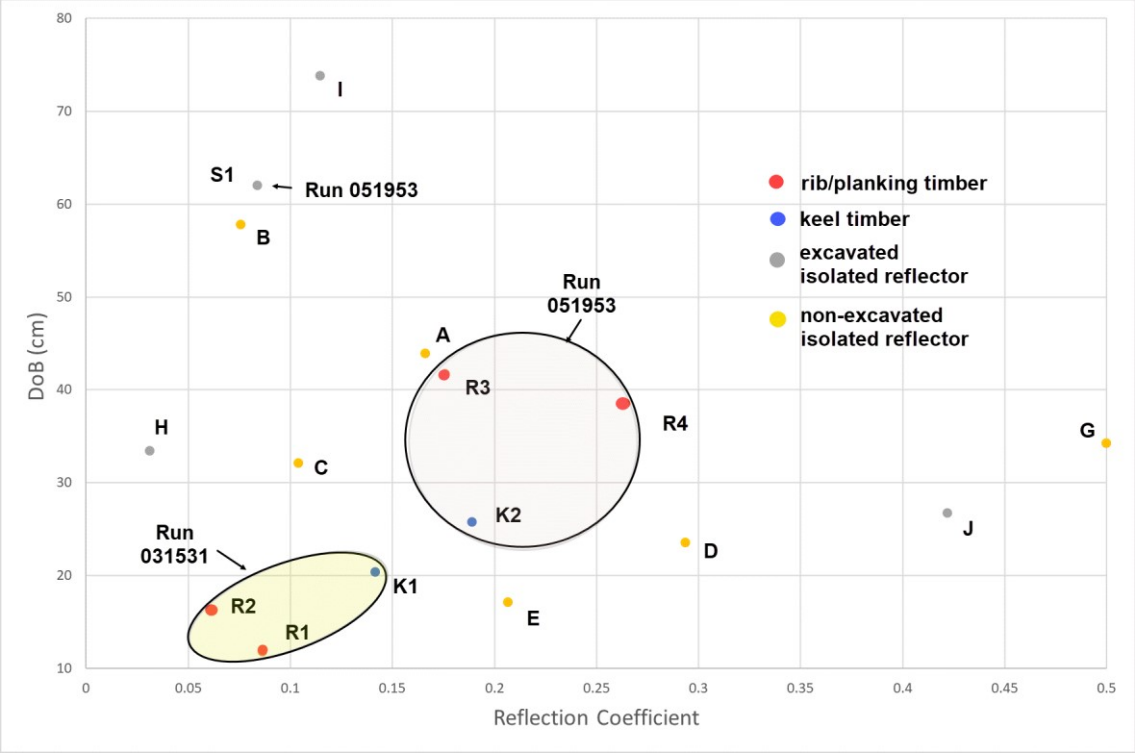

Figure 5.23 Scatter plot of reflection coefficients for *James Matthews* material and isolated reflectors.

The lack of any differentiation between the refection coefficient values for the timbers in the cross sections may simply result from similar acoustic properties in all timbers. The WAM 2000 conservation pre-disturbance survey of the *James Matthews* wrecksite (see Figure 3.31a for trench locations) identified that the keel and keelson were constructed using beech and white oak timbers, and the ceiling planks, ribs and outer planking were constructed of white oak timber (Richards 2001:13). While the timber locations K1 to R4 were not excavated and tested, all the timbers examined in the five test trenches were waterlogged, with some significantly deteriorated. The mean values of the specific gravity (a unitless measure for density) of beech and oak timbers determined by Richards were similar, varying from 0.58 (beech wood in keel) to 0.47– 0.45 (oak timber in ribs and inner planking). Individual radial and tangential acoustic velocities in saturated beech were not found in the literature to compare with those published for saturated oak samples. However, Quinn et al. (1997b:28) reported timber characteristics for beech and oak at 12% moisture content, with densities 15% higher for beech than oak, but with similar radial and tangential velocities for both timber species. These results are associated with moisture contents below FSP and therefore are unlikely to be representative of their fully saturated condition. However, their similarity suggests that any differences in in situ acoustic impedance derived K_{DR} values may well be masked by other factors. These include variability in the surficial seabed characteristics, patchy algal growth, isolated sandbags and other materials subsequently used for site protection, which all may affect the magnitude of reflector amplitudes from the seabed surface and the deeper buried reflector.

A potentially clearer site interpretation was achieved by initially assessing the difference in timber densities from the shipwreck material submerged since 1841 from the adjacent sleepers which were buried in 2017 and recovered 20.5 months later. Richard's density measurements reported as specific gravity could not be back-calculated to bulk or basic density, however the density of the recovered oak blocks at the time of the SBP survey along the adjacent sleepers could be expressed in terms of specific gravity. The reflection coefficients determined from the keel and ribs of *James Matthews* (Table 5.21), and the reflection coefficients for the adjacent oak sleepers measured in 2018 (Table 5.15), were plotted against specific gravity as shown in Figure 5.24a. This figure reveals that following an extended period of submergence, the waterlogged and (partially) degraded white oak had a significantly lower specific gravity, reflecting the loss of cellulose in the timber (Grattan 1987:65–66). These shipwreck timbers also had corresponding lower reflection coefficient values compared to the recently buried, partially-saturated European oak timbers. To expand this analysis to include the results from all sleepers buried adjacent to the *James Matthews* wrecksite, Figure 5.24b displays the relationship between % saturation and specific gravity for all recently buried timber blocks retrieved from both the James Matthews and Swan River

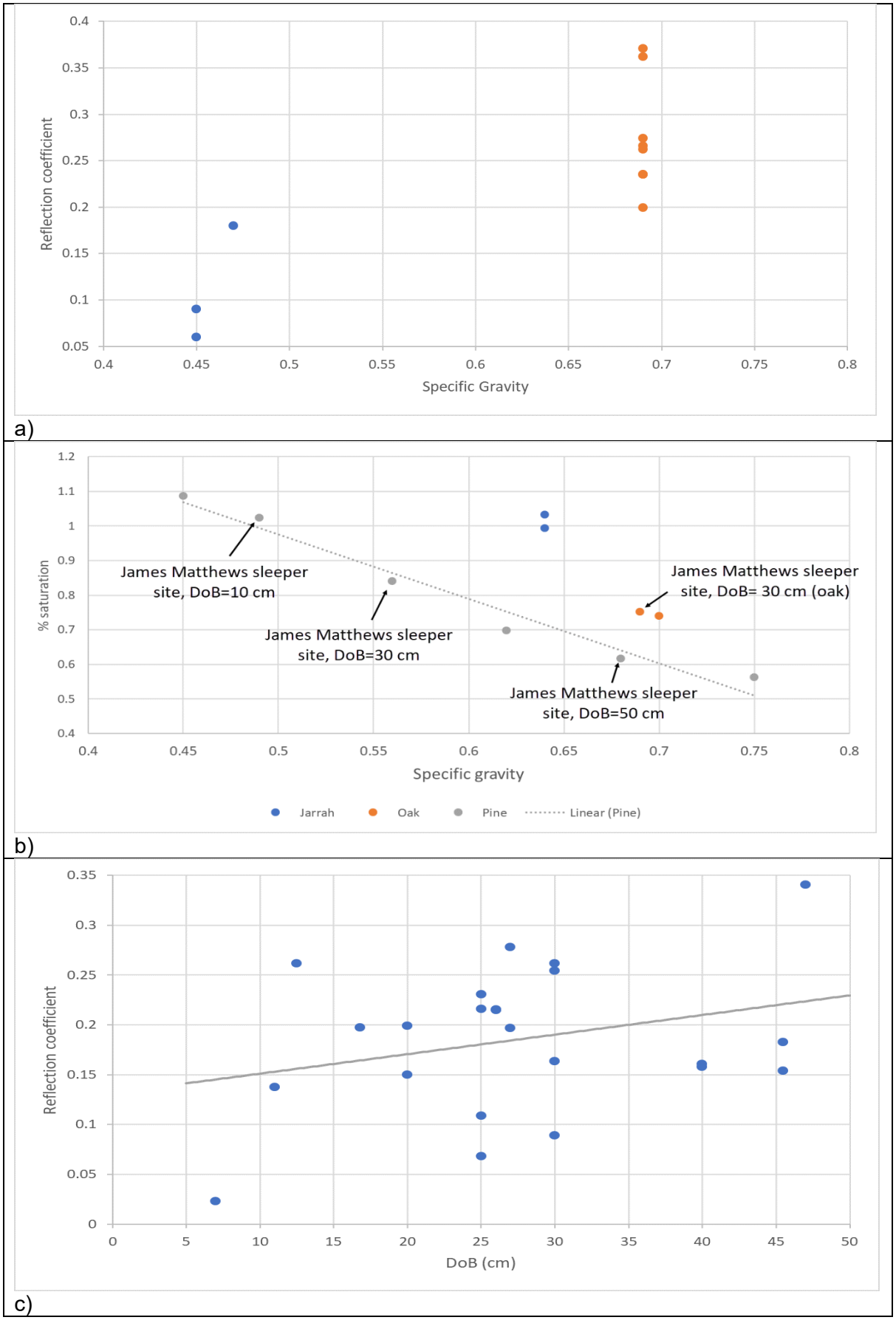

Figure 5.24 Relationships between % saturation, reflection coefficients, specific gravity and depth of burial.

sleeper sites. Here, the % saturation (moisture content/umax) of the timber blocks is shown to rise with decreasing specific gravity. For the pine blocks buried at multiple depths, the highest % saturation of the pine timbers occurred in the shallowest burial depths, with the lowest % saturation in the deepest burial depths. This shows the effect of the relative higher degradation and water penetration rates in the shallower aerobic sediments, and the relative slower rate of degradation/waterlogging in the deeper anaerobic sediments. Reflection coefficients were determined from two SBP runs at the James Matthews sleeper site in 2018 (Table 5.15) for all 16 pine sleepers buried at these same burial depths. These reflection coefficients were plotted against DoB and the results depicted in Figure 5.24c. The results show significant variability. A non-linear regression curve is shown with a general rising trend of reflection coefficient with increasing depth of burial, however its very low R^2 value (0.09) indicates a weak statistical relationship between these parameters. Figure 5.24 demonstrates that SBP-based reflection coefficient values were able to discriminate density, and hence degradation differences, between oak timbers which had been buried in similar sediments for almost 180 years compared with those buried for only 20.5 months. For pine sleepers buried for 20.5 months, direct measurement of % saturation and density (specific gravity) confirmed the higher relative rate of saturation/degradation in the shallower buried sleepers compared to those buried deeper. This trend however was only weakly observed in the SBP derived reflection coefficients due to the high variability associated with the calculation of those reflection coefficient values.

A clear relationship between the type of shipwreck-related material buried at the *James Matthews* site and the acoustic data could not be established. Figure 5.24 however, shows that through the derived reflection coefficient values, parametric SBPs can differentiate changes in density within similar types of timbers. By knowing the burial depth of the timber, inferences can be made regarding the relative state of degradation of that material. In addition, the combination of the burial depth and reflection coefficient values of each reflector, together with site specific sediment DO and Eh profiles, can be used to provide an interpretation of the buried material at a site. This is illustrated in Figure 5.25 for the *James Matthews* wrecksite. The reflection coefficients from both the known ship's timbers and surrounding isolated reflectors were plotted against their respective reflector DoB revealing three identifiable groupings of K_{DR} and DoB reflectors. Reflection coefficients from the known timbers and from two isolated reflectors grouped together (Group 1) to show increasing K_{DR} values with depth of burial. On the assumption that all timbers have similar acoustic impedance properties and have been buried for a similar time period since the wrecking event in 1841, then the SBP data identified increasing timber degradation with decreasing burial depth. One of the two isolated reflectors with these similar properties was located just beyond the 1977 excavation

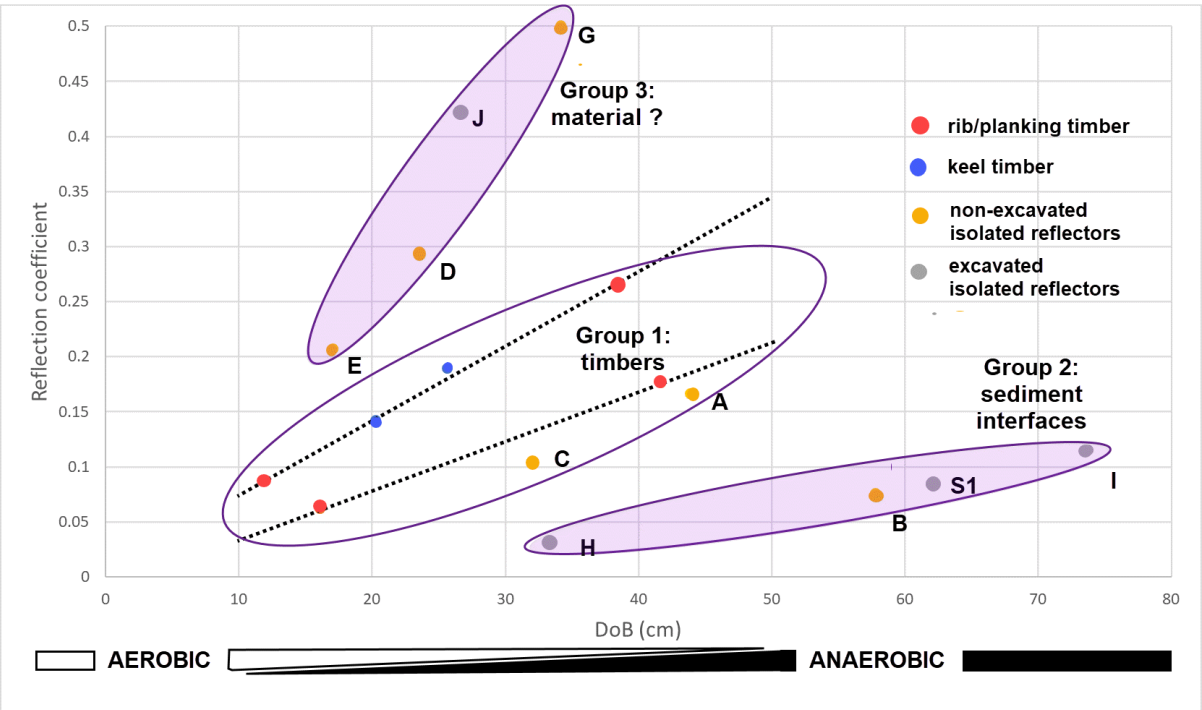

Figure 5.25 *James Matthews* site interpretation.

off the bow of the shipwreck remains at a burial depth of 32 cm, the other located almost 30 m away with a burial depth of 44 cm. This interpretation suggests that these two isolated reflectors may be pieces of timber separated from the hull of *James Matthews* during or post the wrecking event. It is possible that isolated reflectors E and D also belong to this group. The second group of isolated reflectors had low K_{DR} values (0.04–0.11) with burial depths generally in excess of 55 cm (Group 2). At these depths environmental conditions within the sediments would be conducive to timber conservation, so their low K_{DR} values are unlikely to be associated with degraded timber. One of these isolated reflectors (S1) was identified on a cross-section from the AutoCAD model to be located at the bottom of the 1977 excavation trench outside the hull bulwarks. This suggests that the second group of low reflection coefficient with higher depth of burial reflectors is associated with weak sediment interfaces resulting from excavation and backfill of trenches. The third group of isolated reflectors are characterised by higher K_{DR} values (0.2–0.5) with burial depths in the range 18 cm to 35 cm. With the current information it was not possible to interpret the nature of these reflectors, however those reflectors in the upper reflection coefficient range (G and J) are unlikely to be associated with timber as their K_{DR} values exceed all values derived from freshly buried oak, jarrah and pine on the adjacent sleeper site.

The complimentary use of geophysical instruments may also assist in the interpretation of material composition. Magnetometer surveys can identify the presence and general spatial

location of ferrous material on a site, but not the depth nor detailed aerial extent of that material. WAM Department of Maritime Archaeology undertook a 25m wide spaced magnetometer search pattern over the *James Matthews* site in 2018 using a towed Marine Magnetics Explorer magnetometer. The results of this coarse preliminary survey are shown in Figure 5.26 which indicate a significant ferrous anomaly located on the wrecksite. A finer survey pattern and an underwater magnetic hand survey would refine the horizontal position of the ferrous

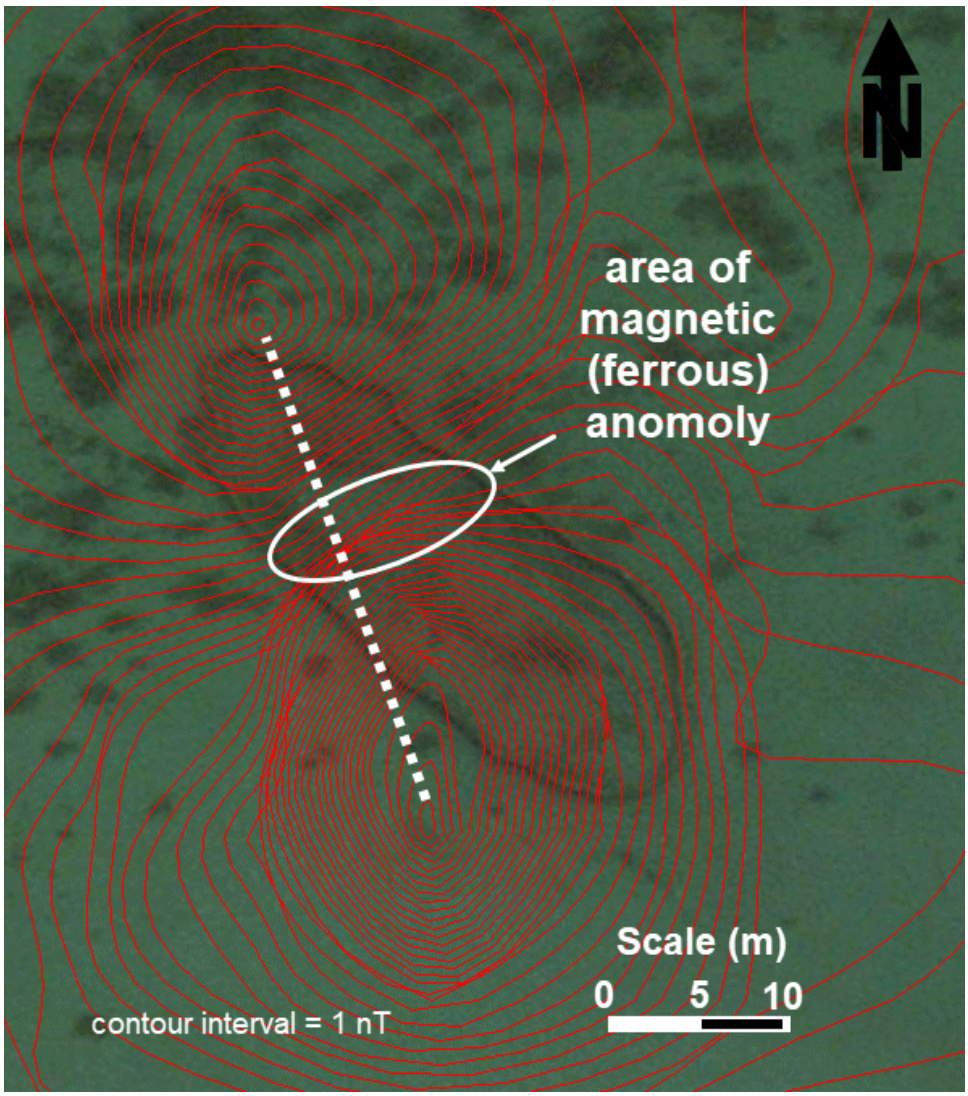

Figure 5.26 Magnetometer survey anomalies over *James Matthews* wrecksite (image by Jeremy Green).

metal located on this site (Dr Jeremy Green pers. comm. 2019). Suffice to say that the complimentary use of SBP and magnetometer instruments would together help interpret both the presence, and horizontal and vertical distribution, of ferrous material on the *James Matthews* site.

3D site interpretation

A quasi 3D visualisation of the site based on interpolation of the SBP data enabled a more holistic interpretation of the seabed-protruding and sub-seabed features on the *James Matthews* wrecksite. While the individual SBP runs have been scrutinised to quantify DoB and thickness of shallow buried ship wreck materials, a broader site interpretation was achieved by interpolating these runs using gridding software. The results of gridding 37 transverse and 10 longitudinal SBP runs into one 'volume' is described in Chapter 4. Horizontal, incremental depth slices through this 'volume' provided the visual interpretation of the site not easily seen in the individual SBP cross sectional runs. Examples include the separated stern post, and the overall shape of the hull remains with the stern end buried slightly deeper than the bow, and the deepest curvature of the remaining starboard hull located just forward of the slate mound.

Complimentary imagery, and the results from a separate geophysical survey using a multibeam echo sounder (MBES), support and reinforce the site interpretation based on the interpolated SBD data. At this site, the ellipsoidal shape of the shallow crash barriers seen in the top slice of the 3D 'volume' is clearly visible in the satellite imagery used as background for the site figures. At times of high turbidity though, or at sites with greater water depths, such surficial features would not be visible through satellite imagery. Such features would however be discernible using MBES acoustic devices. The WA Department of Transport, Marine Survey Branch, undertook a regional MBES survey around Woodman Point in 2017. Figure 5.27a shows an oblique view of a coarse-resolution digital elevation model (DEM) of the *James Matthews* site. The cofferdam, windlass and slate mound are identifiable and align with the interpretation based on the top slices of the 3D 'volume'. A section profile through the site DEM (Figure 5.27b) clearly shows the sloping seabed from bow to slate mound, consistent with the surficial interpretation from the SBP data. These MBES results verify the SBP based site interpretation and demonstrate the value of using multiple non-invasive geophysical tools on complex shipwreck sites.

Key aspects of the performance of the parametric SBP have been validated and verified. These include the ease and flexibility of instrument deployment and data interpretation, the accuracy of estimates for the aerial extent and DoB of buried material, and the site interpretation of buried material through qualitative and quantitative analyses of cross-sections and quasi-3D interpolations. Based on the interpretation of the experimental buried sleepers and the complex *James Matthews* wrecksite, the results from reflection coefficient analyses of the acoustic data cannot be used predictively to determine the nature and degradation state of buried material. However, in conjunction with a magnetometer survey which can identify if

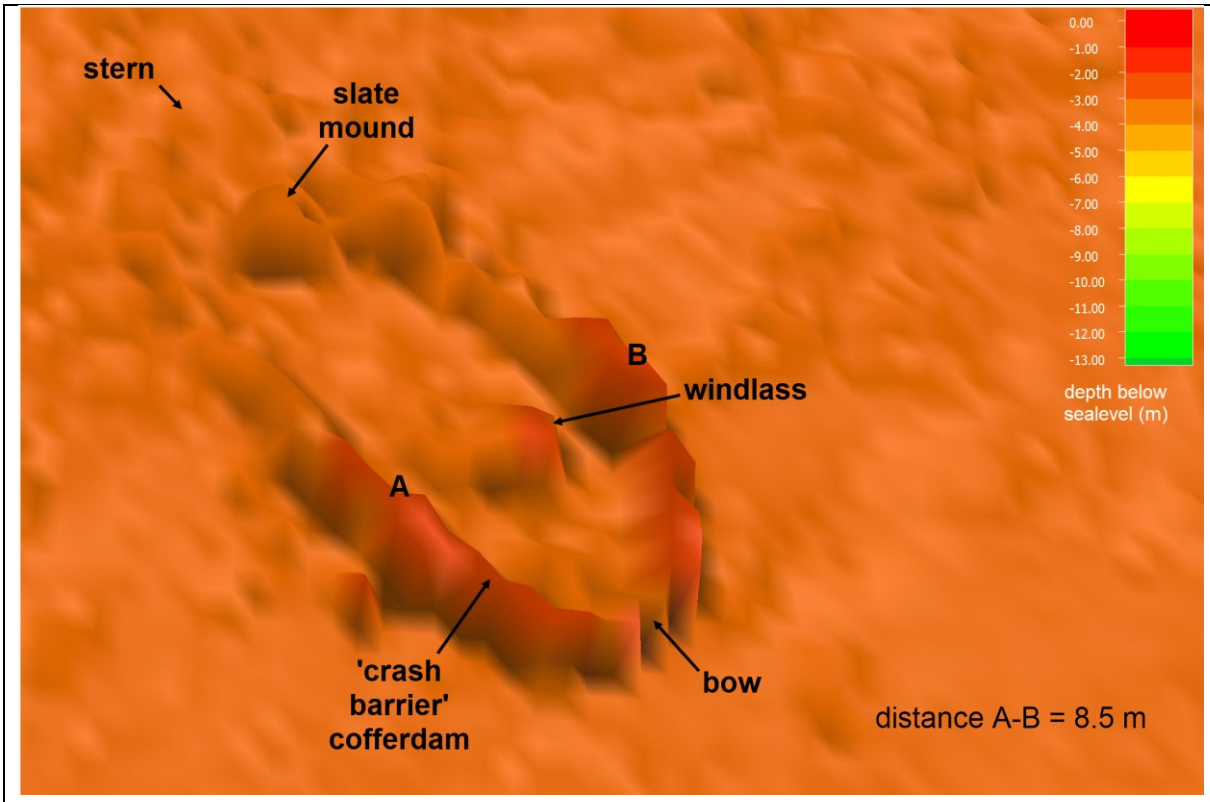

a)

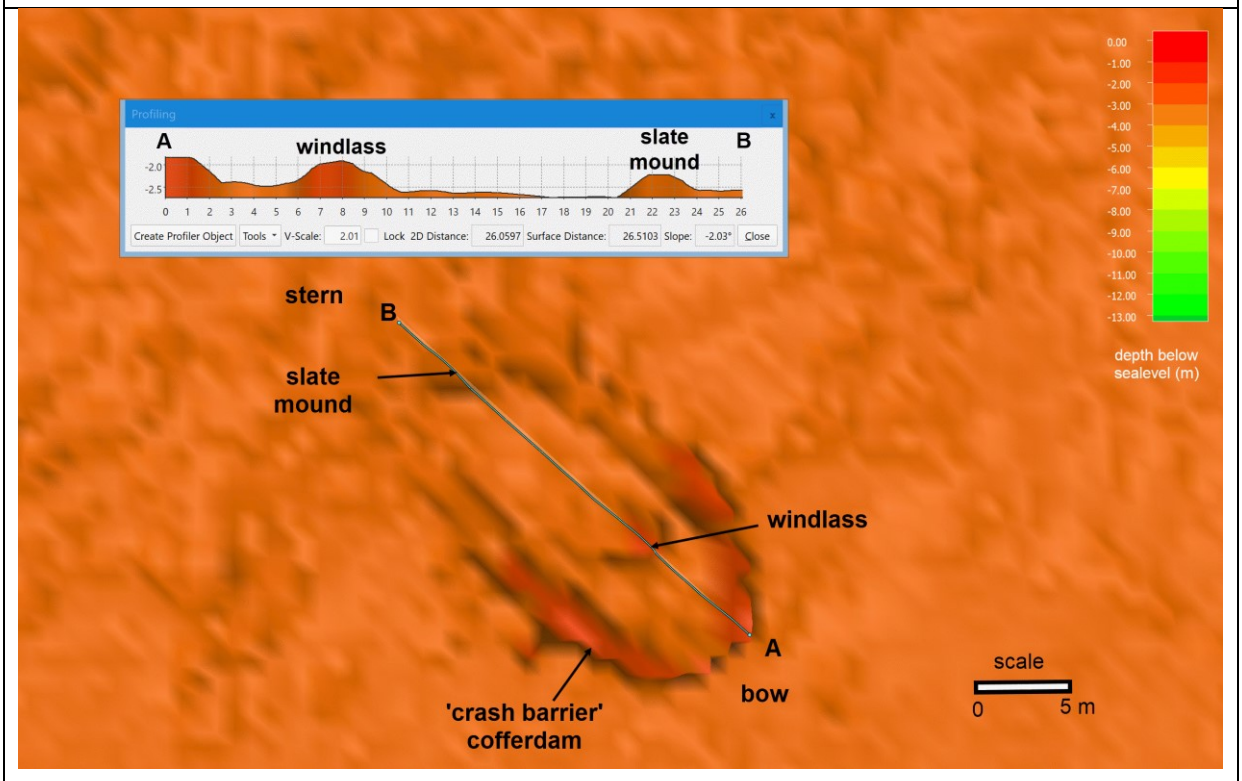

b)

Figure 5.27 MBES DEM of *James Matthews* wrecksite with: a) oblique view; and b) plan view and profile (images provided by John Mullally).

ferrous material is present on a site and if so its general location, the SBP data can provide insight into the vertical and horizontal distribution of that material. The following section provides a context in which these non-invasive performance attributes can be used for in situ management and archaeological research purposes.

Chapter summary

Sub-bottom acoustic data, in situ parameters affecting acoustic performance, and results from measured and/or surveyed buried material were reported in Chapter 4. These data, together with independent magnetometer and MBES surveys, were compared and interpreted within this chapter to firstly validate, then verify the performance of the Innomar SES-2000 *compact* parametric SBP. The ease and speed of operability, and consistency of data interpretation from vessel and underwater sled-mounted SBP in shallow waters from 0.9 m deep, were demonstrated. High confidence in correctly identifying the presence of buried material at the experimental sleeper sites and at the *James Matthews* wrecksite was established, together with the mapping of the aerial extent of the buried material in a complex wrecksite. Following correction for in situ conditions, the depth of burial of sleepers were correctly measured with an accuracy of 6% in the depth range 12 cm to 50 cm, and on the *James Matthews* wrecksite burial depths in the range 14 cm to 60 cm were verified. Complimentary surveys with magnetometers afford insights into the depth and distribution of ferrous material, but SBP data alone could not provide predictive descriptions on the material properties or their state of preservation. These performance attributes were then assessed in terms of their application for in situ management and archaeological research purposes on maritime archaeological sites.

Detailed examination of the SBP echo plots along multiple runs at the James Matthews sleeper site demonstrated that shallow buried material covered by more than 12 cm of sediment can be identified with high confidence. Based on the identification of 27 possible sleepers from each of four opposing SBP runs, the SBP measurements and reflector interpretation procedure correctly mapped sleeper locations 93% of the time. Only one identified reflector did not match a sleeper location, and only three sleeper locations were not correctly identified.

The burial depths of reflectors based on the pre-set acoustic velocity of 1500 m/s used in the SESWIN data acquisition software correlated with, but underestimated the known DoB of the buried sleepers with a proportional bias—the larger the burial depth the larger the underestimate of its true depth. Based on concurrent water temperature and salinity

measurements, acoustic velocities in the water column were corrected to 1535.8–1542.4 m/s. Likewise the acoustic speed in the sediments were also corrected. This was achieved using the known sediment characteristics and quantification of their density, from the combination of bulk density measurements and in situ density penetration force profile tests. The corrected acoustic speeds in the sediments were 1682.1–1787.3 m/s. These corrections were then applied to the acoustically determined seabed level and depth of buried material, resulting in a predictive equation:

$$\text{True burial depth (cm)} = 1.63 + 1.01 \times (d_{DoBcorr}) \quad (14)$$

where $d_{DoBcorr}$ is the velocity-corrected SBP estimate (cm) in the range 10 cm to 50 cm.

From an operational perspective, the accuracy of the DoB estimates appeared similar regardless of survey speed or SBP transducer mounting. Multiple reflectors below the seabed were identified at most sleeper locations. When the amplitude changed phase between successive reflectors, then the difference in depths between these reflectors identified sleeper thickness or gaps between multiple vertically-stacked sleepers. Velocity-corrected sleeper thicknesses in the range 13.9–17.9 cm and gaps of 8.7 and 10.3 cm were calculated, compared with actual sleeper thickness of 12.5 cm and gaps of 7.5 cm gap.

Reflection coefficients for each buried reflector were calculated from acoustic data, and verified from in situ sediment and reflector (sleeper) properties at the James Matthews sleeper site. The resulting high variability of the derived reflection coefficients resulted from the variability of the acoustic amplitudes reflecting from the seabed surface, with no identifiable relationships to the material type and degradation state of the buried material. In order to reduce the influence of the variability in seabed amplitudes, the individual calibration coefficient calculated for each reflector location was replaced by the modal value from the distribution of calibration coefficients determined across all the 96 locations. This lessened the variability, such that the reflection coefficient values for each material type tended to group together, however these groups partially or fully overlapped. Consequently, the reflection value determined for the buried sleepers could not be used predictively to identify their material composition.

The reflection coefficient values derived from material impedance characteristics for ferrous sleepers (0.85–0.87) were much larger than the range derived from the SBP data (0.13–0.19). The reflection coefficient values for timber sleepers were calculated using both bulk and basic densities measured from the recovered blocks. Bulk density was used to represent the timber density in the sleepers as encountered in situ by the acoustic wave, and the basic density used to match experimentally derived radial and tangential velocities. In the timbers the

magnitude of the reflection coefficients based on radial and tangential insonification of pine timbers were higher (0.34–0.38) than the range calculated from the 2018 SBP data (typically 0.11–0.28, but with outliers to 0.45). Similar but closer results were obtained for the oak timbers (0.36–0.42 based on in situ measurements compared to typically 0.19–0.36 from SBP data). For the jarrah timbers, there was a closer alignment between reflection coefficient values derived from the 2018 SBP data (typically 0.22–0.27) and in situ characteristics (0.24–0.28). Despite the variability and overlap in reflection coefficient values for different material types, those values derived from 2018 SBP data were generally within a factor of 1–2 of the values derived from in situ measurements. Contrary to this were the results of the reflection coefficient values determined from the 2017 SBP data, which were an order of magnitude lower. The only potential cause identified for this disparity was a gain setting change, which significantly boosted the acoustic power (sound intensity) in the 2017 survey compared to the 2018 survey.

On the more complex *James Matthews* wrecksite, these SBP performance attributes were validated against archaeological survey data recorded following site excavations in the mid–late 1970s. Interpretation of 47 SBP runs across the wrecksite (10 aligned longitudinally at an average spacing of 1.4 m and 37 aligned transversely at an average spacing of 0.8 m) identified the spatial extent of contiguous and isolated materials buried across the site at depths up to 0.8 to 1.1 m below the seabed. Mapping these locations of buried material identified the outer dimensions of the wrecksite with an accuracy of one metre. The spatial extent of the contiguous reflectors extended beyond the known 26 m x 6 m plan outline of the surviving starboard hull which had been recorded in 1975/76. Together with some of the isolated reflectors, the end of these reflectors aligned with outer edges of the five-metre-wide and 1–1.5 m deep trenches excavated in 1977 along three sides adjacent to the hull. Along the north-eastern side of the wreck, only a one-metre-wide trench was excavated five metres out from the keel. This was due to the presence of broken ship timbers identified during the 1975/76 survey and the placement of ballast stones within four metres of the keel. In addition to the reflectors associated with these trenches, a small number of isolated reflectors located further distant from the site were identified. It is possible that these isolated reflectors indicate locations of buried material which may have come from the *James Matthews* wrecking event and subsequent breakup.

Key features on the *James Matthews* wrecksite that are exposed above the seabed and buried below were mapped and interpreted to a vertical accuracy of +/- 5–10 cm and horizontal accuracy of 0–15 cm. These features, identifiable on high resolution vertical SBP cross-sections, were qualitatively assessed against Henderson's 2D survey plan and the 3D digital

model of the in situ remains of *James Matthews.* Two cross-sections were quantitatively compared to corresponding sections cut through the 3D digital model. The plan structure of the site at multiple depth levels was assessed by interpolating all wave form amplitudes from all SBP runs across the site into one 3D 'volume'. Interpretations at each depth were then made by viewing horizontal slices, cut through the 'volume' and were verified using the results from an independent coarse-resolution MBES survey. The seabed and the remaining hull structure were seen to be sloping upwards from stern to bow, with localised erosional features and seabed protective works occurring around emerged structures. A layer of sediment, from 14 cm to 60 cm deep, covered the frames and ceiling planks of the starboard hull at its deepest point of burial. The slate mound, the top of which is located 80 cm above the localised seabed, iron rods and the keel underneath were visible in the SBP record. The cross-sectional outlines of these features were equally well represented, within a horizontal accuracy of 0–15 cm. However dense seasonally-emergent red algae resulted in localised acoustic interference in the water column and reduced the interpretation accuracy of materials buried underneath these plants. The SBP data also revealed density interfaces which may have resulted from the 1977 excavation and backfilling activities.

A clear relationship between the type of material buried at the *James Matthews* site and the acoustic data could not be found for buried materials at this site. Acoustic data from known locations of ribs and the keel resulted in a range of reflection coefficients from 0.06 to 0.26. Based on timber analyses from the WAM pre-disturbance survey conducted in the year 2000, any variability between reflection coefficients derived for the now-saturated keel and rib timbers is expected to be masked by other factors affecting seabed amplitude variability. However, changes in density within similar types of timbers could be differentiated and by knowing the burial depth of the timber, inferences were made regarding the relative state of degradation of those timbers. In addition, using the combination of the burial depth and reflection coefficient value of reflectors, together with site specific sediment DO and Eh profiles, provided an interpretation of the buried material at a site. The results from an independent coarse-scale magnetometer survey confirmed the presence of ferrous material on the site. Coupled with a localised fine-scale magnetometer survey, the SBP data could be used to map the vertical and horizontal distribution of the ferrous material.

6. DISCUSSION—APPLICATION FOR IN SITU MANAGEMENT AND ARCHAEOLOGICAL RESEARCH PURPOSES

The potential application, and value, of using SBP acoustic methods to map and monitor the sub-seabed material found on UCH sites have been previously reported (Arnott et al. (2002b:699), Gregory (2009:2,6; 2015b:369), Gregory (2015b:369), (Gregory and Manders 2015:37) and Manders et al. (2008:184)). The non-invasive SBP derived data could help inform those responsible for management of UCH sites in three principal areas: 1) identifying the potential level of risk of further material loss from ongoing degradation; 2) providing key information with which to make a sound in situ management plan; and 3) ongoing monitoring feedback regarding the success and stability of the managed site. Despite these apparently significant advantages, Oxley and Keith (2016:8) noted that practitioners have not widely adopted in situ management approaches, despite acknowledging the importance of the underlying site formation theory. These authors argue that the reason for this may arise from 'a lack of funding, limited time and lack of access to the necessary specialists'. The current practice may also come from confusion or lack of confidence on how and when to apply in situ preservation methods, including the use of SBPs, their value and effectiveness.

This research consequently examined the process-oriented approach to in situ preservation and management, and identified how and when SBPs can be effectively applied by archaeologists. To extend the application potential of parametric acoustic SBPs to a broader range of UCH sites that are potentially 'at risk' from loss of archaeological material, it addressed some of the application gaps in different sedimentary environments and buried material types. For the first time, this research quantitatively investigated, in situ, the reliability and accuracy of a parametric SBP to map sites, measure depths of burial (DoB) and differentiate between buried material types and their degradation states. In addition, this thesis demonstrates that the combination of accurate SBP derived DoB estimates and measured sediment chemistry, particularly sediment dissolved oxygen profiles, can provide the basis for a site-based risk assessment of the potential for degradation loss of archaeological materials. This extends earlier laboratory-based outcomes and provides a direction for greater practitioner and research use of parametric SBP instruments. The research also demonstrated the value of SBPs providing preliminary non-invasive data, with which state-of-the-art research designs could be subsequently developed.

Theoretical frameworks for UCH management—the need for non-destructive sub-seabed in situ measurements

Theoretical frameworks for UCH management were reviewed to identify the need and opportunity for SBP use. The influence of the UNESCO 2001 *Convention on the Protection of the Underwater Cultural Heritage* on these frameworks, and the resulting research programs around site formation processes which subsequently evolved, provide the context and the specific need for non-invasive in situ approaches. These methods are required to inform archaeologists regarding the risks of losing UCH material from degradational loss, and to devise and monitor an in situ management plan in response. The 2001 UNESCO Convention also recognises the value of research and the need for limited intrusive methods based on a state-of-the-art archaeological research design. It advocates that the collection of preliminary non-invasive data improves the efficacy of subsequent site investigations. SBP derived data can provide information required for both purposes.

The principles of in situ management arose from the challenge to understand the transformational (site formation) processes acting on underwater and submerged archaeological sites in order to interpret the archaeological record. Muckelroy (1976) developed a theoretical site model in the mid-1970s based on his systematic study of shipwreck site formation processes. This model represented the evolution of a shipwreck from the process of wrecking through to the observed sea-bed distribution of artefacts. Subsequent site formation research focussed on predictive models to explain the presence of artefacts using correlations between the observed distribution of shipwreck sites and their environmental attributes. These models may have been non-predictive and misleading, as their theoretical constructs did not allow for temporal affects and failed to identify the underlying processes which affected a site. Gregory (1996) proposed an alternate model where the natural environment is studied to define the processes which currently affect shipwreck sites, in order to understand the current state of material degradation. He advocated that using this knowledge, methods could then be developed to mitigate these effects, and today there is a large volume of published research on the inter-relationship between cultural, physical, chemical and biological site formation processes, materials conservation and site assessment.

The ratification of the 2001 UNESCO *Convention on the Protection of the Underwater Cultural Heritage*, together with the earlier European Valetta Convention, delivered the galvanizing impetus to protect and manage UCH material in situ. Rules incorporated within the UNESCO 2001 convention directed that in situ preservation be considered as the first option, ahead of but not to the exclusion of other activities directed at the UCH. For sites where UCH material

is deemed at risk, a conservation plan addressing in situ protection, needs to be prepared and implemented. The UNESCO 2001 convention also recognizes that research and in situ management are dependent upon data, and that non-destructive techniques come first and are preferred over intrusive methods—but intrusive methods remain important and their efficacy will be significantly improved if informed by preliminary data gathered using non-invasive techniques.

As a consequence of the UNESCO and Valetta Conventions extensive scientific research was undertaken to effectively implement the intentions of both conventions. Specifically, data was needed to answer questions relating to the mechanisms and speed of shipwreck deterioration, the time period that shipwrecks could be protected in situ, and the validity of approaches for long term management. To determine the degradation risk for buried organic and metallic materials, the relationship between sediment depth, sediment chemistry and biological and chemical activity, was needed. Based on this new scientific data, and in accordance with the principles of the UNESCO 2001 and Valetta Conventions, Gregory and Matthiessen (2012a) argued for a process-driven approach to in situ preservation—one that identifies the site threats, uses in situ data to assess and quantify these threats and uses baseline and ongoing data to identify if the site is safe and if mitigation measures or modification to the in situ management plan is required. This approach encompassed Gregory's (2009) proposed five step process to successfully deliver the in situ preservation framework. These steps require in situ data to be collected using non-destructive techniques on sites where UHC material is found exposed on the seabed and in the water column, and/or where materials are buried below the seabed. Information is required on:

- the extent of the site to be preserved;
- the most significant physical, chemical and biological threats to the site;
- the type of materials located on the site and their state of preservation;
- the strategies to mitigate deterioration and stabilise the site from natural impacts; and
- the subsequent monitoring of a site and implemented mitigation strategies.

For those materials buried on and below the seabed, marine geophysical equipment, particularly SBPs, have been recognised as powerful tools which could provide key information required in the successful delivery of the in situ preservation framework. Specifically, SBPs have the potential to collect data on the lateral extent of buried UHC material, and the depth of sediment cover to provide greater insight into major site threats as shown by this research. SBPs have previously been able to detect density (degradation) differences in timbers in laboratory studies, and this has now been quantitatively demonstrated

in situ. These SBP derived data help inform decisions regarding in situ management strategies, and repeated subsequent surveys can monitor the location of buried material, its depth of burial and material densities to assess site stability.

SBP performance verification—quantified results meeting UHC in situ management and research needs

To assess, manage or undertake research related to shallow-buried material in a manner consistent with binding international conventions and current best practice, practitioners and researchers need to obtain preliminary non-invasive data which provide information on the following sub-seabed site characteristics:

- confirmation of the presence of buried material, and if confirmed, the spatial location of that material;
- the lateral extent of the site, encompassing all contiguous and isolated materials;
- the depth of burial, relative to the seabed level, of those materials; and
- the nature of those materials, and their degradation state.

To further understand the archaeological potential of the sub-seabed material, information on the overall shape and dimensions of contiguous components is beneficial. Together, these data are used to make a preliminary risk assessment of the potential for ongoing materials degradation and in situ management plans in response, as well as inform subsequent site investigations, if warranted. Subsequent monitoring of the depth of material burial, relative to the seabed level, provides routine data with which to assess the stability of the site and/or success of in situ management actions. The following sections discuss how the application of verified parametric SBP performance characteristics can provide these preliminary and on-going site data requirements with relative ease.

Applicability to determining site extent

The initial results from the experimental validation trials quantified the high accuracy and reliability of identifying and locating various timber and ferrous sleepers 12.5 cm wide buried at various depths between 11 cm and 50 cm in medium-grained calcareous and siliceous sediments. The position of the known sleeper locations (measured independently by tape and by RTK DGPS) and the interpreted SBP reflector locations were co-plotted in GIS for comparison. Based on the identification of 27 possible sleepers from each of four separate SBP runs, sleeper locations were correctly identified 94% of the time. Only one reflector identified as a possible sleeper did not match a sleeper location, and five very shallow (DoB < 11 cm) sleeper locations weren't detected across the four runs. The shallowest range of sleeper burial depths (5.5–11 cm) corresponds to the upper portion of a band of high acoustic

wave amplitudes associated with the reflection of the acoustic waves at the seawater/seabed interface. This background acoustic noise masks the identification of any reflector surface in this range, however reflection signals can be progressively discerned below this depth range. The reliability of the SBP measuring correct sleeper locations was assessed using the Watson and Petrie method agreement analysis for categorical variables. The 95% confidence intervals on the proportion of correctly predicted locations were calculated using the Wilson interval estimation method. The 95% confidence level range associated with correctly predicting sleeper locations for all burial depths was 88% to 97%, around a mean value of 94%. Excluding the sleepers with DoB < 11 cm the confidence levels rose to range from 94% to 100% around a mean of 99%. This means that there is high confidence and reliability in using the SBP to identify the locations of a variety of shallow-buried materials, and very high confidence of identifying those with burial depths greater than 11 cm.

The measured horizontal location accuracy for these sleepers, determined over the four separate SBP runs, fell in the range 5–21 cm. A significant component of this variability was attributed to very poor water visibility conditions affecting the positioning of the RTK DGPS sled directly above the centre line of each 12 cm wide sleeper.

Quantitative verification of the lateral site extent of a complex, contiguous wrecksite was achieved with a measurement accuracy on one metre by analysis of reflectors from 47 SBP runs across the *James Matthews* wrecksite. Additional isolated reflectors at varying distances from the known hull location were also identified—subsequent analyses were undertaken in order to interpret whether-or-not these isolated buried material signatures were associated with the wrecking event and/or with post degradation losses. Of the 47 SBP runs surveyed over the site, 37 tracked 'loosely parallel' and transversely across the buried wrecksite material at an average spacing of 0.8 m, and 10 runs crossed longitudinally at an average spacing of 1.4 m. Contiguous and isolated reflectors were identified at depths up to 0.8 to 1.1 m below the seabed, and their lateral extent compared against the WAM's 2D survey plan of the buried remains (Figure 5.20). The spatial dimensions of the contiguous reflectors extended beyond the known 26 m x 6 m plan outline of the surviving starboard hull which had been archaeologically recorded following excavation in 1975/76. Together with some of the isolated reflectors, the extent of these reflectors aligned with the outer edges of relocated ballast stones and the surrounding one-metre or five-metre wide, by 1.5 m deep, trenches excavated by WAM in 1977. These trenches were subsequently reburied at the end of the excavation season, providing greater complexity for SBP interpretation to this site. Similar to Quinn et al's (1997c) Chirp SBP recording of infilled scour holes adjacent to the *Mary Rose,* the parametric mapping of the aerial extent of *James Matthews* appeared to identify sediment density

interfaces associated with the bottom of the backfilled trenches, in addition to the buried UCH material from *James Matthews*. Without prior knowledge of these outer trenches, the lateral extent of the materials associated with the wrecksite would have been over-estimated. Never-the-less, the overall outer dimensions of this complex wrecksite were interpreted to be 36 m x 16 m, with an accuracy of one metre.

Applicability to measuring DoB

As described in Chapter 2 for sites with buried UHC materials, their DoB is one of the most influential site variables affecting physical, chemical and biological threats to those items. The rate of degradation and loss of timber structure is significantly lessened in anoxic, reducing conditions (Gregory 1996; Gregory et al. 2008a), likewise for isolated buried metals (Godfrey et al. 2005). In conditions with overlying aerobic waters, dissolved oxygen diffuses into the upper shallow layers of the seabed due to sediment dynamics and biological activity. The depth of burial, conducive to material preservation, has been experimentally studied in the numerous reburial and site formation process studies (Björdal and Nilsson 2008; Gregory 1998; Nyström Godfrey et al. 2011; Richards 2011a). A depth of 50 cm has generally been adopted, but in most circumstances the researchers have identified that site specific conditions dictate the optimum depth. Hence to assess site risk to material degradational loss, accurate measurement of the DoB of that material is required.

At the James Matthews experimental sleeper site, the parametric SBP accurately measured the true DoB of sleepers buried from 10 cm to 50 cm below the seabed within a 95% confidence range of 0.6–2.5 cm. The reflector burial depths for each of the buried sleepers at the James Matthews sleeper site were determined across two SBP runs by subtracting their respective mean seabed depth estimates from their mean buried reflector depth estimates. When multiple reflectors were identified below the seabed, the thickness of, or possible gap between the material was calculated by subtracting the depth estimates of the first reflector from the second, provided that there was a corresponding phase change. The Bland-Altman method comparison technique was applied to quantify the accuracy of the SBP derived sleeper burial depth estimates against their known DoB. The burial depths of reflectors based on the pre-set acoustic velocity of 1500 m/s in water and sediments used in the Innomar SESWIN data acquisition software correlated with, but underestimated the known DoB of the buried sleepers. The Passing-Bablok regression analysis test concluded that proportional bias existed (the larger the burial depth the larger the underestimate of its true depth) in this data set, and that the methods (direct seabed measurement and uncorrected SBP DoB estimates) did not result in equal outcomes.

To improve the measurement interpretation accuracy, concurrent water temperature and salinity measurements were used to correct the acoustic velocities in the water column to 1535.8–1542.4 m/s, respectively. Likewise the acoustic speed in the sediments were also corrected. This was achieved using the known sediment characteristics, and quantification of their density from the combination of bulk density measurements and in situ density penetration force profile tests. The corrected acoustic speeds in the sediments were 1682.1–1787.3 m/s. These corrections were then applied to the acoustically determined mean seabed depths and mean buried reflector depth estimates. The subsequent results from the Passing-Bablok regression analyses identified that with corrected acoustic velocities, there was no proportional bias and that the measurement methods (seabed direct versus corrected SBP estimates) provided the same DoB result within the limits of agreement (0.6–2.5 cm). The Passing-Bablok linear regression relationship between the true and corrected SBP estimates resulted in a predictive equation:

True burial depth (cm) = 1.63 + 1.01 x ($d_{DoBcorr}$)

where $d_{DoBcorr}$ is the velocity-corrected SBP estimate (cm) in the range 10 cm to 50 cm.

Velocity-corrected sleeper thicknesses, based on SBP measurements, fell in the range 13.9–17.9 cm and vertical gaps between sleepers were estimated to be 8.7 cm and 10.3 cm. These compare with actual sleeper thickness of 12.5 cm and gaps of 7.5 cm.

These experimental outcomes demonstrate that it is possible to use velocity corrected parametric SBP data to accurately measure the depth of sediment cover of shallow-buried materials, below 10 cm depths, with a vertical resolution to sub-decimeter accuracy. These results included measurements for timber and ferrous sleepers with upper surfaces flat and longitudinal timber grain horizontal, and for pine sleepers, two inclined by 22.5^0 to the horizontal and three rotated with their longitudinal grain oriented vertically. The significance of this result for other similar sites is that the orientation and grain direction of timbers buried in sediments appears to have minimal effect on the accuracy of measuring their respective burial depths using a parametric SBP. This is an important practical outcome as timber orientation and grain is not known ‘a priori’ during preliminary site surveys.

Verified depth of burial measurements on the *James Matthews* wrecksite indicated a high risk of ongoing degradation to the remaining upper hull timbers and metal rods. The DoB measurements were verified using the 3D AutoCAD model of the buried remains constructed from WAM’s archived records of the 1975/76 excavation and archaeological survey (Figures 5.21 and 5.22). Two SBP echo plots were quantitatively compared by co-plotting, at the same horizontal and vertical scale, corresponding cross-sections cut through the 3D digital model.

Isolated dense seasonally-emergent red algae growing across the site at the time of survey resulted in localised acoustic interference in the water column, and reduced the interpretation accuracy of materials buried directly underneath these plants. Never-the-less SBP reflectors identified the outline of the exposed slate mound and the buried keel and ribs/planking within a horizontal accuracy of 0–15 cm and a +/- 5–10 cm relative vertical accuracy. A layer of sediment, from near zero to 30 cm deep covered the remains of the starboard hull along one cross-section, and from 14 cm to a maximum of 60 cm along the other section of the hull was recorded. The sediment/timber interface over the buried ribs/planking was closely aligned (+/- 2 cm) to the upper side of the model cross sections. The slate mound, the top of which was located 80 cm above the localised seabed, iron rods and the keel underneath were clearly visible in the SBP record. On the starboard side of the exposed slate mound, the SBP data indicated a higher surface level, however this may simply represent a sandbag more recently placed as part of the WAM's temporary site protection activities. Beyond the starboard bulwarks, a number of reflectors were identified between 30–55 cm below the seabed level. These may reveal the legacy of the 1977 excavation and backfilling activities along and under the starboard bulwarks.

In an open aerobic environment, using concurrent DO profiles determined from sediment cores collected in adjacent reference (undisturbed) locations, these DoB measurements would indicate a high risk of ongoing degradation to the upper hull timbers and metal rods. The conservators at WAM are fully aware of this situation and have previously collected timber samples and undertaken in situ metal corrosion potential measurements. The results of those analyses confirmed the material degradation. The museum conservators consequently devised and implemented an in situ management plan for the *James Matthews* wrecksite (Richards 2003; Richards et al. 2007; Richards et al. 2014). This included the installation of the surrounding crashbarrier cofferdam, sterile sediment backfilling, placement of a geotextile cover to reduce sediment DO levels above and within the immediate surrounds of the wreck, and monitoring of sediment chemistry and sacrificial timber samples.

Estimating buried material types and their density

Relationships between SBP data and the material properties, including density, of the buried materials provide key inputs into in situ management and research plans. In this study, these were investigated using SBP acoustically derived reflection coefficients for the buried oak, pine, jarrah and ferrous sleepers, and for timbers and isolated reflectors on the *James Matthews* wrecksite. Importantly the density, and hence degradation state, of similar timber species from the *James Matthews* and from the sleepers were shown to be significantly different, with the former more saturated and degraded than the latter.

All reflection coefficients for were derived using the modal value for the calibration coefficient (x), rather than the 50th percentile value in Plets et al's (2008:Appendix A) methodology, due to high skewness of the distribution of amplitudes associated with the seabed surface and seabed 1st multiple reflections. This approach resulted in identifiable groupings for each of the sleeper material types (Figure 5.16), these groups however overlapped and hence limited any resulting predictive capacity. This was predominantly due to the variability in amplitude returns from adjacent reflections representing the buried sleepers, and possibly due to the relatively low levels of degradation in these timbers at the time of SBP measurement. Unexpectantly the reflection coefficients for the ferrous sleepers were similar to or lower than those from timber. The reasons for this discrepancy are unknown, but may have resulted from the composite structure of the ferrous sleepers and/or non-uniform backfilling above the recently buried ferrous sleepers causing significant amplitude variations on top of these sleepers.

Of particular note for future in situ acoustic site surveys, the reflection coefficients for the pine sleepers with different orientations and grain directions were similar, which results in an advantageous situation. Within the pine group of reflection coefficients (Figure 5.12) reflection coefficients associated with sleepers which were buried with their long grain oriented vertically, and those with their upper surfaces tilted 22.5^{0} from the horizontal, were identifiable, but not significantly different to those buried flat with their long grain horizontal. These results indicate that differing orientations of buried timbers, and their associated varying longitudinal, radial and tangential compressional P-wave velocities, may have little impact on the identification of buried shipwreck materials and their state of degradation, using in situ SBP measurements. This tentative conclusion is further discussed later, and its implication for site interpretation expanded.

Reflection coefficients for these sleepers were also independently derived for comparison purposes using ex situ measured material properties of the sediments and timber sleepers, and literature reported ferrous properties. The reflection coefficient values for timber sleepers were calculated using both bulk and basic densities measured from representative recovered timber blocks. Bulk density was used to characterise the timber density in the sleepers as encountered in situ by the acoustic wave, and the basic density used to match experimentally derived radial and tangential velocities. Sediment bulk density was determined from sediment cores collected within the disturbed zone of the buried sleepers and sediment velocities determined from the regression line for siliclastic + calcareous sands presented by Richardson and Jackson (2017:506, 511). Despite the variability and overlap in reflection coefficient values for different material types, reflection coefficient values derived from 2018 SBP data were generally within a factor of 1–2 of the values derived from in situ measurements (Figure 5.17).

The exception were reflection coefficient values for ferrous material which were 4.5–6.5 times lower than the material derived values. Contrary to these were the results of the reflection coefficient values for timbers determined from the 2017 SBP data, reported in Winton (2019), which were an order of magnitude lower. The only potential cause identified for this disparity was a gain setting change in the SBP transmitter, which significantly boosted the acoustic power (sound intensity) in the 2017 survey compared to the 2018 survey.

The in situ derived reflection coefficients were also compared to those derived under laboratory conditions by Zisi (2016:173–175) to further assess their applicability. The comparison, as shown in Table 6.1, revealed similar outcomes. For oak (*Quercus* petraea) samples with a basic density of 478 Kg/m^3 in sand, Zisi obtained absolute reflection coefficient values in the range 0.26 to 0.30 depending on the insonification angle, compared with the in situ measured oak (*Quercus* robur) value of 0.28. The absolute reflection coefficients derived in the laboratory for pine (*Pinus* sylvestris) with a basic density of 429 Kg/m^3 in sand were higher than those measured in situ for *Pinus* radiata. The small difference in derived reflection coefficients for pine may result from the testing of two different pine species. Zisi did not test jarrah timber, but developed a 'combined' wood curve across a broad range of density values. For a timber in sand with a jarrah equivalent basic density of 559 Kg/m^3, Zisi estimated absolute reflection coeffients from 0.20 to 0.25 corresponding to flat and quarter sawn timbers. The in situ and materials derived jarrah values of 0.27 and 0.26, compared very well.

Table 6.1 Comparison of in situ and laboratory derived timber reflection coefficients

in situ SBP derived reflection coefficients						Zisi's laboratory derived reflection coefficients		
timber	mean	SD	n	basic density (Kg/m^3)	material derived	all results (Figures 6.1, 6.2)	insonification angle (Figure 6.3)	
							0–30^0	60–90^0
pine (all sleepers)	0.20	0.09	24	429	0.36	0.29	0.28	0.33
pine (22.5^0)[a]	0.18	0.03	3					
pine (vertical)[b]	0.16	0.08	6					
oak (sleepers)	0.28	0.06	8	478	0.38	0.26	0.26	0.30
oak (*James Matthews* ribs)	0.11	0.06	3	na	na			
Jarrah (sleepers)	0.27	0.06	4	559	0.26		0.20	0.25

[a] sleeper rotated 22.5^0 to horizontal; [b] sleeper longitudonal grain horizontal; SD=standard deviation; n=number of observations

The similarity between the in situ, laboratory and materials derived reflection coefficient values provides greater confidence in the values derived from the parametric SBP survey. These quantified in situ results, for the first time, confirm Zisi's (2016:176) laboratory based conclusion 'that the orientation of the wood, either flat-sawn (0–30°) or quarter sawn (60–90°), does not seem to influence the reflection coefficient'. If this was not the case, then interpretation of density differences, and possibly material differences between types of buried materials measured using acoustic means, would be more difficult. The variability of in situ derived reflection coefficients is primarily affected by the irregularity in the seabed and seabed surface. Reflection coefficient values are also affected by the density of the timber and the relative orientation of the timber when insonified by the SBP acoustic wave. Timbers are sawn along different grain axes for use in ship construction. The controlled laboratory work by Zisi and others have demonstrated the effect on laboratory derived reflection coefficient values when the insonification angle is aligned to the timbers' longitudinal, tangential or radial grain directions. In situ, these alignments, relative to the in situ acoustic waves, reflect the type of sawn timber cut, the timber's initial location within the ship's construction, and the timber's final orientation following the wrecking and burial events. If the orientation of the buried timbers resulted in significant differences in the reflection coefficients derived from in situ acoustics, then differences due to timber density would be much harder to identify. This is an important outcome since researchers do not know, a priori, the likely grain orientation of buried shipwreck timbers when gathering initial site data for research or in situ management purposes.

Reflection coefficient values derived from SBP measurements over the *James Matthews* shipwreck demonstrated the ability to identify different density, and hence degradation state, for oak from ship timbers compared with oak used in the adjacent sleepers. A preliminary model using reflection coefficient values was also developed to interpret in situ conditions on the *James Matthews* wrecksite. Reflection coefficients were derived from the SBP data for the known keel and rib timbers of *James Matthews*, and for a number of the isolated reflectors directly adjacent to, and further separated from, the intact hull remains. The magnitude of the coefficients for the rib and keel timbers ranged from 0.06, corresponding to burial depths from 11 to 20 cm, to 0.26 for timbers with burial depths of 25–42 cm. This suggests higher levels of timber degradation associated with shallower burial depths. Reflection coefficients derived for the isolated reflectors generally spanned a similar range (0.03–0.29), the exception to this were two values (0.42 and 0.5) which were associated with reflectors located on the edge of the 1977 excavation trenches.

The WAM 2000 conservation pre-disturbance survey of the *James Matthews* wrecksite identified that the keel and keelson were constructed using beech and white oak timbers, and the ceiling planks, ribs and outer planking were constructed of white oak timber. All timbers examined in five test trenches were waterlogged, with some significantly deteriorated. Timber density (expressed as specific gravity) ranged from 0.45–0.47 for the oak in the ribs and inner planking. This compares to a value of 0.69 calculated for the European oak blocks purposely-buried and recovered 20.5 months later at the adjacent James Matthews sleeper site. A plot of reflection coefficients vs specific gravity for oak timbers (Figure 5.24a) showed a significant difference with low reflection coefficient values (0.06–0.18) associated with the water logged lower specific gravity shipwreck timbers, and higher values (0.2–0.37) associated with the non-water logged higher specific gravity timber sleepers. This figure confirmed, as expected, that following an extended period of submergence, the waterlogged and (partially) degraded white oak had a significantly lower specific gravity, reflecting the loss of cellulose in the timber (Grattan 1987:65–66). These shipwreck timbers also had corresponding lower reflection coefficient values (Table 6.1) compared to the recently buried, partially-saturated European oak timbers.

A site interpretation of the buried materials at the *James Matthews* wrecksite was achieved using the known relationships between DoB, DO and degradation potential. The reflection coefficients from both the known ship's timbers, and the surrounding isolated reflectors, were plotted against reflector DoB (Figure 5.25). Reflection coefficients from the known timbers and from two isolated reflectors grouped together to show increasing reflection coefficient values with depth of burial. Assuming that the saturated beech and oak timbers hull have similar acoustic impedance properties, then the SBP data demonstrated the expected increase in timber degradation with decreasing burial depth. One of the two isolated reflectors with these similar properties was located off the bow of the shipwreck remains at a burial depth of 32 cm, the other located almost 30 m away with a burial depth of 44 cm. The above relationship suggests that these two isolated reflectors may be pieces of timber separated from the hull of *James Matthews* during or post the wrecking event. A second group of isolated reflectors shown on Figure 5.25 had low reflection coefficient values (0.04–0.11) but with burial depths typically in excess of 55 cm. At these depths, environmental conditions within the sediments should be conducive to timber conservation. The low reflection coefficient values are hence unlikely to be associated with degraded timber. One of these isolated reflectors in this group was located at the bottom of the 1977 excavation trench outside the starboard bulwarks. This suggests that the second group (with low reflection coefficients and higher depth of burial reflectors) is associated with weak sediment interfaces resulting from excavation and backfill of trenches. A third group of isolated reflectors shown on Figure 5.25 are characterised by

higher reflection coefficient values (0.2–0.5) with burial depths in the range 18 cm to 35 cm. With the current information it was not possible to interpret the nature of these reflectors. Those reflectors in the upper reflection coefficient range are unlikely to be associated with timber as their reflection coefficient values exceed all values derived from freshly buried oak, jarrah and pine on the adjacent sleeper site. It is possible that the isolated reflector with the highest reflection coefficient (G) may represent ballast stones which were relocated beyond the keel during the WAM excavation surveys.

This model provides a preliminary interpretation of the site which could be used to guide further investigations under either an in situ management or research plan. If further tested, this approach may provide a unique way in which to assess the archaeological potential and composition of complex shipwreck sites.

Site structure and field logistics

In addition to the preceding site interpretations from in situ SBP data, it is also possible to visualise an interpolated quasi-3D structure of the buried site remains. This provides more information with which to plan additional non-invasive or limited invasive investigations for archaeological research and in situ management purposes. In addition, such visualisation would permit a greater focus on further detailed analyses using existing data from specific SBP runs. In a similar manner to that used by Plets et al. (2009:411–412) the amplitudes from the continuous vertical echo plot traces along all 47 SBP runs which crossed the *James Matthews* wrecksite were interpolated into a 29 m x 28 m x 1.45 m 'volume' using gridding software. Within this 'volume' interpolated amplitudes were calculated at the corners of almost 65,000 elements (voxels), each 0.5 m x 0.5 m x 0.05 m in the horizontal (x and y) and vertical (z) dimensions. The reflector amplitudes within the 'volume' were plotted in horizontal layers starting from the upper surface, with each slice representing a progressively deeper depth level (Figure 4.50). Examination of these sequentially deeper amplitude layers revealed the plan shape of the surrounding cofferdam, the locations of surficial features, the shallowing slope of the seabed within the cofferdam from stern to bow, the keel and starboard hull buried deeper at the stern than the bow, and the general concave shape of the hull. The isolated stern post separated from the damaged stern was also identified. The localised sediment features and the stern to bow seabed slope were verified using the results from an independently acquired coarse-resolution MBES survey. The mass of iron bars between the slate mound and the keel was identifiable, the general location for which was indicated by a coarse magnetometer survey undertaken by WAM.

The ease of setup and use, together with fast survey vessel speeds which permit the acquisition of multiple closely spaced runs over a site in a time period of only hours, should

lessen practitioners' concerns regarding field costs and survey times. From an operational perspective, the quality of the DoB data appeared similar regardless of survey speed or transducer mounting. The 2017 survey of the *James Matthews* wrecksite and preliminary survey of the James Matthews sleeper site were conducted using a vessel mounted transducer, with the vessel travelling at 2m/s during survey. On-board satellite navigational systems acquired decimeter accurate positional data and heave compensation data which were fed directly into the proprietary data collection software. The transducer mounted amidships on a vertical pole and just below the waterline permitted shallow water access (less than two metres) and avoided all propeller wash noise, except during hard turns at the ends of each run. In 2018 measurements were undertaken at the completed James Matthews sleeper site, and at the Swan River sleeper site, with the SBP transducer mounted to a purpose-built seabed sled. The transducer head was positioned 90.5 cm and 71.5 cm above the seabed and riverbed, respectively, at these sites. The sled was remotely controlled moving at an average speed of 0.15 m/s across each site, with positioning achieved using Bluetooth© connectivity between an RTK DGPS antennae mounted on the sled mast, and the onboard proprietary data collection software. Surveys were undertaken within two days from the time of equipment mobilisation on the survey vessel or seabed sled through to demobilisation—actual onsite SBP surveys took only hours.

The non-invasive data presented from this research successfully addressed the identified needs and applications for in situ monitoring and archaeological research purposes at the experimental and *James Matthews* sites. It also extended the range of material types investigated and sediment environments used in the SBP testing. The results provide a direction for archaeologists to assess, manage or undertake research related to shallow-buried material in a manner consistent with binding international conventions and current best practice. Recommendations to extend the research and interpretations undertaken here are provided in the following final chapter.

7. CONCLUSIONS AND RECOMMENDATIONS

For the first time, this research provides quantified in situ validation and verification of parametric SBP measurement performance on a historic shipwreck site and on purpose-built testing or control sites. This work extends the application potential of parametric acoustics to in situ management at sites that are potentially 'at risk' from loss of archaeological material. It also identifies that SBP data can provide preliminary evidence for archaeological research planning. Both outcomes are in accordance with the requirements of the 1992 European Valetta Convention and UNESCO 2001 *Convention on the Protection of the Underwater Cultural Heritage,* and the UCH management frameworks that subsequently evolved.

The present study has significantly contributed to new knowledge regarding the applicability of parametric SBPs for in situ management of UHC sites and for archaeological research purposes. Parametric SBPs can be used with high confidence and reliability to identify the locations of a variety of shallow-buried materials with widths greater than 12 cm in medium grained calcareous and siliceous sands. A very high level of detection accuracy was quantified in situ for multiple oak (*Quercus* robur), pine (*Pinus* radiata), jarrah (*Eucalyptus* marginata) and ferrous sleepers buried at different depths from 5 cm to 50 cm in medium-fine grained calcareous sediments. The 95% confidence level range associated with correctly predicting sleeper locations for all burial depths was 88% to 97%, around a mean value of 94% based on the Watson and Petrie method agreement analysis for categorical variables and the Wilson interval estimation method. Excluding the sleepers with DoB < 11 cm the confidence levels rose to a range 94% to 100% around a mean of 99%. Sleeper locations buried in medium grained siliceous were also identified, but not quantified due to recording failure of their precise location.

Determining the lateral site extent of UCM material is the first requirement in the five-step process to successfully deliver the in situ preservation framework. In relation to UCH requirements, the parametric SBP provided decimeter accuracy for locating individual isolated sleepers, and one metre accuracy for the lateral site extent on a complex shipwreck site. On the James Matthews sleeper site, a horizontal SBP measurement accuracy of 5–21 cm was achieved across 104 independent sleeper measurements. A significant component of this variability was attributed to very poor water visibility conditions affecting the positioning of the RTK DGPS sled directly above the centre line of each 12.5 cm wide sleeper. The extent of the *James Matthews* shipwreck site was interpreted to be 36 m x 16 m with a measurement accuracy of one metre, not including a small number of isolated and potentially related reflectors identified up to 30 m from the known extent of the intact hull remains. This was

based on interpreting contiguous and isolated reflectors associated with buried features from 47 SBP measurement runs across the previously excavated and archaeologically surveyed site. The outer site dimensions determined from the SBP data included reflectors associated with WAM's 1977 excavated and backfilled trenches surrounding the known hull remains, and reflectors possibly associated with relocated ballast stones. Like Quinn's 1977 Chirp investigations on infilled scour holes associated with *Mary Rose,* the parametric SBP identified weak acoustic reflections from sediment density interfaces. The implication then for determining site extent is to carefully assess any differences in acoustic reflection coefficient signatures across sites where localised seabed scouring events may have occurred.

Accurate DoB measurements of shallow-buried material meets an important need to assess the risk associated with potential degradational loss of that material. Parametric SBPs provide highly accurate depth measurements in surficial medium grained calcareous sediments with sub-decimeter vertical resolution. Within a 95% confidence range of 0.6–2.5 cm, using water and sediment corrected acoustic velocities, the parametric SBP accurately measured the true DoB of identified materials buried from 10 cm to 50 cm below the seabed. The Bland-Altman method comparison technique was applied to quantify the accuracy of the SBP derived sleeper burial depth estimates against their known DoB. This included sleepers with flat upper surfaces and surfaces inclined 22.5^0 to the horizontal. The Passing-Bablok regression analyses identified that there was no proportional bias and that the measurement methods (seabed direct versus corrected SBP estimates) provided the same DoB result, as per the following predictive equation, within the limits of agreement.

True burial depth (cm) = $1.63 + 1.01 \times (d_{DoBcorr})$

where $d_{DoBcorr}$ is the velocity-corrected parametric SBP estimate (cm) in the range 10 cm to 50 cm.

This is a key outcome as DoB is one of the most important variables assessing degradation risk to buried materials, and extends SBP applicability as Chirp SBPs have difficulty in identifying any material in the top 30 cm layer. The vertical resolution of the parametric SBP was determined to be at least 10 cm, based on measurement of the thickness of all buried sleepers (13.9–17.9 cm versus actual 12.5 cm) and gaps between multiple stacked sleepers (8.7–10.3 cm versus 7.5 cm actual).

SBP measurements of the depth of burial of keel, ribs and planking timber on the *James Matthews* shipwreck site were confidently interpreted, and identified a high risk of ongoing materials degradation. A layer of sediment from zero to 30 cm and from 14 cm to 60 cm was identified by direct comparison to a 3D AutoCAD model constructed from the 1975/76

archaeological survey of the timber remains of *James Matthews*. In an open aerobic environment, using DO profiles determined from adjacent sediment cores, these shallow burial depths in aerobic–sub-oxic sediments would indicate a high risk of ongoing degradation to the upper hull timbers and metal rods. The conservators at WAM have been fully aware of this situation and have previously analysed samples and undertaken in situ testing which confirmed these levels of degradation. They consequently have devised and implemented an in situ management plan for the *James Matthews* wrecksite.

Reflection coefficient analyses using the in situ SBP data verified the ability to differentiate density, and hence degradation state, between the fully saturated and degraded white oak used in the frame construction of *James Matthews,* and the adjacent partially saturated European oak used in the buried sleepers. The timber density results were obtained from WAM's analyses of timber samples collected from wreck timbers, and sleeper densities were determined by analyses of recovered sacrificial blocks which were concurrently buried with the sleepers.

Analyses of reflection coefficients to identify distinct buried material types was not successful as identified reflection coefficient groupings for oak, pine, jarrah and iron sleepers overlapped, or partially overlapped, with each other. This was in part a result of the high variability in reflected seabed and buried reflector amplitudes across adjacent wave traces, and possibly as a result of the recent and non-uniform backfilling of sediments on top of the sleepers. The variability in reflection coefficients derived for all sleepers was improved using the modal value for the calibration coefficient (x), rather than the 50^{th} percentile value due to high skewness of the distribution of amplitudes associated with the seabed surface and seabed 1^{st} multiple reflections. The results of this approach matched (within a factor of 1–2) independently derived reflection coefficient values based on in situ sediment and sleeper impedance properties. The exception were reflection coefficients for iron which were up to 6.5 times lower than their materials derived equivalent.

The reflection coefficient results also provide a valuable insight into the sensitivity of timber grain orientation on in situ acoustic measurements. The pine sleepers were predominantly buried with their longitudinal grain in a horizontal position, however for three sleepers the grain direction was rotated vertically, and two other sleepers were buried with their long grain horizontal but the upper surface tilted at 22.5^0. The reflection coefficients for these sub-groups were statistically similar and fell within the broader range of all pine sleepers. The mean values of each of the in situ derived reflection coefficient timber groups were similar to laboratory derived values obtained by Zisi in 2019 (0.28 for oak vs. 0.26–0.30; 0.20 vs. 0.28–0.33 for pine; and 0.27 vs. 0.20–0.25 for jarrah equivalent timber). The range in Zisi's values

represented differences in insonification angles, equivalent to different orientations of the timber grain exposed to acoustic measurement. This is the first quantified in situ result which confirms Zisi's laboratory-based conclusion 'that the orientation of the wood, either flat-sawn (0–30°) or quarter sawn (60–90°), does not seem to influence the reflection coefficient'. This is an important outcome since researchers do not know, a priori, the likely grain orientation of buried shipwreck timbers when gathering initial site data for research or in situ management purposes. If in situ reflection coefficients were highly sensitive to longitudinal–radial–tangential grain orientation, then site interpretations would become more difficult.

Acoustically derived reflection coefficients, plotted against the known relationships between DoB, DO and degradation potential, provide a tentative model with which to interpret a site for in situ management purposes. A model was derived for the *James Matthews* shipwreck site which displayed three separate groupings. The first group included measurements associated with the known hull timbers and two unknown isolated reflectors, one in close proximity and one at distance from the intact hull timbers. This group displayed the expected decrease in reflection coefficient and decrease in burial depth associated with the increase in timber degradation, and represents the intact and potentially dispersed hull timbers. A second group with low reflection coefficients but with higher depths of burial was interpreted to represent weaker sediment reflection interfaces from the backfilling of excavated trenches. The third group, comprising isolated reflectors surrounding the hull timbers, was characterised by high reflection coefficients and high depths of burial. These may possibly be associated with ballast stones relocated during the 1975/76 site excavation.

The ease and speed of parametric SBP field data collection should lessen practitioners' concerns regarding field costs and survey time. Of equal importance, fast survey vessel speeds (2 m/s) permit the acquisition of multiple closely spaced runs over a site. With each run providing a very high density of continuous amplitude recordings through the seabed, interpolation software can successfully convert these discrete records into a quasi-3D interpretation of the site. Visualisation tools, or a series of plots of sequential horizontal 2D layers, provides an informative data set with which to plan additional non-invasive, or limited invasive, investigations for archaeological research and in situ management purposes. In addition, such visualisation also permits a greater focus on further detailed analyses using the existing SBP data.

The validated characteristics of the parametric SBP provide data which supports the process driven in situ preservation and research frameworks advocated by the 1992 European Valetta Convention and UNESCO 2001 *Convention on the Protection of the Underwater Cultural Heritage*.

A number of recommendations for future research evolve from this current work. These include:

- expand the relationship between reflection coefficient values and timber density. This can be achieved by parametric SBP measurements on different sites and by returning to the sleeper sites in this study, once further waterlogging and degradation has occurred in the European oak, radiata pine and jarrah sleepers buried at different levels.
- extend the evaluation of parametric SBP performance in fine-grained sediment environments.
- evaluate the performance of the parametric SBP for interpretation of submerged settlement sites, specifically those with large stone constructed features.
- assess the comparative advantages and optimum use of the SES-2000 *quattro* vs the single beam SES-2000 *compact* SBP for in situ management purposes.
- undertake further parametric SBP measurements to guide minimal invasive investigations at the isolated reflectors identified at the *James Matthews* wrecksite. The purpose of this would be to validate the current site interpretation, especially around the possible timber pieces separated from the intact hull.
- use the parametric SBP in combination with other complimentary geophysical instruments, measure in situ water quality parameters and undertake ex situ analysis of sediment cores in future applications. These complimentary data sets add value to site interpretation and in situ management and archaeological research planning. Specifically, use a magnetometer to identify if ferrous metal is located on site and its location, and then use the SBP to identify the depth and structure of the buried materials under the identified magnetic anomaly. If using the single beam SBP, then undertake a combined MBES survey to add a full 3D interpretation of the surface features across the site to tie in with the 2D or quasi 3D interpretation of the buried material. A limited number of 50 cm long sediment cores collected for ex situ dissolved oxygen and redox profiling will provide insight into the optimal depth of burial, below which the conditions are conducive to preservation of timbers. Subsequent analysis of these cores for sediment facies, grain size and bulk density, and collecting in situ measurements of water salinity and temperature, will enable site specific adjustments to the in situ acoustic wave speed in the water column and within the sediments. This will permit accurate estimates of the depth of material buried located below the seabed.
- use demodulated high frequency data for absolute seabed depth estimates, and demodulated low frequency data for depth of seabed and depths of reflectors associated with buried material—subtraction of these two sets of low frequency values

give the depth of burial for that material. Given the high intra-trace amplitude variability associated with seabed and deeper reflectors, reflection coefficients should be calculated based on the average of depth and amplitude values from 3–5 adjacent traces, with the calibration coefficient calculated from the modal value derived from a large number (>30) of traces.

BIBLIOGRAPHY

Alevizos, E., M. Snellen, D. Simons, K. Siemes and J. Greinert 2018 Multi-angle backscatter classification and sub-bottom profiling for improved seafloor characterization. *Marine Geophysical Researches* 39(1):289–306.

AmesWeb 2019 *Density of steel*. Retrieved 19/07/2019 from <https://www.amesweb.info/Materials/Density of Steel.aspx>.

Anuskiewicz, R. 1998 Technology, Theory and Analysis Using Remote Sensing as a Tool for Middle-Range Theory Building in Maritime and Nautical Archaeology. In L.E. Babits and H. Van Tilburg (eds), *Maritime Archaeology A Reader of Substantive and Theoretical Contributions*. New York, NY Springer US : Imprint: Springer.

applanix 2019 *POS MV Datasheet*. Retrieved 28/05/2019 from <https://www.applanix.com/products/posmv.htm>.

Arnott, S., A. Best, J. Dix and D. Gregory 2002a *Acoustical properties of waterlogged wood*. Proceedings of the Sixth European Conference on Underwater Acoustics, Gdansk, Poland.

Arnott, S., J. Dix, A. Best and D. Gregory 2002b Acoustic propagation in waterlogged wood. *Acta Acustica united with Acustica* 88(5):699–702.

Arnott, S., J. Dix, A. Best and D. Gregory 2005 Imaging of buried archaeological materials: The reflection properties of archaeological wood. *Marine Geophysical Researches* 26(2):135–144.

Astrup, P., M. , C. Skriver, J. Benjamin, F. Stankiewicz, I.A.K. Ward, J.K. McCarthy, P. Ross, P. Baggaley, S. Ulm and G. Bailey, N 2019 Underwater Shell Middens: Excavation and Remote Sensing of a Submerged Mesolithic site at Hjarnø, Denmark. *The Journal of Island and Coastal Archaeology* 0:1–20.

Australian-Government 2018 *Underwater Cultural Heritage Act 2018*. Retrieved from <https://www.legislation.gov.au/Details/C2018A00085>.

Baker, P. and G. Henderson 1979 *James Matthews* excavation. A second interim report. *International Journal of Nautical Archaeology* 8(3):225–244.

Barklage, M., P. Puleo, Y. Axford and B. Curry 2019 *Application of sub bottom profiling to image the structure and stratigraphy of glacial sediments in geneva lake, wi*. SAGEEP 2019-32nd Annual Symposium on the Application of Geophysics to Engineering and Environmental Problems.

Benjamin, J. 2019 *Clarification of in situ preservation at UNESCO Brest Conference June 2019*: Tweet @jon_benj - 18 Jun 2019.

Bergstrand, T. 2010 The Danish 17th-Century Man-of-War *Stora Sofia*: Documentation and in situ preservation. *International Journal of Nautical Archaeology* 39(1):56–65.

Bergstrand, T. and N. Godfrey (eds) 2007 *Reburial and analyses of archaeological remains: Studies on the effect of reburial on archaeological materials performed in Marstrand, Sweden 2002–2005. The RAAR project*: Bohusläns Museum and Studio VästSvensk Konservering, Uddevalla, Sweden.

Björdal, C.G. 2012a Evaluation of microbial degradation of shipwrecks in the Baltic Sea. *International Biodeterioration & Biodegradation* 70:126–140.

Björdal, C.G. 2012b Microbial degradation of waterlogged archaeological wood. *Journal of Cultural Heritage* 13(3):S118–S122.

Björdal, C.G. and T. Nilsson 2008 Reburial of shipwrecks in marine sediments: a long-term study on wood degradation. *Journal of Archaeological Science* 35(4):862–872.

Bjørnø, L. 2017a Finite-amplitude waves. In T. Neighbors and D. Bradley (eds), *Applied underwater acoustics*, p.857–888. Amsterdam, Netherlands: Elsevier.

Bjørnø, L. 2017b Scattering of sound. In T. Neighbors and D. Bradley (eds), *Applied underwater acoustics*, p.297–362. Amsterdam, Netherlands: Elsevier.

Bjørnø, L. 2017c Sonar systems. In T. Neighbors and D. Bradley (eds), *Applied underwater acoustics*, pp.587–742. Amsterdam, Netherlands: Elsevier.

Bjørnø, L. 2017d Underwater acoustic measurements and their applications. In T. Neighbors and D. Bradley (eds), *Applied underwater acoustics*, p.889–947. Amsterdam, Netherlands: Elsevier.
Bucur, V. and R.C. Chivers 1991 Acoustic properties and anisotropy of some Autralian wood species. *ACUSTICA* 75:69–74.
Bull, J.M., M. Gutowski, J.K. Dix, T.J. Henstock, P. Hogarth, T.G. Leighton and P.R. White 2005 Design of a 3D chirp sub-bottom imaging system. *Marine Geophysical Researches* 26(2–4):157–169.
Bull, J.M., R. Quinn and J.K. Dix 1998 Reflection coefficient calculation from marine high resolution seismic reflection (chirp) data and application to an archaeological case study. *Marine Geophysical Researches* 20(1):1–11.
Caiti, A., O. Bergem and J. Debedal 1999 Parametric sonars for seafloor characterization. *Measurement Science and Technology* 10:1105–1115.
Camidge, K., P. Holt, C. Johns, L. Randall and A. Schmidt 2010 *Developing Magnetometer Techniques to Identify Submerged Archaeological Sites – Theoretical Study Report*.
Caporaso, A. 2017 A dynamic processual maritime archaeological landscape formation model. In A. Caporaso (ed.), *Formation processes of maritime archaeological landscapes*, pp.7–30. Where the Land meets the Sea. Springer.
Cawthra, H.C., R.J. Anderson, J.C. De Vynck, Z. Jacobs, A. Jerardino, K. Kyriacou and C.W. Marean in press Migration of Pleistocene shorelines across the Palaeo-Agulhas Plain: Evidence from dated sub-bottom profiles and archaeological shellfish assemblages. *Quaternary Science Reviews*.
Chronis, A., T. Hasiotis and J. Lowag 2014 Relationship between gas-bearing sediments and biogenic mounds, student research, project in hydrography. *Hydro International* Novermber/December:22–25.
Class Instrumentation 2019 *Ultrasonic Sound Velocity Chart*. Retrieved from <htpp://www.classltd.com/sound velocity table.html>.
Clément, E. 1996 Current developments at UNESCO concerning the protection of the underwater cultural heritage. Presentation made at the first and the second national maritime museum conferences on the protection of underwater cultural heritage (Greenwich, 3 and 4 February 1995) (London, IMO, 25 and 26 January 1996). *Marine Policy* 20(4):309–323.
Council-of-Europe 1992 *European Convention on the Protection of the Archaeological Heritage (Revised)*. Retrieved from <https://www.coe.int/en/web/conventions/full-list/-/conventions/treaty/143>.
Cunningham, J.J. 2008 Middle range approaches. In, *Encyclopedia of Archaeology*, p.1620–1622. New York: Academic Press.
Cvikel, D., O. Grøn and L.O. Boldreel 2017 Detecting the Ma'agen Mikhael B shipwreck. *Underwater Technology* 34(2):93–98.
Delgado, J.P. 1997 Site formation processes. In J.P. Delgado (ed.), *Encylcopaedia of Underwater and Maritme Archaeology*, p.386–388. London: British Museum Press.
Department of Water and Environmental Regulation, G.o.W.A. 2018 *Annual Swan Canning Estuarine Data Report June 2017–May 2018*.
Dix, J.K., A. Bastos, R.M.K. Plets, J.M. Bull and T.J. Henstock 2008 High resolution sonar for the archaeological investigation of marine aggregate deposits. *Project Report* 3365.
Edgetech. Retrieved from <https://www.edgetech.com/product-category/sub-bottom-profiling/>.
Firth, A. 1999 Making archaeology: the history of the Protection of Wrecks Act 1973 and the constitution of an archaeological resource. *International Journal of Nautical Archaeology* 28(1):10–24.
Forrest, J., J. Homer and G. Hooper 2005 The application of acoustic remote sensing to maritime archaeological site surveys. *AIMA Bulletin* 29:1–8.

Ghinassi, M., A. D'Alpaos, L. Tommasini, L. Brivio, A. Finotello and C. Stefani 2019 Tidal currents and wind waves controlling sediment distribution in a subtidal point bar of the Venice Lagoon (Italy). *International Journal of Sedimentology* 66(7):2926–2949.

Gibbs, M. 2006 Cultural site formation processes in maritime archaeology: disaster response, salvage and muckelroy 30 years on. *International Journal of Nautical Archaeology* 35(1):4–19.

Gibbs, M. and B. Duncan 2016 Cultural site formation processes affecting shipwrecks and shipping mishap sites. In M.E. Keith (ed.), *Site formation processes of submerged shipwrecks*, p.179–207. Gainesville Florida: University Press of Florida.

Godfrey, I.M., E. Reed, V. Richards, N.F. West and T. Winton 2005 The *James Matthews* shipwreck—conservation survey and in situ stabilisation. In P. Hoffman, K. Straetkvern, J.A. Spriggs and D. Gregory (eds), *Proceedings of the 9th ICOM Group on Wet Organic Archaeological Materials Conference, Copenhagen, 2004*, p.40—76. Bremerhaven: The International Council of Museums, Committee for Conservation on the protection and management of underwater cultural heritage.

González, A.W., P. O'Keefe and M. Williams 2009 The UNESCO Convention on the Protection of the Underwater Cultural Heritage: a Future for our Past? *Conservation and Management of Archaeological Sites* 11(1):54—69.

Government-of-Western-Australia 1973 *Maritime Archaeology Act 1973*. Retrieved from <http://museum.wa.gov.au/research/departments/maritime-archaeology/maritime-archaeology-legal-requirements>.

Grattan, D.W. 1987 Waterlogged wood. In C. Pearson (ed.), *Conservation of Marine Archaeological Objects*. London: Butterworths.

Gregory, D. 1996 Formation processes in underwater archaeology: A study of chemical and biological deterioration, School of Archaeological Studies, University of Leicester,

Gregory, D. 1998 Re-burial of timbers in the marine environment as a means of their long-term storage: experimental studies in Lynaes Sands, Denmark. *International Journal of Nautical Archaeology* 27(4):343–358.

Gregory, D. 1999 Monitoring the effect of sacrificial anodes on the large iron artefacts on the Duart Point wreck, 1997. *International Journal of Nautical Archaeology* 28(2):164—173.

Gregory, D. 2007 Monitoring of the environment in the reburial trench at Marstrand, Report no 12725-003006, June 2006. In T. Bergstrand and I.N. Godfrey (eds), *Reburial and Analyses of Archaeological Remains. Studies on the effects of reburial on archaeological materials performed in Marstrand, Sweden 2002—2005, The RAAR project*, p.59—90. Bohuslans Museums.

Gregory, D. 2009 In situ preservation of marine archaeological sites: out of sight but not out of mind. In V. Richards and J. McKinnon (eds), *Open seawater public, professionals and preservation: in situ conservation of cultural heritage*, p.1—16. Flinders University: Past Foundation.

Gregory, D. 2012 Development of tools and techniques to survey, assess, stabilise, monitor and preserve underwater archaeological sites: SASMAP. *International Journal of Heritage in the Digital Era* 1(1 suppl):367—371.

Gregory, D. 2015a Development of tools and techniques to survey, assess, stabilise, monitor and preserve underwater archaeological sites: SASMAP. *International Archives of the Photogrammetry, Remote Sensing and Spatial Information Sciences* XL—5/W7:173—177.

Gregory, D. 2015b Development of Tools and Techniques to Survey, Assess, Stabilise, Monitor and Preserve Underwater Archaeological Sites: SASMAP. *The International Archives of the Photogrammetry, Remote Sensing and Spatial Information Sciences* XL-5-W7(5):173–177.

Gregory, D., A.C. Helms and H. Matthiesen 2008a The use and deployment of modern wood samples as a proxy indicator for biogeochemical processes on archaeological sites preserved in situ in a variety of environments of differing saturation level. *Conservation and Management of Archaeological Sites* 10(3):204—222.

Gregory, D., P. Jensen, H. Matthiesen and K. Straetkvern 2007 The correlation between bulk density and shock resistance of waterlogged archaeological wood using the pilodyn. *Studies in Conservation* 52(4):289–298.

Gregory, D. and M. Manders 2015 *Best practices for locating, surveying, assessing, monitoring and preserving underwater archaeological sites, SASMAP Guideline Manual 2*.

Gregory, D. and H. Matthiesen 2012a The 4th International Conference on Preserving Archaeological Remains In Situ (PARIS4): 23–26 May 2011, the National Museum of Denmark, Copenhagen. *Conservation and Management of Archaeological Sites* 14(1–4):1–6.

Gregory, D. and H. Matthiesen 2012b Nydam Mose: In situ preservation at work. *Conservation and Management of Archaeological Sites* 14(1–4):479–486.

Gregory, D., H. Matthiesen, P. Jensen, I. Nyström Godfrey and T. Bergstrand (eds) 2008b *Reburial and analyses of archaeological remains: Monitoring in the marine environment*. Preserving archaeoloigcal remains in situ. Proceedings of the 3rd conference 7 - 9 december 2006, Amsterdam. Amsterdam: Institue for Geo and Bioarchaeology, VU University.

Grøn, O. and L.O. Boldreel 2013 *Sub-bottom profiling for large-scale maritime archaeological survey. An experience-based approach*. OCEANS 2013 MTS/IEEE Bergen: The Challenges of the Northern Dimension.

Grøn, O. and L.O. Boldreel 2014 Chirping for large-scale maritime archaeological survey: A strategy developed from a practical experience-based approach. *Journal of Archaeology* 2014:11.

Grøn, O., L.O. Boldreel, D. Cvikel and J.P. Hermand 2015 *Subbottom profiling in shallow water: The* Akko 4 *test case*. Rio de Janeiro, Brazil.

Grøn, O. and J.P. Hermand 2015 *Settlement archaeology under water: Practical, strategic and research perspectives*. Rio Acoustics 2015 IEEE/OES Acoustics in Underwater Geosciences Symposium, Rio de Janeiro, Brazil.

Grøn, O., A.N. Jørgensen and G. Hoffmann 2007 Marine archaeological survey by high-resolution sub-bottom profilers. *Norsk Sjøfartsmuseums Årbok* 2007:115–144.

Gutowski, M., J. Malgorn and M. Vardy 2015 *3D sub-bottom profiling—High resolution 3D imaging of shallow subsurface structures and buried objects*. MTS/IEEE OCEANS 2015 Genova: Discovering Sustainable Ocean Energy for a New World.

Hamilton, E.L. 1969 *Sound velocity, elasticity, and related properties of marine sediments, North Pacific, III. Prediction of in situ properties*, Department of the Navy, Naval Undersea Research and Development Centre, San Diego, California.

Heldtberg, M., I. MacLeod and V. Richards 2004 Corrosion and cathodic protection of iron in seawater: a case study of *James Matthews* (1841). *Proceedings of the Metal*.

Henderson, G. 1975 *James Matthews* excavation summer 1974–75. *Australian Archaeology* No. 3:40–45.

Henderson, G. 1976 *James Matthews* excavation, summer 1974. Interim report. *International Journal of Nautical Archaeology* 5(3):245–251.

Henderson, G. 1977a *Day Book Number 72, Eglinton and James Matthews 1971–1977, Includes: Vergulde Draeck, Exmouth-Fairy Queen, Batavia, Albany wreck inspection and Hadda*: Department of Maritime Archaeology, Western Australian Museum.

Henderson, G. 1977b *Four seasons of excavation on the James Matthews wreck*. First Southern Hemisphere Conference on Maritime Archaeology, Fremantle, WA.

Henderson, G. 2008 The wreck of the ex-slaver *James Matthews*. *International Journal of Historical Archaeology* 12(1):39–52.

Henderson, G. 2009 *Redemption of a slave ship: James Matthews*. Welshpool, Western Australia: Western Australian Museum.

Henderson, G. and M. Stanbury 1983 The excavation of a collection of cordage from a shipwreck site. *The International Journal of Nautical Archaology and Underwater Exploration* 12(1):15–26.

Hoffman, P. and M.A. Jones 1989 Structure and degradation process for waterlogged archaeological wood. In, *Advances In Chemistry*, pp.35–65.
ICOMOS, I.C.o.M.a.S. 1996 *Charter on the protection and management of underwater cultural heritage (1996)*. Retrieved from <http://www.icomos.org/charters/underwater_e.pdf>.
Innomar 2017 *SES-2000 Narrow beam parametric sub-bottom profiler: User's guide ISE 2.9.5 post processing software Revision 8 October 2017*.
Innomar 2018 *Innomar SES-2000 compact sub-bottom profiler product sheet*. Retrieved 19 November 2018 from <https://www.innomar.com/innomar-flyer/Innomar-ses2000-compact.pdf>.
Jensen, P. and D. Gregory 2006 Selected physical parameters to characterize the state of preservation of waterlogged archaeological wood: a practical guide for their determination. *Archaeological Science* 33(4):551–559.
Johnson, A.L. 2008 Processual Archaeology. In D.M. Pearsall (ed.), *Encyclopedia of Archaeology*, p.1894─1896. New York: Academic Press.
Keith, M.E. 2016 *Site formation processes of submerged shipwrecks*. Gainesville, Florida: University Press of Florida.
Killick, D. 2015 The awkward adolescence of archaeological science. *Journal of Archaeological Science* 56:242─247.
Kozaczka, E., G. Grelowska, S. Kozaczka and W. Szymczak 2013 Detection of objects buried in the sea bottom with the use of parametric echosounder. *Archives of Acoustics* 38(1):99–104.
Lafferty, B., R. Quinn and C. Breen 2006 A side-scan sonar and high-resolution chirp sub-bottom profile study of the natural and anthropogenic sedimentary record of Lower Lough Erne, northwestern Ireland. *Journal of Archaeological Science* 33(6):756–766.
Lawrence, M.J. and C.R. Bates 2001 Acoustic ground discrimination techniques for submerged archaeological site investigation. *Marine Technology Society Journal* 35(4):65–73.
Lovett, J.R. 1978 Merged seawater sound-speed equations. *Acoustical Society of America* 63(6):1713–1718.
Lunne, T., P.K. Robertson and J.J.M. Powell 1997 *Cone Penetration Testing in Geotechnical Practice*. London: Blackie Academic & Professional.
MacLeod, I. and V.L. Richards 2011 In situ conservation surveys of iron shipwrecks in Chuuk Lagoon and the impact of human intervention. *Australian Institute for the Conservation of Cultural Materials Bulletin* 32:106─122.
MacLeod, I.D. 2016 Corrosion products and site formation processes. In M.E. Keith (ed.), *Site formation processes of submerged shipwrecks*, p.90─113. Gainesville Florida: University press of Florida.
MacLeod, I.D. and J.S. Killingley 1982 The use of barnacles to establish past temperatures on historic shipwrecks. *International Journal of Nautical Archaeology* V 11(3):1057–2414.
Manders, M. 2004 Protecting common maritime heritage. The Netherlands involved in two EU-projects: MoSS and BACPOLES. In F. Maniscalco (ed.), *Mediterraneum*, p.279─292. Italy: Massa Editore.
Manders, M. 2008 In situ preservation: 'the preferred option'. *Museum International* 60(4):31─41.
Manders, M. 2010a Chirp and sonar In M. Manders (ed.), *MACHU final report Nr.3 - Managing cultural heritage underwater*, pp.71–72.
Manders, M. 2010b *MACHU – Managing Cultural Heritage Underwater*. Retrieved from <https://www.machuproject.eu/>.
Manders, M., D. Gregory and V. Richards 2008 The in situ preservation of archaeological sites underwater. An evaluation of some techniques. In M. May, M. Jones and J. Mitchell (eds), *Proceedings of the 2nd Heritage, Microbiology and Science, Microbes, Monuments and Maritime Materials Conference, 28 June–1 July 2005*, p.179─203. Portsmouth, UK: RSC Publishing, London.

Mason, B. 2018 *End of the rainbow? New map scale is more readable by people who are colour blind.* Retrieved from < https://www.scientificamerican.com/article/end-of-the-rainbow-new-map-scale-is-more-readable-by-people-who-are-color-blind/>.
McCarthy, M. 2000 *Iron and steamship archaeology : success and failure of SS Xantho*. New York: New York : Kluwer Academic/Plenum Publishers.
McCarthy, M. 2019 Metal detection: an essential aid in maritime archaeology. *Current Science* 117(10, 25 November 2019, Special Section: Shipwrecks):1628–1634.
Menard, E., N. Nasser, R. Patterson, J. Galloway, P. Cott, B. Hanna and H. Falck 2019 Sub-bottom acoustic profiling as a remediation assessment tool for contaminated lakes. *SN Applied Sciences* 1(6):572.
Mindell, D.A. and B. Bingham 2001 *A high-frequency, narrow-beam sub-bottom profiler for archaeological application*. IEEE Oceans 2001, Honolulu, Hawaii.
Missiaen, T. 2005 VHR marine 3D seismics for shallow water investigations: Some practical guidelines. *Marine Geophysical Researches* 26(2):145–155.
Missiaen, T. 2010a The potential of seismic imaging in marine archaeological site investigations. *Relicta* 6:219–236.
Missiaen, T. 2010b Seismic imaging in marine archaeological site investigations. In M. Manders (ed.), *MACHU final report Nr.3 - Managing cultural heritage underwater*, pp.67–70.
Missiaen, T., I. Demerre and V. Verrijken 2012 Integrated assessment of the buried wrecksite of the Durch East Indiaman '*t Vliegent Hart*. *Relicta* 9:191–208.
Missiaen, T., D. Evangelinos, C. Claerhout, M. De Clercq, M. Pieters and I. Demerre 2017a Archaeological prospection of the nearshore and intertidal area using ultra-high resolution marine acoustic techniques: Results from a test study on the Belgian coast at Ostend-Raversijde. *Geoarchaeology*:1–15.
Missiaen, T., D. Sakellariou and N.C. Flemming 2017b Survey strategies and techniques in underwater geoarchaeological research: An overview with emphasis on prehistoric sites. In, *Under the sea: Archaeology and palaeolandscapes of the continental shelf*, pp.21–37. Springer.
Missiaen, T., E. Slob and M.E. Donselaar 2008 Comparing different shallow geophysical methods in a tidal estuary, Verdronken Land van Saeftinge, Western Scheldt, the Netherlands. *Netherlands Journal of Geosciences - Geologie en Mijnbouw* 87(2):151–164.
Muckelroy, K. 1976 The integration of historical and archaeological data concerning an historic wrecksite: The 'Kennemerland'. *World Archaeology* 7(3):280–290.
Muckelroy, K. 1977 Historic wrecksites in Britain and their environments. *International Journal of Nautical Archaeology* 6(1):47-57.
Muckelroy, K. 1978 *Maritime archaeology*. Cambridge UK: Cambridge University Press.
Müller, S. and J. Wunderlich 2003 Detection of embedded objects using parametric sub-bottom profilers. *The International Hydrographic Review* 4(3).
Müller, S., J. Wunderlich, P. Hümbs and S. Erdmann 2005 *High-resolution sub-bottom profiling for the "shallow survey" common data set using the parametric echosounder SES-2000*. Shallow Survey 2005 4th International Conference, Plymouth 12–15 September 2005.
NATA 2018 *General accreditation guidance—Validation and verification of quantitative and qualitative test methods*. Retrieved 5 November 2018 from <https://www.nata.com.au/phocadownload/gen-accreditation-guidance/Validation-and-Verification-of-Quantitative-and-Qualitative-Test-Methods.pdf>.
Novak, A., A. Šmuc, S. Poglajen and M. Vrabec 2020 Linking the high-resolution acoustic and sedimentary facies of a transgressed Late Quaternary alluvial plain (Gulf of Trieste, northern Adriatic). *Marine Geology* 419:106061.
NSW Department of Primary Industries, O.o.W. 2015 *Validation & verification–What's the difference?* Retrieved 19/11/2018 from
Nyström Godfrey, I., T. Bergstrand and H. Petersson (eds) 2011 *Reburial and analyses of archaeological remains—Phase II results from the 4th retrieval in 2009 from*

Marstrand, Sweden. The RAAR project: Bohusläns Museum and Studio VästSvensk Konservering, Uddevalla, Sweden.
Nyström Godfrey, I., T. Bergstrand, H. Petersson, C. Bohm, E. Christensson, C.G. Björdal, D. Gregory, I. MacLeod, E.E. Peacock and V. Richards 2012 The RAAR project—heritage management aspects on reburial after ten years of work. *Conservation and Management of Archaeological Sites* 14(1─4):360─371.
O'Keefe, P. 1996 Protecting the underwater cultural heritage: The International Law Association Draft Convention. *Marine Policy* 20(4):297–307.
O'Reilly, R. 2007 *Australian built wooden sailing vessels of the South Australian intrastate trade*: Flinders University, Department of Archaeology.
OEMGGlobal. Retrieved 23/10/2019 from <http://oemg-global.com/aquares-and-geotechnical-studies/>.
Oniz, H. 2018 Harbour of Soli-Pompeiopolis: recent underwater archaeological research. *The International Journal of Nautical Archaeology* 47.2:337–342.
Ortmann, N. 2009 Exploring practitioners' attitudes towards in situ preservation and storage for underwater cultural heritage. Unpublished Masters Thesis thesis, Department of Archaeology, Flinders University, South Australia,
Ortmann, N., J.F. McKinnon and V. Richards 2010 In situ preservation and storage: Practitioner attitudes and behaviours. *AIMA Bulletin* 34:27–44.
Oxley, I. 1998 *The in situ preservation of underwater sites*. Preserving Archaeological Remains *in situ*; Proceedings of the Conference of 1st–3rd April 1996, United Kingdom: Museum of London Archaeology Service.
Oxley, I. 2001 Towards the integrated management of Scotland's cultural heritage: Examining historic shipwrecks as marine environmental resources. *World Archaeology* 32(3):413–426.
Oxley, I. 2016 English Heritage and shipwreck site formation processes. In M.E. Keith (ed.), *Site Formation Processes of Submerged Shipwrecks*, p.212–234. Gainesville Florida: University Press of Florida.
Oxley, I. and M.E. Keith 2016 Introduction: Site formation processes of submerged shipwrecks. In M.E. Keith (ed.), *Site formation processes of submerged shipwrecks*, p.1─14. Gainesville, Florida: University Press of Florida.
Pemberton, B. 1979 *Australian coastal shipping*. Carlton, Victoria: Melbourne University Press.
Plets, R.M.K., J.K. Dix, J.R. Adams and A.I. Best 2008 3D reconstruction of a shallow archaeological site from high-resolution acoustic imagery: *Grace Dieu*. *Applied Acoustics* 69(5):399–411.
Plets, R.M.K., J.K. Dix, J.R. Adams, A.I. Best and D.A. Mindell 2005 *High resolution acoustic imagery from a shallow archaeological site: Grace Dieu-a case study*. Proceedings of the International Conference Underwater Acoustic Measurements: Technologies & Results, Heraklion, Crete, Greece.
Plets, R.M.K., J.K. Dix, J.R. Adams, J.M. Bull, T.J. Henstock, M. Gutowski and A.I. Best 2009 The use of a high-resolution 3D chirp sub-bottom profiler for the reconstruction of the shallow water archaeological site of *Grace Dieu* (1439), River Hamble, UK. *Journal of Archaeological Science* 36(2):408–418.
Plets, R.M.K., J.K. Dix, A. Bastos and A.I. Best 2007a Characterization of buried inundated peat on seismic (chirp) data, inferred from core information. *Archaeological Prospection* 14(4):261–272.
Plets, R.M.K., J.K. Dix and A.I. Best 2007b Mapping of the buried Yarmouth Roads wreck, Isle of Wight, UK, using a chirp sub-bottom profiler. *International Journal of Nautical Archaeology* 37(2):360–373.
Quinn, R. 2006 The role of scour in shipwreck site formation processes and the preservation of wreck-associated scour signatures in the sedimentary record ─ evidence from seabed and sub-surface data. *Journal of Archaeological Science* 33(10):1419─1432.

Quinn, R. 2012 Acoustic remote sensing in maritime archaeology. In A. Catsambis, B. Ford and D.L. Hamilton (eds), *The Oxford handbook of maritime archaeology*, pp.68–89. Oxford, UK: Oxford University Press.
Quinn, R., J.R. Adams, J.K. Dix and J.M. Bull 1998a The *Invincible* (1758) site—an integrated geophysical assessment. *International Journal of Nautical Archaeology* 27(2):126–138.
Quinn, R., C. Breen, W. Forsythe, K. Barton, S. Rooney and D. O' Hara 2002 Integrated geophysical Surveys of the French frigate *La Surveillante* (1797), Bantry Bay, Co. Cork, Ireland. *Journal of Archaeological Science* 29(4):413–422.
Quinn, R., J.M. Bull and J.K. Dix 1997a Buried scour marks as indicators of palaeo-current direction at the *Mary Rose* wrecksite. *Marine Geology* 140(3–4):405–413.
Quinn, R., J.M. Bull and J.K. Dix 1997b Imaging wooden artefacts using chirp sources. *Archaeological Prospection* 4(1):25–35.
Quinn, R., J.M. Bull and J.K. Dix 1998b Optimal processing of marine high-resolution seismic reflection (chirp) data. *Marine Geophysical Researches* 20(1):13–20.
Quinn, R., J.M. Bull, J.K. Dix and J.R. Adams 1997c The *Mary Rose* site—geophysical evidence for palaeo-scour marks. *International Journal of Nautical Archaeology* 26(1):3–16.
Raab, L., M. and A. Goodyear, C. 1998 Middle-Range Theory in Archaeology, A critical review of origins and applications. In L.E. Babits and H. Van Tilburg (eds), *Maritime Archaeology A Reader of Substantive and Theoretical Contributions*. New York, NY Springer US : Imprint: Springer.
Richards, V. 2001 *James Matthews* (1841) conservation pre-disturbance survey report. *Department of Materials Conservation, Western Australian Museum*.
Richards, V. 2003 *James Matthews (1841) reburial project, conservation research design*, Department of Materials Conservation, Western Australian Museum, Fremantle.
Richards, V. 2011a *In situ preservation—application of a process-based approach to the management of underwater cultural heritage*. Asia-Pacific Regional Conference on Underwater Cultural Heritage, Manila, Philippines.
Richards, V. 2011b In situ preservation and reburial of the ex-slave ship *James Matthews*. *AICCM Bulletin* 32(1):33–43.
Richards, V. 2012 In situ preservation and monitoring of the *James Matthews* shipwreck site. *Conservation and Management of Archaeological Sites* 14(1–4):169–181.
Richards, V., I.M. Godfrey, R.A. Blanchette, B. Held, D. Gregory and E. Reed 2007 *In situ monitoring and stabalisation of the James Matthews shipwreck site*. Proceedings of the 10th ICOM Group on Wet Organic Archaeological Materials Conference, Amsterdam: rijksdienst archeologie, cultuurlandschap en monumenten.
Richards, V., D. Gregory, I. MacLeod and H. Matthiesen 2012 Reburial and Analyses of Archaeological Remains in the Marine Environment — Investigations into the Effects on Metals. *Conservation and Management of Archaeological Sites* 14(1–4):35–47.
Richards, V., I. MacLeod and P. Veth 2013 *The Australian historic shipwreck protection project–In situ preservation of the Clarence (1850) shipwreck site*. Proceedings of the 12th ICOM Group on Wet Organic Archaeological Materials Conference, Istanbul, Turkey: The International Council for Museums, Committee for Conservation Working Group on Wet Organic Archaeological Materials.
Richards, V., I. MacLeod and P. Veth 2014 *The Australian historic shipwreck preservation project—In situ preservation and long-term monitoring of the Clarence (1850) and James Matthews (1841) shipwreck sites*. Preceedings of the 2nd Asia-Pacific Regional Conference on Underwater Cultural Heritage, 13-16 May 2014, Honolulu, Hawaii: Asia-Pacific Regional Conference on Underwater Cultural Heritage Planning Committee.
Richardson, M.D. and D.R. Jackson 2017 The seafloor. In T. Neighbors and D. Bradley (eds), *Applied underwater acoustics*, pp.469–552. Amsterdam: Elsevier.
Robb, G.B.N., J.K. Dix, A.I. Best, J.M. Bull, T.G. Leighton, P.R. White and A. Seal 2005 *The compressional wave and physical properties of inter-tidal marine sediments*.

Underwater Acoustic Measurements: Technologies & Results, Heraklion, Crete, Greece.
Schiffer, M.B. 1972 Archaeological context and systemic context. *American Antiquity* 37(2):156–165.
Schiffer, M.B. 1987 *Formation processes of the archaeological record*. Albuquerque: University of New Mexico Press.
Schniewind, A.P. 1989 Physical and mechanical properties of archaeological wood. In, *Advances in chemistry, archaeological wood: Properties chemistry and preservation*, pp.87–109.
Sexton, R.T. 1991 Some composite-built ships compared. *Bulletin of the Australian Institue for Maritime Archaeology* 15(2):59–79.
Shefi, D. 2013 Heritage today, gone tomorrow: *in situ* preservation of underwater cultural heritage in law and practice. Unpublished PhD thesis, Department of Archaeology, Flinders University, South Australia,
Shefi, D. and P. Veth 2015 A critical analysis and philosophical review of 'Rapid Reburial': the *Clarence* project. *International Journal of Nautical Archaeology* 44(2):371–381.
Shefi, D., P. Veth, C. Philippou, J. Rodrigues, P. Harvey and J. Carpenter 2014 The Australian historic shipwreck preservation project: An interim progress report. *AIMA Bulletin* 38:31–40.
Shott, M. 1998 Status and Role of Formation Theory in Contemporary Archaeological Practice. *Journal of Archaeological Research* 6(4):299-329.
Simyrdanis, K., M. Bailey, I. Moffat, A. Roberts, W. van Duivenvoorde, A. Savvidis, G. Cantoro, K. Bennett and J. Kowlessar 2019 Resolving Dimensions: A comparison between ERT imaging and 3D modeling of the barge *Crowie*, South Australia. In J.K. McCarthy, J. Benjamion, T. Winton and W. van Duivenvoorde (eds), *3D recording and interpretation for maritime archaeolgy*, pp.175–186. Springer.
Simyrdanis, K., N. Papadopoulos and G. Cantoro 2016 Shallow off-shore archaeological prospection with 3-D electrical resistivity tomography: the case of Olous (modern Eloundra), Greece. *Remote Sensing* 8(11):897–911.
Sitkiewicz, P., S. Rudowski, R. Wróblewski and J. Dworniczak 2020 New insights into the nearshore bar internal structure using high-resolution sub-bottom profiling: The Vistula Spit case study. *Marine Geology* 419:106078.
Staniforth, D.M., J. Hunter and E. Jateff 2009 *International Approaches to Underwater Cultural Heritage*: Nova Science Publishers, Inc.
Staniforth, M. and D. Shefi 2014 *Shipbuilding in the Australian Colonies before 1850*. 2014 ACUA Underwater Archaeology Proceedings: Advisory Council on Underwater Archaology.
Stanish, C. 2008 Explanation in Archaeology, Overview In D.M. Pearsall (ed.), *Encyclopedia of Archaeology*, p.1358–1364. New York: Academic Press.
Stewart, D.J. 1999 Formation processes affecting submerged archaeological sites: An overview. *Geoarchaeology: An International Journal* 14(6):565–587.
Telford, W.M., L.P. Geldart and R.E. Sheriff 1990 *Applied geophysics second edition*. Cambridge: Cambridge University Press.
UNESCO 2001 *UNESCO Convention on the Protection of the Underwater Cultural Heritage*. Retrieved 17/07/2018 from <http://www.unesco.org/new/en/culture/themes/underwater-cultural-heritage/2001-convention/>.
UNESCO 2013 *Manual for Activities directed at Underwater Cultural Heritage. Guidelines to the Annex of the UNESCO 2001 Convention*. Retrieved 12/10/2019 from <http://www.unesco.org/culture/en/underwater/pdf/UCH-Manual.pdf>.
UNESCO 2017 *Best Practices of Underwater Cultural Heritage*. Retrieved from <http://www.unesco.org/new/en/culture/themes/underwater-cultural-heritage/underwater-cultural-heritage/best-practices-of-underwater-cultural-heritage/>.

UNESCO 2019a *Legal Instruments*. Retrieved from <http://www.unesco.org/eri/la/convention.asp?KO=13520&language=E&order=alpha >.

UNESCO 2019b *Niue ratifies UNESCO Convention on the Protection of the Underwater Cultural Heritage*. Retrieved from <http://www.unesco.org/new/en/culture/themes/underwater-cultural-heritage/dynamic-content-single-view/news/niue_ratifies_unesco_convention_on_the_protection_of_the_und/ >.

Vardy, M., M. Vanneste, T. Henstock, J. , M. Clare, I A. , C. Forsberg, F. and G. Provenzano 2017 State-of-the-art remote characterization of shallow marine sediments: the road to a fully integrated solution. *Near Surface Geophysics* 15 387-402.

Vardy, M.E., J.K. Dix, T.J. Henstock, J.M. Bull and M. Gutowski 2008 Decimeter-resolution 3D seismic volume in shallow water: A case study in small-object detection. *Geophysics* 73(2):B33–B40.

Vasudevan, M., K.M. Sivakholundu, D. Venkata Rao and S. Kathiroli 2006 *Application of parametric acoustics for shallow-water near-surface geophysical investigations*. OCEANS 2006 - Asia Pacific.

Veth, P. 2006 Theoretical approaches. In M. Staniforth and M. Nash (eds), *Maritime archaeology Australian approaches*. The Springer Series in Underwater Archaeology. Springer US.

Veth, P., C. Philippou, V. Richards, M. Staniforth, J. Rodrigues, A. Khan, D. Creagh, A. Viduka, A. Barham, I. MacLeod and P. Harvey 2013 The Australian historic shipwreck preservation project 2012: First report on the background, reburial and 'in-situ' preservation at the '*Clarence*' (1841–50). *AIMA Bulletin* 37:1–19.

Veth, P., A. Viduka, M. Staniforth, I. MacLeod, V. Richards and A. Barham 2011 *The Australian historic shipwreck protection project*. Asia-Pacific Regional Conference on Underwater Cultural Heritage, Manilla, Philippines.

von Deimling, J.S., P. Held, P. Feldens and D. Wilken 2016 Effects of using inclined parametric echosounding on sub-bottom acoustic imaging and advances in buried object detection. *Geo-Marine Letters*:1–7.

Wang, F., L. Dong, J. Ding, X. Zhou, C. Tao, X. Lin and G. Liang 2019 An Experiment of the Actual Vertical Resolution of the Sub-bottom Profiler in an Anechoic Tank. *Archives Of Acoustics* 44(1):185–194

Ward, I., P. Larcombe and P. Veth 1998 Towards new process-orientated models for describing wreck disintegration An example using the *Pandora* wreck. *Bulletin of the Australian Institute for Maritime Archaeology* 22:109─114.

Ward, I.A.K., P. Larcombe and P. Veth 1999 A new process-based model for wrecksite formation. *Journal of Archaeological Science* 26(5):561─570.

Warner, M. 1990 Absolute reflection coefficients from deep seismic reflections. *Tectonophysics* 173:15–23.

Wheeler, A.J. 2002 Environmental controls on shipwreck preservation: The Irish context. *Journal of Archaeological Science* 29(10):1149–1159.

Wilken, D., T. Wunderlich, H. Hollmann, M. Schwardt, W. Rabbel, C. Mohr, D. Schulte-Kortnack, O. Nakoinz, J. Enzmann, F. Jurgens and F. Wilkes 2019 Imaging a medieval shipwreck with the new PingPong 3D marine reflection seismic system. *Archaeological Prospection*:1,13.

Winton, T. 2015 Understanding the interactive nature of *in-situ* processes for management of submerged cultural heritage material. *AIMA Bulletin* 39:71–83.

Winton, T. 2019 Quantifying depth of burial and composition of shallow buried archaeological material: Integrated sub-bottom profiling and 3D survey approaches. In J.K. McCarthy, J. Benjamin, T. Winton and W. Van Duivenvoorde (eds), *3D Recording and interpretation for maritime archaeology*, pp.155–174. Springer.

Winton, T. and V. Richards 2005 In situ containment of sediment for shipwreck reburial projects. In P. Hoffmann, K. Strætkvern, J.A. Spriggs and D. Gregory (eds), *Proceedings of the 9th ICOM Group on Wet Organic Archaeological Materials*

Conference, Copenhagen, 7-11 June 2004, pp.77–89. Bremerhaven: The International Council of Museums, Committee for Conservation Working Group on Wet Organic Archaeological Materials.
Wunderlich, J. and S. Müller 2003a High-resolution sub-bottom profiling using parametric acoustics. *International Ocean Systems* 7(4):6–11.
Wunderlich, J. and S. Müller 2003b Non-linear echo sounders for high-res sub-bottom profiling. *Sea Technology* 44(9):23–26.
Wunderlich, J., S. Müller, S. Erdmann, T. Buch, P. Hümbs and R. Endler 2005a *High-resolution acoustical site exploration in very shallow water—a case study*. EAGE Near Surface 2005, Palermo, Italy.
Wunderlich, J., G. Wendt and S. Müller 2005b High-resolution echo-sounding and detection of embedded archaeological objects with nonlinear sub-bottom profilers. *Marine Geophysical Researches* 26(2):123–133.
Zisi, A. 2016 Relationship between wood density and ultrasound propogation velocity: A non-destructive evaluation of waterlogged archaeological wood state of preservation based on its underwater acoustic properties. Unpublished PhD thesis, Faculty of Natural and Environmental Sciences, School of Ocean and Earth Science, University of Southampton, United Kingdom.,

A. SITE LOGISTICS

Field record

Tables A.1 and A.2 summarise all field trips, site access, personnel involved, dive times and water depths at the *James Matthews* wreck-site and adjacent James Matthews sleeper site, and at the Swan River Sleeper site, respectively.

Sleeper positions

Tables A.3 and A.4 list the tape measured seabed distances from the reference picket to each sleeper buried at the James Matthews and Swan River sleeper sites, respectively, together with the seabed level relative to the end plate slot and the actual burial depth at times of SBP measurement. Tables A.5 and A.6 list positions of all James Matthews sleeper locations and the Swan River sleeper endplate locations measured using the Leica GS16 High Precision GNSS RTK Rover on 19th June 2019 and 20th May 2018, respectively.

Positions of key features on *James Matthews* wrecksite

Table A.7 lists the mean (centroid) seabed location of the slate mound and windlass measured using the Leica GS16 High Precision GNSS RTK Rover on 18th May 2018.

Table A.1 Field record, *James Matthews* wrecksite and James Matthews sleeper site

date	site	main purpose	dive details									vessel	max water depth (m)
			field team members	dive 1			surface interval (mins)	dive 2			total dive time for day (mins)	dive equipment	
				time entry	time exit	total dive time (mins)		time entry	time exit	total dive time (mins)			
7/02/2017	James Matthews sleeper	sleeper site setup	Jeremy Green										Dirk Hartog	1.5-2.0
			Ross Anderson											
			Deb Shefi	10.36	10.54	18					18	SCUBA		
			Nic Bigourdan	12.35	13.39	64					64	SCUBA		
			Rebecca Ryan	10.36	10.54	18					18	SCUBA		
			Trevor Winton	12.35	13.39	64					64	SCUBA		
8/02/2017	James Matthews sleeper	sleeper site setup and test sled	Mack McCarthy										Dirk Hartog	1.5-2.0
			Ross Anderson											
			Deb Shefi	12.45	13.00	15					15	SSBA		
			Rebecca Ryan	12.45	13.00	15					15	SSBA		
			Vicki Richards											
			John Carpenter	11.54	13.11	77					77	SCUBA		
			Trevor Winton	11.54	12.54	60	68	14.02	14.25	23	83	SCUBA		
9/02/2017	James Matthews sleeper	install star pickets and concrete blocks	Mack McCarthy										Dirk Hartog	1.5-2.0
			Vicki Richards											
			John Carpenter	11.05	12.36	91					91	SCUBA		
			Trevor Winton	11.05	12.36	91					91	SCUBA		
13/02/2017	James Matthews sleeper	dredging - sleeper burial	Mack McCarthy					13.39	14.00	21	21	SSBA	Dirk Hartog	1.5-2.0
			Ross Anderson											
			Deb Shefi	11.00	13.11	131.00					131	SSBA		
			Trevor Winton	11.00	13.11	131.00	28	13.39	14.00	21	152	SSBA		

Table A.1 Field record, *James Matthews* wrecksite and James Matthews sleeper site (cont'd)

date	site	main purpose	dive details									vessel	max water depth (m)
			field team members	dive 1			surface interval (mins)	dive 2			total dive time for day (mins)	dive equipment		
				time entry	time exit	total dive time (mins)		time entry	time exit	total dive time (mins)				
14/02/2017	James Matthews sleeper	dredging - sleeper burial	Mack McCarthy										Dirk Hartog	1.5-2.0
			John Carpenter	10.51	14.00	189					189	SCUBA		
			Rebecca Ryan											
			Trevor Winton	10.47	14.00	193					193	SSBA		
15/02/2017	James Matthews sleeper	dredging - sleeper burial	Mack McCarthy	11.27	15.15	228					228	SSBA	Dirk Hartog	1.5-2.0
			Trevor Winton	11.15	15.15	240					240	SSBA		
			Jeremy Green											
			John Carpenter											
16/02/2017	James Matthews sleeper	dredging - sleeper burial	Ross Anderson										Dirk Hartog	1.5-2.0
			Mack McCarthy	11.15	13.20	125.00	20	13.40	15.15	95	220	SSBA		
			Rebecca Ryan									SSBA		
			Trevor Winton	11.15	13.20	125.00	10	13.30	15.15	105	230			
17/02/2017	James Matthews sleeper	dredging - sleeper burial	Mack McCarthy	10.45	12.25	100.00	35	13.00	13.30	30	65	SSBA	Dirk Hartog	1.5-2.0
			Deb Shefi											
			Trevor Winton	11.00	12.25	85.00	25	12.50	13.40	50	135.00	SSBA		
8/03/2017	James Matthews sleeper	site levelling, recording distances, photographic record	Pat Baker	10.15	11.00	45					45	SCUBA	Sea Squirt	1.5-2.0
			Mack McCarthy											
			Trevor Winton	10.15	11.45	90					90	SCUBA		
30/05/2017	James Matthews sleeper	inspect site, trial sled	Mack McCarthy	11.50	12.00	10					10	SSBA	Dirk Hartog, Wally, surf ski	1.5-2.0
			Trevor Winton	12.30	2.00	90	5	2.05	3.45	100	190	SCUBA		
			Kalle Kasi											
			Kevin Edwards											

Table A.1 Field record, *James Matthews* wrecksite and James Matthews sleeper site (cont'd)

date	site	main purpose	dive Details									vessel	max water depth (m)
			field team members	dive 1			surface interval (mins)	dive 2			total dive time for day (mins)	dive equipment		
				time entry	time exit	total dive time (mins)		time entry	time exit	total dive time (mins)				
6/06/2017	James Matthews sleeper	install side pickets, calibrate GNSS positioning system	Patrick Morrison	1.25	2.30	65					65	SCUBA	Dirk Hartog	1.5-2.0
			Trevor Winton	12.50	2.30	100					100	SCUBA		
			Mack McCarthy											
			Doug Bergerson											
7/07/2017	*James Matthews,* James Matthews sleeper	SBP measurements	Mack McCarthy										Dirk Hartog	1.5-2.0
			Doug Bergersen											
			Patrick Morisson	11.00	11.30	30					30	SCUBA		
			Steve Wells	11.00	11.30	30					30	SCUBA		
			Trevor Winton	10.45	11.30	45					45	SCUBA		
28/06/2017	*James Matthews,* James Matthews sleeper	measure height and location of besser blocks, and trial magnetometer survey	Jeremy Green										Dirk Hartog	1.5-2.0
			Ross Anderson	10.06	10.23	17					17			
			Deb Shefi											
			Trevor Winton	9.55	10.23	28					28			
15/03/2018	*James Matthews*, James Matthews sleeper	sediment coring for pore water analyses. Inspected sleeper site and *James Matthews* site for geo-reference marks.	Mack McCarthy										Dirk Hartog	2.5-3.0
			Vicki Richards											
			Jon Carpenter											
			Iva Cirkovick									snorkel		
			Mitch Cadden	11.45	12.45	60						snorkel/SSBA		
			Trevor Winton	11.32	13.08	96	66	14.14	14.27	8	104	SCUBA		

Table A.1 Field record, *James Matthews* wrecksite and James Matthews sleeper site (cont'd)

date	site	main purpose	dive details									vessel	max water depth (m)
			field team members	dive 1			surface interval (mins)	dive 2			total dive time for day (mins)	dive equipment		
				time entry	time exit	total dive time (mins)		time entry	time exit	total dive time (mins)				
11/04/2018	James Matthews sleeper	burial of additional sleepers	Trevor Winton	10.54	11.15	21	18	11.33	12.16	43		SCUBA	Dirk Hartog	2.7 - 2.9
			Trevor Winton				24	12.4	14.18	98	162	SCUBA		
			Mack McCarthy											
			Maddy Fowler					12.41	14.18	98	98	SCUBA		
			Patrick Morrison	10.54	11.15	21	18	11.33	12.16	43	61	SCUBA		
			Tash Trenear											
			Kalle Kasi											
18/04/2018	James Matthews sleeper	completion of burial of additional sleepers, clean endplates, remove site tapes	Trevor Winton	10.32	10.59	27	14	11.13	12.12	59		SCUBA	Dirk Hartog	2.5-2.8
			Trevor Winton				18	12.31	13.55	85	171	SCUBA		
			Mack McCarthy											
			Maddy Fowler					12.31	13.55	85	85	SCUBA		
			Patrick Morrison	10.45	12.15	90					90	SSBA		
			Kalle Kasi											
9/05/2018	James Matthews sleeper	trialled new sled, cut end plate lengths, drove extra star pickets, collected extra cores for in situ density analyses	Trevor Winton	11.01	11.09	9	53	12.02	12.59	57			Dirk Hartog	2.6 - 2.8
			Trevor Winton				30	13.27	13.41	14	80	SCUBA		
			Jeremy Green											
			Ross Anderson											
			Ian McCann					12.02	12.59	57	57	SCUBA		
			Mitch Cadden					12.02	12.59	57	57	SCUBA		

Table A.1 Field record, *James Matthews* wrecksite and James Matthews sleeper site (cont'd)

date	site	main purpose	dive details									vessel	max water depth (m)
			field team members	dive 1 time entry	dive 1 time exit	dive 1 total dive time (mins)	surface interval (mins)	dive 2 time entry	dive 2 time exit	dive 2 total dive time (mins)	total dive time for day (mins)	dive equipment		
18/05/2018	*James Matthews,* James Matthews sleeper	SBP measurements using sled, geo-referencing *James Matthews* site	Ross Anderson										Dirk Hartog and Seaspray	2.8 - 3.1
			Trevor Winton	15.52	11.03	11	74	12.17	12.41	24				
			Trevor Winton	13.31	13.34	3	60	14.34	15.14	40				
			Trevor Winton	16.07	16.24	17					95	SCUBA		
			Patrick Morrison											
			Ian McCann	12.17	12.41	24	110	14.34	15.14	40	64			
			Doug Bergerson											
			Mack McCarthy	16.07	16.24	17					17			
7/11/2018	James Matthews sleeper	retrieved 8 timber blocks and 3 additional sediment cores	Trevor Winton	11.41	11.54	13	65	12.59	13.28	29	42	SCUBA	Dirk Hartog	2.4 m
			Mack McCarthy											
			Deb Shefi											
			Patrick Morrison	11.41	11.54			12.59	13.28	29	29	Snorkelling/ SCUBA		
19/06/2019	James Matthews sleeper	sleeper positional measurements with sled and RTK DGPS	Trevor Winton	10.46	11.21	35		1.43	1.58	15	50	SCUBA	Dirk Hartog	2.5 m
			Ross Anderson											
			Deb Shefi	12.34	1.06	42					42	SCUBA		
			Patrick Morrison	12.34	1.06	42					42	SCUBA		
			Iva Cirkovick											

Table A.2 Field record, Swan River sleeper site.

date	site	main Purpose	field team members	site access	max water depth (m)
6/02/2017	Swan River, East Fremantle	test sled buoyancy	Trevor Winton	car	wading
15/09/2017	Point Roe, Swan River	investigate suitable site for burial of sleepers in fine sediments	Trevor Winton	car	wading
29/09/2017	Coffee Point, South of Perth Yacht club, Swan River	investigate suitable site for burial of sleepers in fine sediments	Trevor Winton	car	wading
2/01/2018	Coffee Point	low tide burial of sleepers	Trevor Winton David Winton Ian Warne Alan Stephens	car	wading
3/01/2018	Coffee Point	low tide burial of sleepers	Trevor Winton David Winton Ian Warne Alan Stephens	car	wading
4/01/2018	Coffee Point	low tide burial of sleepers & blocks	Trevor Winton David Winton Ian Warne	car	wading
5/01/2018	Coffee Point	measure sleeper positions, smoothed seabed	Trevor Winton	car	wading
29/01/2018	Coffee Point	trial sled, smoothed seabed	Trevor Winton	car	wading
30/01/2018	Coffee Point	Re-trialled sled, modified end plate heights	Trevor Winton	car	wading
10/04/2018	Coffee Point	sediment coring	Trevor Winton	car	wading
6/05/2018	Coffee Point	placed star pickets	Trevor Winton	car	wading
8/05/2018	Coffee Point	trialled new sled	Trevor Winton Ian McCann Ian Warne	car	wading
17/05/2018	Coffee Point	SBP measurements using sled	Trevor Winton Doug Bergerson Ian McCann Helen & Sandy	cars	wading
20/05/2018	Coffee Point	RTK DGPS measurement of endplates	Trevor Winton	car	wading
29/05/2018	Coffee Point	in situ density cores	Trevor Winton	car	wading
11/10/2018	Coffee Point	sediment coring, removal of timber blocks	Trevor Winton	car	wading

Table A.3 Sleeper locations and burial depths, James Matthews sleeper site.

sleeper number	distance from NE star-pickets (m)	sleeper type	date of burial	at time of SBP measurements			
				7/06/2018		18/05/2018	
				average height of slot above seabed (cm)	Actual burial depth (cm)	average height of slot above seabed (cm)	actual burial depth (cm)
Besser Block	0.6		May 18				
1	1	P20 $_{(22)}$	11/04/2018			3.25	16.75
2	1.9	P20	11/04/2018			7.5	12.5
Besser Block	2.2		Jun 2017, removed May 2018				
3	2.8	P20 $_{(22)}$	11/04/2018			0	20
4	3.7	P^30	9/02/2017	2	28	0	30
5	4.7	P30	9/02/2017	1	29	4	26
6	6.05	P30	13/02/2017	3	27	5	25
7	7.3	P10	13/02/2017	3	7	3	7
8	8.35	P50	13/02/2017	9	41	10	40
9	9.15	P30	13/02/2017	1	29	3	27
10	10.26	P10	14/02/2017	0	10	0.5	9.5
11	11.16	O30	14/02/2017	3	27	7.5	22.5
12	12.26	P^30 [a]	14/02/2017	1	29	5	25
Besser Block	13.01		May 2018				
13	13.85	O30	15/02/2017	0	30	0	30
14	15.6	P^30	15/02/2017	0	30	0	30
15	16.35	P50	15/02/2017	1	49	3	47
16	17.25	P50	15/02/2017	5	45	4.5	45.5
17	18.6	O30	15/02/2017	1	29	0	30
18	19.72	P10/30	15/02/2017	0	10	2	8
19	21.55	P10/30/50	15/02/2017	1	9	4.5	5.5
20	23.23	P10	15/02/2017	0	10	-1	11
21	24.23	O20	18/04/2018			-3.5	23.5
22	25.03	J20	18/04/2018			-3	23
23	25.73	J30	18/04/2018			-5	35
24	26.53	S20	18/04/2018			-7.5	27.5
25	27.33	S30	18/04/2018			0	30
26	28.23	S50	11/04/2018			4	46

[a] plus Besser Block until May 2018
P20 $_{(22)}$: pine sleeper inclined 22.5 degrees to horizontal
P^30: pine sleeper with vertical grain
P10/30/50: multi-stacked pine sleepers with 10, 30 and 50 cm DoB
10/20/30/50: nominal burial depth (cm)

Table A.4 Sleeper locations and burial depths, Swan River sleeper site.

sleeper/block number	sleeper/block type	distance from western stake (m)	burial depth at time of SBP measurements	
			average height of slot above riverbed (cm)	actual burial depth (cm)
	Besser Block	0.5	14.0	
1	S20	1.02	- 0.5	20.5
2	J30	2.26	4.5	25.5
3	P30	4.72	2.5	27.5
4	S50	6.00	4.5	45.5
5	P10	6.82	1.0	9.0
6	O30	7.80	2.5	27.5
7	P20	8.81	0.5	19.5
8	O30	10.28	5.0	25.0
9	J30	11.77	4.0	26.0
10	P10	12.90	1.0	9.0
11	S30	13.94	-1.5	31.5
12	J50	14.73	2.0	48.0
13	P50	15.27	7.5	42.5
14	J50	15.83	8.0	42.0
15	P30	16.87	3.0	27.0
16	J20	17.80	0.0	20.0
17	P20	18.76	4.0	16.0
18	J20	19.87	0.0	20.0
	Besser Block		13.0	
19a, b	$J20_B$ / $J30_B$	20.54	4.0 / 11.0	16.0 / 19.0
20a, b	$P20_B$ / $P30_B$	21.07	2.0 / 10.0	18.0 / 20.0
21a, b	$O30_B$ / $P50_B$	21.82	1.0 / 20.0	29.0 / 30.0
22a, b	$P20_B$ / $J20_B$	22.66	3.0 / 7.0	17.0 / 13.0

P: pine, O: oak, J: jarrah, S: steel
10/20/30/50: nominal burial depth (cm)
$_B$ block

Table A.5 James Matthews sleeper location, sleeper positions

RTK ID	sleeper #	latitude (MGA50)	longitude (MGA50)
GS0002	1	-32°07'54.7086	115°44'38.5827
GS0003	2	-32°07'54.7194	115°44'38.5999
GS0004	3	-32°07'54.7406	115°44'38.6260
GS0005	4	-32°07'54.7655	115°44'38.6542
GS0006	5	-32°07'54.7874	115°44'38.6795
GS0007	6	-32°07'54.8201	115°44'38.7231
GS0008	7	-32°07'54.8525	115°44'38.7527
GS0009	8	-32°07'54.8702	115°44'38.7811
GS00010	9	-32°07'54.9131	115°44'38.8411
GS00011	10	-32°07'54.9375	115°44'38.8696
GS00012	11	-32°07'54.9571	115°44'38.8898
GS00013	12	-32°07'54.9833	115°44'38.9222
GS00014	BB	-32°07'54.9999	115°44'38.9443
GS00015	13	-32°07'55.0001	115°44'38.9445
GS00016	14	-32°07'55.0224	115°44'38.9743
GS00017	15	-32°07'55.0326	115°44'38.9889
GS00018	16	-32°07'55.0704	115°44'39.0469
GS00019	17	-32°07'55.0841	115°44'39.0700
GS00020	18	-32°07'55.1105	115°44'39.1073
GS00021	19	-32°07'55.1102	115°44'39.1074
GS00022	20	-32°07'55.1368	115°44'39.1385
GS00023	21	-32°07'55.1790	115°44'39.1900
GS00024	22	-32°07'55.1792	115°44'39.1890
GS00025	23	-32°07'55.2166	115°44'39.2362
GS00026	24	-32°07'55.2396	115°44'39.2590
GS00027	25	-32°07'55.2768	115°44'39.3099
GS00028	26	-32°07'55.3140	115°44'39.3670
GS00029	27	-32°07'55.3428	115°44'39.3928

BB: Besser Block

Table A.6 Swan River sleeper location, endplate positions

RTK ID	location	latitude (MGA50)	longitude (MGA50)
GS0002	Western Besser Block	-32°00'14.516"	115°50'45.913"
GS0003	Sleeper 1 (Nth EP)	-32°00'14.517"	115°50'45.937"
GS0004	Sleeper 1 (Sth EP)	-32°00'14.531"	115°50'45.926"
GS0005	Sleeper 2 (Sth EP)	-32°00'14.557"	115°50'45.962"
GS0006	Sleeper 2 (Nth EP)	-32°00'14.544"	115°50'45.974"
GS0007	Sleeper 3 (Nth EP)	-32°00'14.597"	115°50'46.044"
GS0008	Sleeper 3 (Sth EP)	-32°00'14.611"	115°50'46.031"
GS0009	Sleeper 4 (Nth EP)	-32°00'14.618"	115°50'46.086"
GS0010	Sleeper 4 (Sth EP)	-32°00'14.631"	115°50'46.076"
GS0011	Sleeper 5 (Nth EP)	-32°00'14.639"	115°50'46.110"
GS0012	Sleeper 5 (Sth EP)	-32°00'14.652"	115°50'46.097"
GS0013	Sleeper 6 (Nth EP)	-32°00'14.654"	115°50'46.138"
GS0014	Sleeper 6 (Sth EP)	-32°00'14.668"	115°50'46.128"
GS0015	Sleeper 7 (Nth EP)	-32°00'14.678"	115°50'46.168"
GS0016	Sleeper 7 (Sth EP)	-32°00'14.691"	115°50'46.156"
GS0017	Sleeper 8 (Nth EP)	-32°00'14.708"	115°50'46.214"
GS0018	Sleeper 8 (Sth EP)	-32°00'14.720"	115°50'46.200"
GS0019	Sleeper 9 (Nth EP)	-32°00'14.735"	115°50'46.259"
GS0020	Sleeper 9 (Sth EP)	-32°00'14.748"	115°50'46.246"
GS0021	Sleeper 10 (Nth EP)	-32°00'14.760"	115°50'46.291"
GS0022	Sleeper 10 (Sth EP)	-32°00'14.772"	115°50'46.279"
GS0023	Sleeper 11 (Nth EP)	-32°00'14.779"	115°50'46.323"
GS0024	Sleeper 11 (Sth EP)	-32°00'14.792"	115°50'46.310"
GS0025	Sleeper 12 (Nth EP)	-32°00'14.796"	115°50'46.345"
GS0026	Sleeper 12 (Sth EP)	-32°00'14.809"	115°50'46.332"
GS0027	Sleeper 13 (Nth EP)	-32°00'14.805"	115°50'46.361"
GS0028	Sleeper 13 (Sth EP)	-32°00'14.819"	115°50'46.349"
GS0029	Sleeper 14 (Nth EP)	-32°00'14.816"	115°50'46.379"
GS0030	Sleeper 14 (Sth EP)	-32°00'14.829"	115°50'46.367"
GS0031	Sleeper 15 (Nth EP)	-32°00'14.837"	115°50'46.410"
GS0032	Sleeper 15 (Sth EP)	-32°00'14.850"	115°50'46.399"
GS0033	Sleeper 16 (Nth EP)	-32°00'14.860"	115°50'46.438"
GS0034	Sleeper 16 (Sth EP)	-32°00'14.871"	115°50'46.425"
GS0035	Sleeper 17 (Nth EP)	-32°00'14.878"	115°50'46.465"
GS0036	Sleeper 17 (Sth EP)	-32°00'14.891"	115°50'46.452"
GS0037	Sleeper 18 (Nth EP)	-32°00'14.902"	115°50'46.497"
GS0038	Sleeper 18 (Sth EP)	-32°00"14.914"	115°50'46.485"
GS0039	Eastern Besser Block	-32°00'14.914"	115°50'46.503"

EP: endplate

Table A.7 James Matthews wrecksite, mean (centroid) seabed location of slate mound and windlass

RTK ID	location	latitude (MGA50)	longitude (MGA50)
GS0003	windlass	-32°07'54.922"	115°44'37.836"
GS0004		-32°07'54.923"	115°44'37.843"
GS0005	slate mound	-32°07'54.571"	115°44'37.448"
GS0006		-32°07'54.571"	115°44'37.451"
GS0007		-32°07'54.570"	115°44'37.451"

B. SEDIMENT CHARACTERISTICS

Sediment descriptions and Particle Size Distribution (PSD)

Tables B.1 to B.8 provide down-core sediment descriptions, and photographs of shell/fragments greater than 1 mm for each10 cm sub-core level or for entire core, for sediment cores collected at the James Matthews sleeper site. Corresponding PSD plots are shown in Figures B.1 to B.8.

Tables B.9 to B.16 provide down-core sediment descriptions, and photographs of shell/fragments greater than 1 mm for each10 cm sub-core level or for entire core, for sediment cores collected at the Swan River sleeper site. Corresponding PSD plots are shown in Figures B.9 to B.16.

Sediment bulk density and porosity calculations

Tables B.17 and B.18 present all sediment core measurements and calculations for sediment bulk density and sediment porosity from cores collected at the James Matthews sleeper site and the Swan River sleeper site, respectively.

Sediment chemistry profiles

Dissolved oxygen (DO) profiles and redox (Eh) profiles along the sediment cores collected at the James Matthews sleeper site are presented in Figures B17 to B.26. Similar DO and Eh profiles along the sediment cores collected at the Swan River sleeper site are displayed in Figures B.27 to B.34.

Table B.1 Down-core sediment description, core 20, James Matthews sleeper site.

Depth (cm)	Description		shell/frags >1mm at sub-core depth levels (photographs by Trevor Winton)
0	yellow	medium-fine grained calcareous sand 1.7% shell/frags >1 mm	
1			
2	grading grey with depth		
3			
4			
5			
6			
7			
8			
9			
10		medium-fine grained calcareous sand 11.9% shell/frags > 1mm	
11			
12			
13			
14			
15			
16			
18			
20	lighter yellow grains	medium grained calcareous sand 16.5% shell/frags >1 mm	
22			
24			
28			
30		medium grained calcareous sand 1.8% shell/frags >1 mm	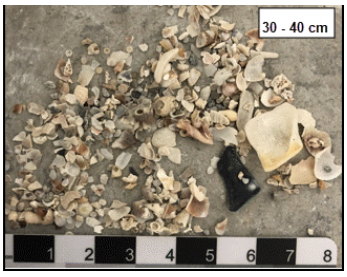
32			
34	yellowish grey		
36			
40			
42		medium grained calcareous sand 0.7% shell/frags >1 mm	
43			
44			
45			
46			
47			

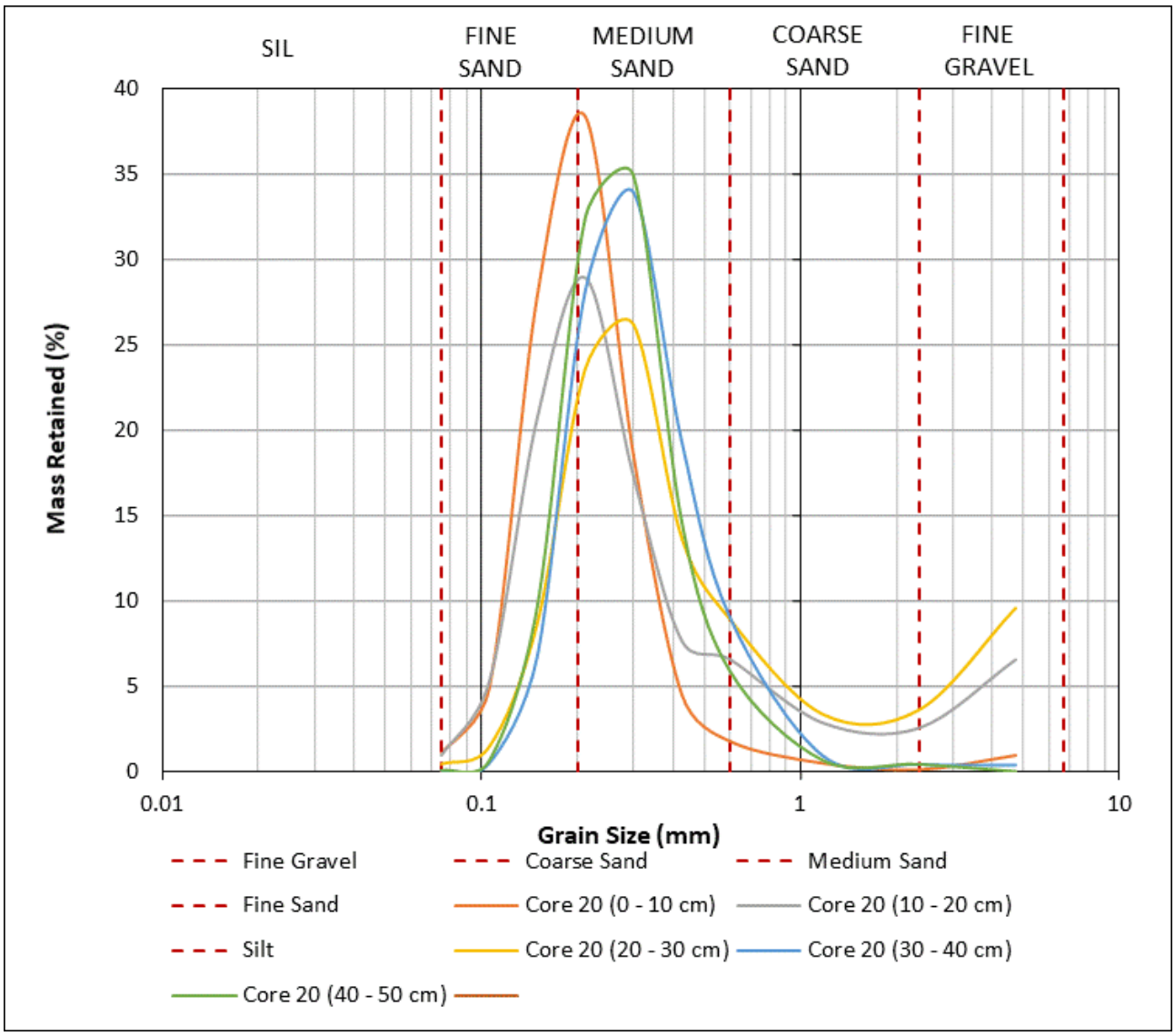

Figure B.1 PSD, core 20, James Matthews sleeper site.

Table B.2 Down-core sediment description, core 122, James Matthews sleeper site.

Depth (cm)	Description		shell/frags >1mm at sub-core depth levels (photographs by Trevor Winton)
0	yellowish band	Medium-Fine grained calcareous sands, 0.7 % shell/frags > 1mm	
1	grey		
2			
3			
4	dark grey, fine in appearance		
5			
6			
7			
8			
9	darker yellowish grey		
10		Medium-Fine grained calcareous sands, 4.4 % shell/frags > 1mm	
11			
12			
13			
14			
15	lighter yellowish grey, fine in appearance		
16			
18			
20		Medium grained calcareous sands, 5.3 % shell/frags > 1mm	
22			
24			
28	darker yellowish grey, coarser in appearance		
32		Medium grained calcareous sands, 0.7 % shell/frags > 1mm	
33			
36			
40			
42		Medium grained calcareous sands, 2.1 % shell/frags > 1mm	
44			
46	darker grey		
47			
48			
49			
50			
51			

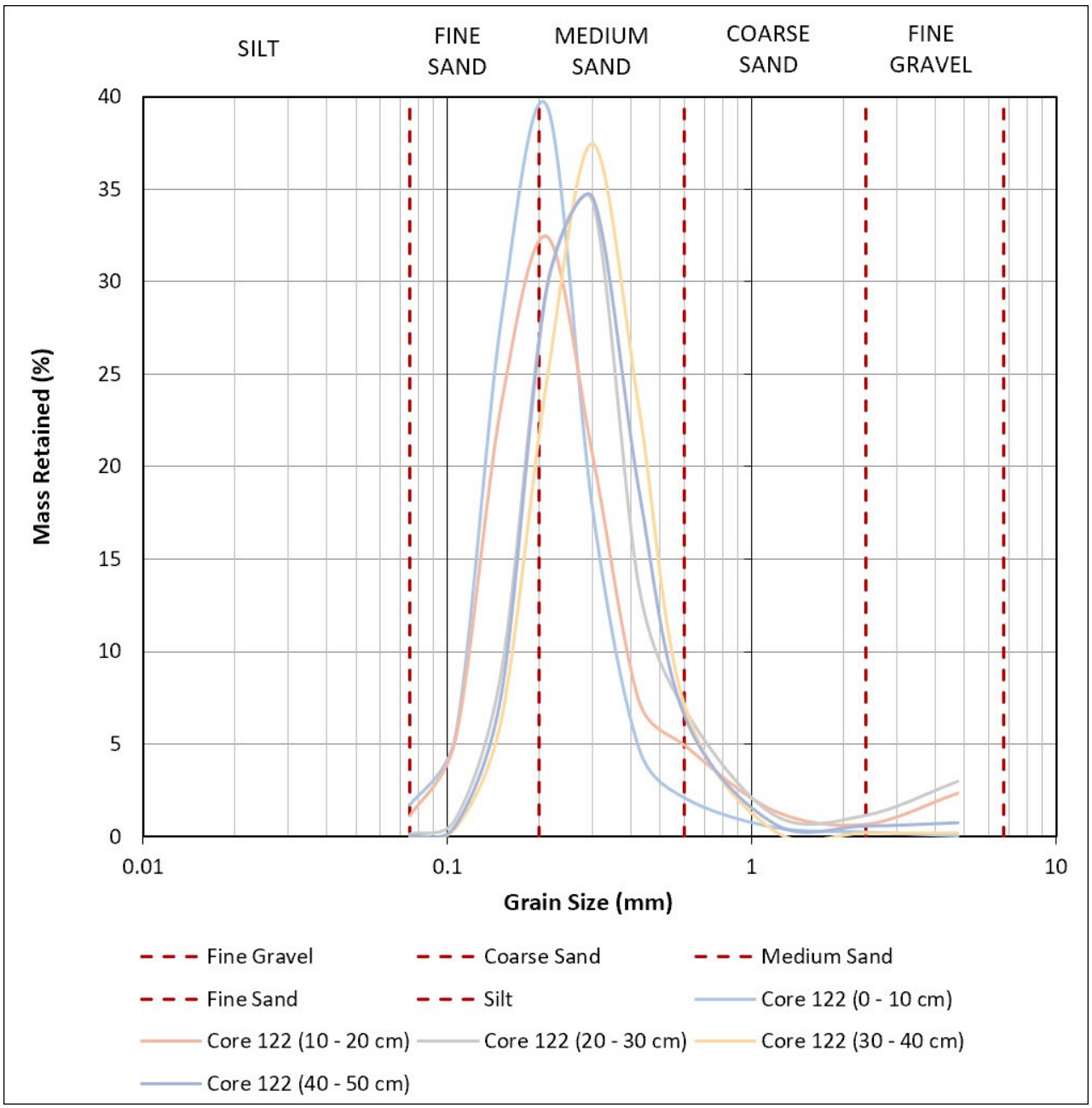

Figure B.2 PSD, core 122, James Matthews sleeper site.

Table B.3 Down-core sediment description, core 192, James Matthews sleeper site.

Depth (cm)	Description		shell/frags >1mm at sub-core depth levels (photographs by Trevor Winton)
0	greyish yellow	Medium to fine grained calcareous sand, 2.2 % shell/frags > 1mm	
1			
2			
3			
4			
5			
6			
7			
8			
9			
10		Medium to fine grained calcareous sand, 8.8 % shell/frags > 1mm	
11			
12			
13			
14	lightens to yellowish-grey		
15			
16			
18			
20		Med-Fine grained calcareous sand, 2.7% shell/frags > 1mm	
22	light – mid grey		
24			
26			
30		Medium grained calcareous sand, 1.2% shell/frags > 1mm	
31			
32			
33			
34			
36			
38			
40		Medium grained calcareous sand, 0.8 % shell/frags > 1mm	
41			
42			
43			
44			
45			
46			

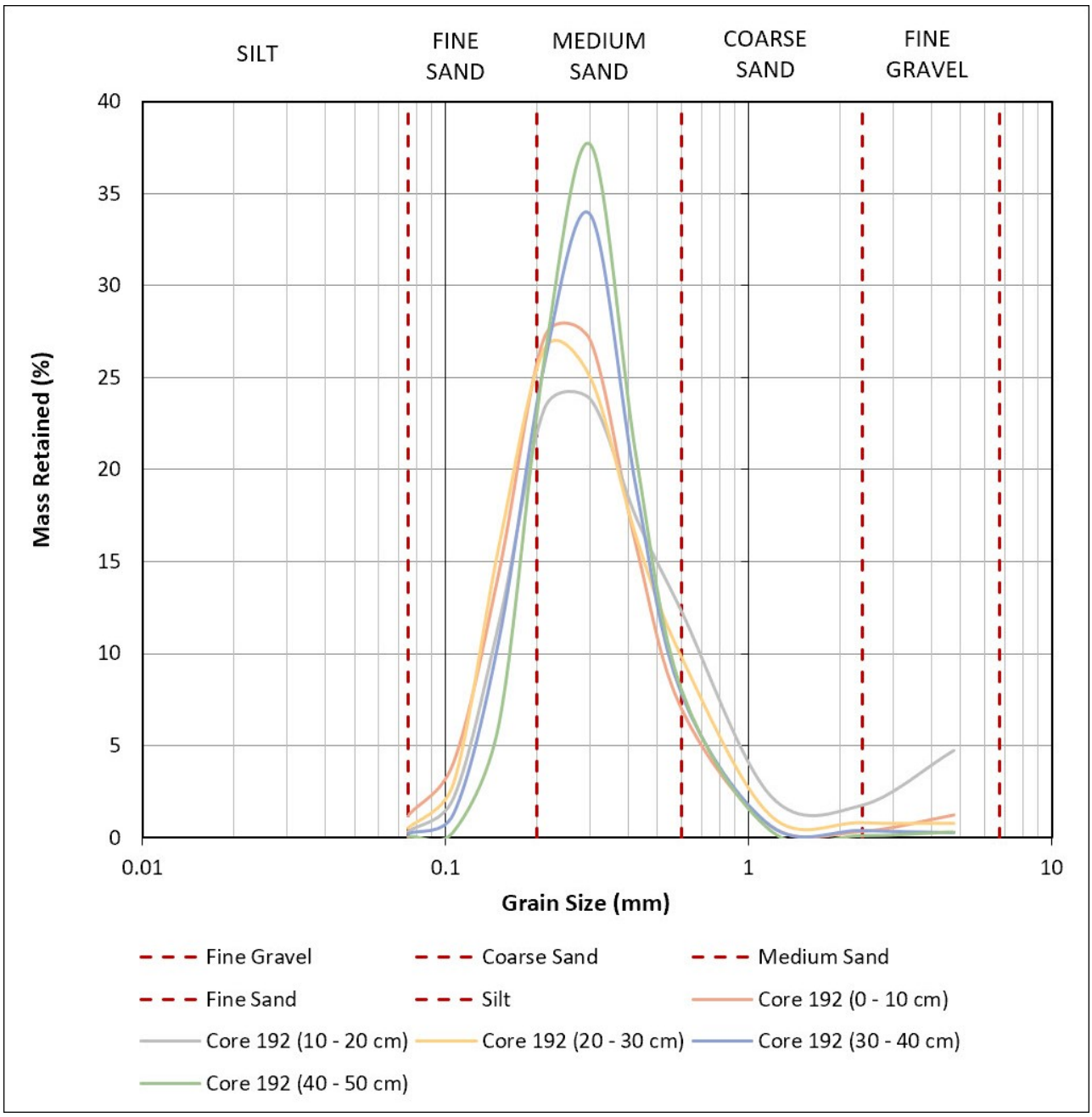

Figure B.3 PSD, core 192, James Matthews sleeper site.

Table B.4 Down-core sediment description, core 193, James Matthews sleeper site.

Depth (cm)	Description		shell/frags >1mm at sub-core depth levels (photographs by Trevor Winton)
0	light grey, slightly yellowish	Medium to fine grained calcareous sands, 3.4 % shell/frags >1mm	
1			
2			
3			
4	darker grey, appears coarser towards 15		
5			
6			
7			
8			
9			
10		Medium grained calcareous sands, 6.5 % shell/frags >1mm	
11			
12			
13			
14			
15			
16	slightly yellowish, finer appearance		
18			
20		Medium grained calcareous sands, 10.8 % shell/frags >1mm	
22			
24			
25			
26	greyer, coarser appearance		
28			
30	lighter colour, finer in appearance	Medium grained calcareous sands, 5.5 % shell/frags >1mm	
32			
34			
35	darker		
38			
39			
40			
41			

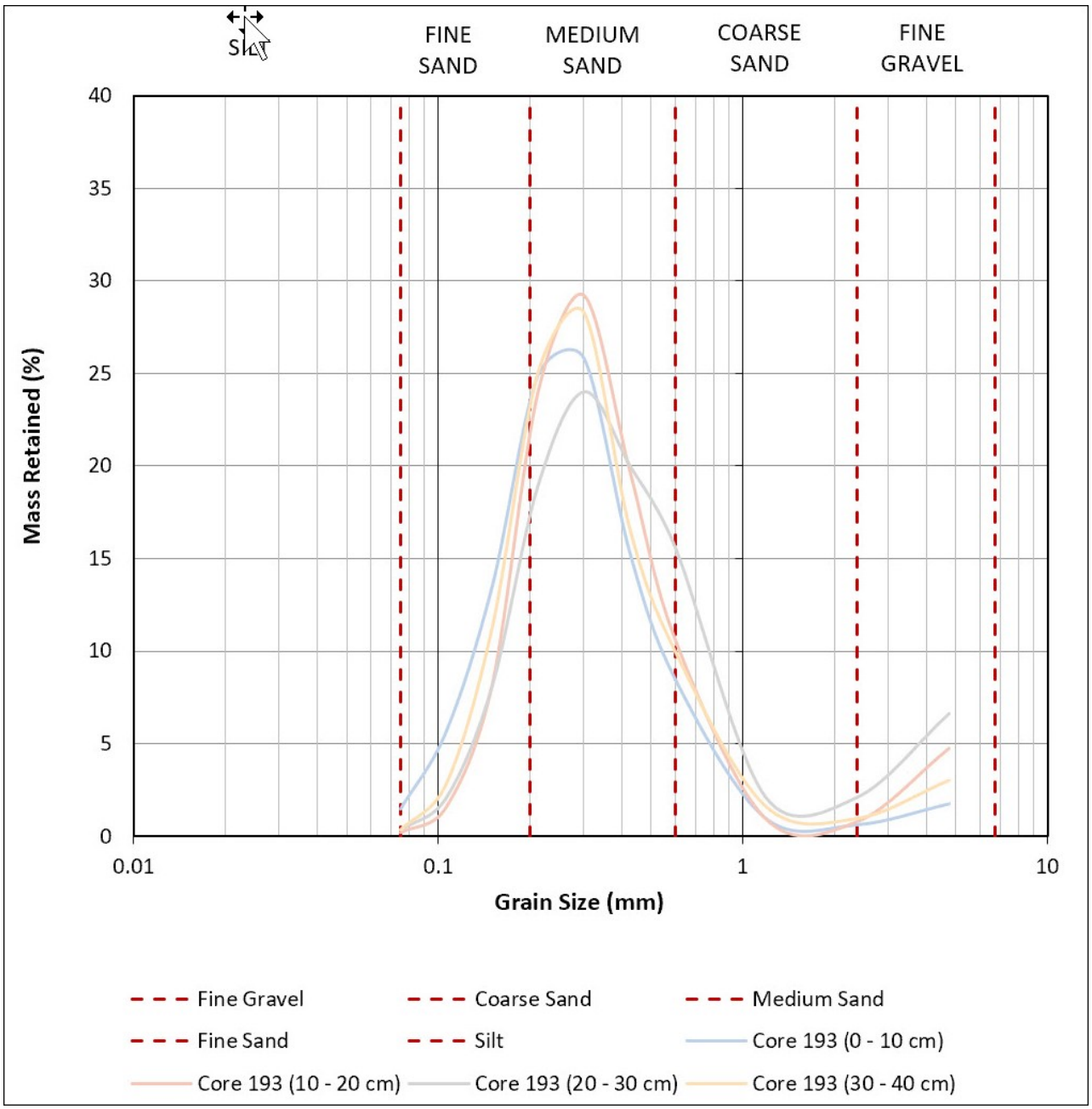

Figure B.4 PSD, core 193, James Matthews sleeper site.

Table B.5 Down-core sediment description, core 214, James Matthews sleeper site.

Depth (cm)	Description	shell/frags >1mm at sub-core depth levels (photograph by Trevor Winton)
0	medium calcareous sand, 2.1 % shell/frags > 1mm	
2		
4		
6		
8		
10		
12		
14		
16		
18		
20		
22		
24		
26		
28		
30		
32		
34		
36		
38		
40		
42		
44		
46		
48		
50		

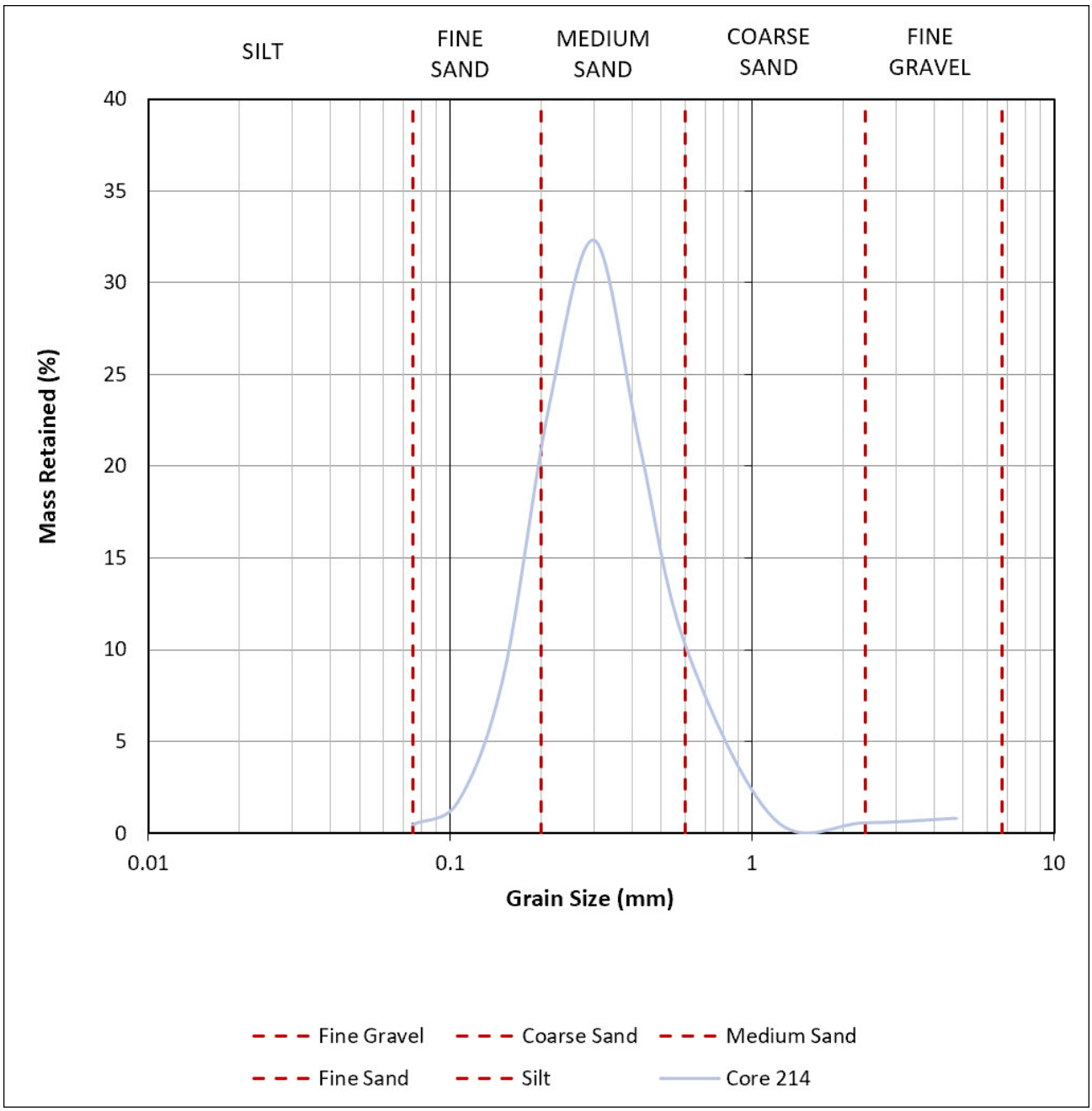

Figure B.5 PSD, core 214, James Matthews sleeper site.

Table B.6 Down-core sediment description, core 217, James Matthews sleeper site.

Depth (cm)	Description	shell/frags >1mm at sub-core depth levels (photograph by Trevor Winton)
0	medium to fine grained calcareous sand, 4.6 % shell/frags > 1mm	
2		
4		
6		
8		
10		
12		
14		
16		
18		
20		
22		
24		
26		
28		
30		
32		
34		
36		
38		
40		
42		
44		
46		
48		
50		

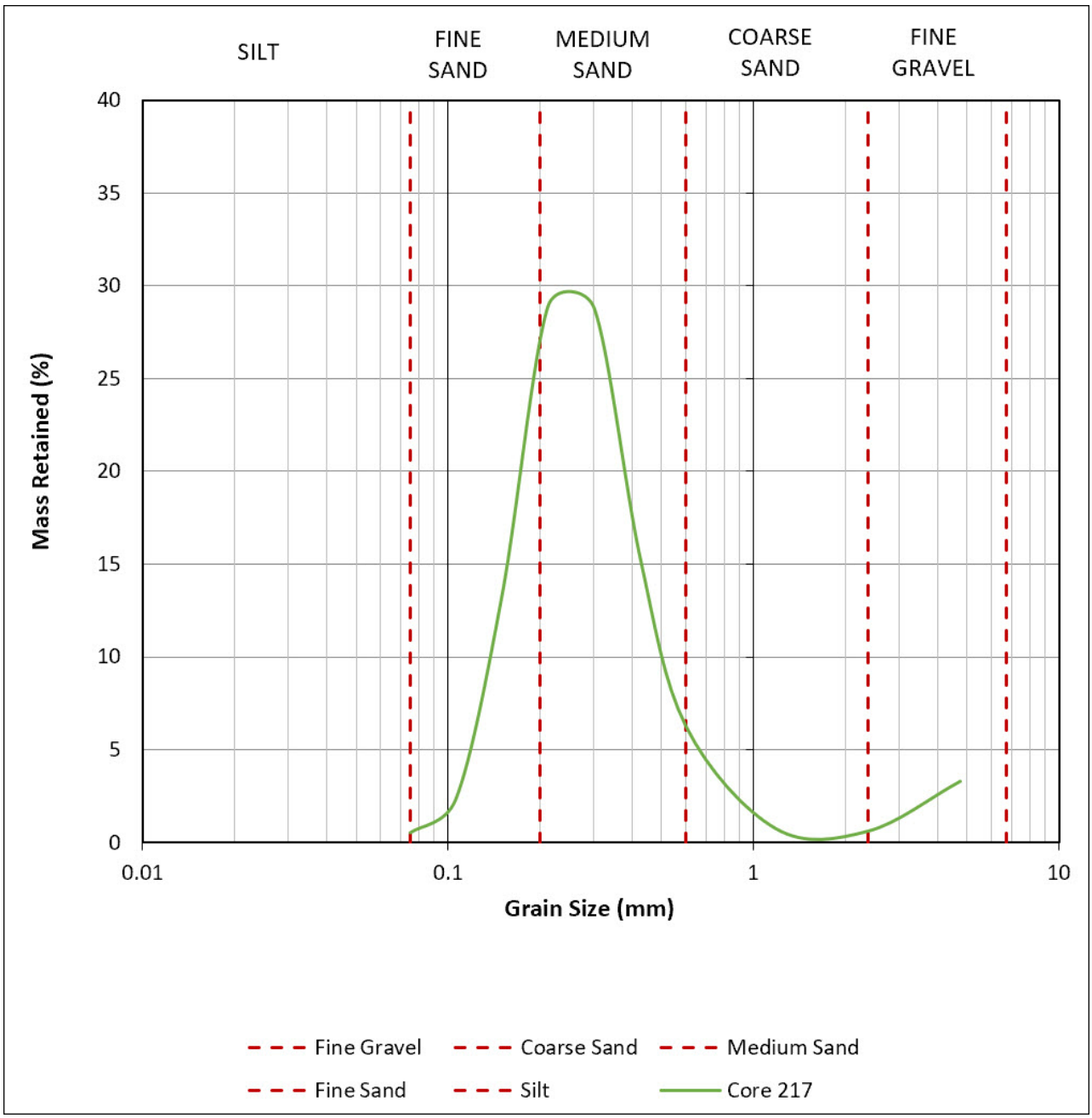

Figure B.6 PSD, core 217, James Matthews sleeper site.

Table B.7 Down-core sediment description, core 218, James Matthews sleeper site.

Depth (cm)	Description	shell/frags >1mm at sub-core depth levels (photograph by Trevor Winton)
0	medium to fine grained calcareous sand, 2.1 % shell/frags > 1mm	
2		
4		
6		
8		
10		
12		
14		
16		
18		
20		
22		
24		
26		
28		
30		
32		
34		
36		
38		
40		
42		
44		
46		
48		
50		

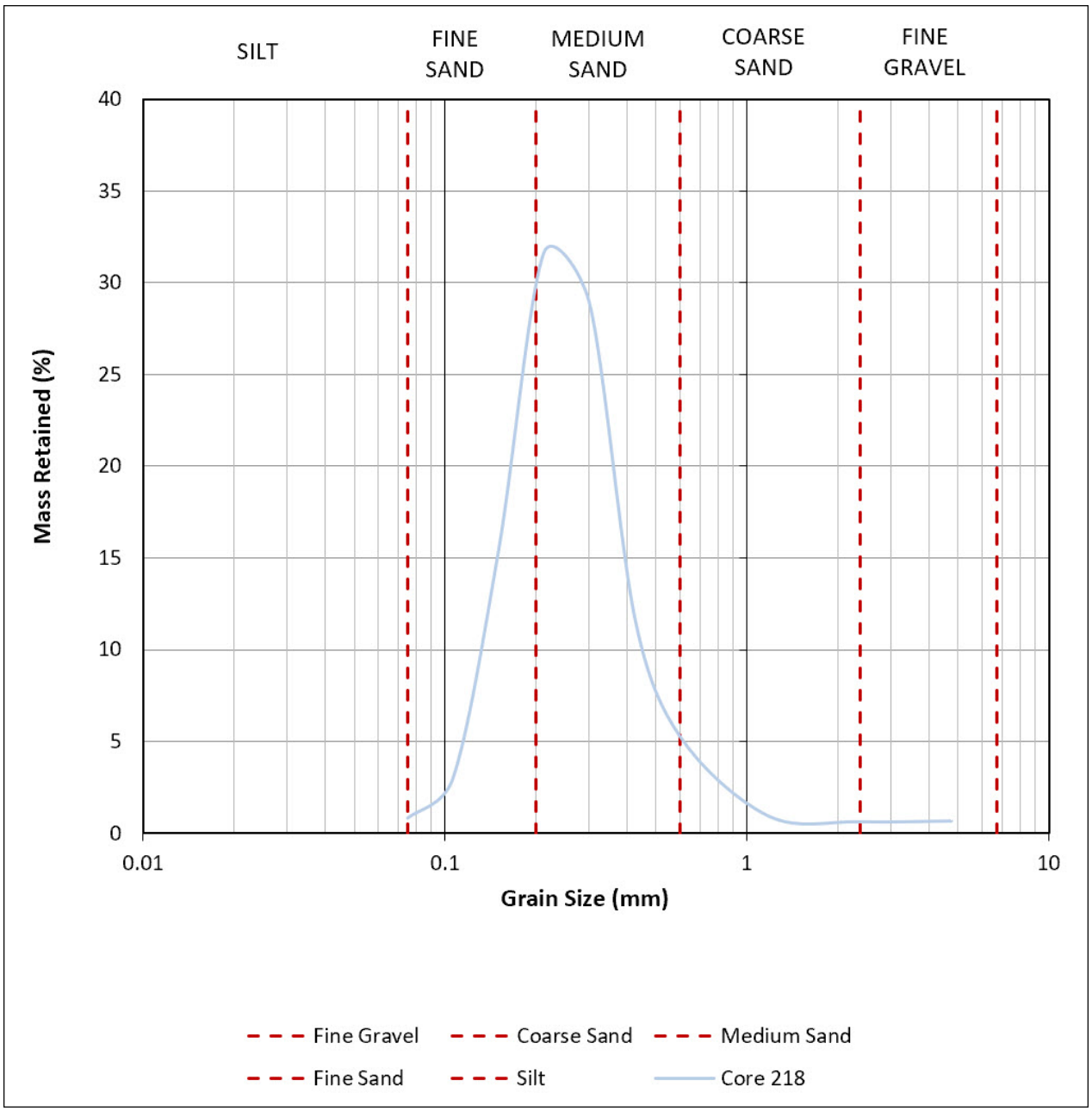

Figure B.7 PSD, core 218, James Matthews sleeper site.

Table B.8 Down-core sediment description, core 300, James Matthews sleeper site.

Depth (cm)	Description	shell/frags >1mm at sub-core depth levels (photograph by Trevor Winton)
0	medium to fine grained calcareous sand, 1.9 % shell/frags> 1mm	
2		
4		
6		
8		
10		
12		
14		
16		
18		
20		
22		
24		
26		
28		
30		
32		
34		
36		
38		
40		
42		
44		
46		
48		
50		

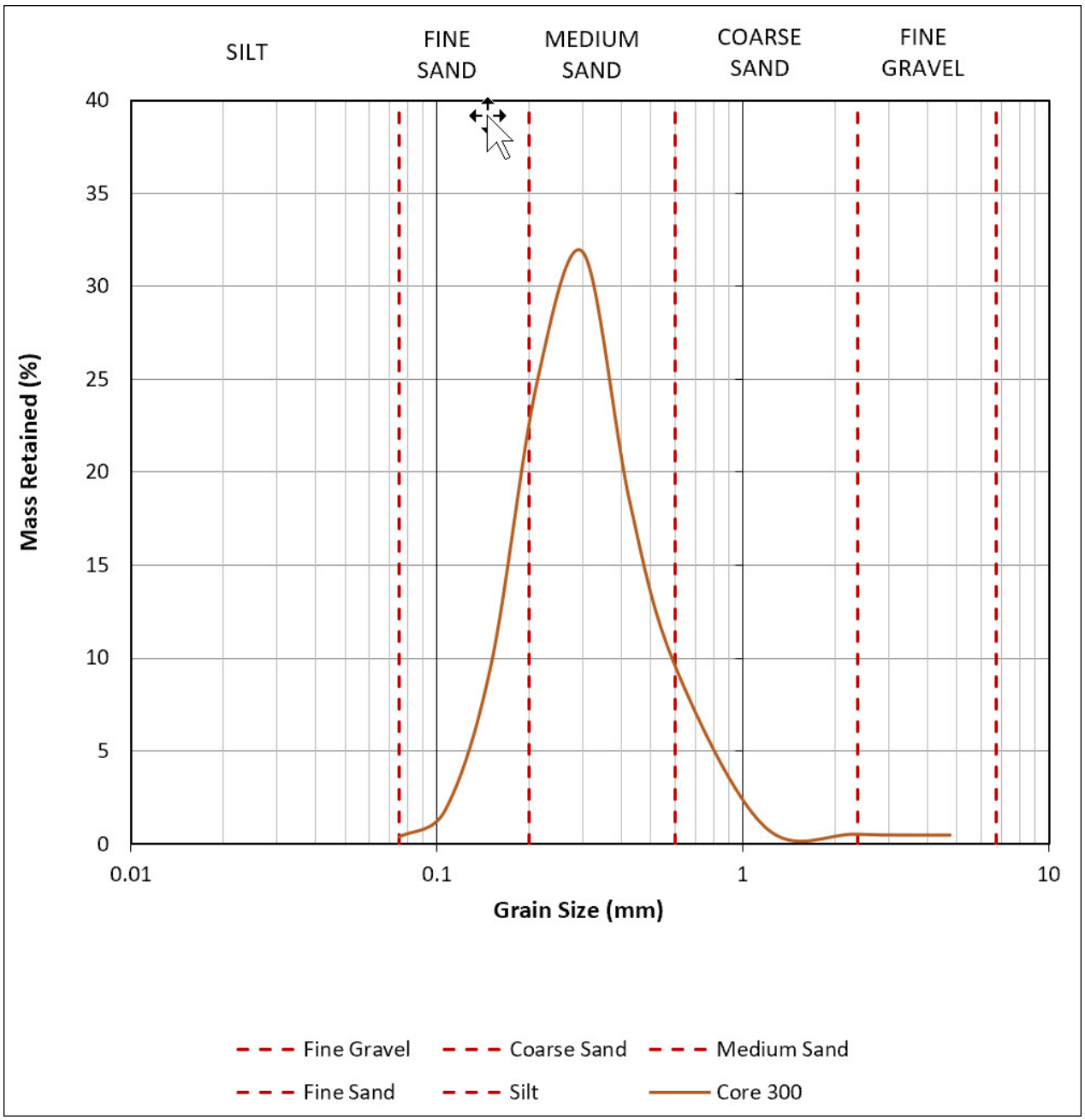

Figure B.8 PSD, core 300, James Matthews sleeper site.

Table B.9 Down-core sediment description, core 12, Swan River sleeper site.

Depth (cm)	Description		shell/frags >1mm at sub-core depth levels (photographs by Trevor Winton)
0	yellow, coarser in appearance	Medium to coarse grained siliceous sand, 2.3% shell/frags > 1mm	
1			
2			
3			
4			
5	black, yellow on opposite (lower) side		
6			
7			
8			
9			
10		Medium to coarse grained siliceous sand, 3.1% shell/frags > 1mm	
11			
12			
13			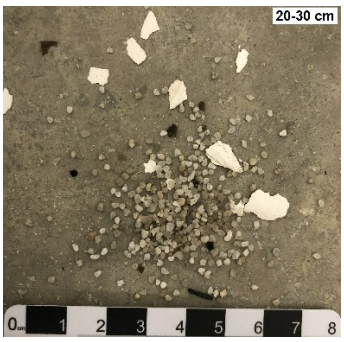
14			
15			
16			
17	yellowish grey, coarser in appearance		
18			
19			
20		Medium grained siliceous sand, 0.6% shell/frags > 1mm	
21			
22			
26	yellow, finer appearance		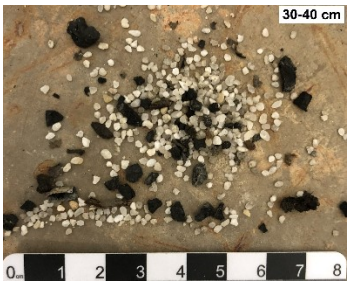
32			
34		Medium grained siliceous sand, 1.2% shell/frags > 1mm	
38			
42			
44		Medium grained siliceous sand, 0.7% shell/frags > 1mm	
46			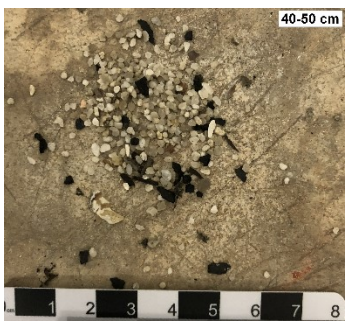
48			
50			
51			
52			
53			

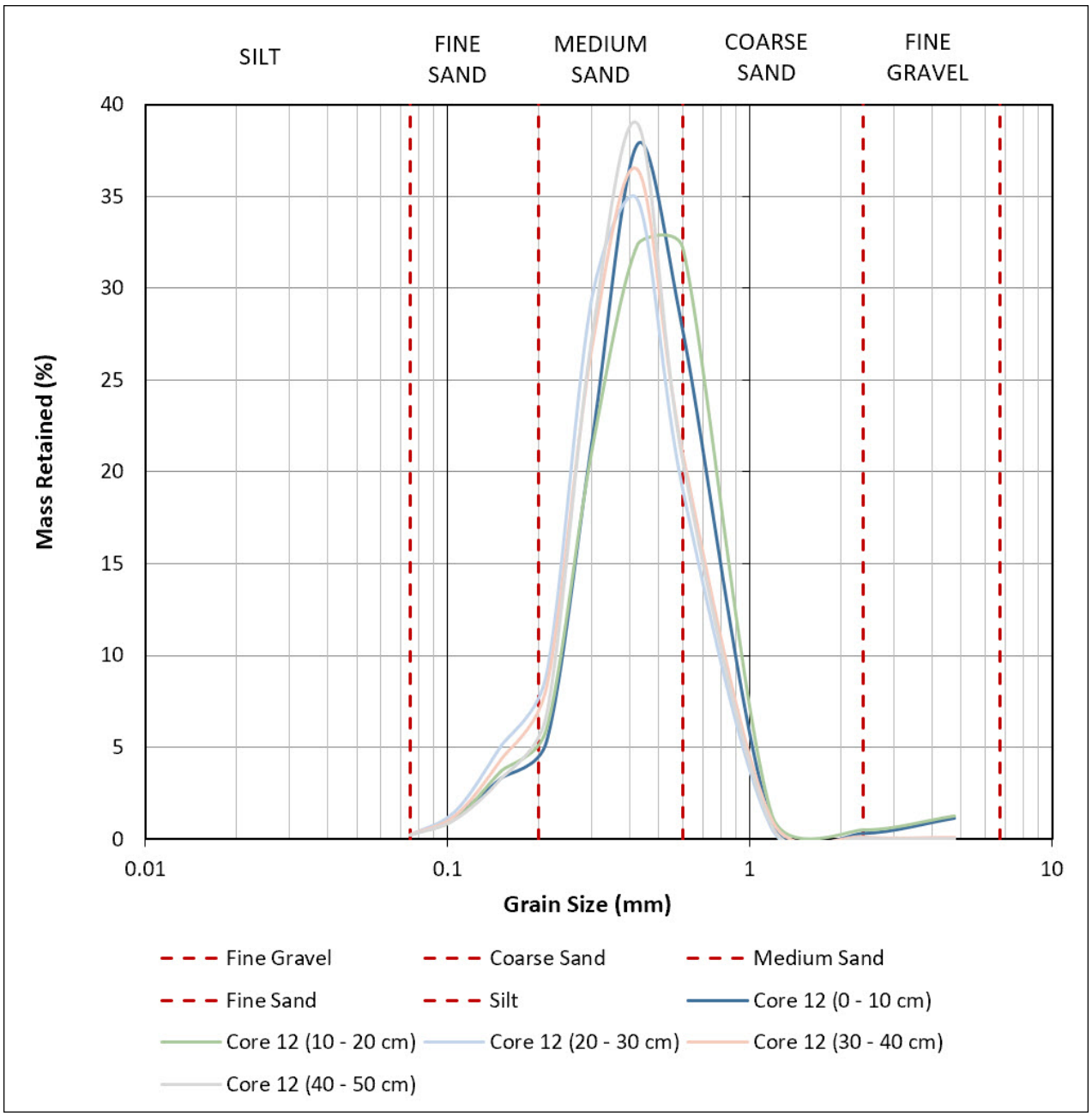

Figure B.9 PSD, core 12, Swan River sleeper site.

Table B.10 Down-core sediment description, core 17, Swan River sleeper site.

Depth (cm)	Description		shell/frags >1mm at sub-core depth levels (photographs by Trevor Winton)
0	yellow, coarser in appearance	Medium to coarse grained siliceous sand, 3.1% shell/frags > 1mm	
1			
2			
3	black band		
4	yellow, coarser in appearance		
5			
6			
7	grey intermixed with black		
8			
9			
10	black	Medium to coarse grained siliceous sand, 7.2% shell/frags > 1mm	
11			
12			
13			
14			
15			
16			
17	grey, finer in appearance		
18			
19			
20			
21	yellowish, finer in appearance	Medium grained siliceous sand, 0.6% shell/frags > 1mm	
22			
26			
30	yellowish with small black spots	Medium grained siliceous sand, 1.0% shell/frags > 1mm	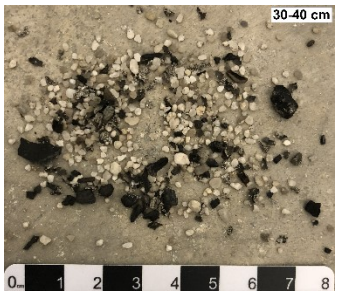
34			
38			
42			
44			
46			
47			
48	yellowish, finer in appearance	Medium grained siliceous sand, 0.4% shell/frags > 1mm	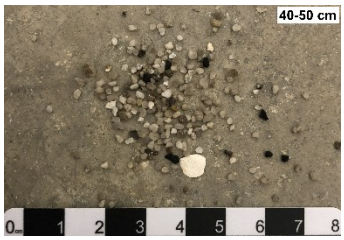
49			
50			

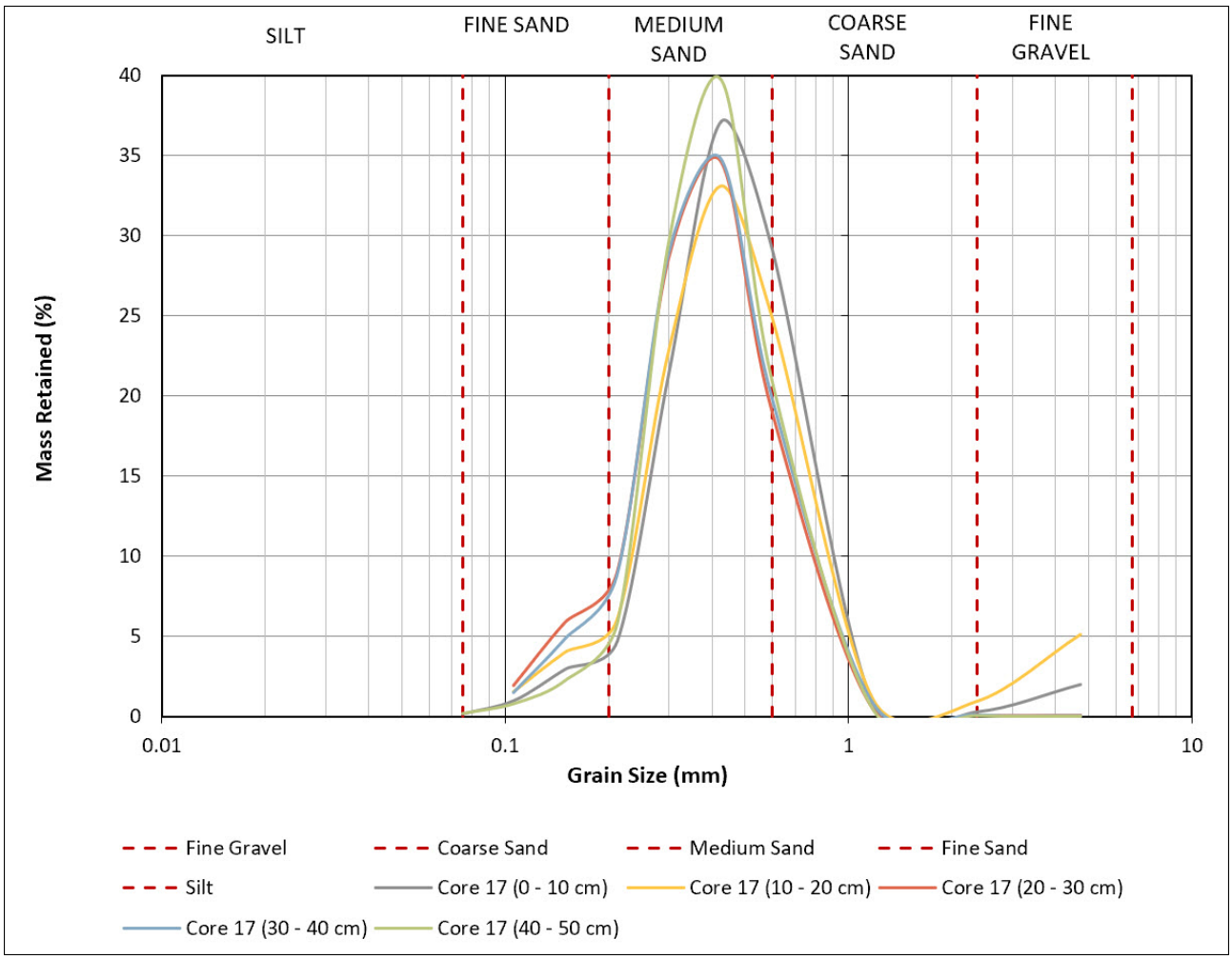

Figure B.10 PSD, core 17, Swan River sleeper site.

Table B.11 Down-core sediment description, core 169, Swan River sleeper site.

Depth (cm)	Description		shell/frags >1mm at sub-core depth levels (photographs by Trevor Winton)
0	yellow, coarse in appearance	medium grained siliceous sand, 2.1 % > 1mm	
1			
2			
3	greyish yellow		
4			
5			
6			
7			
8			
9			
10		medium grained siliceous sand, 1.1 % > 1mm	
11			
12	darker band, light shell (?) fragments		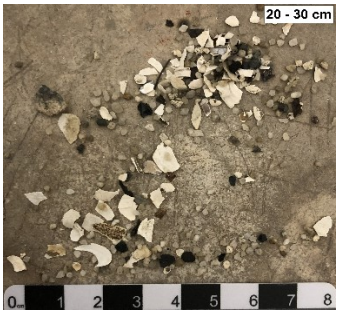
13			
14			
15			
16	darkish grey		
17			
18			
19			
20	yellowish grey	medium grained siliceous sand, 0.9 % > 1mm	
21			
23	darker yellowish grey, finer in appearance		
25			
26			
30	yellowish grey, occasional darker spot	medium grained siliceous sand, 2.2 % > 1mm	
34			
38			
42			
46		medium grained siliceous sand, 3.8 % > 1mm	
48			
49			
50			

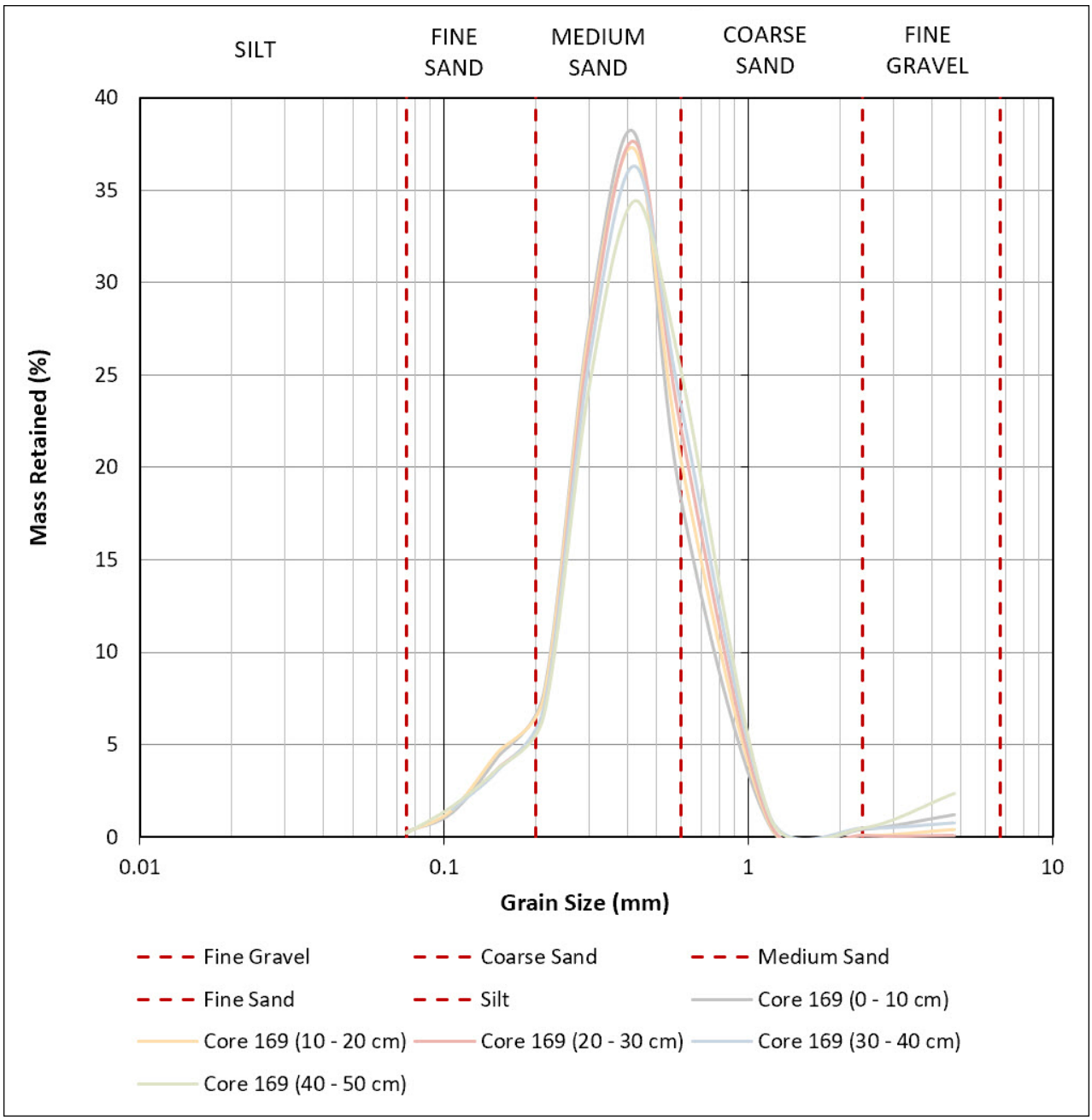

Figure B.11 PSD, core 169, Swan River sleeper site.

Table B.12 Down-core sediment description, core 176, Swan River sleeper site.

Depth (cm)	Description		shell/frags >1mm at sub-core depth levels (photographs by Trevor Winton)
0	yellow colour	medium grained siliceous sand, 2.4 % > 1mm	
1			
2			
3	dark grey		
4			
5			
6			
7			
8			
9			
10		medium grained siliceous sand, 1.8 % > 1mm	
11			
12			
13			
14			
15	dark grey–yellow		
16			
18			
20	dark grey	medium grained siliceous sand, 2.6 % > 1mm	
22			
24			
26	yellowy-grey		
28			
30	dark grey	medium grained siliceous sand, 2.3 % > 1mm	
32			
34			
36			
38	yellowy-grey		
40		medium grained siliceous sand, 2.9 % > 1mm	
42			
44	dark grey–yellow, very soft		
46			
48			
49			
50			

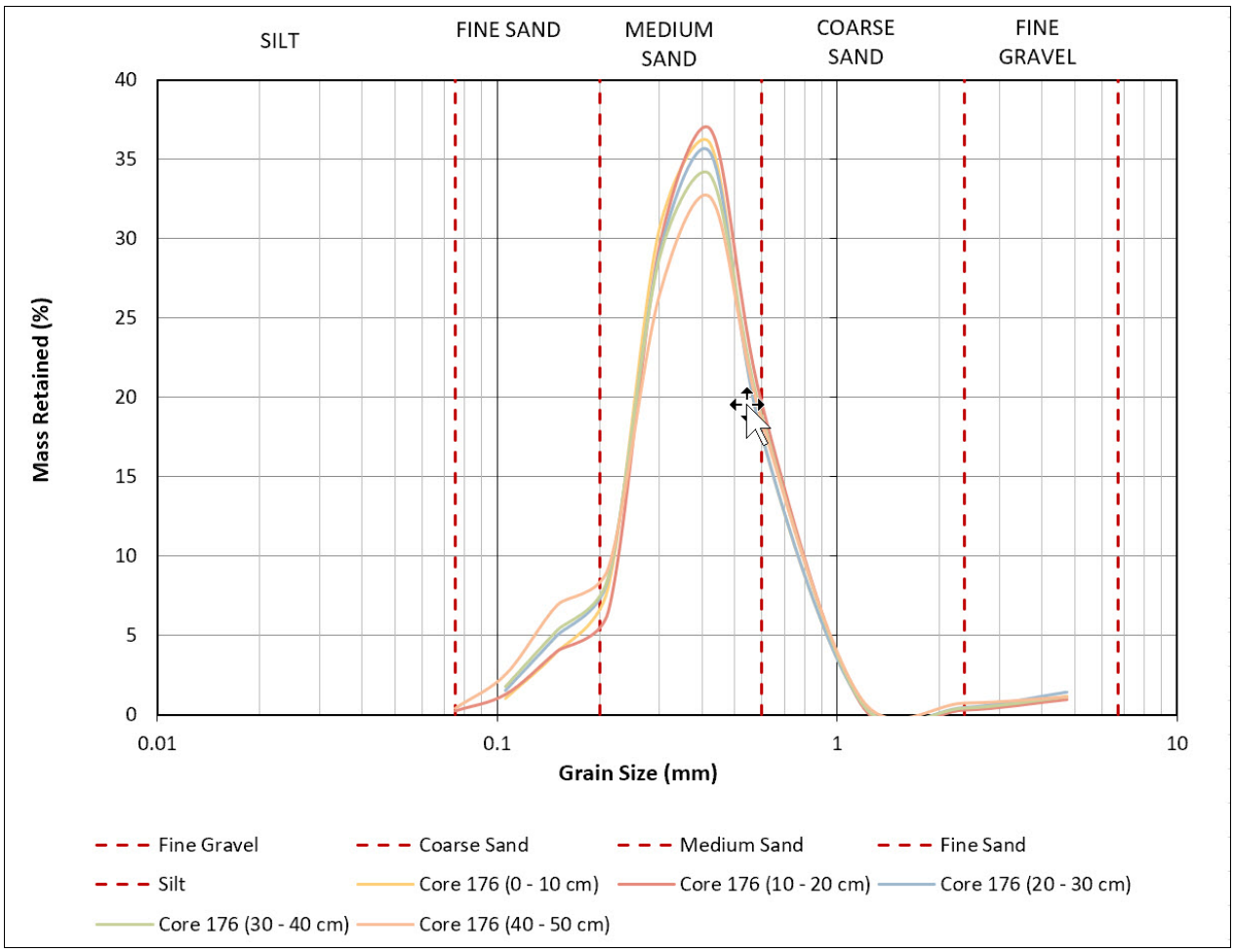

Figure B.12 PSD, core 176, Swan River sleeper site.

Table B.13 Down-core sediment description, core 301, Swan River sleeper site.

Depth (cm)	Description	shell/frags >1mm at sub-core depth levels (photograph by Trevor Winton)
0	medium grained siliceous sand, 5.3 % shell/frags > 1mm	
1		
2		
3		
4		
5		
6		
7		
8		
9		
10		
11		
12		
13		
14		
15		
16		
17		
18		
19		
20		
21		
22		
26		
32		
34		
38		
42		
44		
46		
48		
50		
51		
52		
53		

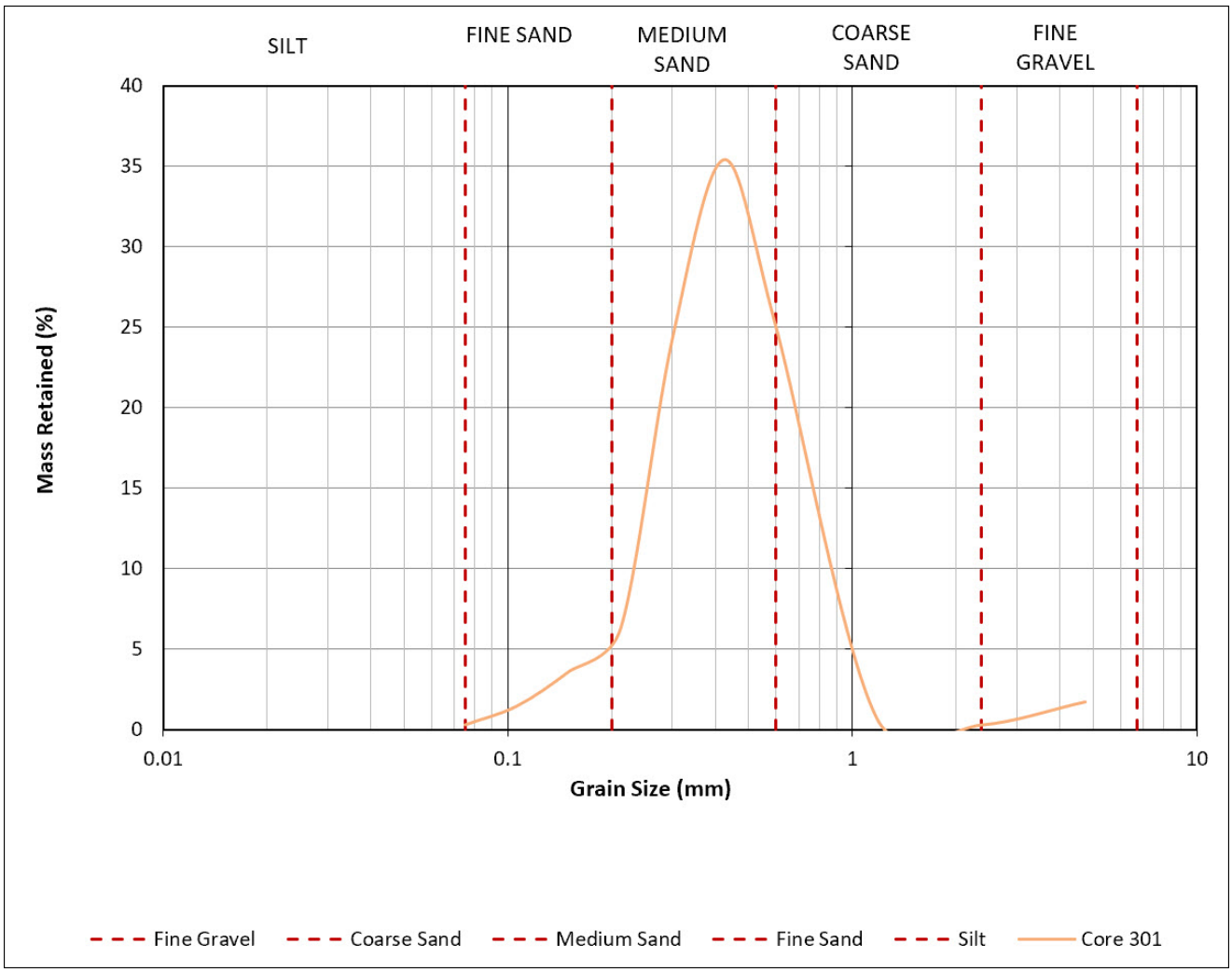

Figure B.13 PSD, core 301, Swan River sleeper site.

Table B.14 Down-core sediment description, core 302, Swan River sleeper site.

Depth (cm)	Description	shell/frags >1mm at sub-core depth levels (photograph by Trevor Winton)
0	medium siliceous sand, 1.3 % shell/frags > 1mm	
1		
2		
3		
4		
5		
6		
7		
8		
9		
10		
11		
12		
13		
14		
15		
16		
17		
18		
19		
20		
21		
22		
26		
32		
34		
38		
42		
44		
46		
48		
50		
51		
52		
53		

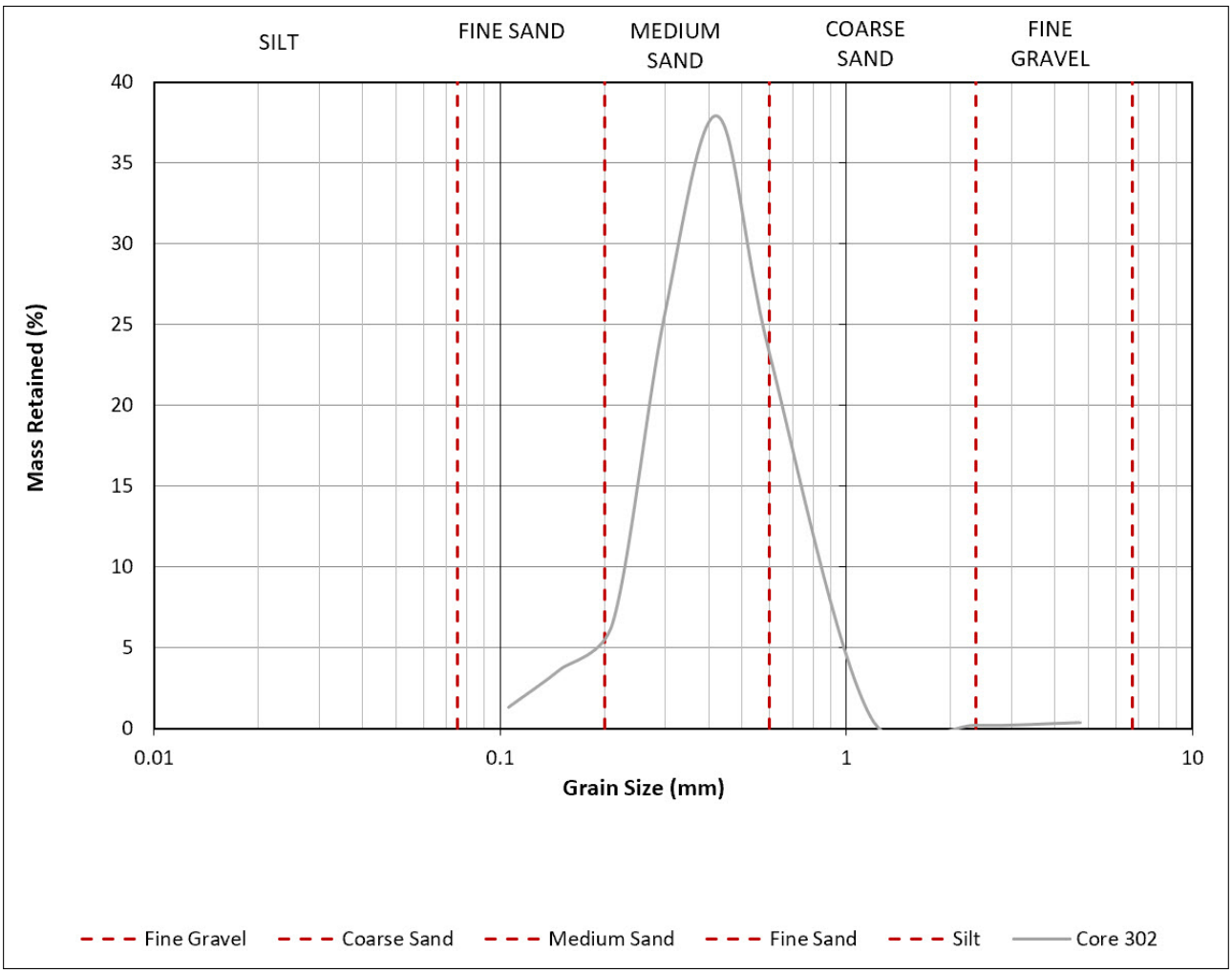

Figure B.14 PSD, core 302, Swan River sleeper site.

Table B.15 Down-core sediment description, core 303, Swan River sleeper site.

Depth (cm)	Description	shell/frags >1mm at sub-core depth levels (photograph by Trevor Winton)
0	medium grained siliceous sand, 5.3 % shell/frags > 1mm	
1		
2		
3		
4		
5		
6		
7		
8		
9		
10		
11		
12		
13		
14		
15		
16		
17		
18		
19		
20		
21		
22		
26		
32		
34		
38		
42		
44		
46		
48		
50		
51		
52		
53		

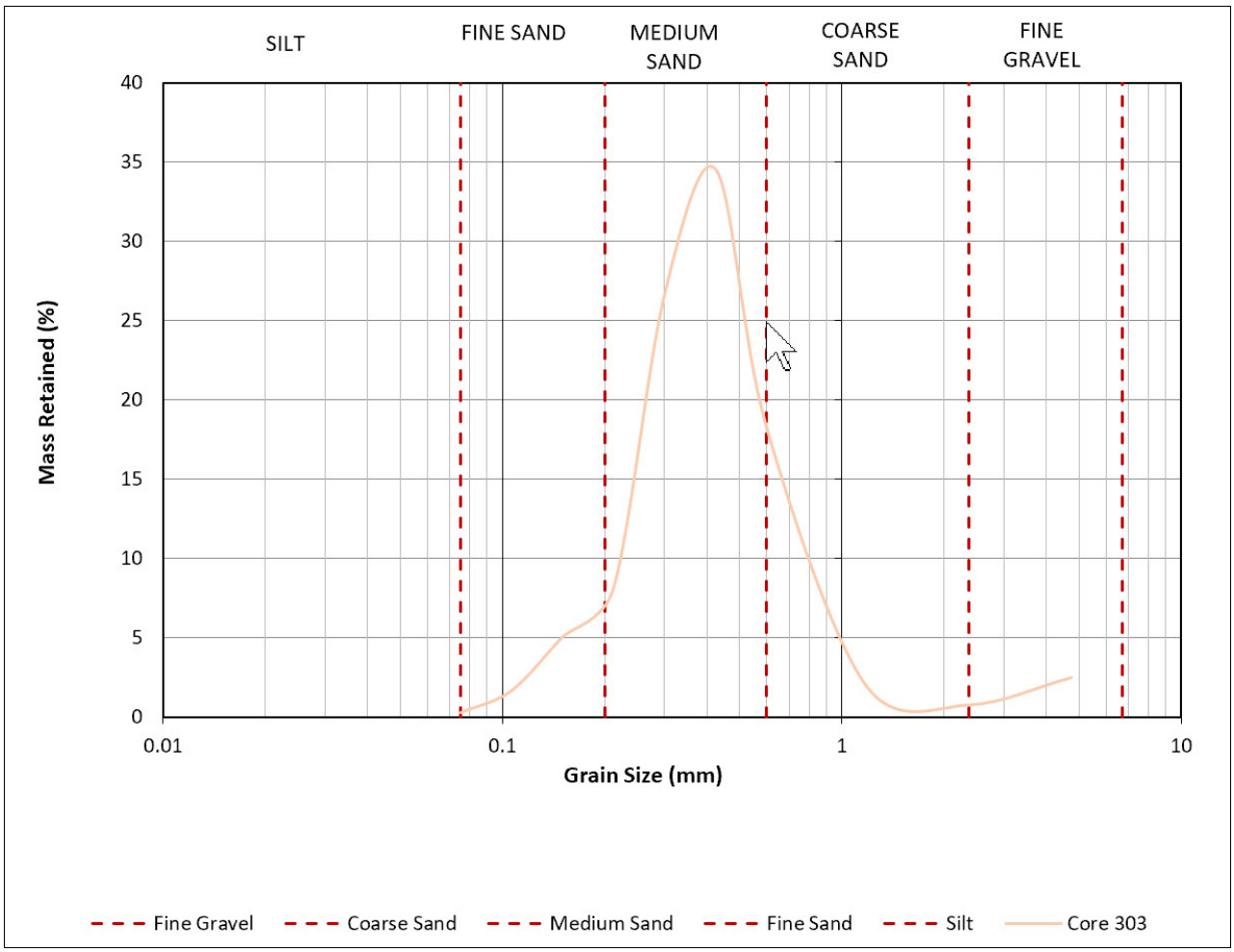

Figure B.15 PSD, core 303, Swan River sleeper site.

Table B.16 Down-core sediment description, core 304, Swan River sleeper site.

Depth (cm)	Description	shell/frags >1mm at sub-core depth levels (photograph by Trevor Winton)
0	medium grained siliceous sand, 2.1 % shell/frags > 1mm	
1		
2		
3		
4		
5		
6		
7		
8		
9		
10		
11		
12		
13		
14		
15		
16		
17		
18		
19		
20		
21		
22		
26		
32		
34		
38		
42		
44		
46		
48		
50		
51		
52		
53		

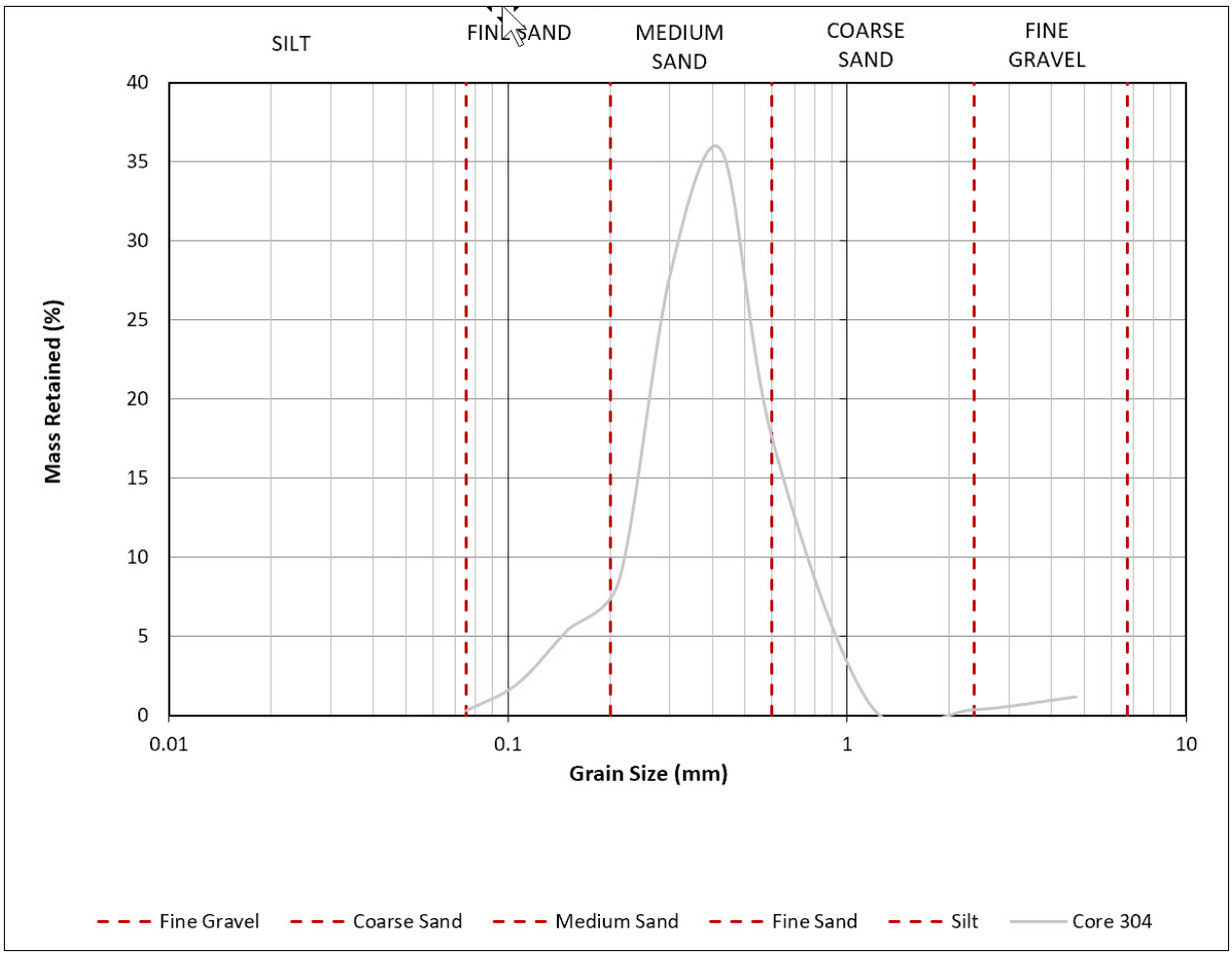

Figure B.16 PSD, core 304, Swan River sleeper site.

Table B.17 Sediment bulk density and porosity calculations, James Mathews sleeper site.

sediment core	total core weight (tube, bungs, sediment and water) (gm)	internal tube diameter (mm)	tube weight (gm)	weight of bungs (gm)	height of water above sediment (mm)	volume of water above sed (mm^3)	weight of water above sediment (gm)	wet weight of sediment (gm)	Height of (saturated) sediment (mm)	sediment wet (bulk) density (kg/m^3)
214	2238.5	43	381.5	187.2	124	180073.4	184.6	1485.2	487	2100.1
215	2081.4	43	355.6	188	108	156838.1	160.8	1377.0	455	2084.0
216	1854	43	358.2	182	8	11617.6	11.9	1301.9	430	2084.9
217	2181.4	43	337.5	187.5	52	75514.6	77.4	1579.0	512	2123.7
218	2103.8	43	357.2	181.5	62	90036.7	92.3	1472.8	485	2091.1
218*l1*	2118.7	43	357.2	181.5	28	40661.7	41.7	1538.3	540	1961.7
218*t1*	2090.0	43	357.2	181.5	86	124889.6	128.0	1423.3	474	2067.7
218*l2*	2098.5	43	357.2	181.5	24	34852.9	35.7	1524.1	536	1958.0
218*t2*	2099.1	43	357.2	181.5	85	123437.4	126.5	1433.9	476	2074.3

sediment core	sediment dry weight (gm)	wet volume of sediment (m3)	weight of evaporated water (gm)	uncorrected[a] porosity (%)	weight of seawater lost (gm)	volume of seawater (cm^3)	salt corrected[b] porosity (%)
214	1179.7	0.000707	305.5	43.2	316.6	309.2	43.7
215	1079.6	0.000661	297.4	45.0	308.2	301.0	45.6
216	1023.6	0.000624	278.3	44.6	288.4	281.7	45.1
217	1235.2	0.000743	343.8	46.2	356.3	347.9	46.8
218	1120.18	0.000704	352.6	50.1	365.4	356.9	50.7
218*l1*	1120.18	0.000784	418.2	53.3	433.3	423.2	54.0
218*t1*	1120.18	0.000688	303.1	44.0	314.1	306.8	44.6
218*l2*	1120.18	0.000778	403.9	51.9	418.6	408.8	52.5
218*t2*	1120.18	0.000691	313.7	45.4	325.1	317.5	45.9

a: Hamilton (1969:25)
b: Hamilton (1969:26, Method A)

l1,2: light compaction test 1,2
t1,2: tight compaction test 1,2

Table B.18 Sediment bulk density and porosity calculations, Swan River sleeper site.

sediment core	total core weight (tube, bungs, sediment and water) (gm)	internal tube diameter (mm)	tube weight (gm)	weight of bungs (gm)	height of water above sediment (mm)	volume of water above sed (mm^3)	weight of water above sediment (gm)	wet weight of sediment (gm)	Height of (saturated) sediment (mm)	sediment wet (bulk) density (kg/m^3)
301	2238.8	47.5	173.1	188.1	31			1877.6	502	2110.7
302	2152.5	47.5	172.7	187.4	60			1792.4	462	2189.3
303	2241.9	47.5	170.5	188.0	39	69110.3	70.8	1812.6	495	2066.4
304	1966.2	47.5	171.5	188.2	36	63794.1	65.4	1541.1	428	2031.9
304*t*	2070.2	47.5	171.5	188.2	110	194926.5	199.8	1510.7	410	2079.3
304*l*	2083.8	47.5	171.5	188.2	79	139992.6	143.5	1580.6	451	1977.7

sediment core	sediment dry weight (gm)	wet volume of sediment (m3)	weight of evaporated water (gm)	uncorrected[a] porosity (%)	weight of seawater lost (gm)	volume of seawater (cm^3)	salt corrected[b] porosity (%)
301	1483.2	0.000889	394.4	44.3	408.7	399.1	44.9
302	1371.2	0.000819	421.2	51.5	436.5	426.3	52.1
303	1519.5	0.000877	293.1	33.4	303.7	296.6	33.8
304	1251.5	0.000758	289.6	38.2	300.1	293.1	38.7
304*t*	1251.5	0.000726	259.2	35.7	268.6	262.3	36.1
304*l*	1251.5	0.000799	329.1	41.2	341.0	333.1	41.7

a: Hamilton (1969:25)
b: Hamilton (1969:26, Method A)

l: light compaction test
t: tight compaction test

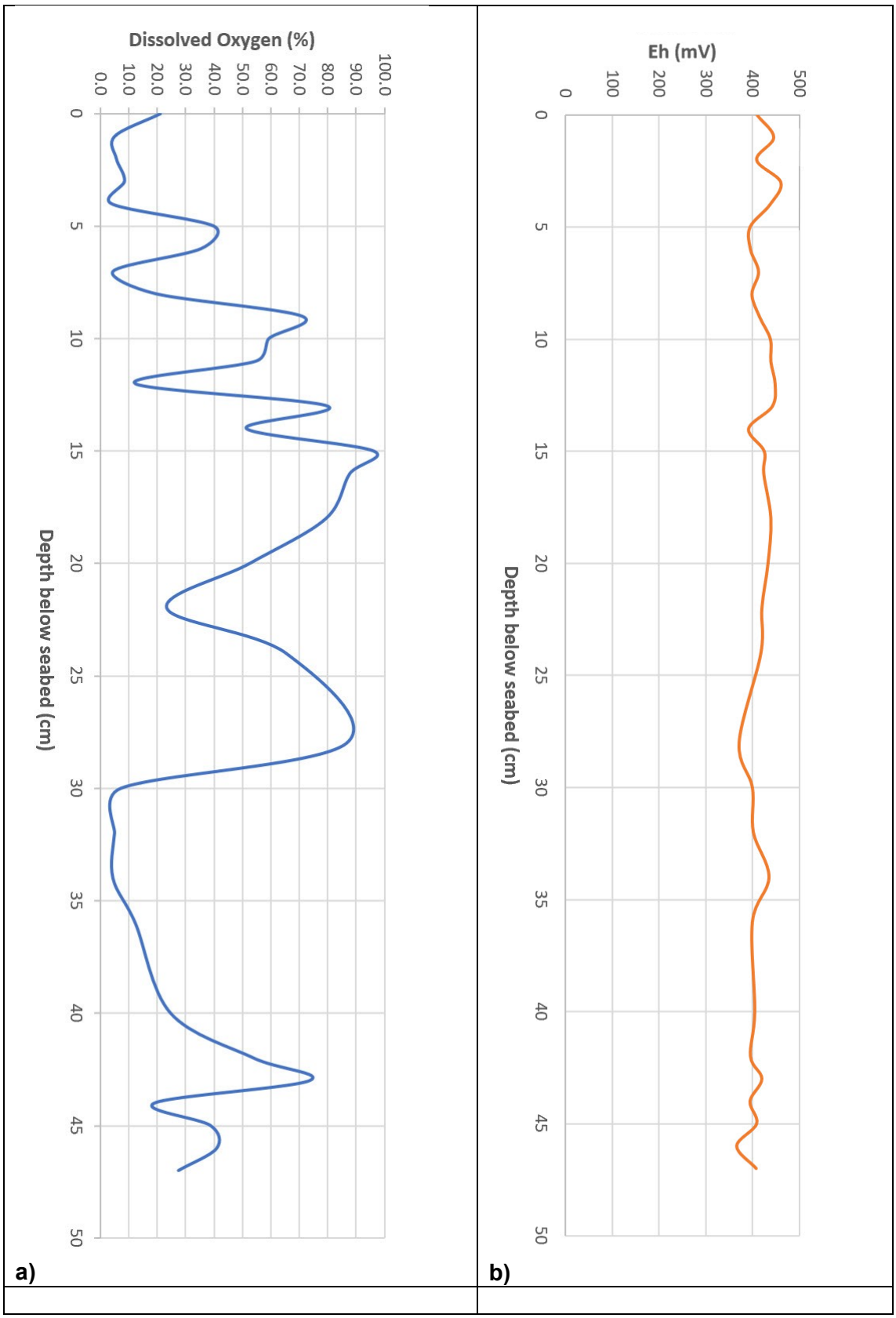

Figure B.17 Down-core profiles in core 20, James Matthews sleeper site: (a) DO; and (b) Eh.

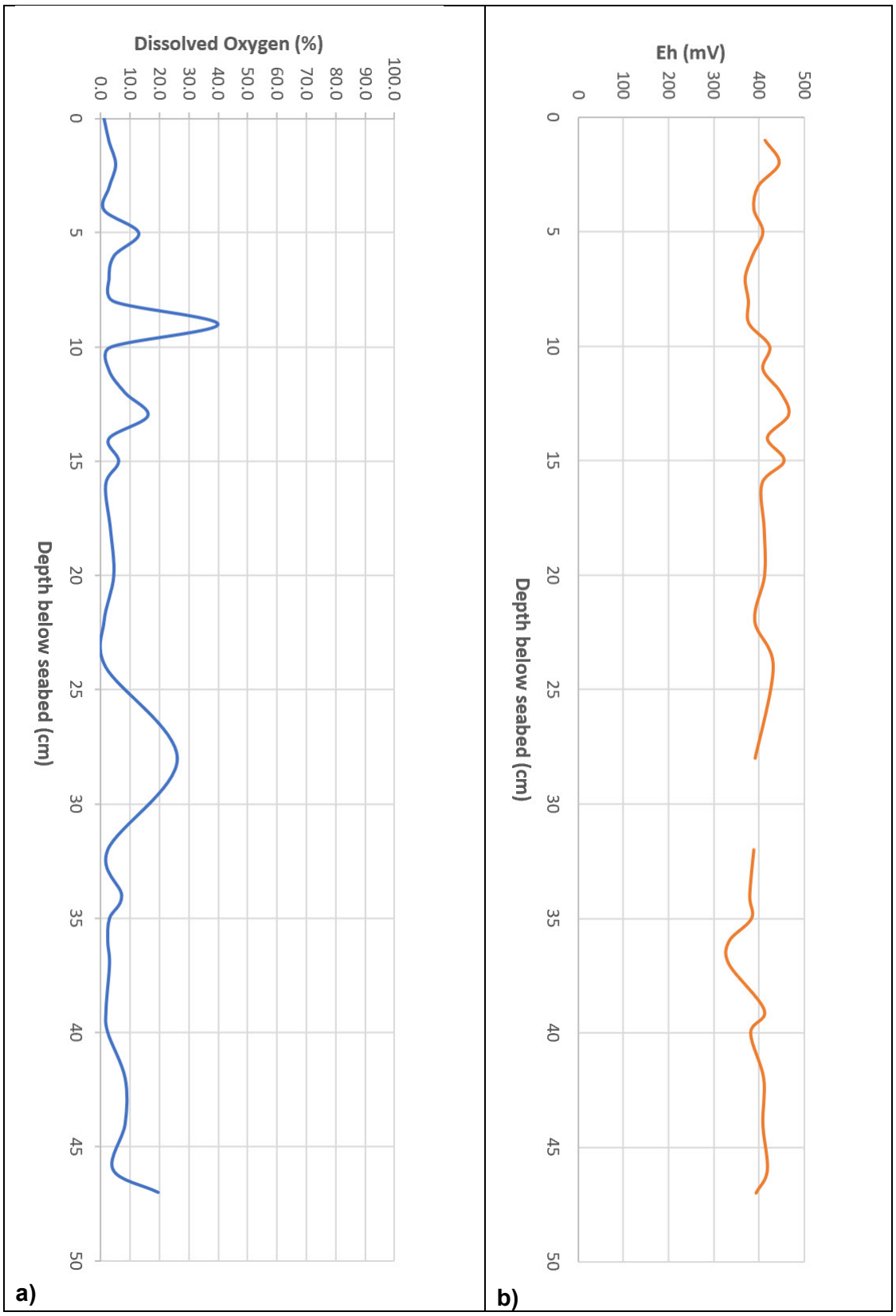

Figure B.18 Down-core profiles in core 100, James Matthews sleeper site: (a) DO; and (b) Eh.

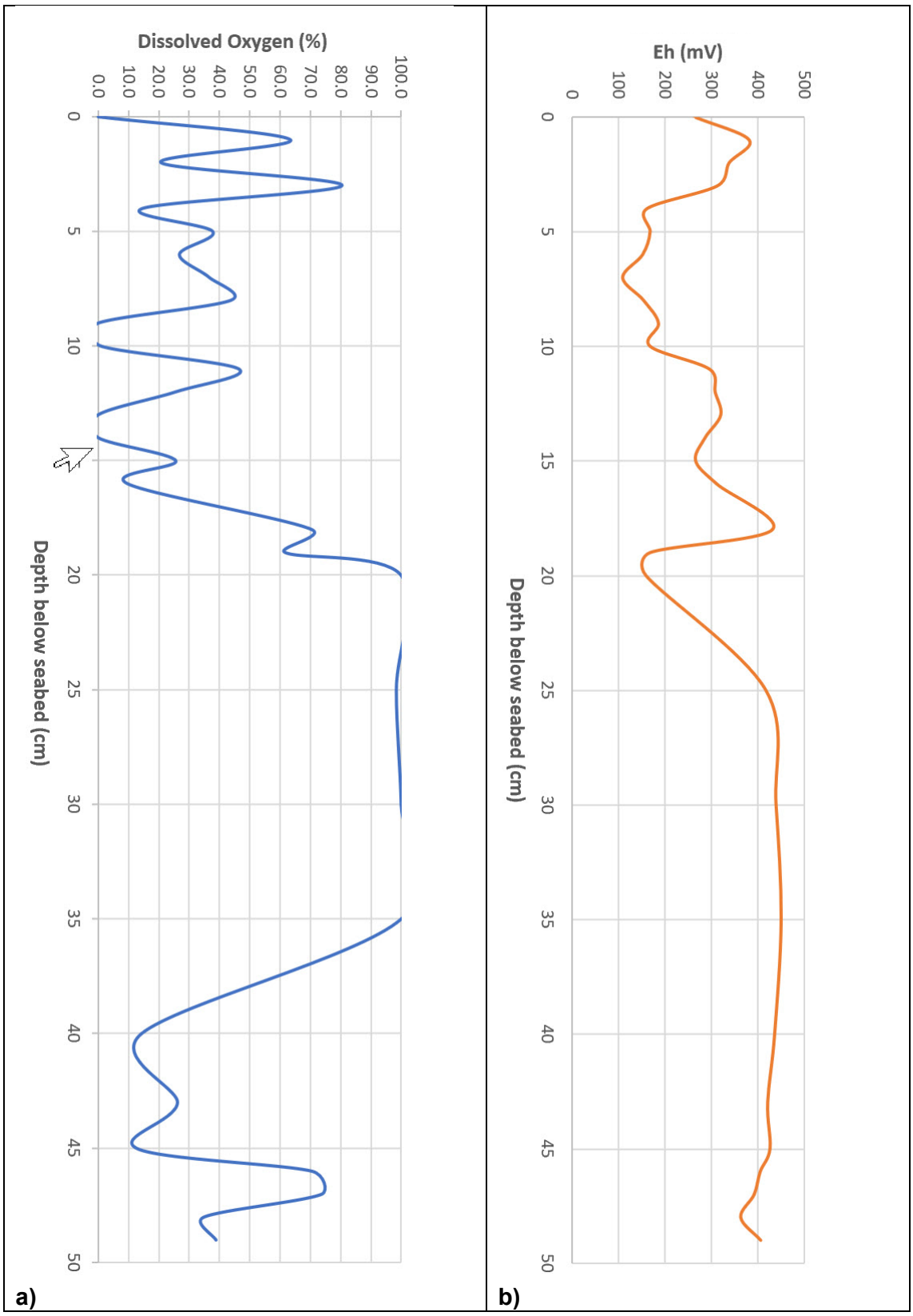

Figure B.19 Down-core profiles in core 112, James Matthews sleeper site: (a) DO; and (b) Eh.

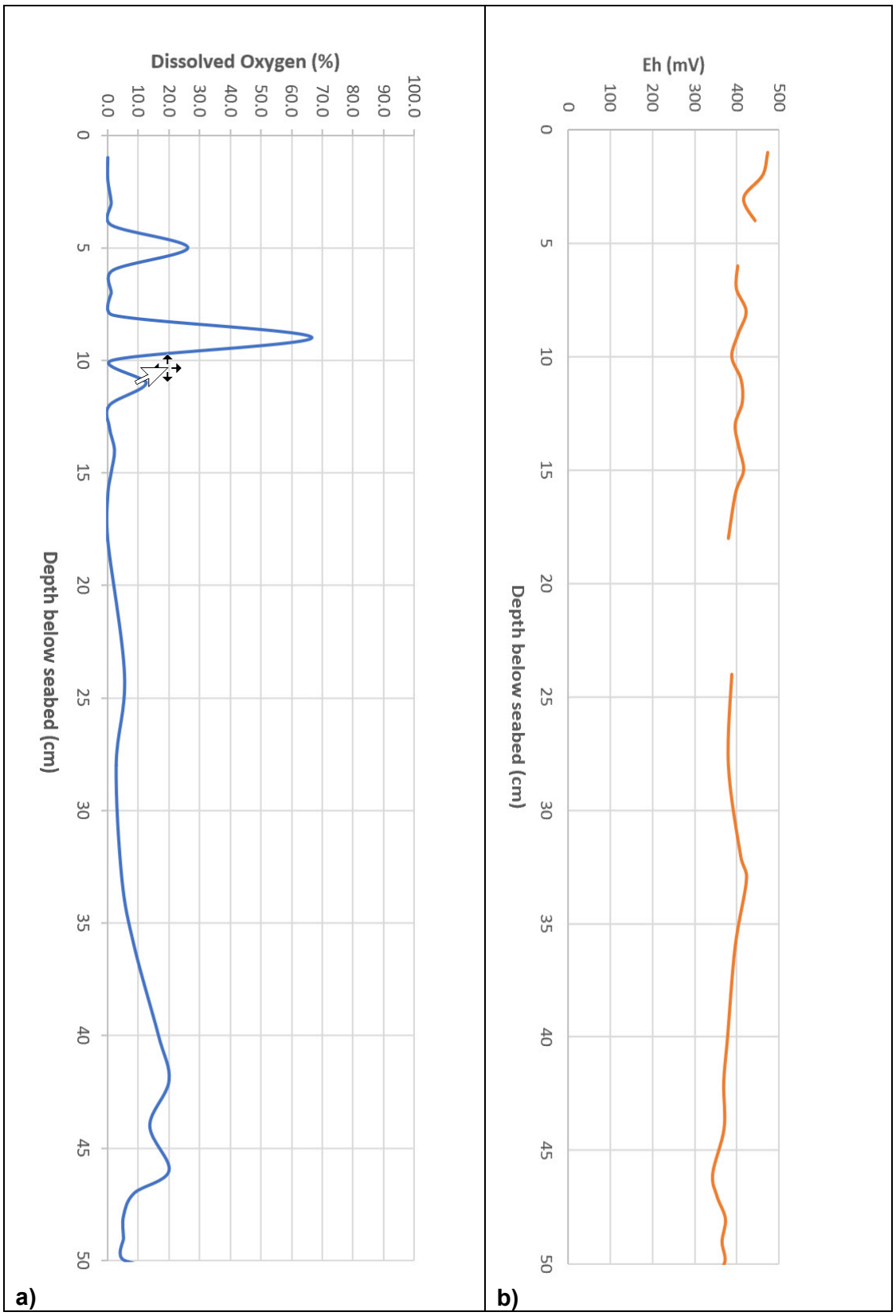

Figure B.20 Down-core profiles in core 122, James Matthews sleeper site: (a) DO; and (b) Eh.

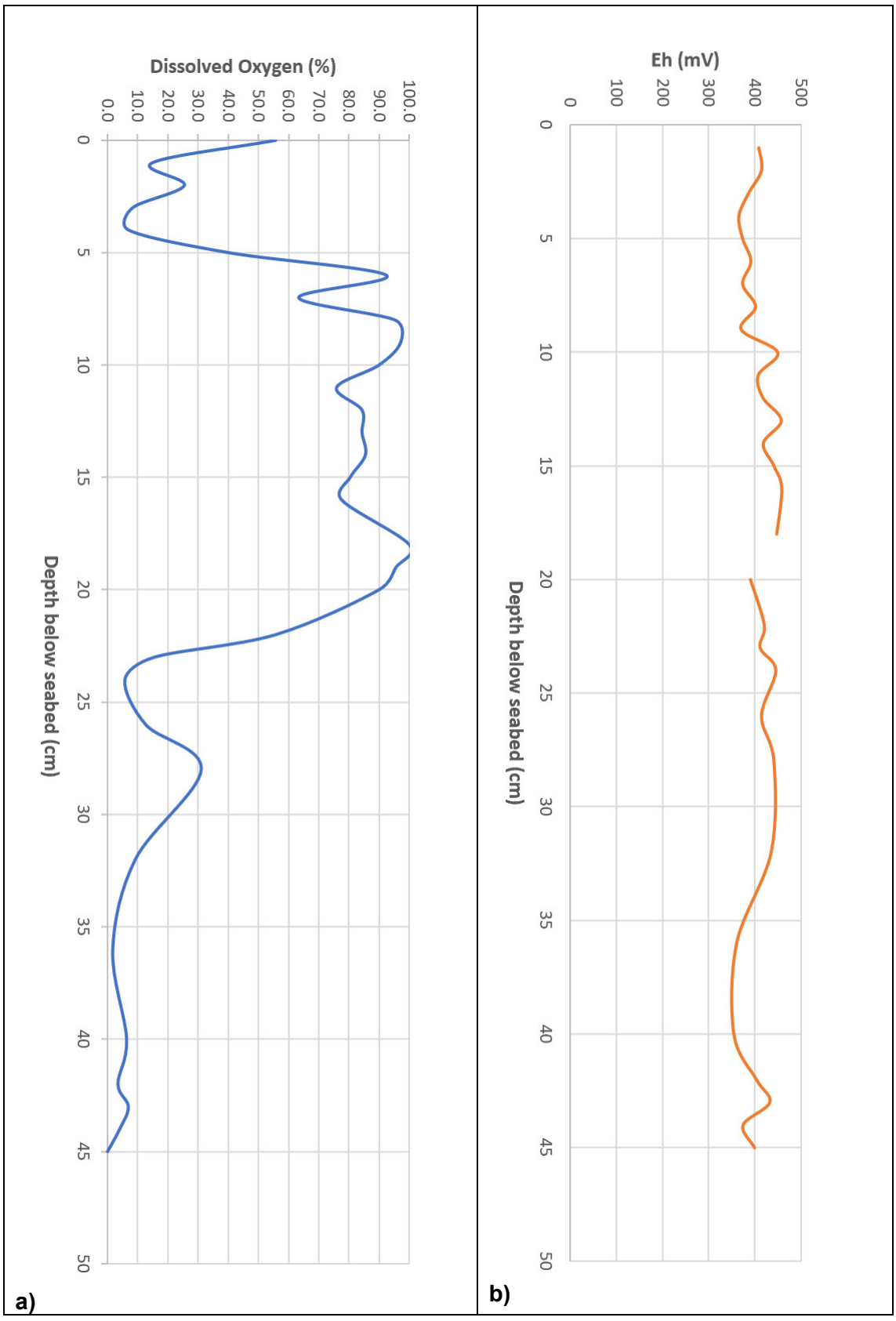

Figure B.21 Down-core profiles in core 155, James Matthews sleeper site: (a) DO; and (b) Eh.

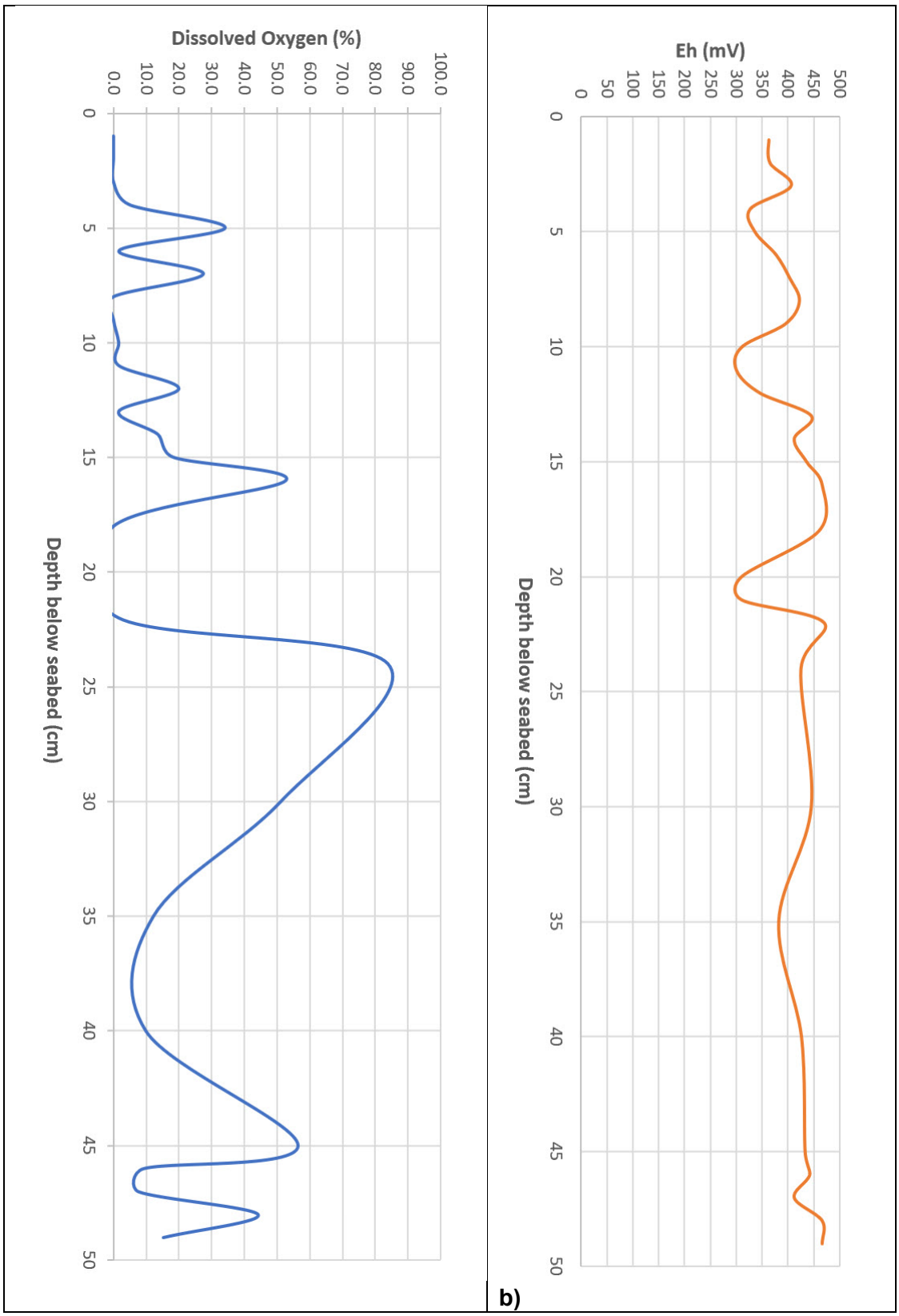

Figure B.22 Down-core profiles in core 170, James Matthews sleeper site: (a) DO; and (b) Eh.

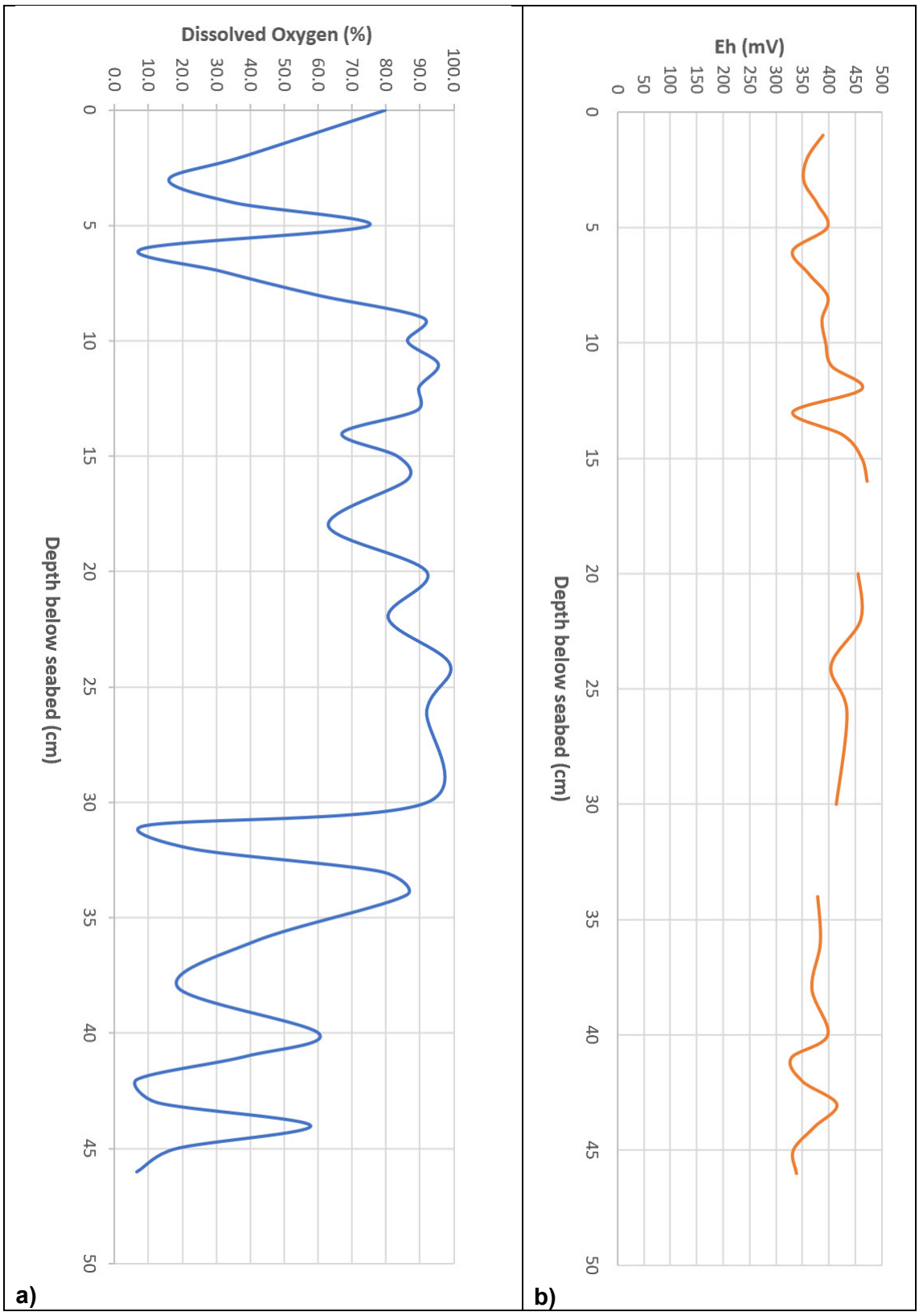

Figure B.23 Down-core profiles in core 192, James Matthews sleeper site: (a) DO; and (b) Eh.

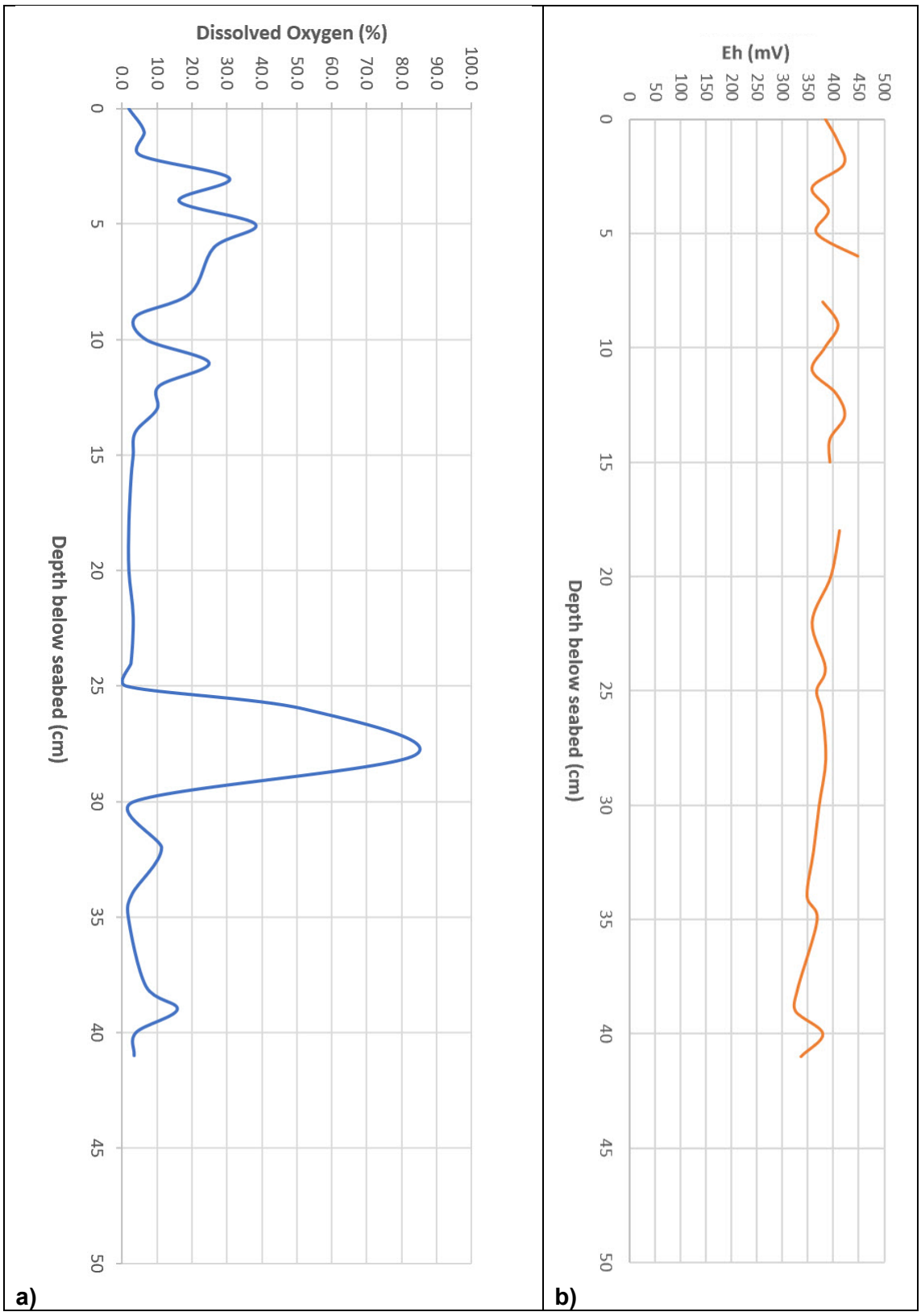

Figure B.24 Down-core profiles in core 193, James Matthews sleeper site: (a) DO; and (b) Eh.

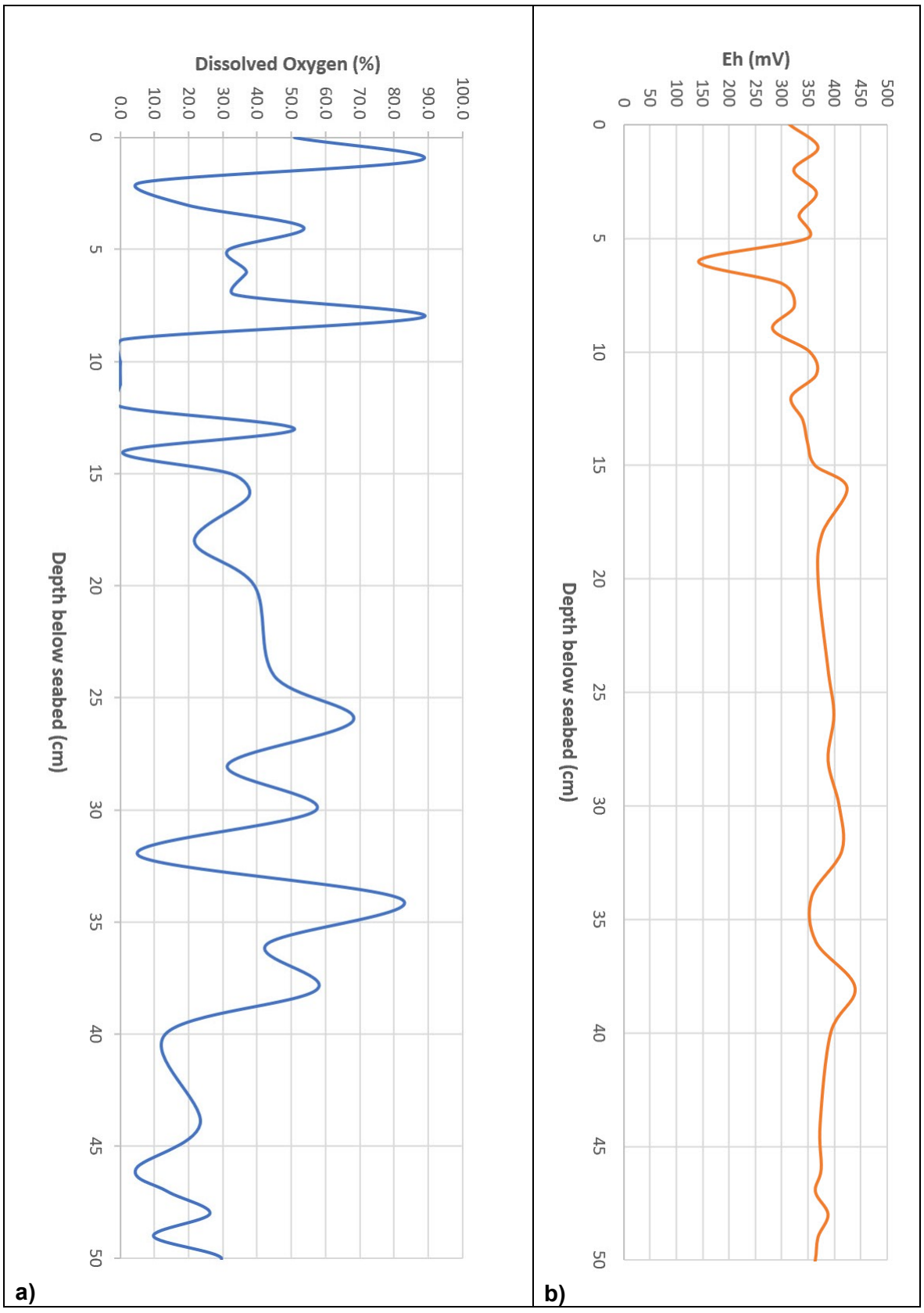

Figure B.25 Down-core profiles in core 194, James Matthews sleeper site: (a) DO; and (b) Eh.

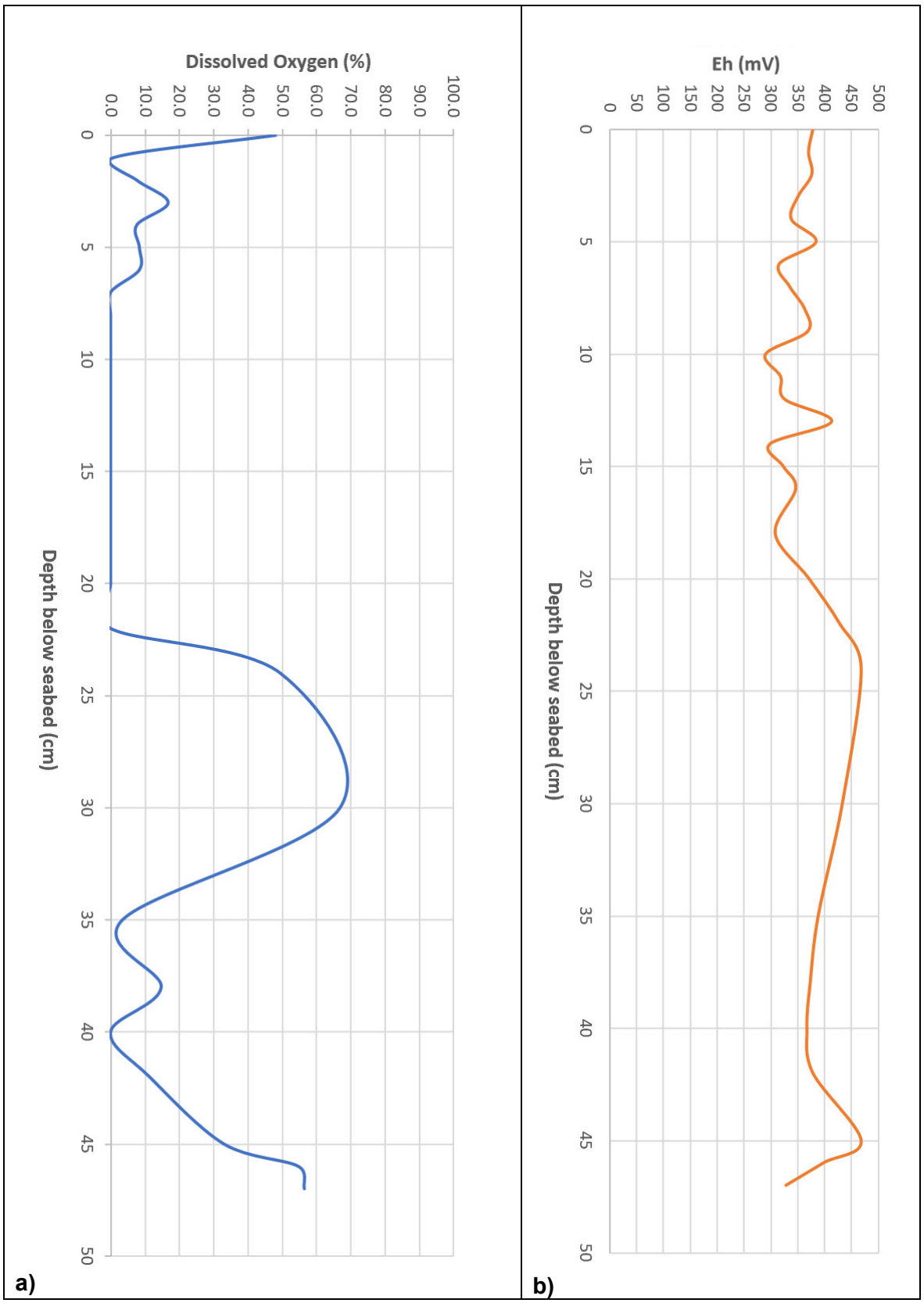

Figure B.26 Down-core profiles in core 195, James Matthews sleeper site: (a) DO; and (b) Eh.

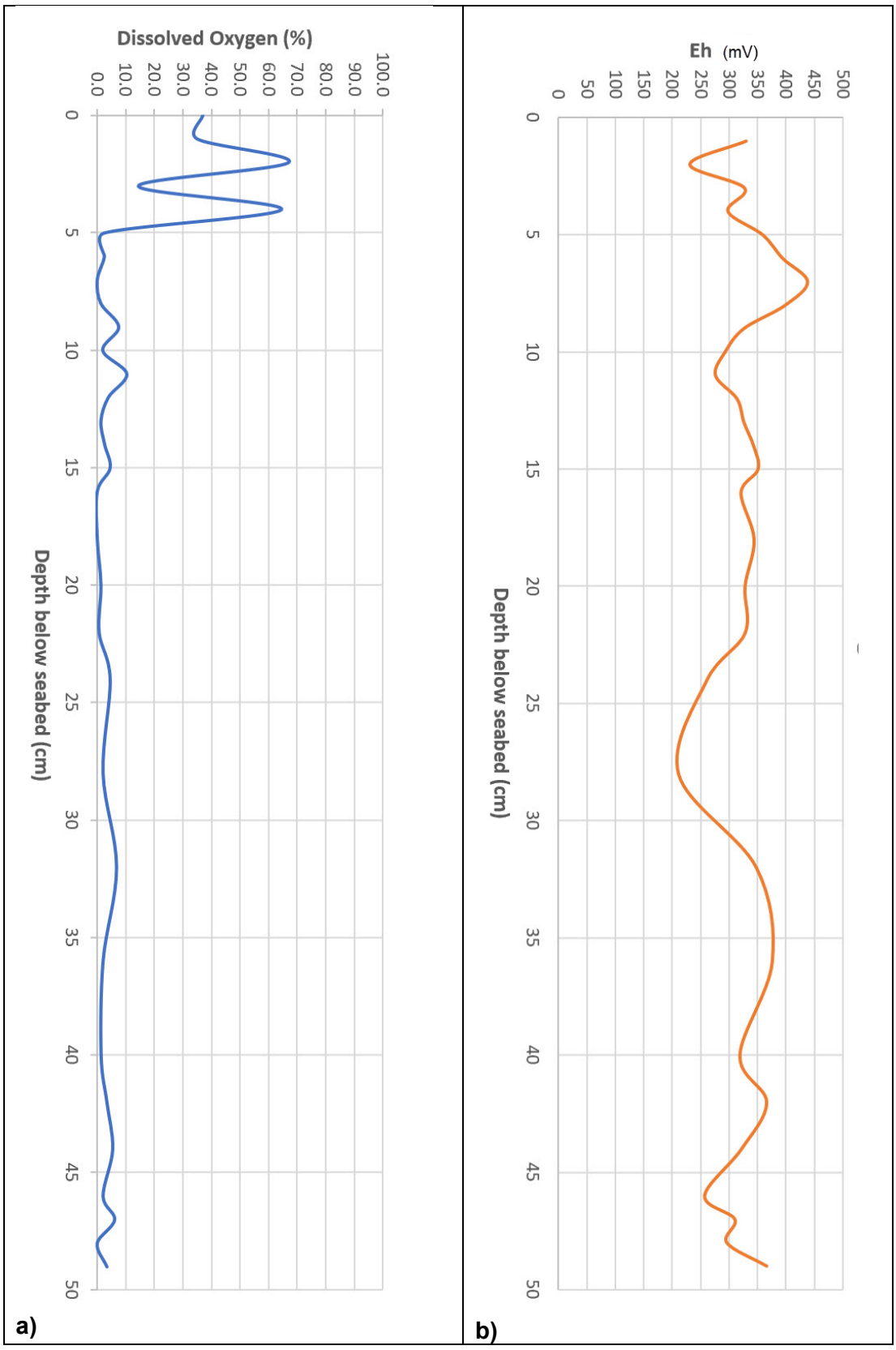

Figure B.27 Down-core profiles in core 10, Swan River sleeper site: (a) DO; and (b) Eh.

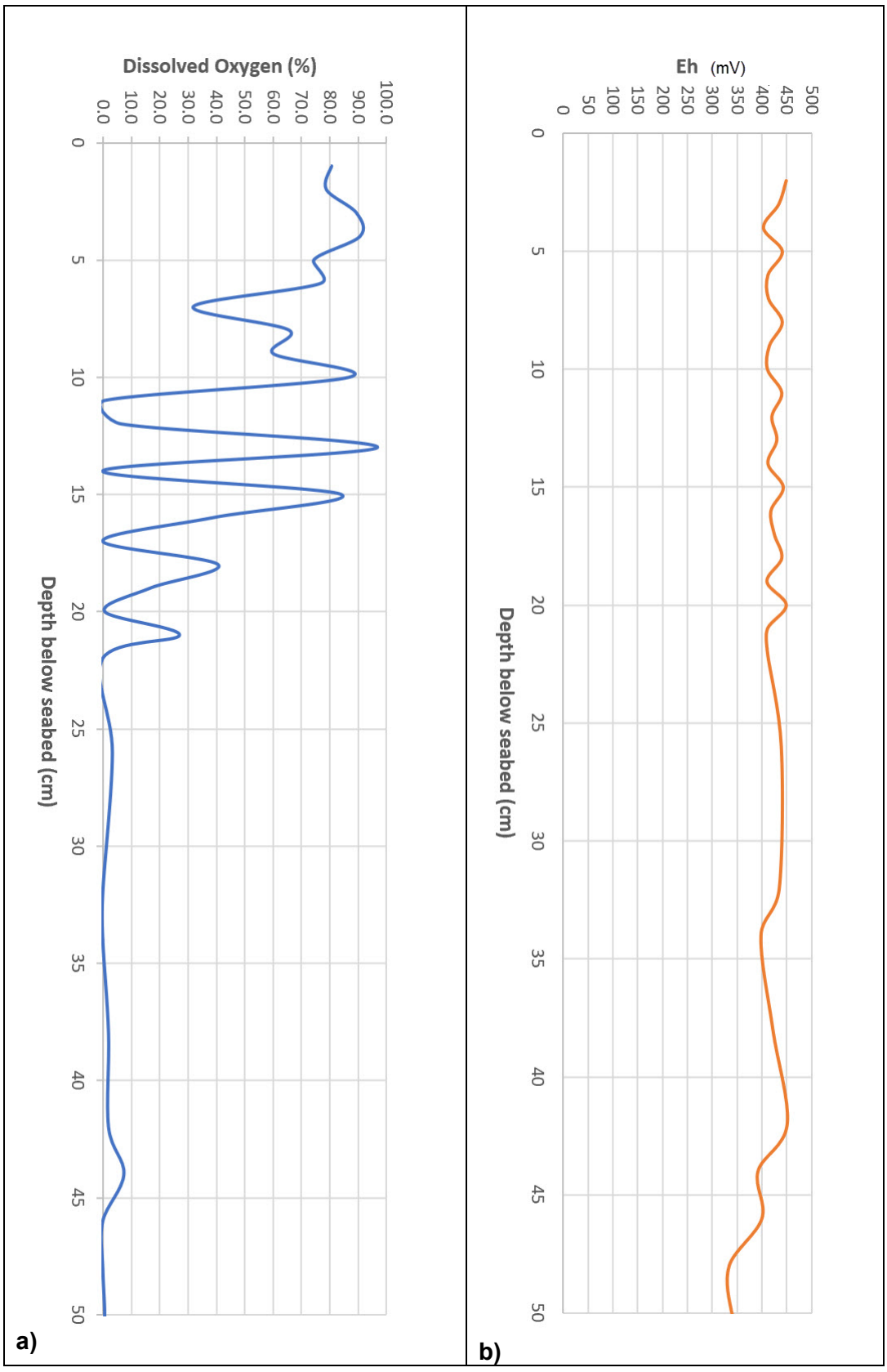

Figure B.28 Down-core profiles in core 12, Swan River sleeper site: (a) DO; and (b) Eh.

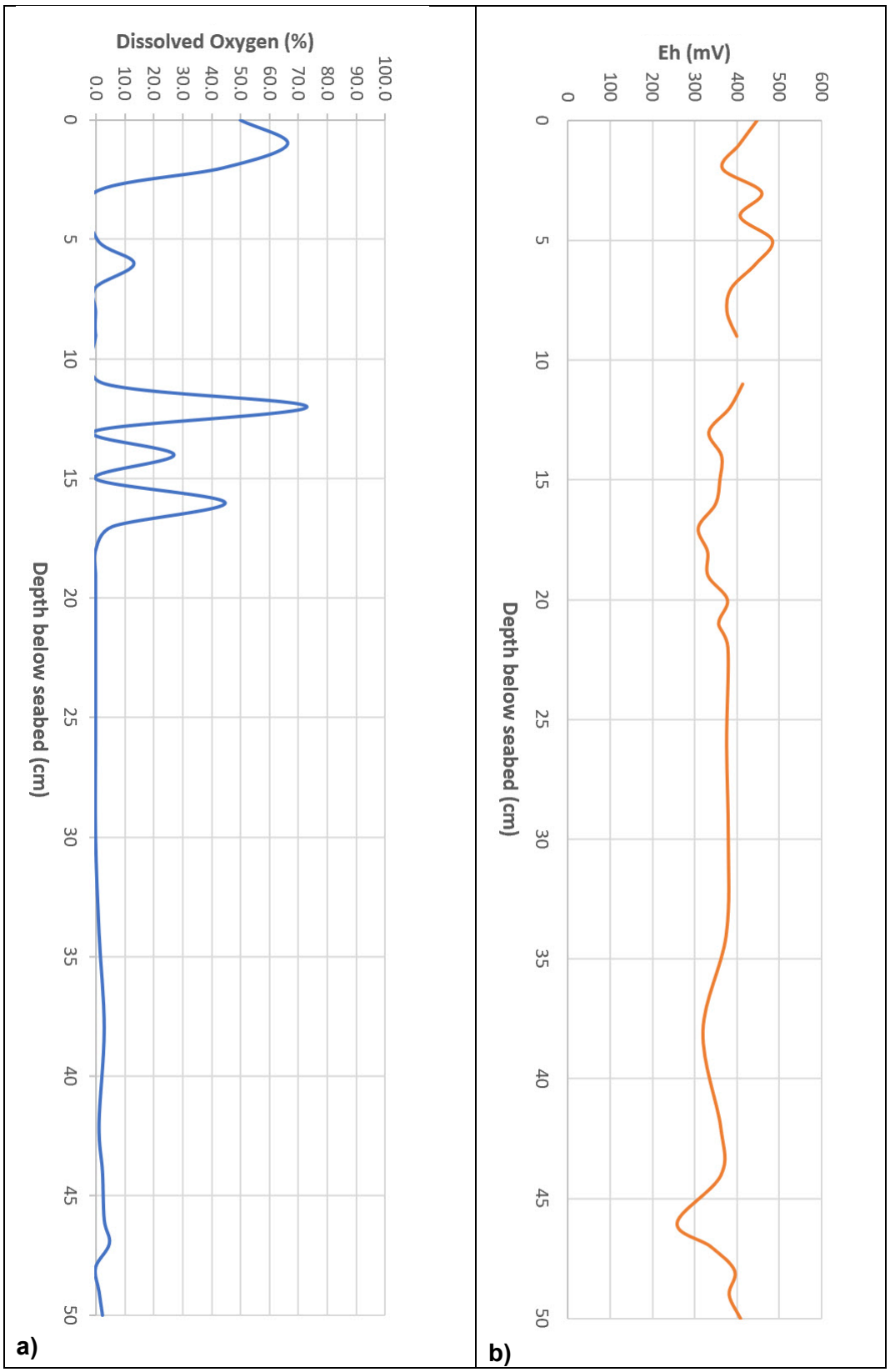

Figure B.29 Down-core profiles in core 17, Swan River sleeper site: (a) DO; and (b) Eh.

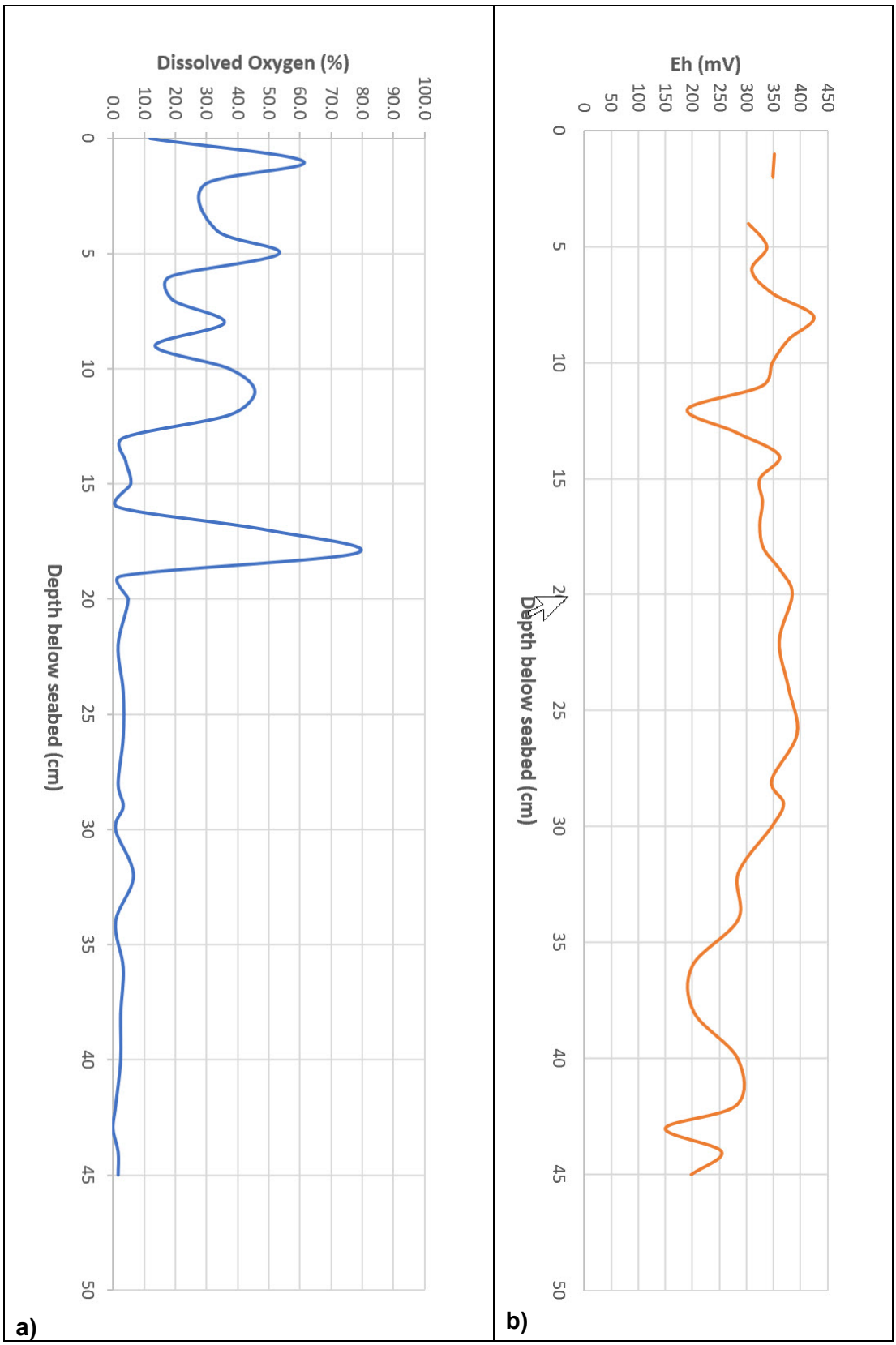

Figure B.30 Down-core profiles in core 156, Swan River sleeper site: (a) DO; and (b) Eh.

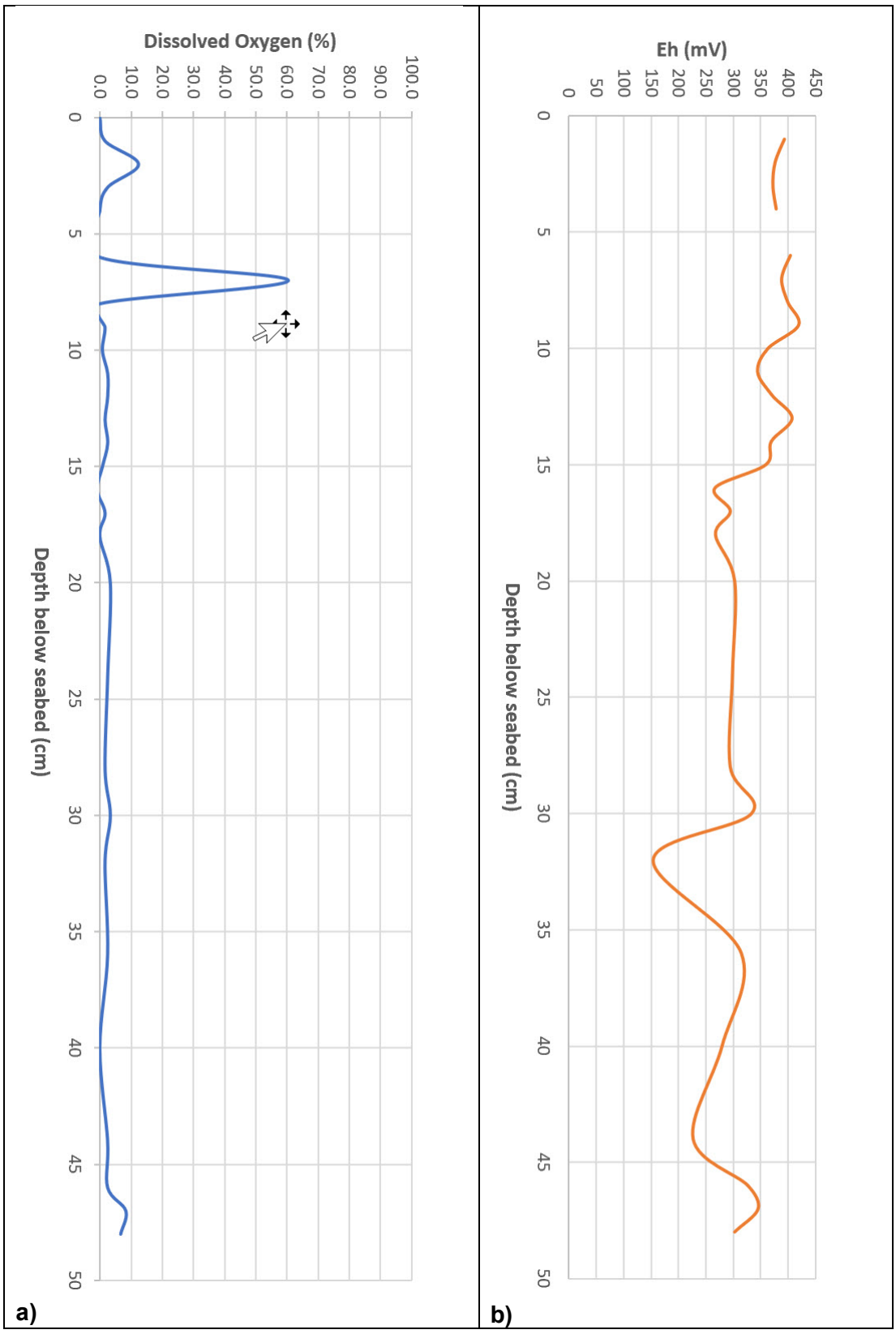

Figure B.31 Down-core profiles in core 162, Swan River sleeper site: (a) DO; and (b) Eh.

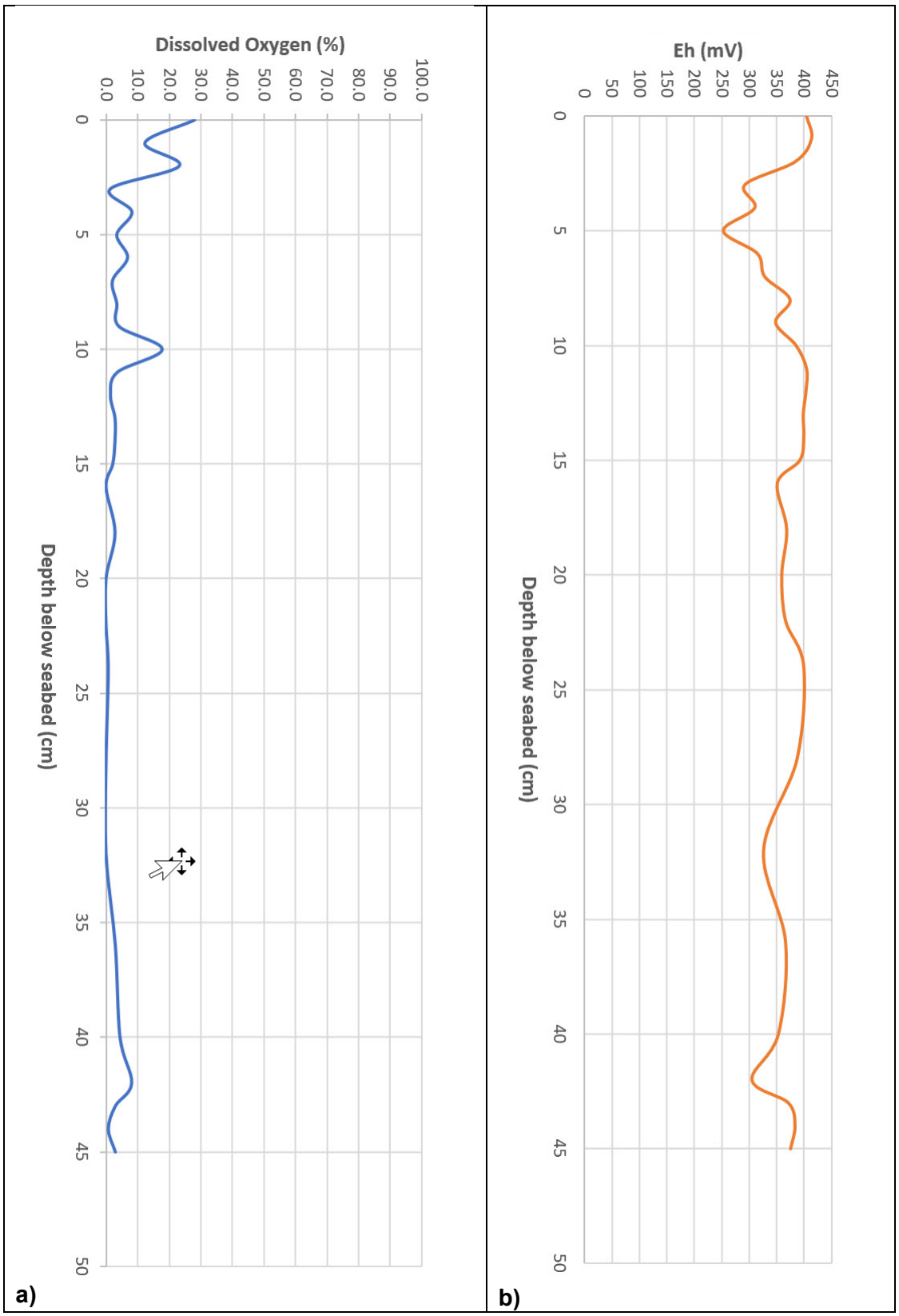

Figure B.32 Down-core profiles in core 163, Swan River sleeper site: (a) DO; and (b) Eh.

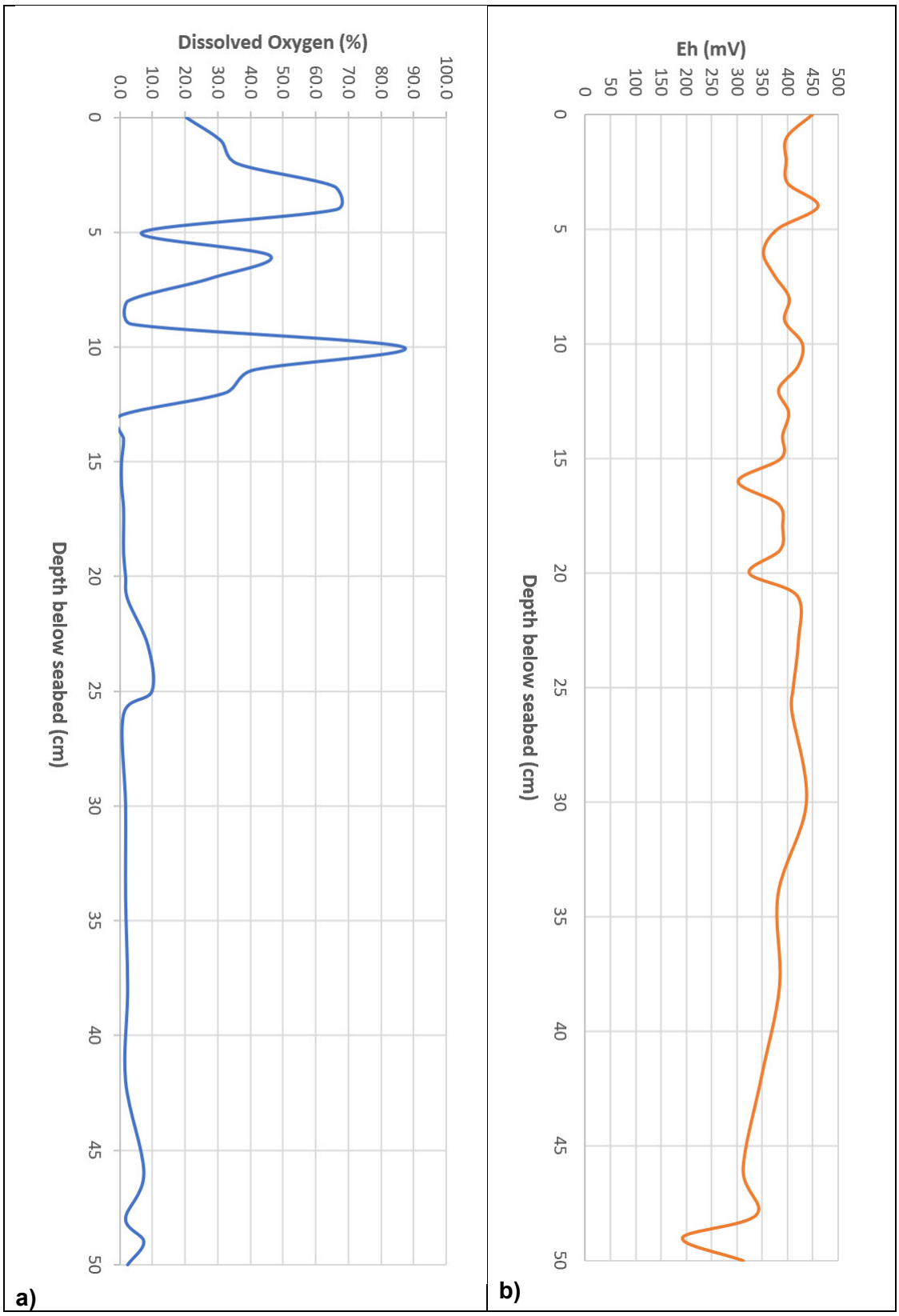

Figure B.33 Down-core profiles in core 169, Swan River sleeper site: (a) DO; and (b) Eh.

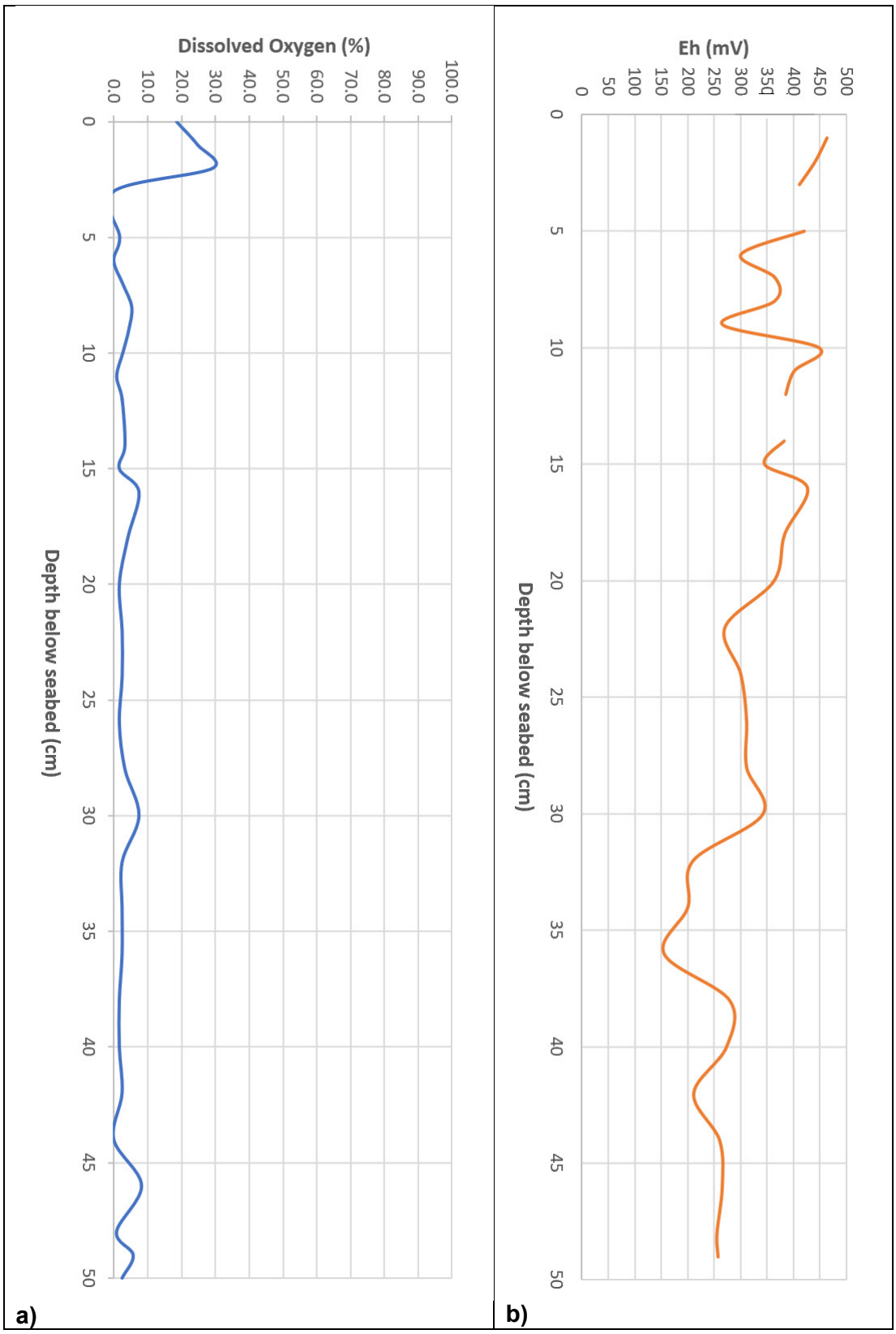

Figure B.34 Down-core profiles in core 176, Swan River sleeper site: (a) DO; and (b) Eh.

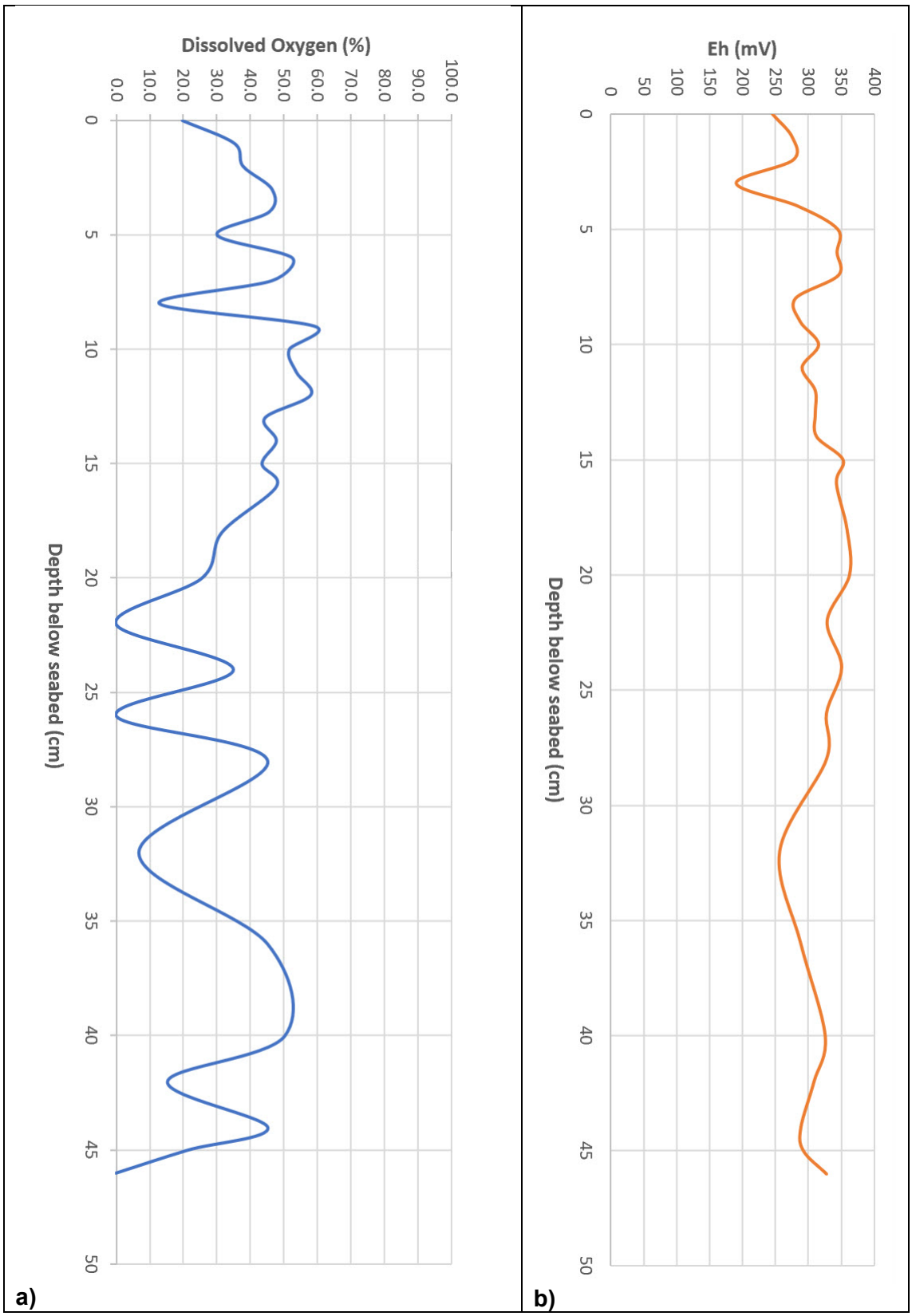

Figure B.35 Down-core profiles in core 177, Swan River sleeper site: (a) DO; and (b) Eh.

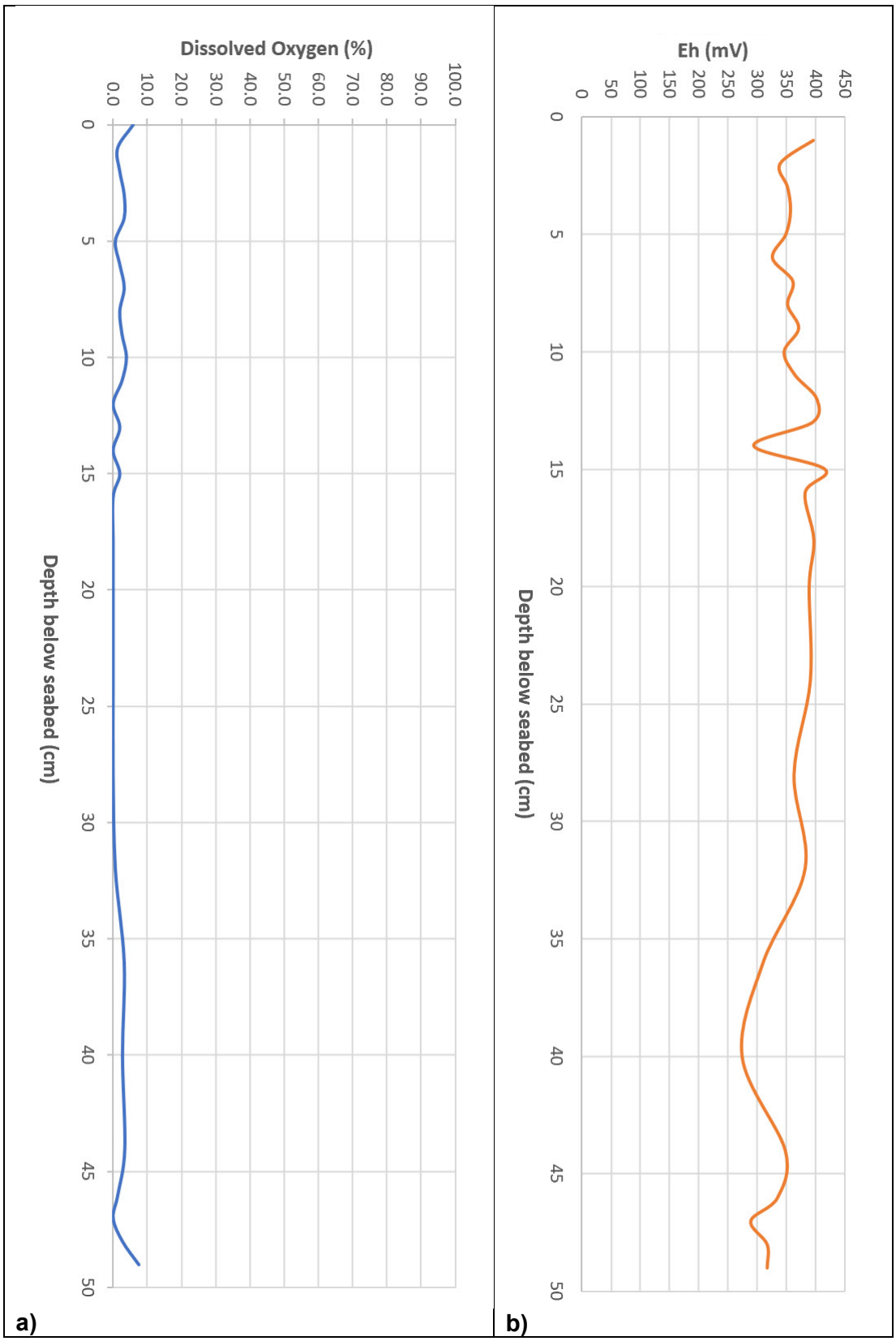

Figure B.36 Down-core profiles in core 183, Swan River sleeper site: (a) DO; and (b) Eh.

C. TIMBER CHARACTERISTICS

Pre-burial timber characteristics

Table C.1 displays the results of measurements and calculations of basic density, bulk density, and maximum % moisture content in replicated jarrah, oak and pine timber samples prior to sub-seabed burial at the sleeper sites.

Post-burial and recovery timber characteristics

Table C.2 displays the results of measurements and calculations of basic density, bulk density, moisture content and specific gravity in sub-samples cut from jarrah, oak and pine timber blocks buried and recovered 20.5 months later from the James Matthews sleeper site.

Table C.3 displays the results of measurements and calculations of basic density, bulk density, moisture content and specific gravity in sub-samples cut from jarrah, oak and pine timber blocks buried and recovered 9.25 months later from the Swan River sleeper site.

Table C.1 Pre-burial timber basic density, bulk density and maximum % moisture content

timber cube	measured weight (g)					average volume (cm^3)	basic density		bulk density		max % moisture content
	petrie dish	petrie dish and wet sample	wet sample	petrie dish and dry sample	dry sample		(gm/cm^3)	(kg/m^3)	(gm/cm^3)	(kg/m^3)	
J11	50.0738	59.9740	9.9002	55.4622	5.3884	9.13	0.590	590.2	0.760	759.5	83.73
J12	43.4913	53.0443	9.5530	48.6488	5.1575	8.75	0.589	589.4	0.863	863.1	85.23
J13	43.2923	53.1268	9.8345	48.4659	5.1736	8.95	0.578	578.1	0.872	872.4	90.09
J21	42.4188	52.1280	9.7092	47.2700	4.8512	9.04	0.537	536.6	0.809	809.5	100.14
J22	58.1958	69.0092	10.8134	63.8874	5.6916	9.36	0.608	608.1	0.986	986.5	89.99
J23	39.6803	49.7722	10.0919	44.7125	5.0322	8.97	0.561	561.0	0.972	972.4	100.55
O11	50.1106	60.5352	10.4246	55.1357	5.0251	8.57	0.586	586.4	0.645	645.3	107.45
O12	48.0445	57.8128	9.7683	52.4202	4.3757	8.39	0.522	521.5	0.579	578.9	123.24
O13	48.0565	58.6054	10.5489	53.1624	5.1059	8.81	0.580	579.6	0.643	643.2	106.60
O21	43.2160	54.7307	11.5147	49.2874	6.0714	8.92	0.681	680.7	0.751	751.2	89.65
O22	49.1714	59.6725	10.5011	54.3298	5.1584	9.11	0.566	566.2	0.623	622.7	103.57
O23	49.6519	60.0355	10.3836	54.8264	5.1745	9.39	0.551	551.1	0.609	608.8	100.67
P11	37.6383	47.8217	10.1834	42.2708	4.6325	8.88	0.522	521.7	0.595	594.9	119.83
P12	48.4967	58.5605	10.0638	52.9734	4.4767	8.61	0.520	519.9	0.596	596.2	124.80
P13	42.1904	51.9217	9.7313	46.0841	3.8937	8.48	0.459	459.2	0.503	502.8	149.92
P21	65.9351	76.0510	10.1159	69.7279	3.7928	8.85	0.429	428.6	0.464	464.0	166.71
P22	36.9474	47.3460	10.3986	40.9504	4.0030	8.84	0.453	452.8	0.494	493.7	159.77
P23	42.2314	52.0113	9.7799	46.1624	3.9310	8.55	0.460	459.8	0.501	500.9	148.79

J: jarrah; O: oak; P: pine

Table C.2 Post-burial and recovery timber basic density, bulk density, % moisture content and specific gravity, James Matthews sleeper site.

block	P10 (D1)							P10 (D2)						
sub-sample ID	wet volume (cm^3)	wet weight (gm)	dry weight (gm)	bulk density (kg/m^3)	basic density (kg/m^3)	% moisture content	specific gravity	wet volume (cm^3)	wet weight (gm)	dry weight (gm)	bulk density (kg/m^3)	basic density (kg/m^3)	% moisture content	specific gravity
T4														
T3														
T2	13.99	15.4217	5.8650	1102.7	419.3	162.9	0.44	14.05	14.1430	5.1605	1006.4	367.2	174.1	0.42
T1	13.23	14.3823	5.5598	1086.9	420.2	158.7	0.44	13.76	13.1823	5.0875	958.2	369.8	159.1	0.44
C	14.96	14.9543	5.7768	999.9	386.2	158.9	0.44	14.47	13.8062	5.2551	954.4	363.3	162.7	0.44
B1	12.87	9.9449	6.1066	773.0	474.6	62.9	0.77	14.59	14.5152	5.3866	995.1	369.3	169.5	0.42
B2	13.15	10.8199	6.8956	822.9	524.4	56.9	0.81	14.12	14.5948	5.1926	1033.3	367.6	181.1	0.40
L2	11.54	12.5935	4.5600	1091.5	395.2	176.2	0.41	11.01	9.2532	4.9960	840.3	453.7	85.2	0.66
L1	11.82	12.0884	4.5804	1022.6	387.5	163.9	0.43	11.29	9.2313	4.4715	817.9	396.2	106.4	0.58
R1	11.75	11.7287	4.4574	998.3	379.4	163.1	0.44	12.01	12.6086	4.6813	1050.2	389.9	169.3	0.42
R2	11.47	12.3926	4.3750	1080.8	381.5	183.3	0.40	10.55	11.9192	4.3277	1129.5	410.1	175.4	0.41

block	P30 (D1)							P30 (D2)						
sub-sample ID	wet volume (cm^3)	wet weight (gm)	dry weight (gm)	bulk density (kg/m^3)	basic density (kg/m^3)	% moisture content	specific gravity	wet volume (cm^3)	wet weight (gm)	dry weight (gm)	bulk density (kg/m^3)	basic density (kg/m^3)	% moisture content	specific gravity
T4								14.84	15.1648	6.9518	1022.0	468.5	118.1	0.54
T3	10.58	10.6049	4.0926	1002.2	386.8	159.1	0.44	13.94	12.1613	6.4700	872.5	464.2	88.0	0.65
T2	14.18	13.8852	5.5069	979.2	388.3	152.1	0.46	12.63	10.8582	5.8030	859.5	459.3	87.1	0.65
T1	12.89	12.5065	5.1762	970.2	401.5	141.6	0.48	15.27	13.2876	7.1700	870.3	469.6	85.3	0.66
C	13.18	12.4119	5.0490	942.0	383.2	145.8	0.47	13.85	12.0870	6.5793	872.7	475.0	83.7	0.66
B1	14.74	14.0723	5.4991	954.8	373.1	155.9	0.45	12.46	10.7116	5.9211	859.6	475.2	80.9	0.68
B2	13.18	13.5203	4.9322	1025.9	374.2	174.1	0.42	12.90	13.6472	6.2045	1057.7	480.9	120.0	0.54
L2	12.28	12.3168	4.5132	1002.9	367.5	172.9	0.42	12.32	9.2130	5.2815	747.8	428.7	74.4	0.71
L1	12.41	12.7772	4.5820	1030.0	369.4	178.9	0.41	13.66	9.5485	6.5730	698.8	481.1	45.3	0.89
R1	11.17	7.9748	5.0526	713.6	452.1	57.8	0.80	12.76	13.7476	4.8718	1077.1	381.7	182.2	0.40
R2	10.86	8.3417	4.5180	768.2	416.1	84.6	0.66	13.28	14.9260	5.9997	1123.9	451.8	148.8	0.46

P10/30: pine block buried with 10/30 cm DoB; D1/D2: duplicate blocks

Table C.2 Post-burial and recovery timber basic density, bulk density,% moisture content and specific gravity, James Matthews sleeper site (cont'd).

block	P50 (D1)							P50 (D2)						
sub-sample ID	wet volume (cm^3)	wet weight (gm)	dry weight (gm)	bulk density (kg/m^3)	basic density ($kg/m^{3)}$	% moisture content	specific gravity	wet volume (cm^3)	wet weight (gm)	dry weight (gm)	bulk density (kg/m^3)	basic density (kg/m^3)	% moisture content	specific gravity
T4								13.49	13.8754	6.2281	1028.3	461.6	122.8	0.53
T3	23.07	22.0359	10.2214	955.1	443.0	115.6	0.55	13.48	10.7457	6.2708	797.0	465.1	71.4	0.72
T2	15.88	12.9901	6.9815	818.1	439.7	86.1	0.65	15.29	10.9980	7.4150	719.4	485.1	48.3	0.87
T1	14.18	11.5517	6.4221	814.5	452.8	79.9	0.68	15.80	11.1100	7.5491	703.2	477.8	47.2	0.88
C	15.54	12.1731	7.0596	783.4	454.3	72.4	0.72	15.47	10.4806	7.1036	677.6	459.3	47.5	0.88
B1	14.93	12.0255	6.9480	805.2	465.2	73.1	0.72	14.15	10.1633	6.6228	718.1	467.9	53.5	0.83
B2	14.55	14.7725	6.5963	1015.3	453.4	124.0	0.52	14.34	15.1520	6.8604	1056.4	478.3	120.9	0.53
L2	11.64	8.9376	5.8891	767.6	505.8	51.8	0.84	11.02	8.4703	5.1493	768.6	467.3	64.5	0.76
L1	14.64	8.7390	6.0812	597.1	415.5	43.7	0.91	11.60	8.2383	5.6326	710.0	485.5	46.3	0.89
R1	15.42	16.8965	6.2233	1095.4	403.5	171.5	0.42	11.85	12.1554	4.7228	1025.9	398.6	157.4	0.45
R2	14.95	16.8170	6.8208	1124.8	456.2	146.6	0.47	11.06	12.1565	4.6031	1099.4	416.3	164.1	0.43

block	O30 (D1)							O30 (D2)						
sub-sample ID	wet volume (cm^3)	wet weight (gm)	dry weight (gm)	bulk density (kg/m^3)	basic density (kg/m^3)	% moisture content	specific gravity	wet volume (cm^3)	wet weight (gm)	dry weight (gm)	bulk density (kg/m^3)	basic density (kg/m^3)	% moisture content	specific gravity
T4														
T3														
T2	12.62	12.1039	5.7038	959.2	452.0	112.2	0.56	9.89	10.8285	6.4035	1094.6	647.3	69.1	0.74
T1	10.73	8.5851	4.5285	800.1	422.1	89.6	0.64	9.45	9.0004	5.1317	952.0	542.8	75.4	0.70
C	11.58	9.0522	5.3036	781.8	458.0	70.7	0.73	10.22	8.5072	4.9477	832.5	484.2	71.9	0.72
B1	11.12	8.782	4.9951	790.0	449.3	75.8	0.70	8.95	7.7291	4.3826	863.8	489.8	76.4	0.70
B2	11.16	10.1951	5.5914	913.2	500.8	82.3	0.67	9.86	10.2224	5.5994	1037.0	568.1	82.6	0.67
L2	10.85	9.5321	4.831	670.8	445.4	97.3	0.61	10.22	8.1874	4.5526	801.2	445.5	79.8	0.68
L1	12.04	9.42	5.5222	782.4	458.7	70.6	0.73	9.48	7.7762	4.7144	820.0	497.1	64.9	0.76
R1	10.82	7.7863	4.6188	719.7	426.9	68.6	0.74	11.63	9.4325	5.5874	810.9	480.4	68.8	0.74
R2	9.46	7.5621	4.0345	799.7	426.6	87.4	0.65	11.42	9.7202	5.4095	850.8	473.5	79.7	0.68

P50/O30: pine/oak blocks buried with 50/30 cm DoB; D1/D2: duplicate blocks

Table C.3 Post-burial and recovery timber basic density, bulk density,% moisture content and specific gravity, Swan River sleeper site.

block	P20							P30						
sub-sample ID	wet volume (cm^3)	wet weight (gm)	dry weight (gm)	bulk density (kg/m^3)	basic density ($kg/m^{3)}$	% moisture content	specific gravity	wet volume (cm^3)	wet weight (gm)	dry weight (gm)	bulk density (kg/m^3)	basic density (kg/m^3)	% moisture content	specific gravity
T4								10.89	11.6520	5.3253	1069.9	489.0	118.8	0.54
T3								11.07	8.1778	5.6195	738.6	507.6	45.5	0.89
T2	12.07	10.7067	5.4264	886.7241	449.4	97.3	0.61	10.87	7.5365	5.4651	693.4	502.8	37.9	0.96
T1	10.75	10.9707	4.4374	1020.671	412.8	147.2	0.47	11.52	7.7497	5.7060	673.0	495.5	35.8	0.98
C	12.18	13.3222	4.7747	1093.511	391.9	179.0	0.41	11.95	7.8468	5.6813	656.6	475.4	38.1	0.95
B1	11.24	12.8652	4.8736	1144.228	433.5	164.0	0.43	11.66	8.0483	5.0251	690.2	431.0	60.2	0.79
B2	10.52	11.9539	4.5521	1136.417	432.8	162.6	0.44	12.11	12.7749	5.0450	1054.7	416.5	153.2	0.45
L2	15.16	17.2003	6.6111	1134.56	436.1	160.2	0.44	10.98	7.6408	4.9054	695.6	446.6	55.8	0.82
L1	16.54	18.7044	7.0877	1131.046	428.6	163.9	0.43	10.80	7.8258	5.7665	724.7	534.0	35.7	0.98
R1	15.09	17.176	6.3163	1138.44	418.6	171.9	0.42	10.70	12.1683	4.4734	1136.7	417.9	172.0	0.42
R2	16.14	18.3263	6.7689	1135.751	419.5	170.7	0.42	10.63	12.1351	4.9713	1141.5	467.7	144.1	0.47

block	P50							O30						
sub-sample ID	wet volume (cm^3)	wet weight (gm)	dry weight (gm)	bulk density (kg/m^3)	basic density (kg/m^3)	% moisture content	specific gravity	wet volume (cm^3)	wet weight (gm)	dry weight (gm)	bulk density (kg/m^3)	basic density (kg/m^3)	% moisture content	specific gravity
T4	10.89	11.5816	4.7074	1063.9	432.4	146.0	0.47							
T3	10.19	8.6641	4.4734	850.2	439.0	93.7	0.62	10.72	10.8182	5.1418	1008.9	479.5	110.4	0.56
T2	11.66	9.0791	4.9928	778.3	428.0	81.8	0.67	13.20	10.8298	6.2800	820.4	475.7	72.4	0.72
T1	10.95	8.6558	4.7289	790.5	431.9	83.0	0.67	10.02	7.6080	4.9362	759.6	492.9	54.1	0.83
C	11.55	8.9112	5.0008	771.2	432.8	78.2	0.69	10.83	8.0988	5.2627	747.7	485.8	53.9	0.83
B1	10.31	7.9819	4.5221	774.3	438.7	76.5	0.70	10.94	9.1806	5.2886	839.1	483.4	73.6	0.71
B2	14.37	14.6201	6.4529	1017.7	449.2	126.6	0.52	11.74	11.7243	5.6988	998.7	485.5	105.7	0.58
L2	11.11	8.5848	5.1904	772.5	467.1	65.4	0.76							
L1	10.82	7.7711	5.4311	717.9	501.7	43.1	0.91	19.59	14.3776	7.9210	734.0	404.4	81.5	0.67
R1	12.06	13.6451	5.1645	1131.5	428.2	164.2	0.43	14.48	11.5942	6.8052	800.7	470.0	70.4	0.73
R2	12.14	13.6112	5.348	1121.0	440.5	154.5	0.45							

P/O/20/30/50: pine/oak blocks buried with 20/30/50 cm DoB

Table C.3 Post-burial and recovery timber basic density, bulk density,% moisture content and specific gravity, Swan River sleeper site (cont'd).

block	J20							J30						
sub-sample ID	wet volume (cm^3)	wet weight (gm)	dry weight (gm)	bulk density (kg/m^3)	basic density (kg/m^3)	% moisture content	specific gravity	wet volume (cm^3)	wet weight (gm)	dry weight (gm)	bulk density (kg/m^3)	basic density (kg/m^3)	% moisture content	specific gravity
T4	15.66	11.5816	8.6873	739.7	554.8	33.3	1.00	15.77	15.7665	7.4300	1482.9	698.8	112.2	0.56
T3	12.19	13.3824	6.7821	1097.4	556.1	97.3	0.61	11.66	11.6633	5.8459	1091.8	547.3	99.5	0.60
T2	12.33	13.6298	6.8102	1105.0	552.1	100.1	0.60	10.28	11.1172	5.6164	1081.7	546.5	97.9	0.61
T1	11.55	12.9279	6.3828	1119.8	552.8	102.5	0.59	10.62	10.5447	5.4158	992.6	509.8	94.7	0.62
C	13.30	14.9900	7.4307	1126.8	558.6	101.7	0.59	10.83	11.4766	6.0369	1059.3	557.2	90.1	0.64
B1	12.95	14.6331	7.1370	1129.8	551.0	105.0	0.58	9.49	9.6287	5.2663	1014.3	554.8	82.8	0.67
B2	13.34	15.1172	7.1769	1133.2	538.0	110.6	0.56	10.10	11.0020	5.6835	1089.5	562.8	93.6	0.62
L2	13.83	14.5743	7.7177	1053.7	558.0	88.8	0.64	13.14	12.9521	7.4623	985.9	568.0	73.6	0.71
L1	14.13	16.0137	7.9173	1133.2	560.3	102.3	0.59	13.70	14.4981	7.6654	1058.2	559.5	89.1	0.64
R1	13.23	14.9391	7.2572	1129.4	548.6	105.9	0.58	15.33	16.1041	8.5196	1050.6	555.8	89.0	0.64
R2	12.77	13.7163	7.0991	1074.3	556.0	93.2	0.63	14.58	14.5783	8.1555	985.0	551.0	78.8	0.69

J20/30: jarrah block buried with 20/30 cm DoB

D. SBP DATA

Location of identified sub-surface reflectors, James Matthews sleeper site

Tables D.1 to D.6 identify the latitude and longitude locations for sub-surface reflectors identified along SBP runs over buried sleepers at the James Matthews sleeper site.

Location of sub-surface reflectors identified across the *James Matthews* wrecksite

Table D.7 identifies the latitude and longitude of the ends of contiguous and isolated sub-surface reflectors along transverse SBP runs across the *James Matthews* wrecksite. Table D.8 identifies the same features for longitudinal SBP runs across the *James Matthews* wrecksite.

SBP reflector characteristics

Tables D.9 to D.12 summarise amplitude and depth mean, SD and RSD values for each reflector, coded by the central trace number, extracted from SBP runs at the James Matthews sleeper site. Tables D.13 and D.14 summarize the same characteristics for SBP runs at the Swan River site.

Table D.1 Reflector locations for SBP run 20170608-024600

Reflector (trace) ID	WGS84		decimal degrees	
	latitude	longitude	latitude	longitude
787	-32^0 07.91948’	115^{0}44.65473’	-32.131991	115.744246
826	-32^0 07.91890’	115^{0}44.65359’	-32.131982	115.744227
850	-32^0 07.91833’	115^{0}44.65251’	-32.131972	115.744209
898	-32^0 07.91775’	115^{0}44.65149’	-32.131963	115.744192
936	-32^0 07.91706’	115^{0}44.65057’	-32.131951	115.744176
954	-32^0 07.91706’	115^{0}44.65057’	-32.131951	115.744176
1005	-32^0 07.91538’	115^{0}44.65885’	-32.131923	115.744148
1041	-32^0 07.91445’	115^{0}44.65802’	-32.131908	115.744134
BB1	-32^{0}07.91203'	115^{0}44.64512'	-32.131867	115.7440853
BB2	-32^{0}07.91706'	115^{0}44.65057'	-32.131951	115.7441762

BB: besser block

Table D.2 Reflector locations for SBP run 20170608-025024

Reflector (trace) ID	WGS84		decimal degrees	
	latitude	longitude	latitude	longitude
799	-32^0 07.91710’	115^{0}44.65133’	-32.131952	115.744189
829	-32^0 07.91710’	115^{0}44.65133’	-32.131952	115.744189
850	-32^0 07.91650’	115^{0}44.65029’	-32.131942	115.744172
900	-32^0 07.91570’	115^{0}44.64927’	-32.131928	115.744155
940	-32^0 07.91500’	115^{0}44.64825’	-32.131917	115.744138
973	-32^0 07.91420’	115^{0}44.64722’	-32.131903	115.744120
1016	-32^0 07.91330’	115^{0}44.64617’	-32.131888	115.744103
1042	-32^0 07.91330’	115^{0}44.64617’	-32.131888	115.744103
1062	-32^0 07.91260’	115^{0}44.64509’	-32.131877	115.744085
1079	-32^0 07.91260’	115^{0}44.64509’	-32.131877	115.744085
BB1	-32^{0}07.91259'	115^{0}44.64509'	-32.131877	115.535531
BB2	-32^{0}07.91645'	115^{0}44.65029'	-32.131941	115.535532

Table D.3 Reflector locations for SBP run 18052018-135105.

Reflector (trace) ID	WGS84		decimal degrees	
	latitude	longitude	latitude	longitude
428	-32^0 07.92177’	115^{0}44.65614’	-32.132030	115.744269
595	-32^0 07.92155’	115^{0}44.65584’	-32.132026	115.744264
903	-32^0 07.92121’	115^{0}44.65528’	-32.132020	115.744255
1145	-32^0 07.92086’	115^{0}44.65469’	-32.132014	115.744245
1426	-32^0 07.92056’	115^{0}44.65426’	-32.132009	115.744238
1723	-32^0 07.92016’	115^{0}44.65370’	-32.132003	115.744228
2081	-32^0 07.91970’	115^{0}44.65308’	-32.131995	115.744218
2522	-32^0 07.91899’	115^{0}44.65222’	-32.131983	115.744204
2810	-32^0 07.91862’	115^{0}44.65177’	-32.131977	115.744196
3073	-32^0 07.91814’	115^{0}44.65113’	-32.131969	115.744186
3126	-32^0 07.91810’	115^{0}44.65108’	-32.131968	115.744185
3366	-32^0 07.91780’	115^{0}44.65065’	-32.131963	115.744178
3909	-32^0 07.91719’	115^{0}44.64974’	-32.131953	115.744162
4227	-32^0 07.91693’	115^{0}44.64934’	-32.131949	115.744156
4528	-32^0 07.91644’	115^{0}44.64874’	-32.131941	115.744146
4782	-32^0 07.91596’	115^{0}44.64819’	-32.131933	115.744137
5273	-32^0 07.91521’	115^{0}44.64724’	-32.131920	115.744121
5695	-32^0 07.91458’	115^{0}44.64637’	-32.131910	115.744106
6005	-32^0 07.91424’	115^{0}44.64587’	-32.131904	115.744098
6330	-32^0 07.91375’	115^{0}44.64532’	-32.131896	115.744089
6724	-32^0 07.91314’	115^{0}44.64471’	-32.131886	115.744079
7152	-32^0 07.91274’	115^{0}44.64427’	-32.131879	115.744071
7301	-32^0 07.91257’	115^{0}44.64407’	-32.131876	115.744068
7428	-32^0 07.91244’	115^{0}44.64392’	-32.131874	115.744065
7729	-32^0 07.91202’	115^{0}44.64342’	-32.131867	115.744057
7937	-32^0 07.91178’	115^{0}44.64312’	-32.131863	115.744052

Table D.4 Reflector locations for SBP run 18052018-135516.

Reflector (trace) ID	WGS84		decimal degrees	
	latitude	longitude	latitude	longitude
162	-32^0 07.921883’	115^{0}44.65630’	-32.132031	115.744272
364	-32^0 07.921574’	115^{0}44.65586’	-32.132026	115.744264
717	-32^0 07.921268’	115^{0}44.65540’	-32.132021	115.744257
1004	-32^0 07.920949’	115^{0}44.65486’	-32.132016	115.744248
1252	-32^0 07.920590’	115^{0}44.65430’	-32.132010	115.744238
1523	-32^0 07.920367’	115^{0}44.65395’	-32.132006	115.744233
3545	-32^0 07.918689’	115^{0}44.65189’	-32.131978	115.744198
3763	-32^0 07.918476’	115^{0}44.65162’	-32.131975	115.744194
3945	-32^0 07.918128’	115^{0}44.65121’	-32.131969	115.744187
4243	-32^0 07.917767’	115^{0}44.65074’	-32.131963	115.744179
4714	-32^0 07.917251’	115^{0}44.64999’	-32.131954	115.744167
4915	-32^0 07.916943’	115^{0}44.64947’	-32.131949	115.744158
5646	-32^0 07.916038’	115^{0}44.64821’	-32.131934	115.744137
6106	-32^0 07.915264’	115^{0}44.64735’	-32.131921	115.744123
6501	-32^0 07.914607’	115^{0}44.64646’	-32.131910	115.744108
7119	-32^0 07.913881’	115^{0}44.64543’	-32.131898	115.744091
7482	-32^0 07.913299’	115^{0}44.64479’	-32.131888	115.744080
7703	-32^0 07.912913’	115^{0}44.64434’	-32.131882	115.744072
7956	-32^0 07.912492’	115^{0}44.64386’	-32.131875	115.744064
8309	-32^0 07.912077’	115^{0}44.64344’	-32.131868	115.744057
8581	-32^0 07.911960’	115^{0}44.64334’	-32.131866	115.744056

Table D.5 Reflector locations for SBP run 18052018-132252.

Reflector (trace) ID	WGS84		decimal degrees	
	latitude	longitude	latitude	longitude
234	-32^0 07'54.703''	115^{0}44'38.582''	-32.131862	115.744051
384	-32^0 07'54.710''	115^{0}44'38.593''	-32.131864	115.744054
592	-32^0 07'54.754''	115^{0}44'38.644''	-32.131876	115.744068
972	-32^0 07'54.774''	115^{0}44'38.666''	-32.131882	115.744074
1355	-32^0 07'54.814''	115^{0}44'38.710''	-32.131893	115.744086
1774	-32^{0}07'54.843"	115^{0}44'38.744''	-32.131901	115.744096
1981	-32^0 07'54.860''	115^{0}44'38.764''	-32.131906	115.744101
2302	-32^0 07'54.899''	115^{0}44'38.814''	-32.131916	115.744115
2534	-32^0 07'54.926''	115^{0}44'38.850''	-32.131924	115.744125
2702	-32^0 07'54.943''	115^{0}44'38.873''	-32.131929	115.744131
2931	-32^0 07'54.974''	115^{0}44'38.912''	-32.131937	115.744142
3226	-32^0 07'55.003''	115^{0}44'38.947''	-32.131945	115.744152
4489	-32^0 07'55.028''	115^{0}44'38.979''	-32.131952	115.744161
5164	-32^0 07'55.062''	115^{0}44'39.027''	-32.131962	115.744174
5353	-32^0 07'55.075''	115^{0}44'39.050''	-32.131965	115.744181
5654	-32^0 07'55.102''	115^{0}44'39.089''	-32.131973	115.744191
5890	-32^0 07'55.128''	115^{0}44'39.125''	-32.131980	115.744201
6704??	-32^0 07'55.161''	115^{0}44'39.167'	-32.131989	115.744213
7121	-32^0 07'55.170''	115^{0}44'39.178''	-32.131992	115.744216
7853	-32^0 07'55.234''	115^{0}44'39.252''	-32.132009	115.744237
8242	-32^0 07'55.251''	115^{0}44'39.275''	-32.132014	115.744243
8484	-32^0 07'55.263''	115^{0}44'39.295''	-32.132018	115.744249
8807	-32^0 07'55.286''	115^{0}44'39.338''	-32.132024	115.744261
9280	-32^0 07'55.309''	115^{0}44'39.373''	-32.132030	115.744270

Table D.6 Reflector locations for SBP run 18052018-135912.

Reflector (trace) ID	WGS84		decimal degrees	
	latitude	longitude	latitude	longitude
290	-32^0 07'54.702'	115^{0}44'38.582''	-32.131862	115.744050
502	-32^0 07'54.710''	115^{0}44'38.593''	-32.131865	115.744054
732	-32^0 07'54.754''	115^{0}44'38.644''	-32.131871	115.744063
970	-32^0 07'54.774''	115^{0}44'38.666''	-32.131876	115.744068
1262	-32^0 07'^{0}54.814''	115^{0}44'38.710''	-32.131883	115.744076
1567	-32^0 07'54.743''	115^{0}44'38.744''	-32.131893	115.744086
1868	-32^0 07'54.860''	115^{0}44'38.764''	-32.131901	115.744094
2186	-32^0 07'54.899''	115^{0}44'38.814''	-32.131906	115.744102
2620	-32^0 07'54.926''	115^{0}44'38.850''	-32.131917	115.744118
3227	-32^0 07'54.943''	115^{0}44'38.873''	-32.131930	115.744134
3525	-32^0 07'54.974''	115^{0}44'38.912''	-32.131936	115.744142
3981	-32^0 07'55.003''	115^{0}44'38.947''	-32.131944	115.744154
4154	-32^0 07'55.028''	115^{0}44'38.979''	-32.131949	115.744159
4543	-32^0 07'55.062''	115^{0}44'39.027''	-32.131959	115.744173
4747	-32^0 07'55.0^{0}75''	115^{0}44'39.050''	-32.131966	115.744181
5071	-32^0 07'55.102''	115^{0}44'39.089''	-32.131974	115.744192
5450??	-32^0 07'55.128''	115^{0}44'39.125''	-32.131982	115.744202
5804	-32^0 07'55.161''	115^{0}44'39.167'	-32.131991	115.744213
6224	-32^0 07'55.170''	115^{0}44'39.178''	-32.132002	115.744228
6507	-32^0 07'55.234''	115^{0}44'39.252''	-32.132009	115.744236
6743	-32^0 07'55.251''	115^{0}44'39.275''	-32.132013	115.744242
6975	-32^0 07'55.263''	115^{0}44'39.295''	-32.132017	115.744248
7228	-32^0 07'55.286''	115^{0}44'39.338''	-32.132024	115.744259
7433	-32^0 07'55.309''	115^{0}44'39.373''	-32.132028	115.744266

Table D.7 Latitude and longitude of ends of contiguous and isolated sub-surface reflectors along transverse SBP runs, *James Matthews* wrecksite.

Transverse tracks SBP run ID	western end of contiguous reflector		eastern end of contiguous reflector		western end of isolated reflector		eastern end of isolated reflector	
	longitude	latitude	longitude	latitude	longitude	latitude	longitude	latitude
JM_12kHz_20170607_045617								
JM_12kHz_20170607_045828								
JM_12kHz_20170607_050037	115.733508	-32.1169215	115.73351	-32.1169210				
JM_12kHz_20170607_050357	115.733508	-32.1169213	115.73351	-32.1169207				
JM_12kHz_20170607_050504	115.733506	-32.1169194	115.733508	-32.1169186	115.733505	-32.1169195	115.733506	-32.1169194
JM_12kHz_20170607_050619	115.733508	-32.1169209	115.73351	-32.1169203				
JM_12kHz_20170607_050821	115.733506	-32.1169193	115.733507	-32.1169191	115.733507	-32.1169189	115.733508	-32.1169185
JM_12kHz_20170607_050945	115.733508	-32.1169210	115.733509	-32.1169205	115.733503	-32.1169233	115.733504	-32.1169231
JM_12kHz_20170607_051048	115.733506	-32.1169200	115.733508	-32.1169194	115.733505	-32.1169202	115.733505	-32.1169201
JM_12kHz_20170607_051228	115.733508	-32.1169210	115.733509	-32.1169205				
JM_12kHz_20170607_051421	115.733506	-32.1169197	115.733508	-32.1169192	115.733506	-32.1169198	115.733506	-32.1169198
JM_12kHz_20170607_051619	115.733506	-32.1169208	115.733509	-32.1169196				
JM_12kHz_20170607_051745	115.733507	-32.1169204	115.733509	-32.1169196	115.733507	-32.1169206	115.733507	-32.1169204
51745 cont'd					115.733509	-32.1169195	115.73351	-32.1169193
JM_12kHz_20170607_051953	115.733506	-32.1169202	115.733508	-32.1169190	115.733508	-32.1169188	115.733509	-32.1169187
JM_12kHz_20170607_052110	115.733507	-32.1169203	115.733509	-32.1169200	115.733506	-32.1169207	115.733507	-32.1169206
JM_12kHz_20170607_052310	115.733506	-32.1169186	115.733507	-32.1169183				
JM_12kHz_20170607_052451	115.733508	-32.1169212	115.73351	-32.1169208				
JM_12kHz_20170607_052644	115.733507	-32.1169212	115.73351	-32.1169205				
JM_12kHz_20170607_052801	115.733508	-32.1169220	115.733509	-32.1169217				
JM_12kHz_20170607_052937	115.733506	-32.1169184	115.733507	-32.1169182				
JM_12kHz_20170607_053048	115.733508	-32.1169218	115.73351	-32.1169214	115.733512	-32.1169204	115.733513	-32.1169202
JM_12kHz_20170607_053203	115.733505	-32.1169189	115.733506	-32.1169184	115.733333	-32.1166667	115.733333	-32.1166667
JM_12kHz_20170607_053316	115.733508	-32.1169216	115.73351	-32.1169215	115.733333	-32.1166667	115.733333	-32.1166667
JM_12kHz_20170607_053543	115.733506	-32.1169188	115.733506	-32.1169184	115.733333	-32.1166667	115.733333	-32.1166667
JM_12kHz_20170607_053700	115.733506	-32.1169187	115.733507	-32.1169184	115.733333	-32.1166667	115.733333	-32.1166667

Table D.7 Latitude and longitude of ends of contiguous and isolated sub-surface reflectors, *James Matthews* wrecksite (cont'd).

Transverse tracks SBP run ID	western end of contiguous reflector		eastern end of contiguous reflector		western end of isolated reflector		eastern end of isolated reflector	
	longitude	latitude	longitude	latitude	longitude	latitude	longitude	latitude
JM_12kHz_20170607_053833			115.733507	-32.1169188	115.733333	-32.1166667	115.733333	-32.1166667
JM_12kHz_20170608_031353								
JM_12kHz_20170608_031531	115.733506	-32.1169195	115.733507	-32.1169187	115.733506	-32.1169201	115.733506	-32.1169197
JM_12kHz_20170608_031818	115.733507	-32.1169198	115.733508	-32.1169193	115.733506	-32.1169204	115.733507	-32.1169202
JM_12kHz_20170608_032227	115.733508	-32.1169207	115.733509	-32.1169201	115.733508	-32.1169211	115.733508	-32.1169209
JM_12kHz_20170608_032410	115.733508	-32.1169213	115.733509	-32.1169203				
JM_12kHz_20170608_032550	115.733509	-32.1169220	115.733509	-32.1169214	115.733509	-32.1169212	115.73351	-32.1169209
JM_12kHz_20170608_032823	115.733507	-32.1169200	115.733508	-32.1169187				
JM_12kHz_20170608_033023	115.733509	-32.1169219	115.73351	-32.1169216				
JM_12kHz_20170608_033710	115.733509	-32.1169218	115.733509	-32.1169208				
JM_12kHz_20170608_040920	115.733508	-32.1169221	115.733509	-32.1169215	115.733509	-32.1169212	115.733509	-32.1169208

Table D.8 Latitude and longitude of ends of contiguous and isolated sub-surface reflectors along longitudinal SBP runs, *James Matthews* wrecksite.

Longitudinal tracks SBP run ID	Northern end of contiguous reflector		Southern end of contiguous reflector		Northern end of isolated reflector		Southern end of isolated reflector	
	longitude	latitude	longitude	latitude	longitude	latitude	longitude	latitude
JM_12kHz_20170608_041131	115.733509	-32.1169213	115.733507	-32.1169208	115.73351	-32.1169219	115.73351	-32.1169218
41131 cont'd					115.733507	-32.1169207	115.733507	-32.1169205
JM_12kHz_20170608_041258	115.733506	-32.1169204	115.73351	-32.1169218	115.73351	-32.1169219	115.73351	-32.1169219
JM_12kHz_20170608_041421	115.733506	-32.1169197	115.73351	-32.1169213				
JM_12kHz_20170608_041554	115.733506	-32.1169199	115.73351	-32.1169216				
JM_12kHz_20170608_041720	115.733507	-32.1169190	115.733509	-32.1169198	115.733505	-32.1169183	115.733506	-32.1169187
41720 cont'd	115.733509	-32.1169200	115.73351	-32.1169201	115.733506	-32.1169187	115.733506	-32.1169189
JM_12kHz_20170608_041837	115.733506	-32.1169182	115.733509	-32.1169198				
JM_12kHz_20170608_042015	115.733507	-32.1169190	115.73351	-32.1169209				
JM_12kHz_20170608_042312	115.733507	-32.1169185	115.733509	-32.1169204				
JM_12kHz_20170608_042455	115.733507	-32.1169200	115.73351	-32.1169215	115.733506	-32.1169193	115.733507	-32.1169197
JM_12kHz_20170608_042734	115.733506	-32.1169190	115.733509	-32.1169208				

Table D.9 Summary variability, James Matthews sleeper site, SBP run 20170608-024600.

trace	seabed level* (m)		1st reflr	DoB (cm)		sleeper thickness (cm)	depth seabed mult (m) (HF)	depth variability					
								seabed (m) (HF)		DoB (cm) (LF/LF)		seabed mult (m) (HF)	
	LF demod	HF demod	LF demod	LF/LF	HF/LF			SD	RSD	SD	RSD	SD	RSD
787	2.468	2.455	2.909	44.1	45.4	-	4.801	0.033	1.3%	3.16	7.2%	0.014	0.3%
826	2.444	2.419	2.633	18.8	21.4	12.0	4.824	0.006	0.2%	3.08	16.4%	0.039	0.8%
850	2.474	2.438	2.779	29.7	34.1	14.7	4.794	0.012	0.5%	3.07	10.4%	0.022	0.5%
898	2.457	2.444	2.969	50.5	52.5	17.1	4.807	0.005	0.2%	0.90	1.8%	0.009	0.2%
936	2.444	2.423	2.738	29.3	31.5	-	4.801	0.025	1.0%	2.89	9.9%	0.023	0.5%
954	2.427	2.402	2.733	29.1	33.1	-	4.781	0.008	0.3%	1.91	6.6%	0.021	0.4%
1005	2.455	2.395	2.658	20.3	26.3	12.0	4.674	0.016	0.7%	1.69	8.3%	0.006	0.1%
1041	2.457	2.436	2.832	37.4	39.6	-	4.803	0.018	0.7%	1.07	2.9%	0.012	0.3%
mean	*2.453*	*2.426*				*14.0*		*0.015*	*0.6%*	*2.22*	*7.9%*	*0.018*	*0.4%*
SD	*0.015*	*0.021*				*2.5*							

trace	amplitude variability								
	Seabed (LF)			1st reflr (LF)			seabed mult (LF)		
	amp	SD	RSD	amp	SD	RSD	amp	SD	RSD
787	16354	3208	19.6%	934	186	19.9%	-354	65	18.3%
826	28856	4841	16.8%	3981	1365	34.3%	-149	65	43.3%
850	-21066	6393	30.3%	1771	509	28.7%	-53	12	22.9%
898	23010	9220	40.1%	-1643	207	12.6%	-193	153	79.3%
936	21160	4133	19.5%	6092	125	2.1%	462	134	29.1%
954	-31266	3172	10.1%	-17499	1714	9.8%	130	21	15.8%
1005	-23133	8072	34.9%	-6438	1584	24.6%	-666	211	31.7%
1041	15577	5093	32.7%	-949	82	8.6%	-115	55	48.0%
mean		*5516*	*25.5%*		*722*	*17.6%*		*89*	*36.0%*

Table D.10 Summary variability, James Matthews sleeper site, SBP run 20170608-025024.

trace	seabed level* (m)		1st reflr	DoB (cm)		sleeper thickness (cm)	depth seabed mult (m)	depth variability					
								seabed (m) (HF)		DoB (cm) (LF/LF)		seabed mult (m) (HF)	
	LF demod	HF demod	LF demod	LF/LF	HF/LF			SD	RSD	SD	RSD	SD	RSD
799	2.622	2.577	2.896	27.4	31.9	18.8	4.953	0.014	0.6%	2.46	9.0%	0.016	0.3%
829	2.609	2.569	2.851	24.2	28.2	18.2	4.935	0.012	0.5%	4.82	19.9%	0.021	0.4%
850	2.592	2.605	2.986	39.4	38.1	19.0	4.938	0.028	1.1%	2.32	5.9%	0.011	0.2%
900	2.650	2.571	2.843	19.3	27.2	-	4.863	0.021	0.8%	2.00	10.4%	0.015	0.3%
917	2.622	2.592	2.866	24.4	27.4	-	4.970	0.023	1.05	0.01	0.0%	0.025	0.55
940	2.652	2.603	2.883	23.1	28.0	11.8	4.965	0.005	0.2%	1.62	7.0%	0.010	0.2%
973	2.629	2.586	3.012	38.3	42.6	12.2	4.938	0.005	0.2%	2.06	5.4%	0.008	0.2%
992	2.661	2.440	2.817	15.6	37.7	-	4.777	0.023	1.0%	1.90	12.0%	0.210	0.4%
1016	2.654	2.631	2.870	21.6	23.9	12.6	4.991	0.023	0.9%	3.33	15.4%	0.000	0.0%
1042	2.635	2.599	2.877	24.2	27.8	12.4	4.955	0.023	0.9%	1.79	7.4%	0.021	0.4%
1062	2.648	2.590	2.858	21.0	26.8	-	4.944	0.006	0.2%	6.45	30.7%	0.022	0.4%
mean	*2.633*	*2.593*				*15.0*		*0.0*	*0.5%*	*2.99*	*11.9%*	*0.0*	*0.3%*

trace	amplitude variability								
	seabed			1st reflr			seabed mult		
	amp	SD	RSD	amp	SD	RSD	amp	SD	RSD
799	-19735	11944	60.5%	-5561	660	11.9%	361	39	10.9%
829	17655	5997	34.0%	-2804	207	7.4%	-195	75	38.4%
850	-17330	9819	56.7%	1288	224	17.4%	-194	122	62.9%
900	28298	6144	21.7%	-16330	2146	13.1%	-142	16	11.2%
917	14656	4594	31.0%	2866	1069	37.0%	-315	105	49.0%
940	-23745	7131	30.0%	-5494	1235	22.5%	310	94	30.5%
973	-21707	7777	35.8%	-6032	1252	20.8%	168	83	49.8%
992	28779	4772	17.0%	-5058	1055	21.0%	-90.8	44.4	49.0%
1016	20788	8303	39.9%	-8925	1347	15.1%	215	109	50.7%
1042	27772	7241	26.1%	-18498	1817	9.8%	461	0	0.0%
1062	19372	7197	37.2%	7204	418	5.8%	807	258	32.0%
mean		*7356*	*35.4%*		*1039*	*16.5%*		*86*	*34.9%*

Table D.11 Summary variability, James Matthews sleeper site, SBP run 18052018-135105.

trace	seabed level* (m)		1st reflr	DoB (cm)		sleeper thickness (cm)	phase reversal	depth seabed mult (m) (HF)	depth variability					
									seabed (m) (HF)		DoB (cm) LF/LF		seabed mult (m) (HF)	
	LF demod	HF demod	LF demod	LF/LF	HF/LF				SD	RSD	SD	RSD	SD	RSD
428	0.978	1.020	1.232	25.5	21.2	-	-	1.850	0.025	2.4%	2.06	8.1%	0.008	0.4%
595	1.016	0.963	1.226	21.0	26.3	12.0	yes	1.855	0.000	0.0%	0.59	2.8%	0.005	0.3%
903	1.022	0.963	1.264	24.2	30.1	12.6	yes	1.825	0.000	0.0%	0.59	2.4%	0.006	0.3%
1145	1.001	0.963	1.196	19.5	23.3	10.1	yes	1.850	0.000	0.0%	2.32	11.9%	0.000	0.0%
1426	1.001	0.993	1.196	19.5	20.3	10.1	yes	1.842	0.005	0.5%	2.32	11.9%	0.005	0.3%
1723	1.046	0.984	1.119	7.3	14.6	17.3	yes	1.874	0.000	0.0%	1.51	17.7%	0.005	0.3%
2081	1.050	0.993	1.251	20.1	25.8	15.6	yes	1.893	0.005	0.5%	2.89	17.5%	0.0	0.0%
2522	1.031	0.980	1.179	14.8	19.9	8.6^	2/5	1.861	0.006	0.6%	0.48	3.2%	0.000	0.0%
2810	1.012	0.978	1.262	25.0	28.4	9.8	yes	1.870	0.006	0.6%	1.94	7.8%	0.026	1.4%
3126	1.020	0.975	1.375	35.5	40.0	12.8	yes	1.884	0.005	0.5%	0.48	1.3%	0.005	0.3%
3366	0.960	0.967	1.273	31.2	30.6	16.0	yes	1.859	0.010	1.0%	3.24	10.4%	0.005	0.3%
3909	0.984	0.952	1.230	22.9	27.8	-	-	1.807	0.000	0.0%	1.22	5.3%	0.008	0.4%
4227	0.978	0.973	1.236	25.9	26.3	9.4	yes	1.869	0.000	0.0%	2.06	7.9%	0.010	0.5%
4528	0.963	0.986	1.206	24.4	22.0	-	-	1.863	0.005	0.5%	0.62	2.6%	0.005	0.3%
4782	1.055	0.990	1.209	15.4	21.9	-	-	1.910	0.006	0.6%	1.94	12.6%	0.006	0.3%
5273	1.018	0.973	1.226	20.7	25.3	-	-	1.882	0.000	0.0%	3.43	16.5%	0.000	0.0%
5695	1.010	0.969	1.335	32.5	36.6	11.8	yes	1.919	0.006	0.6%	2.22	6.8%	0.014	0.7%
6002	1.025	1.061	1.153	12.8	9.2	-	-	1.919	0.005	0.5%	1.07	8.3%	0.006	0.3%
6330	1.027	0.973	1.215	18.8	24.2	14.3	2/5	1.893	0.000	0.0%	0.96	5.1%	0.000	0.0%
6724	1.003	1.003	1.221	21.8	21.8	11.8	yes	1.904	0.009	0.9%	2.22	10.2%	0.013	0.7%
7152	1.014	0.958	1.234	22.0	27.6	-	-	1.855	0.006	0.6%	1.79	8.1%	0.006	0.3%
7301	1.027	0.963	1.305	27.8	34.2	-	-	1.872	0.000	0.0%	0.87	3.1%	0.000	0.0%
7428	1.027	0.973	1.185	15.8	21.2	-	-	1.906	0.000	0.0%	2.06	13.0%	0.009	0.5%
7727	1.003	0.952	1.104	10.1	15.2	15.8	yes	1.840	0.000	0.0%	0.59	5.8%	0.000	0.0%
7937	1.010	0.988	1.164	15.4	17.6	-	2/5	1.917	0.035	3.6%	2.58	15.4%	0.026	1.3%
mean	*1.013*	*0.979*				*12.2*			*0.005*	*0.5%*	*1.68*	*8.6%*	*0.007*	*0.4%*
SD	*0.022*	*0.023*				*2.3*								

*depth below transducer head; ^ gap between upper and lower (stacked) sleepers

Table D.11 (cont'd) Summary variability, James Matthews sleeper site, SBP run 18052018-135105.

trace	amplitude variability								
	seabed surface			1st reflector			1st seabed multiple		
	amp	SD	RSD	amp	SD	RSD	amp	SD	RSD
428	5129	1801	35%	-6491	297	5%	719	72	10%
595	-15552	4476	29%	-4598	388	8%	719	72	10%
903	11390	3546	31%	7492	602	8%	1224	62	5%
1145	-12907	3122	24%	-8714	2452	28%	1697	131	8%
1426	12102	4885	40%	-12730	1006	8%	1380	58	4%
1723	-14010	5508	39%	-4920	595	12%	1138	138	12%
2081	21432	8532	40%	8852	1425	16%	633	36	6%
2522	9215	2462	27%	-2973	433	15%	-857	86	10%
2810	-6089	2082	34%	9064	719	8%	-406	33	8%
3126	9940	3902	39%	4632	262	6%	-650	71	11%
3366	9174	5088	55%	11156	552	5%	-715	29	4%
3909	-9619	3629	38%	3021	426	14%	346	14	4%
4227	-6957	2886	41%	8860	943	11%	499	27	5%
4528	11860	1999	17%	3788	415	11%	471	41	9%
4782	-8782	6064	69%	-9236	468	5%	1080	129	12%
5273	-6001	1896	32%	6720	529	8%	963	109	11%
5695	8070	1930	24%	4991	452	9%	180	30	17%
6002	15187	7816	51%	-5599	58	7%	-504	94	19%
6330	12718	6331	50%	-7947	829	10%	-255	16	6%
6724	-6489	411	6%	7424	526	7%	893	109	12%
7152	-21669	10452	48%	-8616	223	3%	516	48	9%
7301	30828	4221	14%	-1984	344	17%	1604	57	4%
7428	-18762	5182	28%	7063	369	5%	946	78	8%
7729	-19552	11582	59%	10025	2036	20%	-1171	46	4%
7937	14867	4209	28%	-7153	617	9%	1092	101	9%
mean		*4416*	*34.9%*		*648*	*9.9%*		*65*	*8.6%*

Table D.12 Summary variability, James Matthews sleeper site, SBP run 18052018-135516.

trace	seabed level* (m)		1st reflr	DoB (cm)		sleeper thickness (cm)	phase reversal	depth seabed mult (m)	depth variability					
									seabed (m) (HF)		DoB (cm) (LF/LF)		seabed mult (m) (LF)	
	LF demod	HF demod	LF demod	LF/LF	HF/LF				SD	RSD	SD	RSD	SD	RSD
162	1.020	0.984	1.23	21	24.6	8.3	yes	1.882	0.000	0.0%	0.96	4.6%	0.000	0.0%
364	1.007	0.980	1.219	21.2	23.9	11.3	no	1.872	0.006	0.6%	1.17	5.5%	0.000	0.0%
717	1.031	0.963	1.273	24.2	31.0	11.8	yes	1.848	0.000	0.0%	0.96	4.0%	0.005	0.3%
1004	1.025	0.96	1.187	16.3	22.7	10.5	no	1.85	0.005	0.5%	0.48	2.9%	0.000	0.0%
1252	0.988	0.963	1.2	18.6	23.7	-	-	1.85	0.000	0.0%	0.59	3.1%	0.000	0.0%
1523	0.969	1.063	1.117	14.8	5.4	10.5	no	1.902	0.006	0.6%	2.66	18.0%	0.005	0.3%
2676	0.971	0.965	1.247	27.6	28.2	-	-	1.874	0.005	0.5%	1.39	5.1%	0.005	0.3%
3291	1.04	0.993	1.183^	14.3^	19.0^	7.3#	-	1.872	0.009	0.9%	1.62	11.3%	0.000	0.0%
3545	1.035	1.02	1.271	23.5	25.1	8.8	yes	1.882	0.006	0.6%	2.14	9.1%	0.000	0.0%
3945	1.035	0.971	1.39	35.5	41.9	10.5	yes	1.884	0.005	0.5%	2.77	7.8%	0.005	0.3%
4243	1.027	0.988	1.478	45.1	49.0	-	-	1.906	0.006	0.6%	0.48	1.7%	0.005	0.3%
4727	0.997	0.997	1.245	24.8	24.8	16	no	1.897	0.005	0.5%	3.81	15.4%	0.006	0.3%
4929	1.022	0.984	1.256	23.3	27.2	7.5	2/5	1.882	0.000	0.0%	2.32	9.9%	0.000	0.0%
5302	1.003	0.984	1.206	20.3	22.2	14.8	no	1.893	0.000	0.0%	2.14	10.5%	0.000	0.0%
5646	1.013	1.042	1.206	19.5	16.4	17.3	yes	1.904	0.022	2.1%	2.20	11.3%	0.000	0.0%
6106	1.031	0.965	1.236	20.5	27.1	17.3	yes	1.882	0.005	0.5%	2.06	10.0%	0.000	0.0%
6501	1.007	0.978	1.33	32.3	35.2	11.3	yes	1.891	0.006	0.6%	1.76	5.4%	0.005	0.3%
6757	0.963	0.960	1.027	6.4	6.7	12.4	yes	1.882	0.009	0.9%	0.00	0.0%	0.000	0.0%
7119	1.027	1.033	1.211	18.4	17.8	8.3	2/5	1.914	0.006	0.6%	0.48	2.6%	0.000	0.0%
7482	1.04	0.984	1.219	18	23.5	10.5	yes	1.904	0.000	0.0%	0.89	5.0%	0.000	0.0%
7703	0.971	0.975	1.234	26.3	25.9	-	-	1.863	0.005	0.5%	1.43	5.5%	0.005	0.3%
7956	1.031	0.973	1.174	14.3	20.1	10.9	yes	1.876	0.000	0.0%	0.59	4.1%	0.006	0.3%
8325	0.948	1.037	1.112	16.5	7.5	11.8	yes	1.949	0.000	0.0%	0.59	7.4%	0.005	0.2%
mean	1.009	0.990				11.7			0.005	0.5%	1.46	7.0%	0.002	0.1%
SD	0.028	0.029				2.9								

^ underside of sleeper; * depth below transducer head; # gap between stacked sleepers

Table D.12 (cont'd) Summary variability, James Matthews sleeper site, SBP run 18052018-135516.

trace	amplitude variability								
	seabed surface			1st reflector			1st seabed multiple		
	amp	SD	RSD	amp	SD	RSD	amp	SD	RSD
162	8683	4110	47%	-4461	329	7%	755	97	13%
364	9857	3010	31%	5306	1499	28%	957	58	6%
717	-6821	2470	36%	7917	877	11%	1221	119	10%
1004	28908	3434	12%	12479	1995	16%	1470	181	12%
1252	15453	5039	33%	8206	5039	14%	1347	72	5%
1523	-7035	2450	35%	-5280	977	19%	840	72	9%
2676	9210	1497	16%	-1850	180	10%	381	55	14%
3291	8971	3895	43%	-2938	167	6%	247	48	20%
3545	5326	1378	26%	12253	285	2%	205	24	12%
3945	-10487	1854	18%	5430	410	8%	-316	80	25%
4243	-16663	2061	2%	-18920	1479	8%	696	52	8%
4727	-11309	6133	54%	5506	345	6%	836	99	12%
4929	-4191	775	18%	-6613	389	6%	365	22	6%
5302	-10713	3414	32%	2371	250	11%	430	71	17%
5646	-6469	2801	43%	8258	368	4%	898	55	6%
6106	8435	837	10%	-9397	212	2%	657	45	7%
6501	-7660	1467	19%	4928	560	11%	240	29	12%
6757	-7731	725	9%	10745	3386	32%	605	53	9%
7119	9395	2474	26%	7539	494	7%	408	52	13%
7482	-7855	899	11%	7399	615	8%	1219	118	10%
7703	-4162	958	23%	-8882	448	5%	266	9	3%
7956	-9778	3316	34%	-5381	488	9%	264	20	7%
8325	-4774	270	6%	17357	2777	16%	-650	57	9%
mean		2403	25%		1025	13%		65	11%

Table D.13 Summary variability, Swan River sleeper site, SBP run 17052018-123344.

trace	seabed level* (m)		total water depth (m)	1st reflr	DoB (cm)		sleeper thickness (cm)	depth seabed mult (m) (HF)	depth variability					
									Seabed (m) (HF)		1st reflector depth (m)		seabed mult (m) (HF)	
	LF demod	HF demod		LF demod	LF/LF	HF/LF			SD	RSD	SD	RSD	SD	RSD
218	0.836	0.772	0.90	0.990	15.4	21.8	-	1.471	0.005	0.6%	0.006	0.6%	0.009	0.6%
1138	0.819	0.761	0.90	1.176	35.7	41.5	-	1.480	0.005	0.6%	0.000	0.0%	0.010	0.6%
1967	0.815	0.764	0.90	0.939	12.4	17.5	-	1.457	0.006	0.8%	0.009	1.0%	0.005	0.3%
2276	0.856	0.740	0.90	0.999	14.3	25.9	-	1.448	0.009	1.2%	0.010	1.0%	0.006	0.4%
2507	0.830	0.761	0.90	1.055	22.5	29.4	10.5	1.478	0.005	0.6%	0.014	1.4%	0.005	0.3%
2896	0.800	0.757	0.90	0.939	13.9	18.2	-	1.463	0.005	0.6%	0.009	1.0%	0.009	0.6%
3245	0.841	0.766	0.90	1.025	18.4	25.9	-	1.467	0.006	0.8%	0.005	0.5%	0.005	0.3%
3413	0.828	0.781	0.90	1.010	18.2	22.9	-	1.474	0.000	0.0%	0.006	0.6%	0.005	0.3%
3574	0.817	0.759	0.90	1.224	40.6	46.5	-	1.461	0.008	1.0%	0.006	0.5%	0.006	0.4%
mean	*0.827*	*0.762*					*10.5*		*0.005*	*0.7%*	*0.007*	*0.7%*	*0.006*	*0.4%*
SD	*0.016*	*0.011*												

trace	amplitude variability								
	seabed			1st reflector			1st seabed multiple		
	amp	SD	RSD	amp	SD	RSD	amp	SD	RSD
218	16460	1276	7.8%	-8920	3298	37.0%	-5475	1195	-21.8%
1138	-24867	5365	21.6%	4297	272	6.3%	6184	338	5.5%
1967	25321	5245	20.7%	4977	610	12.3%	6619	1173	17.7%
2276	21527	6806	31.6%	3260	964	29.6%	-4255	1143	26.9%
2507	-27528	7343	26.7%	-2477	287	11.6%	-5586	599	10.7%
2896	22262	7901	35.5%	5976	1515	25.4%	-7681	613	8.0%
3245	22262	3113	14.0%	-6453	429	6.6%	-4775	380	8.0%
3413	-12435	3180	25.6%	-4090	643	15.7%	-1846	179	9.7%
3574	-17841	8698	48.8%	2302	99	4.3%	-1779	258	14.5%
mean		*5436*	*25.8%*		*902*	*16.5%*		*653*	*8.8%*

Table D.14 Summary variability, Swan River sleeper site, SBP run 17052018-125738.

trace	seabed level* (m)		total water depth (m)	1st reflr	DoB (cm)		sleeper thickness (cm)	depth seabed mult (m) (HF)	depth variability					
									seabed (m) (HF)		DoB (cm) (LF/LF)		seabed mult(m) (HF)	
	LF demod	HF demod		LF demod	LF/LF	HF/LF			SD	RSD	SD	RSD	SD	RSD
185	0.824	0.789	0.90	0.995	17.1	20.6	-	1.474	0.005	0.6%	0.00	0.0%	0.005	0.3%
559	0.806	0.759	0.90	0.997	19.0	23.8	-	1.455	0.000	0.0%	0.48	2.5%	0.000	0.0%
1101	0.824	0.781	0.90	0.933	10.9	15.2	9.8	1.455	0.000	0.0%	0.89	8.2%	0.006	0.4%
1474	0.813	0.749	0.90	0.995	18.2	24.6	12.4	1.427	0.000	0.0%	0.00	0.0%	0.016	1.1%
1837	0.785	0.759	0.90	1.168	38.3	40.9	-	1.448	0.000	0.0%	2.77	7.2%	0.006	0.4%
2068	0.811	0.759	0.90	0.896	8.6	13.7	9.2	1.448	0.000	0.0%	0.98	4.8%	0.006	0.4%
2543	0.804	0.738	0.90	0.971	16.7	23.3	-	1.429	0.000	0.0%	0.96	5.7%	0.021	1.5%
2856	0.817	0.742	0.90	1.084	26.7	34.2	-	1.467	0.006	0.8%	0.01	0.5%	0.014	1.0%
3238	0.802	0.779	0.90	1.037	23.5	25.8	-	1.467	0.018	2.3%	2.73	12.1%	0.009	0.6%
3491	0.832	0.783	0.90	1.123	29.1	34.0	-	1.440	0.005	0.6%	0.48	1.6%	0.006	0.4%
4207	0.804	0.734	0.90	1.097	29.3	36.3	-	1.422	0.006	0.8%	0.96	3.3%	0.011	0.8%
4278	0.821	0.734	0.90	1.102	28.0	36.8	9.0	1.422	0.006	0.8%	0.89	4.0%	0.011	0.8%
4305	0.813	0.77	0.90	1.029	21.6	25.9	-	1.414	0.008	1.0%	1.17	5.4%	0.005	0.3%
4583	0.826	0.761	0.90	1.025	19.9	26.4	-	1.448	0.005	0.6%	1.79	9.0%	0.006	0.4%
4849	0.779	0.772	0.90	0.997	21.8	22.5	-	1.478	0.005	0.6%	0.48	2.0%	0.009	0.6%
5073	0.824	0.781	0.90	0.937	11.3	15.6	12.8	1.440	0.000	0.0%	0.59	5.2%	0.010	0.7%
5383	0.761	0.759	0.90	0.969	20.7	21	12.4	1.435	0.000	0.0%	0.59	2.8%	0.005	0.3%
mean	*0.809*	*0.762*					*10.9*	*1.445*	*0.004*	*0.5%*	*0.93*	*4.4%*	*0.008*	*0.6%*
SD	*0.019*	*0.018*						*0.019*						

Table D.14 (cont'd) Summary variability, Swan River sleeper site, SBP run 17052018-125738.

trace	amplitude variability								
	seabed			1st reflector			1st seabed multiple		
	amp	SD	RSD	amp	SD	RSD	amp	SD	RSD
185	-31670	2433	7.7%	-13021	2436	18.7%	9371	974	10.4%
559	28079	4821	17.2%	2854	620	21.7%	-7005	950	13.6%
1101	11050	1509	13.7%	-3186	603	18.9%	-6397	832	13.0%
1474	27606	2952	10.7%	2260	339	15.0%	-3441	143	4.1%
1837	17800	7113	40.0%	3116	382	12.3%	-2205	249	11.3%
2068	30783	3345	10.9%	21633	3024	14.0%	-2808	184	6.5%
2543	20407	7255	35.6%	3056	367	12.0%	3584	604	16.8%
2856	25534	2714	10.6%	-2315	414	17.9%	-5522	532	9.6%
3238	20293	2605	12.8%	3851	671	17.4%	-3763	285	7.6%
3491	-21414	5186	24.2%	1765	82	4.6%	-2922	211	7.2%
4207	-31812	1505	4.7%	1320	108	8.2%	-3215	540	16.8%
4278	-19917	7812	39.2%	1087	176	16.2%	-2062	235	11.4%
4305	12469	4267	34.2%	-1835	251	13.7%	4870	289	5.9%
4583	-16065	9093	56.6%	-2169	356	16.4%	-4802	1455	30.3%
4849	10731	2200	20.5%	-3023	604	20.0%	-3536	872	24.7%
5073	-26399	6284	23.8%	-16287	2079	12.8%	-5411	572	10.6%
5383	16555	8652	52.3%	-16287	2079	12.8%	-5411	572	10.6%
mean		*4691*	*24.4%*		*858*	*14.9%*		*559*	*12.4%*

Table D.15 Phase variability in amplitudes recorded from seabed and from 1st buried reflector, SBP runs 135105, 135516

		phase from seabed reflector	
		all the same (all + or all -)	not all the same
phase from 1st buried reflector	all the same, and same phase as seabed	2	8
	all the same, but opposite phase to seabed	5	11
	not all the same, but majority similar to seabed majority	3	12
	not all the same, but majority opposite to seabed majority		8